WORKSHOP ON ADVANCES IN SMOOTH PARTICLE HYDRODYNAMICS

Los Alamos National Laboratory,

September 21-23, 1993

WORKSHOP PROCEEDINGS

Organizing Committee:

Chuck Wingate
MS F645
Los Alamos National Laboratory
Los Alamos, NM 87545

email: caw@lanl.gov
phone: 505-667-8954
fax: 505-665-3389

Warner Miller
MS B288
Los Alamos National Laboratory
Los Alamos, NM 87545

email: warn@regge.lanl.gov
phone: 505-667-3747
fax: 505-665-4055

PREFACE

This proceedings contains copies of the viewgraphs presented at the September 1993 Workshop on Advances in Smooth Particle Hydrodynamics held at Los Alamos National Laboratory, Los Alamos, New Mexico. This was the second conference of this series. The first conference in this series was held at Phillips Lab in Albuquerque, New Mexico in January 1993 and was organized jointly by Phillips Lab and Sandia National Laboratory. Proceedings from the first conference, including a videotape of the meeting, can be obtained from Steve Attaway at Sandia.

We are now in the process of planning the third SPH meeting. If anyone has any suggestions for the next meeting please contact Chuck Wingate or Warner Miller at Los Alamos or Steve Attaway at Sandia.

We are indebted to Ms. Jan Muir who worked very diligently to assemble these proceedings, and to the Theoretical Division Office for their administrative assistance. We wish to acknowledge support for this conference from NASA under the High Performance Computing and Communications Program.

<div align="right">

Chuck Wingate (X-1, MS F645)
Warner Miller (T-6, MS B288)

Los Alamos National Laboratory
Los Alamos, NM 87545

December, 1993

</div>

TABLE OF CONTENTS

WORKSHOP ON ADVANCES IN SMOOTH PARTICLE HYDRODYNAMICS

Los Alamos National Laboratory, September 21-22 and September 23, 1993

At the Study Center (top floor of the library)

AGENDA

Tuesday, September 21, 1993

8:30   Welcome and administrative announcements

8:35   Bob Stellingwerf   What is SPH?

9:15   Joe Monaghan   SPH Masters Negative Stress

9:45   Break

10:15   Larry Libersky   Cylindrical SPH / SPH with energetic reactions

10:55   Dave Amdahl   Topics in SPH

11:30   Lunch

1:30   Charles Luehr   Progress on Interface Problems in SPH

2:00   Lou Baker   Boundaries and Interfaces in SPH

2:30   Break

3:00   Mike Owen   Methodology and Tests of Adaptive SPH

3:30   Mike Fisher   SPH Energy Conservation for Viscous Flows

5:30   Reception at the University House (next to the Study Center)

Wednesday, September 22, 1993

8:30	Administrative Announcements	
8:35	Gordon Johnson	Linked Penetration Calculations
9:00	Chuck Wingate	Topics in SPH
9:30	Marv Alme	SPHINX Simulations of Oblique Impact of Steel Fragments onto Steel Armor Plate (with Nick Ferriter)
10:00	Break	
10:30	Jeff Swegle	Stability and Consistency of the SPH Method
11:00	Dave Amdahl, Mike Fisher, Chuck Wingate and Bob Stellingwerf Graphics Demos	
11:30	Lunch	
1:30	Darrell Hicks	SPH: Instabilities, Wall Heating and Conservative Smoothing
2:00	Willy Benz	Tensor H and Fragmentation
2:30	Break	
3:00	Bob Stellingwerf	Workshop on Numerical problems in SPH

Thursday, September 23, 1993

9:00	Wojciech Zurek	Opening Remarks
9:15	Willy Benz	Tidal Disruptions and Elliptic Kernels
9:55	Mike Warren	Breaking the 1.e07 Particle Limit in SPH
10:35	Break	
11:00	Patrick Mann	SPH vs. FEM: Relativistic Spherical Collapse
11:40	Lunch	
1:00	Pablo Laguna	SPH without H
1:40	Warner Miller	Avoidance of Velocity-Biased Kernels
2:30	Break	
3:00	Hanno Sponholz	Tidal Disruptions and Accretion Disks
3:40	Joe Monaghan	Energy and Viscosity in Relativistic SPH

WHAT IS SPH ?

Overview, Comments, Trieste

Smooth Particle Hydrodynamics Workshop

September, 21, 1993, LANL

Bob Stellingwerf

Los Alamos National Laboratory

Applied Theoretical Division

Los Alamos

SPH is a *MONTE CARLO* Technique!

- First proposed as such by Lucy in 1977.

- Many improvements have been made to SPH since then, but it still is based on a Monte Carlo integration step.

- Basic Monte Carlo theorem, uniform sampling, i=1,N, over volume V:

$$\int f(x)dV \approx \frac{V}{N}\sum f_j = \sum f_j \Delta V_j$$

- For random sampling with probability density ρdV (Lucy):

$$\rho(r) \approx \frac{M}{N}\sum w(r-r_j) = \sum w(r-r_j)\Delta m_j$$

where $w(r-r')$ is a *kernel* that provides a local, compact support.

- Then for any specific quantity, Q (something/gm), we can compute the corresponding "density" $q = \rho Q$ (something/cc) via:

$$q(r) \approx \sum Q_j w(r-r_j)\Delta m_j$$

Los Alamos

SPH is a *MONTE CARLO* Technique (continued)

- Now, since Q_j is a constant, and all of the local variation of $Q(r)$ has been transferred to the $w(r-r')$, we have:

$$\nabla q(r) \approx \sum Q_j \nabla w(r - r_j) \Delta m_j$$

- Now, to do physics we interpret the Δm_j as the mass associated with "particle" j, and the interpolated velocity as the mean velocity of that mass, and *presto*, we have a (real) Lagrangian scheme!

- Note, however, that the "particles" are still actually Monte Carlo sampling points, the kernels overlap, and SPH is actually *not* a particle scheme at all, much less a Lagrangian hydro scheme...

- Much progress since Lucy can be attributed to Monaghan, who noted:
    1. Since an interpolation is involved to apply the integral theorem, a considerable body of interpolation theory can be applied.
    2. By applying some algebraic tricks, the SPH equations can be made to conserve mass, momentum, angular momentum and (optionally) total energy.
    3. The sampling error can be reduced by starting with a regular grid of points.

Los Alamos

SPH Volume Element

- **A handy form of the Monte Carlo integral for SPH is:**

$$\langle f(r) \rangle = \int f(r') w (r - r') dV = \sum f_j w (r - r_j) \Delta V_j$$

- **Where <> indicates the interpolated function, and the usual choice for ΔV_j is (m_j / ρ_j).**

- **Other possibilities can be considered: Lucy used** $\langle f_i \rangle = \dfrac{\sum f_j w (r_i - r_j) m_j}{\rho_i}$

  or we could consider $\langle f_i \rangle = \left(\dfrac{m_i}{\rho_i} \right) \sum f_j w (r_i - r_j)$.

- **Another possible choice might be**

$$\langle f_i \rangle = \frac{\sum f_j w (r_i - r_j)}{\sum w (r_i - r_j)}$$

  - **this has the advantage that neither the mass nor the density enters the interpolation, and edge effects are eliminated (functions are constant to the edge of the kernel), but the implied boundary condition at the edge of an object is $\Delta P = 0$, rather than $P = 0$.**

- **Another problem with all of these alternatives is that symmetry (required for momentum and energy conservation) is usually lost, but not all possibilities have been explored.**

Los Alamos

SPH Problem Areas

- Adequate coverage of w(r-r') is needed to approximate the integral. This means lots of neighbors, and preferrably a non-uniform spacing. Interpolation theory, on the other hand, requires regular spacing and gives best results with narrow kernels. A balance is needed.

- Spherical particles impose a maximum 1D strain that can be tolerated, and imply an elasticity limit that can cause premature fracture (tennis ball problem). Widening the kernel fixes this in most cases.

- Instabilities related to the "cell-centered" averaging are sometimes seen. These are most often encountered in quiescent regions under tension, although the analogous compressional instability has never been seen.

- Interfaces in which some quantities (such as mean molecular weight) vary discontinuously can cause large fluctuations when perturbed.

- Density given by the sum of masses formula cannot be constant at the edge of an object. This is incompatible with a solid equation of state.

- Densities given by integrating a continuity equation may not be consistent with the masses used in the integral sums.

Los Alamos

SPH- Some Comments

- **Tennis Ball Problem:** extra viscosity, different kernel, or simply increasing the smoothing length (more neighbors) fixes this. The optimum fix may be to allow non-spherical kernels.

- **Fracture:** very high strain/high fracture experiments are modeled very well for both ductile and brittle materials, even without a fracture model. Benz/Asphaug model shows promise of modeling fracture accurately on all scales.

- **Continuity Equation:** seems to work, but no consistent way of setting the masses, or verifying that mass is conserved has been proposed.

- **Interfaces:** for individual problems a workable solution can often be found by carefully matching masses, sizes and placement of particles. No general treatment is known. Probably the most serious problem now facing the technique.

- **Cell-centered instability:** usually seen at very late time in relaxing problems such as crater formation. Varying the pressure average sometimes helps (Libersky). Not normally a serious problem for most applications.

Los Alamos

SPH
Masters Negative Stress

J. J. Monaghan
Monash University

J. A. Morris
Monash University

PROGRAM

- Why use particle methods

- Different forms of SPH

- Lessons from MHD — <u>stability</u>

- Stability when
$$P_a = \rho_0 r^2 \left[\frac{\rho_a}{\rho_0} - 1 + \mathbb{R} \right]$$

- Adjusting Kernels for the momentum conserving form

- Stability of Pressure difference form .

- Conclusions

Particle Methods

- They provide the natural way to solve the Hyperbolic terms in fluid equs

$$\frac{\partial A}{\partial t} + \vec{v} \cdot \nabla A = \ldots$$

particles carry mass, mom, thermal energy etc.—

- Interfaces can be followed easily

- Errors appear in a physically sensible way e.g.
  (A) Plasma - Incorrect choice → Heating
     of parameters

     parameters now O.k.

  (B) Elastic - Material fractures

- Because the particle method is directly related to the corpuscular nature of the fluid
  conservation good
  complicated physics can be added easily

- Efficient for highly distorted flow
  -splash, fragmentation

S.P.H.

- Particle method without a grid
- Properties from Interpolation from Particles

Mutant Forms

- Different Kernels

- Different arrangement of terms

- Different time stepping

- Different h variations

- Different viscosity - other dissipation

M.H.D. Problems

Mom

$$\frac{d\vec{u}}{dt} = -\frac{\vec{\nabla}P}{\rho} + \frac{\vec{J}\times\vec{B}}{\rho}$$

or

$$\frac{dv_i}{dt} = -\frac{1}{\rho}\frac{\partial P}{\partial x^i} + \frac{1}{\rho}\frac{\partial M_{ij}}{\partial x^j}$$

where

$$M_{ij} = \frac{1}{\mu_0}\left(B_i B_j - \frac{1}{2}B^2 S_{ij}\right)$$

ideal gas

G. Phillips, J.J. Monaghan M.N.R.A.S. 216, 883 (1985)

$\vec{B}$ _____→ x

One D motion · · · · · · · · · ↑ particle
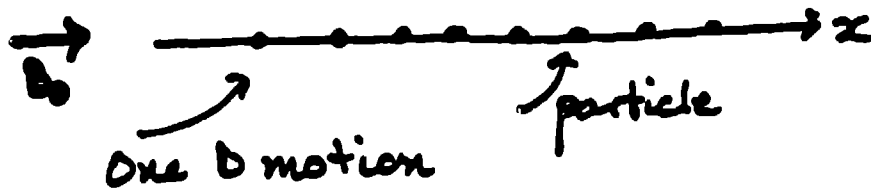
$$\frac{dv_a}{dt} = -\sum_b m_b\left[\frac{P_b}{\rho_b^2} + \frac{P_a}{\rho_a^2} - \frac{1}{3\mu_0}\frac{B^2}{\rho^2}\right]\vec{\nabla}W_{ab}$$

$$\frac{1}{\rho^2} = \frac{1}{\rho_a^2} + \frac{1}{\rho_b^2}$$

Perturbations

keep particles apart

Potential Barrier

$P_0 > \frac{B_0^2}{3\mu_0}$

Potential Well

$P_0 < \frac{B_0^2}{3\mu_0}$

Tries to pull particles together
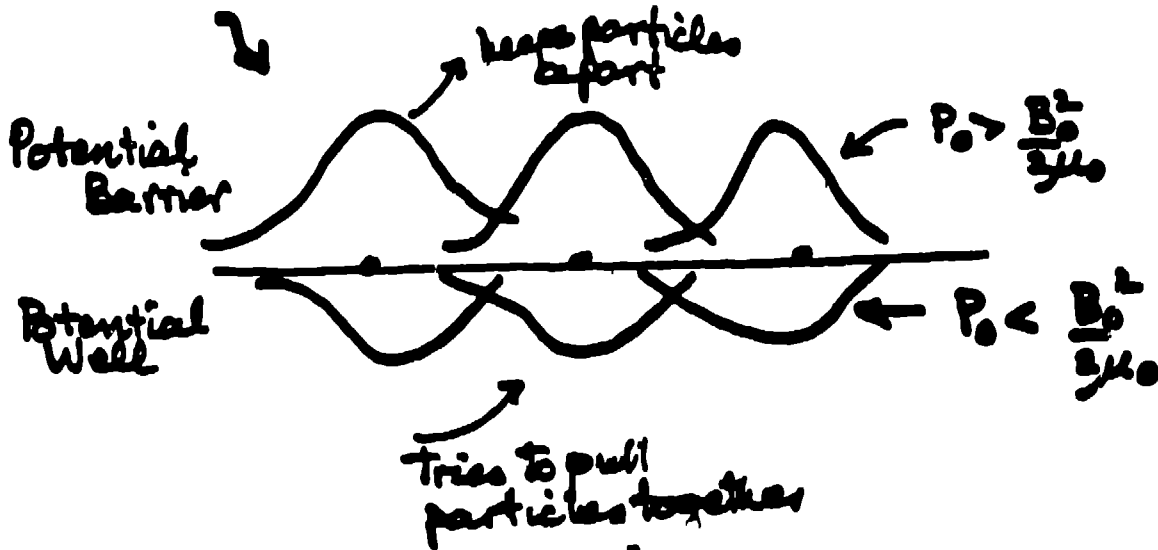
How The Instability
Was Removed

Pressure term
Treated in the usual way

Magnetic term
either

calculate $\vec{J}, \vec{B}$ then $\vec{J} \times \vec{B}$

or

Make $M_{ij} < 0$ by subtracting a constant.

Analysis

Jeff Swegle + others. (Jerry Brackbill ......)
Joe Morris, Willy Benz

$$P_a = \rho_o c^2 \left[\frac{\rho_a}{\rho_o} - 1 + R_b \right]$$

(constant) — pointing to R_b

$R = 1 \rightarrow$ isothermal gas
$R = 0 \rightarrow$ like metal
$R < 0 \rightarrow$ unstable cases
$R = 1 - \frac{B_o^2}{2\mu_o} \rightarrow$ mag. case.

1D Gas

particle

$\leftarrow \Delta x \rightarrow$
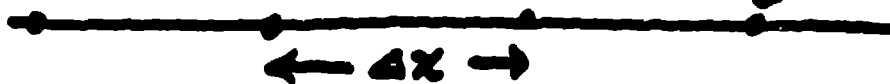
Small Oscillation $\begin{cases} \text{Pert} \propto e^{i(k(a\Delta x) - \omega t)} \\ \rho_a \approx \rho_o \quad \text{background} \end{cases}$

$$\sum_a f_a \sim \int_{-\infty}^{\infty} f(x)\,dx$$

$$U(k,h) = \int_{-\infty}^{\infty} e^{-iku} W(u,h)\,du \qquad \text{If } U=1 \text{ result is exact}$$

Only o.k for $hk \ll 1$.

$$\boxed{\omega^2 = c^2 k^2 \left[2 R_0 \, U(k,h) - (2R_0 - 1) U^2(k,h) \right]}$$

gaussian

$$\omega^2 = c^2 k^2 \, e^{-\left(\frac{hk}{2}\right)^2} \left[2R_0 - (2R_0-1) e^{-\left(\frac{hk}{2}\right)^2} \right]$$

$$< 0 \text{ if } R_0 < 0$$

Recall

$$\begin{cases} P_a = \rho_a c^2 \left[\dfrac{\rho_a}{\rho} - 1 + R_0 \right] \\[2mm] \dfrac{\nabla P_a}{\rho_a} = \sum_b m_b \left(\dfrac{P_a}{\rho_a^2} + \dfrac{P_b}{\rho_b^2} \right) \nabla_a W_{ab} \\[2mm] \rho_a = \sum_b m_b W_{ab} \end{cases}$$

$$\sum_{n=-\infty}^{\infty} f_n = \sum_{l=-\infty}^{\infty} \int_{-\infty}^{\infty} f(x) e^{-2\pi i l x} dx$$

Gives useful expressions

Direct Summation

$$\omega^2 = 2c^2 R \sum_j \Delta x \left(1 - \cos(j k \Delta x)\right)\left(\frac{\partial^2 W}{\partial x^2}\right)_j$$

$$+ c^2(1 - 2R) \left\{ \sum_j \Delta x \cdot \sin(j k \Delta x)\left(\frac{\partial W}{\partial x}\right)_j \right\}^2$$

$h = 1.2$

Normalised numerical sound speed squared

Contour
Sep = 0.1

R →

Unstable

k →

c^2 Normalised numerical sound speed squared

good

Fair

h

good -

k →

R = 1

contour
sep = 0.1
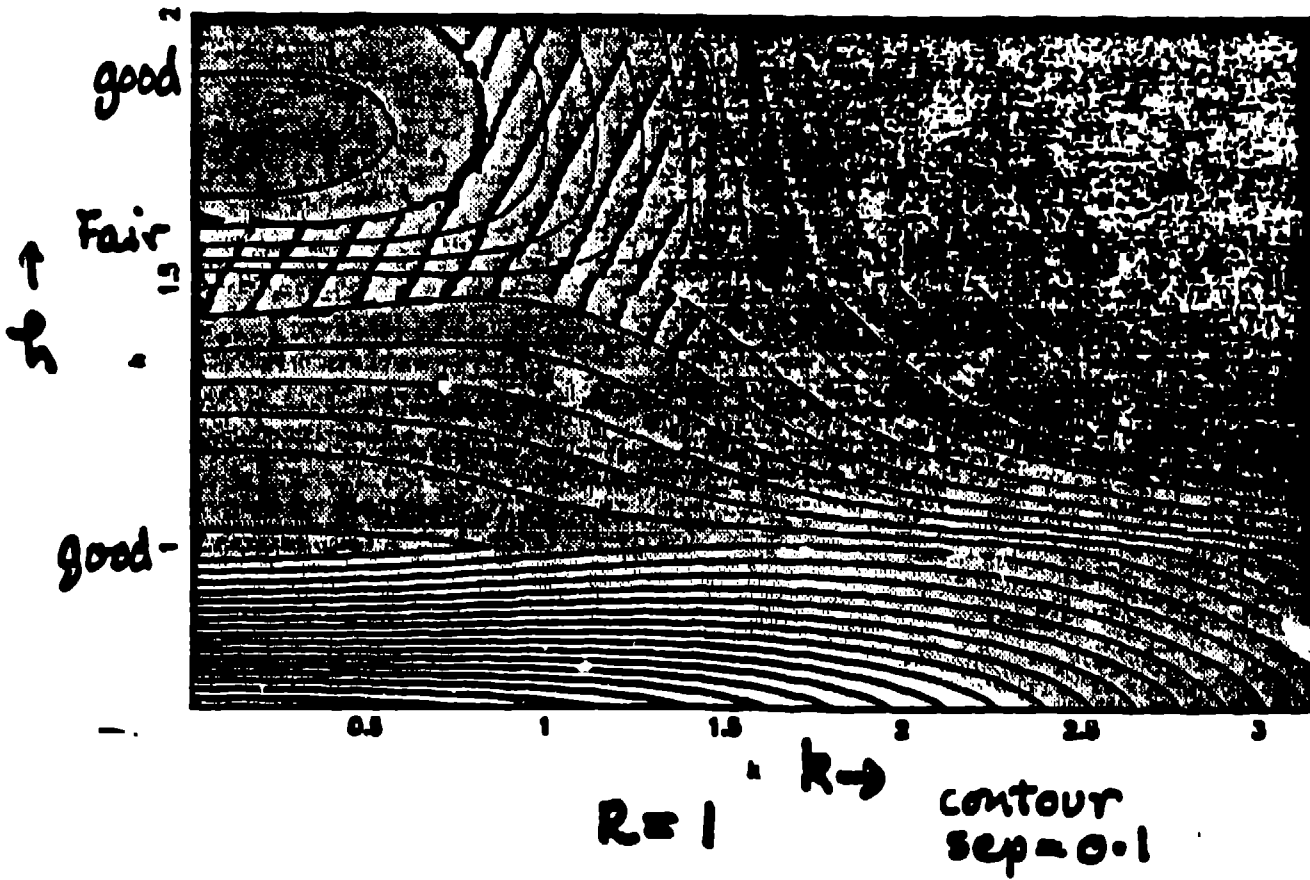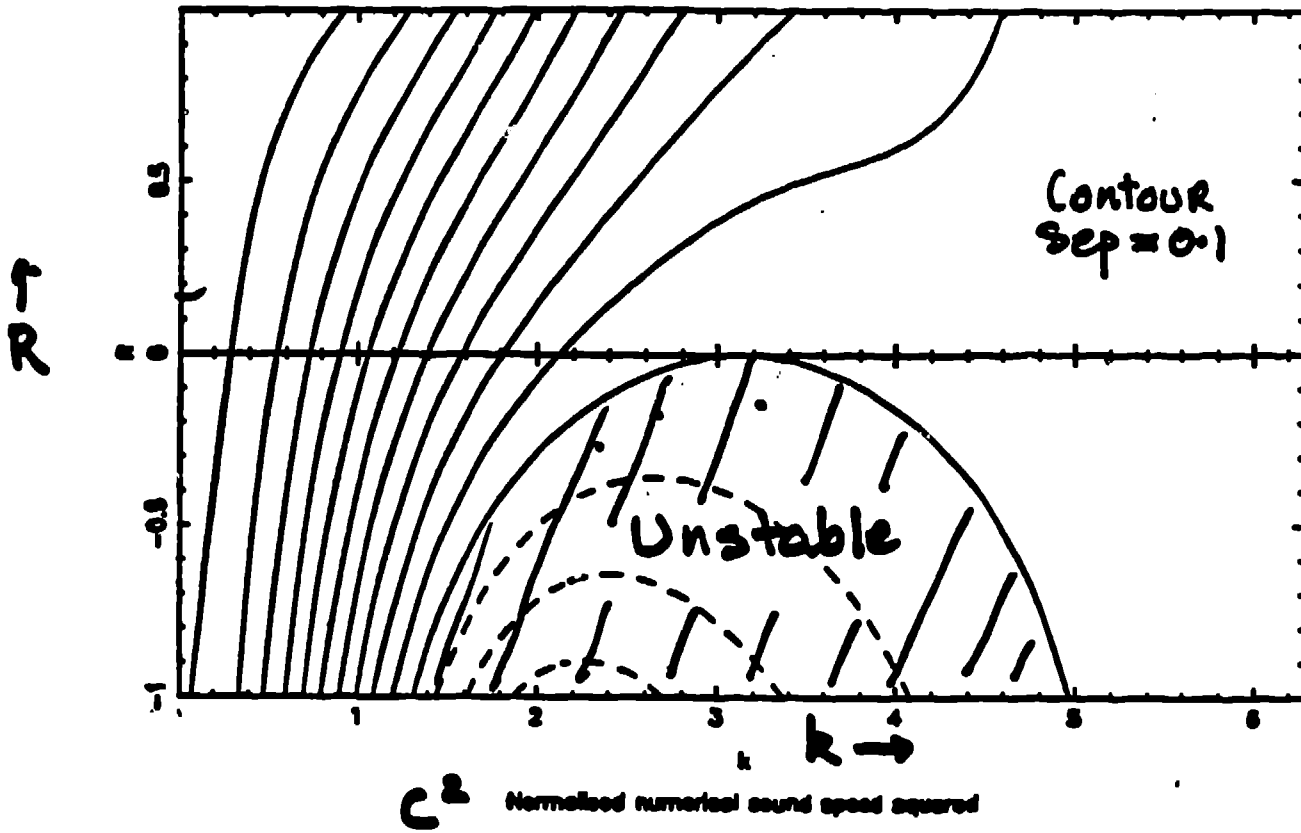
Tailor Made Kernels
'A Pack of Camels'

$$W_n = A_n \left(\frac{x}{h}\right)^{2n} W_0$$

Then

$$W(x,h) = \sum_{n=0}^{N} B_n W_n(x,h)$$

With

$$\sum_n B_n = 1$$

Choose for
- Stability
- Speed of Sound

Example

$R_0 = -0.1$
$h = 1$

$B_0 = 0.6015625$
$B_1 = 0.375$
$B_2 = 0$
$B_3 = 0.0234375$
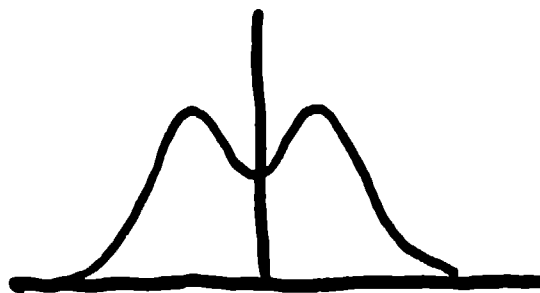
$n=1$
$R=-0.1$

c^2 Normalised numerical sound speed squared

Unstable

Stable for all $R < 0$

$k \rightarrow$

c^2 Normalised numerical sound speed squared

Unstable
$c^2 > -0.05$

Unstable

Unstable

$k \rightarrow$
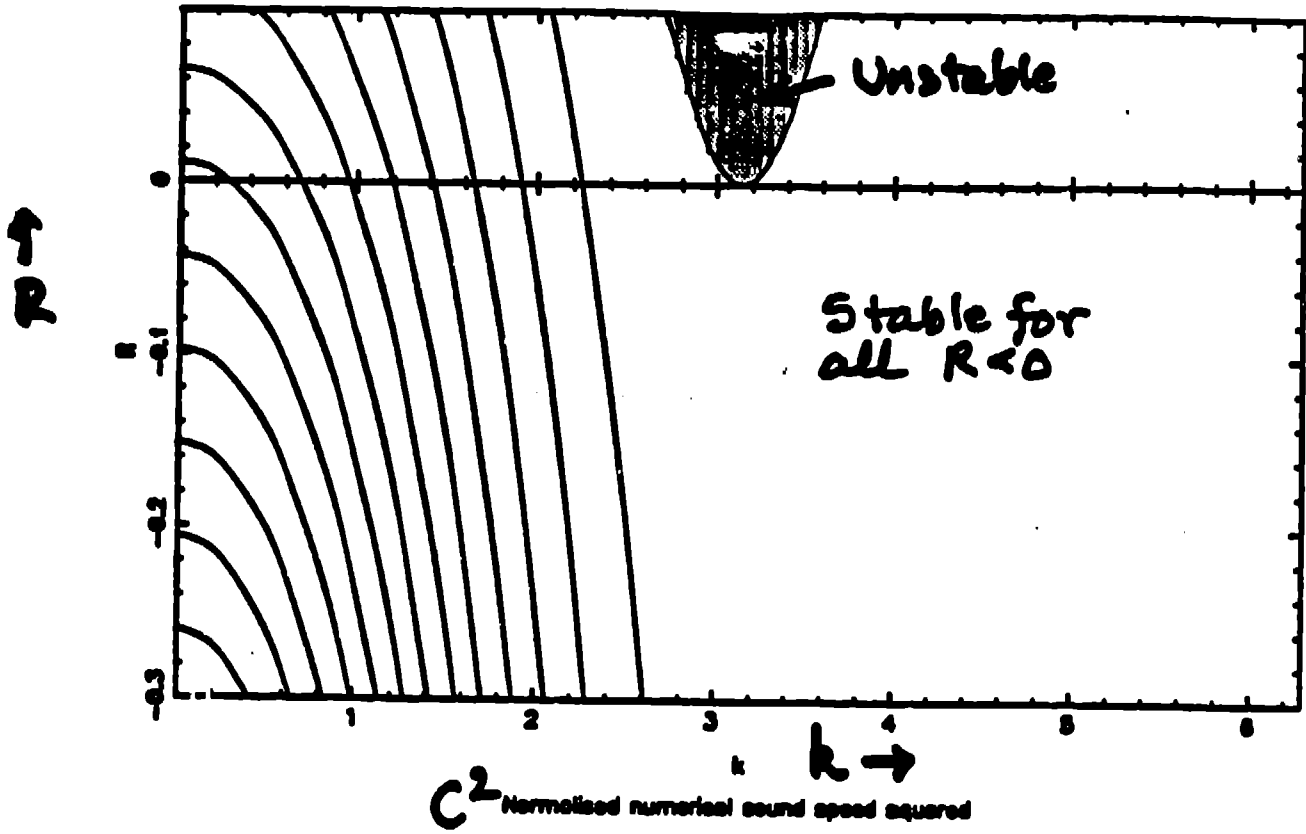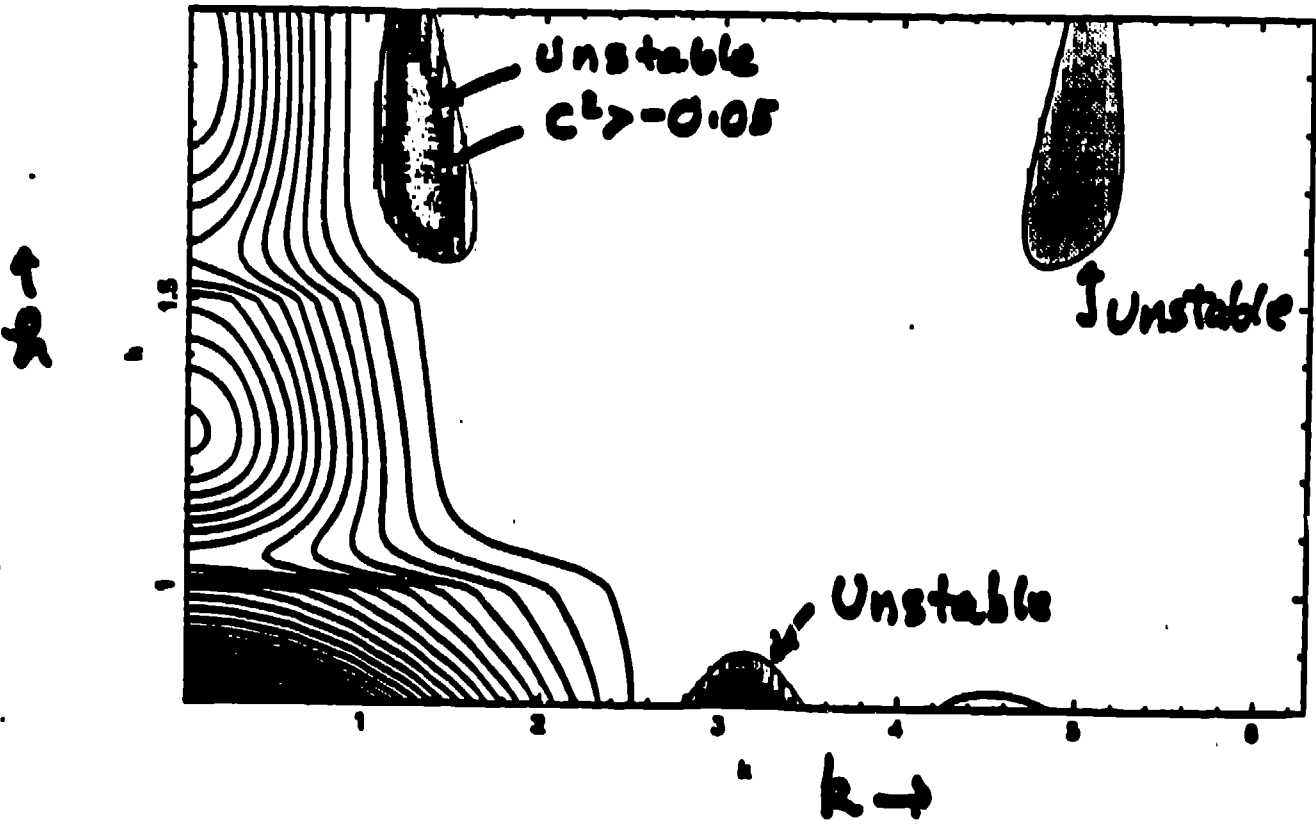
Kernels

$$W_0(x,h) = \frac{1}{h} \begin{cases} \frac{2}{3} - \left(\frac{x}{h}\right)^2 + \frac{1}{2}\left(\frac{|x|}{h}\right)^3 & ; 0 \leq |x| < h \\ \frac{1}{6}\left(2 - \frac{|x|}{h}\right)^3 & ; h \leq |x| \leq 2h \\ 0 & ; |x| > 2h \end{cases}$$
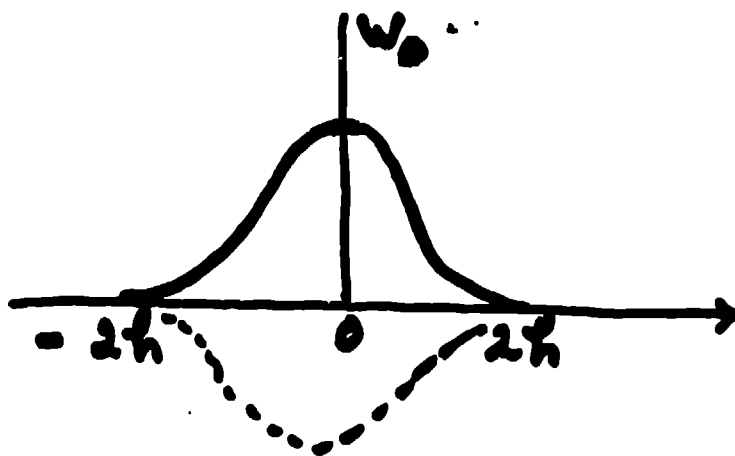
Dromedary Camel
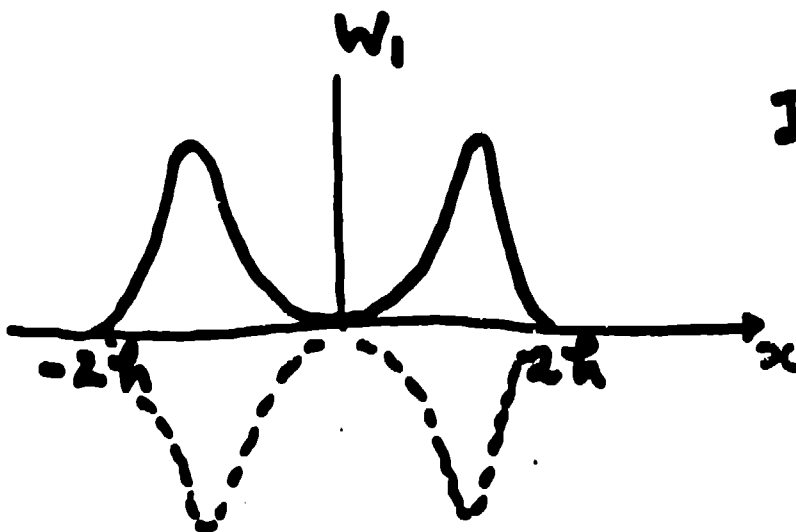
Bactrian Camel

$$W_1 = 3\left(\frac{x}{h}\right)^2 W_0$$

Pressure Difference ∇P

$$\left(\frac{\nabla P}{\rho}\right)_a = \sum_b m_b \left(P_b - P_a\right) \frac{\nabla_a W_{ab}}{\rho_a \rho_b}$$

Stability for 1D

No R_o

$$\omega^2 = \left(\frac{mc}{\rho_o}\right)^2 \left[\sum_{-a}^{\infty} \sin(k a x_j) \frac{\partial W_j}{\partial x} \right]^2$$

ALWAYS STABLE

Excellent C

Thermal Energy Equ. (Not Needed Here).

$$\frac{d u_a}{dt} = -\frac{P_a}{\rho_a} \sum_b m_b \frac{\left(\vec{v}_b - \vec{v}_a\right)}{\rho_b} \cdot \nabla_a W_{ab}$$

Normalised numerical sound speed squared
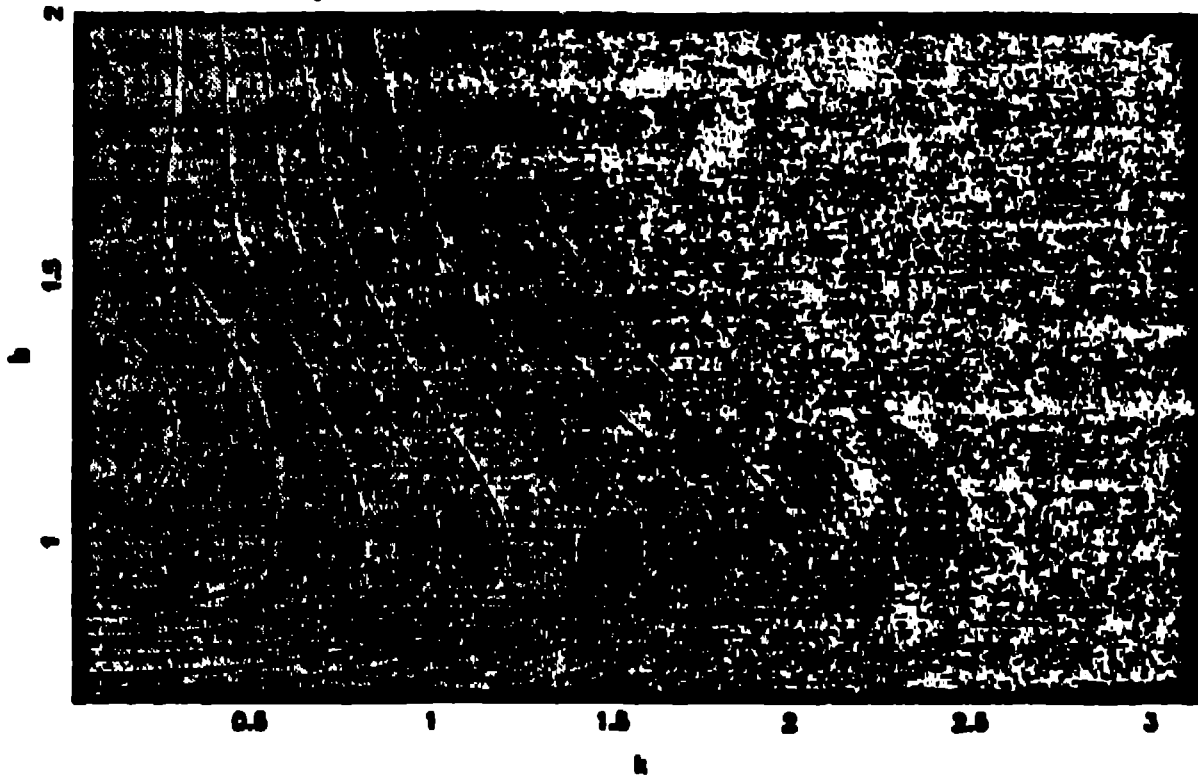
Normalised numerical sound speed squared

C^2 Momentum Conserving Form

$R=1$

Some Oscillation

$\uparrow \int \rho$

[Pressure Difference]

$\uparrow \int \rho$
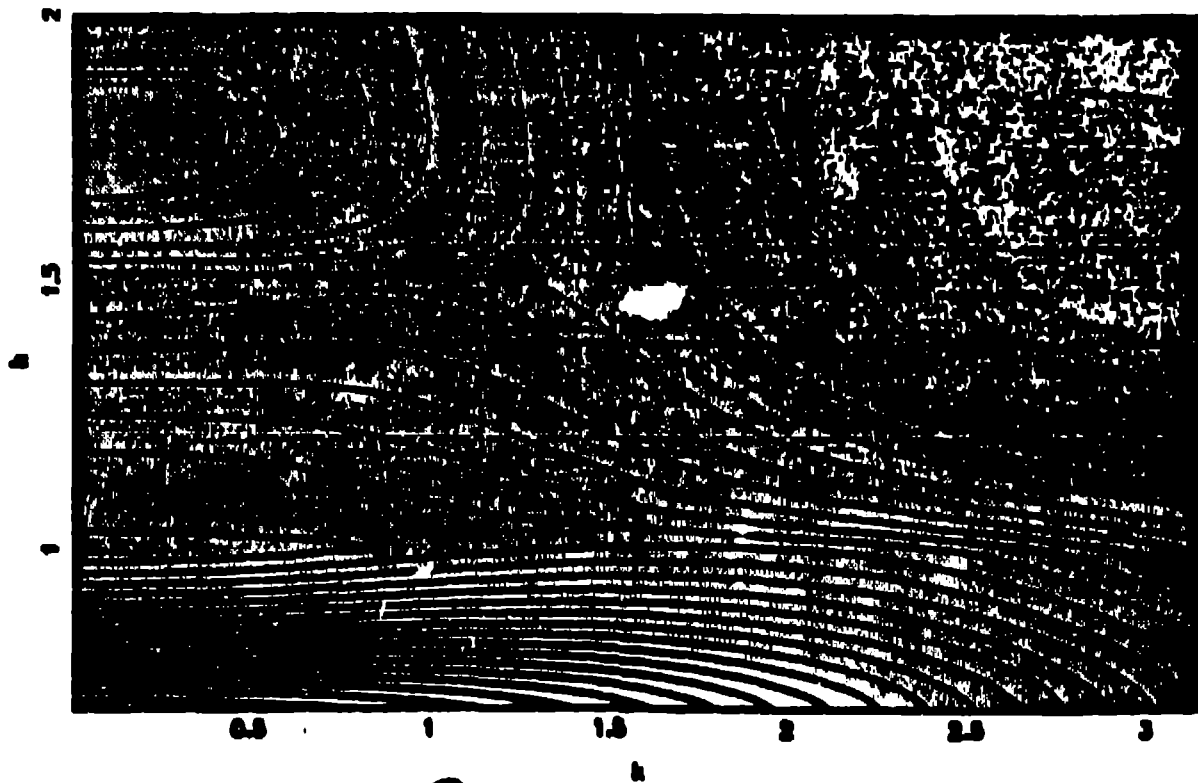
[Momentum Conserving]
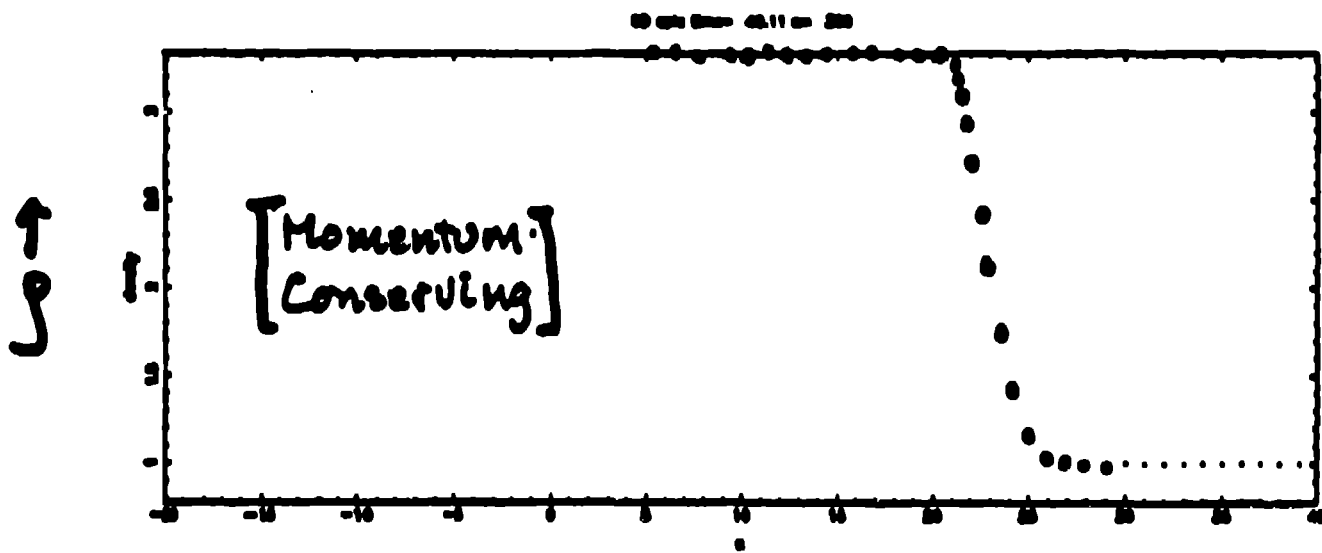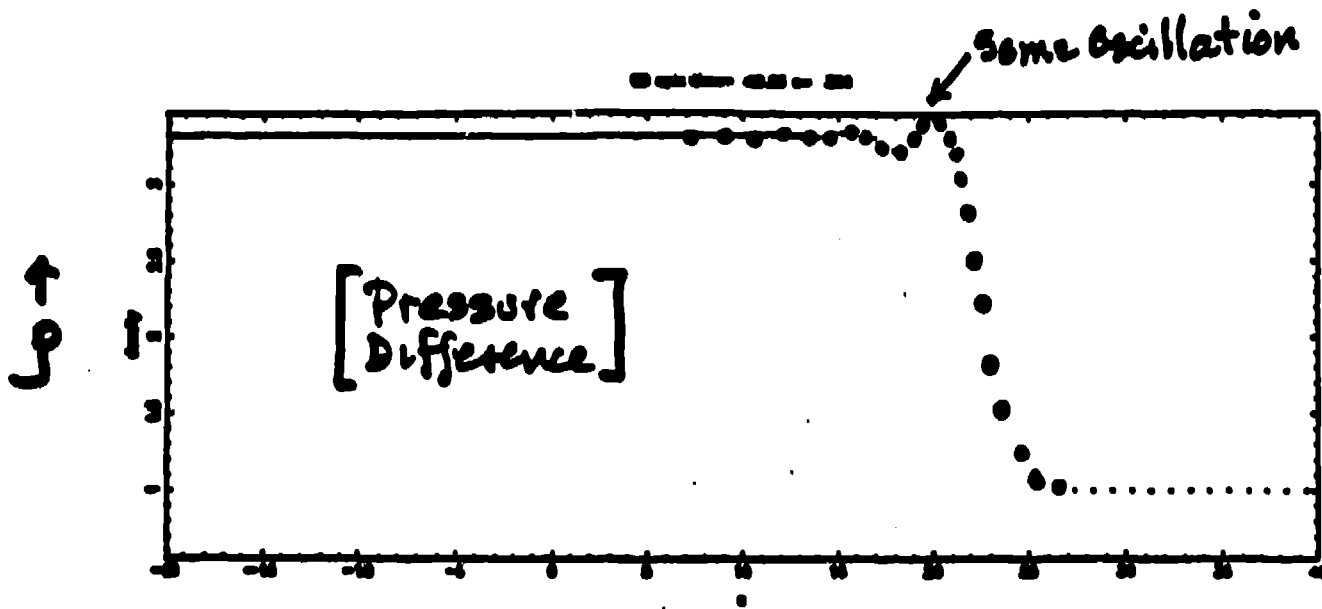
P. Diff

V. Good C
'Good' shock

Conserve mom with Lagrange Mult.

Take Home Message

- If $P \gtrsim 0$ use Mom Conserving form

- If $P < 0$ use Press. Diff form
  $$\text{or}$$
  $$\text{Tailor made Kernels}$$

- IF
  $$\text{stress}: \quad T_{ij} = -P \overset{\nearrow \gtrsim 0}{\delta_{ij}} + M_{ij}$$

$$\frac{d\vec{v}_i}{dt}(a) = -\sum_b m_b \left(\frac{P_a}{\rho_a^2} + \frac{P_b}{\rho_b^2} \right) \nabla_a W_{ab}$$

$$+ \sum_b m_b \left[\frac{M_{ij}(b) - M_{ij}(a)}{\rho_a \rho_b} \right] \nabla_{a,j} W_{ab}$$

CALCULATION OF REACTIVE FLOW USING SMOOTHED PARTICLE HYDRODYNAMICS

L.D. Libersky   A.G. Petschek   Per-Anders Persson

Energetic Materials Research Testing Center (EMRTC) and
Department of Physics
New Mexico Institute of Mining and Technology
Socorro, NM 87801

Reactive flow is incorporated within the framework of Smoothed Particle Hydrodynamics and a mixture rule is formulated which allows for treatment of large grained explosives and propellants. The method is tested using length scales fine enough to resolve the reaction zone. The simulation seems to reproduce ideal detonation theory quite well for planar steady-state detonation in Composition-B.

INTRODUCTION

Smoothed Particle Hydrodynamics (SPH) is a relatively new computational technique that seems well suited to simulation of reactive flow. The method uses Lagrangian fluid elements (particles) that are not tied to any underlying spatial grid. The gridless nature of the technique makes it possible to compute highly distorted flow in a pure Lagrangian frame. The method has other nice features such as the relative ease of adding new physics and of extending calculations to three dimensions. Application of SPH to the calculation of reactive flow has the potential, therefore, for improved accuracy and extended applicability. The main purpose of this paper is to describe the inclusion of reactive flow within the SPH framework. In so doing, we introduce new ways of treating the temperature in which (a) thermal equilibrium is not a mixture rule and (b) the temperature reference curve is determined analytically. A simulation of planar steady-state detonation in Composition-B is shown to reproduce ideal detonation theory quite well.

THEORY

The SPH representation of the fluid conservation equations are given below (see [1] for derivations).

$$\frac{d\rho}{dt} = \rho_i \sum_j \frac{m_j}{\rho_j}(U_i^a - U_j^a)\frac{\partial W_{ij}}{\partial x_i^a} \qquad (1)$$

$$\frac{dU_i^a}{dt} = -\sum_j m_j \left(\frac{P_i}{\rho_i^2} + \frac{P_j}{\rho_j^2} + \Pi_{ij}\right)\frac{\partial W_{ij}}{\partial x_i^a} \qquad (2)$$

$$\frac{dE}{dt} = \sum_j m_j (U_i^a - U_j^a)\left(\frac{P_i}{\rho_i^2} + \tfrac{1}{2}\Pi_{ij}\right)\frac{\partial W_{ij}}{\partial x_i^a} \qquad (3)$$

Variables are coordinates (x), time (t), density (ρ), velocity (U), specific internal energy (E), pressure (P) and artificial viscosity (Π). The subscripts refer to a given particle (i) and its neighbors (j). Interactions between particles are weighted by the interpolation kernel W called the smoothing function. Typically, W is a B-spline whose width Δ is measured by the parameter h, the smoothing length. Notice that only gradients of W appear in these equations. Because of this, no underlying spatial grid is required. The formulation can be extended to include reactive flow by adding a constitutive relation and a rate equation for the unburned fraction (λ) of reacting material. From this point on we drop the particle index in order to use subscript notation for other purposes.

$$P = P(\rho, E, \lambda) \qquad (4)$$

$$\frac{d\lambda}{dt} = f(P, \rho, \lambda) \qquad (5)$$

Reacting material is partitioned into unburned solid (s) and reacted gas (g) phases according to conservation laws for mass and energy.

$$V = \lambda V_s + (1-\lambda)V_g \tag{6}$$

$$E = \lambda E_s + (1-\lambda)E_g \tag{7}$$

Here, $V=1/\rho$ is the specific volume. In order to close the system of equations (1-5) two additional constraints are required. For high density military explosives, it has often been assumed that the chemical reaction occurs homogeneously, therefore one chooses pressure and temperature equilibrium between the solid and gas phases of the burning material. However, for composite reacting materials having grain sizes typical of many explosives and propellants, the assumption of temperature equilibrium is not valid. A more realistic assumption for large grained materials would be that negligible heat transfer occurs between the two phases, i.e., the unreacted solid behaves isentropically. We therefore close the system of equations (1-6) by imposing the constraints of pressure equilibrium and an adiabatic solid.

$$P_s = P_g \tag{8}$$

$$\frac{\partial E_s}{\partial V_s} = -P_s \tag{9}$$

In order to use (9) we must know which isentrope the reacting material is on. For ideal steady state detonations this is the isentrope passing through the von-Neumann point. For transitions to detonation a family of adiabats defined by the solid Hugoniot are encountered by the reacting material. A prognostic equation for the entropy is added for this purpose.

$$\frac{dS}{dt} = \frac{dQ}{T} \tag{10}$$

The heat added (dQ) is the artificial viscous work (Π terms in equation 3). Equation (10) also introduces the temperature T which we compute by linear extrapolation form the principal adiabat.

$$T = T_s + (E - E_s)/C_v \tag{11}$$

Using the First Law

$$dE = TdS - PdV , \tag{12}$$

the following relations can be derived

$$\left.\frac{\partial T}{\partial V}\right)_s = \left.\frac{\partial P}{\partial S}\right)_V \qquad \left.\frac{\partial E}{\partial S}\right)_V = T \tag{13}$$

Assuming a Gruneisen equation of state

$$P(V,E) = P_H(V) + \frac{\gamma}{V}[E - E_H(V)] , \tag{14}$$

the pressure derivative in (13) can be written as

$$\left.\frac{\partial P}{\partial S}\right)_V = \left.\frac{\partial T}{\partial V}\right)_s = \left.\frac{\partial P}{\partial E}\right)_V \left.\frac{\partial E}{\partial S}\right)_V = \frac{\gamma}{V}T \tag{15}$$

An equation for the solid adiabat temperature is, therefore,

$$\left.\frac{\partial T}{\partial V}\right)_s = \frac{\gamma}{V}T \tag{16}$$

which, for $\gamma/V=$const. integrates to

$$T_s e^{(\gamma_o,V_o)V} = T_o e^{\gamma_o} \tag{17}$$

We obtain the adiabat energy E_S by integration.

$$E_s(V) = -\int_{V_o}^{V} PdV =$$

$$\int_{V_o}^{V}\left[P_H + \frac{\gamma}{V}(E - E_H)\right]dV \tag{18}$$

where the Hugoniot pressure and energy are given by

$$P_H = \frac{C^2(V_o - V)}{[V_o - S(V_o - V)]^2} \tag{19}$$

$$E_H = \frac{1}{2}P_H(V_o - V) \tag{20}$$

Here, C and S are coefficients in the linear shock speed - particle speed relationship $U_s = C + SU_p$ and V_o is the normal volume. Choosing $\gamma/V=a$ to be constant, and letting $F = E \exp(aV)$ we have

$$F = -\int_{V_o}^{V} e^{aV}\left[P_H - \frac{\gamma}{V}E_H\right]dV \tag{21}$$

which integrates to

$$F(V) = \frac{1}{2S^2}\left\{-C^2(2S-aV_o)e^{aV_o} + \left[1 + \frac{(2-aV_o/S)}{(SV/V_o - S+1)}\right]\right\} \tag{22}$$

$$+ \frac{C^2(2S^2 - 4aSV_o + a^2V_o^2)}{2S^2}\left\{Ei[a(V_o - V) + aV_o/S] - Ei(aV_o/S)\right\}$$

where Ei is the exponential integral. The adiabat energy is therefore,

$$E_s(V) = F(V)e^{-\frac{I_o V}{V_o}} \quad (23)$$

Equations (11), (17) and (23) are used to calculate the temperature of the solid required in (10). Methods using fits to the Hugoniot temperature for the reference curve [2] have caused us difficulties, apparently because we require temperatures outside the region of validity of the fit. The analytic nature of our method eliminates such problems.

EQUATIONS OF STATE

For the unreacted solid material the Gruneisen equation of state (14,19) is used. A HOM representation of the BKW [2] equation of state is used for the gaseous detonation products.

$$P = P_A + \frac{\gamma}{V}(E - E_A)/V \quad (24)$$

$$\ln(P_A) = A + B(\ln V) + C(\ln V)^2 + D(\ln V)^3 + E(\ln V)^4 \quad (25)$$

$$\ln(E_A) = K + L(\ln P) + M(\ln P)^2 + N(\ln P)^3 + O(\ln P)^4 \quad (26)$$

$$-1/\beta = R + S(\ln V) + T(\ln V)^2 + U(\ln V)^3 \quad (27)$$

Here, the subscript "A" represents the adiabat passing through the CJ point. The coefficients are computed using the "BKW" code [3].

For a partially reacted particle $(0 < \lambda < 1)$ we apply the mixture rules (8,9) in the following way. First we identify which adiabat the particle is on by comparing the particle entropy with the entropy on the solid Hugoniot. The family of adiabats is characterized by the solid Hugoniot curve for the unreacted material. Second, upper limits on the volume (V/λ) and energy (E/λ) of the solid are provided by (6,7) to ensure positive V_g and E_g. Next, we identify the lower limit for the solid volume as $V(E/\lambda)$ on the adiabat. Having an acceptable volume range for the partially reacted solid, we pick the arithmetic mean as the starting guess for V_s and compute V_g using (8). The starting solid energy is $E_s(V_s)$ with (9) providing E_g. A Newton-Raphson iteration is then used toward pressure equilibrium between the solid and gas phases, constraining the solid to move along its adiabat.

CALCULATION

A one-dimensional simulation was performed in order to examine planar steady-state detonation in Composition-B explosive using the new formalism within the framework of Smoothed Particle Hydrodynamics. For this calculation we took the

smoothing length (h) to be 1 μm. Burning was initiated by impacting the explosive with equivalent inert material. The shock pressure input to the sample was kept just below P_{CJ} (290 Kb) so as to minimize the run distance to detonation. A Forest-Fire rate [4] was used to describe the decomposition.

$$\frac{d\lambda}{dt} = \lambda \sum_{i=1}^{14} C_i P^{i-1} \quad (28)$$

The coefficients in (27) were obtained using the ATFIRE code [5] and are listed in Table1. Fits for the Comp-B isentrope (25,26,27) are given in Table 2. Solid parameters used were: $V_o = 0.583$ cc/g, $C = 0.21$ cm/μs, $S = 1.5$ and $\gamma = 2.0$.

i	C_i	i	C_i
1	-1.035458043E+01	8	8.206591093E+09
2	4.734274495E+02	9	-4.298662700E+10
3	-1.675370422E+04	10	1.618379369E+11
4	4.475674643E+05	11	-4.260581743E+11
5	-8.493147134E+06	12	-7.728984899E+11
6	1.195593435E+08	13	7.437676727E+11
7	-1.140256515E+09	14	3.616777570E+11

Table 1. Forest-Fire Rate Coef's for Comp-B

A-E	K-O	Q-U
-3.525848E+00	-1.560876E+00	7.502780E+00
-2.334291E+00	5.331214E-01	-4.412000E-01
5.972673E-01	8.063100E-02	1.912926E-01
3.043104E-02	3.338169E-03	6.778832E-02
-1.752264E-01	-6.843999E-04	-2.424033E-02

Table 2. HOM fit to BKW EOS for Comp-B

Figures 1,2 and 3 show different aspects of the SPH computed steady-state detonation in Composition-B explosive. Only fully or partially reacted particles are plotted for clarity. Inert "flyer plate" particles and particles not yet shocked are omitted. Figure 1 shows the pressure profile. The peak pressure at the shock front is 450 Kb which is the von-Neumann spike. The reaction is 100% complete 400 μm behind the spike at 290 Kb, the Chapman-Jouguet (CJ) state. The reaction is 75% complete 80 μm behind the shock front. These numbers compare well with experimentally measured values for Composition-B.

In Figure 2 the pressure is plotted on the ordinate and the reaction extent on the abscissa. The von-Neumann spike is seen near $\lambda = 1$ and the CJ point is seen near $\lambda = 0$. Notice the large number of particles (~100) comprising the reaction zone. Notice also that adequate resolution of the shock front is achieved in the sense that no substantial reaction takes place until the von-Neumann spike is reached. In Figure 3 the pressure is

again plotted on the ordinate but now the specific volume is used for the abscissa. This representation clearly shows the Rayleigh line extending from the von-Neumann spike to the CJ point. That compression to the von-Neumann point is not abrupt, and that the path to this point is curved, are both due to the artificial viscosity spreading out the shock. In addition to the results presented here we have also modeled cases using lower flyer-plate speeds (reduced shock input) and observe build-up to steady-state detonation consistent with wedge test results. We expect to present this data orally at the conference.

Figure 3. P vs V shows the von-Neumann spike, Rayleigh line and CJ point.
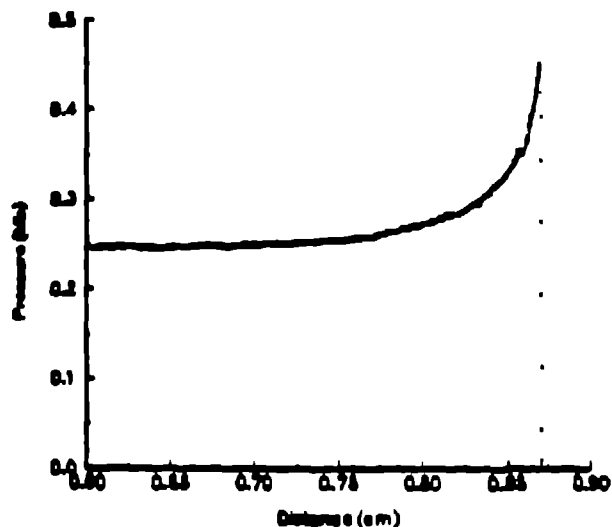
Figure 1. SPH computed pressure profile for steady-state planar detonation in Composition-B explosive.
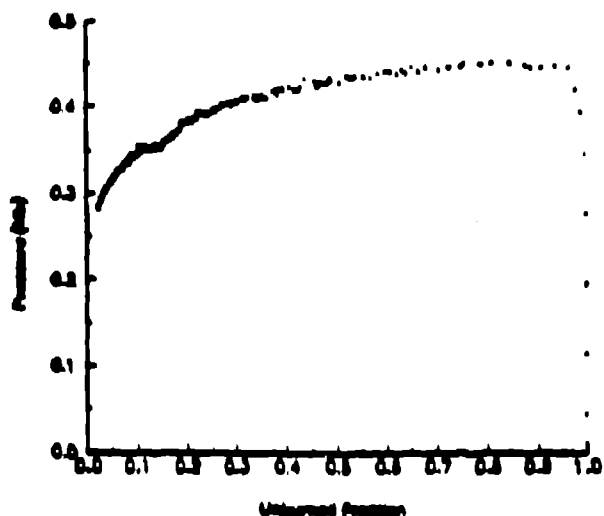
Figure 2. P vs λ shows approximately 100 particles comprising the reaction zone.

CONCLUSIONS

We have derived a new formalism for treating reactive flow and have incorporated it within the framework of Smoothed Particle Hydrodynamics. The mixture rules extend the applicability of reactive flow calculations to large-grained materials and the SPH computing technique allows for easy extension to three-dimensions and improved accuracy. We have tested the approach by calculating planar steady-state detonation in Composition-B. Results show ideal detonation theory to be reproduced quite well.

REFERENCES

1. Libersky, L.D.; Petschek, A.G.; Carney, T.C.; Hipp, J.R.; Allahdadi, F.A.; J. Comput. Phys., accepted for publication., Feb., 1993.

2. Mader, C.L., Numerical Modeling of Detonations, Univ. of Calif. Press, Los Angeles, CA, 1979, p.327.

3. ATBKW Computer Program, Los Alamos Code No. LP-181 Los Alamos National Lab., NM, 1986.

4. Mader, C.L.; Forest, C.A., Two-Dimensional Homogeneous and Heterogeneous Detonation Wave Propagation, LA-6259, Los Alamos National Lab., N.M., 1796.

5. ATFIRE Computer Program, Mader Consultant Co., Honolulu, HI, 1986.

Topics in SPH

Capt David Amdahl

21 September 1993
SPH Meeting
Los Alamos NM

Outline

- **Aero-SPH**
  - Review
  - Revisit the Previous Work
    - Variable H
    - Wall Heating
  - Supersonic Airfoil

Review

- SPH Requires No Grid
    Saves Time and Opens Problem Domain
    of Traditional CFD Methods

- Validate SPH

- Boundary Conditions
    Solid Boundary, In-Flow, and Out-Flow

- Inviscid, Compressible Flow
    Supersonic with Local Sub-Sonic Regions

Ramp Problem

Mach = 2.0

Density = 1.0

Pressure = 1.0

14.75 deg
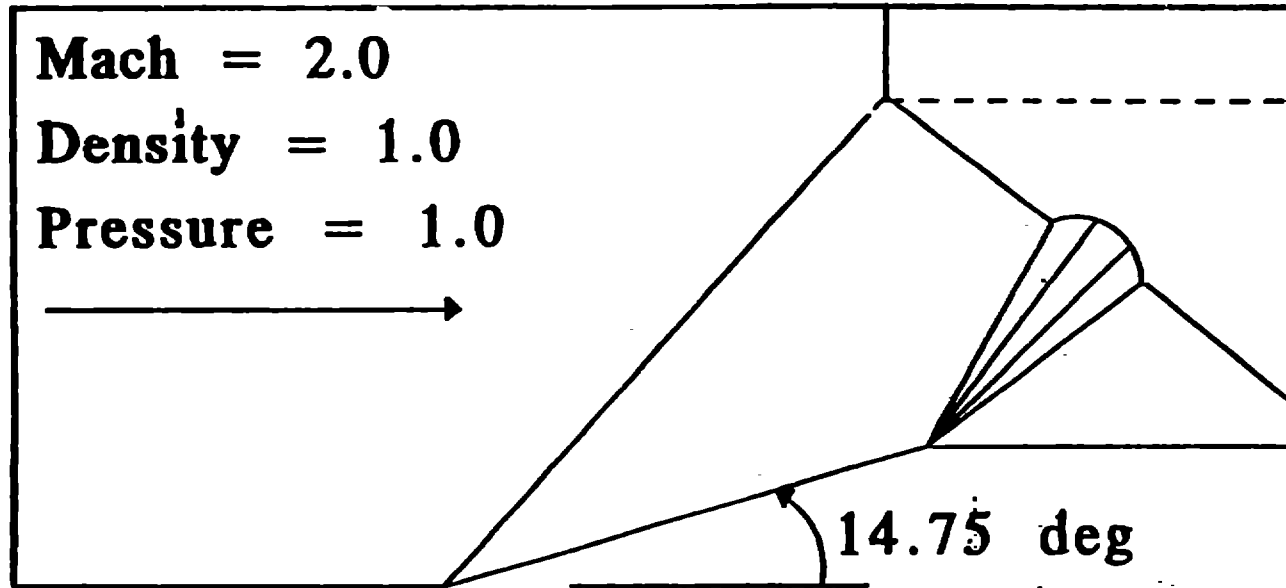
SPH Density Contours (No Wall Heating)
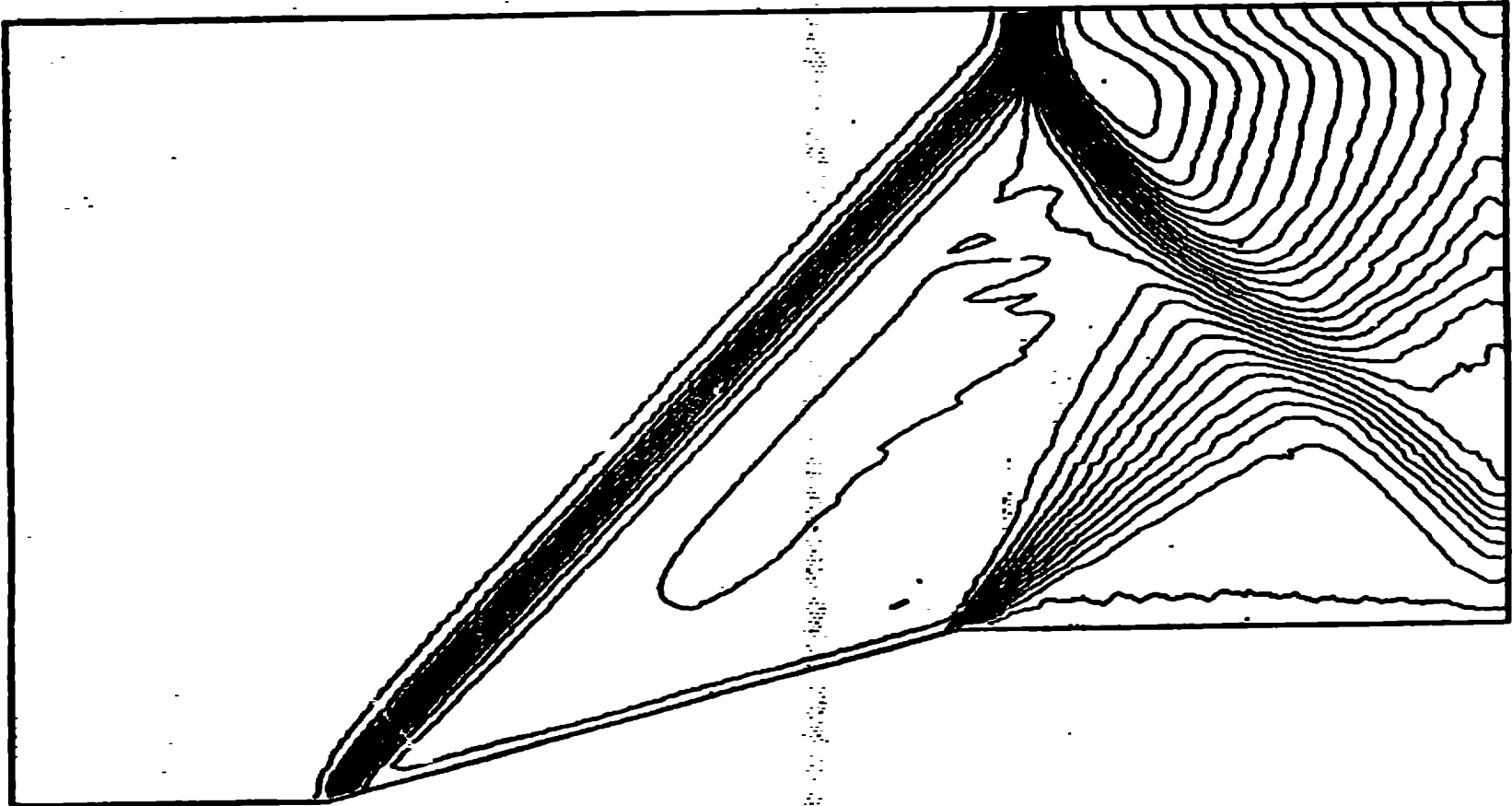
SPH Pressure Contours (No Well Heating)

SPH $\frac{p}{p\tau}$ Contours   (No Well Heating)
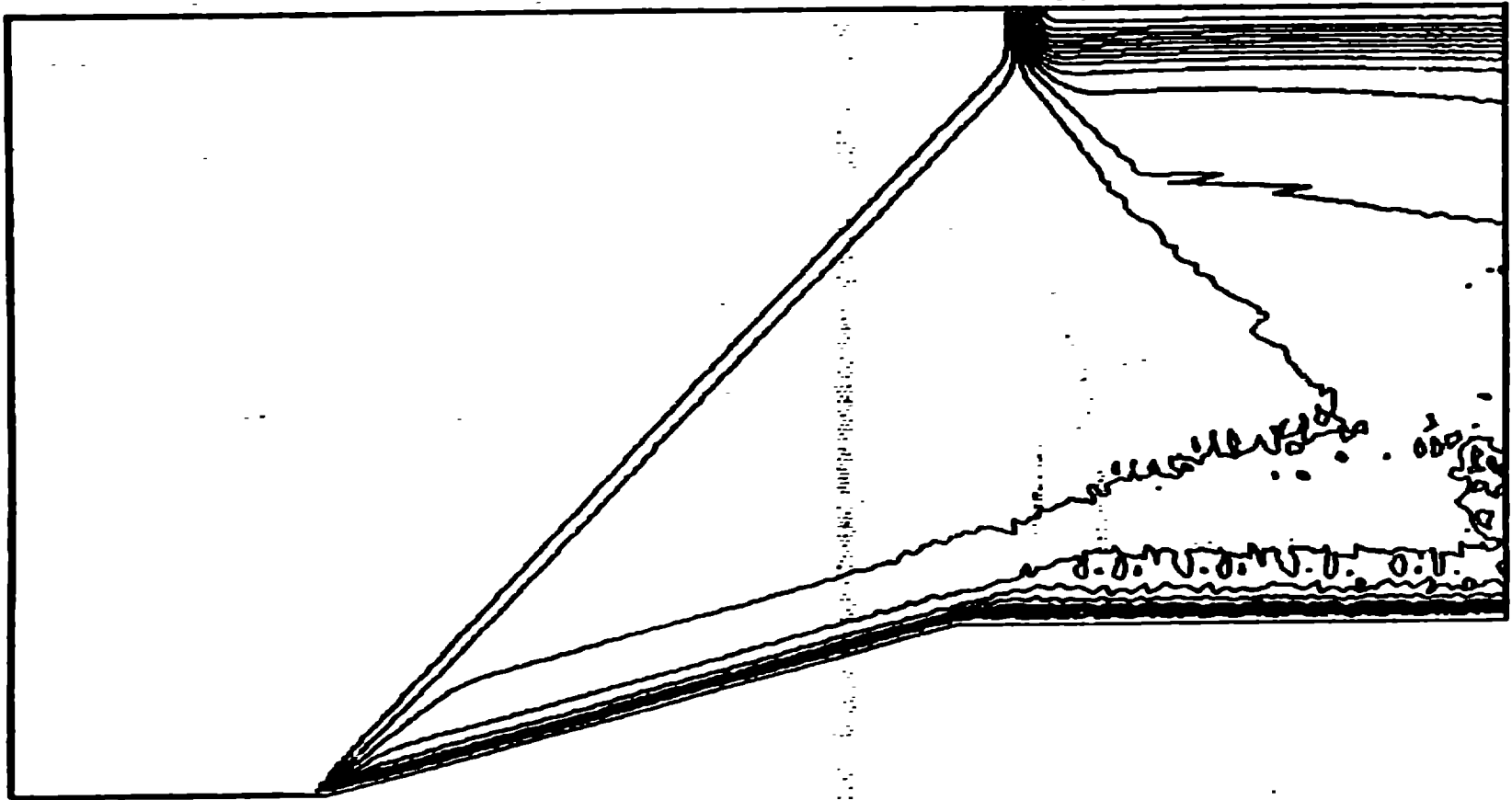
SPH Density Contours (Wall Heating 0.5, 1.0)
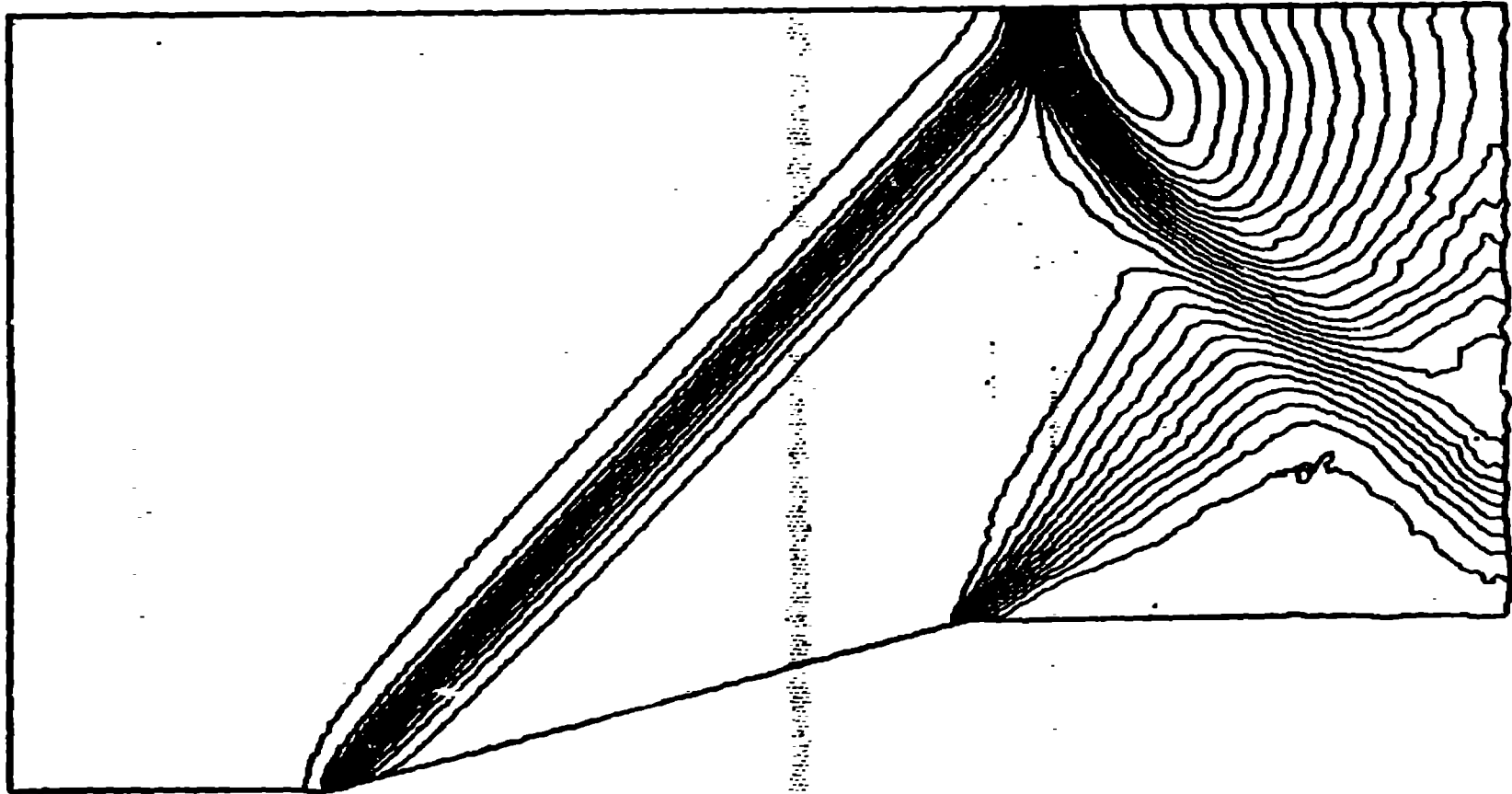
SPH Pressure Contours (Well Heating 0.5, 1.0)
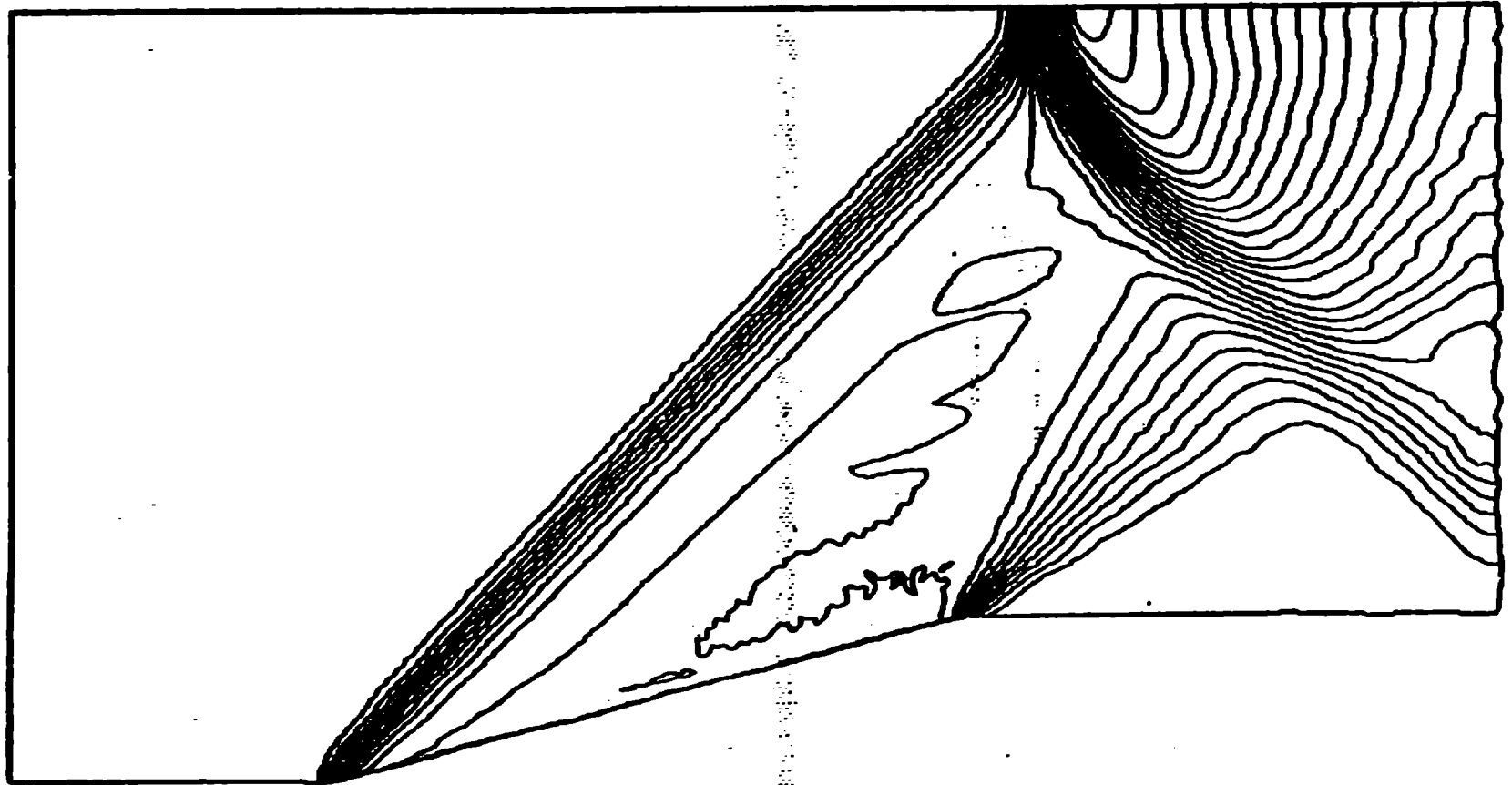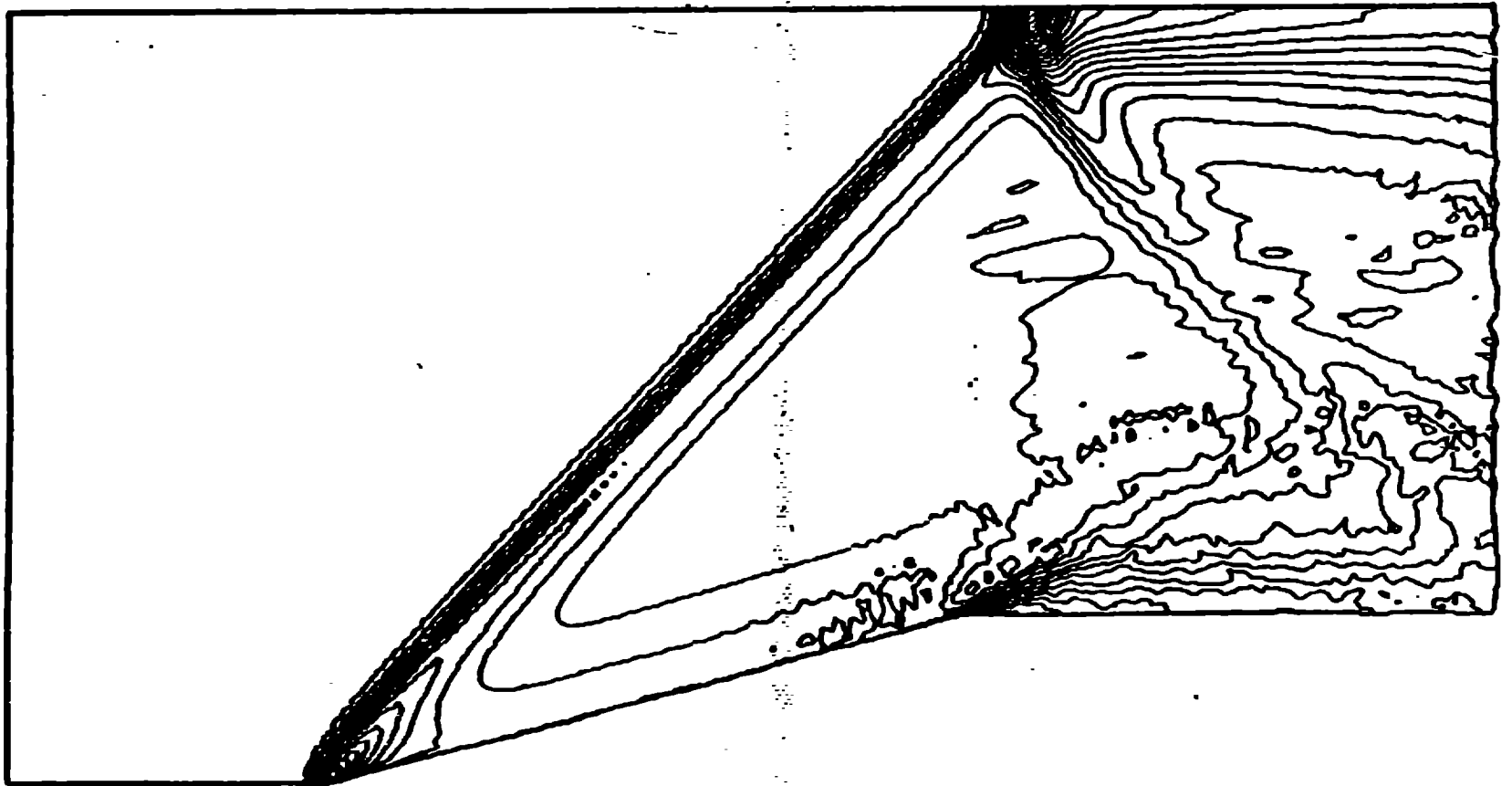
SPH $\frac{P}{\rho^\gamma}$ Contours   (Wall Heating 0.5, 1.0)

Wind Tunnel with a Step
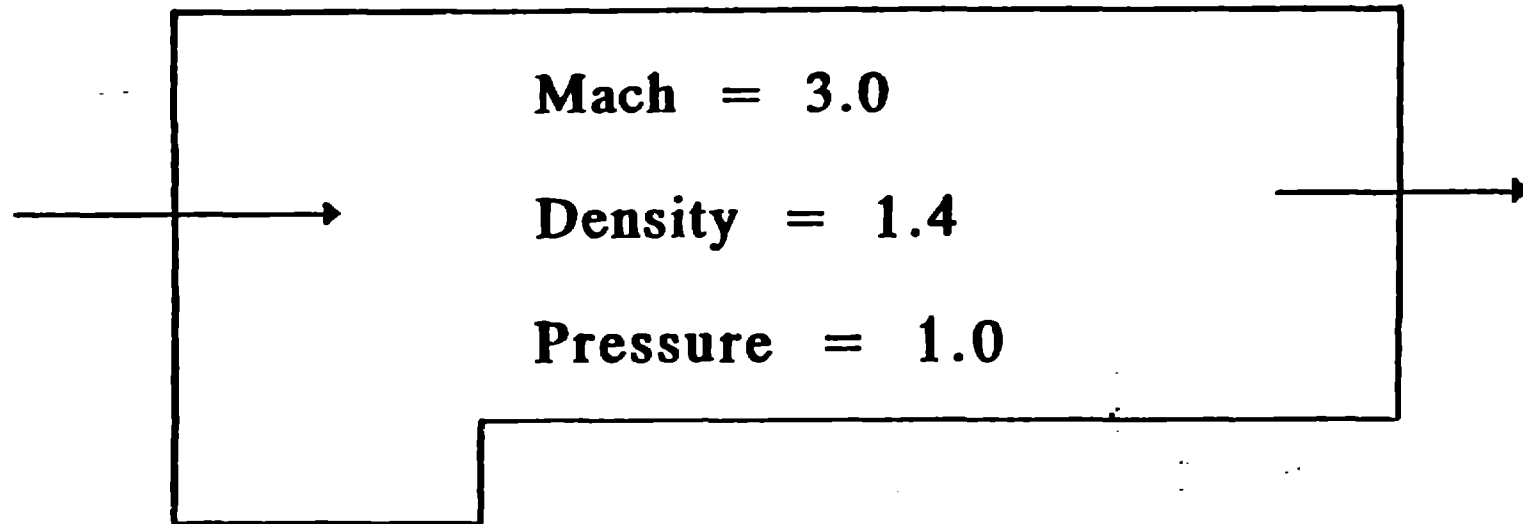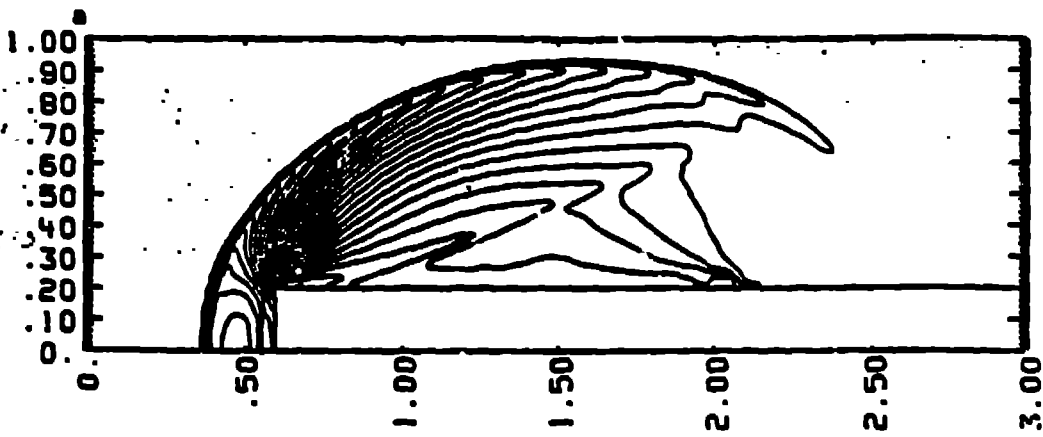
Mach = 3.0

Density = 1.4

Pressure = 1.0

-47-
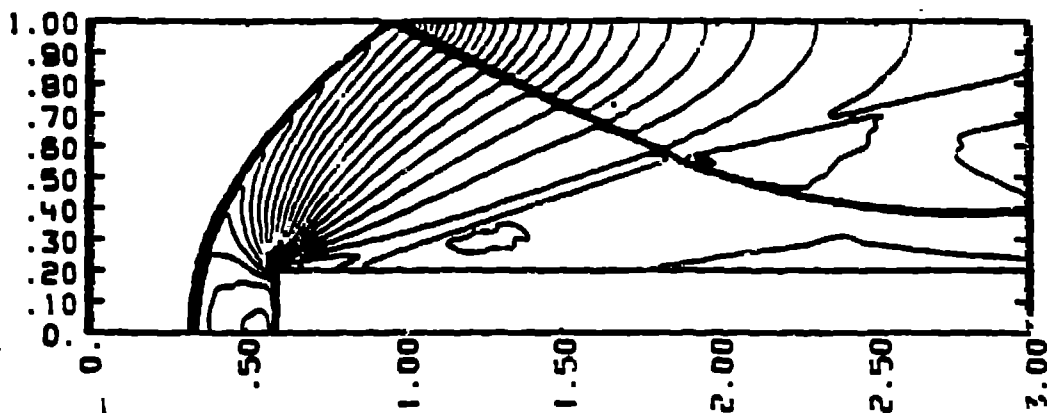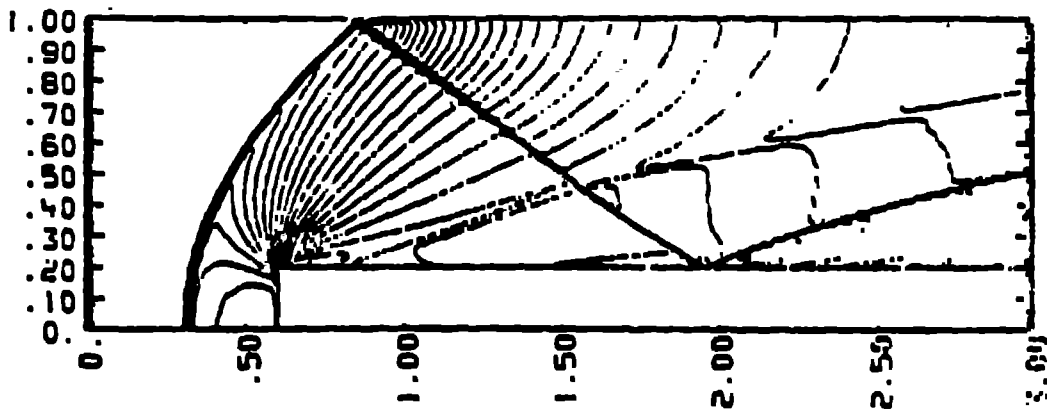
FIG. 3. The time evolution of the Mach 3 wind tunnel problem discussed in Section IVb. The results were obtained with the PPMLR scheme using a uniform grid with $\Delta x = \Delta y = 1/80$. The contours of density are shown at time intervals of 0.5 up to time 3. At time 4, the contours of density, pressure $= p/\rho^\gamma$, v_y, v_x, and $(v_x/c) - 1$ are also plotted. In each plot 30 equally spaced contours are shown with the contour for the lowest level or for any negative level drawn as a dotted line.
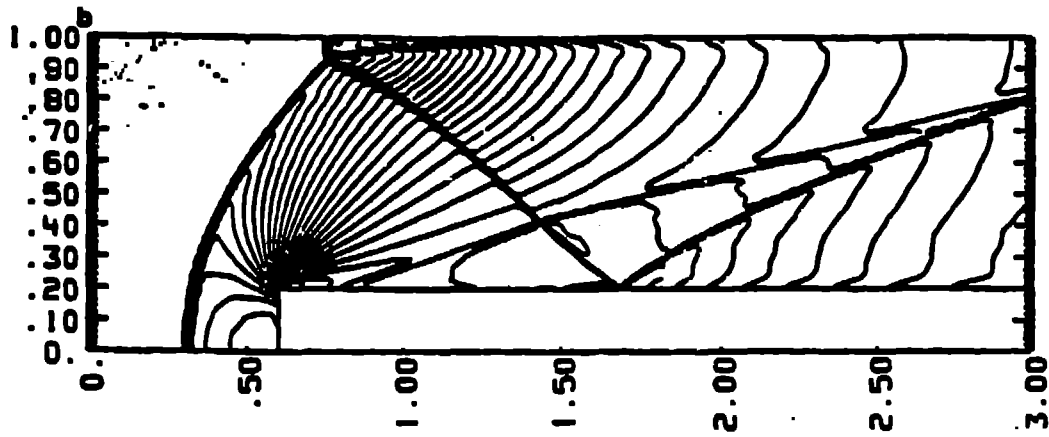
DENSITY   di=2.60e-03 courni=0.800;   PPRLR   4/19/82- 4   180ppl/i
30 contours: 2.660e-01 to 6.450e+00   n =   802   t = 2.00456e+00

DENSITY   di=2.71e-03 courni=0.800;   PPRLR   4/19/82- 4   180ppl/b
30 contours: 2.600e-01 to 6.602e+00   n =   886   t = 2.53107e+00
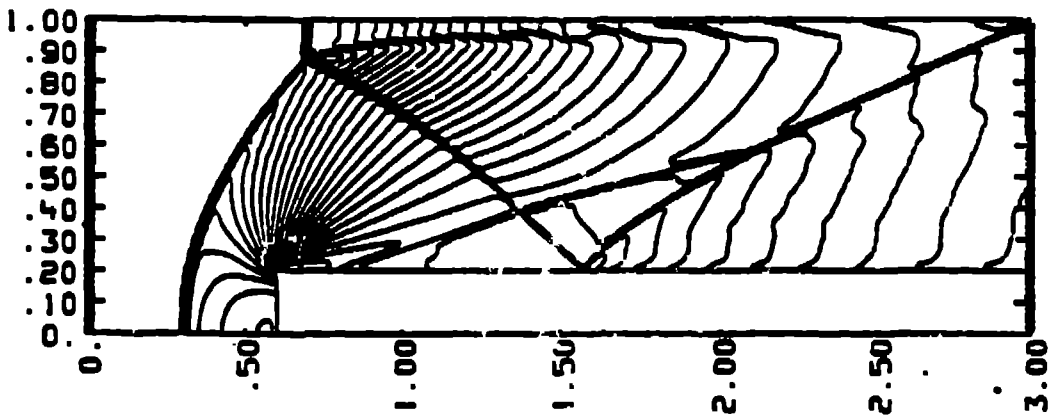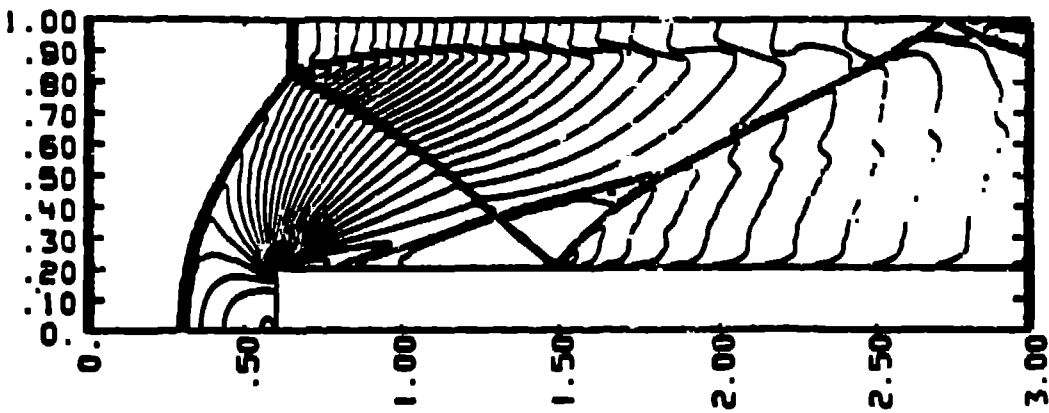
DENSITY   di=2.72e-03 courni=0.800;   PPRLR   4/19/82- 4   180ppl/e
30 contours: 2.673e-01 to 6.383e+00   n = 1170   t = 3.00016e+00

Fig. 3—Continued.
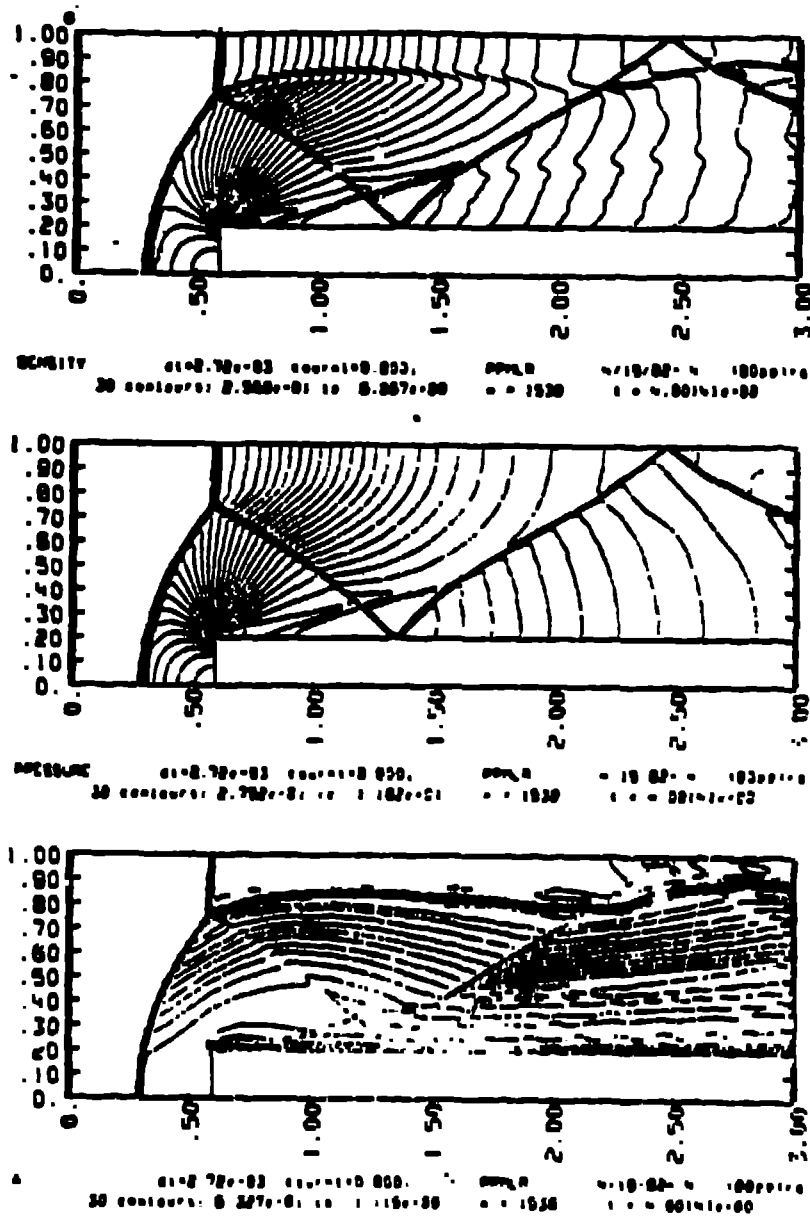
FIG. 3—Continued.

zone used to set the entropy. This condition is based on the assumption of a nearly steady flow in the region near the corner. It is clearly inappropriate at the very outset of the calculation. These conditions remove the grossest errors generated near the corner, but of course large errors in the flow direction there are bound to remain. These errors may be the cause of an overexpansion observed at the corner in all the runs, although similar effects occur in wind tunnel experiments of this type using real viscous air.

The time evolution, up to time 4, of the density distribution in the wind tunnel is displayed in Fig. 3. The flow at time 4 is still unsteady. A steady flow develops by

SPH Density Contours (H Limited)
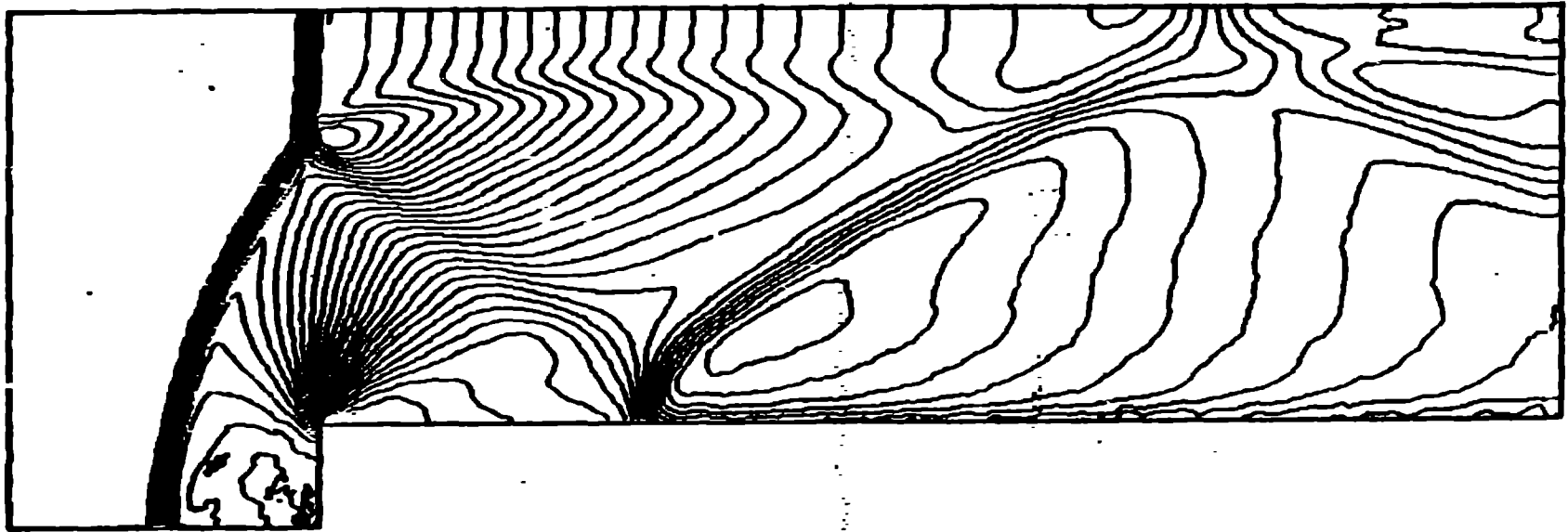
SPH Pressure Contours   (H Limited)
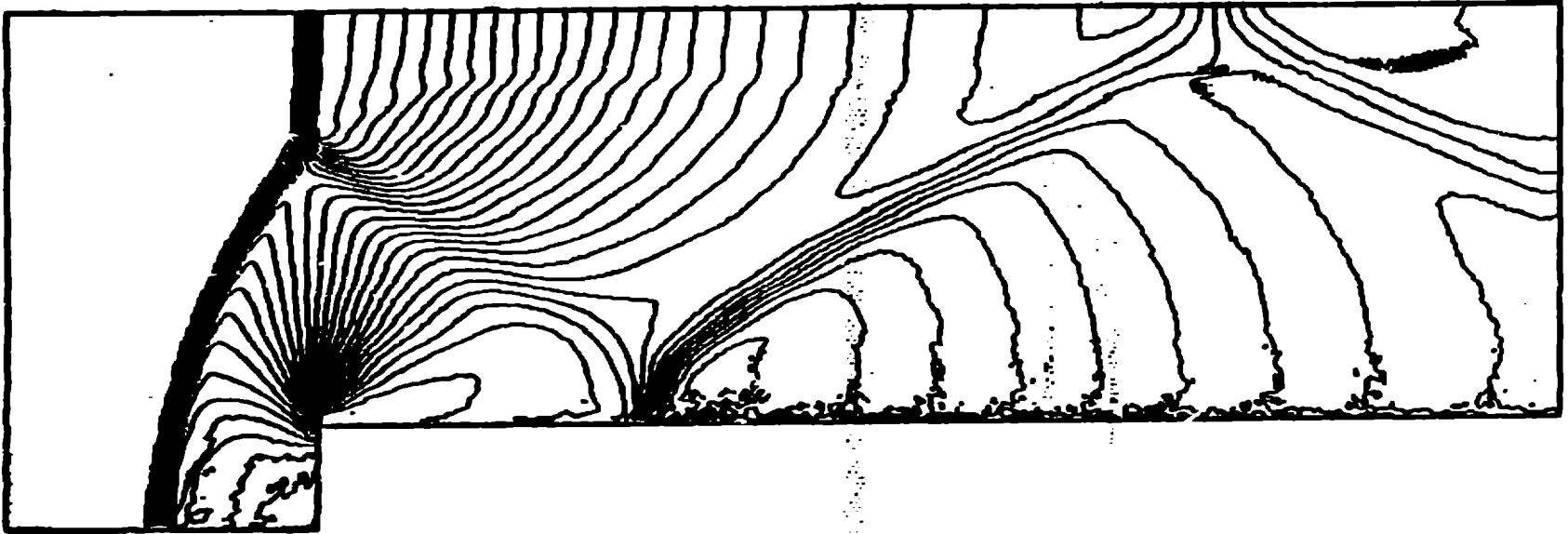
SPH $\frac{P}{P^s}$ Contours   (H Limited)
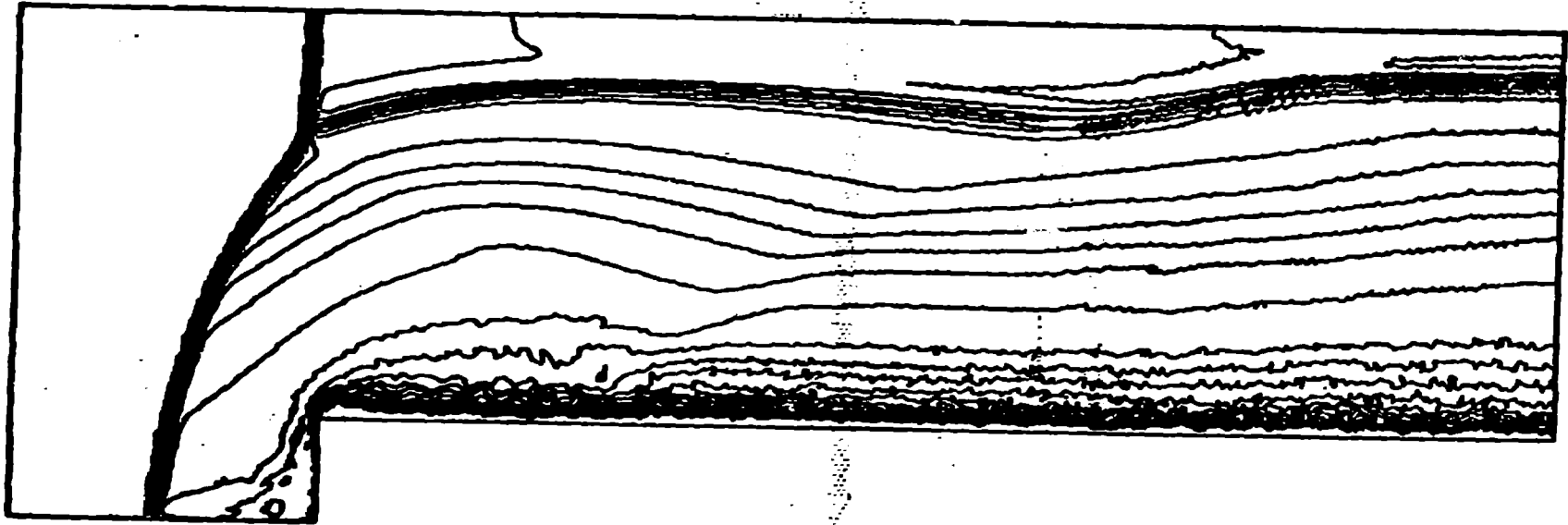
SPH Density Contours (Variable H)
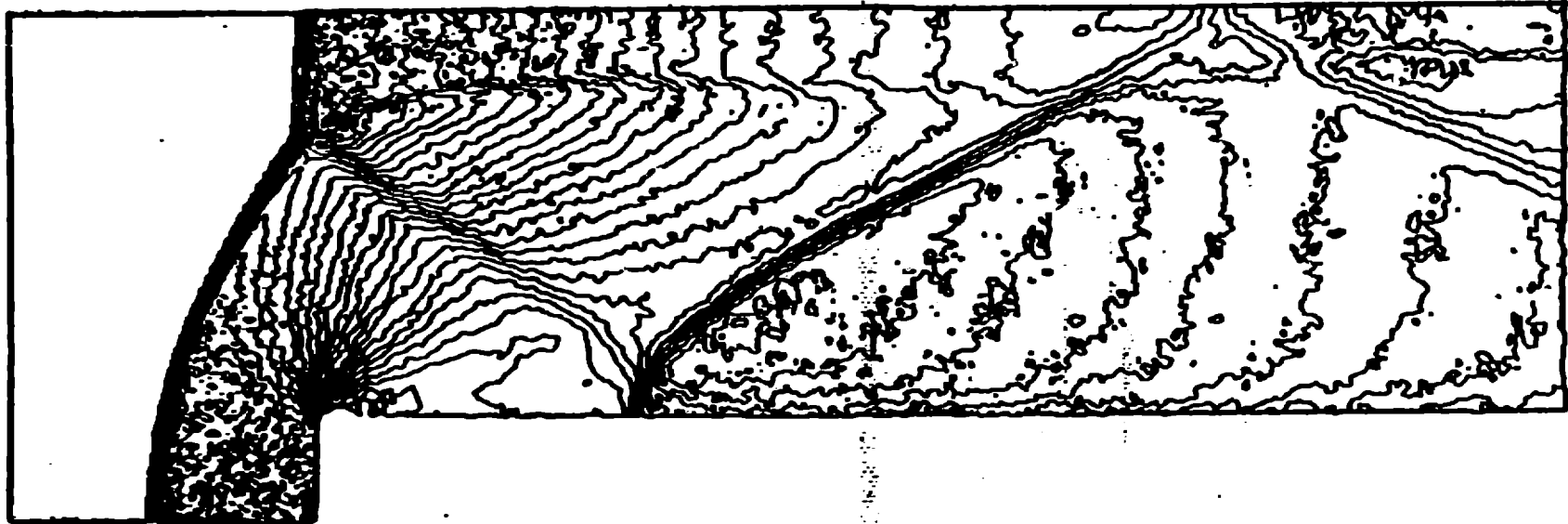
SPH Pressure Contours (Variable H)
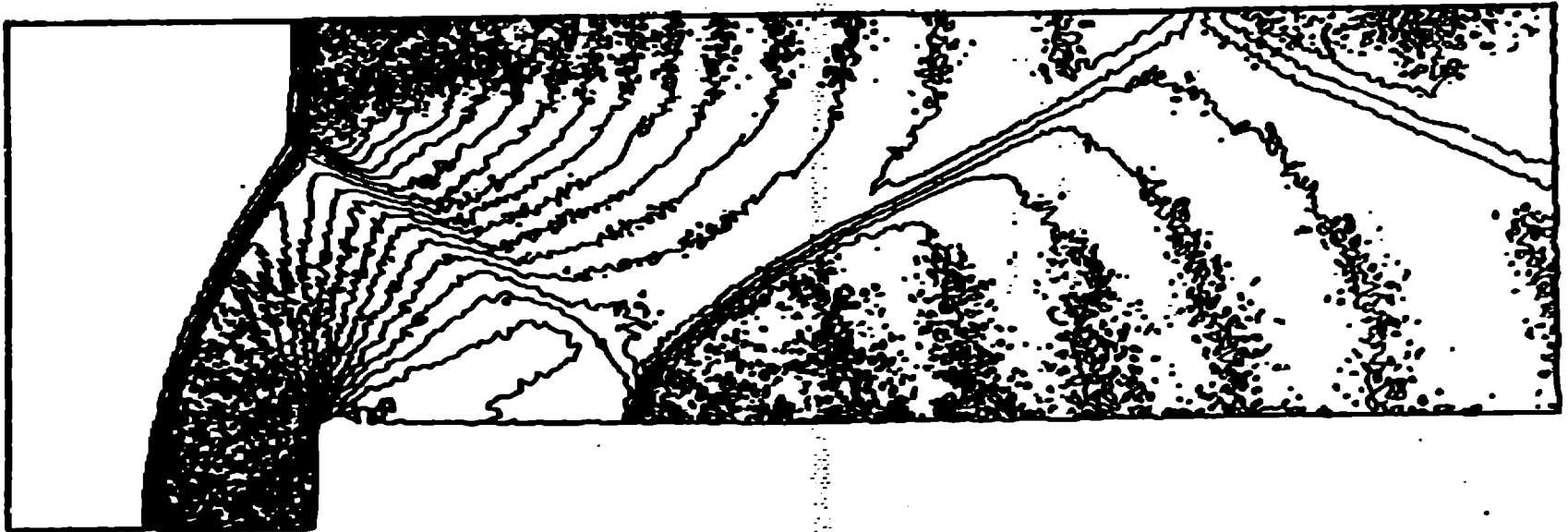
SPH $\frac{P}{\rho^2}$ Contours   (Variable H)
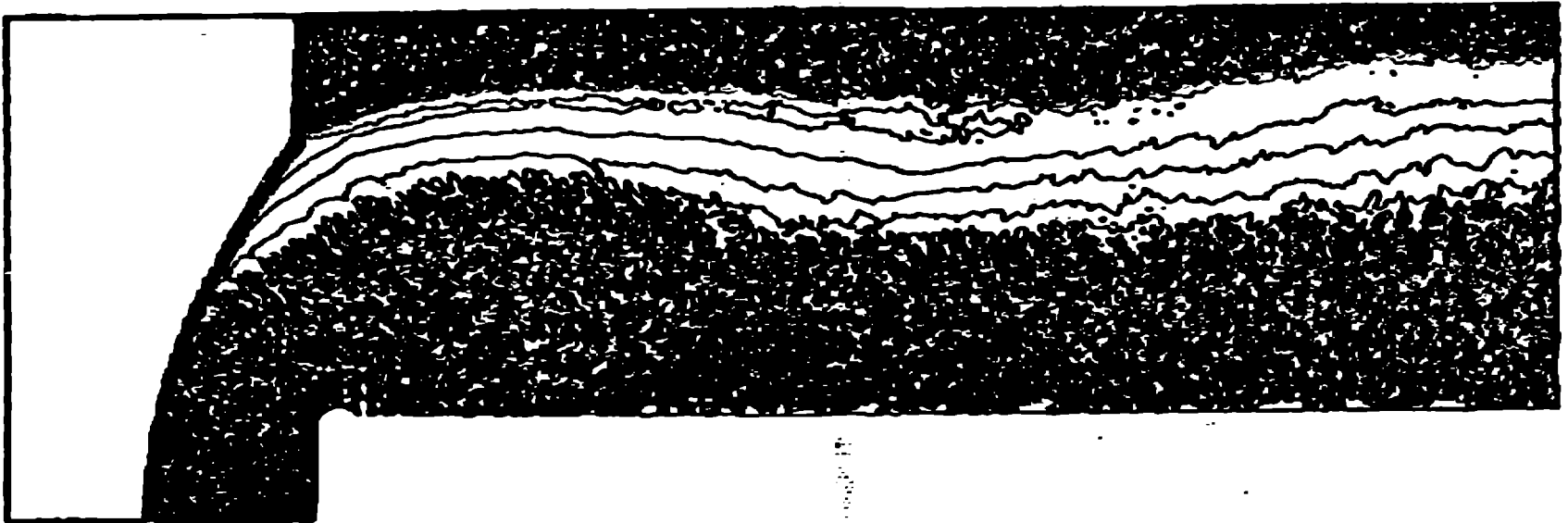
Supersonic Airfoil in a Tunnel

NACA 0012 Airfoil
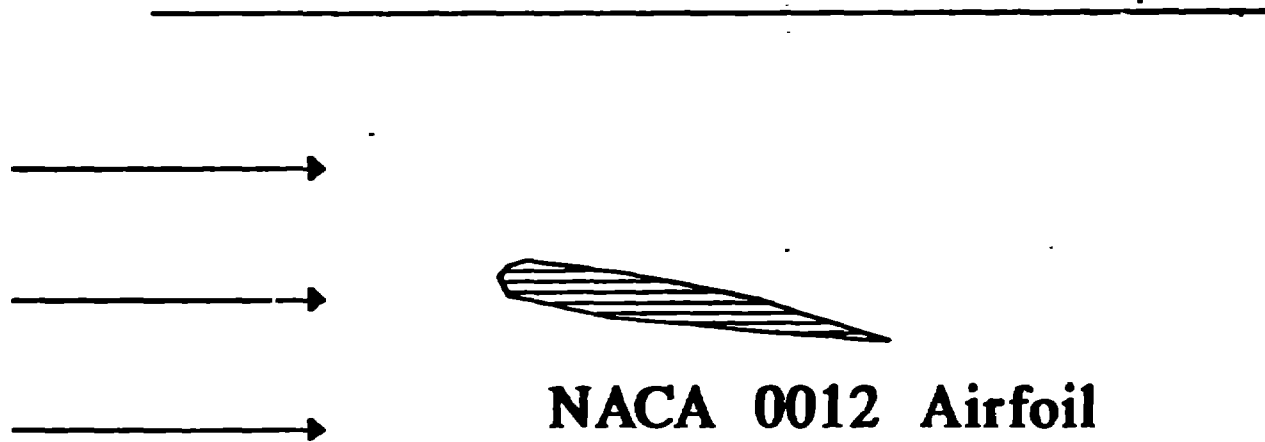
Mach = 1.2
Density = 1.0
Pressure = 1.0
Angle of Attack = 1.25 Deg
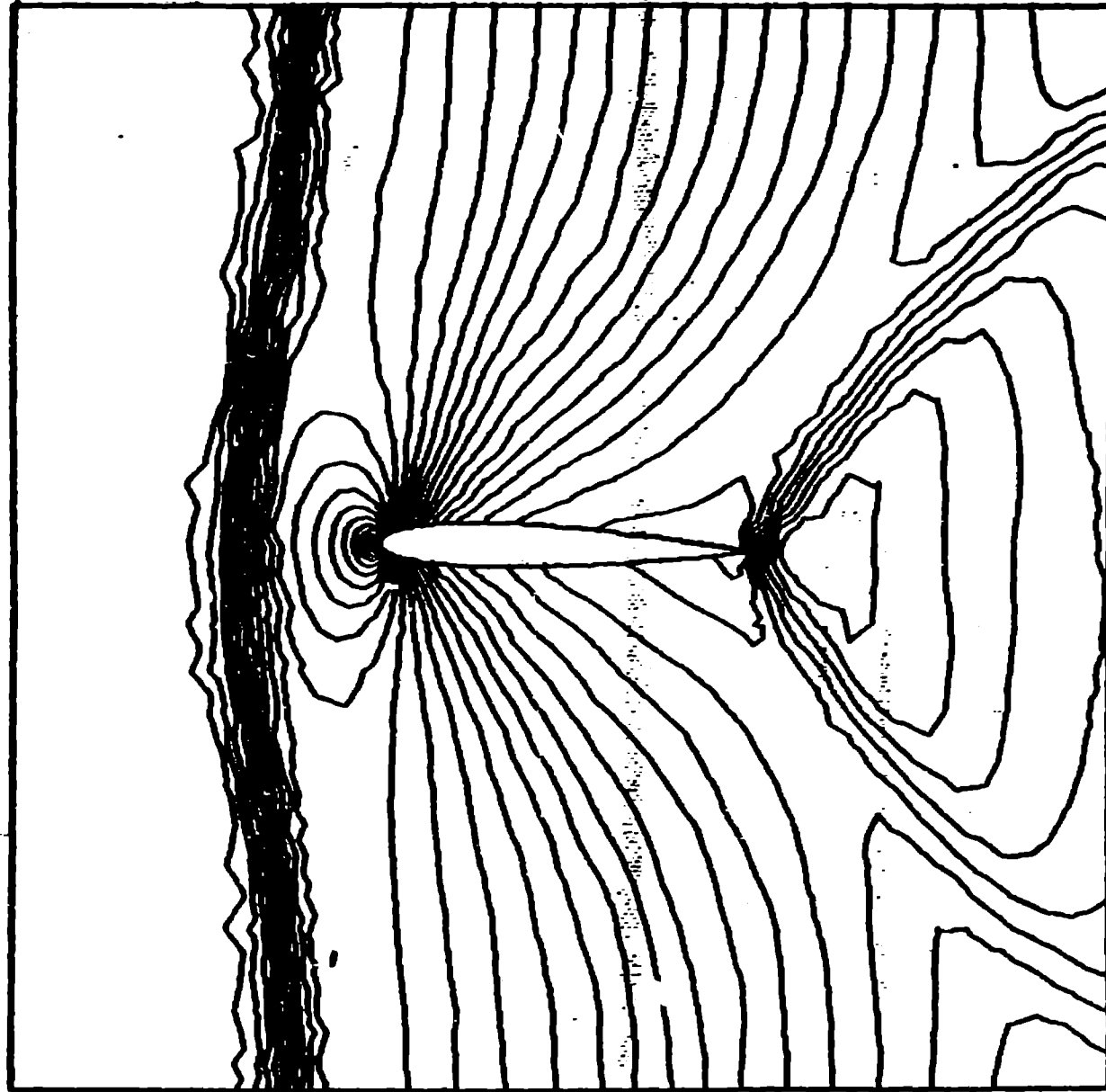
GRID METHOD Density Contours

SPH Density Contours
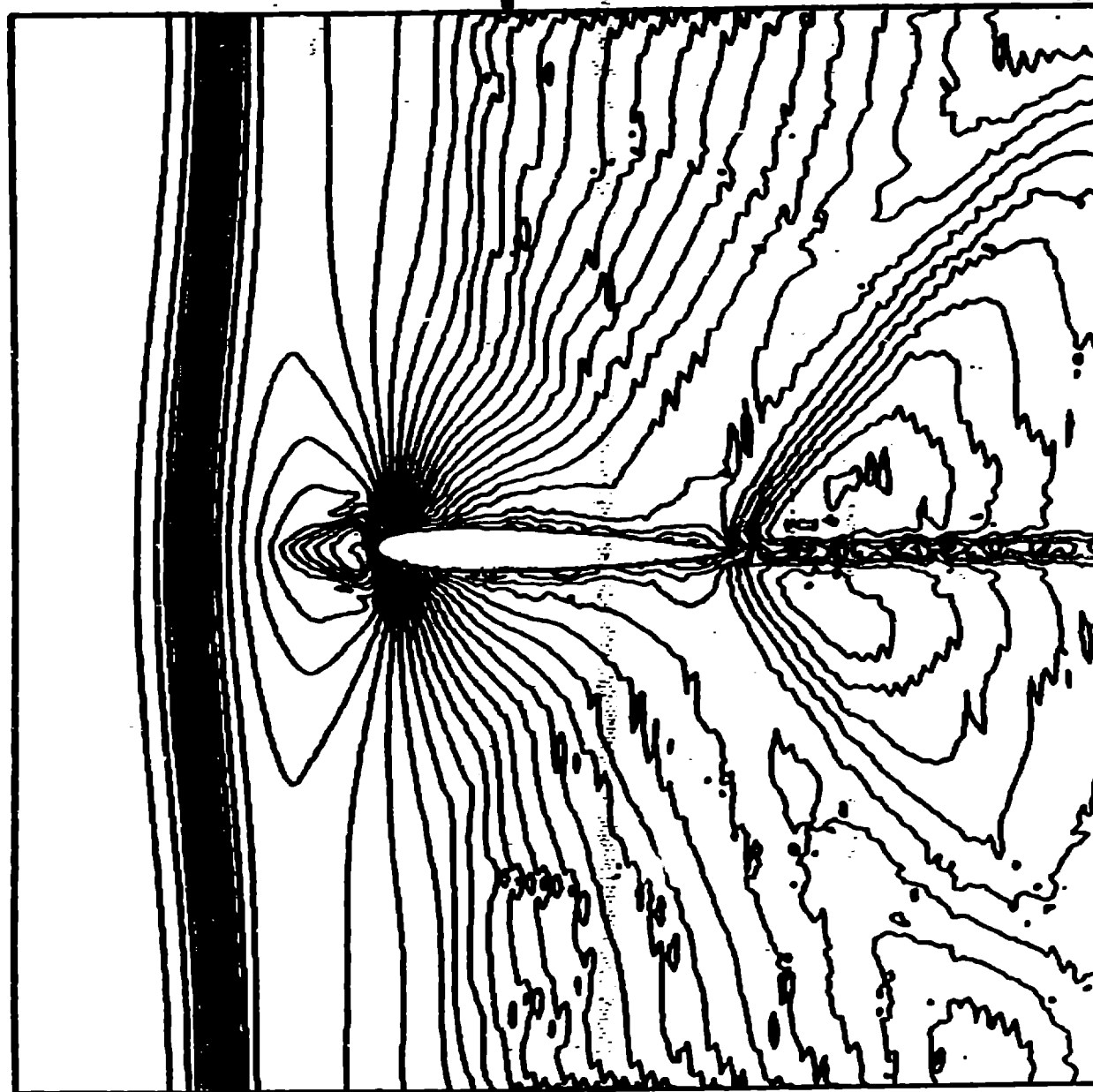
SPH $\frac{1}{\rho^r}$ Contours
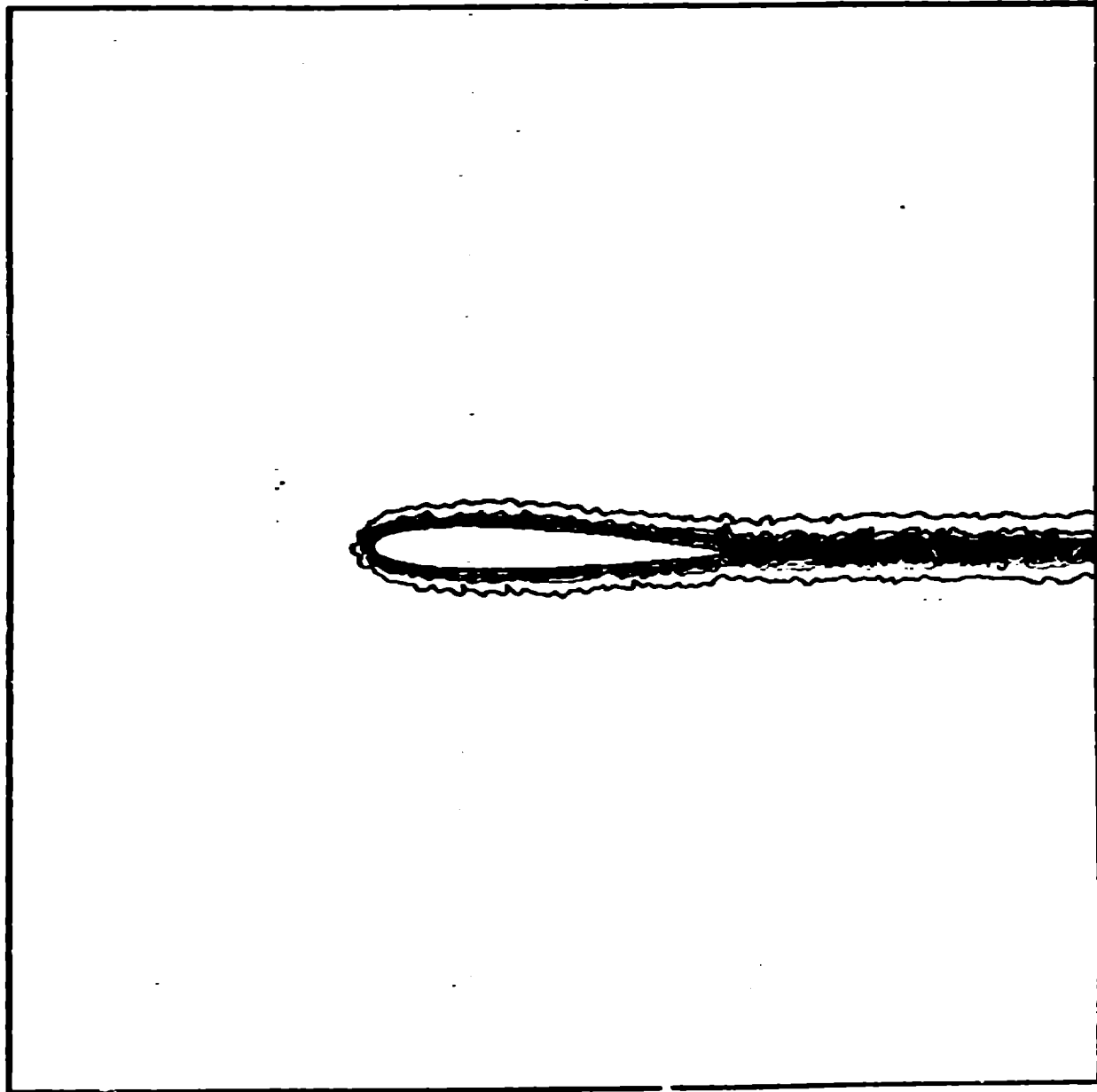
Conclusion

- **Boundary Conditions !!!**

- **Noise Reduction, Sharpen Discontinuities**

- **Overall, Improved Quality of Solution**

PROGRESS ON INTERFACE
PROBLEMS IN SPH

Charles P. Luehr & Firooz A. Allahdadi

USAF Phillips Laboratory, PL/WSSD

OUTLINE:

1. Cutoff Method for Separated Impact

2. Density Deviation Cancellation

3. Effective Relative Velocity Scheme

4. Velocity Divergence Based on
   Estimates Used in Artificial
   Viscosity Theory

CUTOFF METHOD FOR SEPARATED IMPACT

Smoothing function cutoff with shutoff:
  Diff. kinds interact by cutoff method
  Same kinds interact as usual.

Example (see diagram):
  Dim. is 1.   Cutoff dist., $d = 2h/3$.
  No. of particles per h is 3/2.

Procedure:

1. Find active particles (i.e., particles within dist. d from any particle of the other kind).

2. For all i and j of diff. kinds:
    a. If neither is active, they do not interact.
    b. If either is active, they interact as usual.

Before impact

w with cutoff

$v \longrightarrow$

$v = 0$
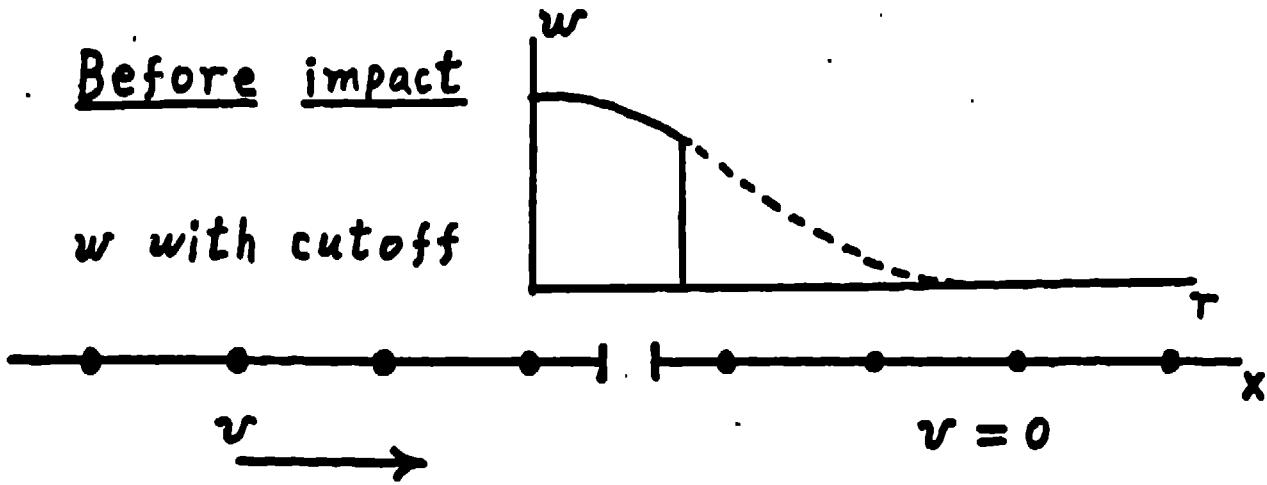
Time of impact

w with cutoff
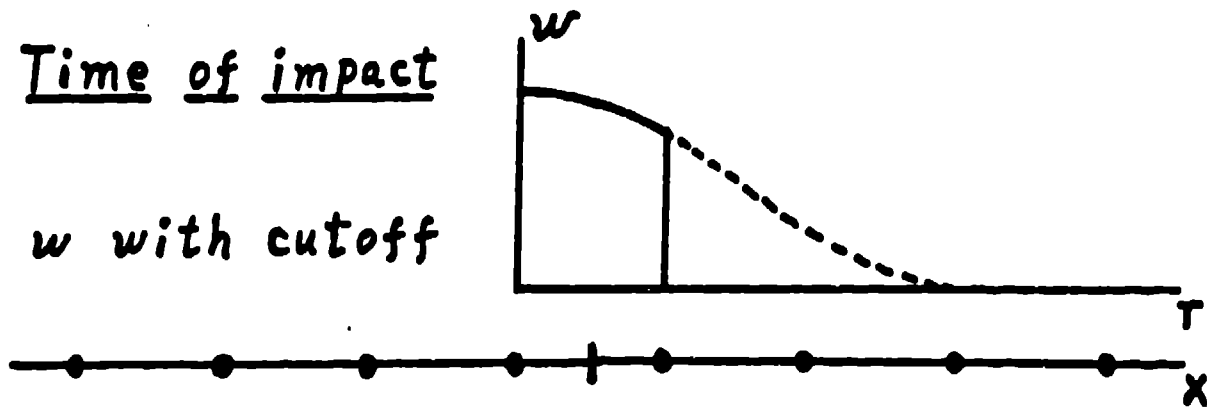
Time of impact

w with shutoff of cutoff
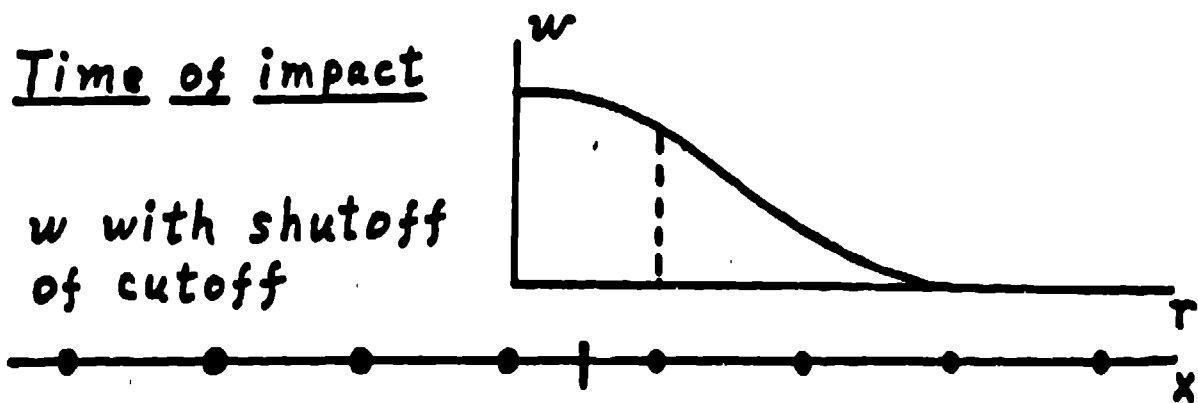
```
-, -, -              [-----(----------,-----,-----,,-----(-----,-----)]
0, 0.0, 3            [H(ignored),NPH(ignored),IEOS(1=PerGas,2=Grun,3=Mie-Grun)]
00, 1                [Number of Iterations,Density(0=Summ,1=Cont)]
5, 2.5, 0.1          [Alpha, Beta, Epsilon, (Artificial Viscosity)]
50, 1.00             [G1, G2 (Wall Heating)]
                     [Interval]
3, 3.0               [CFL No., Stop Time]
.0, 3.0              [Xmin, Xmax (Problem Domain)]
                     [Restart (0=No,1=Yes)]
trt.000000
                     [Number of Lines]
uminum               [Material]
0, 1.0               [Start and End]
71, 1.0E-08, 0.01    [Density, Internal Energy, and Velocity]
01, 1.5              [H,NPH]
uminum               [Material]
02, 2.02             [Start and End]
71, 1.0E-08, 0.0     [Density, Internal Energy, and Velocity]
01, 1.5              [H,NPH]
                     [Number of Time Dump Intervals]
0
trt
```

run G2

Original method
Separated impact
Al on Al at 0.1 km/sec
1 μsec after impact

Density vs. X [NP=300, Time=3.0000, Iter=549]
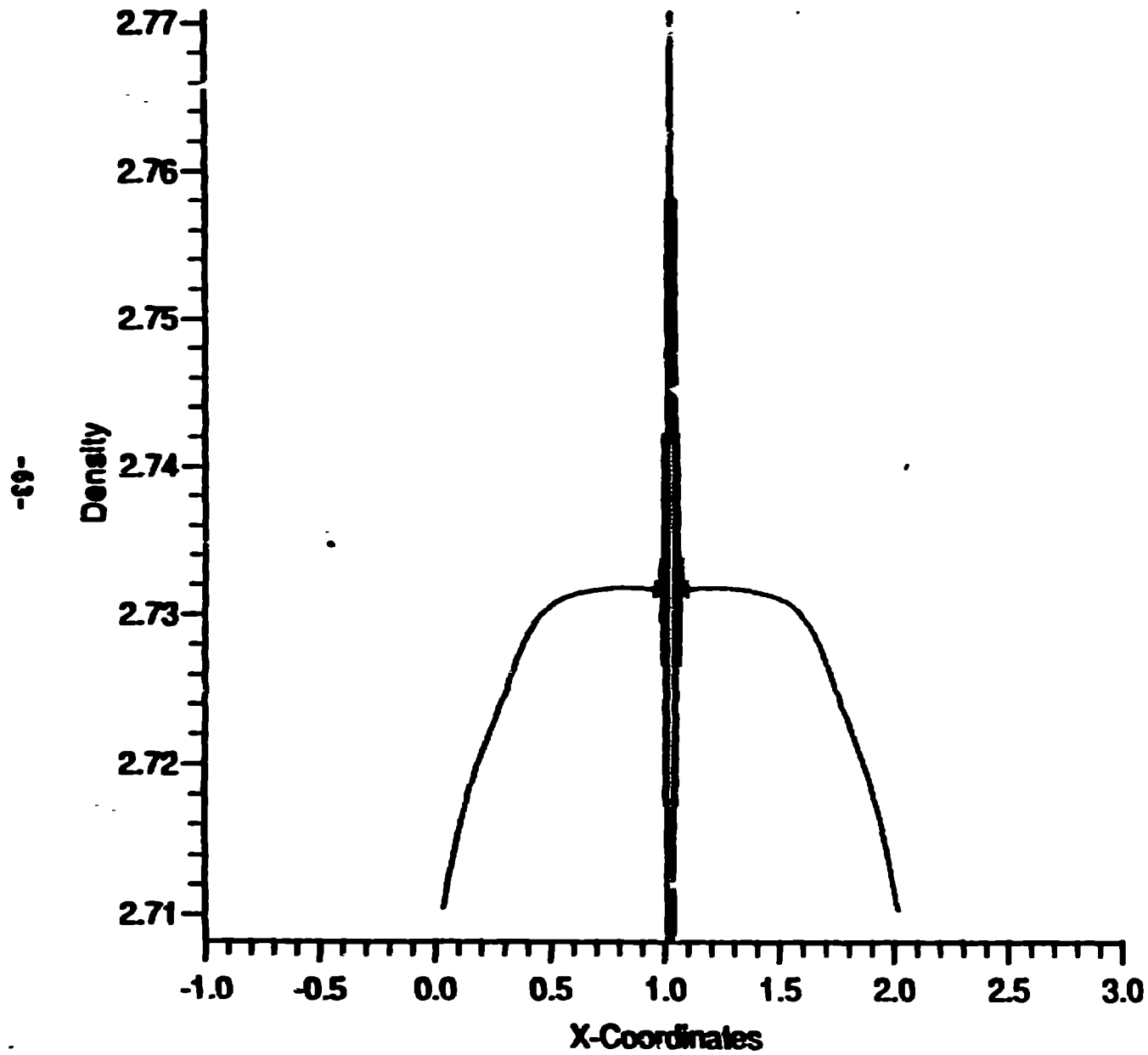
Max Density = 2.770667

Min Density = 2.708231

Alpha = 2.5000
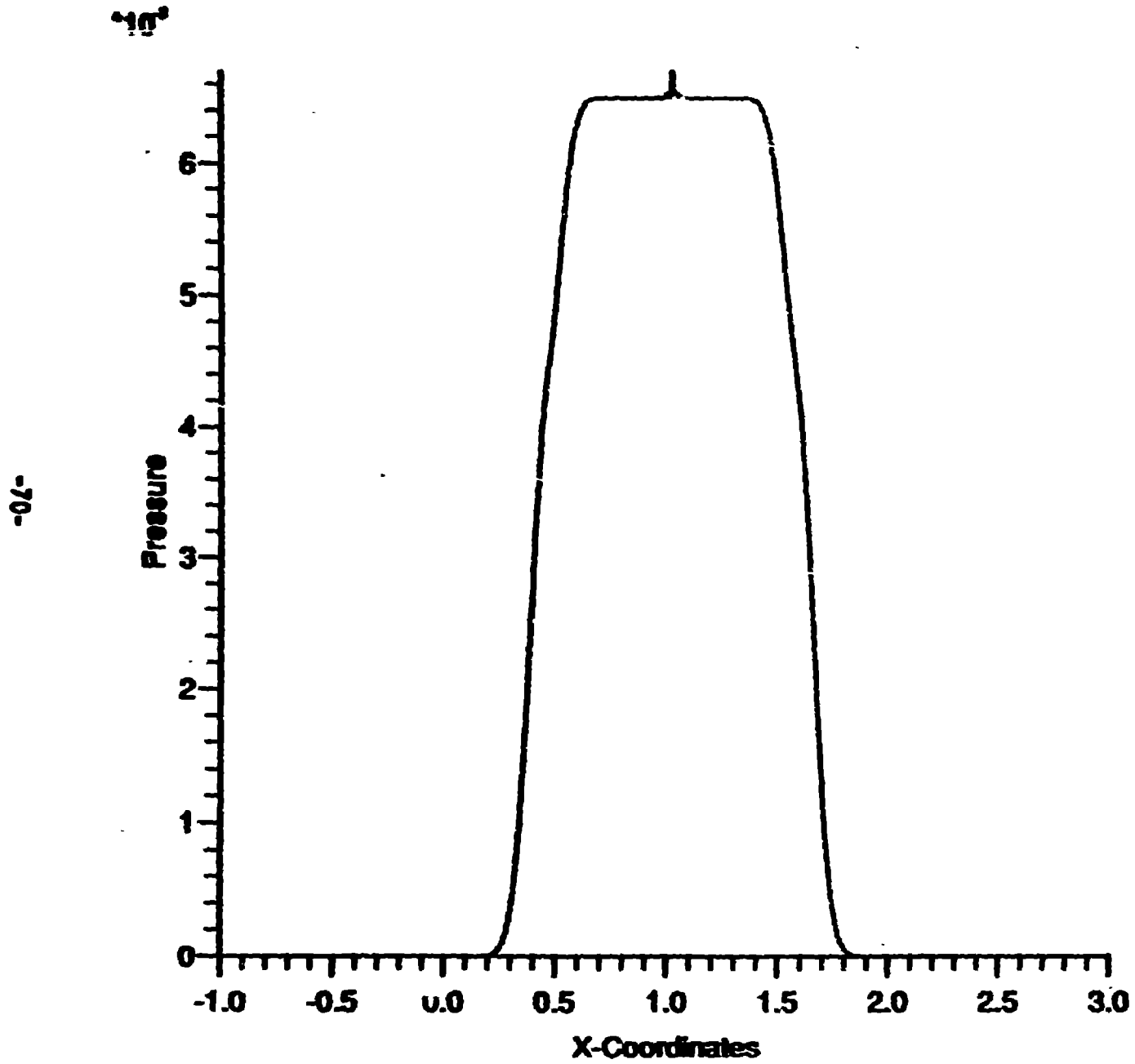
Beta = 2.5000

Eps = 0.1000

G1 = 0.5000

G2 = 1.0000

CFL = 0.3000

———— Calculation

29 December 1992

Pressure vs. X [NP=300, Time=3.0000, Iter=549]

run 62

Max Pressure = 0.017880

Min Pressure = -0.000322

Alpha = 2.5000

Beta = 2.5000

Eps = 0.1000

G1 = 0.5000

G2 = 1.0000

CFL = 0.3000

—————— Calculation

29 December 1992
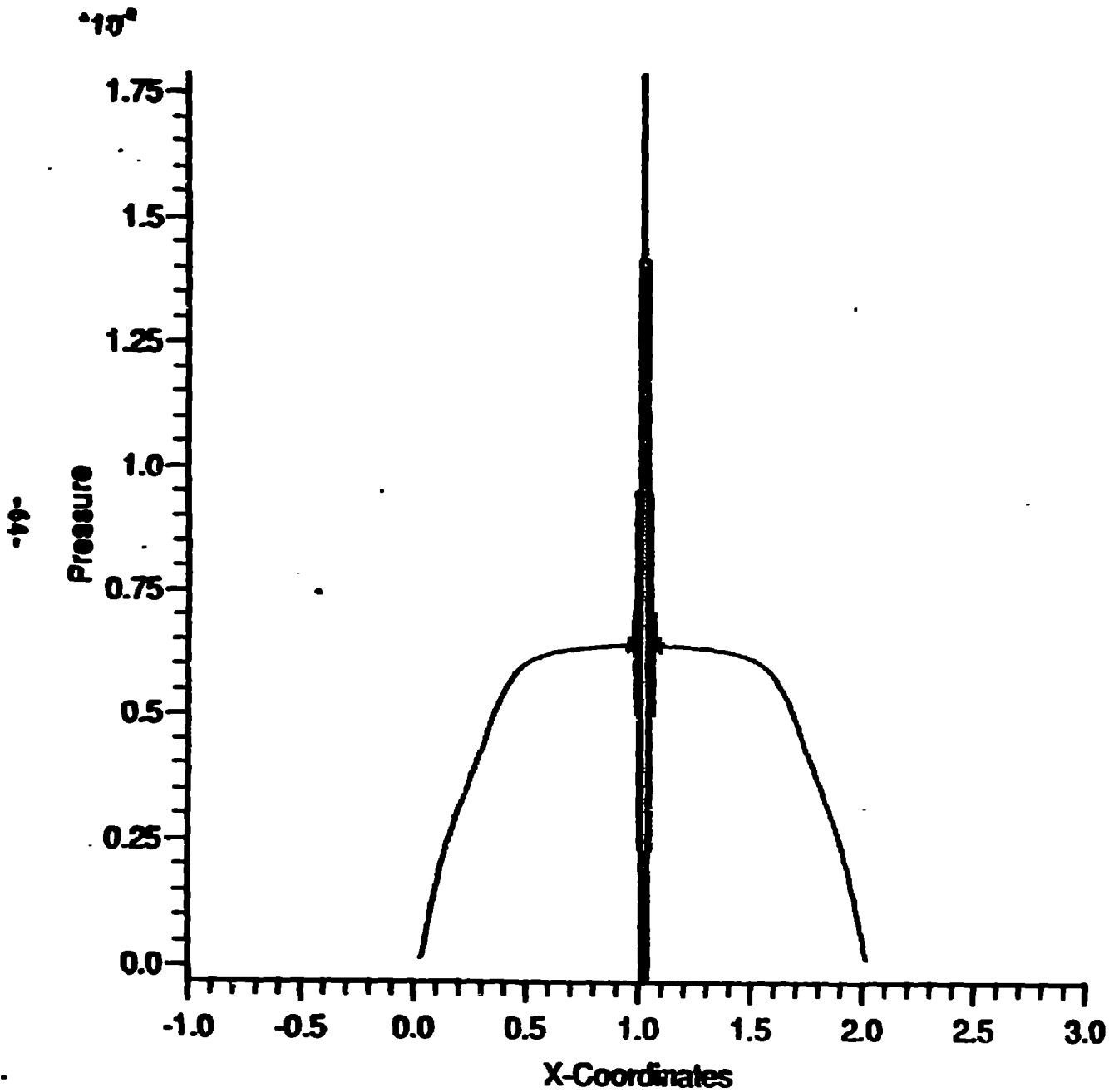
```
0                        [IMOD(0=Original,1=Model,2=Mode2),IVARH(0=Fixed,1=Var)]
, 0.0, 3                 [H(ignored),NPH(ignored),IEOS(1=PerGas,2=Grun,3=Mie-Grun)]
0, 1                     [Number of Iterations,Density(0=Summ,1=Cont)]
, 2.5, 0.1              [Alpha, Beta, Epsilon, (Artificial Viscosity)]
0, 1.00                  [G1, G2 (Wall Heating)]
                         [Interval]
, 3.0                    [CFL No., Stop Time]
0, 3.0                   [Xmin, Xmax (Problem Domain)]
                         [Restart (0=No,1=Yes)]
rt.000000
                         [Number of Lines]
minum                    [Material]
, 1.0                    [Start and End]
1, 1.0E-08, 0.01         [Density, Internal Energy, and Velocity]
1, 1.5                   [H,NPH]
minum                    [Material]
, 2.0                    [Start and End]
1, 1.0E-08, 0.0          [Density, Internal Energy, and Velocity]
1, 1.5                   [H,NPH]
                         [Number of Time Dump Intervals]


rt
```

run G5

Original method
Contact impact
Al on Al at 0.1 km/sec
1 μsec after impact

Density vs. X [NP=300, Time=1.0000, Iter=182]   run 65
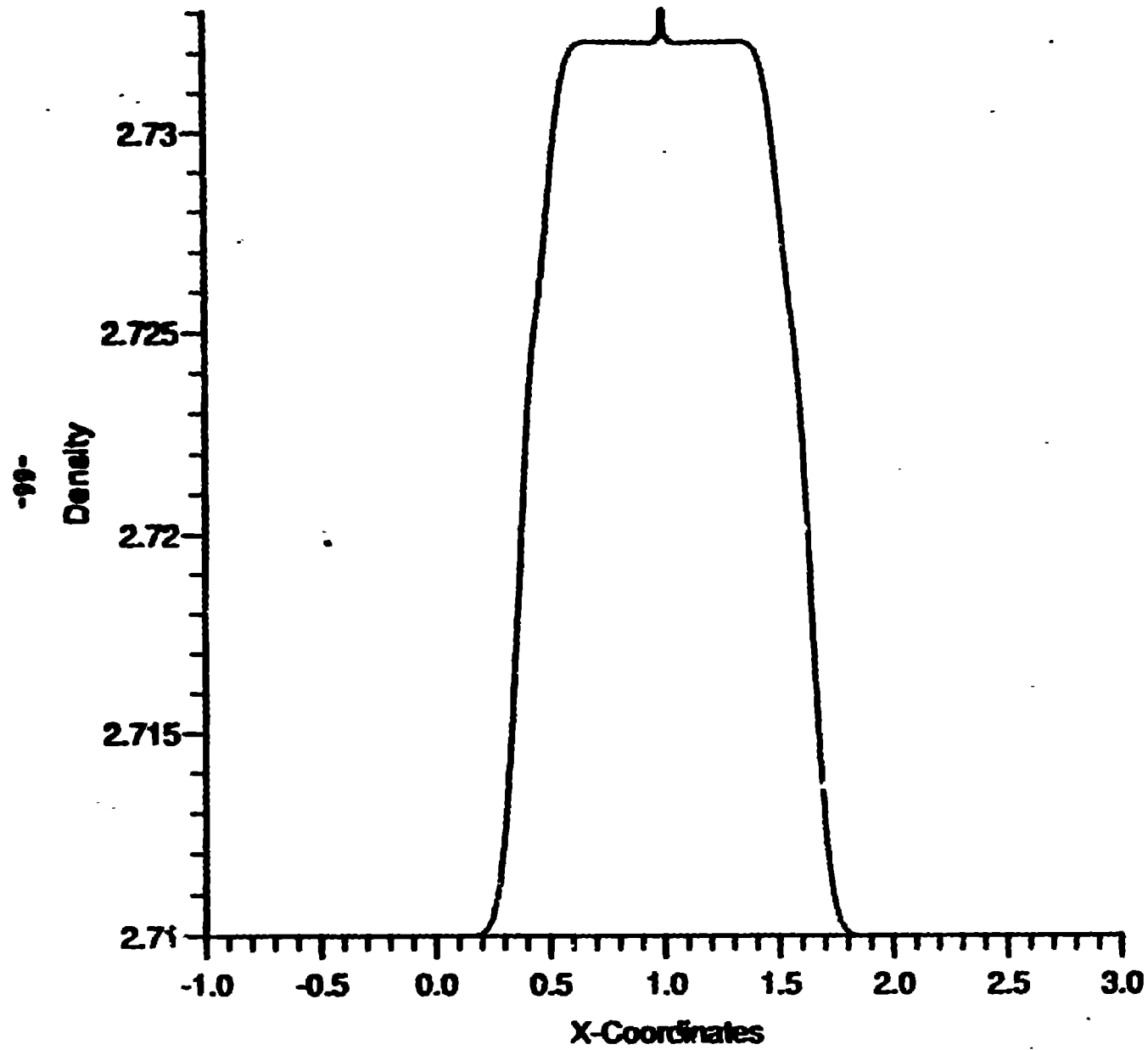
Max Density = 2.733039

Min Density = 2.710000

Alpha = 2.5000

Beta = 2.5000

Eps = 0.1000

G1 = 0.5000

G2 = 1.0000

CFL = 0.3000

——— Calculation

04 January 1993

Pressure vs. X [NP=300, Time=1.0000, Iter=182]   run G5

*10⁶
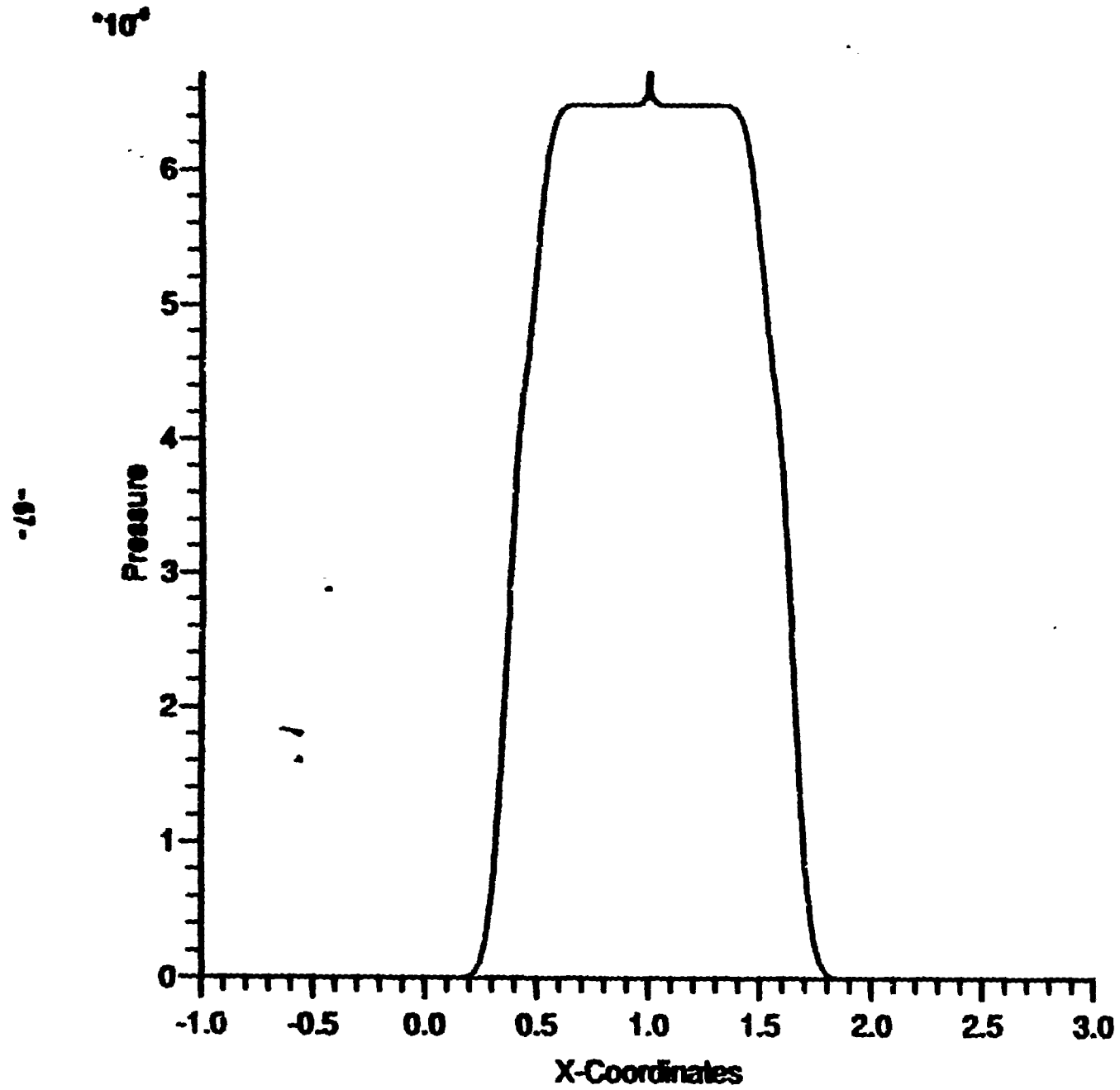
Max Pressure = 0.006720

Min Pressure = 0.000000

Alpha = 2.5000

Beta = 2.5000

Eps = 0.1000

G1 = 0.5000

G2 = 1.0000

CFL = 0.3000

——————   Calculation

04 January 1993

```
, 0                        [IMOD(0=Original,1=Model,2=Mode2),IVARH(0=Fixed,1=Var)]
.0, 0.667                  [HNULT(1.0=usual),DXOHDX(2.0=usual)]
.0, 0.0, 3                 [H(ignored),NPH(ignored),IEOS(1=PerGas,2=Grun,3=Mie-Grun)]
000, 1                     [Number of Iterations,Density(0=Summ,1=Cont)]
.5, 2.5, 0.1               [Alpha, Beta, Epsilon, (Artificial Viscosity)]
.50, 1.00                  [G1, G2 (Wall Heating)]
0                          [Interval]
.3, 3.0                    [CFL No., Stop Time]
1.0, 3.0                   [Xmin, Xmax (Problem Domain)]
                           [Restart (0=No,1=Yes)]
strt.000000
                           [Number of Lines]
luminum                    [Material]
.0, 1.0                    [Start and End]
.71, 1.0E-08, 0.01         [Density, Internal Energy, and Velocity]
.01, 1.5                   [H,NPH]
luminum                    [Material]
.02, 2.02                  [Start and End]
.71, 1.0E-08, 0.0          [Density, Internal Energy, and Velocity]
.01, 1.5                   [H,NPH]
                           [Number of Time Dump Intervals]
.0
strt
```

run K/r1
――――――――
Cutoff method
Separated impact
Al on Al at 0.1 km/sec
1 μsec after impact

Density vs. X [NP=300, Time=3.0000, Iter=559]
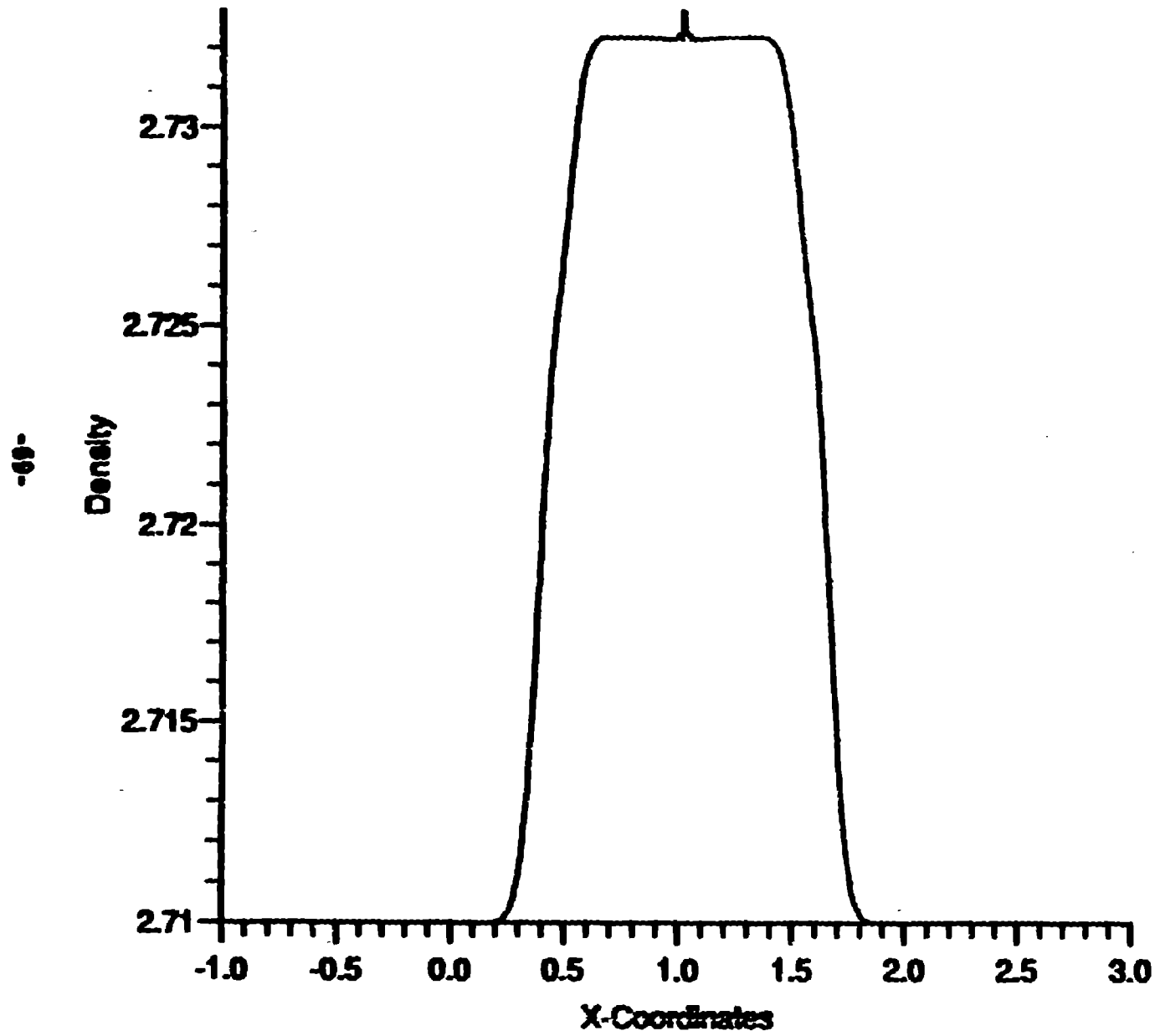
Max Density = 2.732930

Min Density = 2.710000
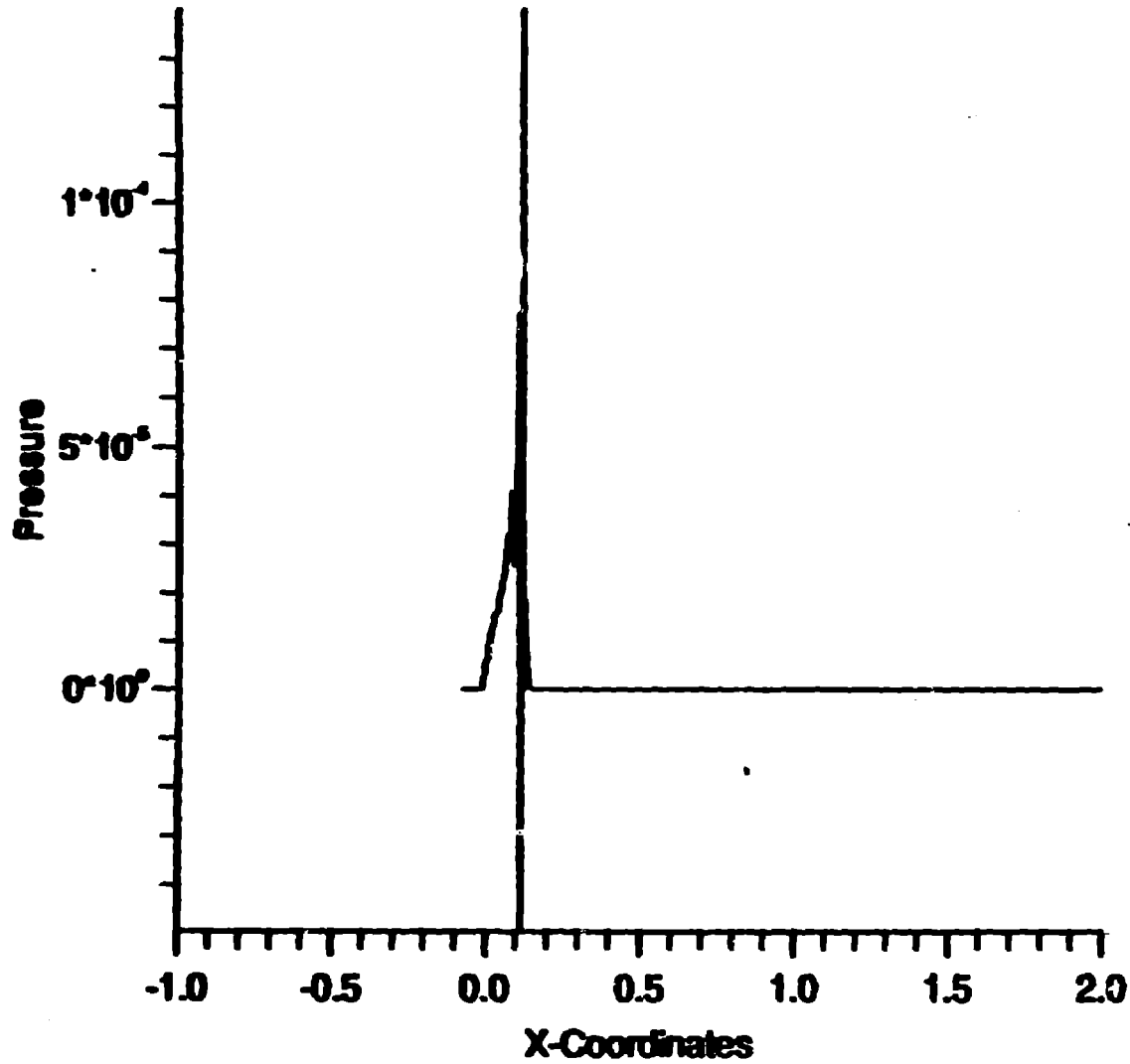
Alpha = 2.5000

Beta = 2.5000

Eps = 0.1000

G1 = 0.5000

G2 = 1.0000

CFL = 0.3000

———————— Calculation

12 July 1993

Pressure vs. X [NP=300, Time=3.0000, Iter=539]

run K/r/

Max Pressure = 0.00669

Min Pressure = 0.00000

Alpha = 2.5000

Beta = 2.5000

Eps = 0.1000

G1 = 0.5000

G2 = 1.0000

CFL = 0.3000

—————— Calculation

12 July 1993

DENSITY DEVIATION CANCELLATION

Continuity Equation:

$$d\rho_i/dt = -\rho_i(\nabla \cdot v)_i$$

with

$$(\nabla \cdot v)_i = -\rho_i^{-1}\sum_j m_j(v_i - v_j) \cdot \nabla_i w_{ij}$$

gives

$$d\rho_i/dt = \sum_j m_j(v_i - v_j) \cdot \nabla_i w_{ij}$$

New velocity divergence:

$$(\nabla \cdot v)_i = -(\sum_j m_j w_{ij})^{-1}\sum_j m_j(v_i - v_j) \cdot \nabla_i w_{ij}$$

Deviation factors due to an interface with a vacuum cancel out.

New Continuity Equation:

$$d\rho_i/dt = \rho_i \left(\sum_j m_j w_{ij} \right)^{-1} \sum_j m_j (\mathbf{v}_i - \mathbf{v}_j) \cdot \nabla_i w_{ij}$$

EFFECTIVE RELATIVE VELOCITY SCHEME

Usual Continuity Equation:

$$d\rho_i/dt = \sum_j m_j(\mathbf{v}_i - \mathbf{v}_j) \cdot \nabla_i w_{ij}$$

Replace m_j with m_i.

Use eff. rel. vel.: $2m_j(m_i + m_j)^{-1}(\mathbf{v}_i - \mathbf{v}_j)$
(for particle i)

Let

$$M_{ij} = 2m_i m_j(m_i + m_j)^{-1}$$

New Continuity Equation:

$$d\rho_i/dt = \sum_j M_{ij}(\mathbf{v}_i - \mathbf{v}_j) \cdot \nabla_i w_{ij}$$

New density by summation:

$$R_i = \sum_j M_{ij} w_{ij}$$

Comparison with usual density by sum:

$$\sum_j M_{ij} w_{ij} \qquad \sum_j m_j w_{ij}$$

$$\text{If } m_j = m_i, \quad \frac{M_{ij}}{m_j} \; = \; \frac{m_j}{m_j} \text{ (just right)}$$

$$\text{If } m_j \gg m_i, \quad 2m_i \; \leq \; m_j \text{ (too large)}$$

$$\text{If } m_j \ll m_i, \quad 2m_j \; \geq \; m_j \text{ (too small)}$$

Continuity Equation with
density deviation cancellation:

$$d\rho_i / dt = \rho_i \left(\sum_j M_{ij} w_{ij}\right)^{-1} \sum_j M_{ij} (\mathbf{v}_i - \mathbf{v}_j) \cdot \nabla_i w_{ij}$$

The resulting SPH equations.

Let

$$N_{ij} = 2m_i(m_i + m_j)^{-1}$$

Density by summation:

$$R_i = \sum_j N_{ij} m_j w_{ij}$$

Velocity Divergence:

$$(\nabla \cdot \mathbf{v})_i = -R_i^{-1} \sum_j N_{ij} m_j (\mathbf{v}_i - \mathbf{v}_j) \cdot \nabla_i w_{ij}$$

Velocity Gradient:

$$\mathbf{L}_i = (\nabla \mathbf{v})_i^T = -R_i^{-1} \sum_j N_{ij} m_j (\mathbf{v}_i - \mathbf{v}_j) \otimes \nabla_i w_{ij}$$

Continuity Equations:

$$d\rho_i/dt = -\rho_i(\nabla \cdot \mathbf{v})_i$$

$$= \rho_i R_i^{-1} \sum_j N_{ij} m_j (\mathbf{v}_i - \mathbf{v}_j) \cdot \nabla_i w_{ij}$$

Energy Equations:

$$de_i/dt = \rho_i^{-1} \mathbf{T}_i \colon \mathbf{L}_i$$

$$= -(\rho_i R_i)^{-1} \sum_j N_{ij} m_j (\mathbf{v}_i - \mathbf{v}_j) \cdot \mathbf{T}_i \cdot \nabla_i w_{ij}$$

Momentum Equations:

$$d\mathbf{v}_i/dt = \sum_j m_j [N_{ij}(\rho_i R_i)^{-1} \mathbf{T}_i \cdot \nabla_i w_{ij}$$

$$+ N_{ji}(\rho_j R_j)^{-1} \mathbf{T}_j \cdot \nabla_i w_{ji}]$$

Comments:

The above equations are for the "Effective Relative Velocity" scheme combined with the "Density Deviation Cancellation" idea.

To get the equations without the "Density Deviation Cancellation" idea, replace all R_i and R_j (on the right side of the equations) with ρ_i and ρ_j respectively.

To get the equations without the "Effective Relative Velocity" scheme, replace N_{ij} and N_{ji} with 1 everywhere.

```
, 1                      [IMOD(0=Orig,1=LouB,2=EffVel),IVARH(0=Fixed,1=Var)]
.0, 0.0, 0               [H(ignr),NPH(ignr),IEOS(ignr)(1=PerGas,2=Grun,3=Mie-Grun)]
500, 1                   [Number of Iterations,Density(0=Summ,1=Cont)]
.5, 2.5, 0.1             [Alpha, Beta, Epsilon, (Artificial Viscosity)]
.50, 1.00                [G1, G2 (Wall Heating)]
n                        [Interval]
.3, 2.0                  [CFL No., Stop Time]
1.0, 2.0                 [Xmin, Xmax (Problem Domain)]
                         [Restart (0=No,1=Yes)]

strt.000000

                         [Number of Lines]
luminum                  [Material]
0.2, 0.0                 [Start and End]
.71, 1.0E-08, 0.6        [Density, Internal Energy, and Velocity]
.01, 1.5, 3              [H,NPH,IEOS(1=PerGas,2=Grun,3=Mie-Grun)]
ir                       [Material]
.0, 2.0                  [Start and End]
.99E-5, 1.0E-8, 0.0      [Density, Internal Energy, and Velocity]
.01, 1.5, 1              [H,NPH,IEOS(1=PerGas,2=Grun,3=Mie-Grun)]
                         [Number of Time Dump Intervals]
.5
.0
strt
```

run L6   PRELIMINARY RESULTS

Eff. Rel. Vel. method with Dens. Dev. Canc.

Piston Problem

Al on air at 6 km/sec

0.2 µsec from start

(Density by continuity equations)

Density vs. X [NP=330, Time=0.2067, Iter=1000]
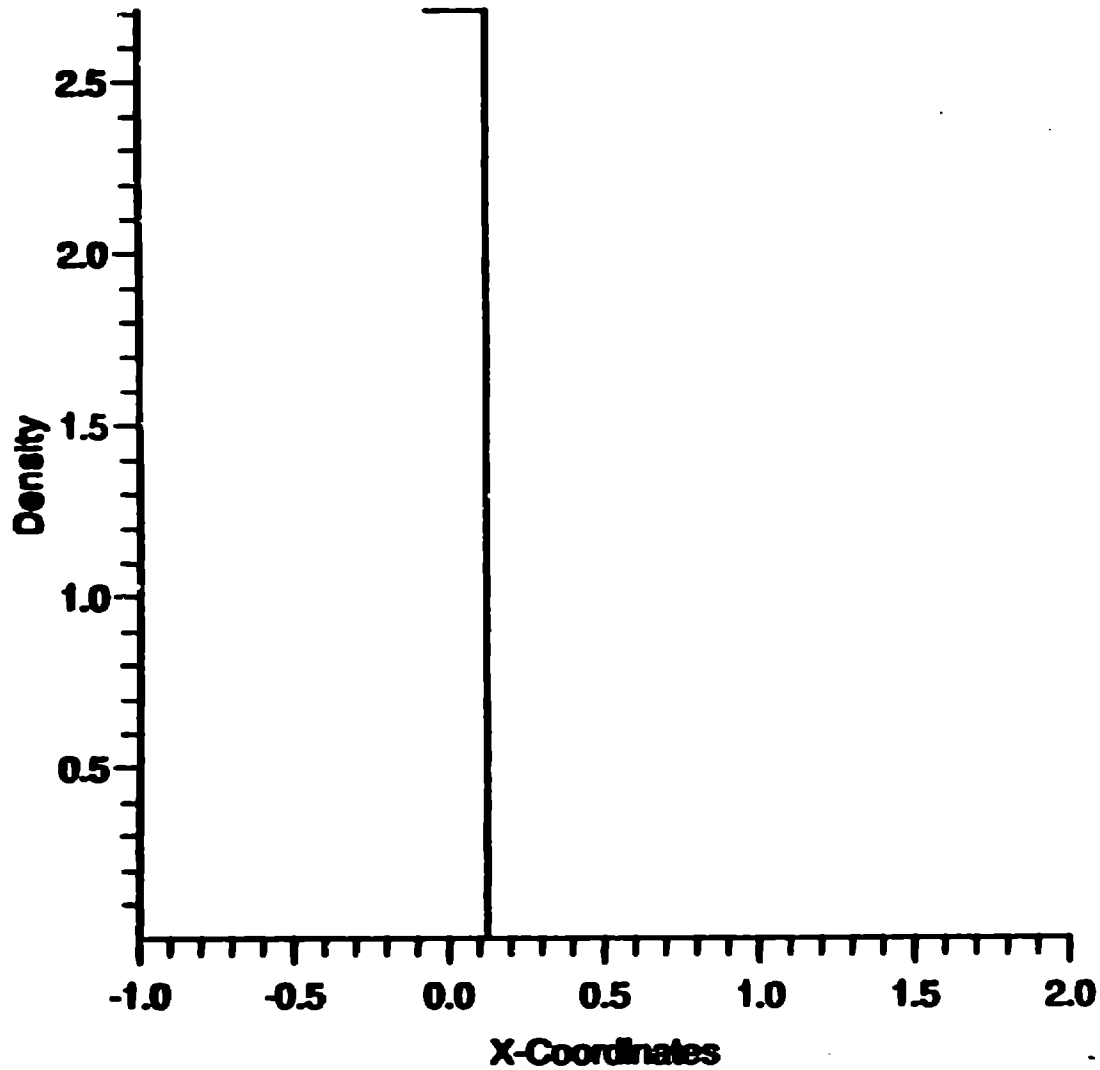
Max Density = 2.710074

Min Density = 0.000090

Alpha = 2.5000
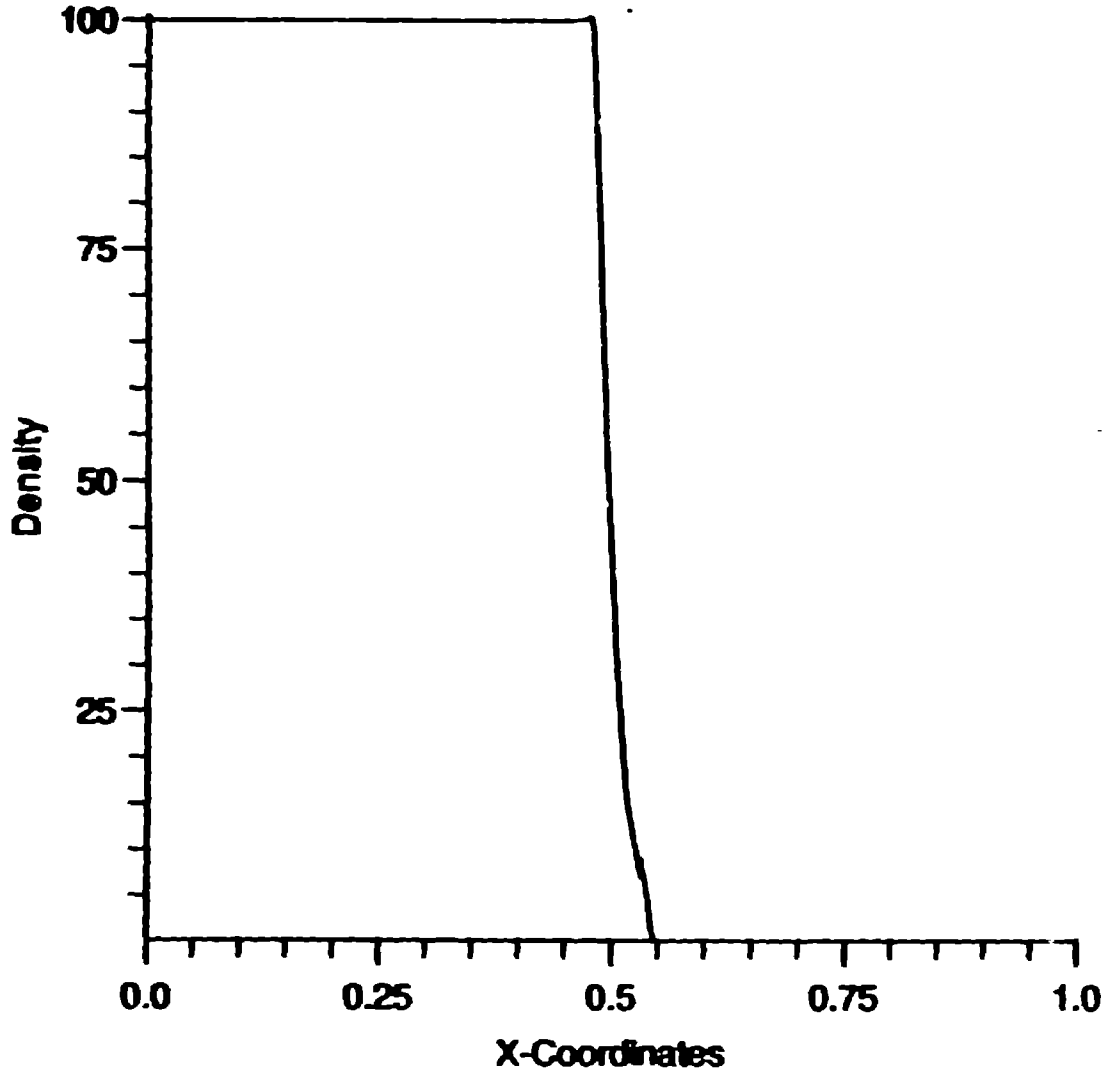
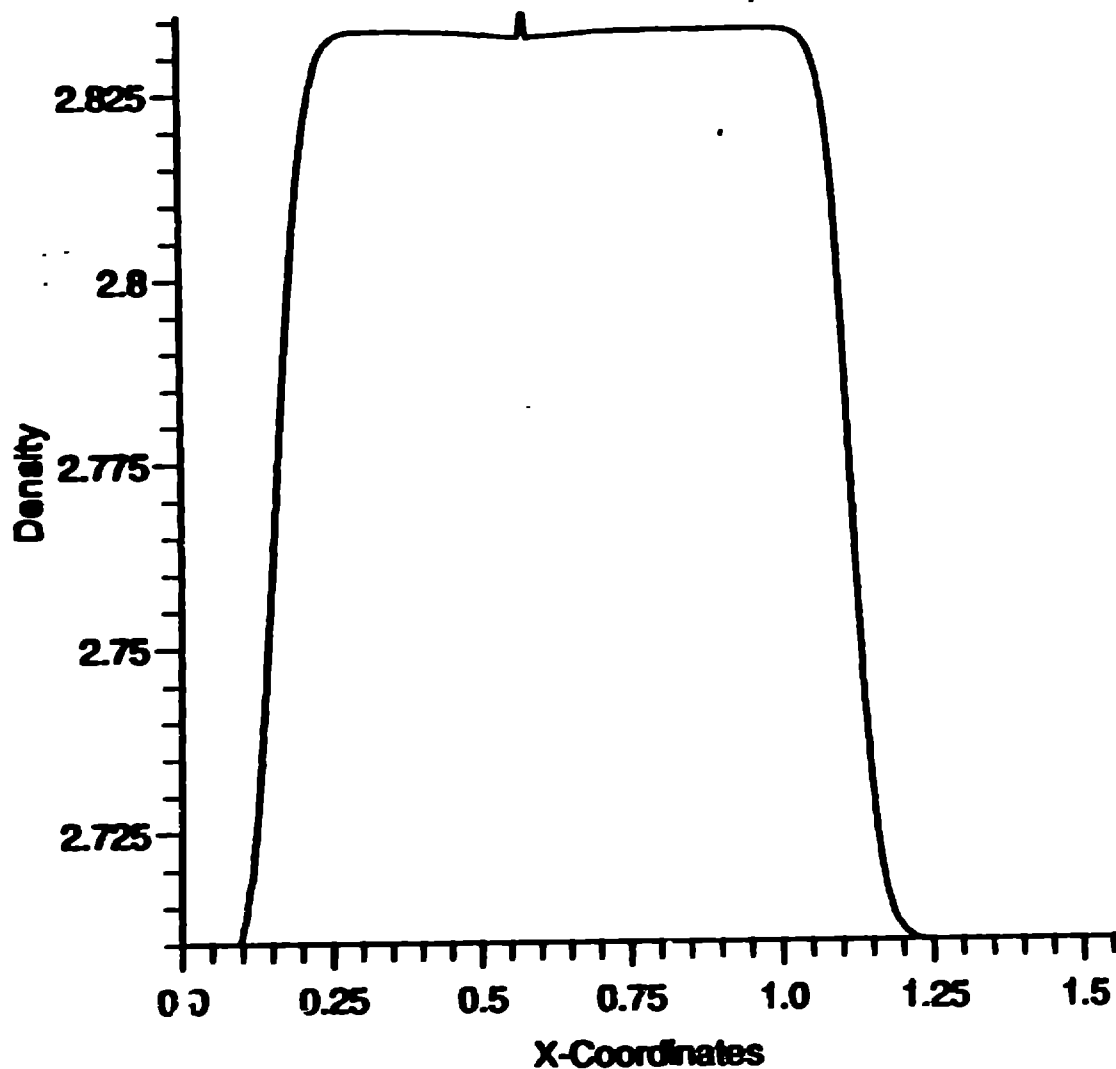Beta = 2.5000

Eps = 0.1000
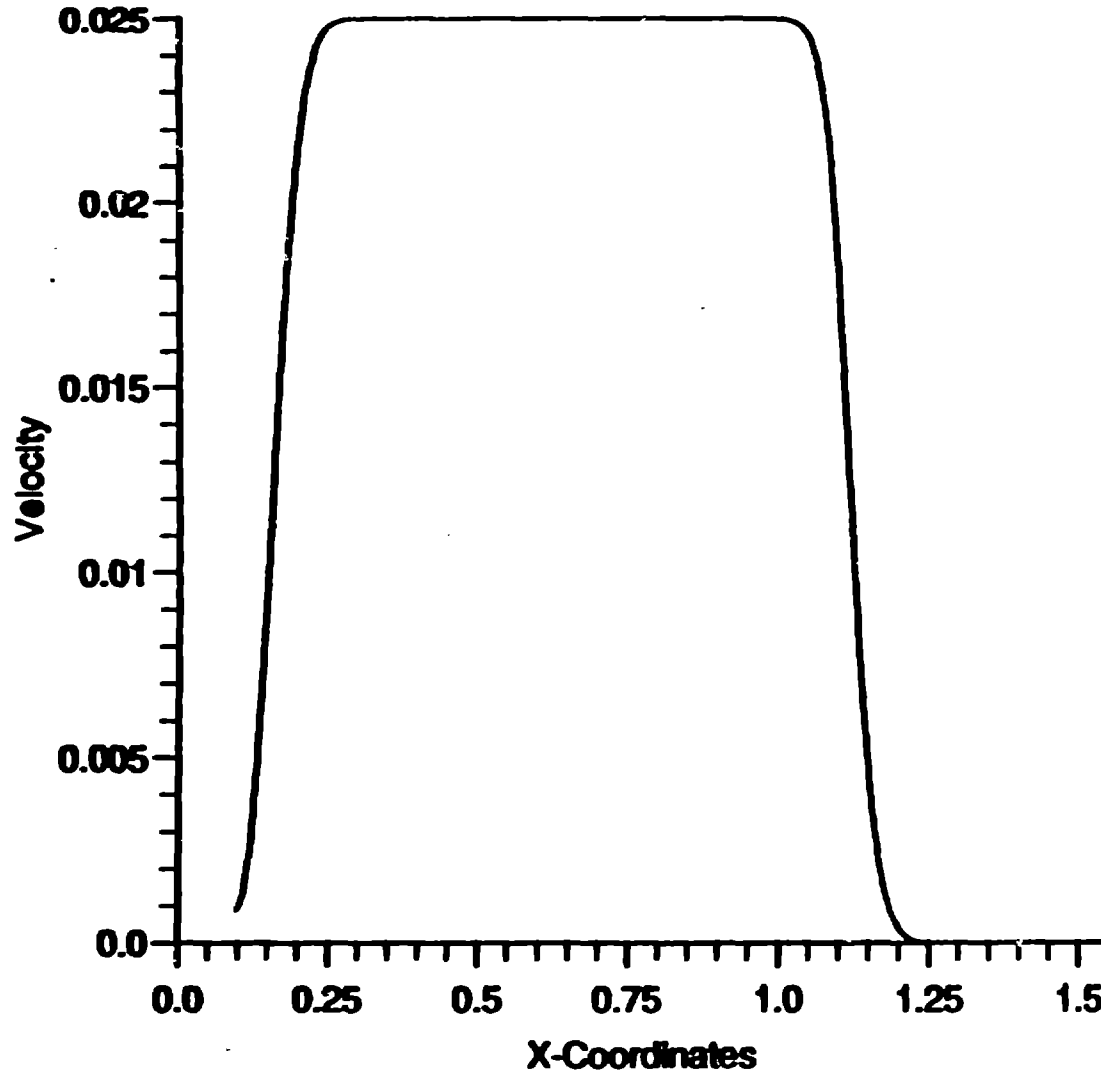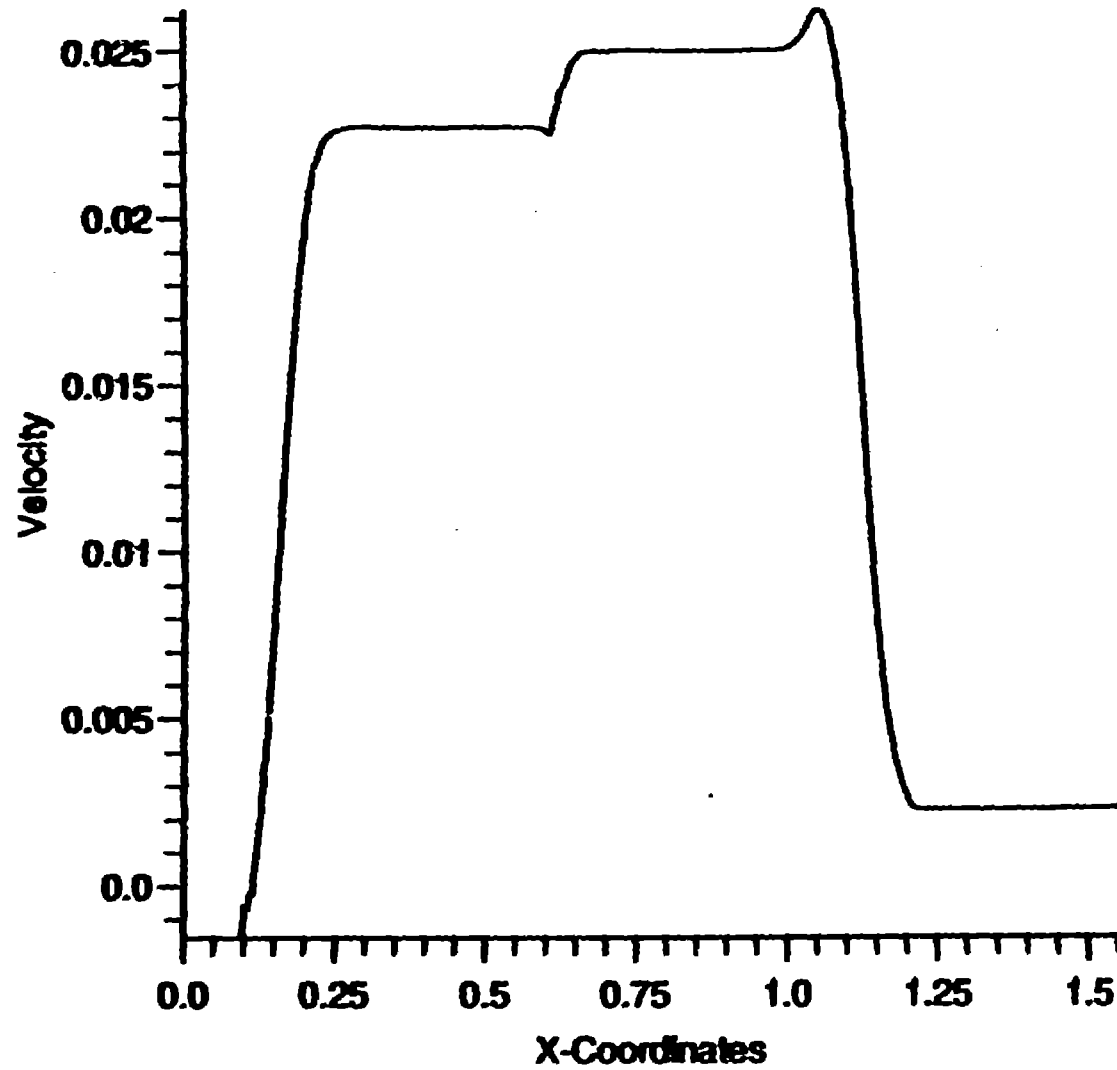
G1 = 0.5000

G2 = 1.0000

CFL = 0.3000

——— Calculation

30 August 1993

Density

X-Coordinates

-1.0 -0.5 0.0 0.5 1.0 1.5 2.0

0.5 1.0 1.5 2.0 2.5

-76-

Pressure vs. X [NP=330, Time=0.2067, Iter=1000]   run L6

Max Pressure = 0.000110

Min Pressure = -0.000050

Alpha = 2.5000

Beta = 2.5000
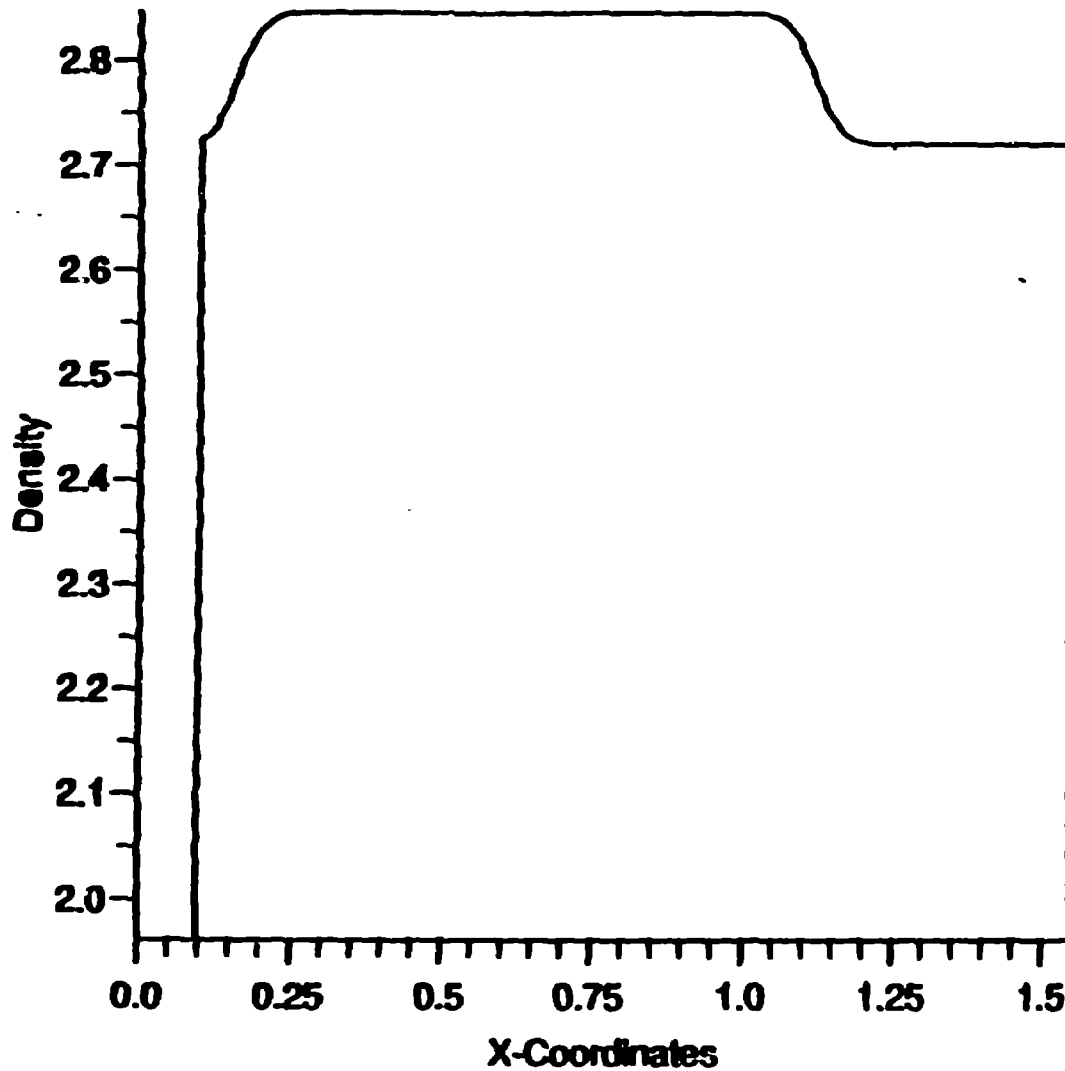
Eps = 0.1000

G1 = 0.5000

G2 = 1.0000

CFL = 0.3000

——————— Calculation

30 August 1993

```
                    [IMOD(0=Orig,1=LouB,2=EffVel),IVARH(0=Fixed,1=Var)]
 0.0, 0             [H(ignr),NPH(ignr),IEOS(ignr)(1=PerGas,2=Grun,3=Mie-Grun)]
0, 1                    [Number of Iterations,Density(0=Summ,1=Cont)]
 2.5, 0.1          [Alpha, Beta, Epsilon, (Artificial Viscosity)]
, 0.00             [G1, G2 (Wall Heating)]
                     [Interval]
 0.2               [CFL No., Stop Time]
, 1.1              [Xmin, Xmax (Problem Domain)]
                   [Restart (0=No,1=Yes)]
t.000000
                   [Number of Lines]
                   [Material]
 0.5               [Start and End]
, 2.5, 0.0      [Density, Internal Energy, and Velocity]
25, 1.5, 1          [H,NPH,IEOS(1=PerGas,2=Grun,3=Mie-Grun)]
                   [Material]
 1.0               [Start and End]
5, 2.0, 0.0     [Density, Internal Energy, and Velocity]
25, 1.5, 1          [H,NPH,IEOS(1=PerGas,2=Grun,3=Mie-Grun)]
                   [Number of Time Dump Intervals]

t
```

runL8 PRELIMINARY RESULTS

Eff. Rel. Vel. method with Dens. Dev. Canc.

Shock tube problem

Air and air, density ratio 8, initially at rest

0.2 µsec from start

(Density by continuity equation)

Density vs. X [NP=600, Time=0.2000, Iter=904]   run L8
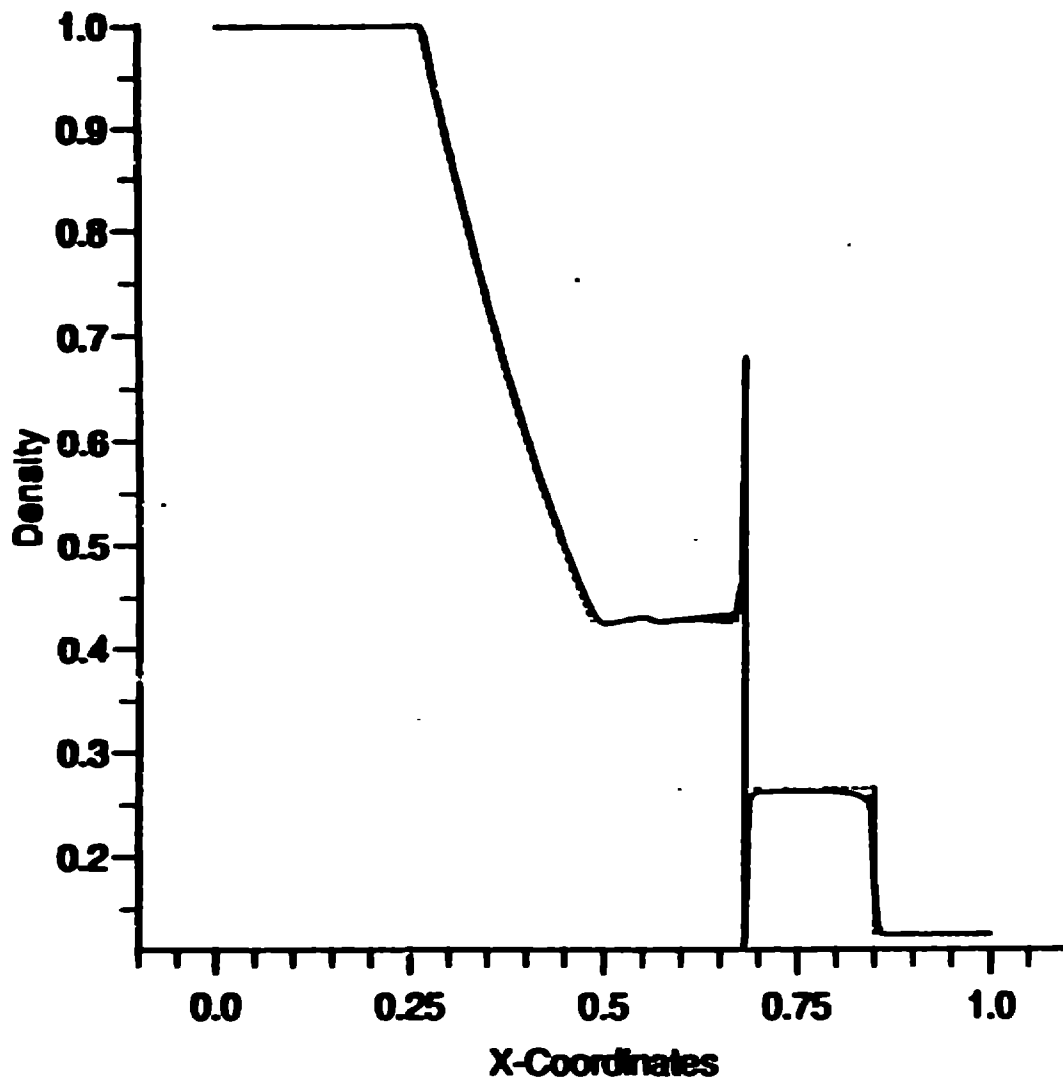
Max Density = 1.00097+

Min Density = 0.110774+

Alpha = 2.5000

Beta = 2.5000

Eps = 0.1000

G1 = 0.0000

G2 = 0.0000

CFL = 0.3000

—— Calculation

----- Analytic

20 September 1993

Pressure vs. X [NP=600, Time=0.2000, Iter=904]   run L8
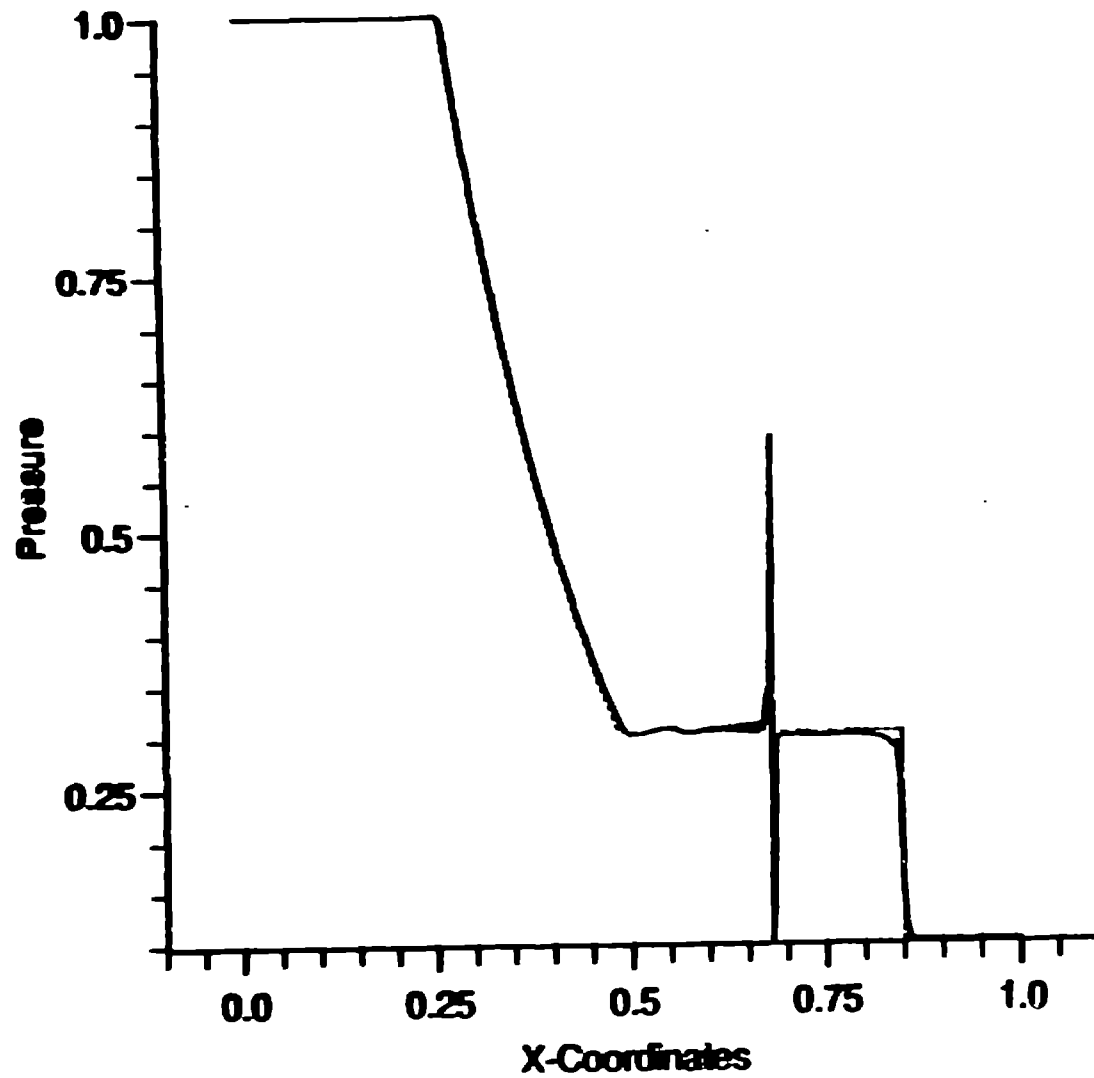
Max Pressure = 1.001363
Min Pressure = 0.097294

Alpha = 2.5000
Beta = 2.5000
Eps = 0.1000
G1 = 0.0000
G2 = 0.0000
CFL = 0.3000

————— Calculation
············· Analytic

20 September 1993

VELOCITY DIVERGENCE BASED ON ESTIMATES USED IN ARTIFICIAL VISCOSITY THEORY

Estimate of contrib. to vel. div. at particle i due to particle j:

$$|\mathbf{r}_i - \mathbf{r}_j|^{-2}(\mathbf{r}_i - \mathbf{r}_j)\bullet(\mathbf{v}_i - \mathbf{v}_j)$$

An averaging procedure weighted by $m_j w_{ij}$ gives:

$$(\nabla\bullet\mathbf{v})_i = -(\sum_j m_j w_{ij})^{-1}\sum_j \{m_j(\mathbf{v}_i - \mathbf{v}_j)$$
$$\bullet[-|\mathbf{r}_i - \mathbf{r}_j|^{-2}(\mathbf{r}_i - \mathbf{r}_j)w_{ij}]\}$$

The result: In the SPH governing equations, $\nabla_i w_{ij}$ is replaced by

$$-|\mathbf{r}_i - \mathbf{r}_j|^{-2}(\mathbf{r}_i - \mathbf{r}_j)w_{ij}$$
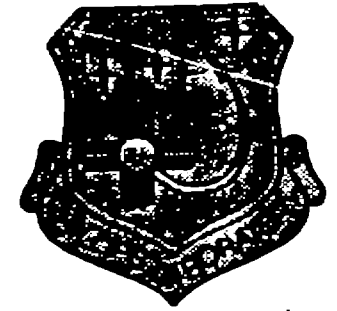
Boundaries and Interfaces in SPH

Louis Baker
Dagonet Software
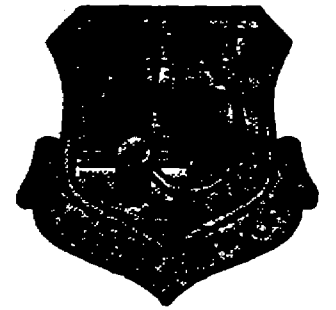
Problem:
Robust SPH for
large density differences
various EOS

Riemann Shock Tube
Aluminum Impact Test Cases
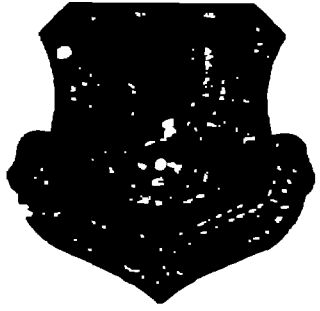
SPH Interpolation

Gibbs Phenomena at Discontinuities
Kernel: Cardinal B-Splines
Ok for uniform spacing, no boundaries
Choice: either
    1) ensure smoothness
    2) modify interpolation for jumps

Cubic Cardinal B-Splines
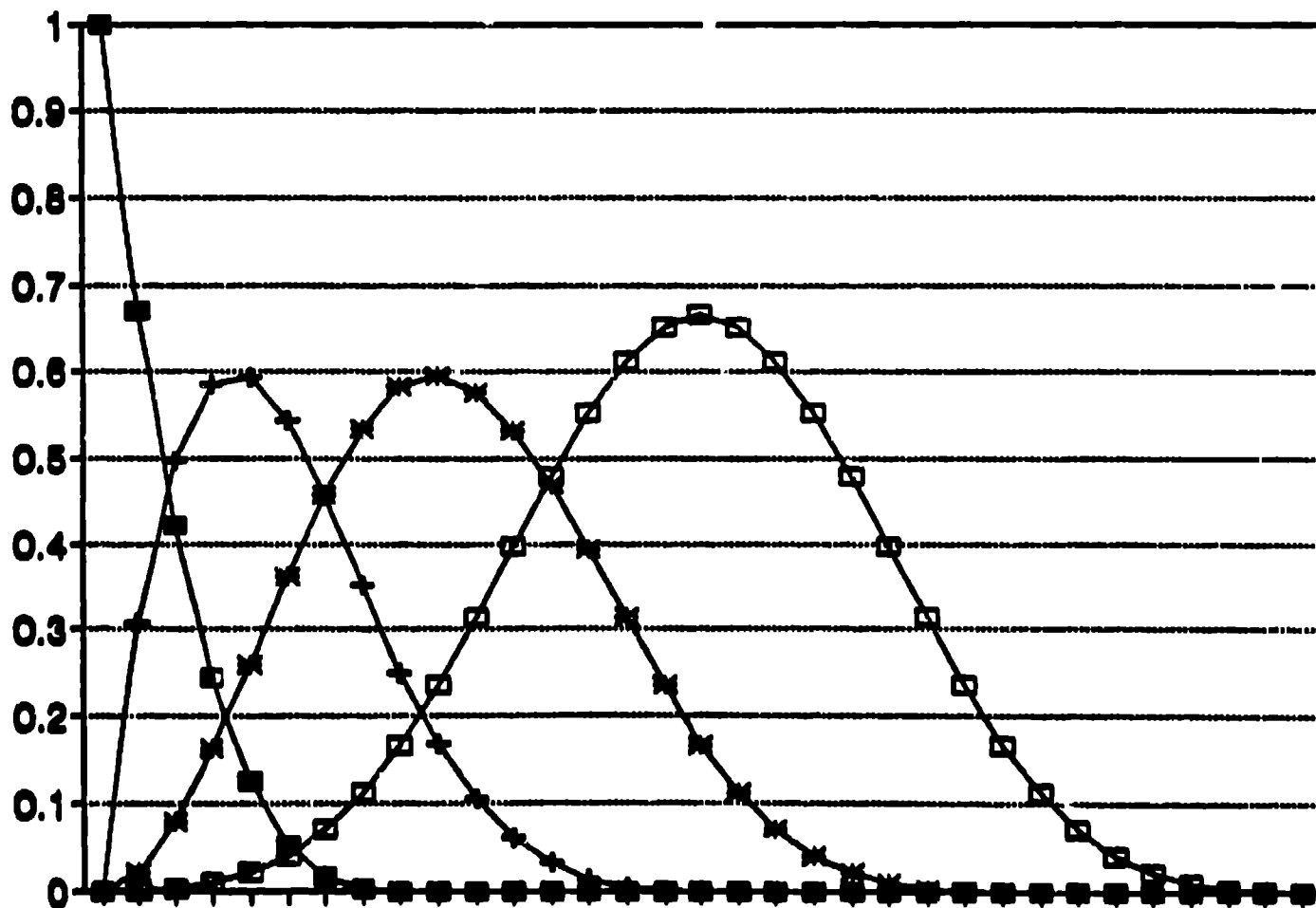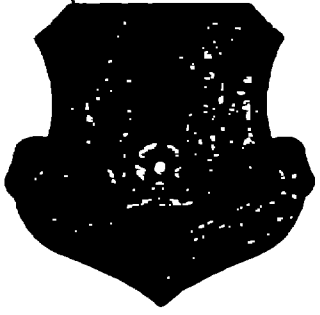
DONT'S

**Mass Match
Mass Adjust
Ratio Zone**
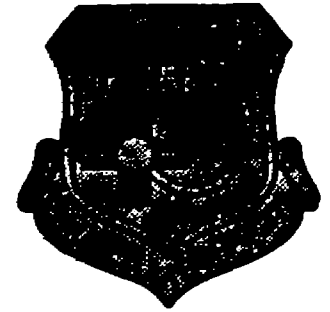
DO's

Use Summation, Not Continuity
Need to re-normalize density for EOS
Volume Match

Density vs. X [NP=800, Time=0.1000, Iter=1706]
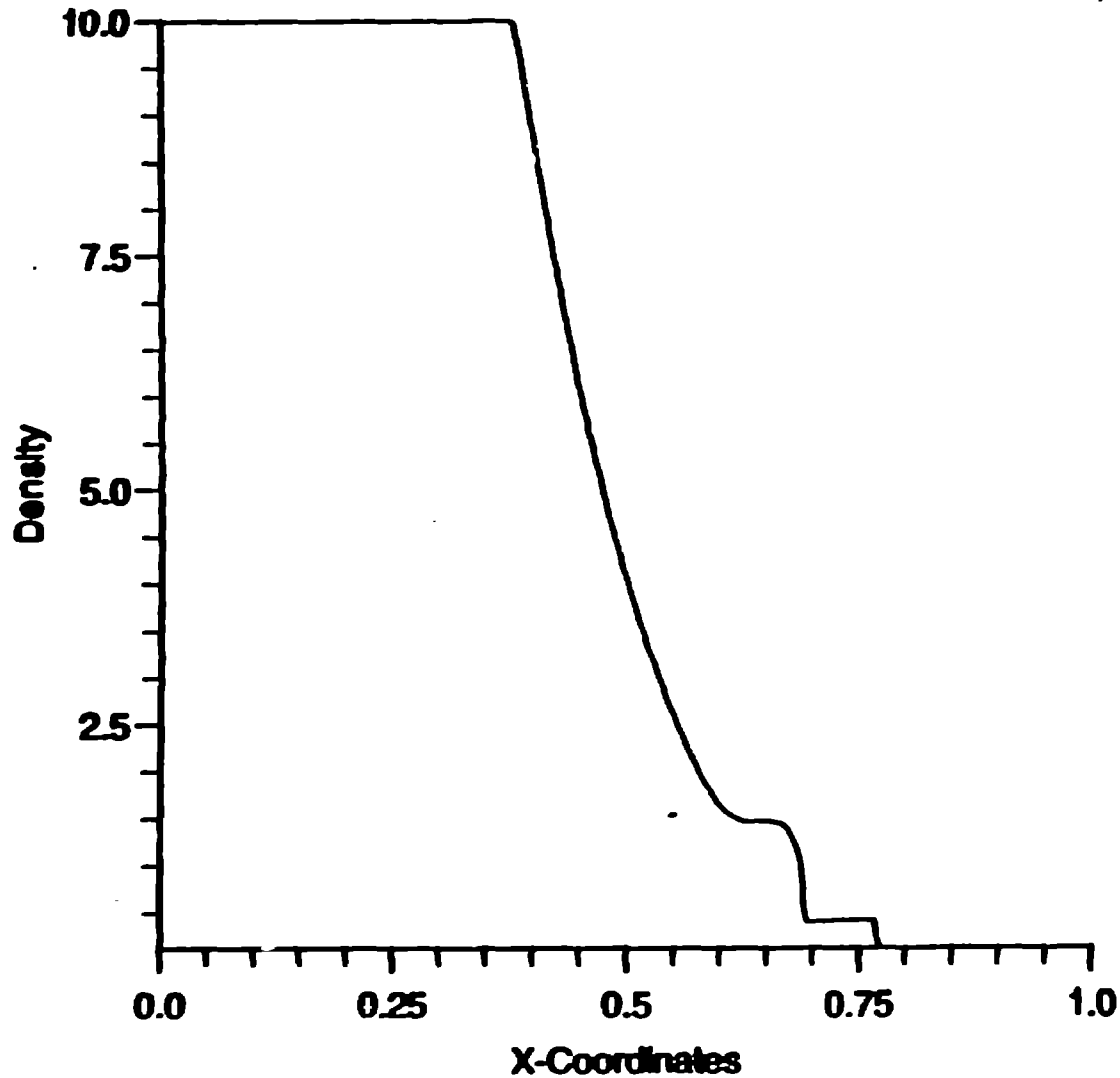
Max Density = 10.0052

Min Density = 0.1249

Alpha = 2.5000

Beta = 2.5000

Eps = 0.1000

G1 = 0.0000

G2 = 0.0000

CFL = 0.2000

——————— Calculation

16 September 1993

80:1 Shock Tube

Density vs. X [NP=800, Time=0.0050, Iter=1651]

Max Density = 100.3448

Min Density = 0.1225

Alpha = 2.5000

Beta = 2.5000

Eps = 0.1000

G1 = 0.0000

G2 = 0.0000

CFL = 0.2000

——————— Calculation

17 September 1993

800:1 Shock Tube

Density vs. X [NP=450, Time=1.0000, Iter=409]

Max Density = 2.8356
Min Density = 2.7100

Alpha = 2.5000
Beta = 2.5000
Eps = 0.1000
G1 = 0.5000
G2 = 1.0000
CFL = 0.3000

—————— Calculation

13 September 1993

Al Impact- Continuity

Al c1

Velocity vs. X [NP=450, Time=1.0000, Iter=409]

Max Velocity = 0.0250

Min Velocity = 0.0000

Alpha = 2.5000
Beta = 2.5000
Eps = 0.1000
G1 = 0.5000
G2 = 1.0000
CFL = 0.3000

——— Calculation

13 September 1993

Pressure vs. X [NP=450, Time=1.0000, Iter=409]
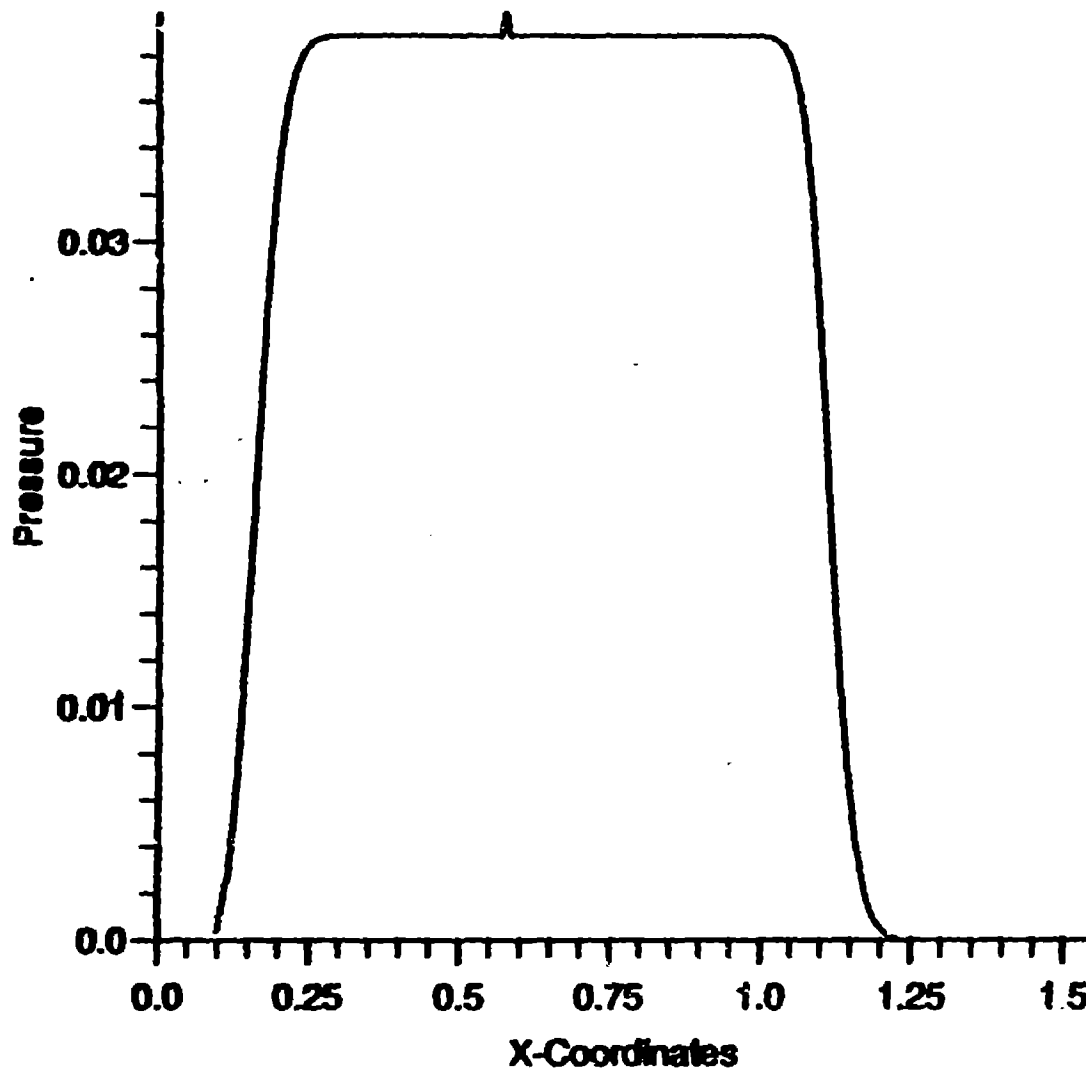
Max Pressure = 0.0397

Min Pressure = 0.0000

Alpha = 2.5000

Beta = 2.5000

Eps = 0.1000

G1 = 0.5000

G2 = 1.0000

CFL = 0.3000

—————— Calculation

13 September 1993

Aℓ

Density vs. X [NP=450, Time=1.0000, Iter=505]
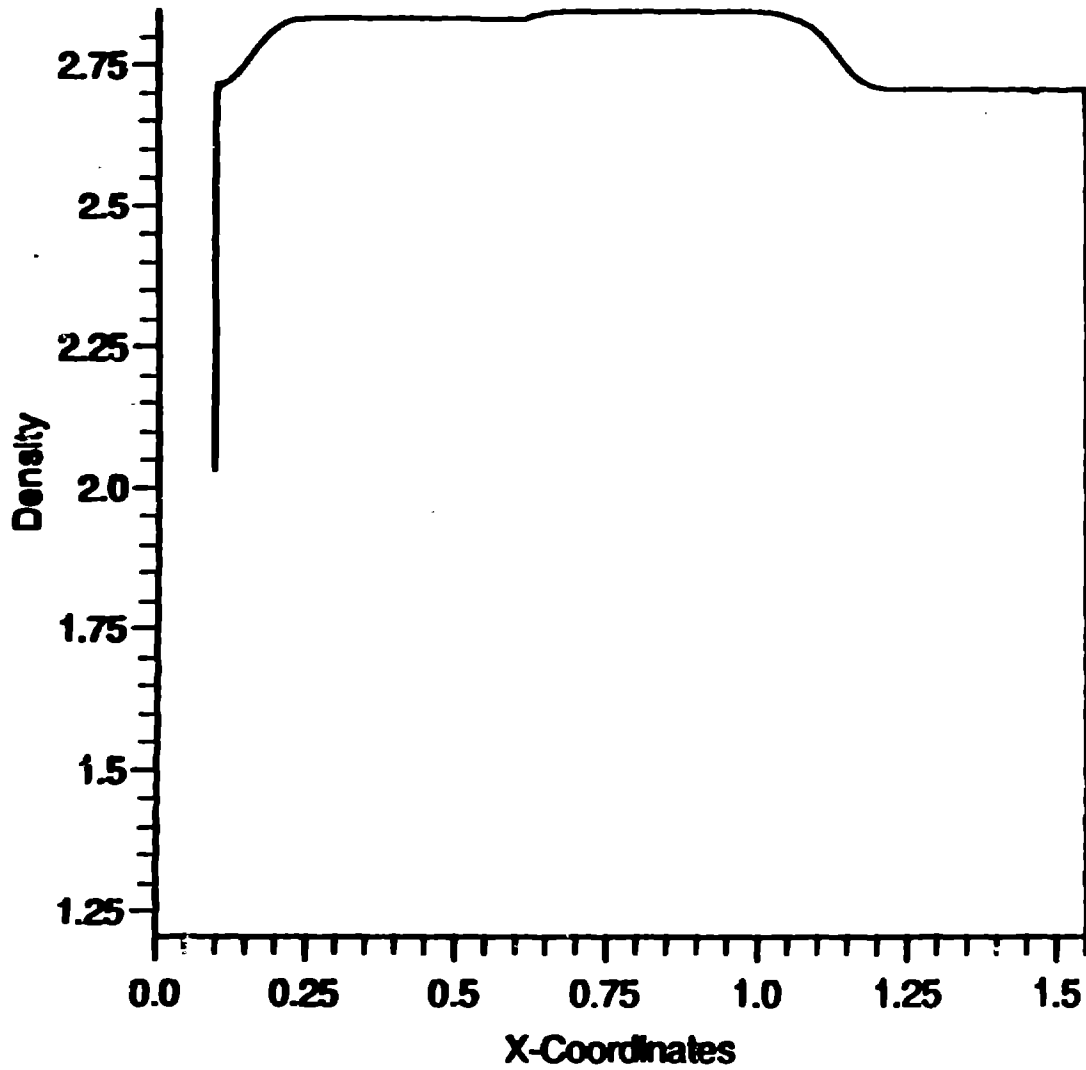
Max Density = 2.8454

Min Density = 1.2357

Alpha = 2.5000

Beta = 2.5000

Eps = 0.1000

G1 = 0.5000

G2 = 1.0000

CFL = 0.3000

——— Calculation

16 September 1993

Al Impact - Naive Summation

Al Cφ

Velocity vs. X [NP=450, Time=1.0000, Iter=505]

Max Velocity = 0.0261
Min Velocity = -0.0015

Alpha = 2.5000
Beta = 2.5000
Eps = 0.1000
G1 = 0.5000
G2 = 1.0000
CFL = 0.3000

———— Calculation

13 September 1993

Pressure vs. X [NP=450, Time=1.0000, Iter=505]
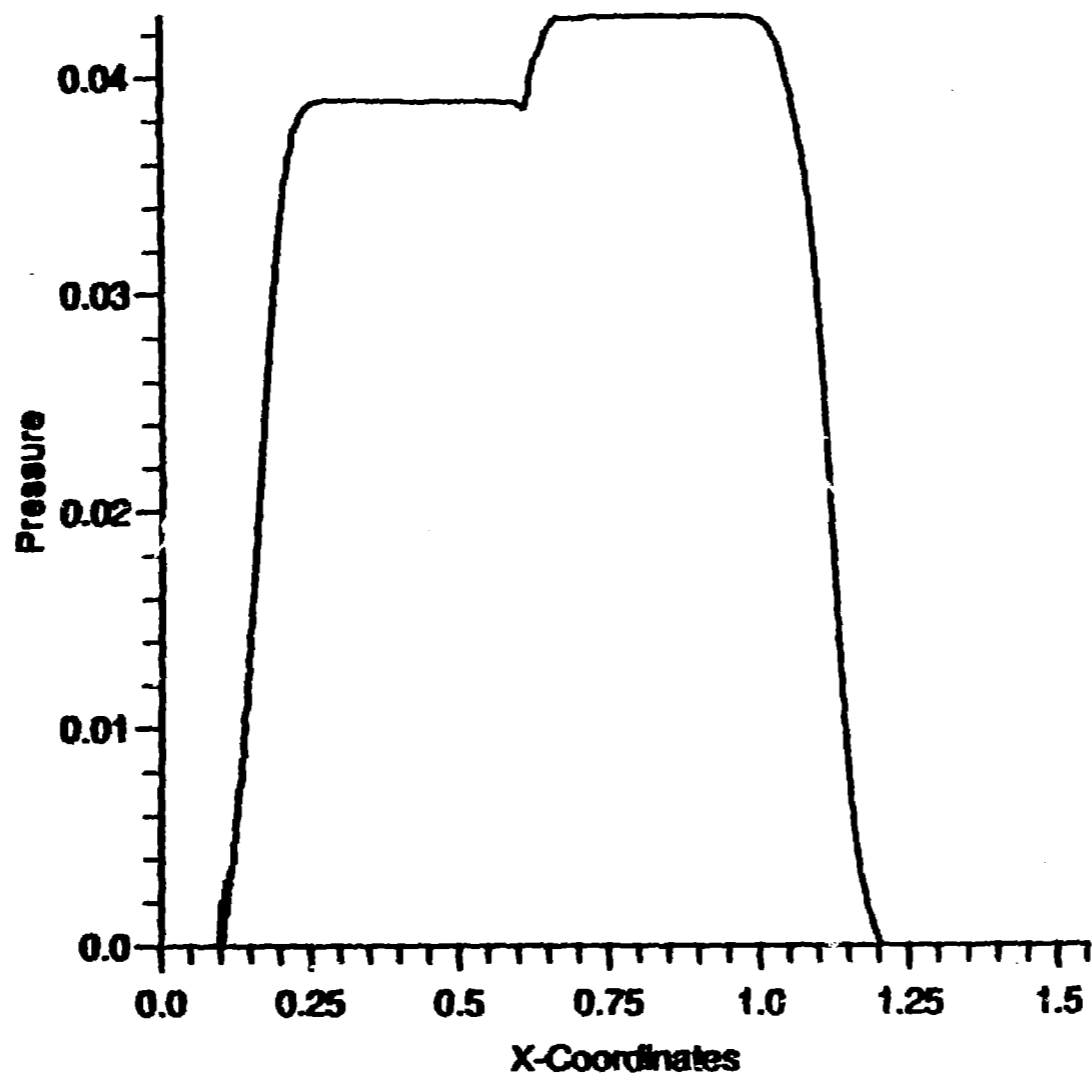
Max Pressure = 0.0428

Min Pressure = 0.0000

Alpha = 2.5000

Beta = 2.5000

Eps = 0.1000

G1 = 0.5000

G2 = 1.0000

CFL = 0.3000

———— Calculation

16 September 1993

Density vs. X [NP=450, Time=1.0000, Iter=413]

Max Density = 2.8463
Min Density = 1.9618

Alpha = 2.5000
Beta = 2.5000
Eps = 0.1000
G1 = 0.5000
G2 = 1.0000
CFL = 0.3000

——— Calculation

13 September 1993

Al Impact - Summation w. Renorm.
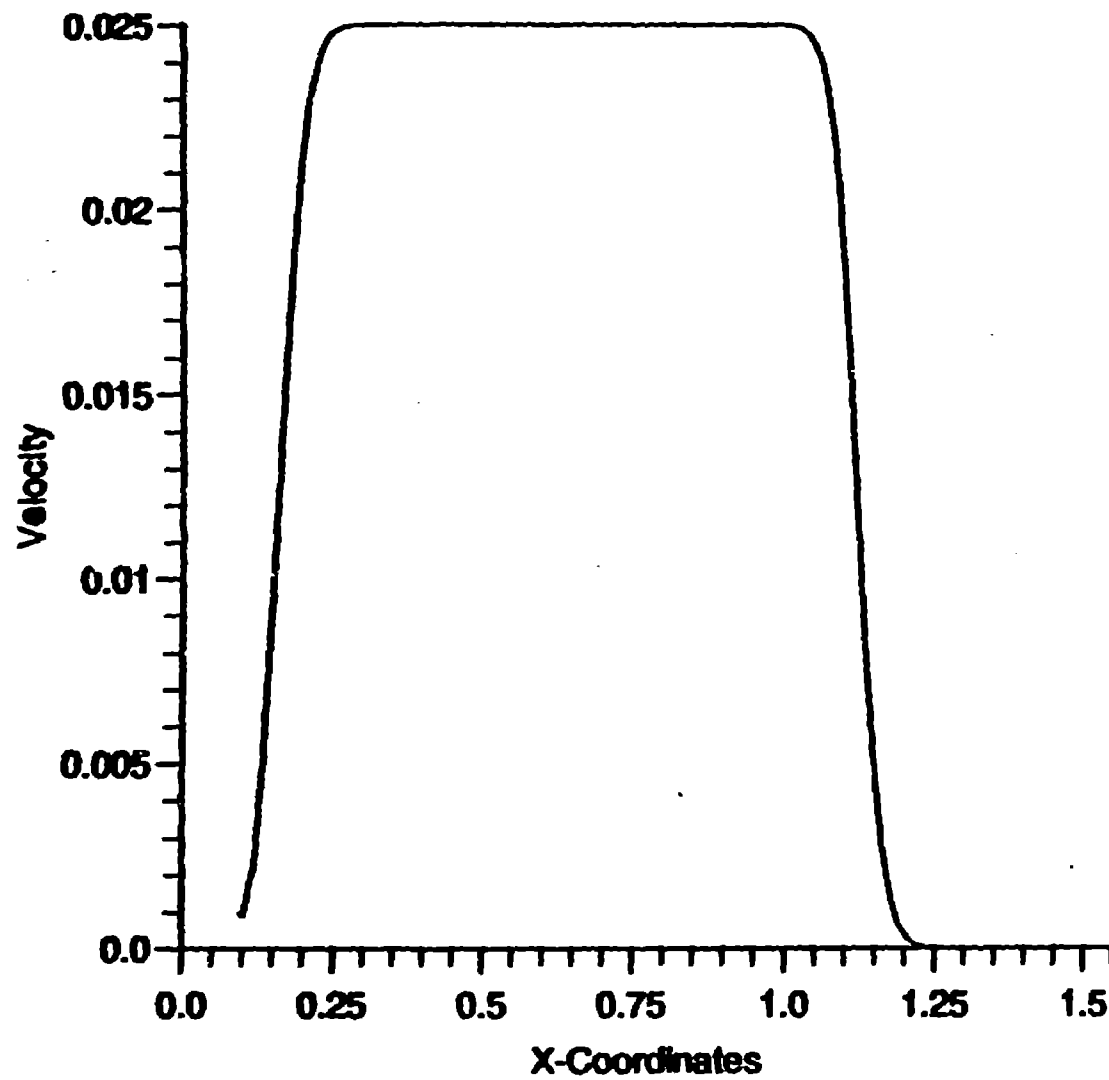
Velocity vs. X [NP=450, Time=1.0000, Iter=413]

Max Velocity = 0.0250

Min Velocity = 0.0000

Alpha = 2.5000

Beta = 2.5000

Eps = 0.1000

G1 = 0.5000

G2 = 1.0000

CFL = 0.3000

———— Calculation

13 September 1993

Alcor4

Pressure vs. X [NP=450, Time=1.0000, Iter=413]
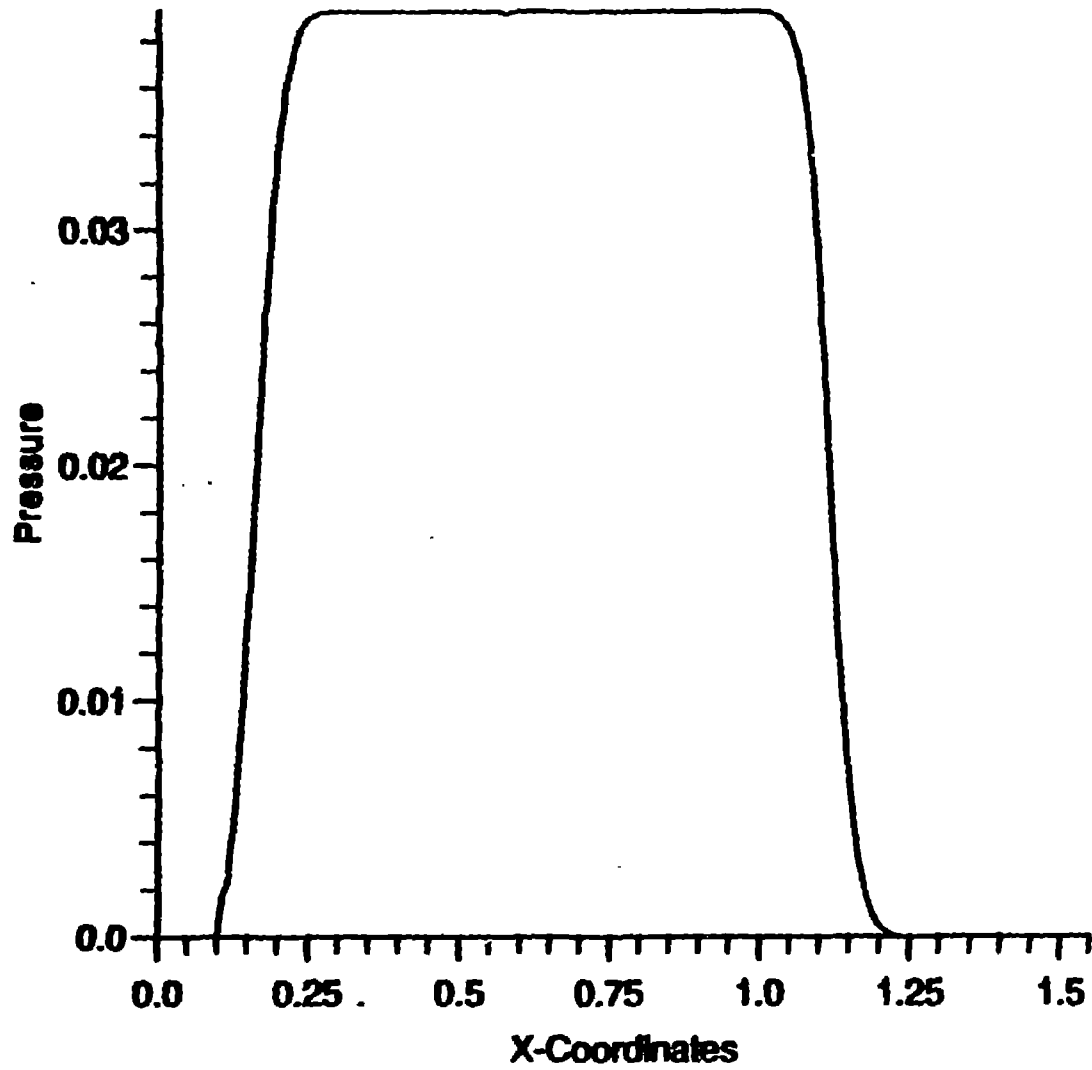
Max Pressure = 0.0392

Min Pressure = 0.0000

Alpha = 2.5000

Beta = 2.5000

Eps = 0.1000

G1 = 0.5000

G2 = 1.0000

CFL = 0.3000

—————— Calculation

16 September 1993

Density vs. X [NP=285, Time=1.0000, Iter=2810]
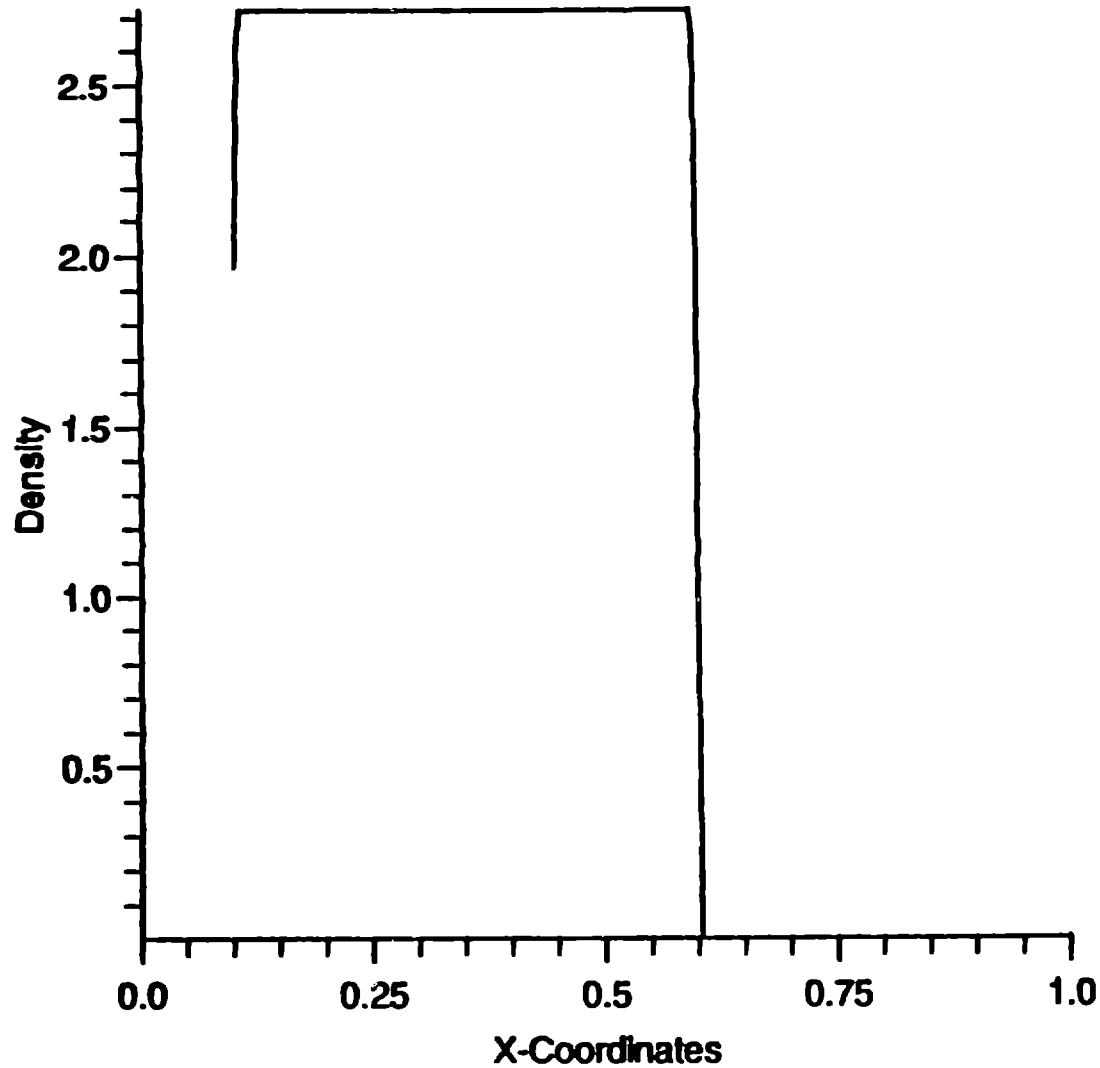
Max Density = 2.7213

Min Density = 0.0001

Alpha = 2.5000

Beta = 2.5000

Eps = 0.1000

G1 = 0.5000

G2 = 1.0000

CFL = 0.1000

——— Calculation

20 September 1993

Al piston pushing Air $\dfrac{P_{Al}}{P_{Air}} \cong 22,000$

Velocity vs. X [NP=285, Time=1.0000, Iter=2810]
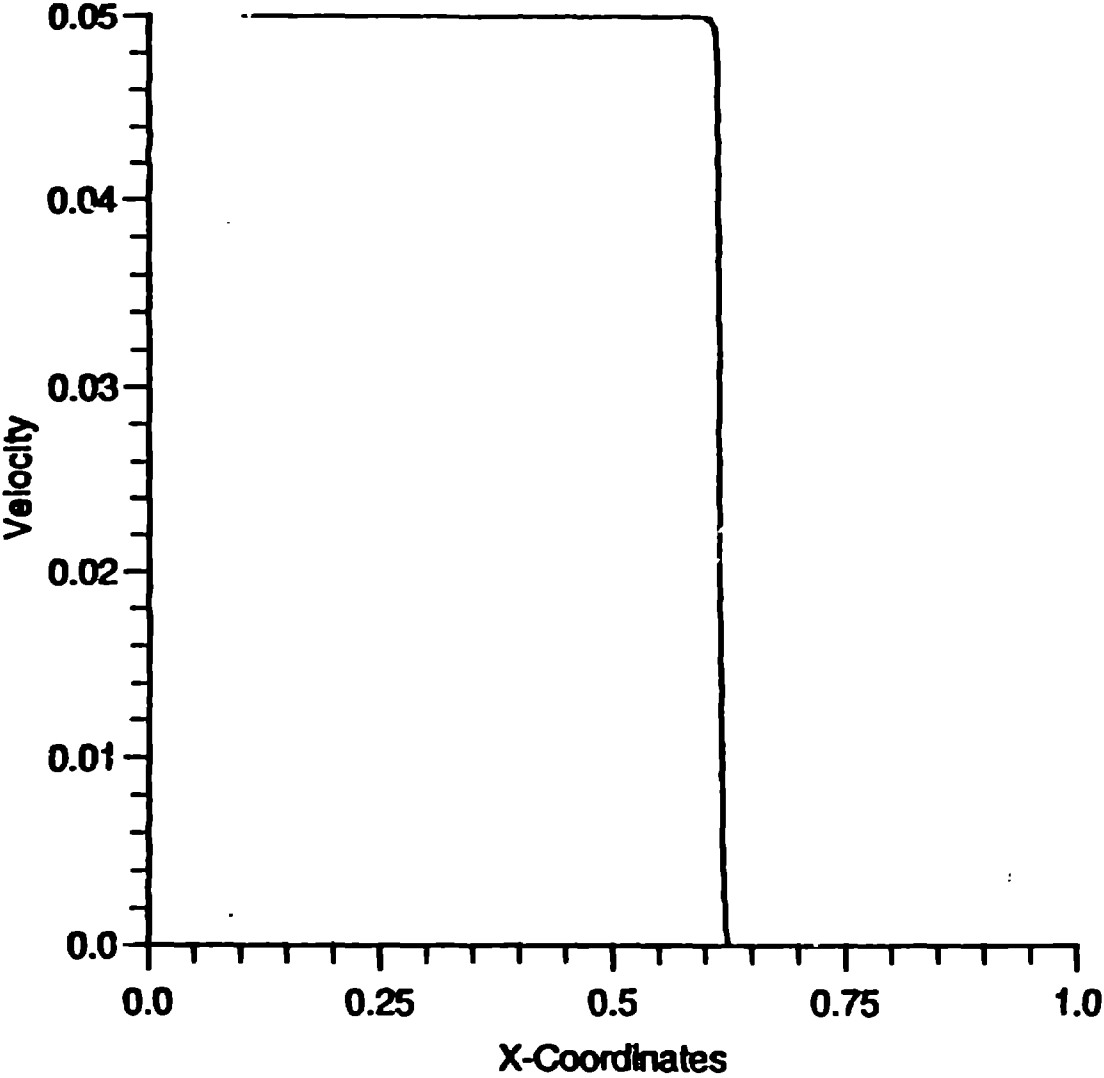
Max Velocity = 0.0500

Min Velocity = -0.0000

Alpha = 2.5000

Beta = 2.5000

Eps = 0.1000

G1 = 0.5000

G2 = 1.0000

CFL = 0.1000

———— Calculation

20 September 1993

Internal Energy vs. X [NP=285, Time=1.0000, Iter=2810]

$\cdot 10^3$

1.25

1.0

0.75

Internal Energy

0.5

0.25

0.0
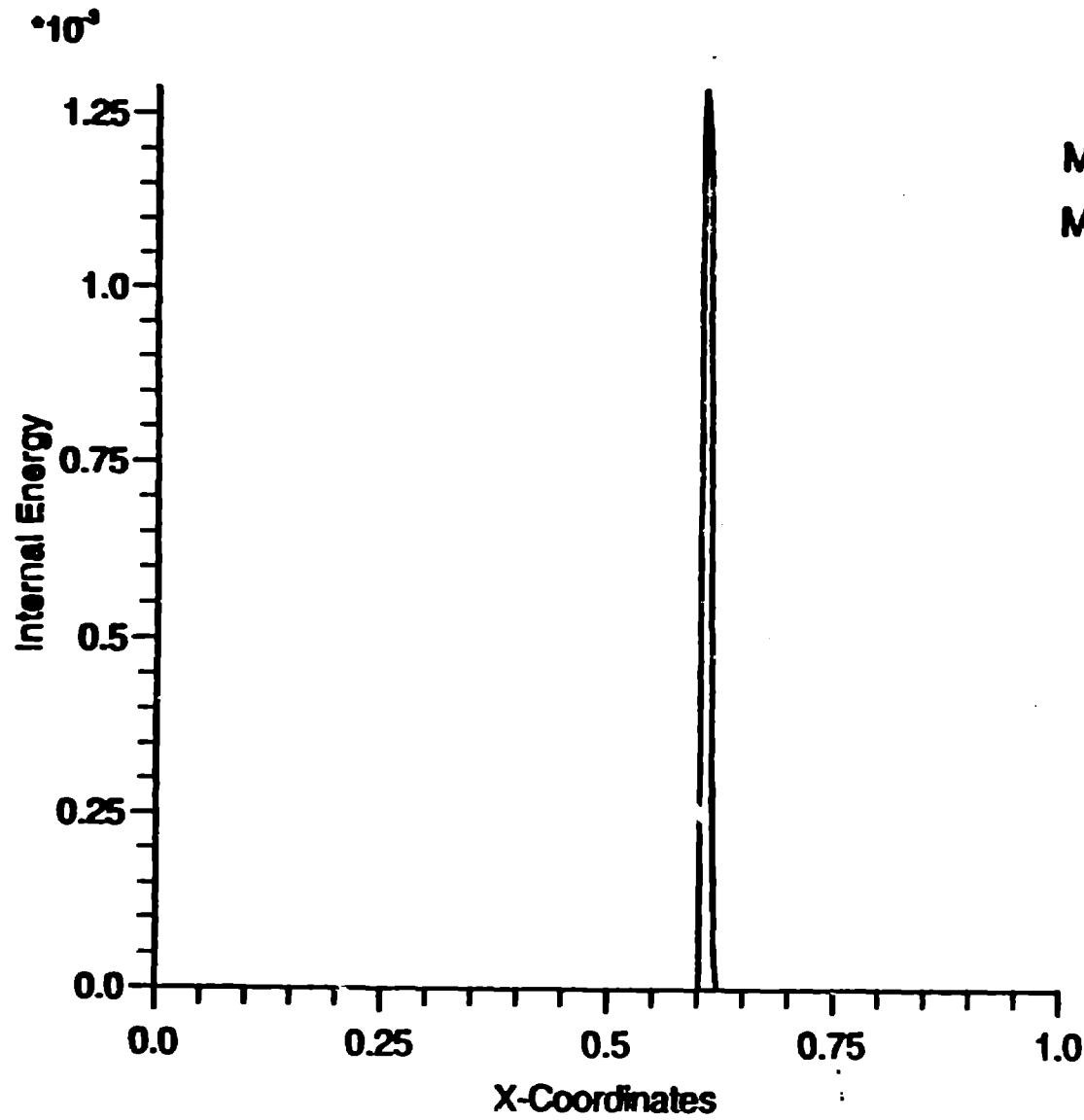
Max Internal Energy = 0.0012

Min Internal Energy = -0.0000

Alpha = 2.5000

Beta = 2.5000

Eps = 0.1000

G1 = 0.5000

G2 = 1.0000

CFL = 0.1000

——— Calculation

20 September 1993

0.0   0.25   0.5   0.75   1.0

X-Coordinates

Methodology and Tests of Adaptive SPH

Mike Owen [*]   Jens Villumsen [†]   Paul Shapiro [‡]

Hugo Martell [§]

September 17, 1993

[*]Dept. of Astronomy, Ohio State University
[†]Dept. of Astronomy, Ohio State University
[‡]Dept. of Astronomy, University of Texas
[§]Dept. of Astronomy, University of Texas

1 Caveat

The Ohio group (Mike Owen and Jens Villumsen) and the Texas group (Paul Shapiro and Hugo Martell) have collaborated on the basic ideas and goals for the development of Asph, but the two groups have independently derived their own Asph theories and algorithms as well as developed entirely independent codes based on those ideas. The bodies of work of both of these groups are based on the same basic principles and should give similar results. All the work presented today is the result of our development in Ohio and any questions on this material should be directed to either Mike Owen or Jens Villumsen; questions pertaining to the Texas development should be referred to Paul Shapiro or Hugo Martell.

2 Definitions

Standard Smoothed Particle Hydrodynamics (Sph)

- Utilizes a single isotropic smoothing scale per particle.
- Interpolation kernel $W(\vec{r}, h)$ may be expressed as

$$W(\vec{r}, h_s) = W\left(\frac{|\vec{r}|}{h_s}\right) \tag{1}$$

- Smoothing scale allowed to vary spatially from particle to particle as well as temporally.
- Artificial viscosity is implemented for any convergent flow within the gas.

Adaptive Smoothed Particle Hydrodynamics (Asph)

- Utilizes an anisotropic smoothing scale per particle, as embodied by the **H** tensor.
- The smoothing tensor is allowed to vary both spatially and temporally, as in Standard Sph.
- The interpolation kernel $W(\vec{r}, \mathbf{H})$ may be expressed as

$$W(\vec{r}, \mathbf{H}) = W(\mathbf{H}\vec{r}) \tag{2}$$

- There are two current variations of Asph, unsuppressed and suppressed:

- **Unsuppressed Asph** utilizes the artificial viscosity for any convergent flow, as in Standard Sph.
- **Suppressed Asph** employs a more restrictive algorithm for implementing the artificial viscosity.

3 Why use Asph?

- Through the use of aspherical kernels, phenomena that are nonisotropic can be better represented (better resolution for a given number of Sph nodes).

  - Standard Sph: $h_s \propto \rho^{-\frac{1}{2}}$ in 2d; $h_s \propto \rho^{-\frac{1}{3}}$ in 3d.

  - Asph: $\mathbf{H}$ is allowed to adapt in arbitrary direction to nonisotropic density evolution, thereby improving resolution; so long as the radius of the anisotropy (shock) is greater than its typical thickness, Asph will have the advantage.

- We are primarily interested in simulating the evolution of structure in the early universe, where in general gravitational instability drives highly nonisotropic evolution. Asph has been tuned to solve the Zeldovich pancake problem as well as possible, as we consider this our canonical problem.

- Asph is in a sense more Lagrangian than Standard Sph, as we are able to more accurately track and maintain a consistent set of neighbors for a given Asph node. The goal of the Asph algorithm is to maintain an equal number of neighboring nodes in all directions from the node of interest.

- Spurious heating resulting from overuse of the artificial viscosity can artificially interfere with the collapse of the Sph gas and influence the development of the fine structure we wish to examine (galaxies, clusters, etc).

4 Disadvantages to Asph

- Asph is more computationally expensive than Standard Sph for a given number of nodes; this is hopefully balanced by the improved resolution.

- Asph is not guaranteed angular momentum conservation since forces are not in general radial. We believe in fact angular momentum conservation will be met so long as the shape of the smoothing kernel faithfully follows the shape of the underlying fluid element, but this remains to be demonstrated; regardless angular momentum conservation is not rigorously guaranteed as in Standard Sph.

- Our current artificial viscosity suppression algorithm mildly violates energy conservation, but this is a small effect.

5 The H tensor transformation

- The H transformation maps from real position space to normalized position space:
  - Standard Sph: $\vec{h} = \vec{r}/h_s$
  - Asph: $\vec{h} = \mathbf{H}\vec{r}$

- Shape of anisotropic smoothing volume as defined by $\mathbf{H}$ is restricted to be elliptical in 2d or ellipsoidal in 3d:
  - 2d: $\mathbf{H}$ is a symmetric 2x2 matrix
  - 3d: $\mathbf{H}$ is a symmetric 3x3 matrix

6 Evolving the H transformation

- The smoothing volume for an individual Asph node is treated analogously to a fluid element, and is therefore evolved in accordance with the changes in the local velocity field as embodied by the rate-of-strain tensor $\sigma = \partial\vec{v}/\partial\vec{r}$

- $\mathbf{H}$ is evolved through a first order treatment of the local velocity field.

$$\Delta\vec{v} = \sigma\Delta\vec{r} \tag{3}$$

Restriction to first order transformations on $\mathbf{H}$ guarantees $\mathbf{H}$ will remain symmetric and therefore elliptical (ellipsoidal).

7 Artificial Viscosity Suppression

We are attempting to develop a more restrictive criterion for the use of the artificial viscosity than the traditional use for any convergent flow. Our reasoning behind this effort is:

- The traditional criterion for the artificial viscosity switch on is overkill in the sense the the artificial viscosity will be active for gas which is not undergoing shocking.

- Overuse of the artificial viscosity can spuriously heat the system, which is potentially a serious problem for collapse simulations.

Some characteristics of our new (and experimental) criterion for the artificial viscosity:

- It distinguishes between the application of the artificial viscosity in the momentum and energy equations.

- It is parameterized in terms of the resolution over the scale of interest and the local velocities–basically a closing time criterion on a pair-by-pair basis.

- The new criterion does not explicitly rely on characteristics of Asph and could in principle be applied in Sph as well. However, it is uncertain whether the lower effective resolution of Sph would negate the usefulness of the criterion; Asph's improved resolution should give it better stopping power (larger $|\partial \vec{v}/\partial \vec{r}|$).

- Our current parameterization of the criterion has been purely empirically calibrated against the 2d Zeldovich pancake problem.

- Much more work is needed here to extend the usefulness (and testing) of the criterion.

8 Technical aspects of the code

- Our current (A)Sph code at Ohio State is maintained under a **make** system and is configurable through preprocessor flags at compile time for a variety of situations. These include:
    - 1, 2, or 3d
    - Standard Sph or Asph
    - Cosmological or Standard space dynamical equations
    - Choice of Cosmological models
    - With or Without gravity
    - Suppressed or Unsuppressed Artificial Viscosity
    - A choice of symmetrization schemes in the dynamical equations

- Individual smoothing scales (h_s) or **H** transformations are maintained for each Sph/Asph node.

- The code features an asynchronous integrator based on a second order Runge-Kutta scheme; this allows us to maintain individual times and timesteps for each Sph node. The asynchronous algorithm has been designed with the following characteristics:
    - implemented with assumption that on "local" scales (scales the size of a local smoothing kernel) times and timesteps will be similar.

- Basic algorithm:
  * Every particle is assigned a current time (t_i) and a target time $(t_i^{targ} = t_i + \Delta t_i)$.
  * The integrator looks globally for the smallest target time.
  * All particles with this smallest target time are selected and integrated (in local groups as batches, if possible).
  * The newly integrated particles are assigned their new current and target times, and the cycle repeats.

- When compiled for cosmology the code integrates all quantities in terms of a power of the expansion factor rather than time $(p = a^{\alpha})$.

- The code has been optimized for use on the Cray YMP at the Ohio SuperComputer Center–typically hits calculation speeds on the order of 100 Mflops or over (problem dependent).

- Current status in development of code:
  - Standard Sph fully implemented and tested in 1, 2, and 3d.
  - Asph fully implemented in 2d; partially in 3d.

9   Tests of Asph and the code

We have run a variety of test problems for the sake of testing both our code and the technique of Asph. In standard space for both Standard Sph and Asph we have run:

- the Riemann shocktube problem in 1, 2, and 3d

- the Sedov blastwave solution for 1d and 2d

In cosmological scenerios we have run (both Sph and Asph):

- the Zeldovich pancake solution for 1d and 2d

- the growth of a void in 1d and 2d (essentially a gravitationally driven blastwave)

- a 2d Hot Dark Matter model

We have focussed on the Zeldovich pancake as our canonical problem, as we expect this to generically represent the sort of situation we are interested in.

10   2d Shocktube Simulation

- High Density region initial conditions:
    - $\rho_i = 1, P_i = 1, v_i = 0 \ \forall x < 0$
- Low Density region initial conditions:
    - $\rho_i = 0.25, P_i = 0.1795, v_i = 0 \ \forall x > 0$
- $t_i = 0, t_f = 0.15$
- Periodic system $(x, y) \in ([-1, 1], [-1, 1])$
- Particles seeded on initial grid
- $\gamma = c_P/c_V = 1.4$

Numerical Simulation Parameters:

- $N_{baryon} = 25000$
    - High density region: $N_x = 100, N_y = 200$
    - Low density region: $N_x = 50, N_y = 100$
- $dt \in [5 \times 10^{-6}, 0.005]$
- $h_s \in [0.005, 0.05]$
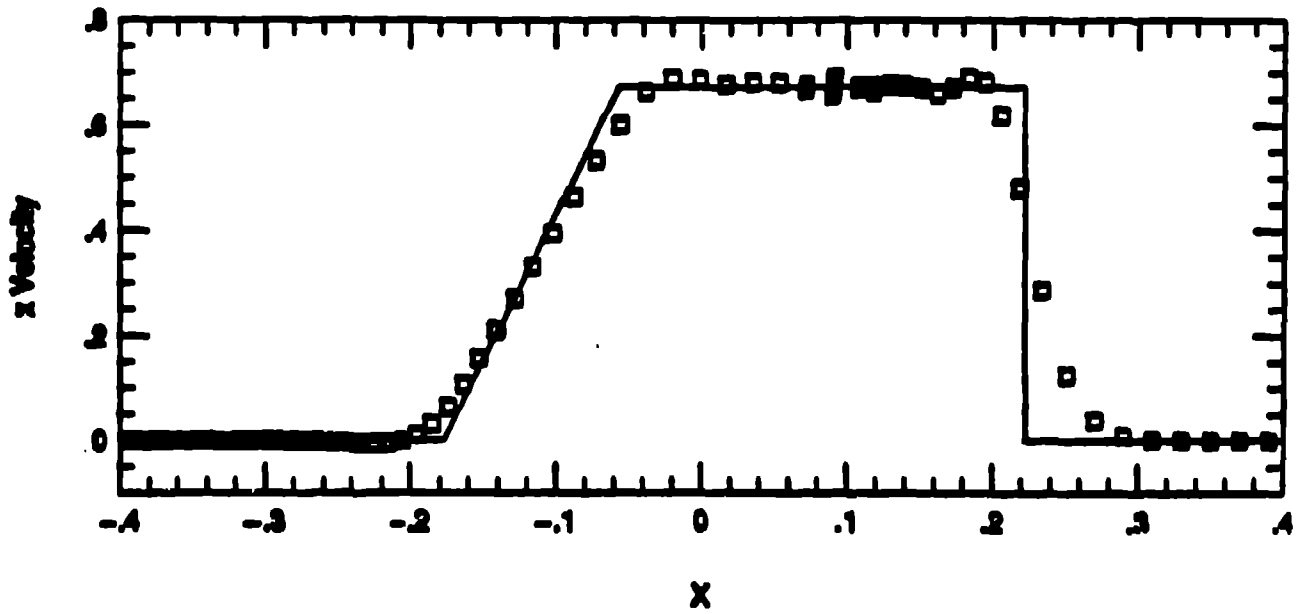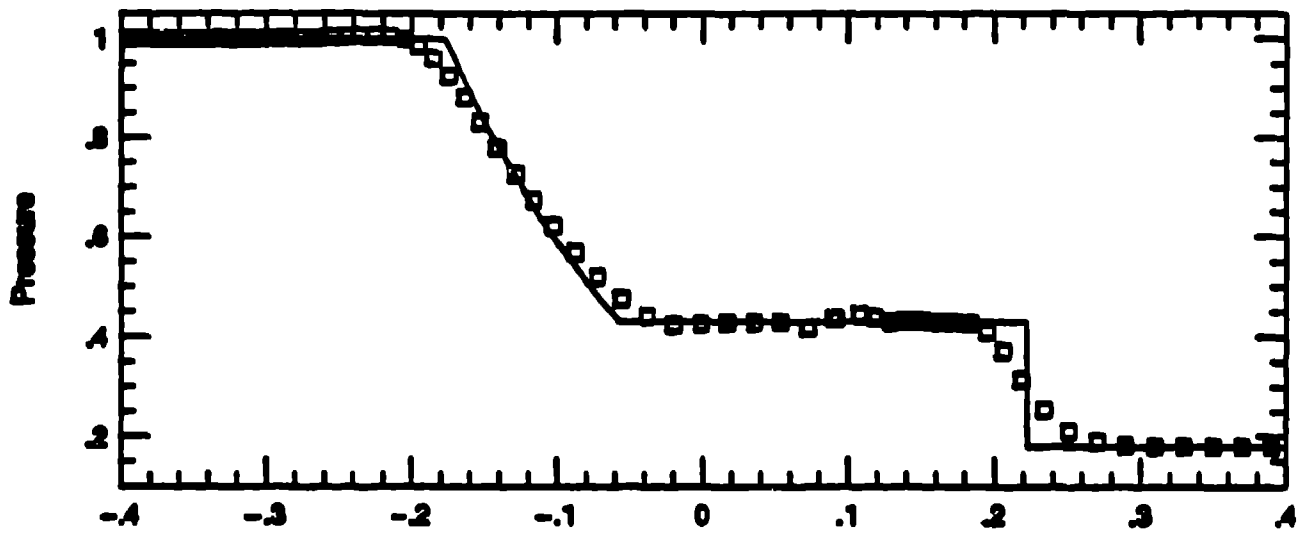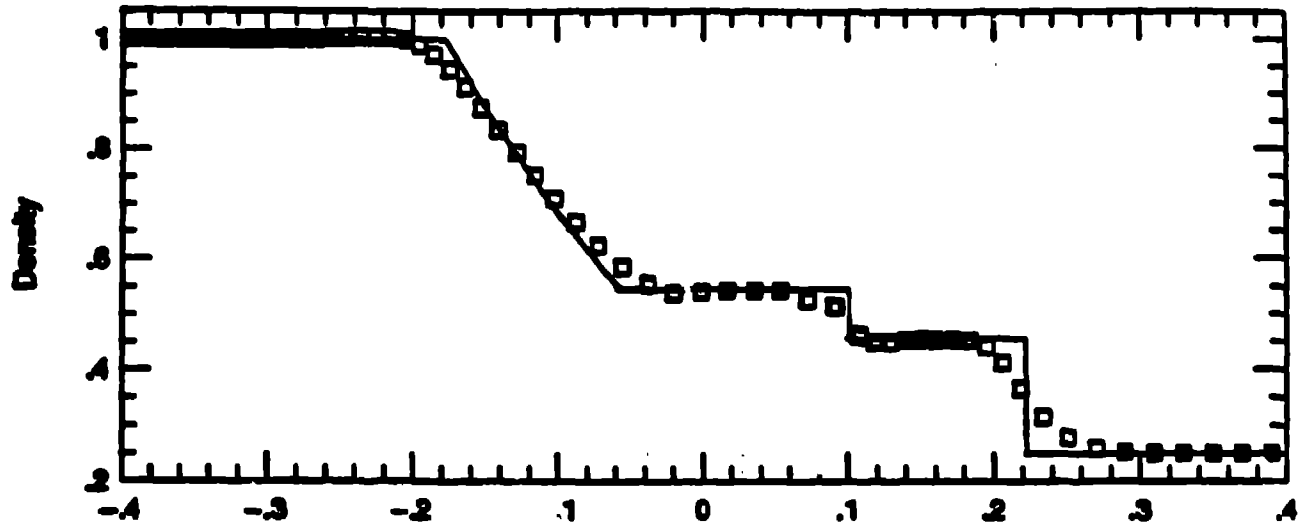
11   Single Wave Planar 2d Zeldovich Pancake Simulations

Background Cosmological and Physical Parameters:

- Einstein-DeSitter cosmology ($\Omega = 1$, $\Lambda = 0$)

- $\Omega_{baryon} = \Omega_{dm} = 0.5$

- $H_0 = 50$ km/sec/Mpc

- $a_{initial} = 1$, $a_{crunch} = 4$, $a_{final} = 5$, $a_0 = 1000$

- $z_{initial} = 999$, $z_{crunch} = 249$, $z_{final} = 199$

- $l_{box} = 10$Mpc @ $a = 1$ $\Rightarrow$ $l_{box} = 50$ Mpc @ $a = 5$

- $k_x = 0$, $k_y = 1$

- $T_i = 3000K$ $\Rightarrow$ $\epsilon_i = 1.49 \times 10^{-13}$

- $\gamma = c_P/c_V = 5/3$

- Pure Hydrogen gas ($\mu = 1$)

- No Radiative Cooling implemented

Numerical Simulation Parameters:

- $N_{baryon} = N_{dm} = 4096$

- $\alpha = 1$, ($p = a^\alpha$)

- $dp \in [10^{-4}, 0.05]$

- $h_s \in [10^{-5}, 0.1]$

- For Asph smoothing kernel axis ratios limited to $h_2/h_1 > 0.01$

2d Single Wavelength Zeldovich pancake: Baryon positions @ a=5.0 (a$_{crunch}$=4.0)
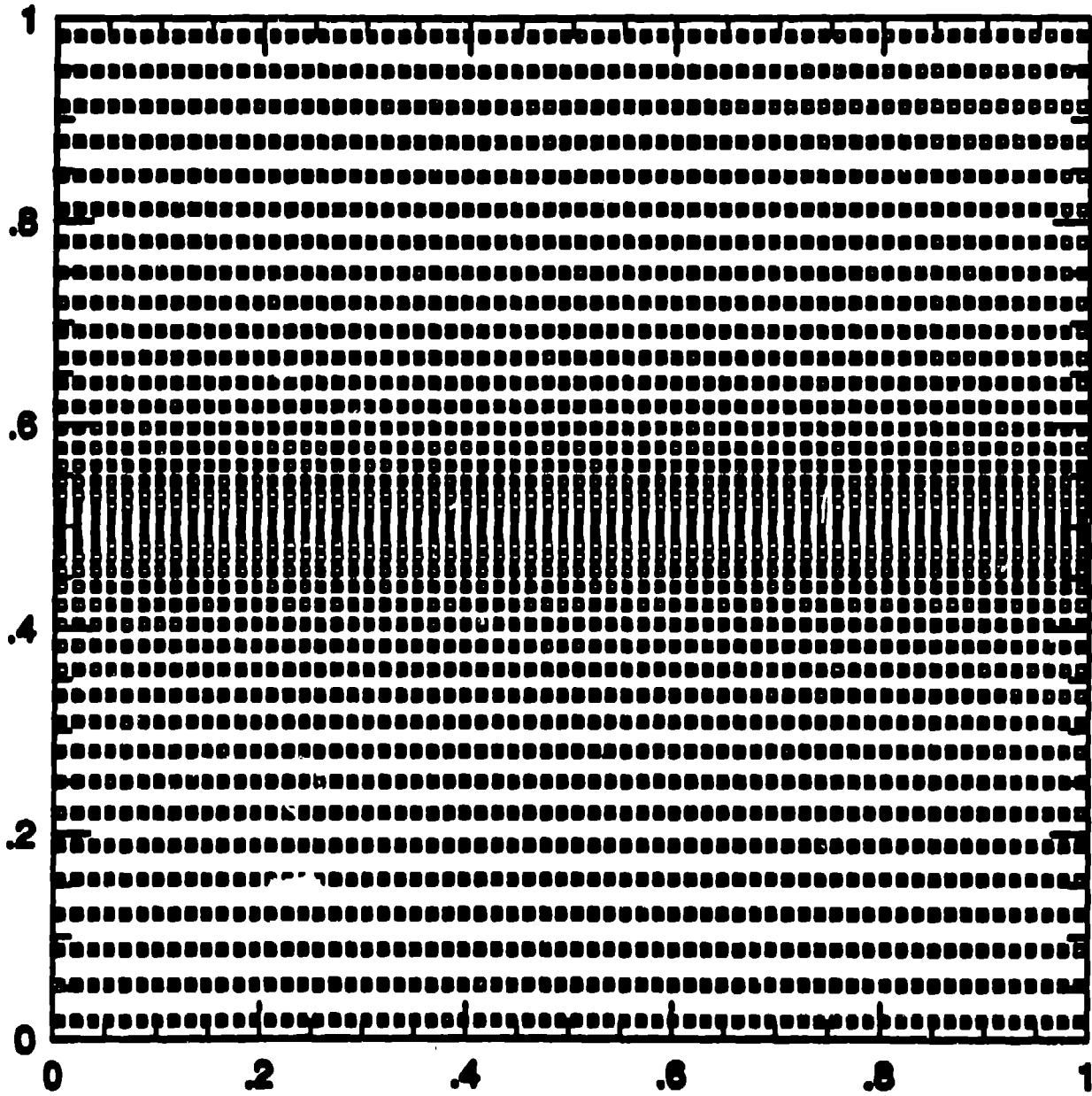
2d pancake @ a=5: Standard Sph

2d pancake @ a=5: Asph with Suppression
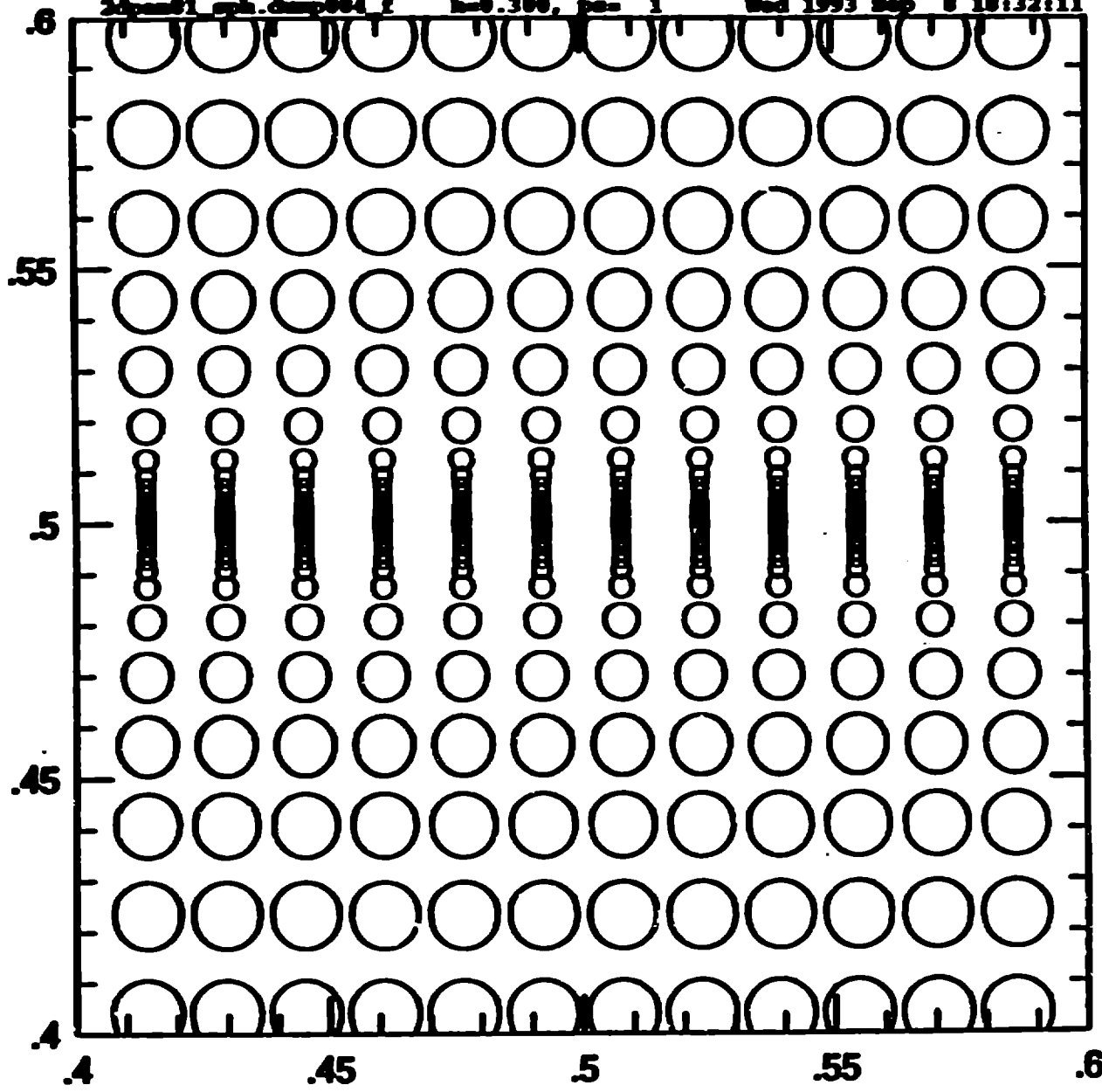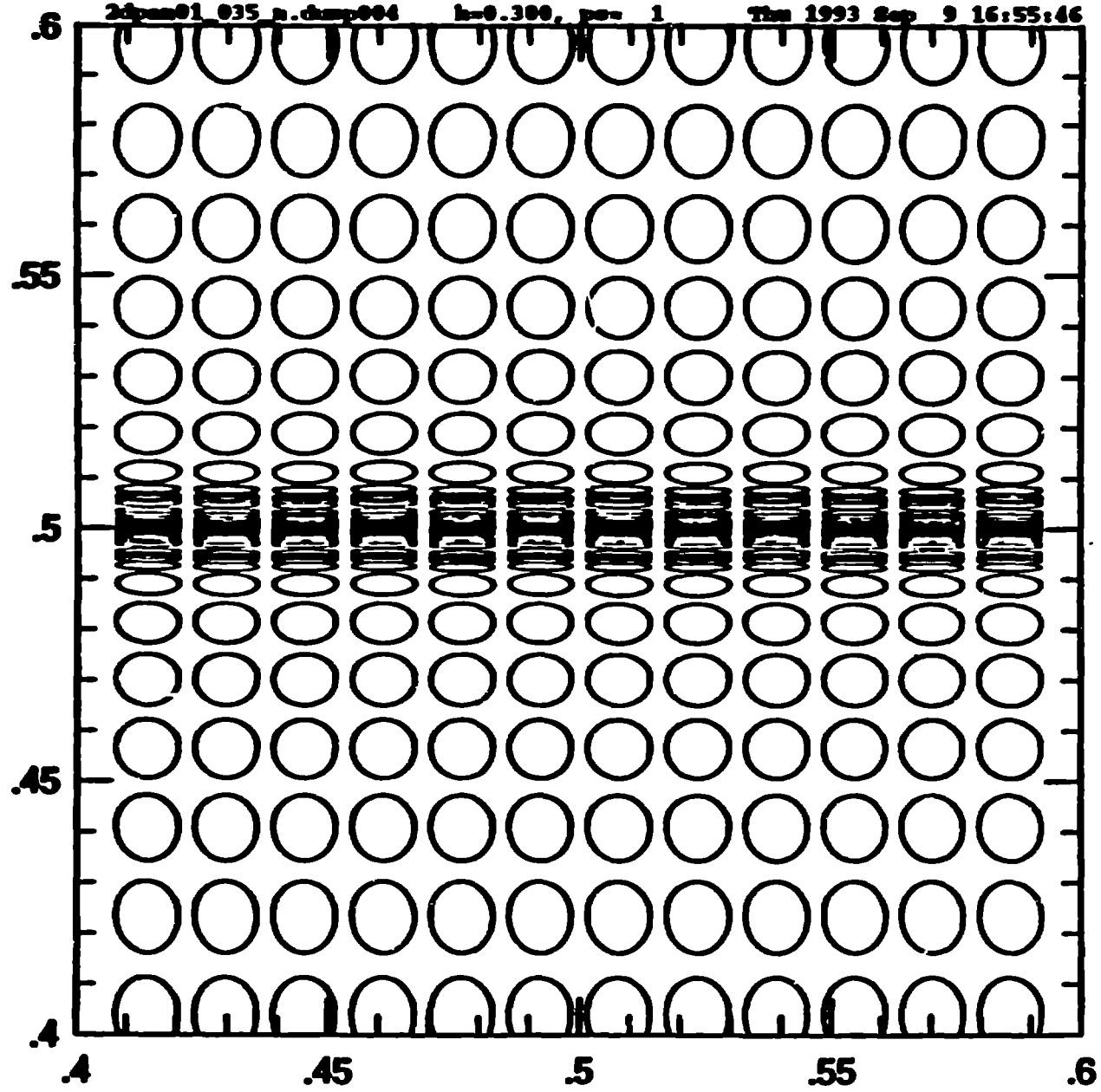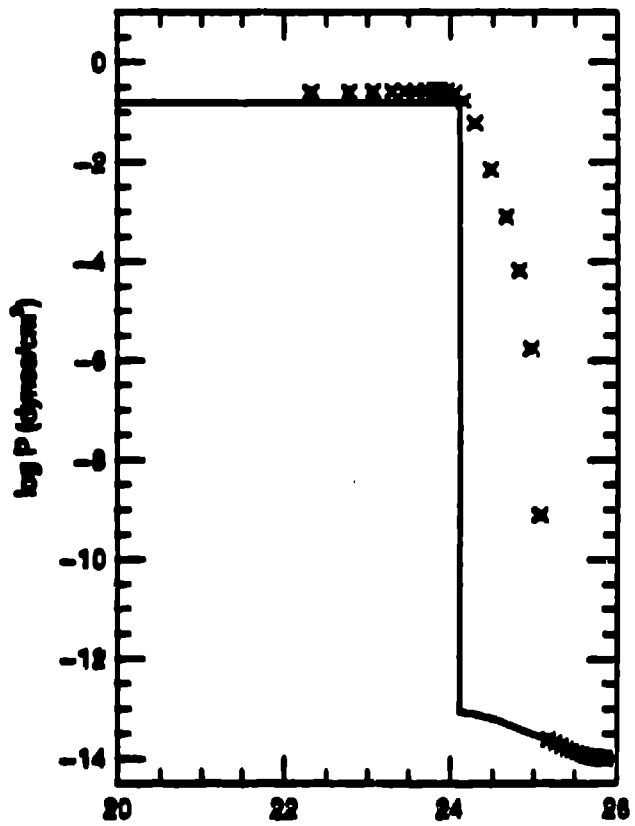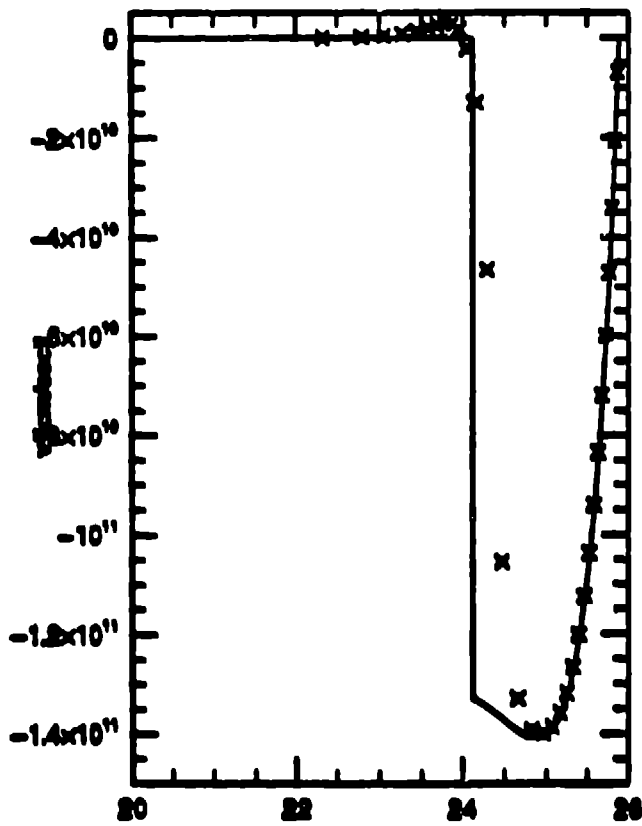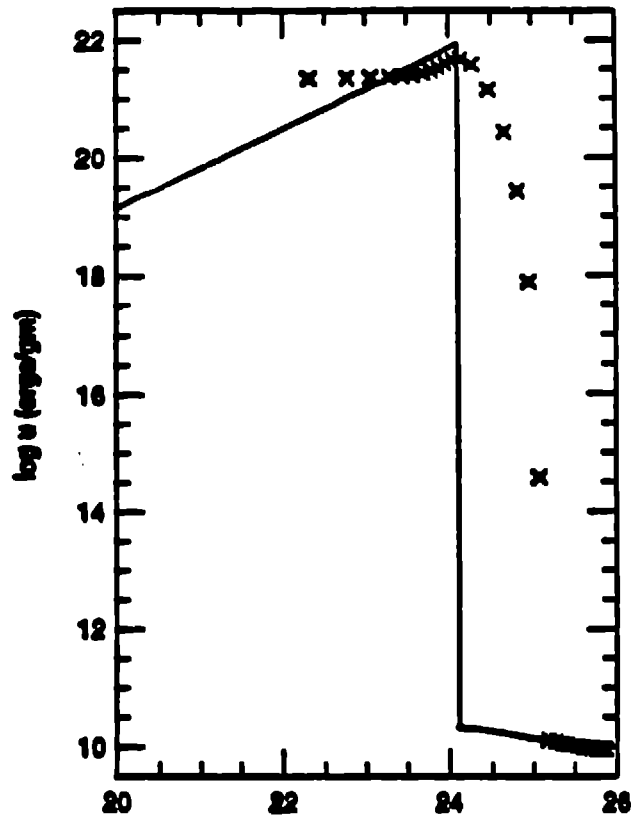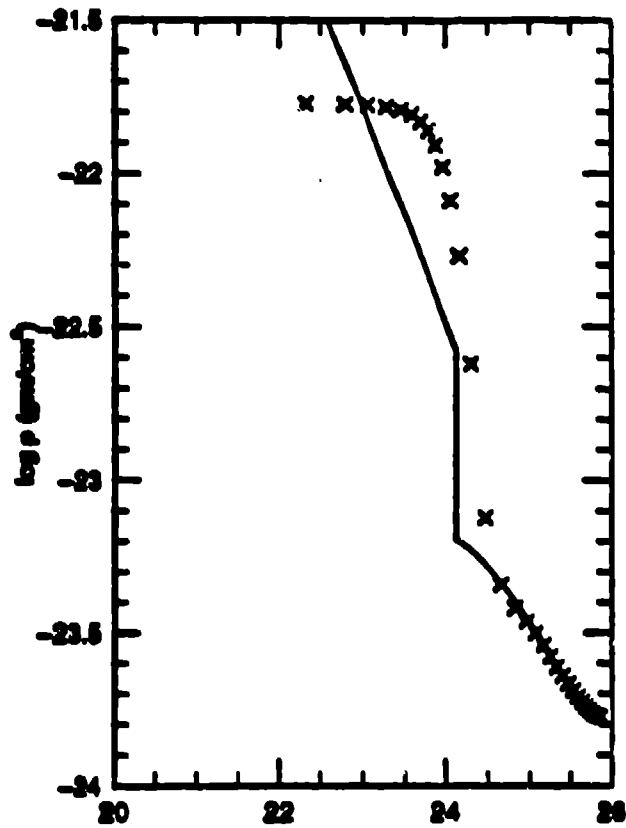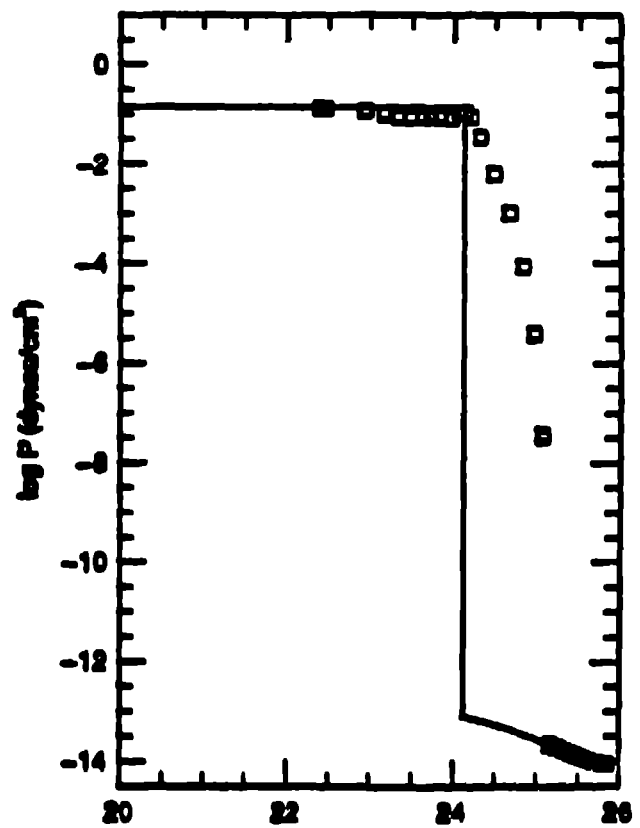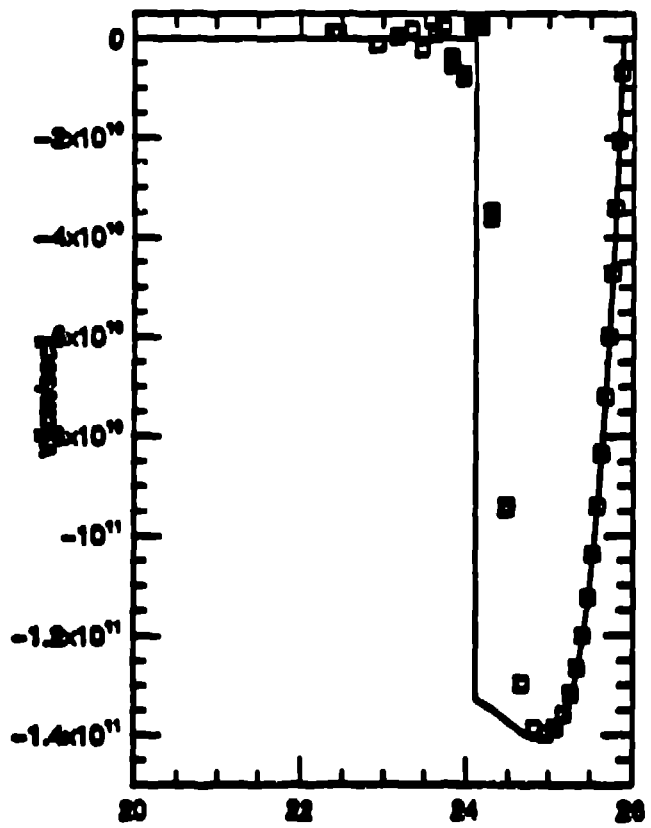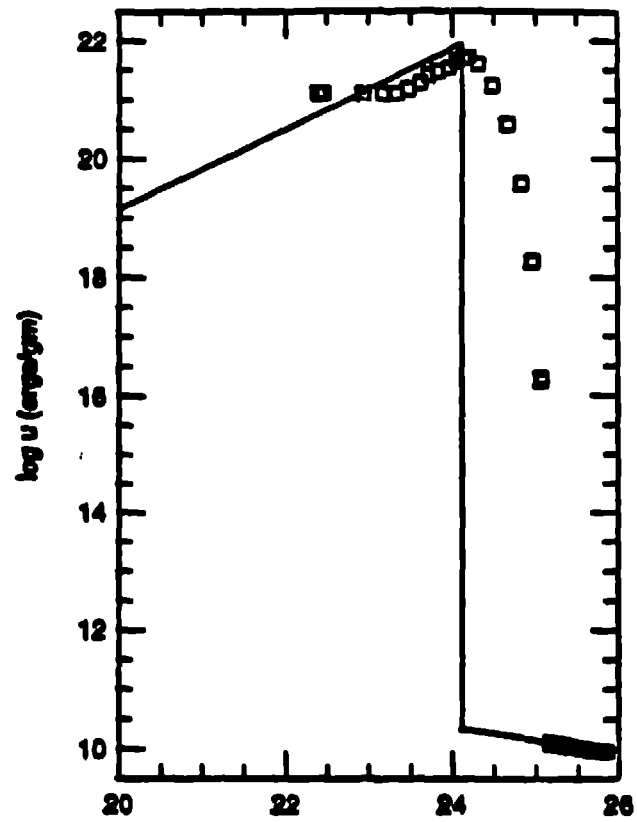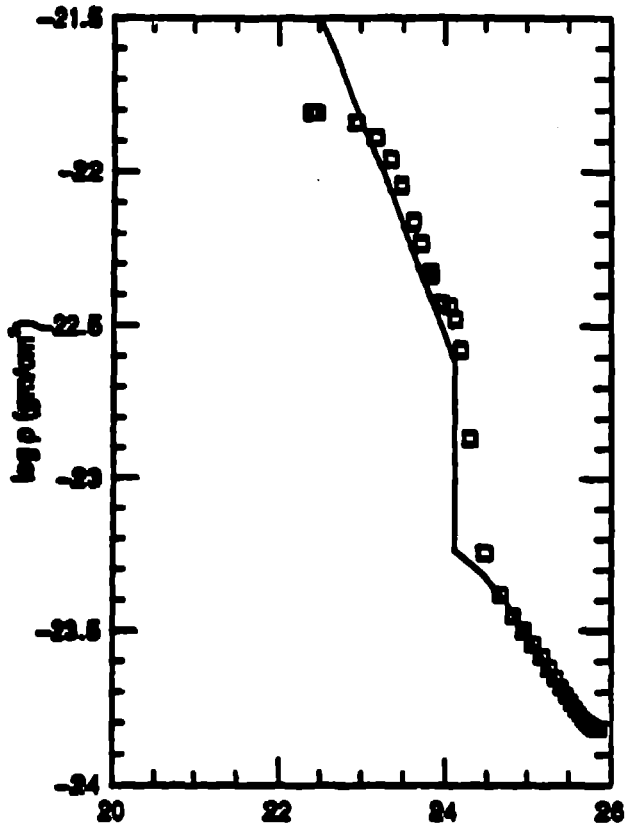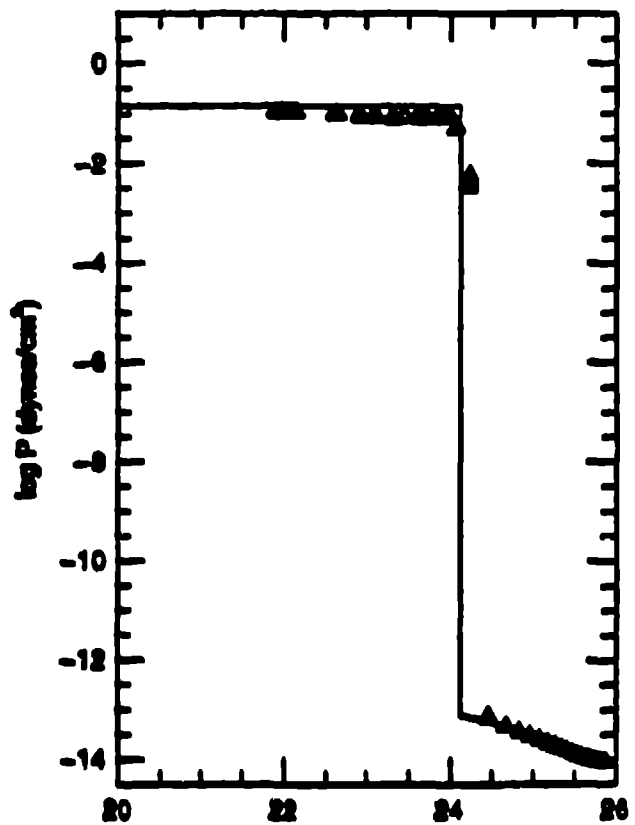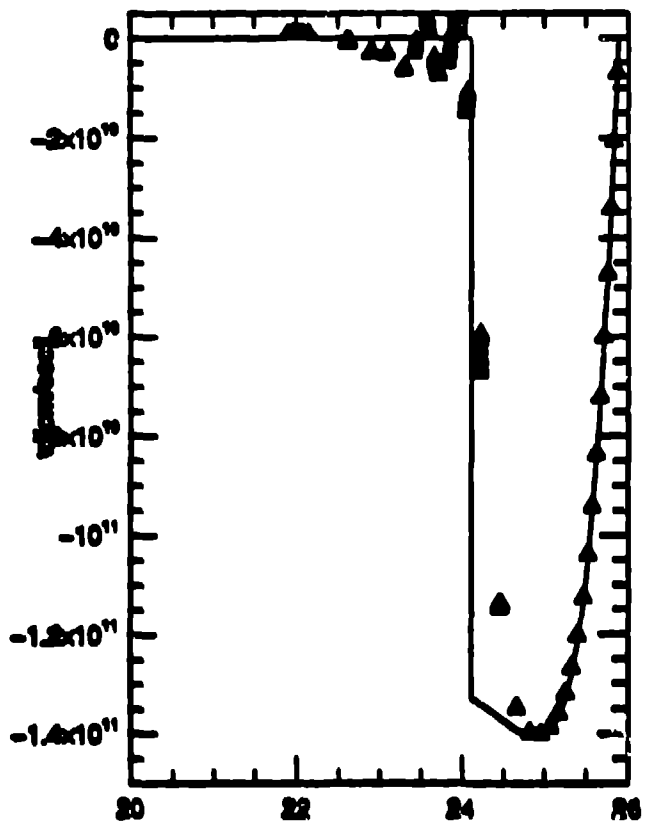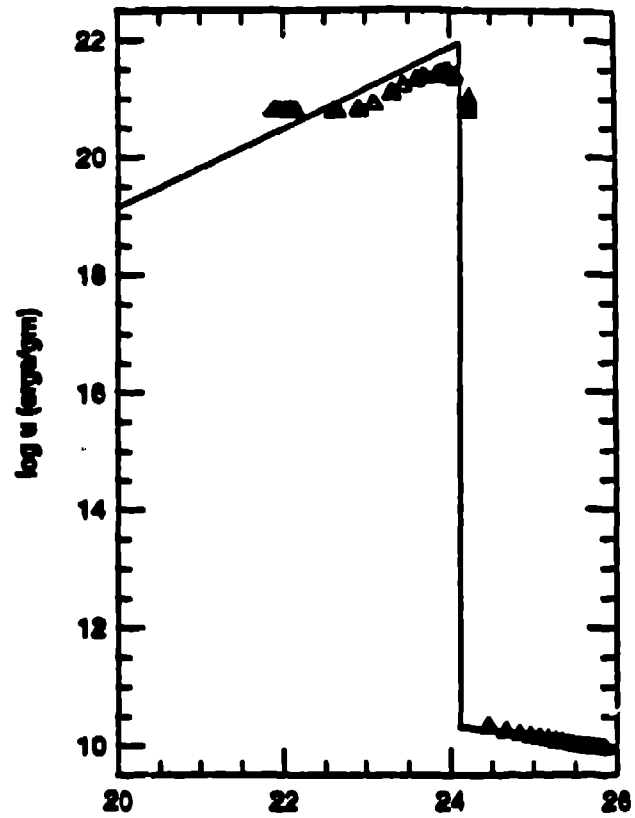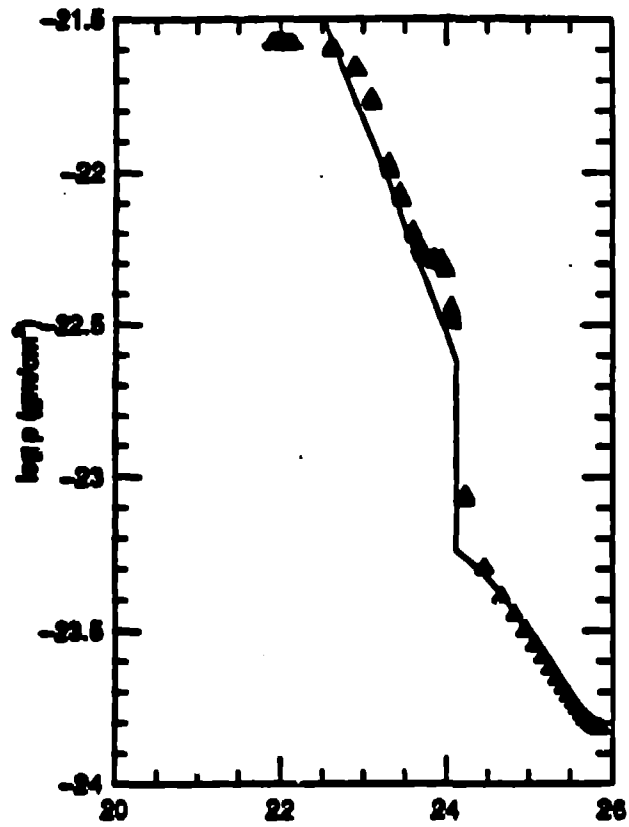
$$\log(x - x_{crunch}) \ (cm)$$

$$\log(x - x_{crunch}) \ (cm)$$

12 Tilted-Shifted Planar 2d Zeldovich Pancake Simulations

Background Cosmological and Physical Parameters:

- Einstein-DeSitter cosmology ($\Omega = 1$, $\Lambda = 0$)

- $\Omega_{baryon} = 0.1$ $\Omega_{dm} = 0.9$

- $H_0 = 50$ km/sec/Mpc

- $a_{initial} = 1$, $a_{crunch} = 4$, $a_{final} = 5$, $a_0 = 1000$

- $z_{initial} = 999$, $z_{crunch} = 249$, $z_{final} = 199$

- $l_{box} = 10$ Mpc @ $a = 1$ $\Rightarrow$ $l_{box} = 50$ Mpc @ $a = 5$

- $k_x = 2$, $k_y = 1$

- $T_i = 3000K$ $\Rightarrow$ $\epsilon_i = 1.49 \times 10^{-13}$

- $\gamma = c_P/c_V = 5/3$

- Pure Hydrogen gas ($\mu = 1$)

- No Radiative Cooling implemented

Numerical Simulation Parameters:

- $N_{baryon} = N_{dm} = 4096$

- $\alpha = 1$, ($p = a^\alpha$)

- $dp \in [10^{-4}, 0.05]$

- $h_s \in [10^{-5}, 0.1]$

- For Asph smoothing kernel axis ratios limited to $h_2/h_1 > 0.01$

2d tilted-shifted pancake: Baryon particle positions @ a=5 (a_{crunch}=4)
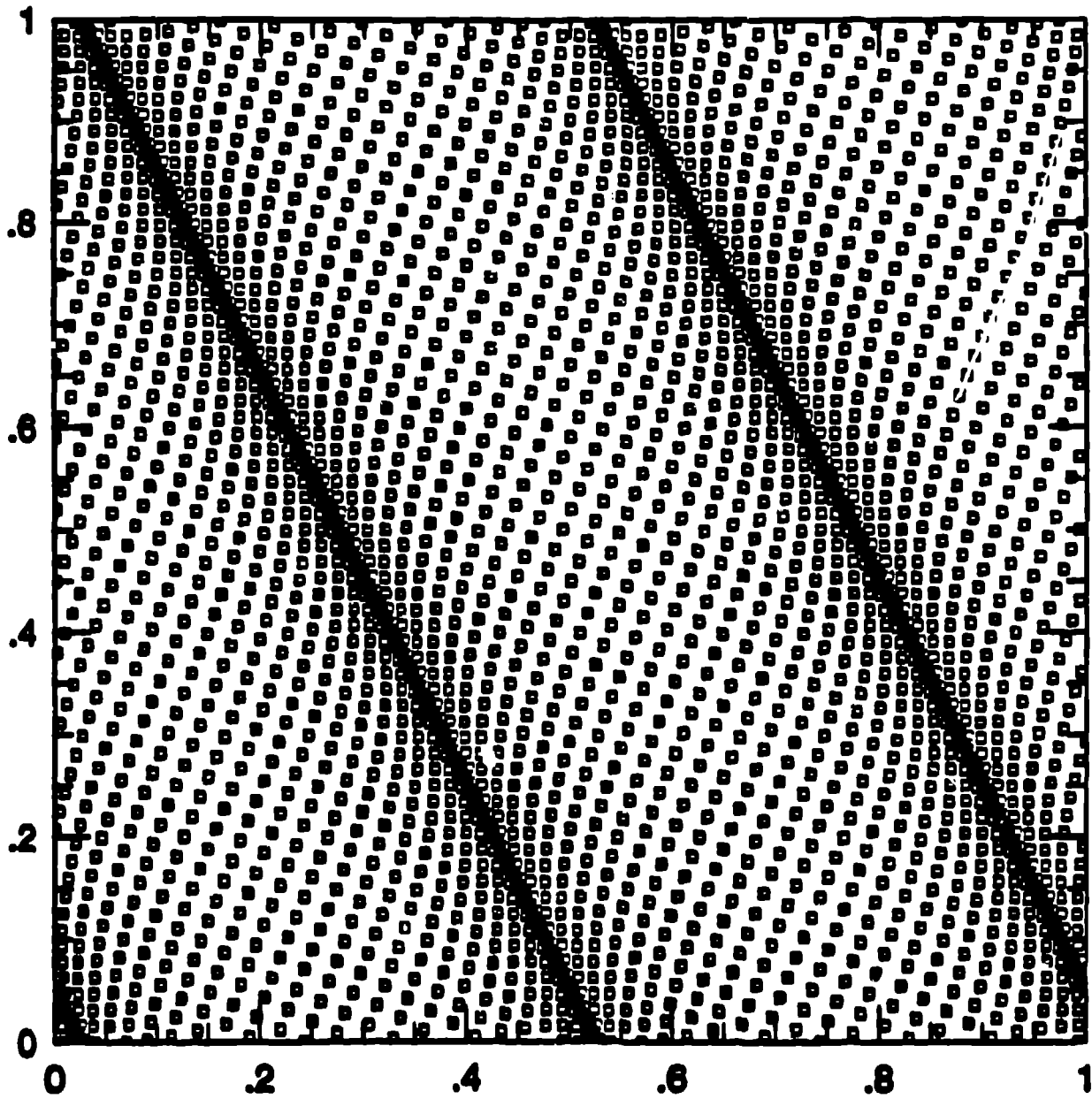
2d tilted-shifted pancake @ a=5: Standard Sph

2d tilted–shifted pancake @ a=5: Asph with suppression

2d tilted-shifted pancake @ a=5 (a_{crunch}=4). Standard SPH
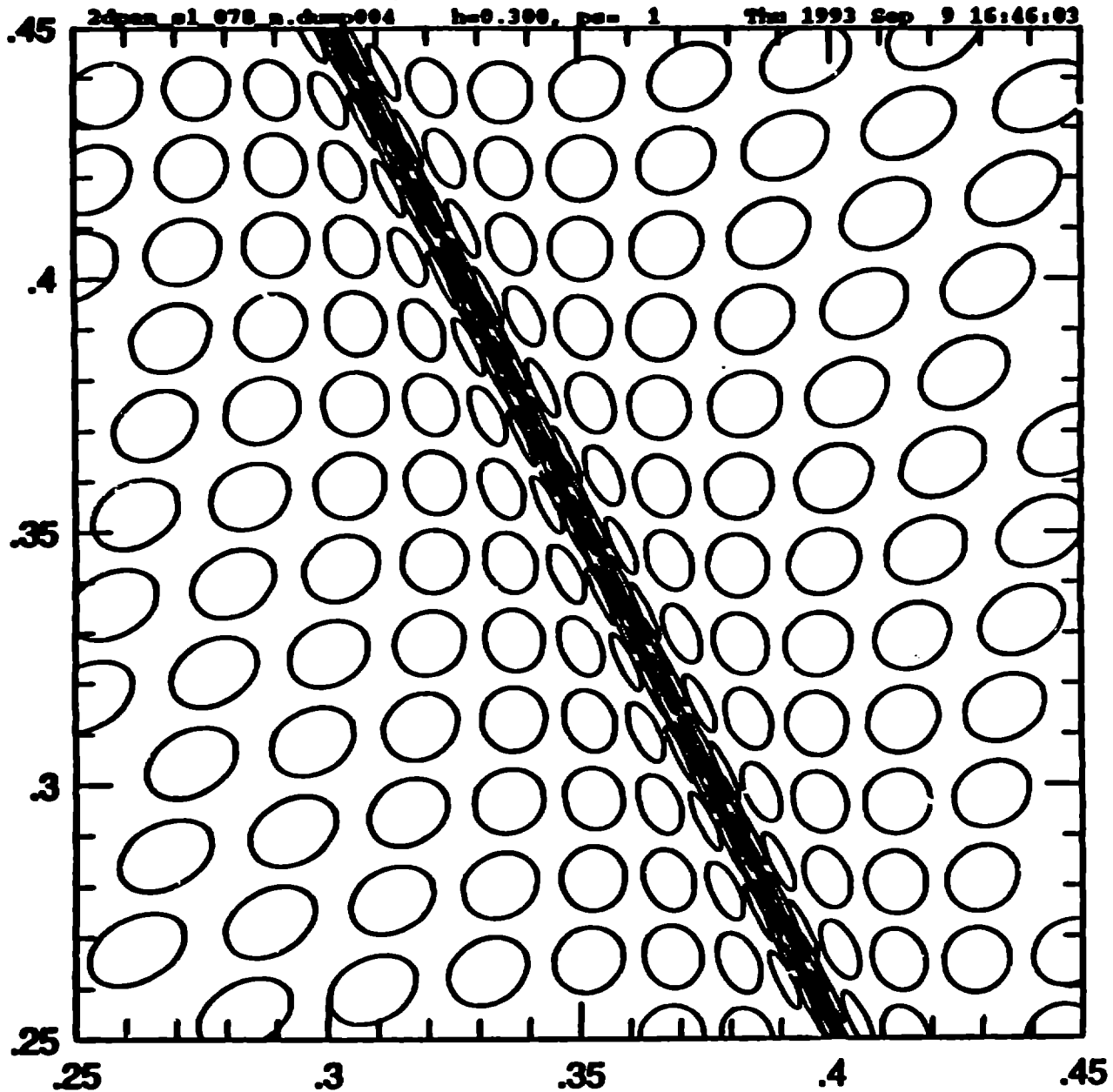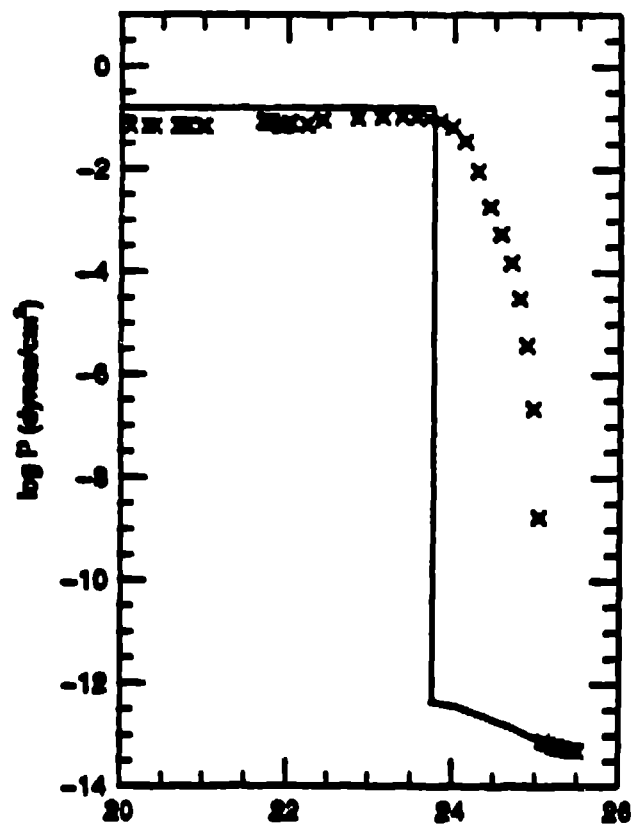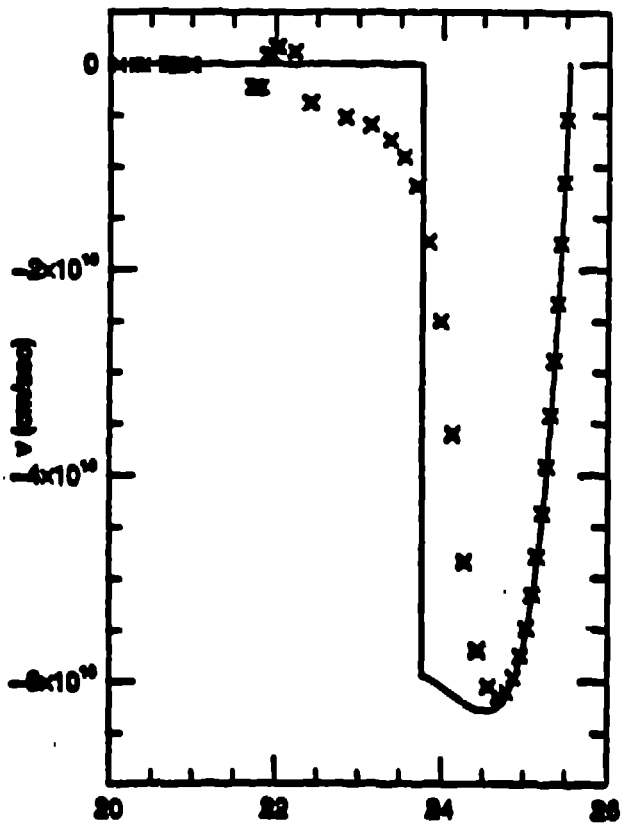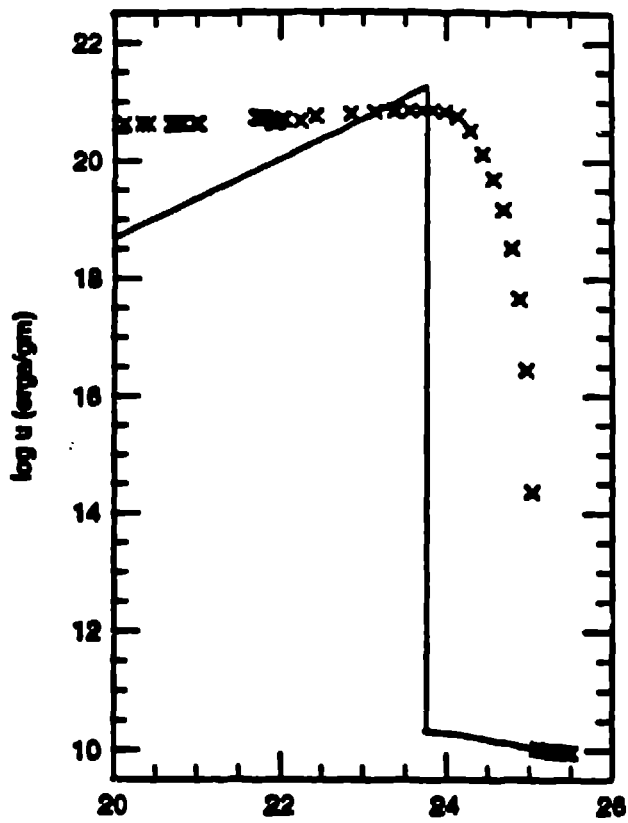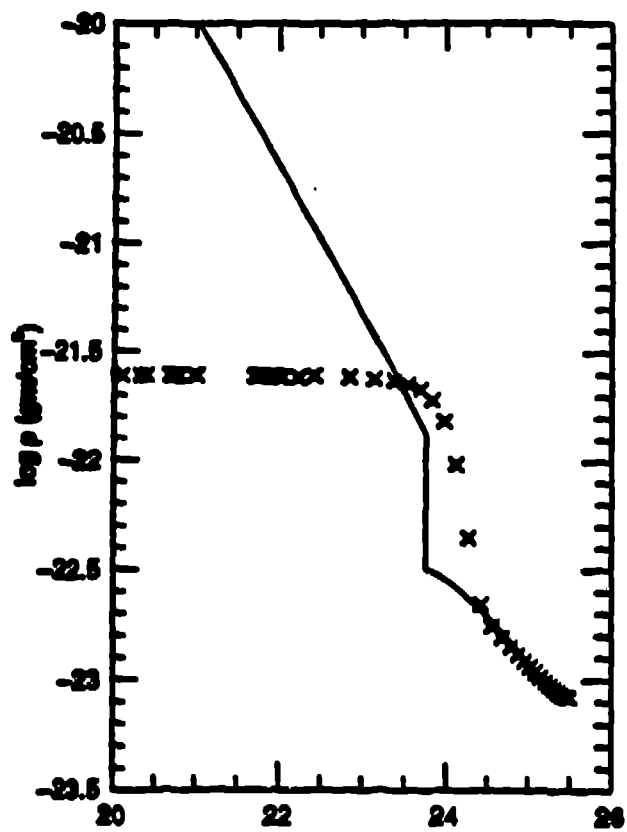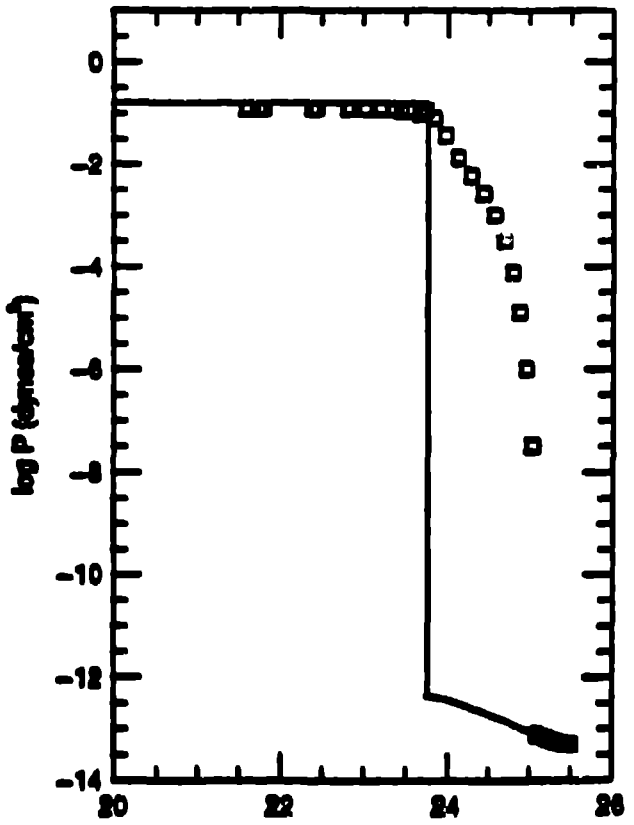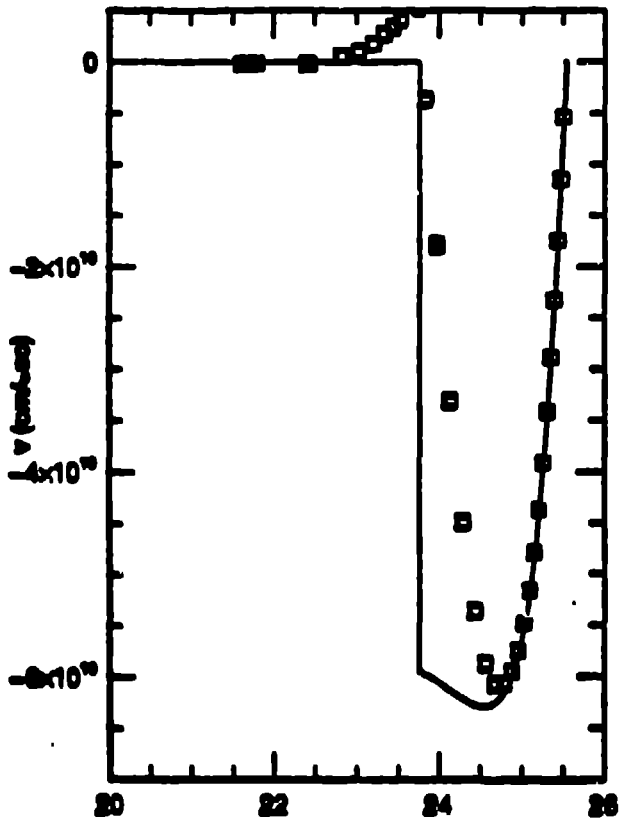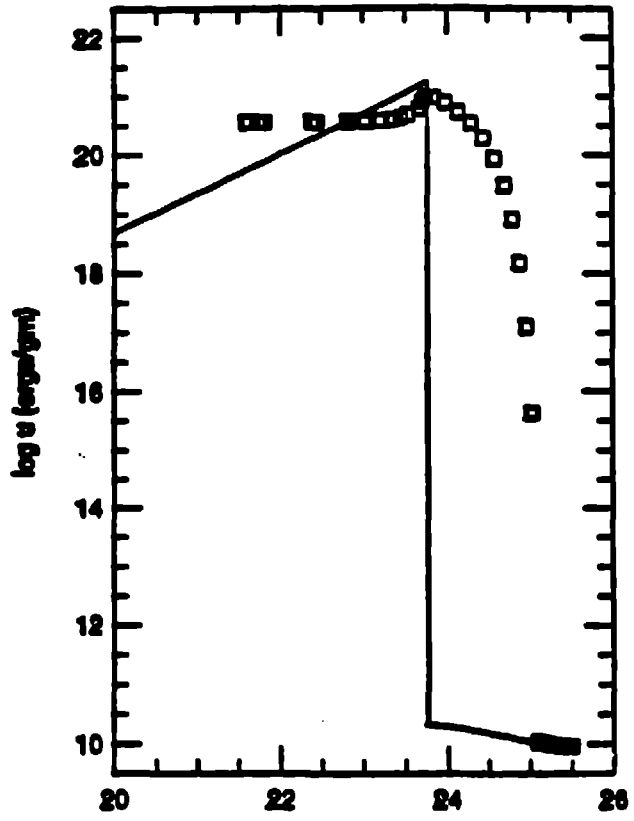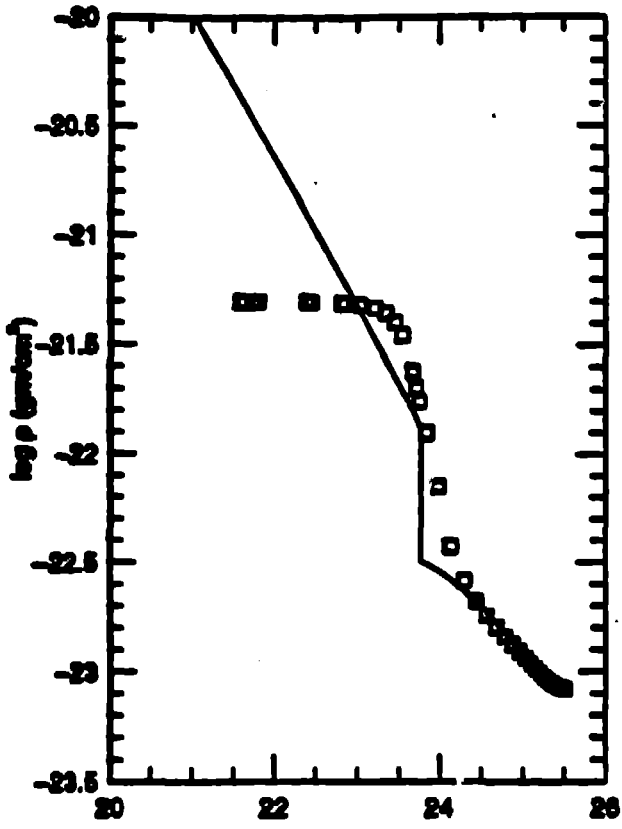
2d tilted–shifted pancake @ a=5 (a_crunch=4): Asph with Art Visc Suppression

$$\log(x - x_{crunch}) \ (cm)$$
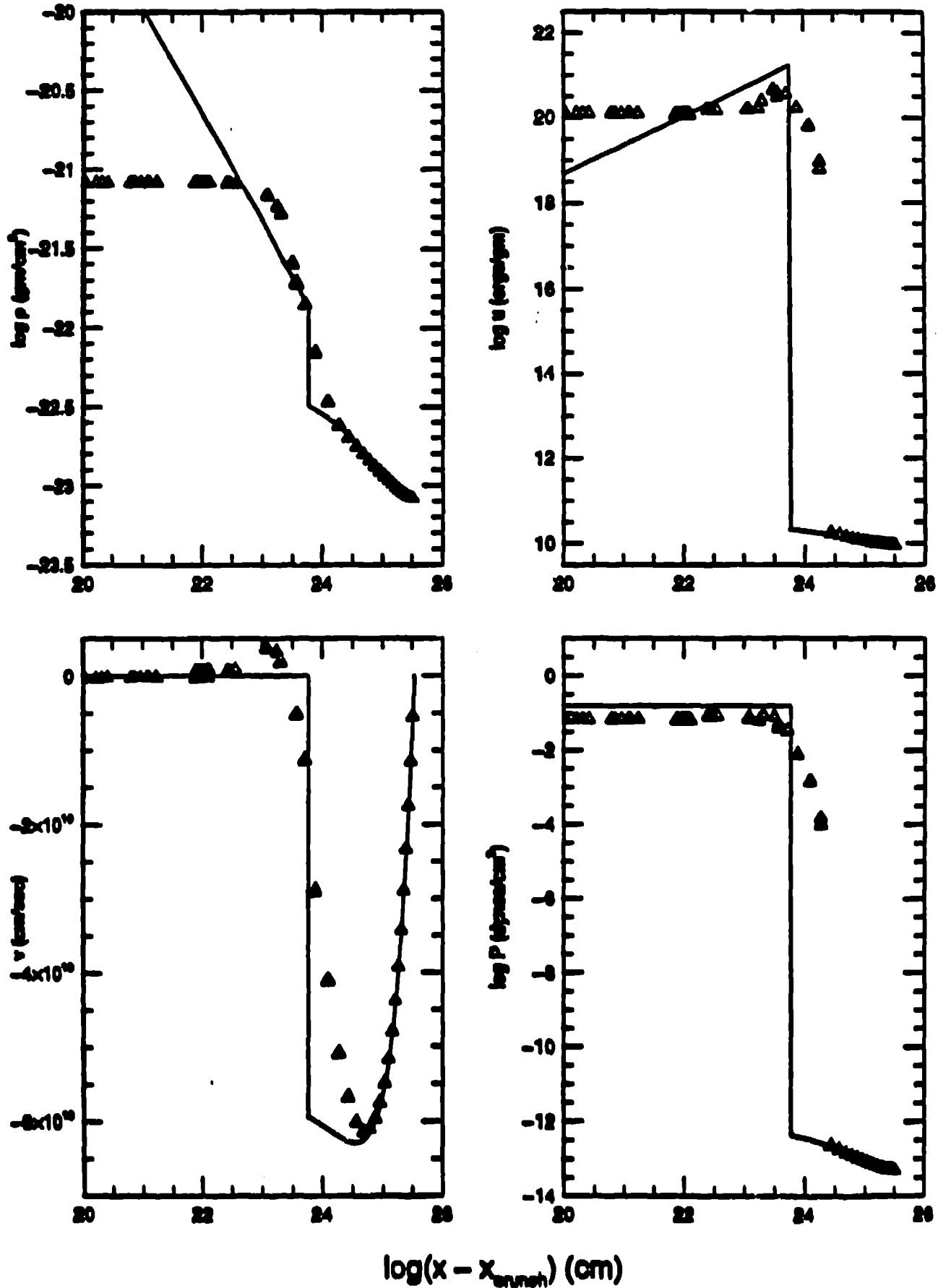
13 2d Hot Dark Matter Simulations

Background Cosmological and Physical Parameters:

- Einstein-DeSitter cosmology ($\Omega = 1$, $\Lambda = 0$)
- $\Omega_{baryon} = 0.1$ $\Omega_{dm} = 0.9$
- $H_0 = 50$ km/sec/Mpc
- $a_{initial} = 1$, $a_{crunch} = 101.7$, $a_{final} = 31$ $a_0 = 31$
- $z_{initial} = 30$, $z_{crunch} = -0.7$, $z_{final} = 0$
- $l_{box} = 6.45$ Mpc @ $a = 1$ $\Rightarrow$ $l_{box} = 200$ Mpc @ $a = 31$
- $k_{wave} \in [1, 64]$
- 4 fundamental waves across periodic box
- HDM density power spectrum slope $= -4$ with extra factor of k to mimic 3d power spectrum
- Particles displaced from regular grid with waves of random amplitude and phase.
- $T_i = 2.88K$ $\Rightarrow$ $\epsilon_i = 1.156 \times 10^{-11}$
- $\gamma = c_P/c_V = 5/3$
- Pure Hydrogen gas ($\mu = 1$)
- No Radiative Cooling implemented

Numerical Simulation Parameters:

- $N_{baryon} = N_{dm} = 16384$
- $\alpha = 1$, $(p = a^\alpha)$
- $dp \in [10^{-4}, 0.05]$, $h_s \in [10^{-5}, 0.1]$, $h_2/h_1 > 0.01$

Baryon positions for 2d Suppressed Asph HDM model @ a=31.0 (z=0.0)
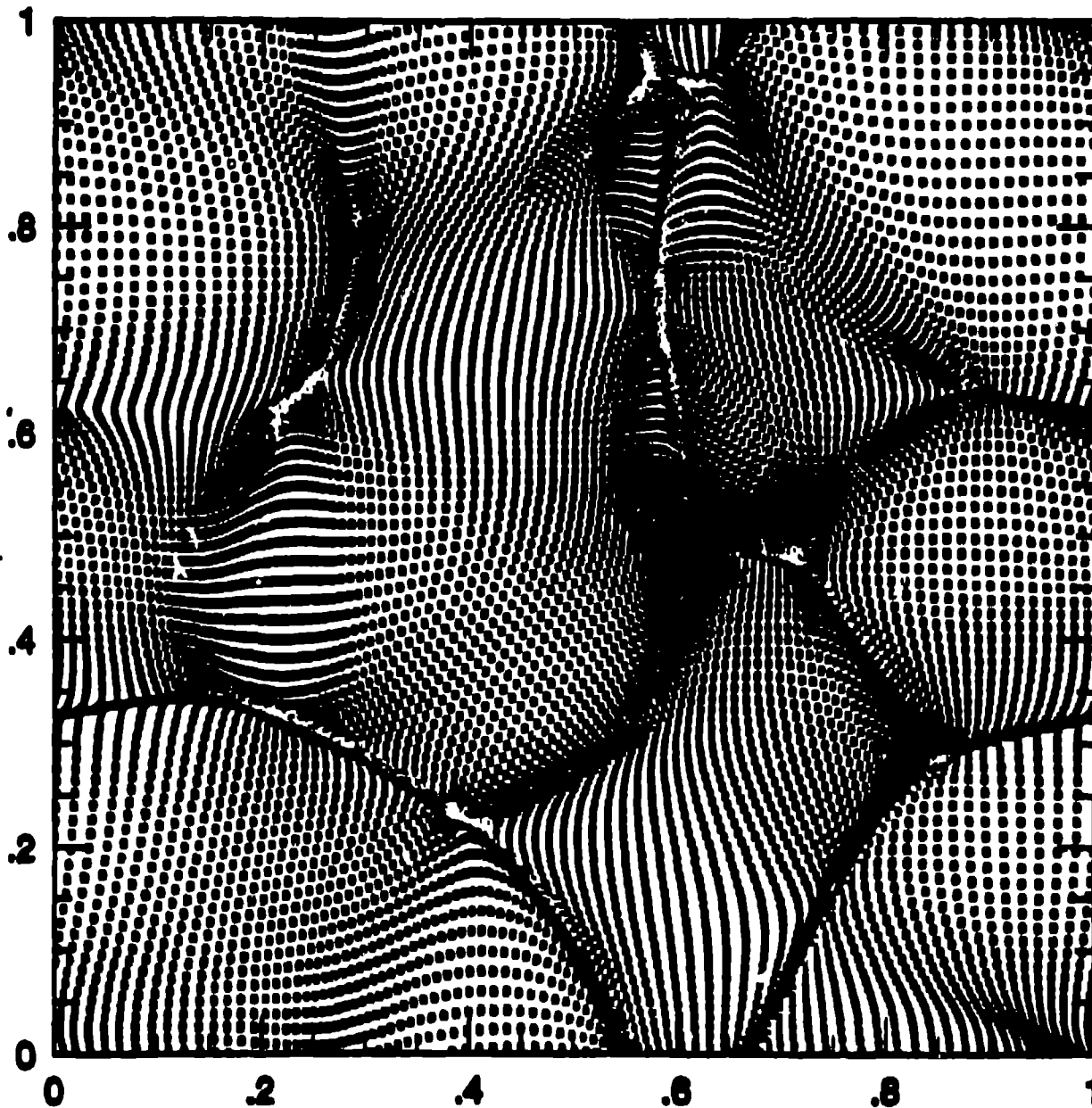
Dark Matter positions for 2d Suppressed Asph HDM model @ a=31.0 (z=0.0)

2d Standard Sph HDM model @ a=25.0 (z=0.24)
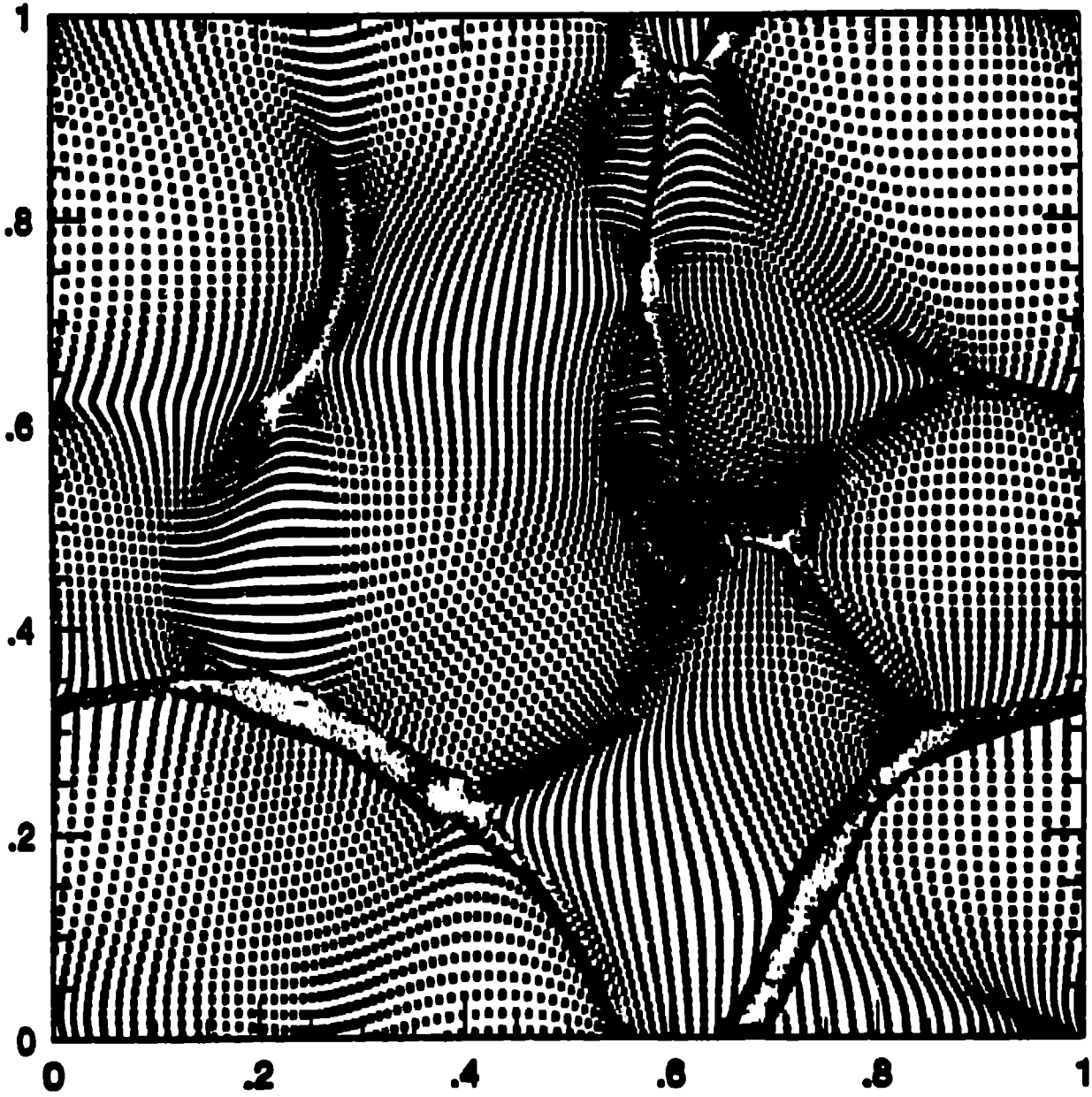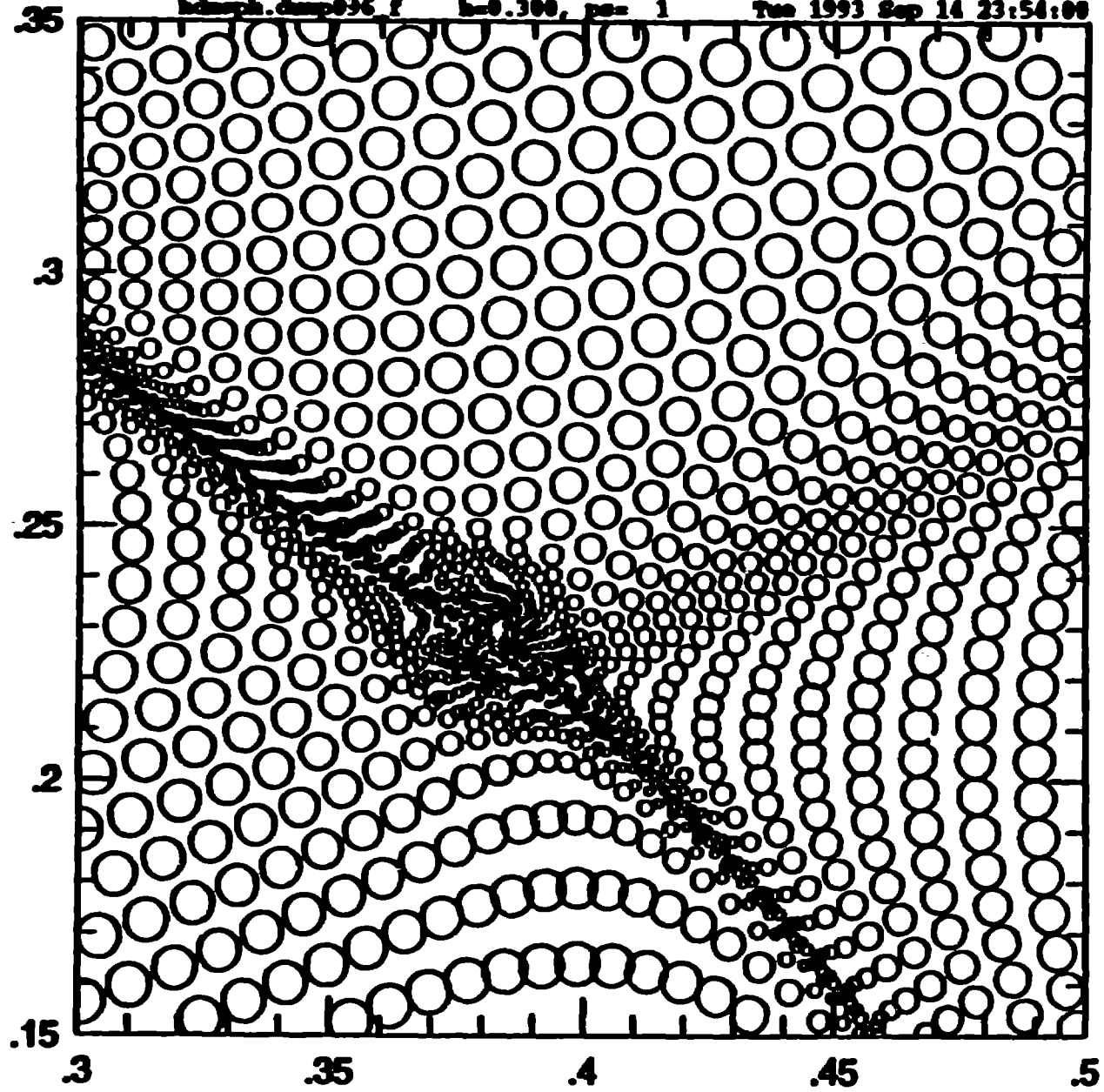
2d Unsuppressed Asph HDM model @ a=25.0 (z=0.24)

hdmaph2_um.dmp096_f   h=0.300, po= 1   Tue 1993 Sep 14 23:56:09

2d Suppressed Asph HDM model @ a=25.0 (z=0.24)
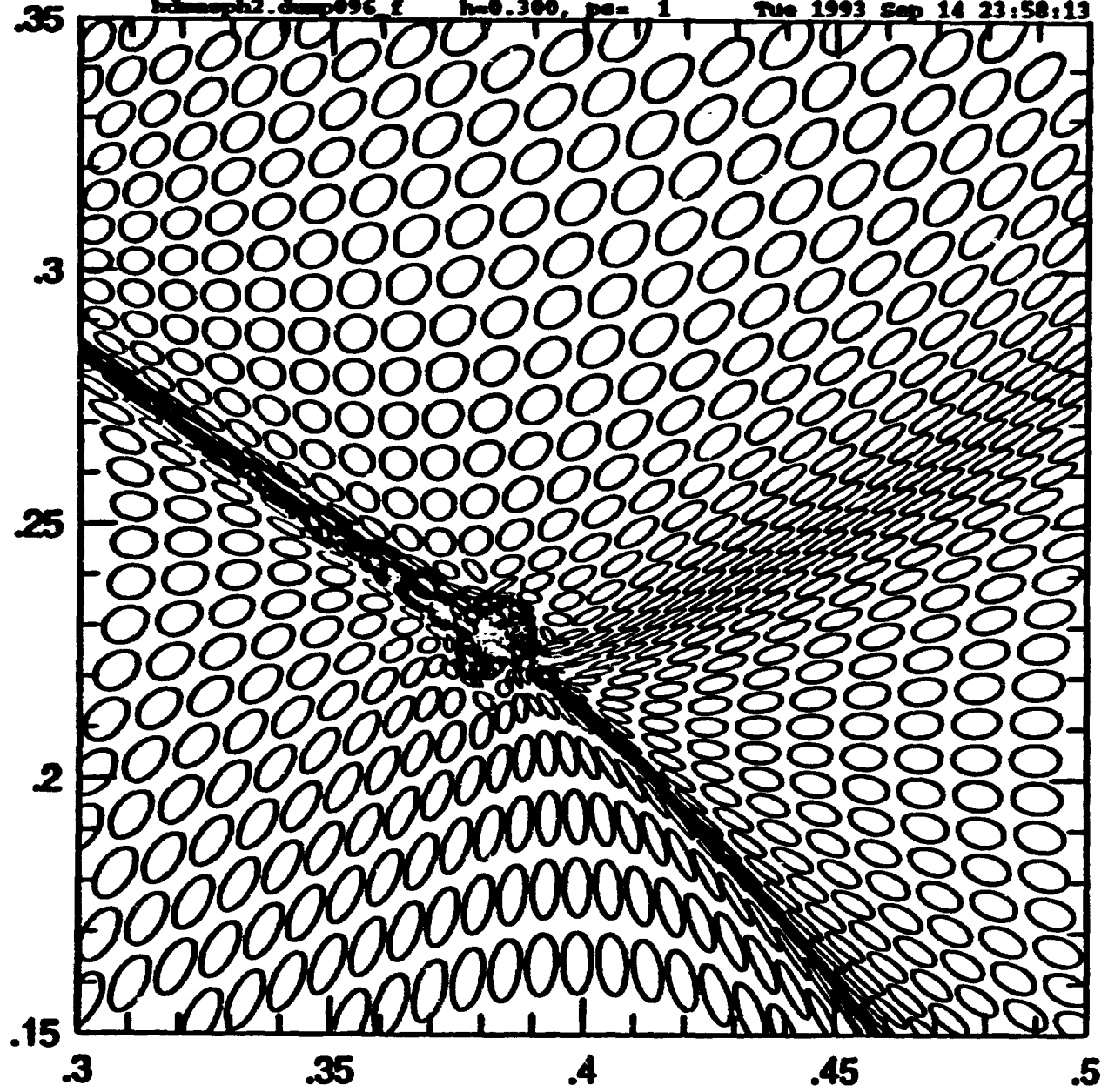
2d Standard Sph HDM model @ a=31.0 (z=0.0)

hdmsph.dump120_f   b=0.300, pa= 1   Fri 1993 Sep 10 14:03:08
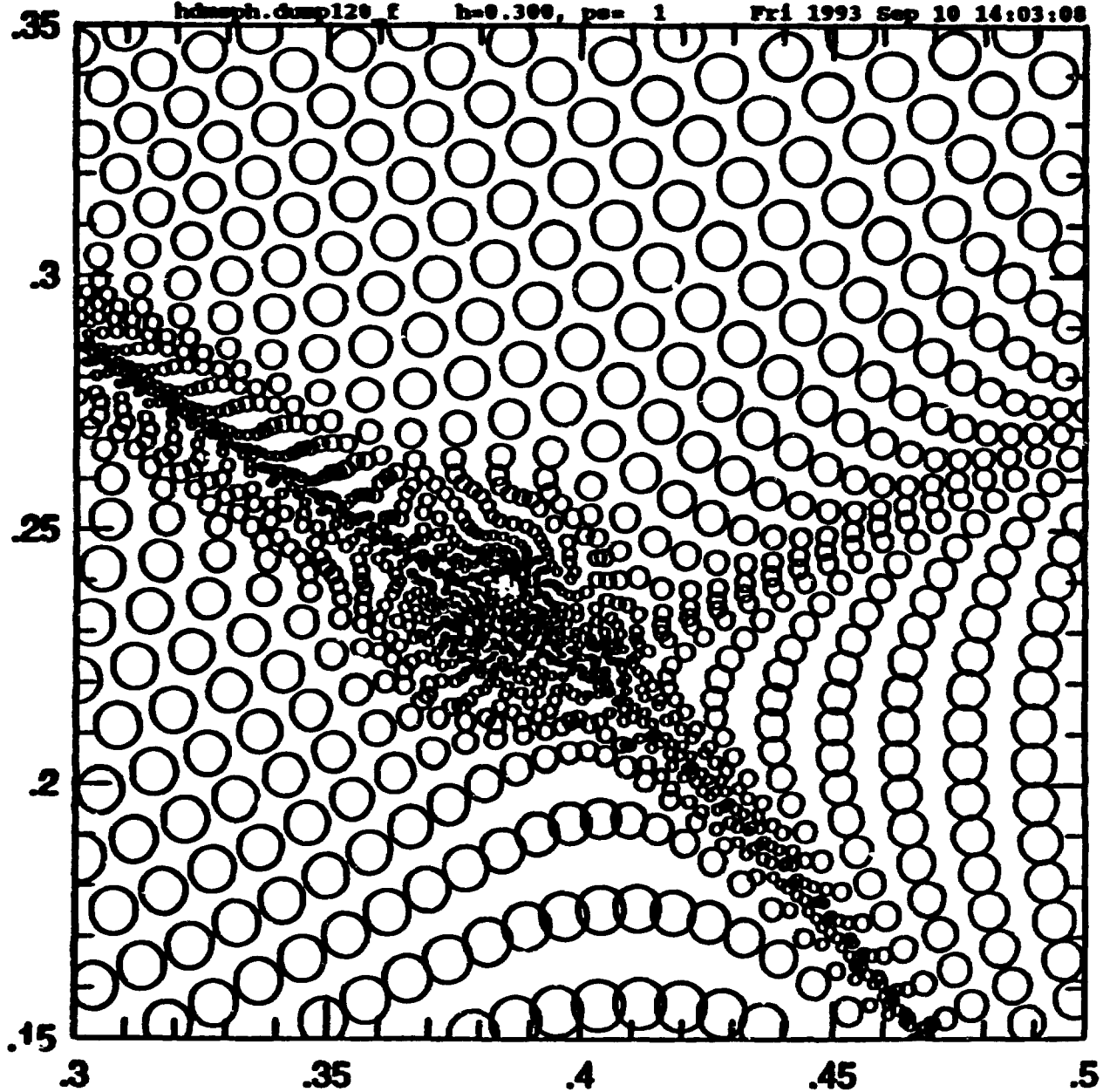
2d Unsuppressed Asph HDM model @ a=31.0 (z=0.0)

2d Suppressed Asph HDM model @ a=31.0 (z=0.0)

hdmasph2.dump120   b=0.300, ps= 1   Fri 1993 Sep 10 13:56:36
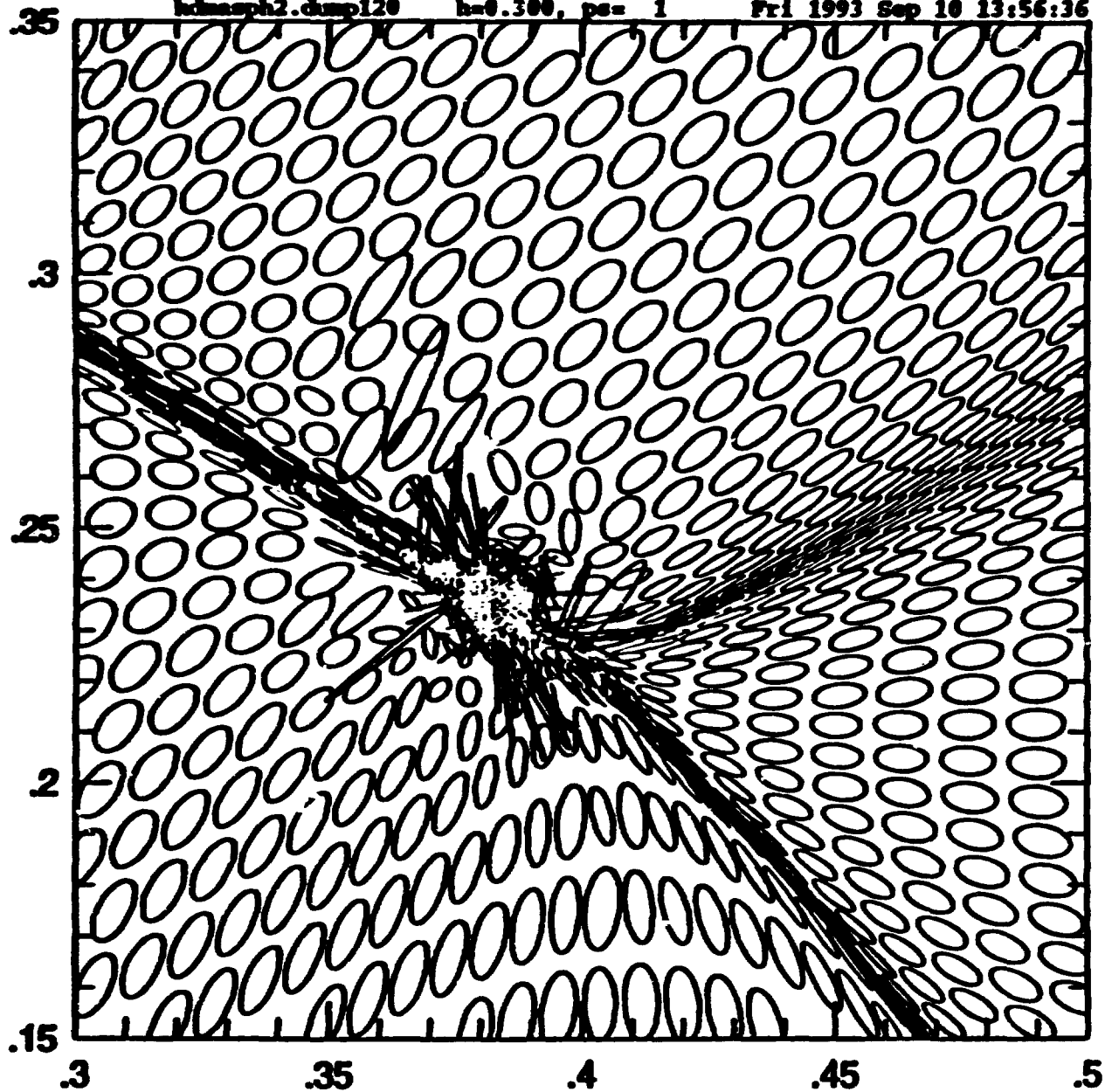
2d HDM Temperature Isocontours for Standard Sph @ a=25
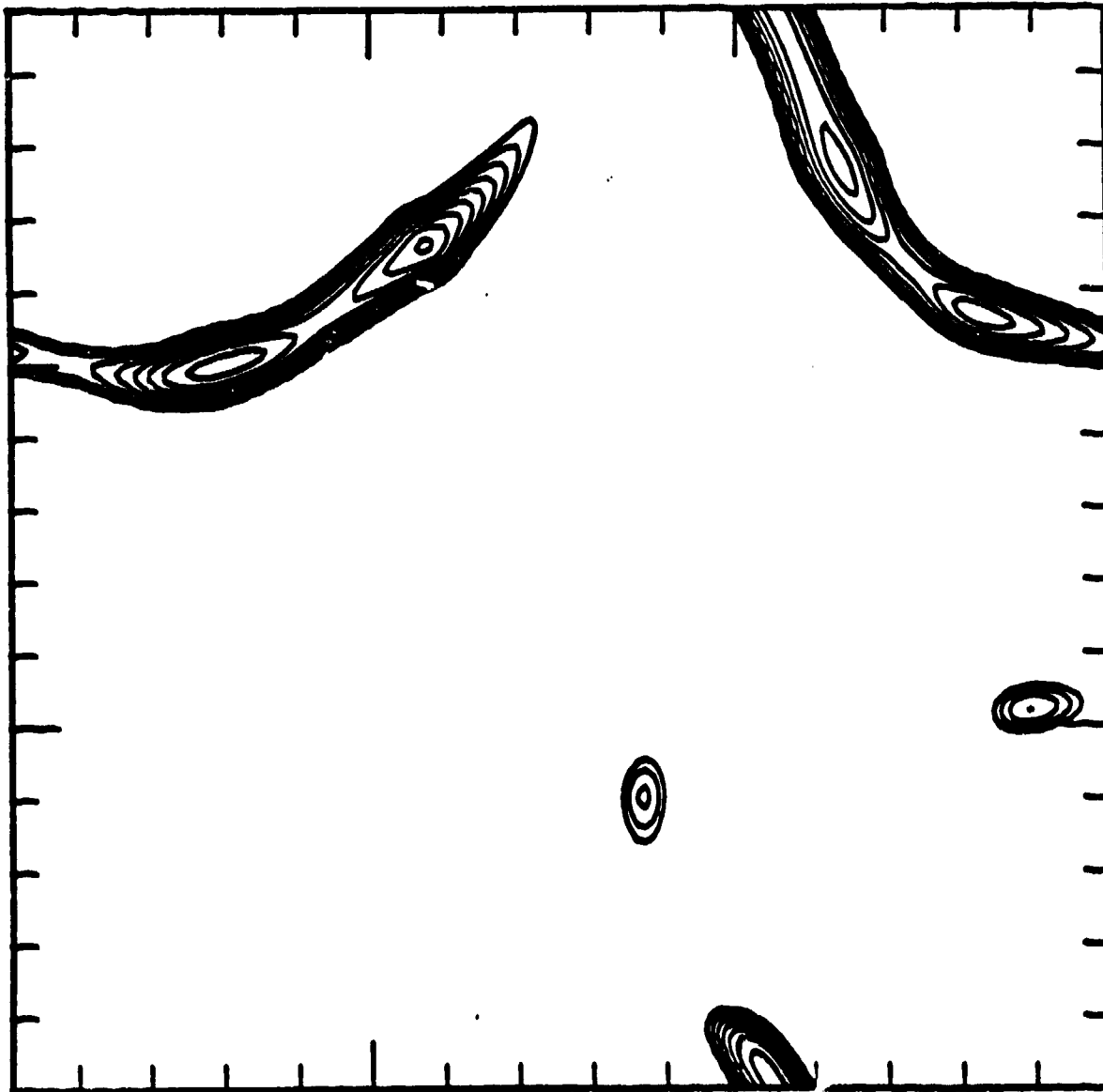
Low contour = $10^5 K$

Contour Ratio = 2

2d HDM Temperature isocontours for Unsuppressed Asph @ a=25
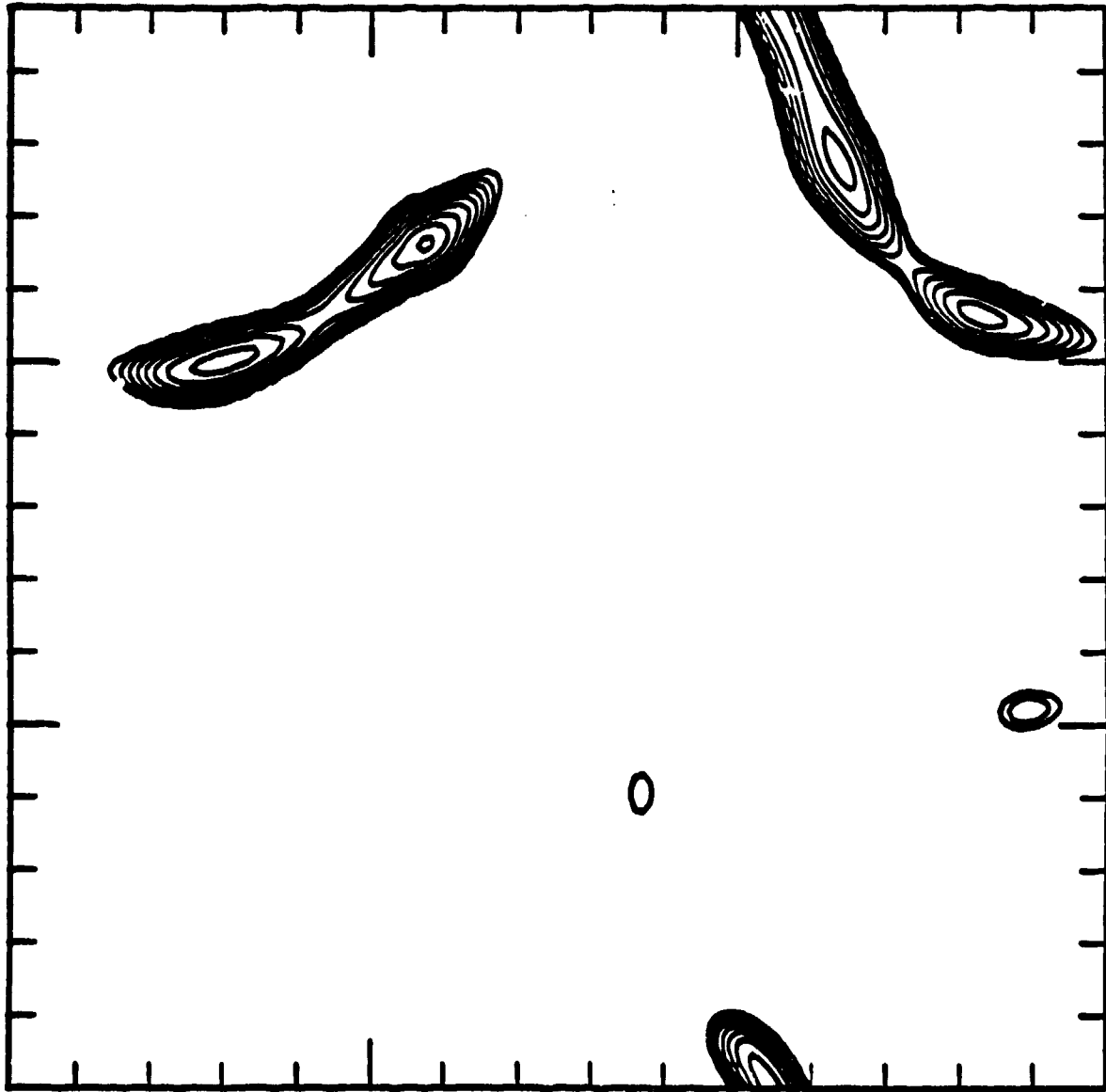
Low contour = $10^5 K$

Contour Ratio = 2

2d HDM Temperature Isocontours for Suppressed Asph @ a=25
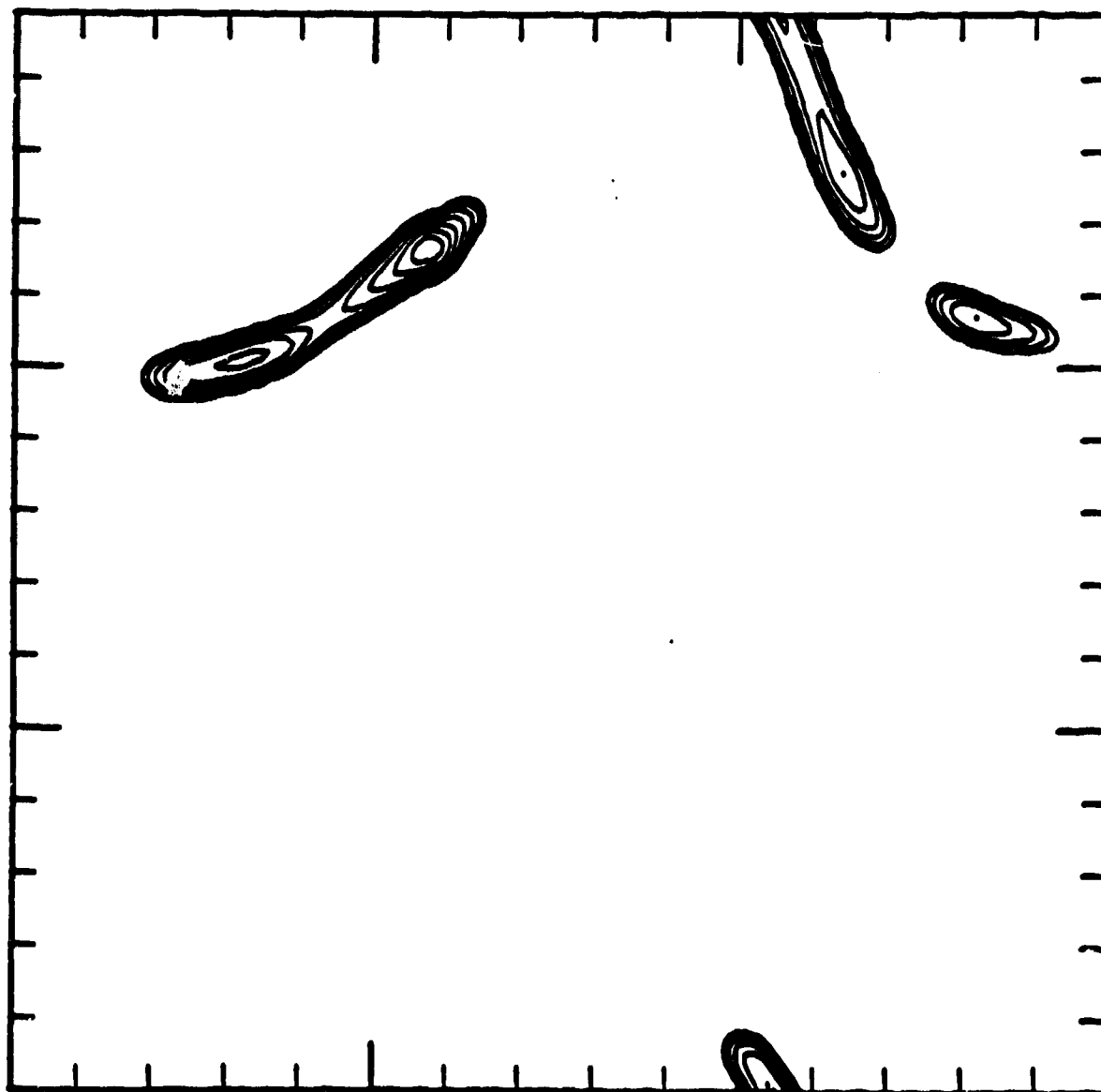
Low   Contour = $10^5 K$

Contour Ratio = 2

15 Conclusions

- Asph shows promise in general for allowing improved resolution within a simulation for a given number of Asph nodes vs. Standard Sph, particularly in intrinsically anisotropic situations.

- The development of an improved criterion for the use of the artificial viscosity in order to reduce spurious heating in combination with the improved resolution of Asph will hopefully allow us to investigate a wider range of scales in cosmological structure formation scenarios.

Future work and considerations:

- The general principles of Asph need to be tried out in a wider range of test problems, in order to explore the benefits and limits of the current technique.

- The question of angular momentum conservation under Asph needs further investigation, since it would seem angular momentum conservation under Asph is dependent upon the H tensor properly following the fluid element approximation.

- The artificial viscosity suppression algorithm needs much more refinement in order to extend its applicability and reliability; most notably it should be converted to an entirely local criterion.

Energy Conservation in Viscous Flows

Mike Fisher

Battelle

-147-

SPH Fluid Equations:

Continuity Equation:

$$\frac{dp_i}{dt} = \sum_j m_j (v_i^\alpha - v_j^\alpha) \frac{\partial W_{ij}}{\partial x_i^\alpha} - \rho_B (v_i^\alpha - v_B^\alpha) n_B^\alpha W_{iB} A_B$$

Momentum Equation:

$$\frac{dv_i^\alpha}{dt} = \sum_j m_j \left(\frac{\Pi_j^{\alpha\beta}}{\rho_j^2} + \frac{\Pi_i^{\alpha\beta}}{\rho_i^2} \right) \frac{\partial W_{ij}}{\partial x_i^\beta}$$

$$- \rho_B \left(\frac{\Pi_B^{\alpha\beta}}{\rho_B^2} + \frac{\Pi_i^{\alpha\beta}}{\rho_i^2} \right) n_B^\beta W_{iB} A_B$$

V

$2h$

Preliminary Results

Legend:
- h = 0.1, without
- h = 0.1, with

x-axis: time (μs)

Preliminary Results

Legend:
- h = 0.2, without
- h = 0.2, with
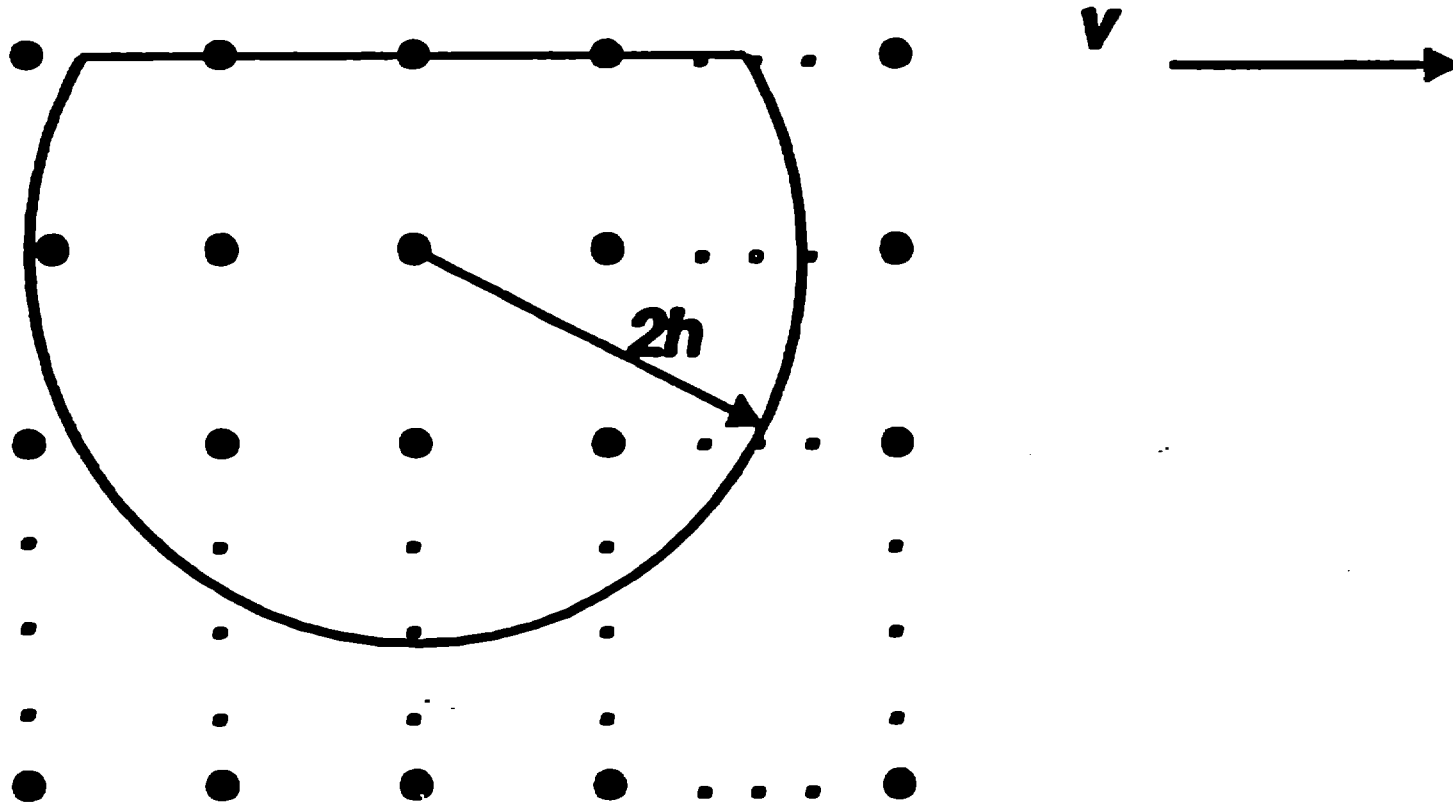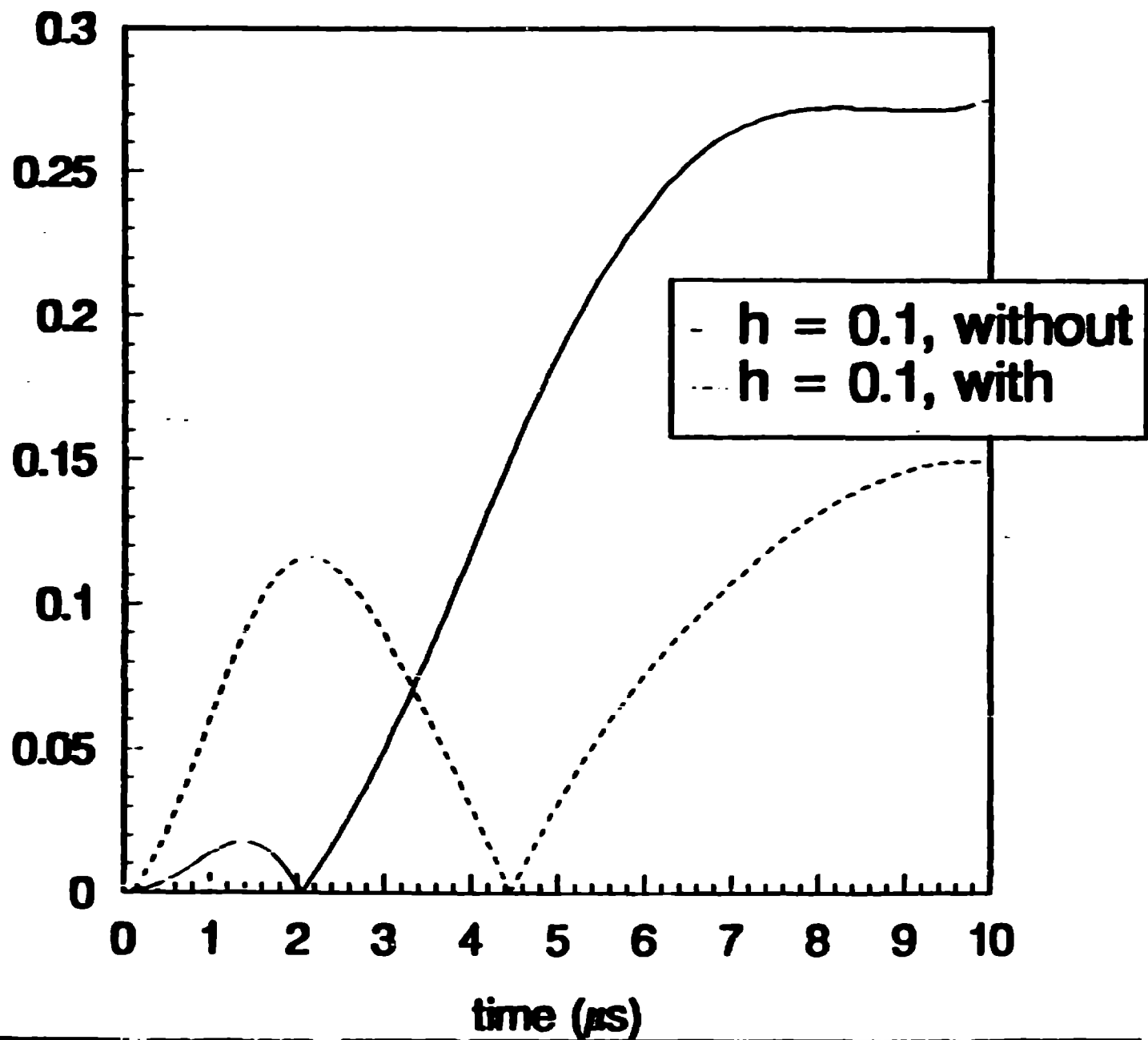
time (μs)
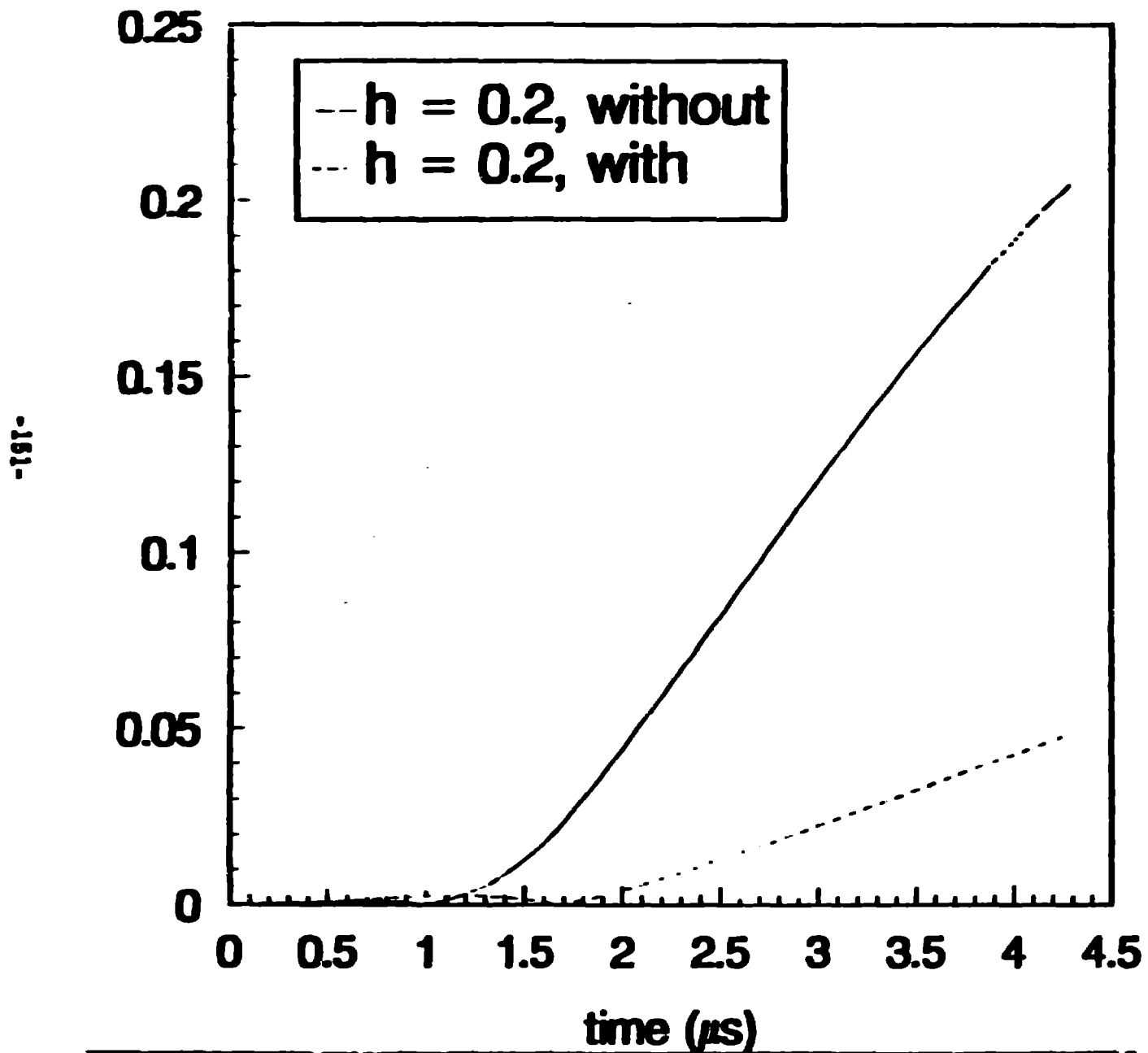
Linked Penetration Computations

Gordon R. Johnson
Alliant Techsystems
Hopkins, Minnesota USA

SPH Workshop
Los Alamos
September 23, 1993

Outline

- **Motivation and discussion**

- **Background**

- **Lagrangian code structure for SPH nodes and standard elements**

- **Examples and discussion**
  - **SPH only**
  - **SPH nodes attached to standard elements**
  - **SPH nodes sliding on standard elements**
  - **SPH nodes automatically generated from standard elements**

- **Summary and conclusions**

eruso

MOTIVATION AND DISCUSSION

- **Desirable to have a Lagrangian code which could accurately handle severe distortions**

- **SPH can handle severe distortions in a Lagrangian framework**
    - **—But what about accuracy and computing time?**

- **It may be a good compromise between Standard Lagrangian codes and Eulerian codes**

- **Linking SPH to a Standard Lagrangian code could have great potential**
    - **—Capability**
    - **—Accuracy**
    - **—Efficiency (Computing time)**

STANDARD ELEMENTS

SPH NODES

Current velocities and displacements of all nodes

Determine strains, strain rates, etc. in all elements

Determine strains, strain rates, etc., in all SPH node

MATERIAL MODELS

Determine stresses from strains, strain rates, etc.

Determine forces on nodes for each element

Determine forces on each SPH node and its neighbor

Collect forces from standard elements and SPH nodes

Update velocities and displacements for all nodes

NTS/11-GJ-015.18pt.TKC

SPH and Standard Element Results
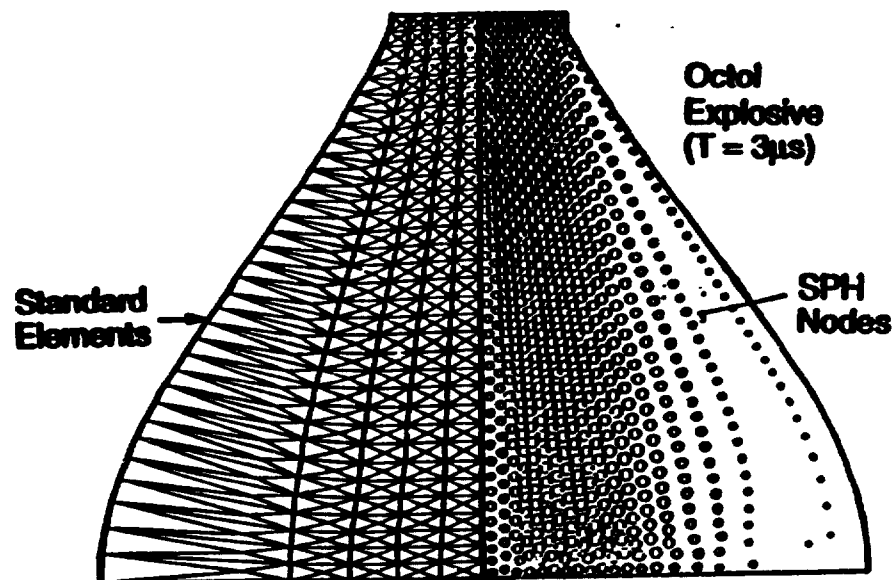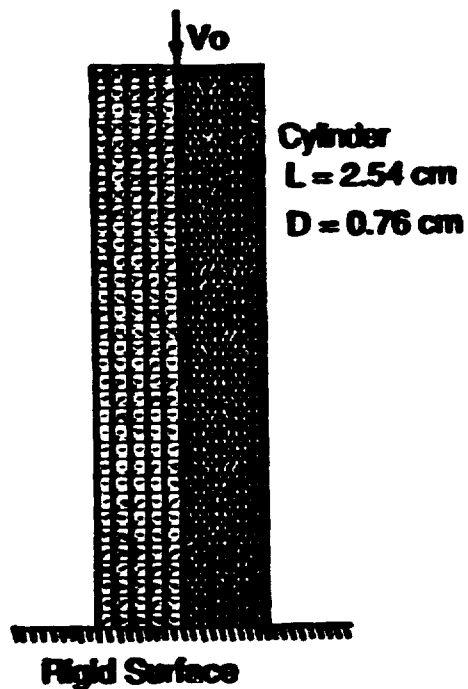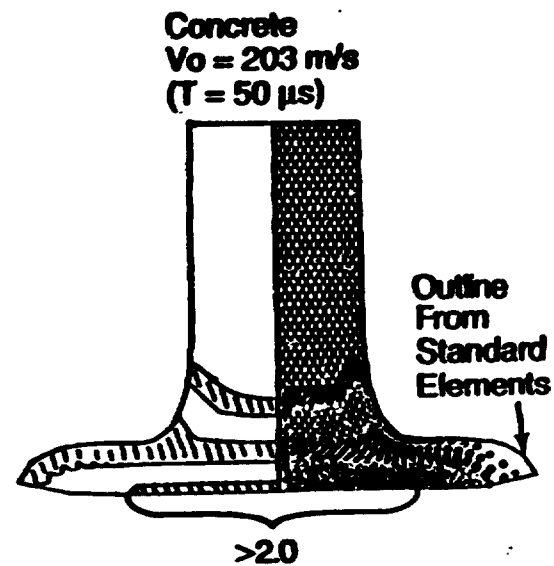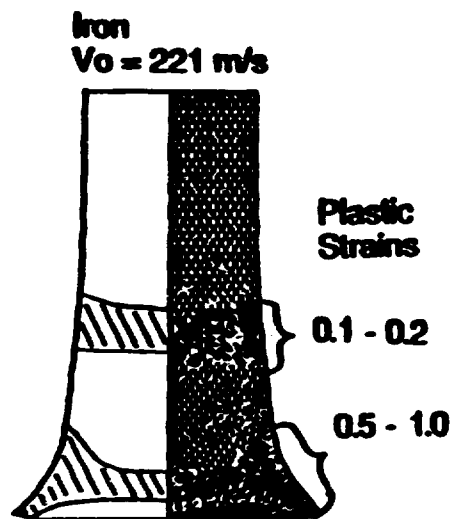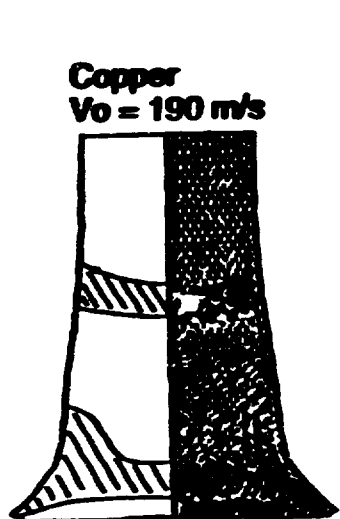
SPH PERFORATION COMPUTATIONS

SPH PENETRATION COMPUTATION

$V_o = 5000$ m/s

Aluminum Rod (6061-T6)
L = 5.1 cm
D = 2.0 cm

Aluminum Plate
(2024-T351)

10 us

Plate Thickness = 12.7 cm

20 μs

40 us
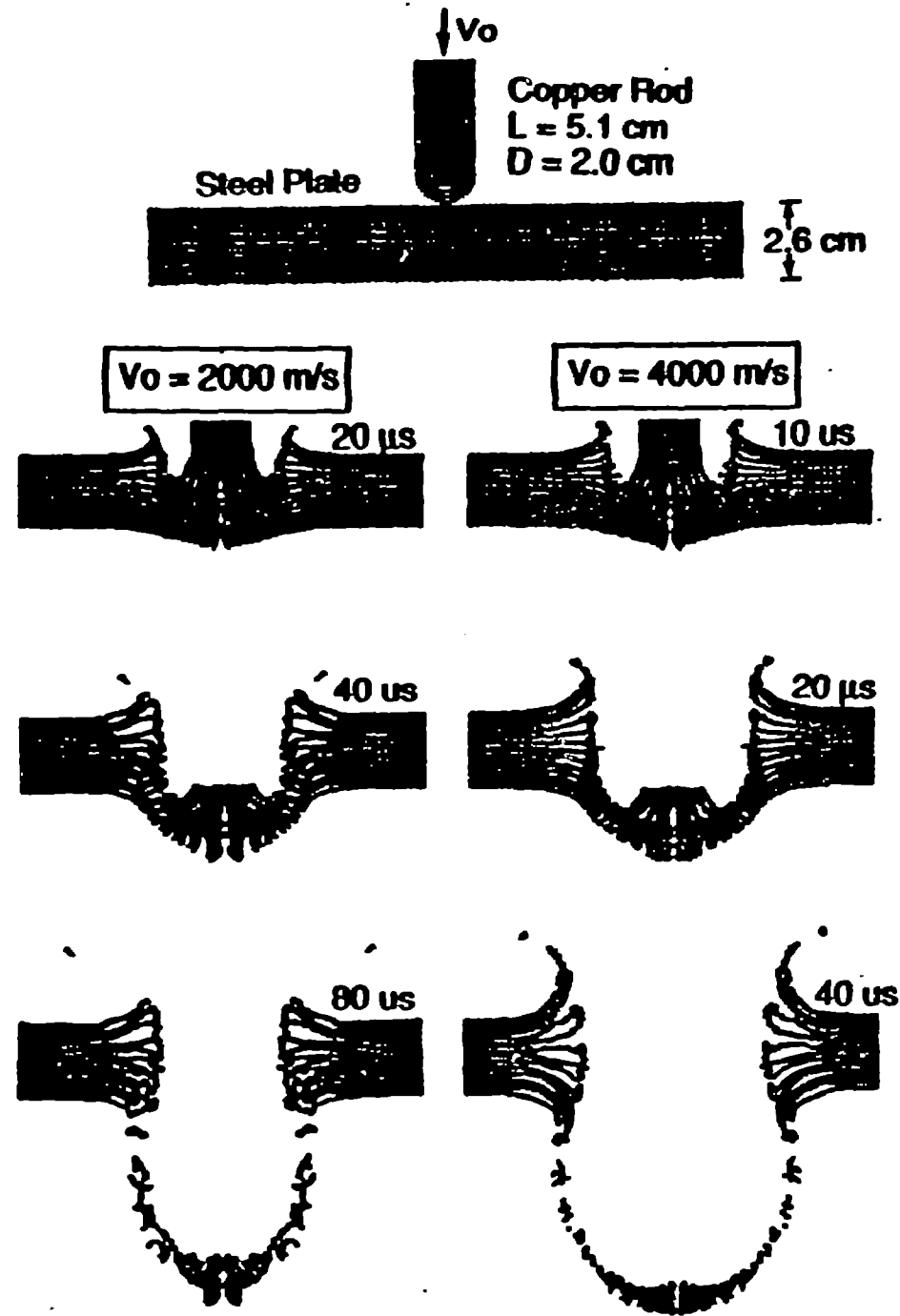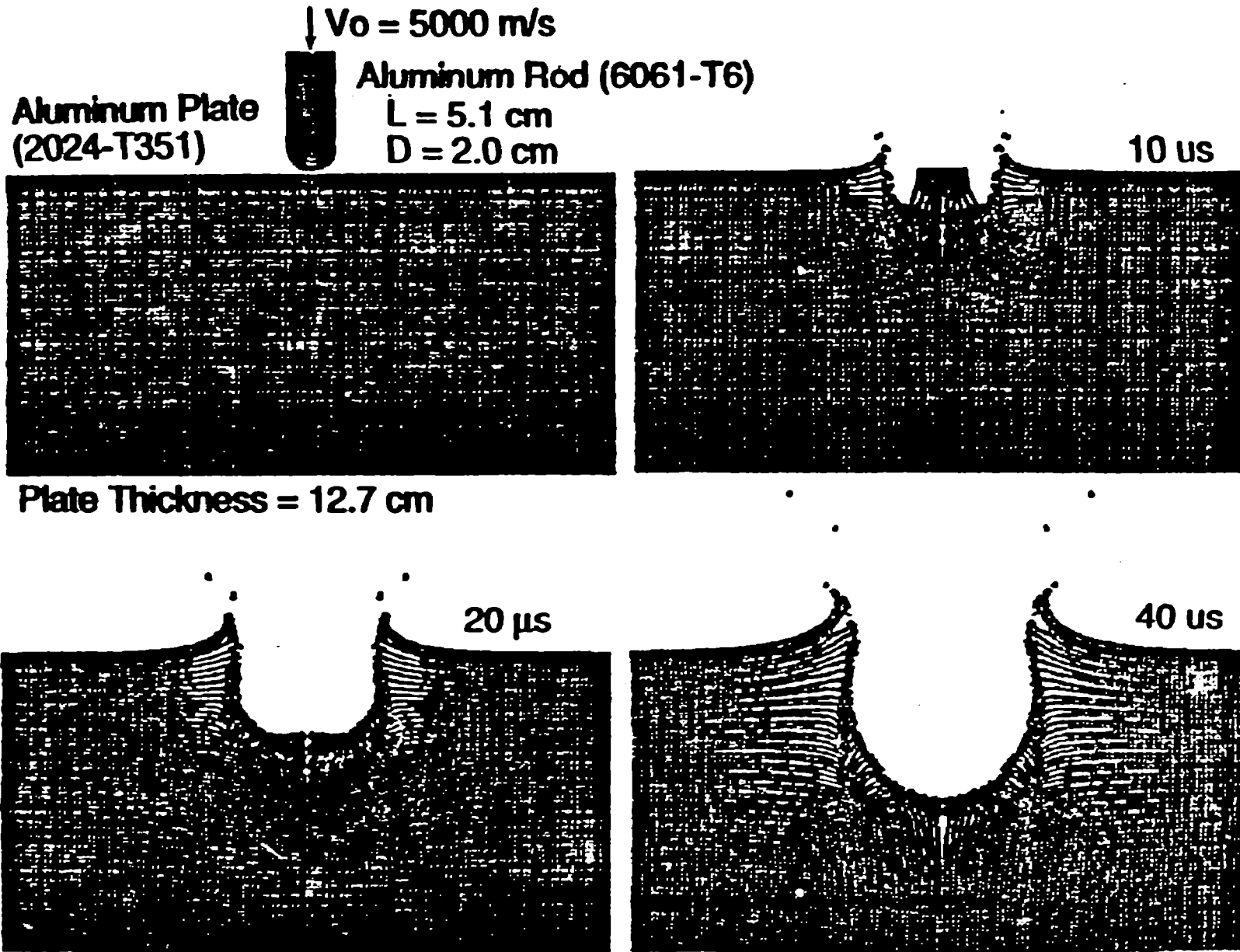
SPH SPALL COMPUTATION

Vo = 4000 m/s

Aluminum Projectile
L = 0.64 cm
D = 1.27 cm

Iron Plate

1.0 µs

Plate Thickness = 2.54 cm
(Full diameter not shown)

2.0 µs

12.0 µs

Solid Nodes Indicate Fracture

Spall
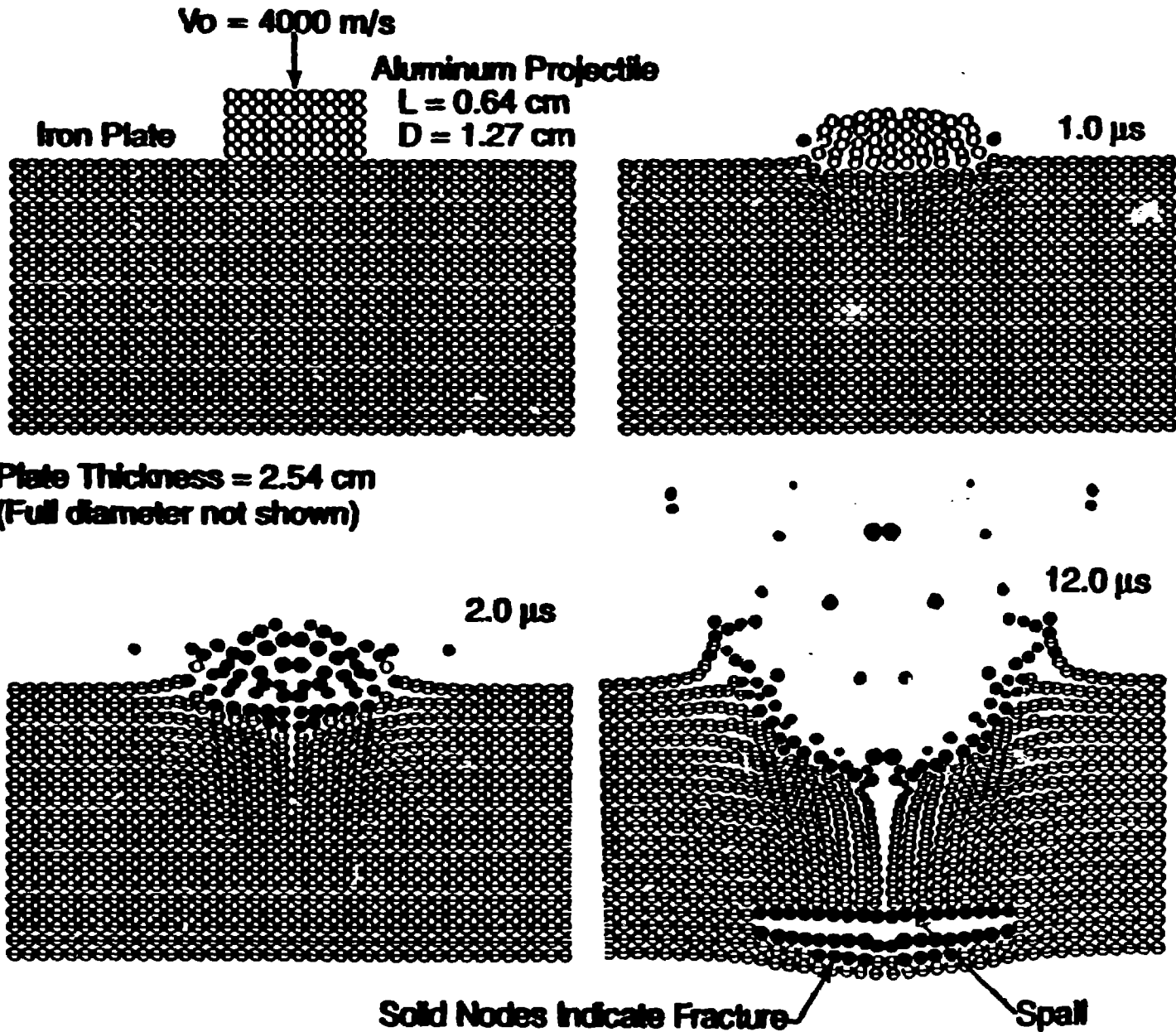
Pointed-Nose Penetrator Computation

Initial Geometry

Final Penetration for V_o = 978 m/s

Grid Deformation

V_o

Steel Rod
L = 71.1mm
D = 7.11mm

SPH Nodes

7075-T651
Aluminum

Linked SPH Results Compared to Test Data

CRU10

Rounded-Nose Penetrator Computation

Initial Geometry

V_o

Steel Rod
L = 71.1mm
D = 7.11mm

SPH Nodes

6061-T651
Aluminum

Final Penetration for V_o = 959 m/s

Grid Deformation

Linked SPH Results Compared to Test Data

GFU82
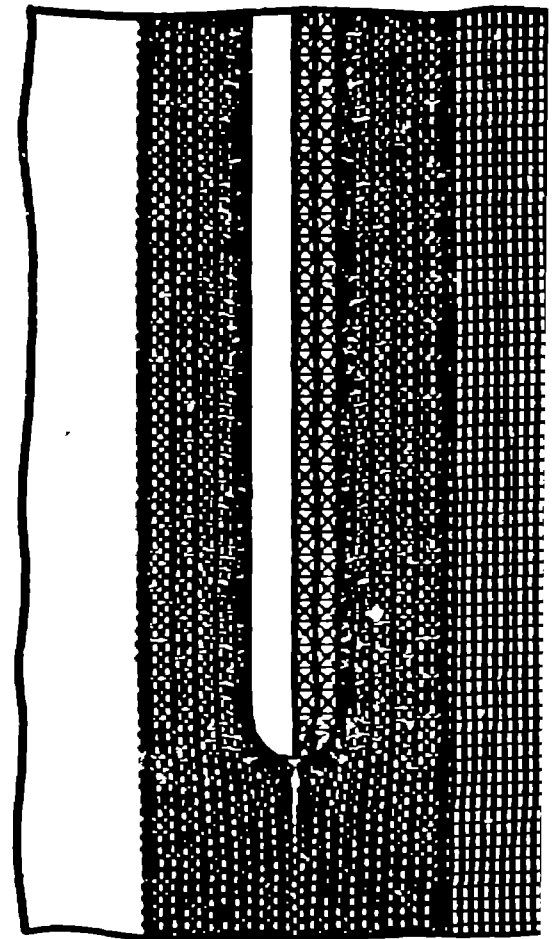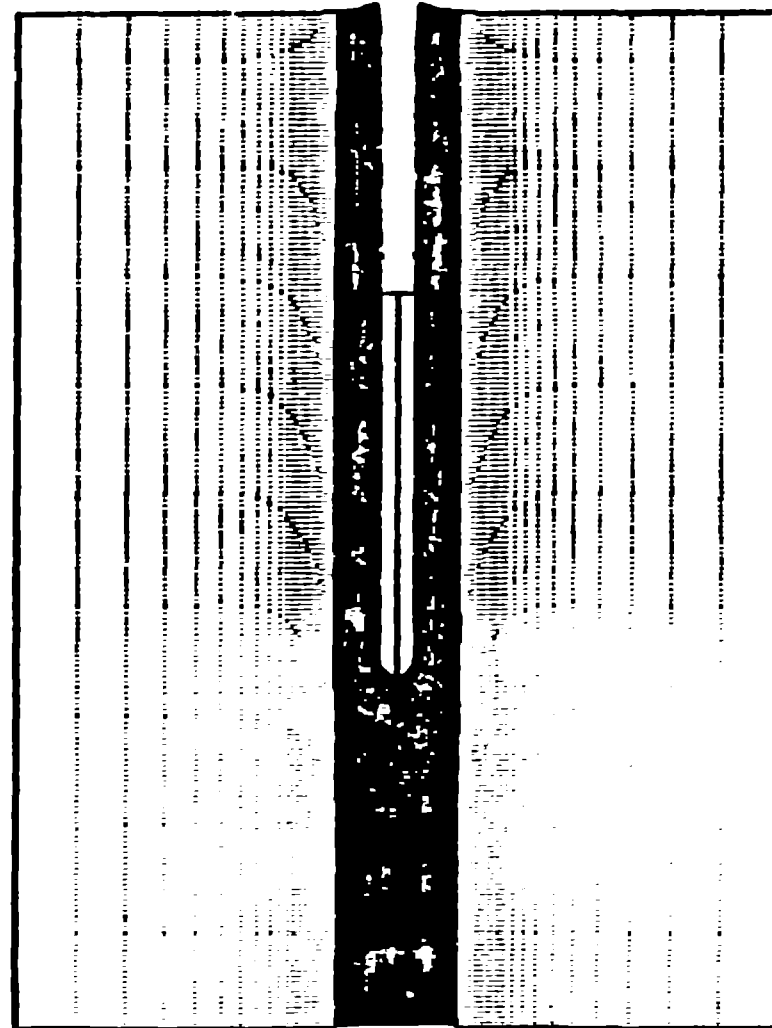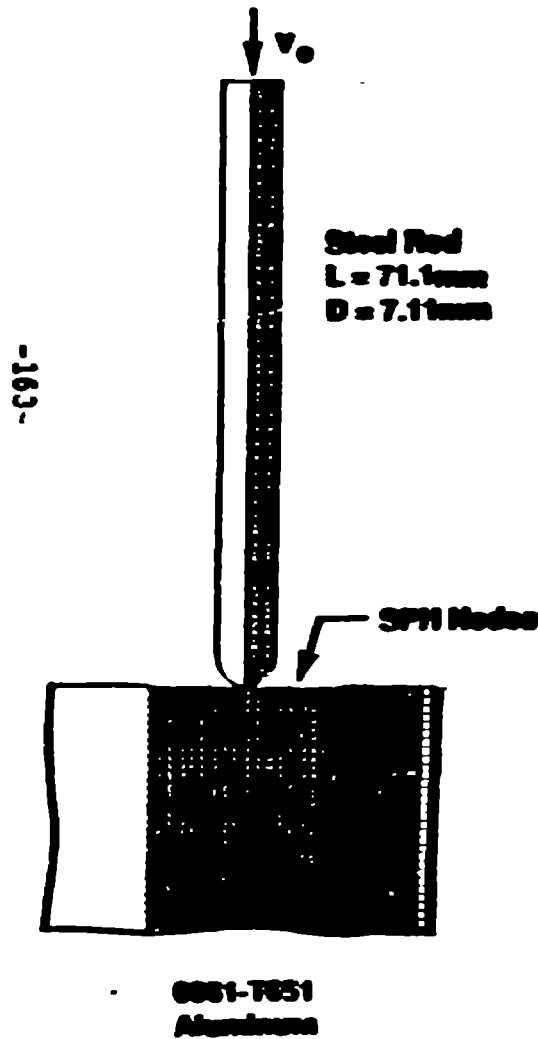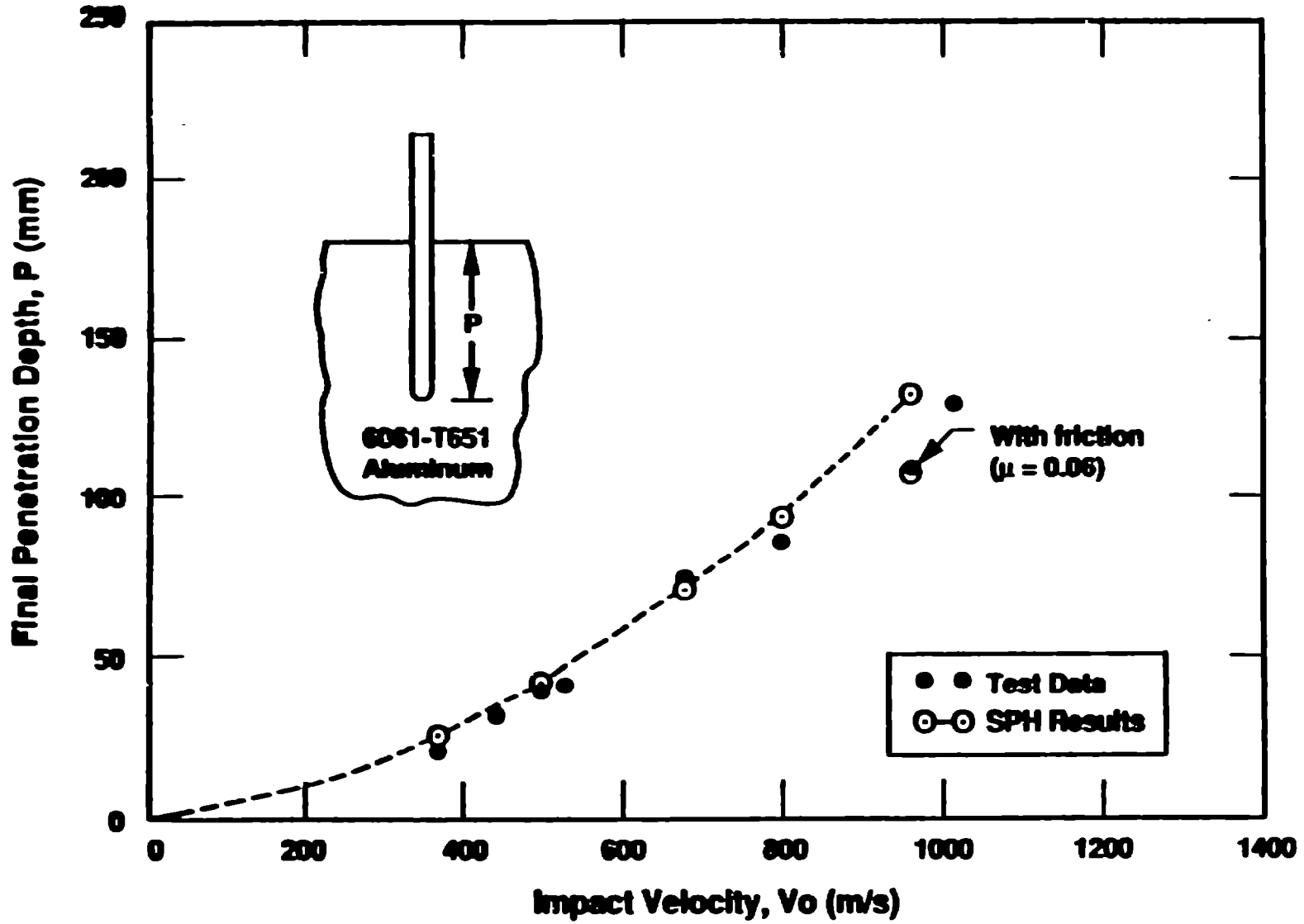
SPH Attachment to Standard Grid
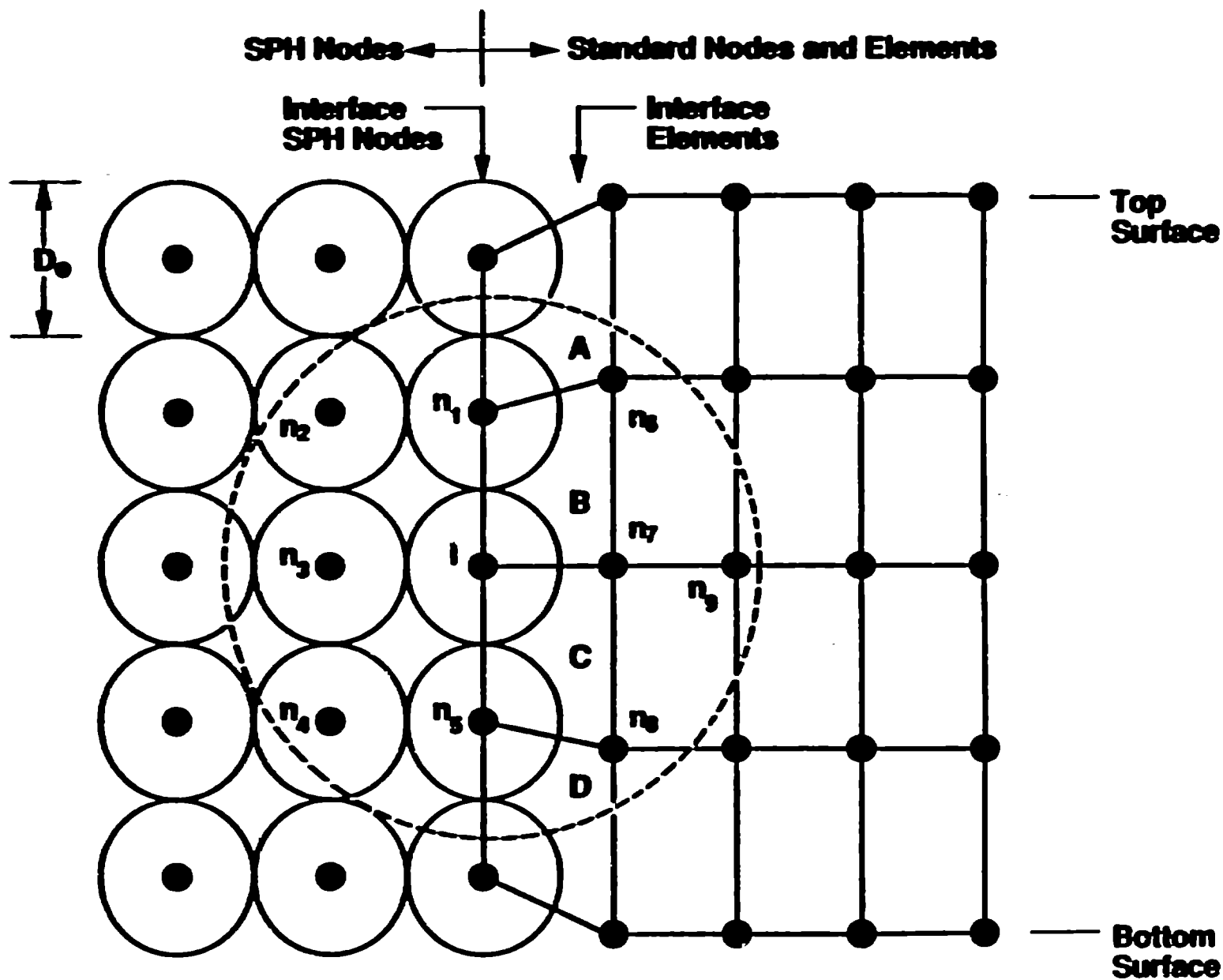
SPH Sliding on Standard Grid

SPH Nodes

Sliding Interface

Standard Elements
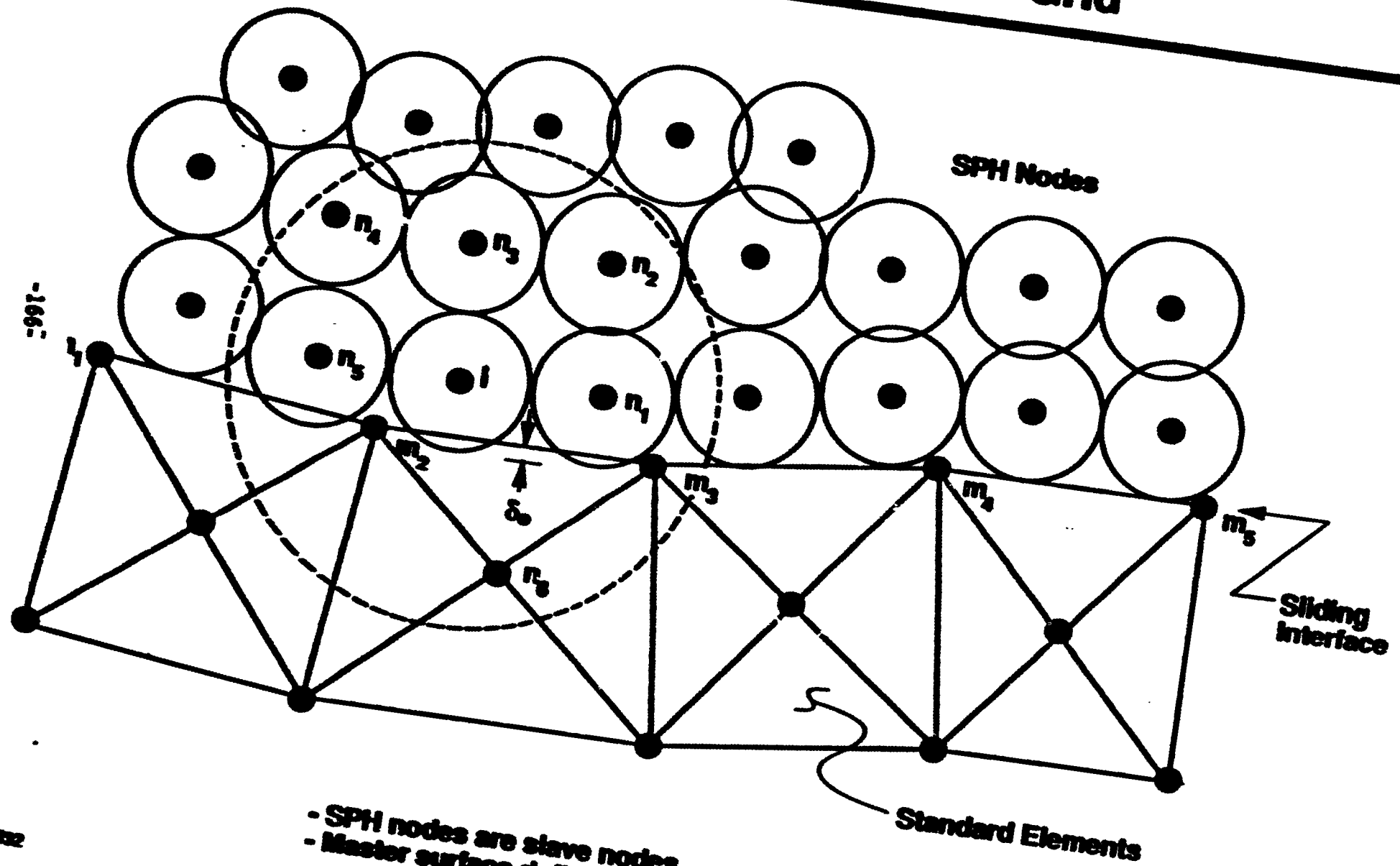
- SPH nodes are slave nodes
- Master surface defined by standard nodes $m_1 - m_5$

Eroding Penetrator Computation
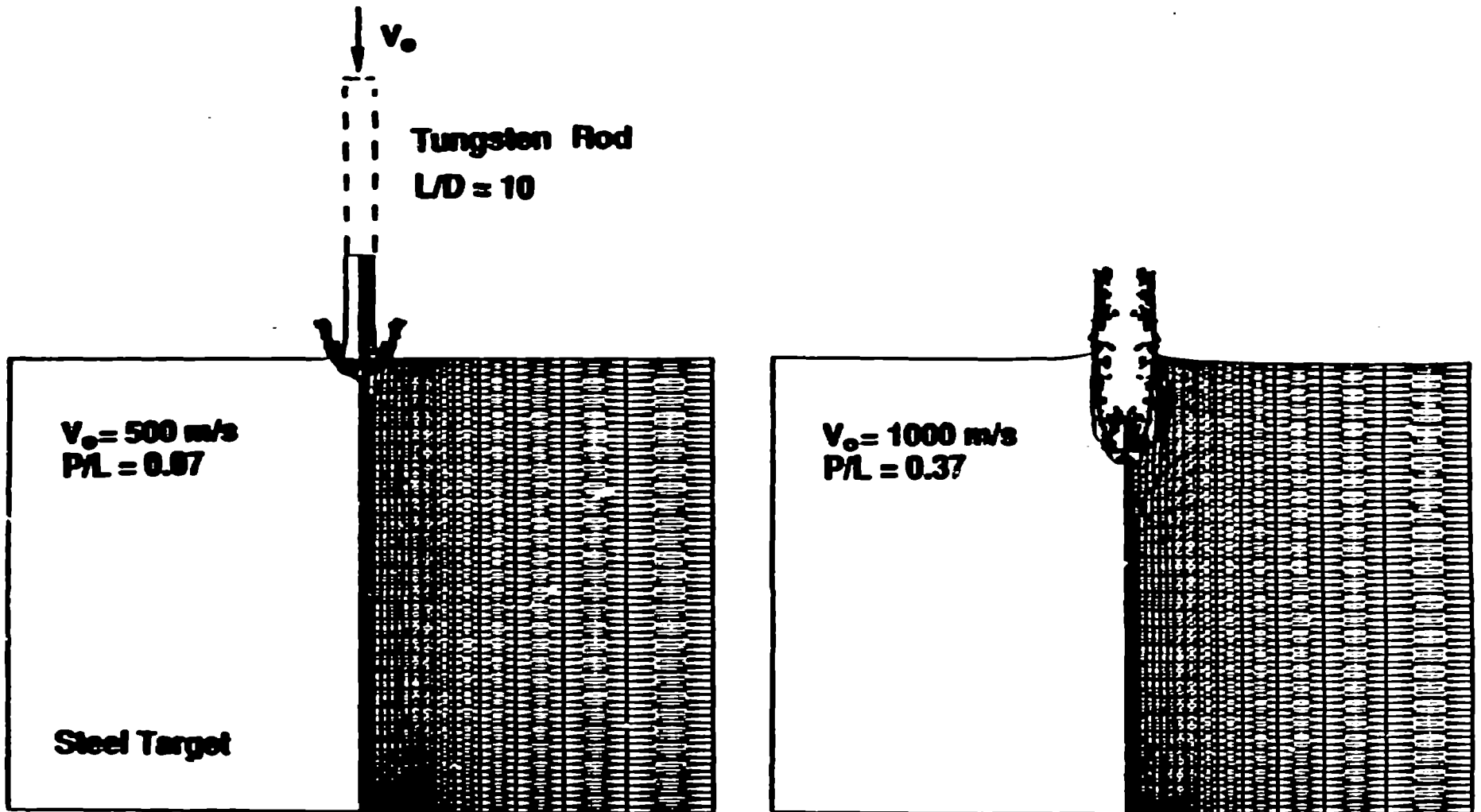
V_0

Tungsten Rod
L/D = 10

V_0 = 500 m/s
P/L = 0.87

Steel Target

V_0 = 1000 m/s
P/L = 0.37

Eroding Penetrator Computation

V_o

Tungsten Rod
L/D = 10

V_o = 1500 m/s
P/L = .78

V_o = 2000 m/s
P/L = 1.18

Eroding Penetrator Computation

V_o

Tungsten Rod

L/D = 10

V_o = 2500 m/s
P/L = 1.36

V_o = 3000 m/s
P/L = 1.48
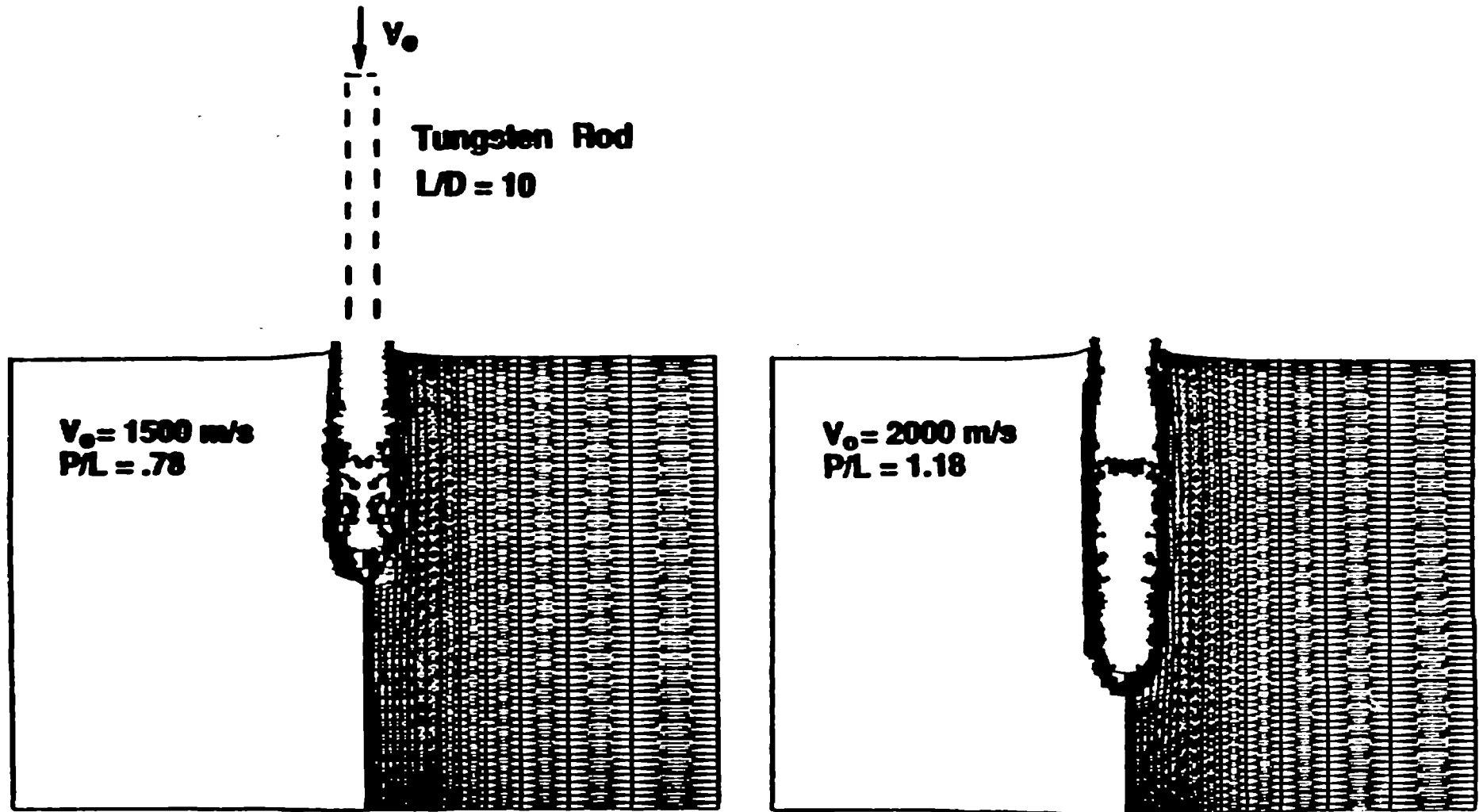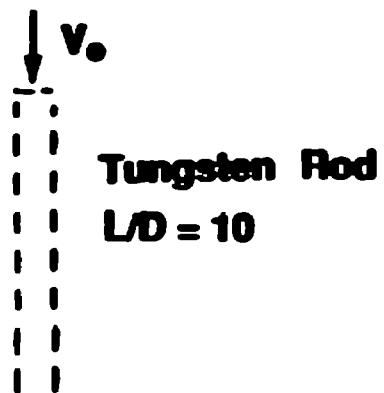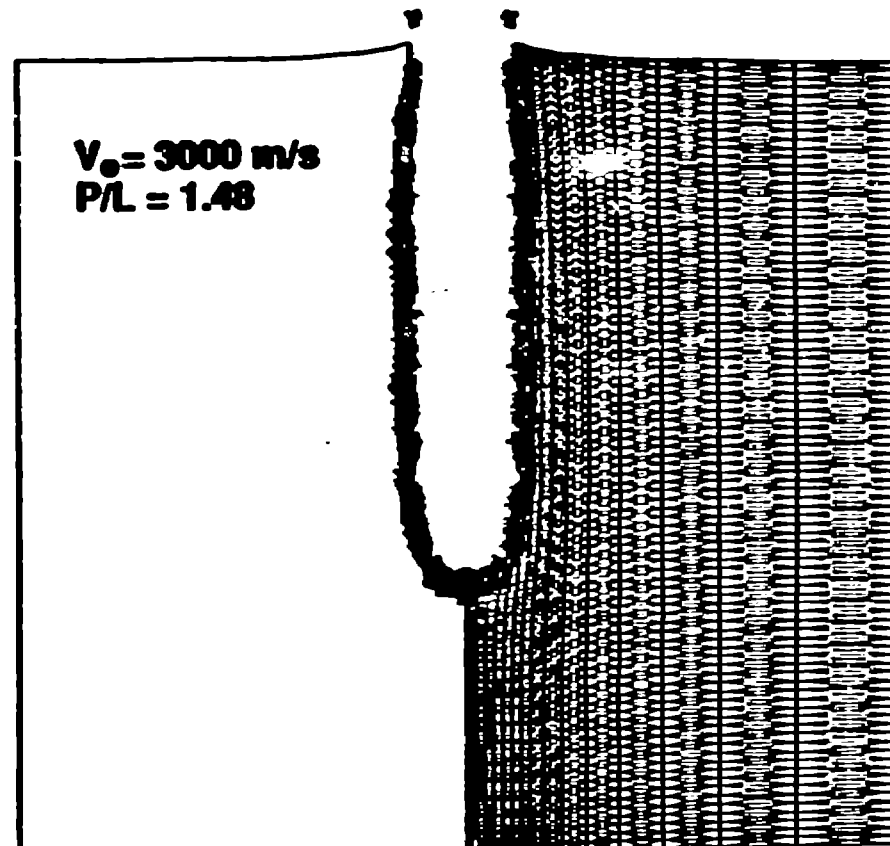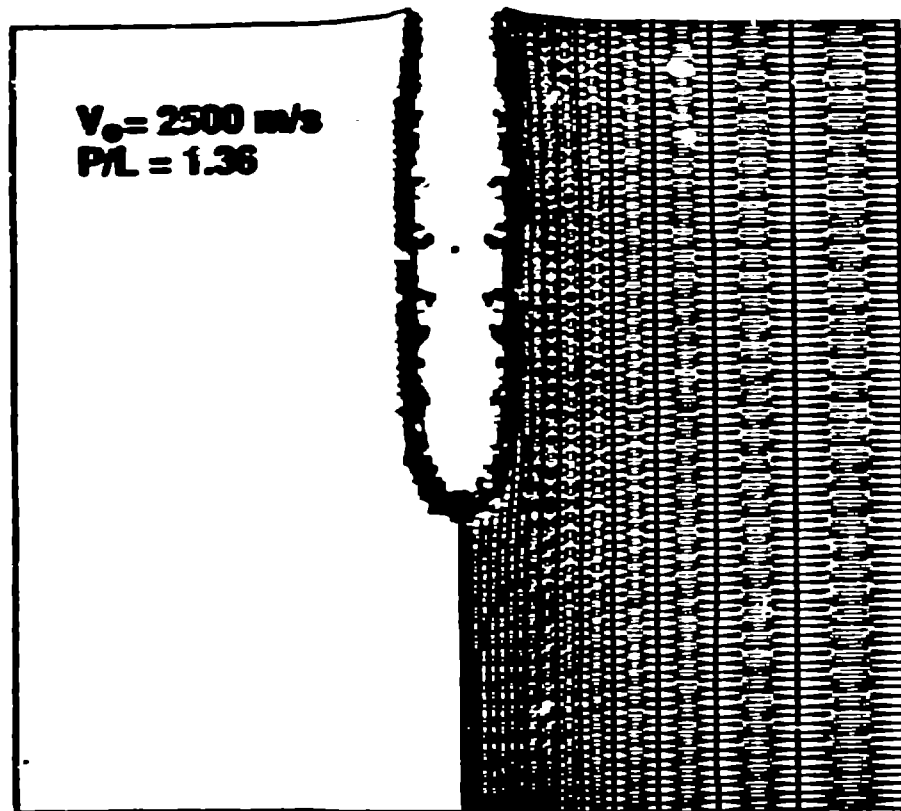
Linked SPH Results Compared to Test Data

GRU00
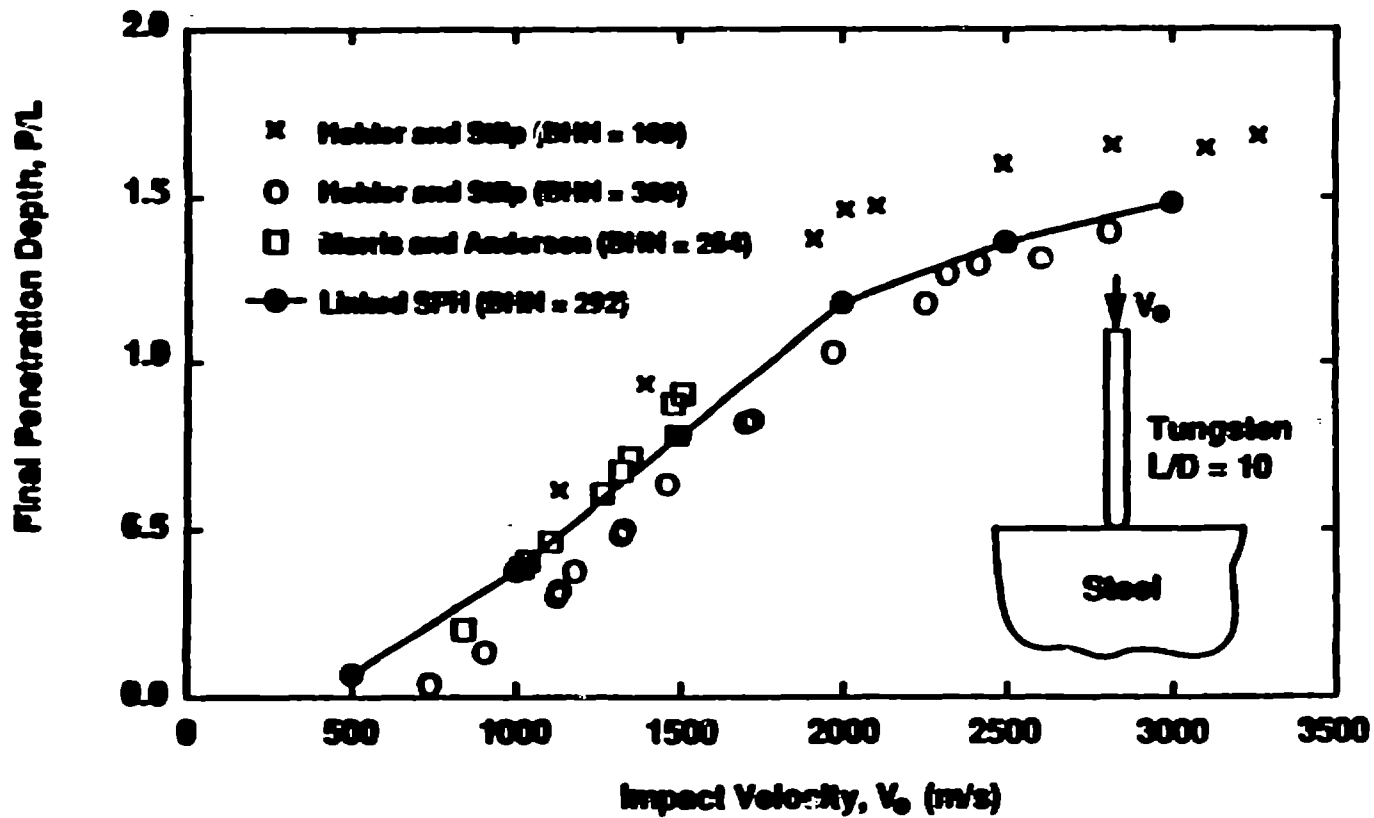
AUTOMATIC SPH NODE GENERATION

STANDARD EROSION ALGORITHM
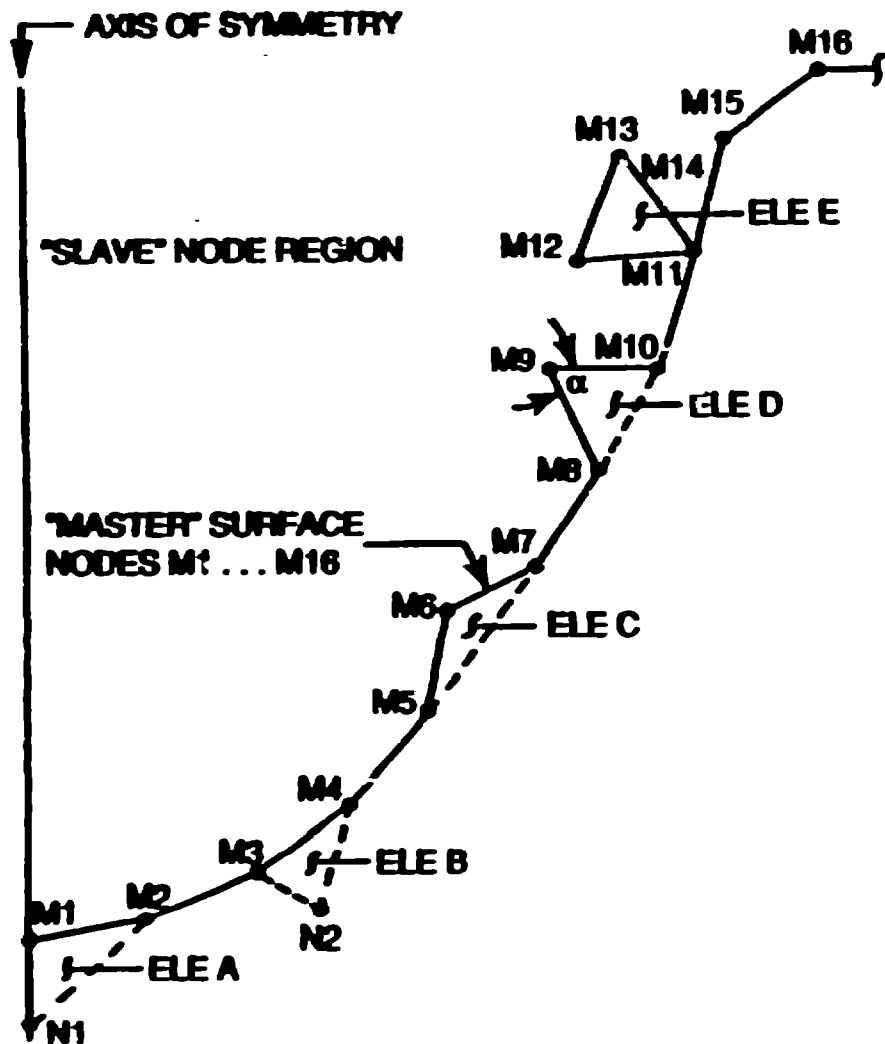
VOLUMES OF ERODED
ELEMENTS ARE DISGARDED

SPH NODE GENERATION

$$\delta_{eff} = \delta - \delta_0$$
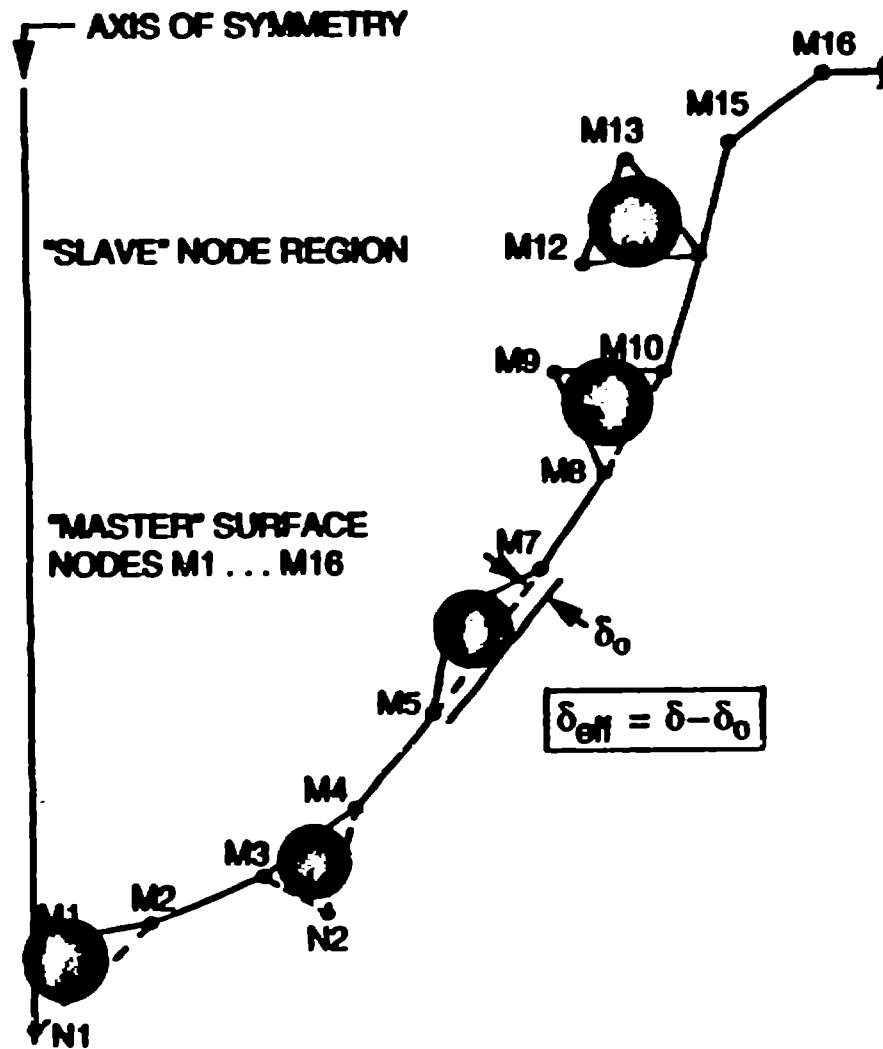
VOLUMES AND MASSES OF ERODED
ELEMENTS ARE REPLACED WITH
SPH NODES

Summary and Conclusions

* **Linked SPH computations show good agreement with test data for three sets of problems**

* **Linked SPH techniques show great potential for some classes of problems**

* **More evaluation and development is required for linked SPH**
  - **Capability**
  - **Accuracy (material interfaces)**
  - **Efficiency (computing time)**

-172-

GRU84

Topics in SPH
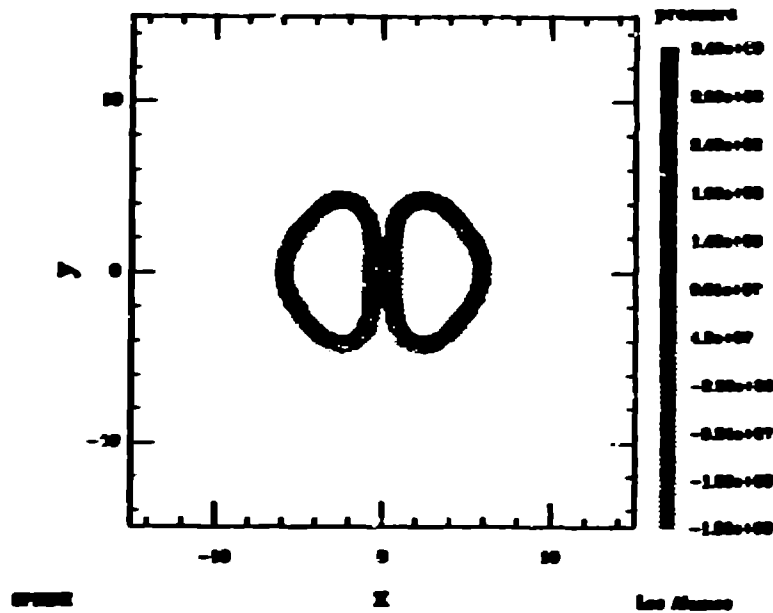
Chuck Wingate

Los Alamos National Laboratory
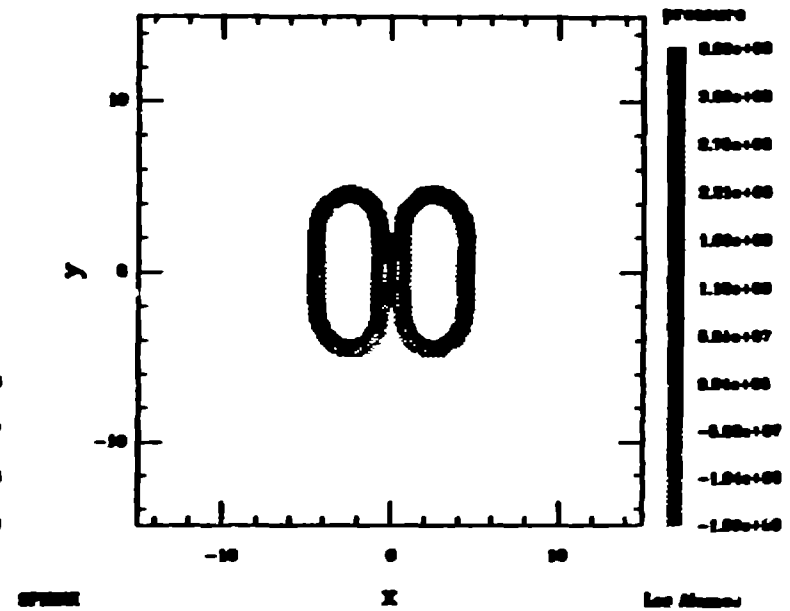
Los Alamos

Tennis/23 Time = 0 μs
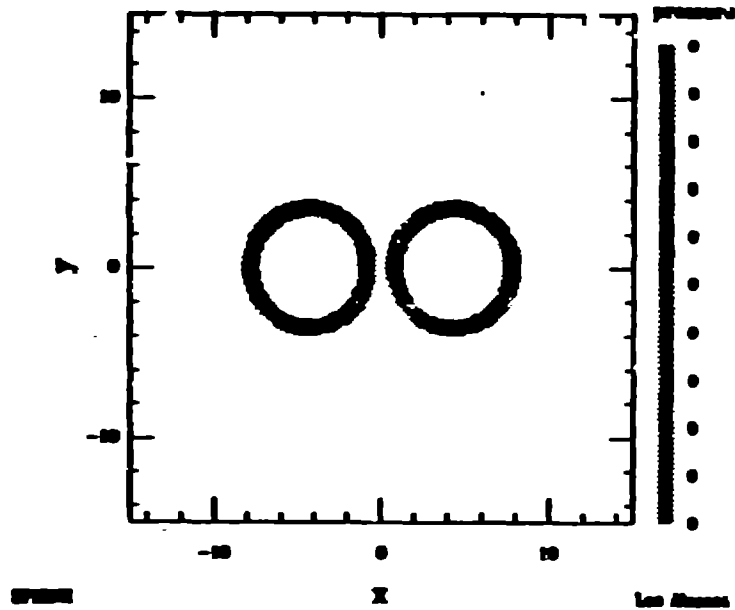
Tennis/23 Time = 201.847 μs
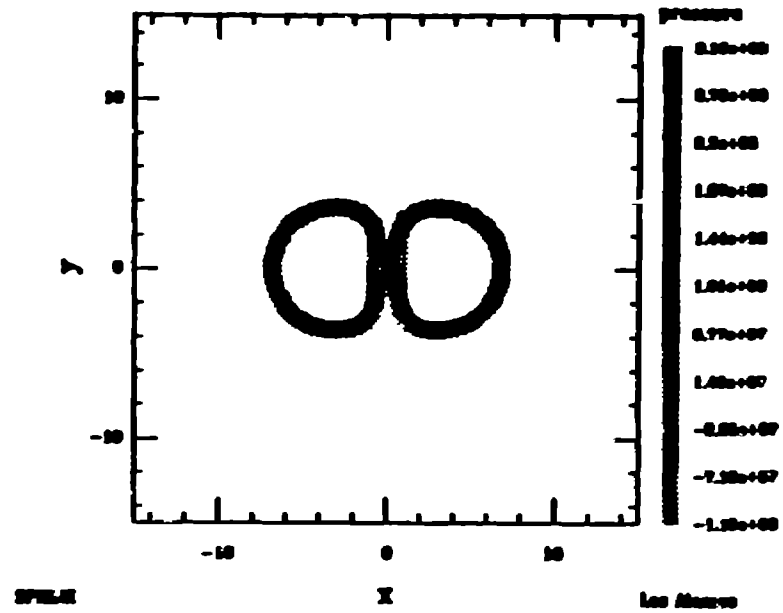
Tennis/23 Time = 400.564 μs

Tennis/23 Time = 603.947 μs

Tennis/23 Time = 802.315 μs

Tennis/23 Time = 1803.77 μs
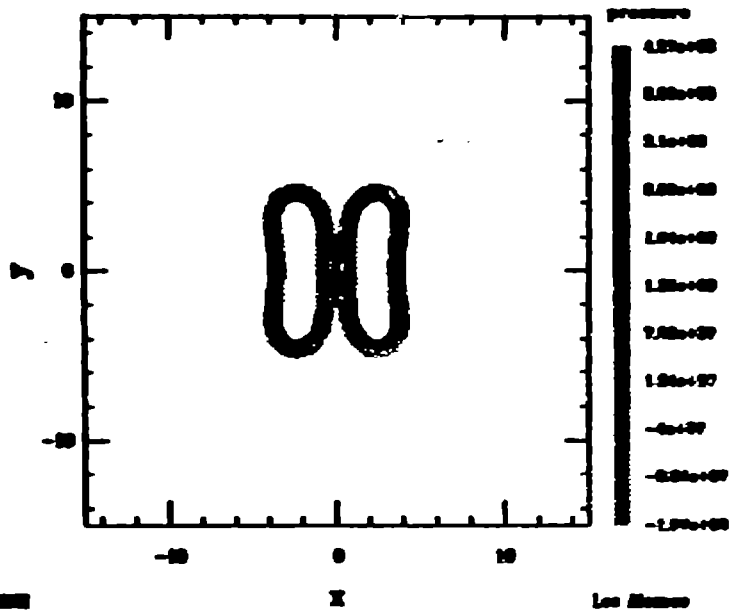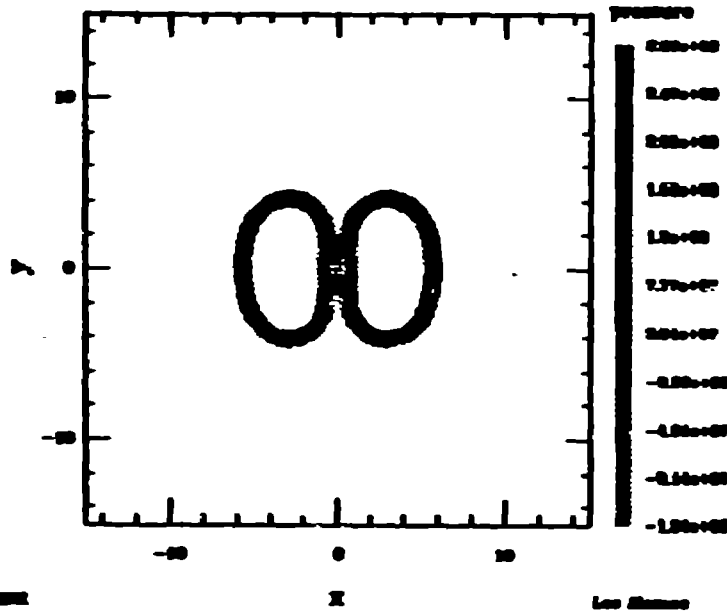
Tennis/23 Time = 1802.94 μs
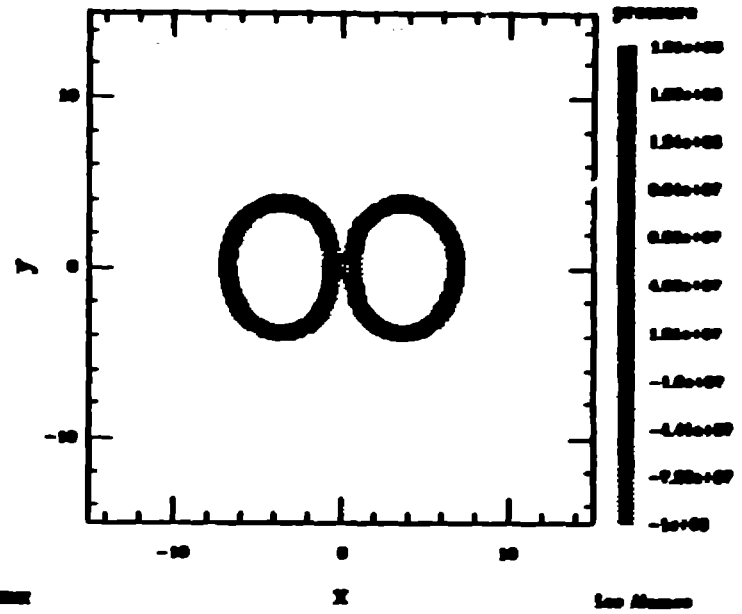
Tennis/23 Time = 2003.66 μs

Tennis/23 Time = 2204.70 μs

Y

X

SPHINX

Los Alamos

pressure
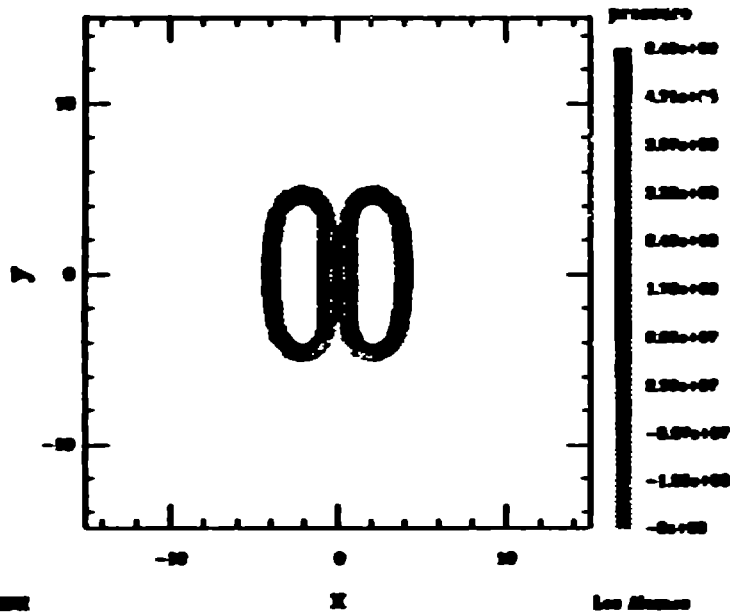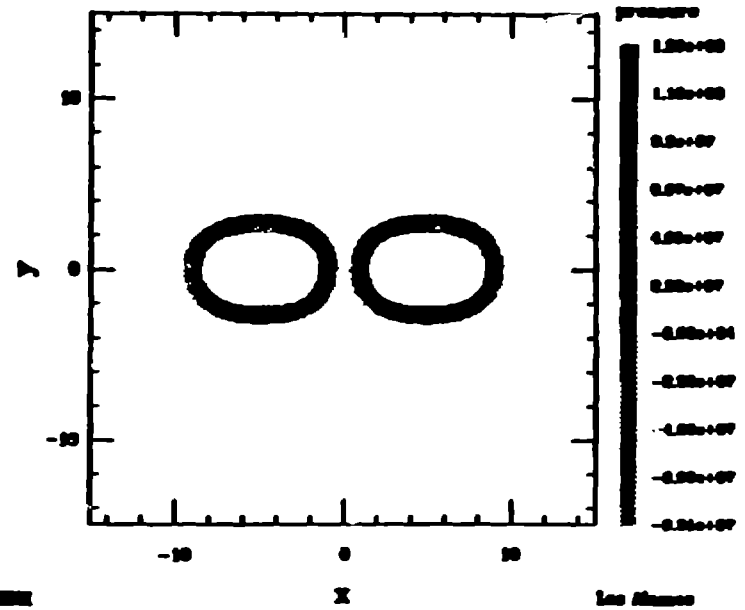
Tennis/23 Time = 2404.71 μs
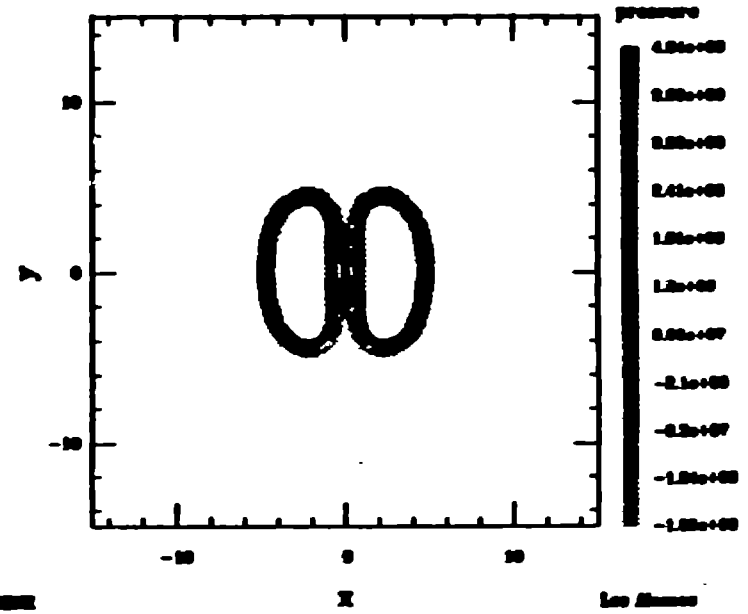
Tennis/23 Time = 2604.22 μs
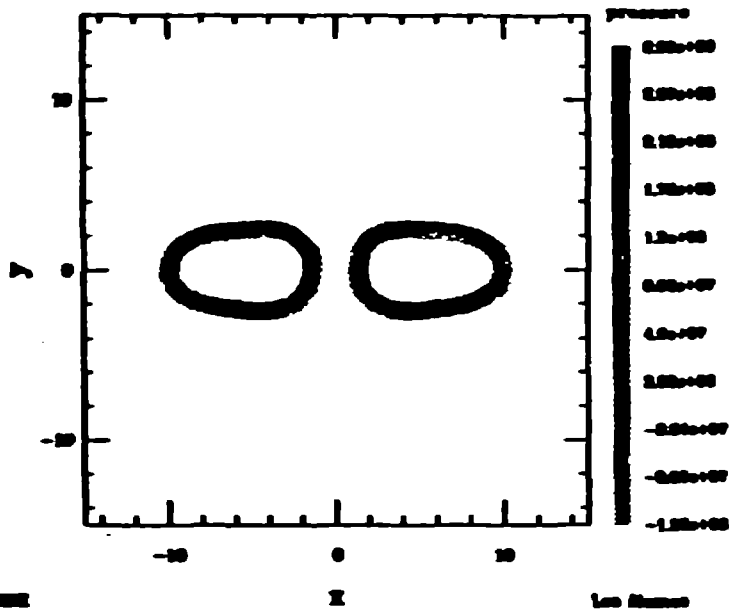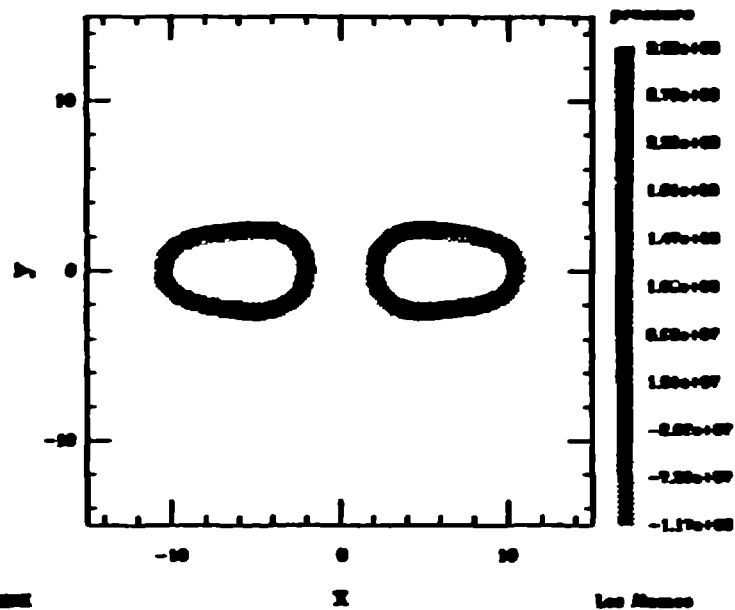
Tennis/23 Time = 2804.14 μs
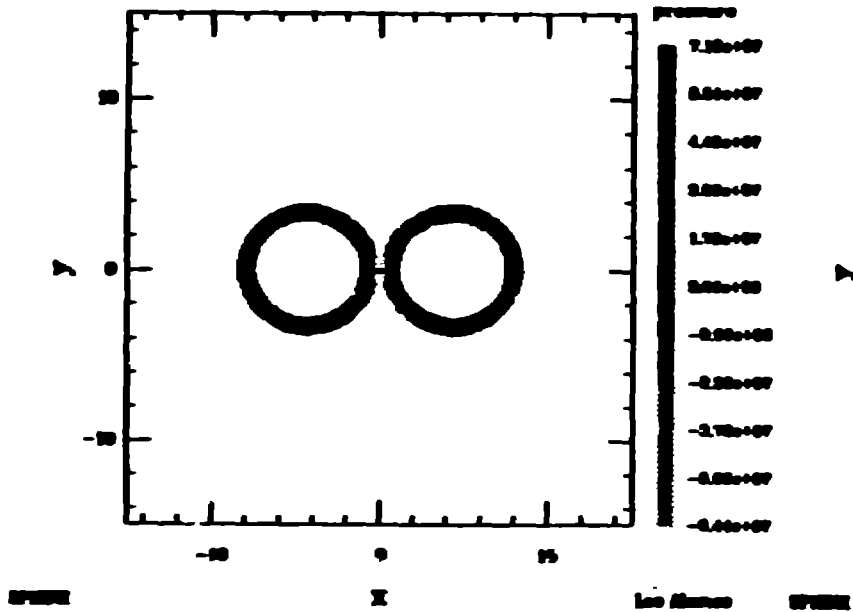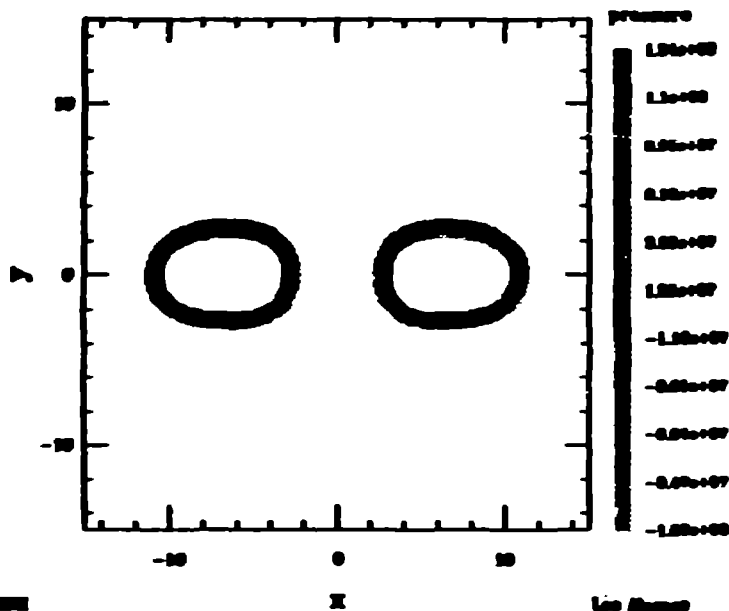
Tennis/23 Time = 3000.06 μs
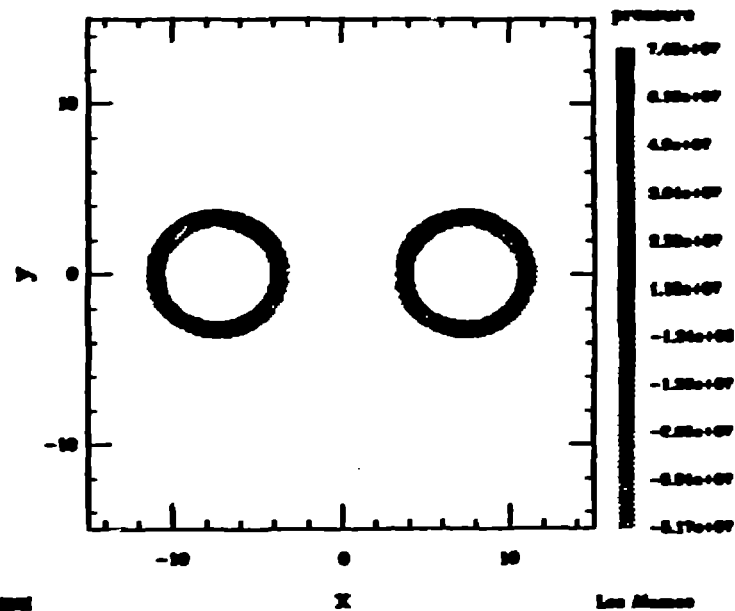
Tennis/23 Time = 3201.15 μs
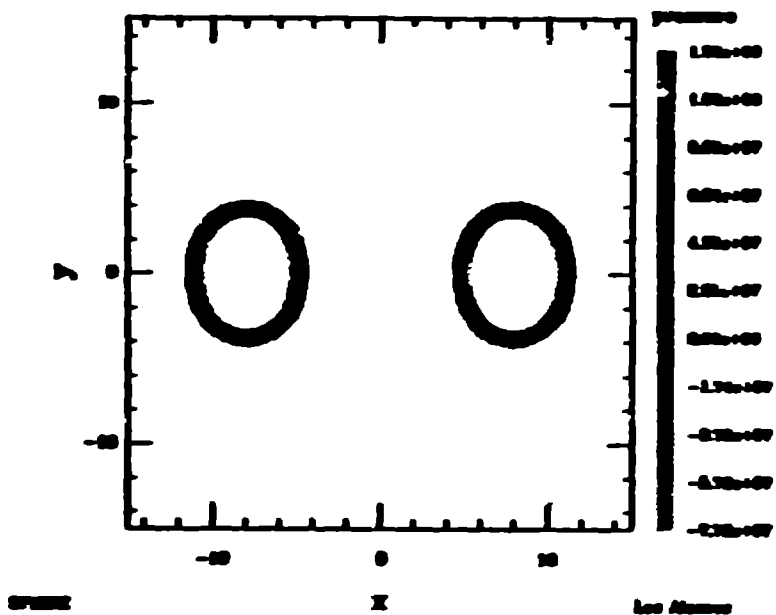
Tennis/23 Time = 3401.98 μs
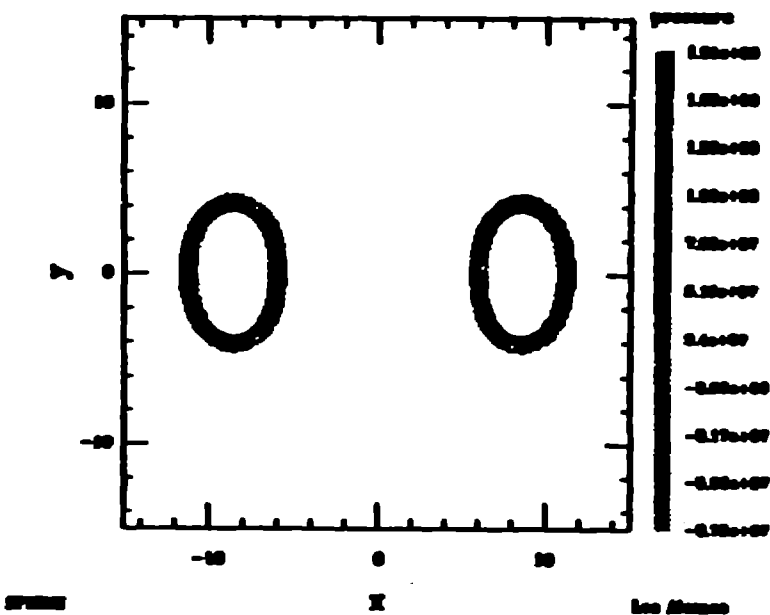
Tennis/23 Time = 3602.23 μs
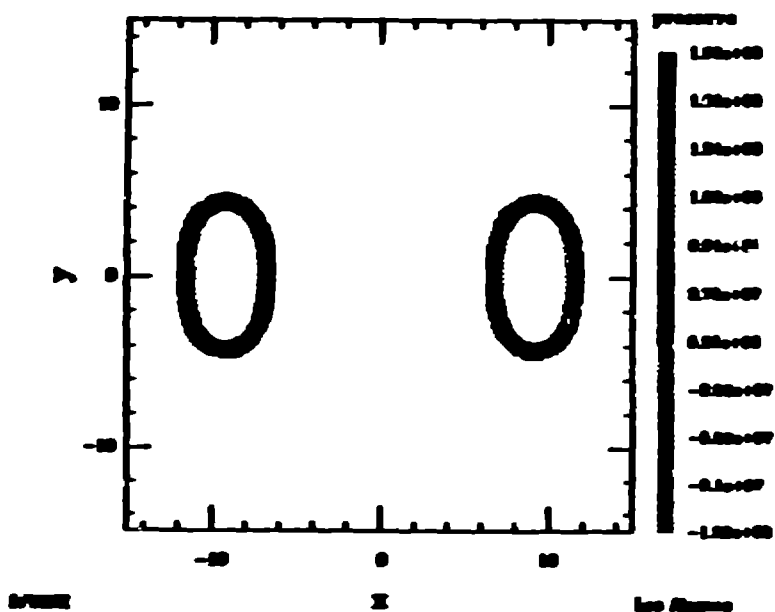
Tennis/23 Time = 4002.66 μs
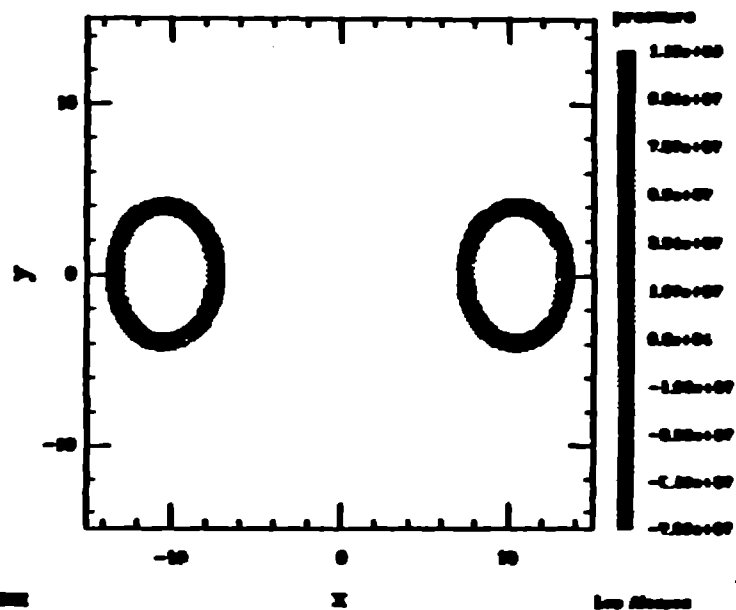
Tennis/16 Time = 2000.03 μs

pressure

3.58e+08
2.99e+08
2.4e+08
1.81e+08
1.22e+08
6.32e+07
4.09e+06
-5.5e+07
-1.14e+08
-1.73e+08
-2.32e+08
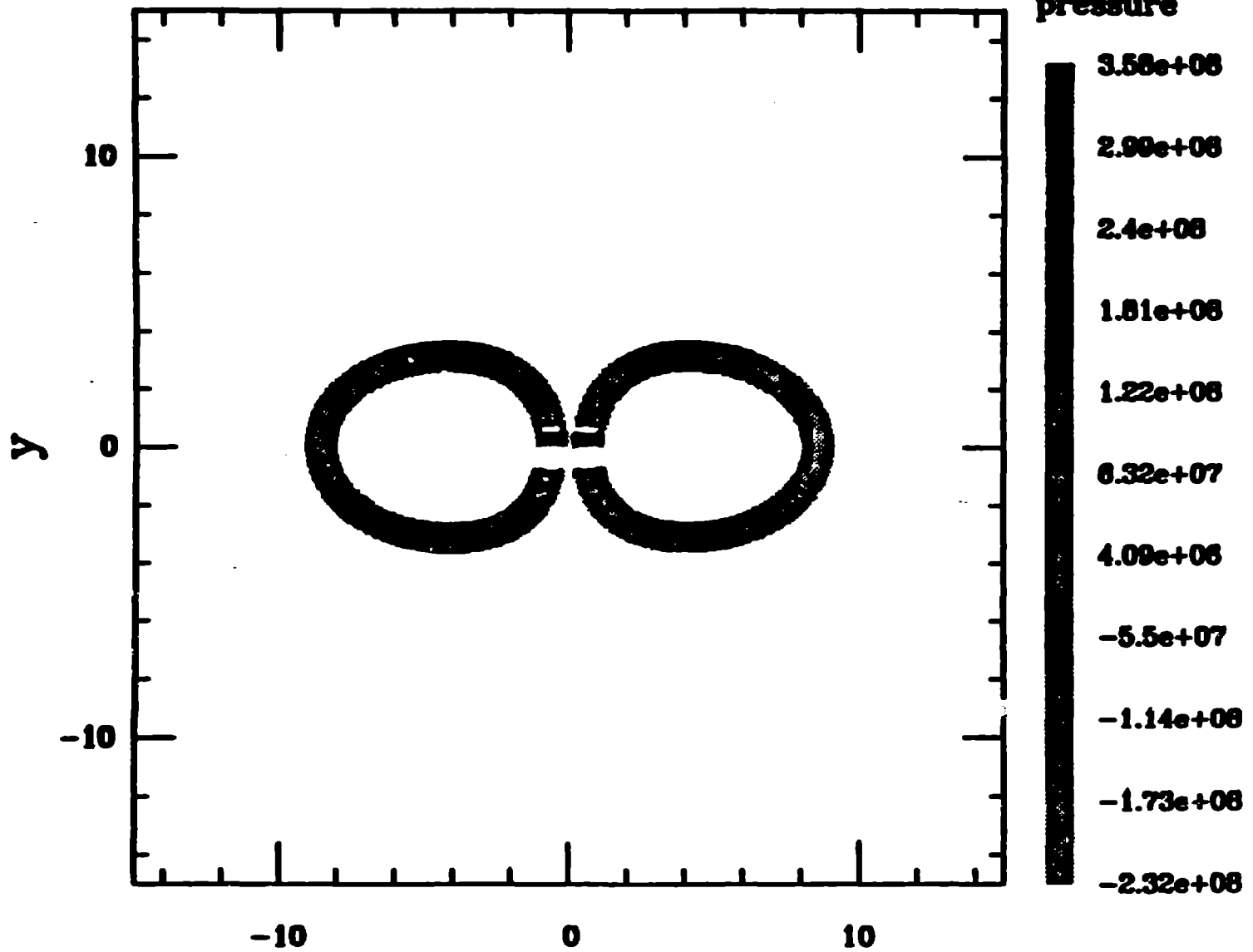
SPHINX   X   Los Alamos

Tennis/22 Time = 2001.14 μs
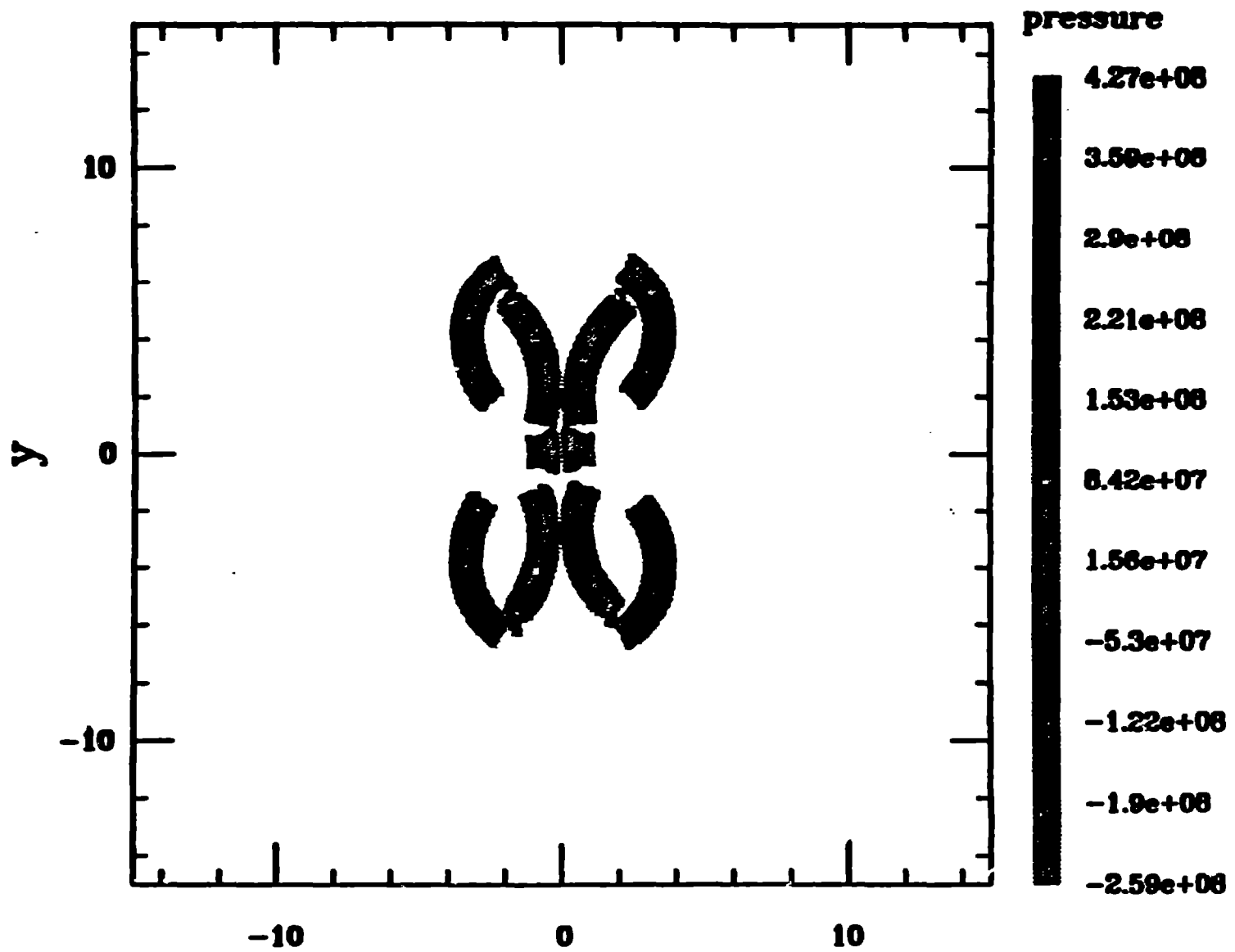
Fe rod impacting a rigid surface at 0.197 km/sec.
SPH calculations - 290 particles, cylindrical symmetry
The Johnson-Cook model matches the data much better.

Elastic Plastic   Johnson-Cook

Calculation

Data

-186-
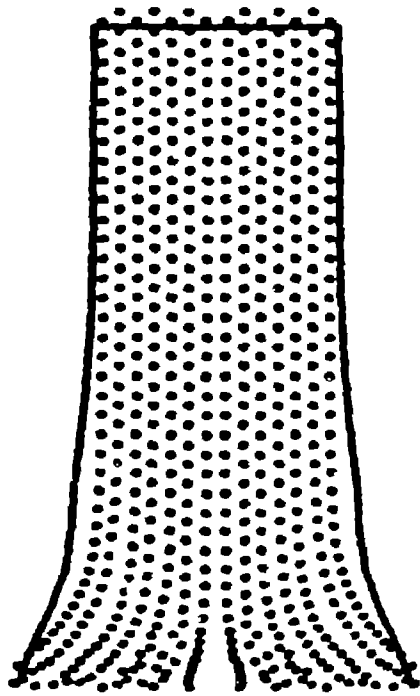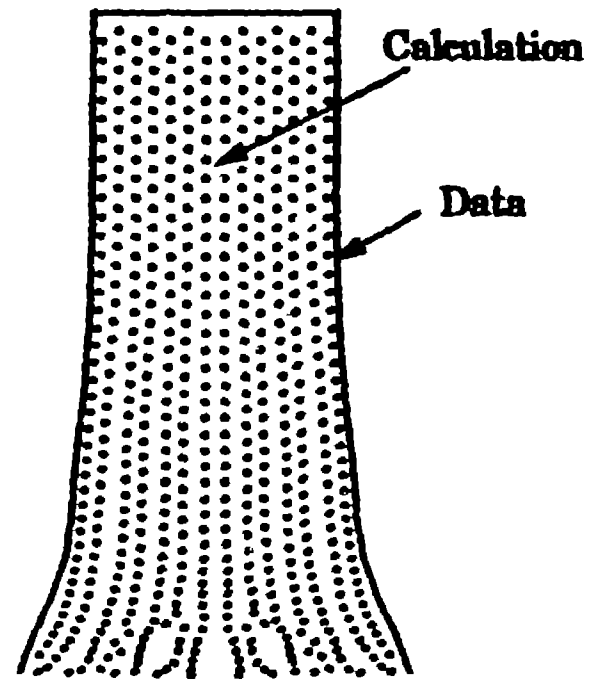
Los Alamos

Taylor Cylinder Problem
Vary Smoothing Length

Data = 2.04

max y (y-axis)

h (x-axis)

x-axis values: 0.00, 0.02, 0.04, 0.06, 0.08

y-axis values: 1.96, 1.98, 2.00, 2.02, 2.04, 2.06

nparticles:
4.12e+03
3.73e+03
3.33e+03
2.94e+03
2.54e+03
2.14e+03
1.75e+03
1.35e+03
957
561
165
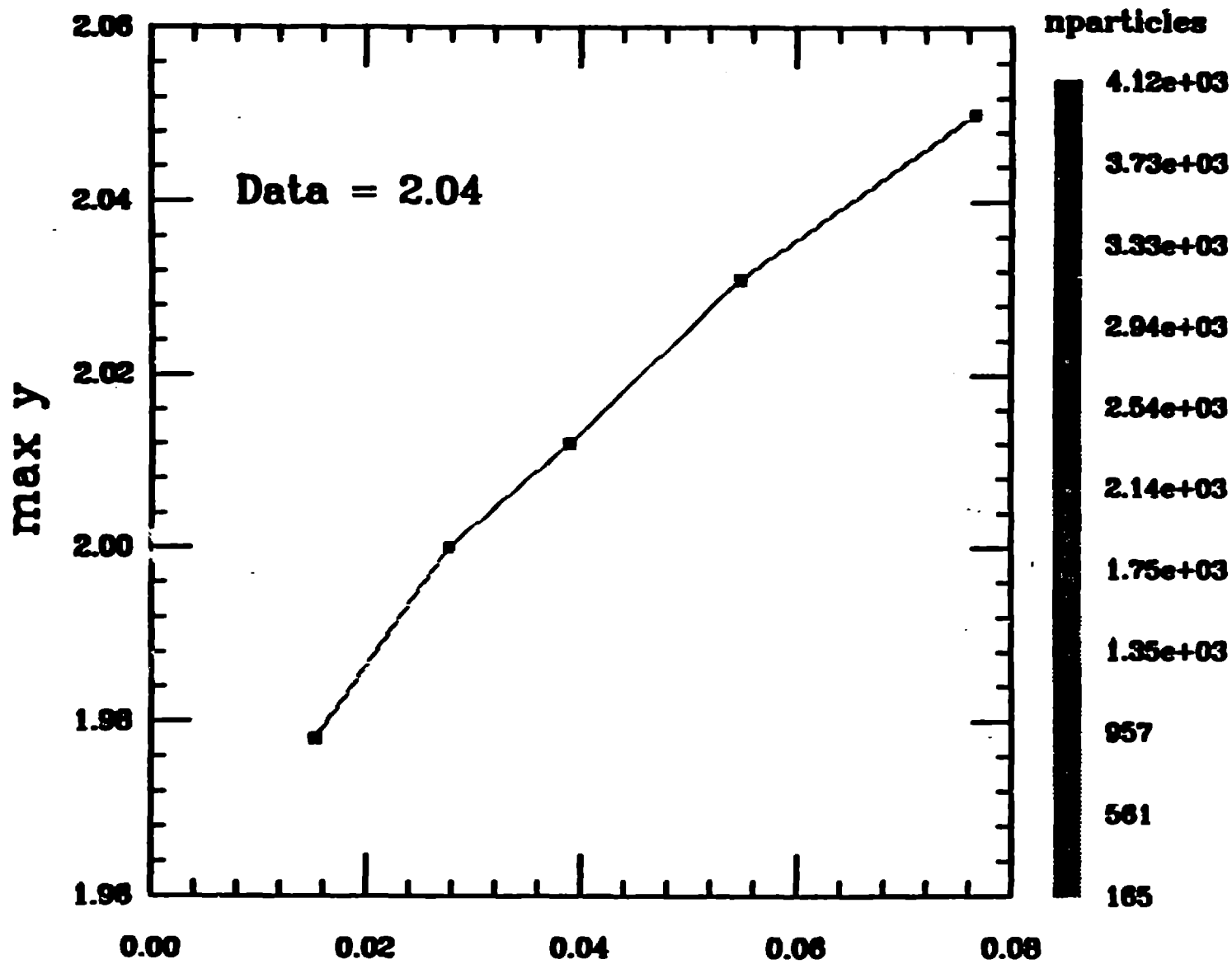
SPHC

Los Alamos

Shock Tube (Density Jump = 4) — SPH Results
90, 180, 360 particles and analytic

1.5 microsec
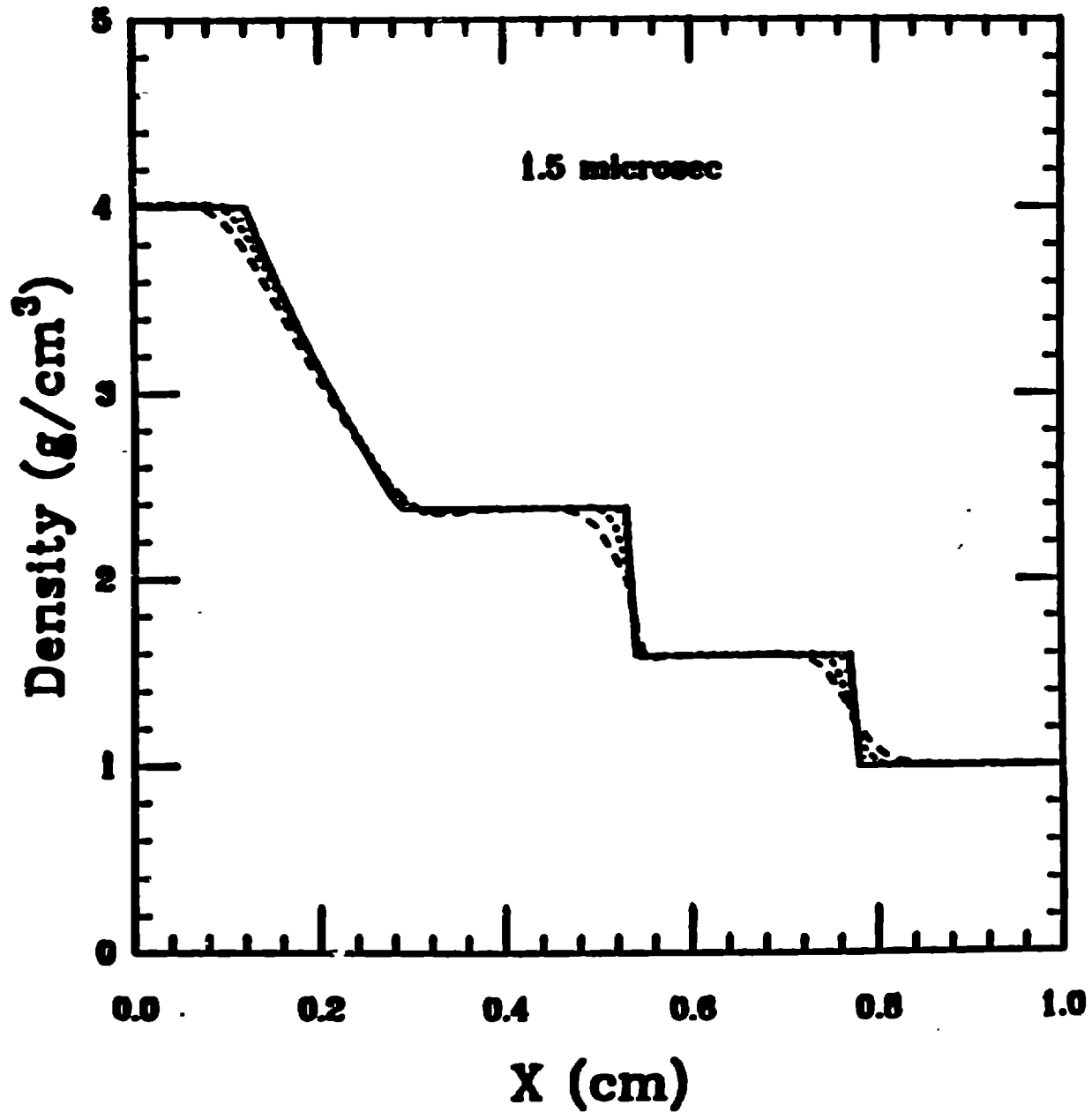
Strong Shock Tube (TP37C) – SPH Results
360 particles
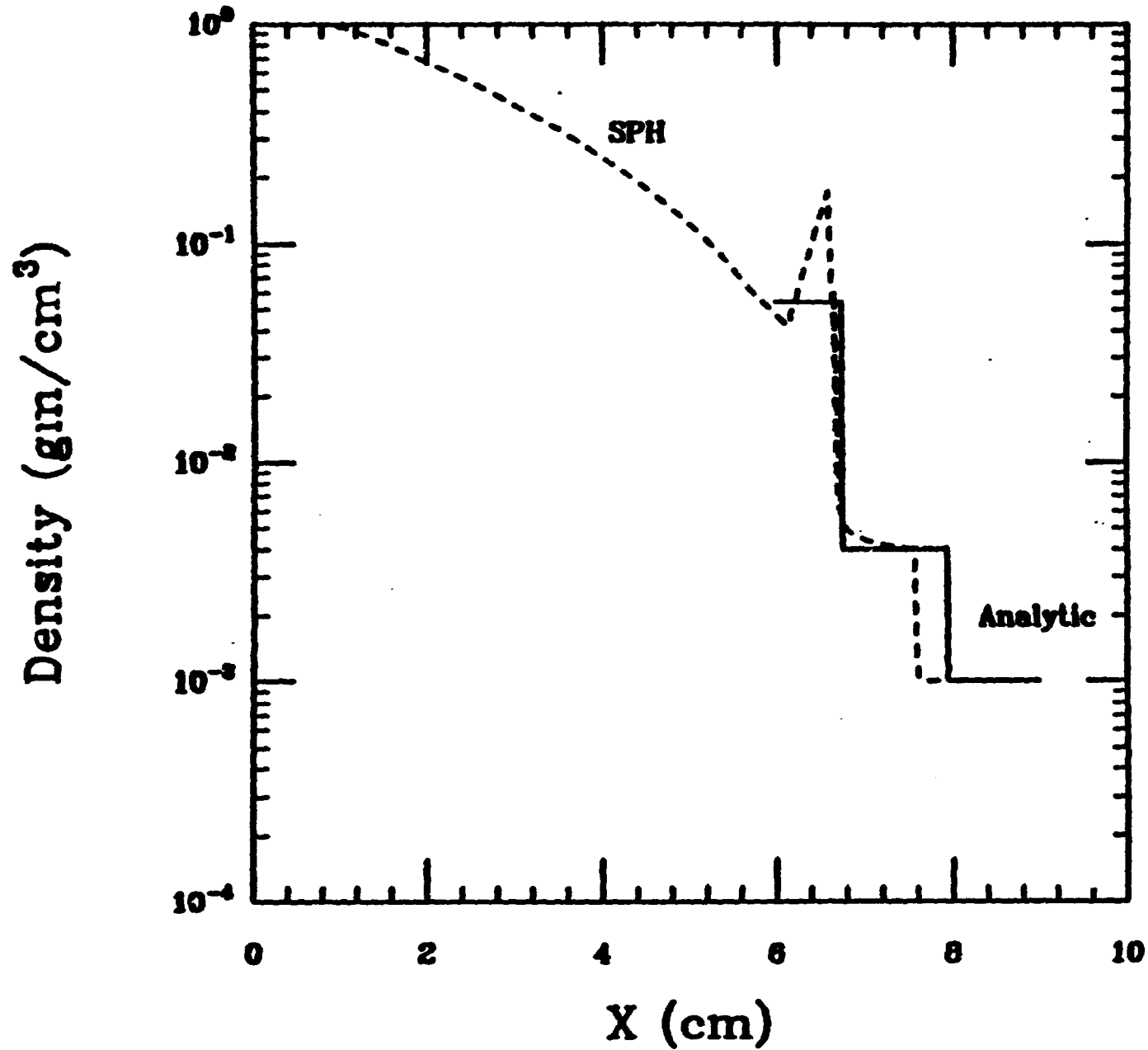
sec/06 Time = 0 μs
Cylindrical
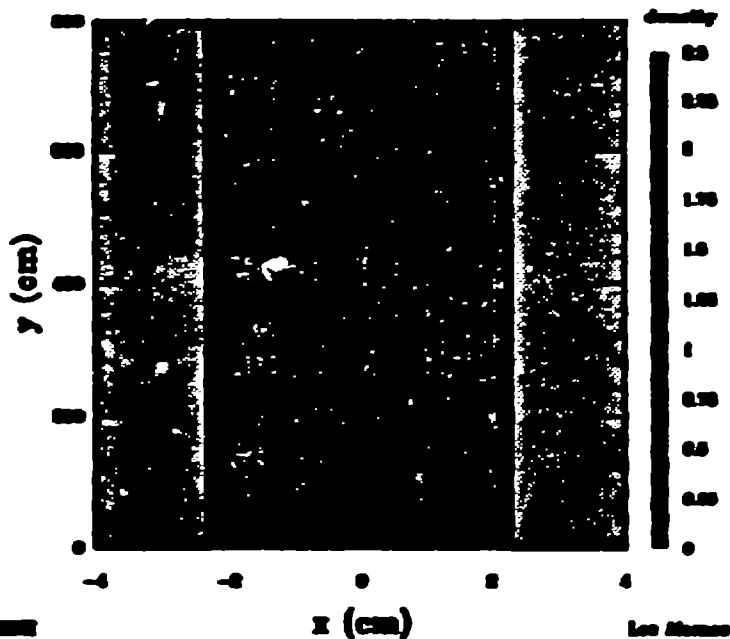
sec/06 Time = 6.00962 μs
Cylindrical
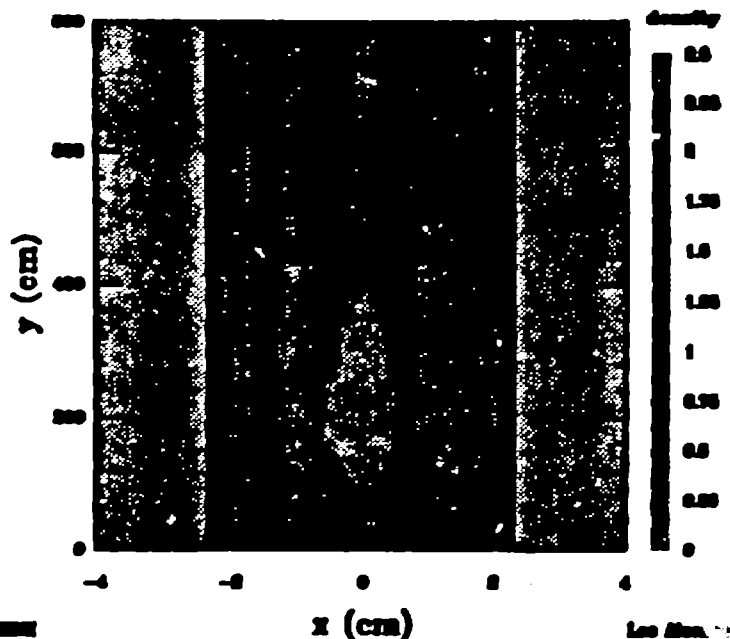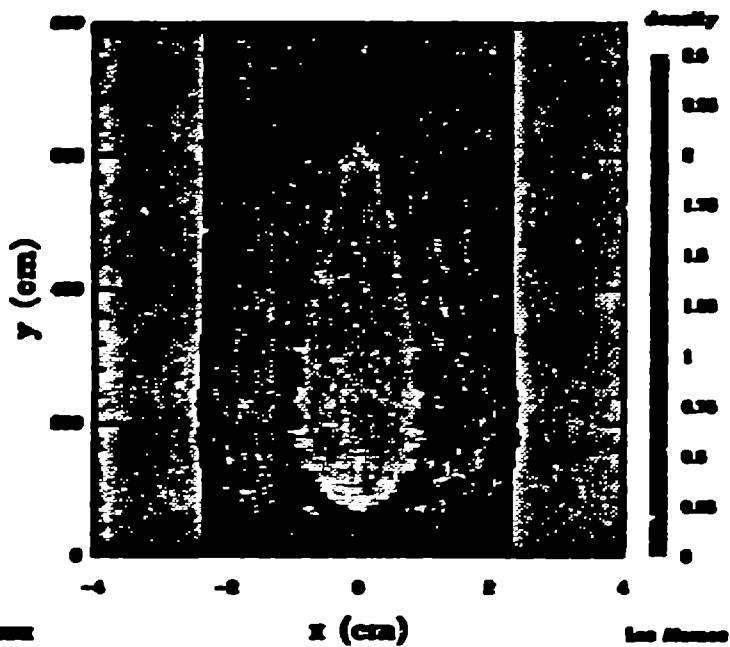
sec/06 Time = 12.0055 μs
Cylindrical

sec/06 Time = 18.0054 μs
Cylindrical
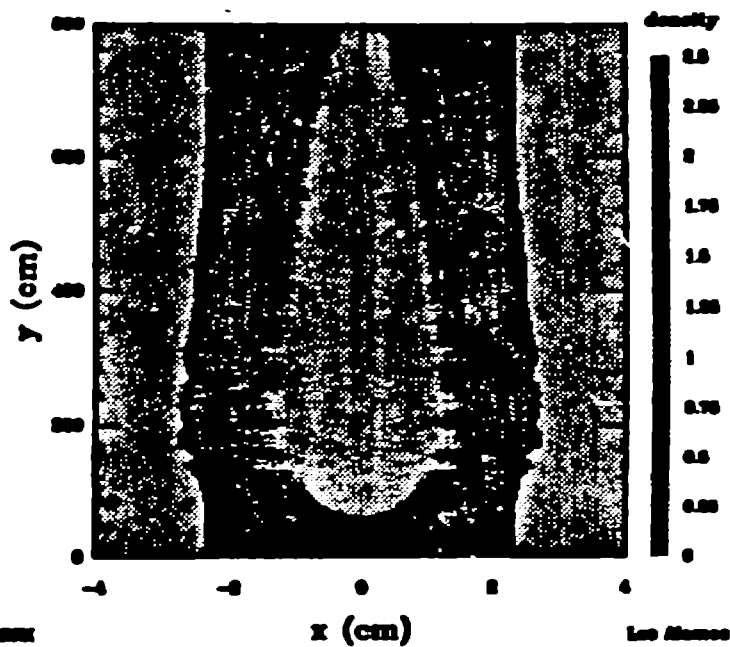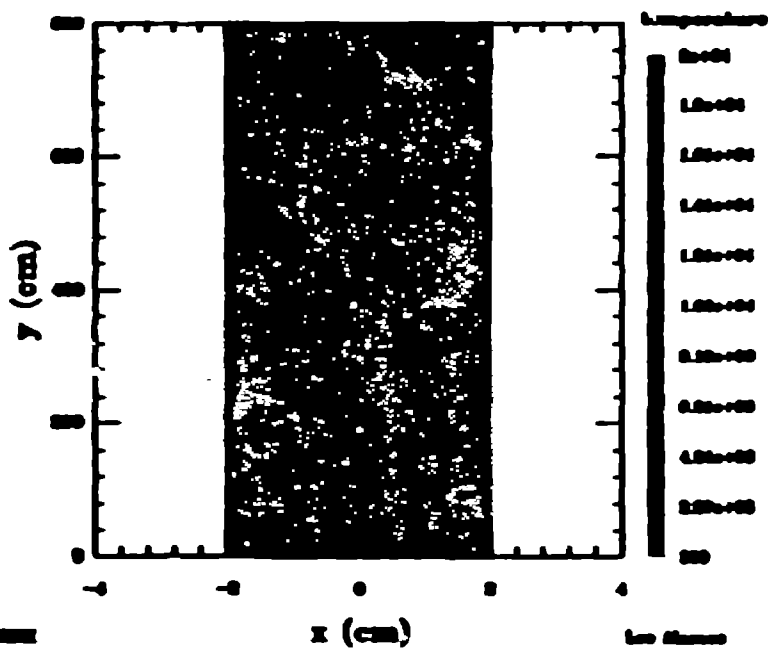
sec/06 Time = 0 μs
Cylindrical

sec/06 Time = 5.00062 μs
Cylindrical
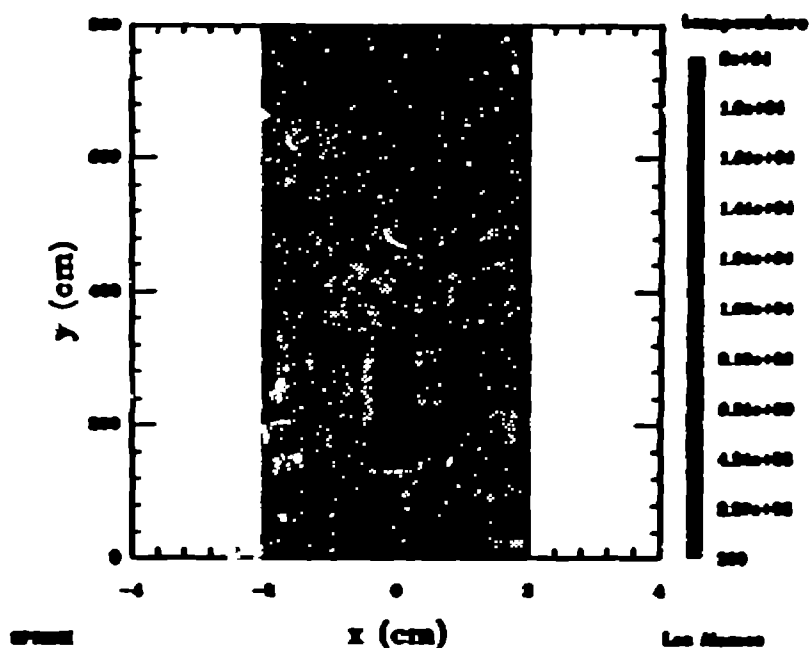
sec/06 Time = 12.0085 μs
Cylindrical
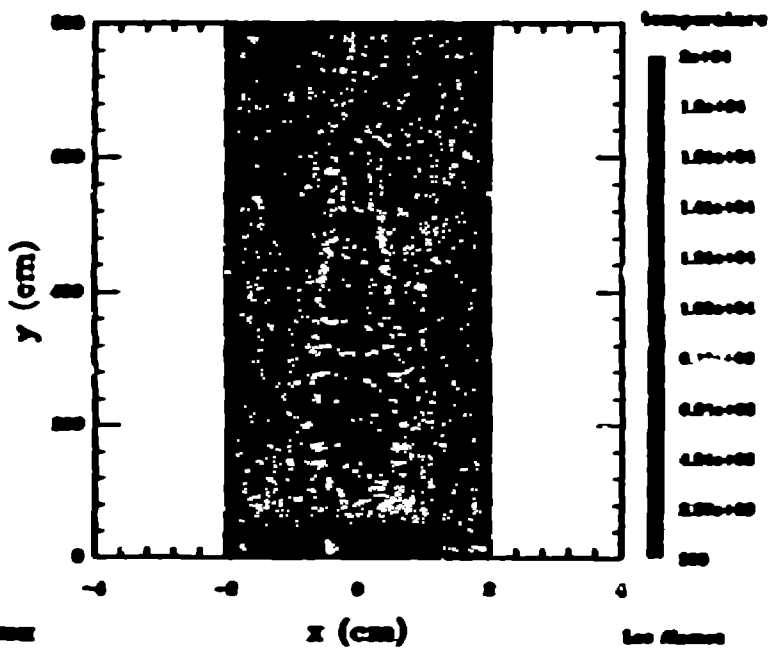
sec/06 Time = 16.0054 μs
Cylindrical
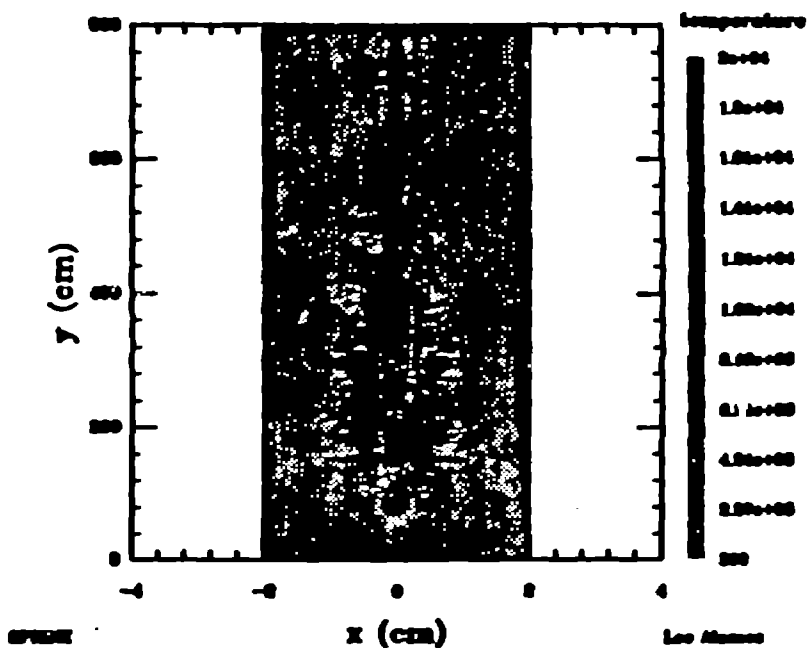
sec/10, x=0 slice, Time = 0 μs
3d, sweep beam z=0-1, 34000 particles
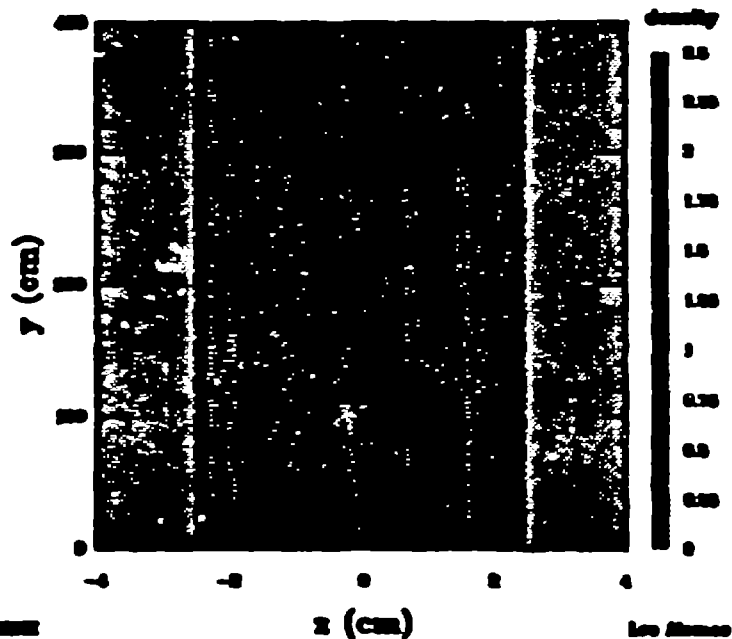
sec/10, x=0 slice, Time = 2.96391 μs
3d, sweep beam z=0-1, 34000 particles
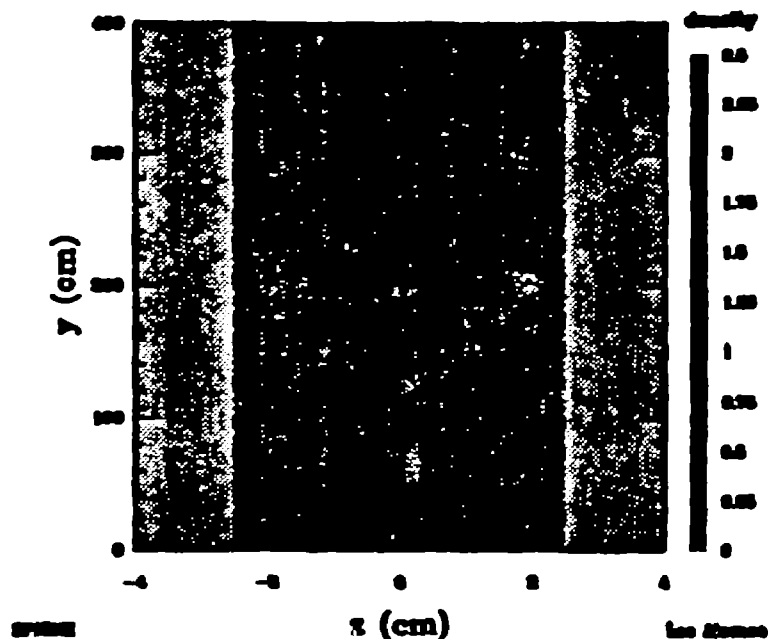
sec/10, x=0 slice, Time = 6.05757 μs
3d, sweep beam z=0-1, 34000 particles
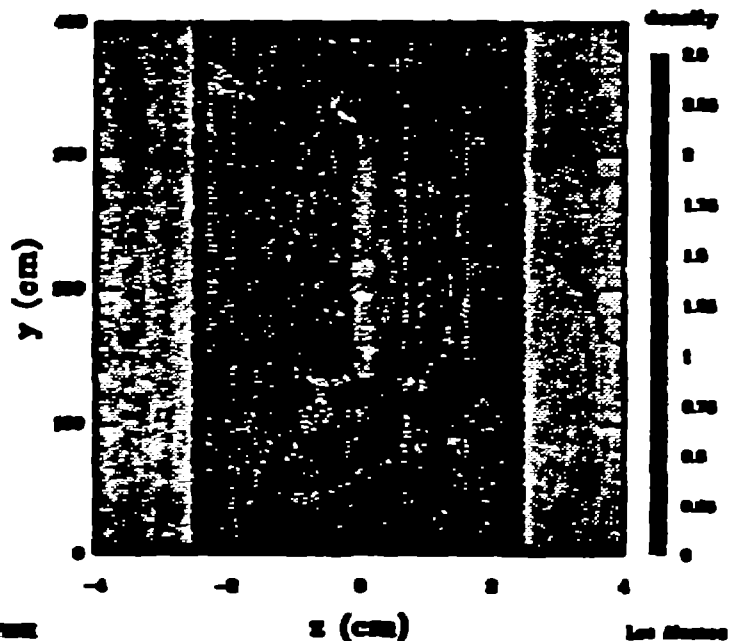
sec/10, x=0 slice, Time = 10.0427 μs
3d, sweep beam z=0-1, 34000 particles
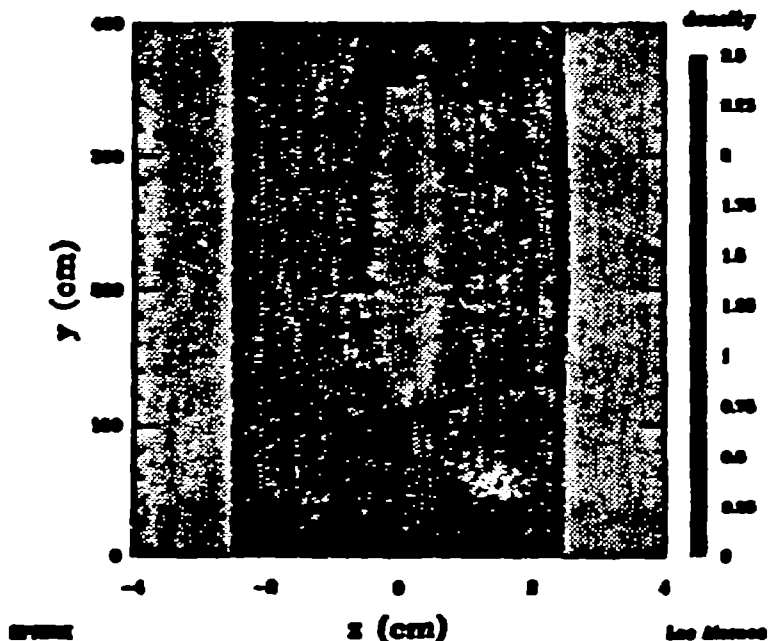
STABILITY AND CONSISTENCY OF THE SPH METHOD

J. W. Swegle[*] and D. L. Hicks[&]

[*]*Sandia National Laboratories*

[&]*Michigan Technological University*

Presented at the
Workshop on Advances in Smoothed Particle Hydrodynamics
LANL, September 21-22, 1993

Outline

1. Short review of stability criterion

2. Stability, the kernel function, and area vectors

3. Consistency of SPH

4. Adjustable factors in SPH numerics

-190-

Sandia
National
Laboratories

File=/net/sahp046/u12/jwswreg/framofiles/sph/wkshp993.vgs

JWS:1562:9/16/93

Stability Regimes

$W''T > 0 \implies$ unstable

$W''T < 0 \implies$ stable

<u>Cubic b-spline kernel</u>
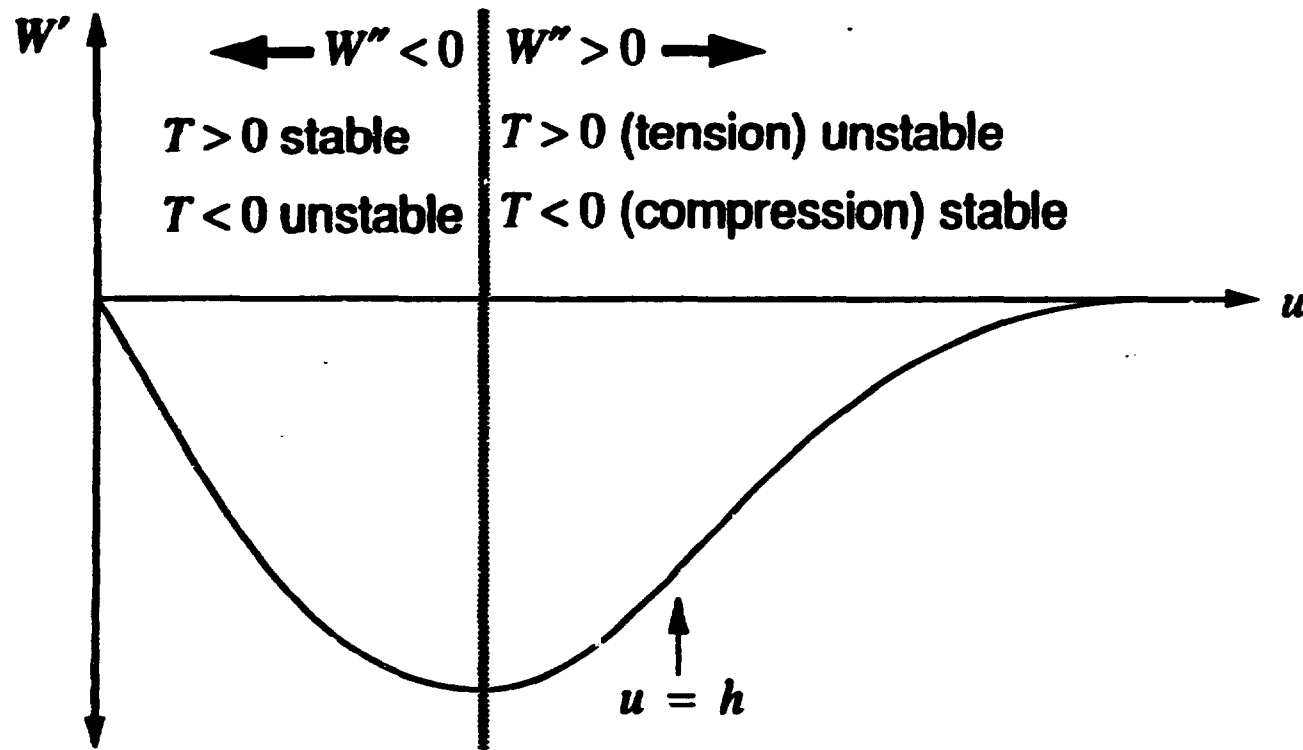
MATERIALS

MATERIALS
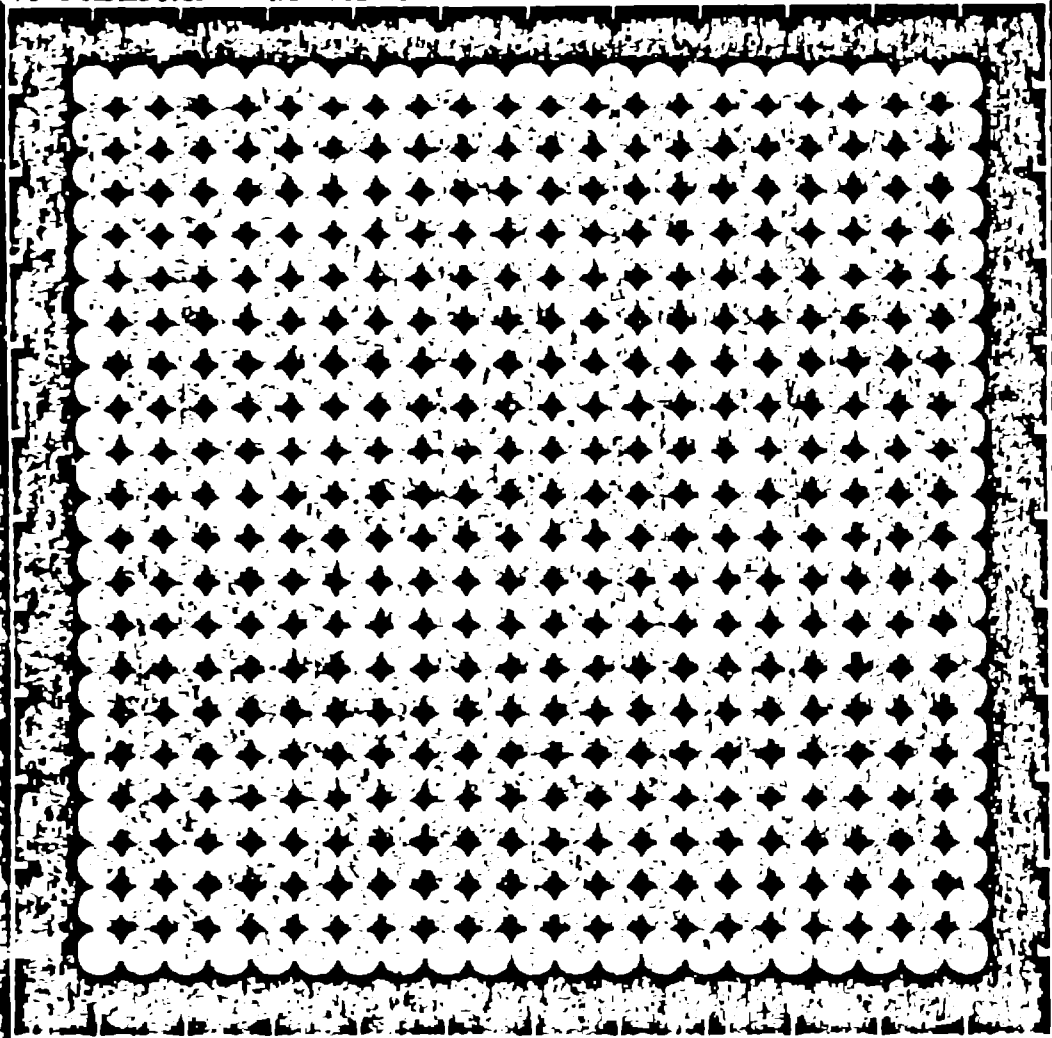
Physical Basis of Instability - Effective Stress

<u>Finite difference eqt of motion</u>

$$\ddot{x} = \frac{\partial \sigma}{\rho_0 \partial X} \approx \frac{\Delta \sigma}{\rho_0 \Delta X} = \frac{\Delta \sigma}{m}$$

<u>SPH eqt of motion</u>

$$\ddot{x} \sim \frac{\Delta(-\sigma W')}{m}$$

$\Rightarrow$ effective stress is $-\sigma(\varepsilon)\, W'(\varepsilon)$

<u>Kernel can cause instabilities</u>

- frequency dependence not taken into account

σ

σ

σ W'

ε

unstable | stable | unstable

-194-
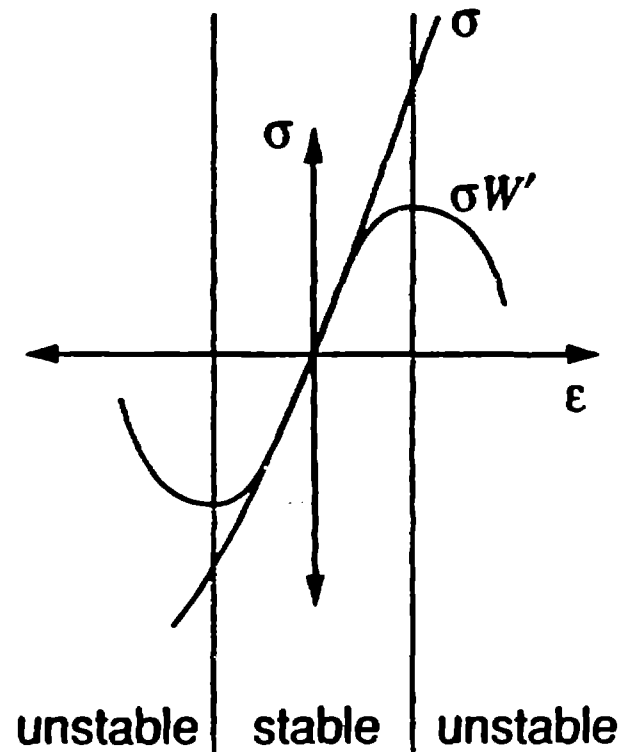
Effective Stress at Noise Frequency

Perturbation equation

$$\delta \ddot{x} \sim \delta(-\sigma W') = -\sigma \delta W' - W' \delta \sigma^{\nearrow 0}$$

$$\delta \ddot{x} = -\sigma \delta W' \text{ at } \lambda_{min}, \ \sigma \text{ constant}$$

$$\Rightarrow \quad \ddot{x} \sim \frac{-\sigma \Delta W'}{m}$$

$$\Rightarrow \quad \sigma_{eff} \sim -W' \ ; \text{ effective stress is a}$$

constant multiple of W' at λ_{min}

Tensile stress decreases with increasing particle separation.

Thus, noise frequency grows unboundedly when $W'' \sigma > 0$, so any level of tensile stress is unstable even at zero strain with cubic b-spline kernel.

Sandia National Laboratories
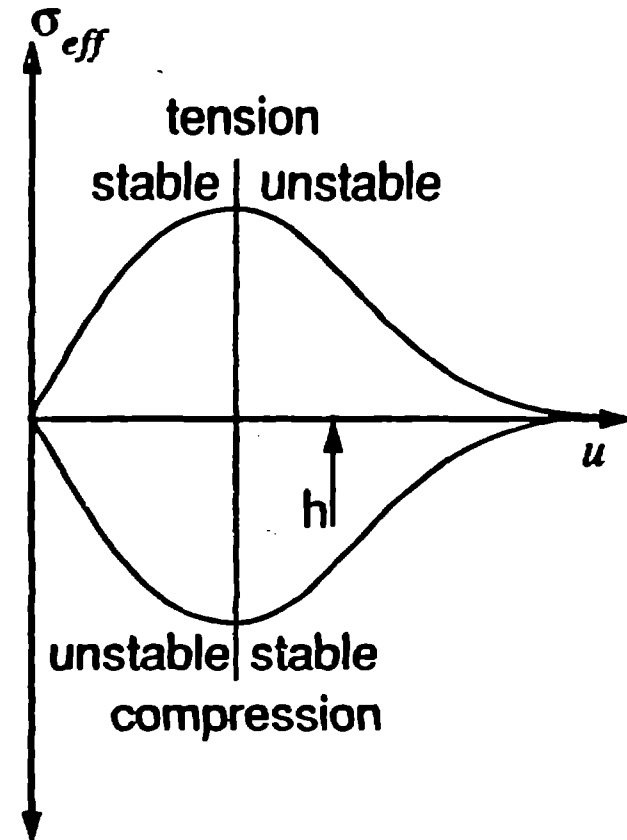
Stability Criterion for Arbitrary Smoothing Length

$$(W^{nd,I+1} + W^{nd,I+3} + W^{nd,I+5} + \ldots)\, T > 0 \qquad \Rightarrow \qquad \text{unstable}$$

$$(W^{nd,I+1} + W^{nd,I+3} + W^{nd,I+5} + \ldots)\, T < 0 \qquad \Rightarrow \qquad \text{stable}$$

Cubic b-spline kernel

$h = \Delta X$

$h = 1.5\Delta X$

$h = 2\Delta X$

$h = 3\Delta X$

JWS:1433:1/20/93
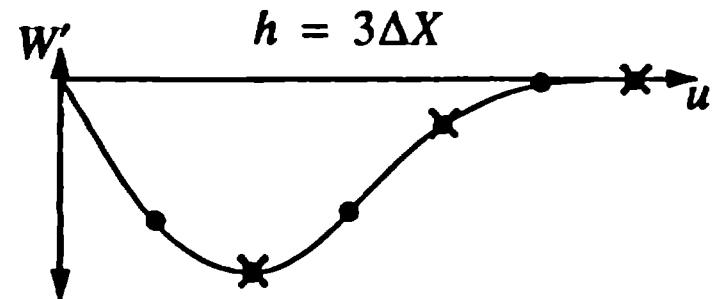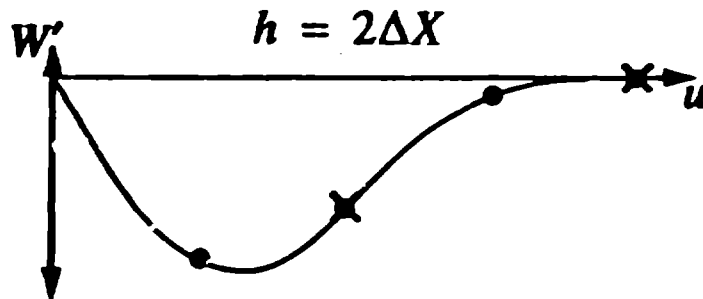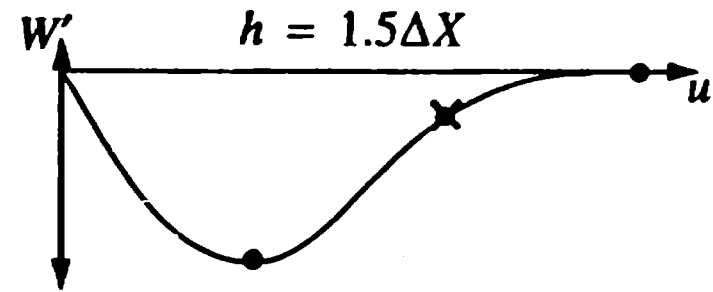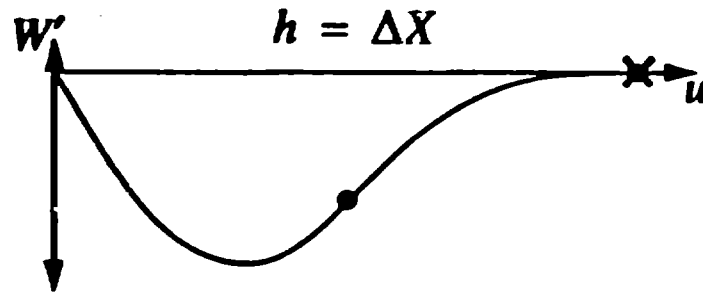
Kernel Function and Instability

Stability is guaranteed in all regimes when $W'' = 0$

- However, such kernels have other difficulties
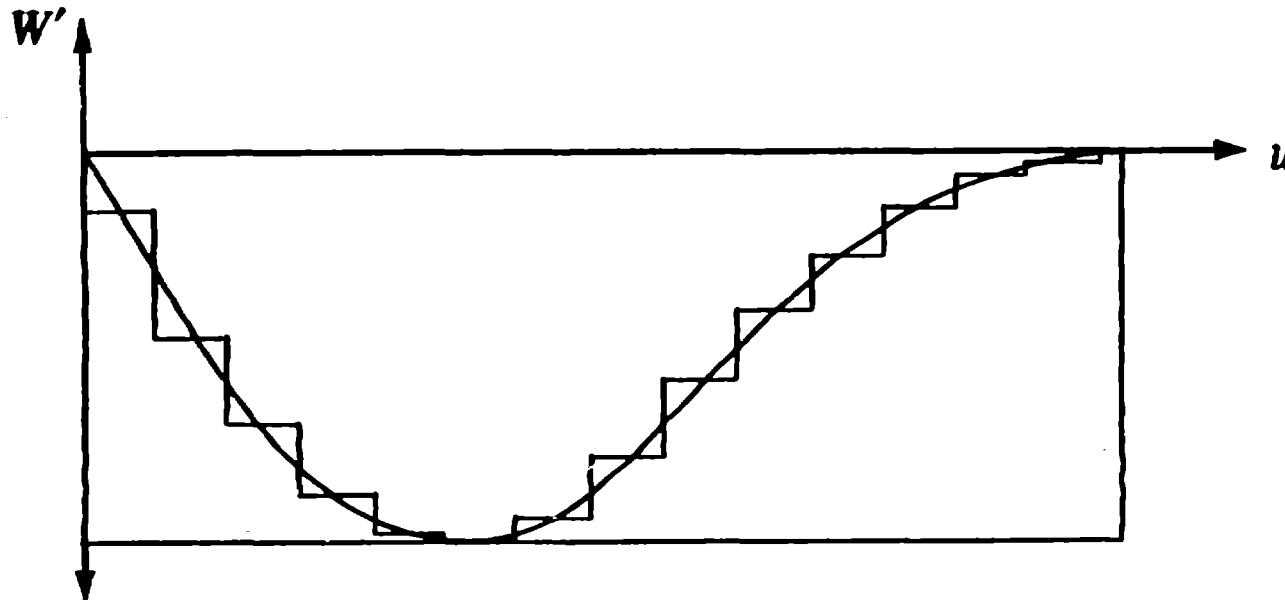
The SPH kernel has a conflict between stability in the tensile regime and the requirement of local support

-197-

CROSS PLOT

ABS(VELOCITY)

ALUMINUM → TENSION
GAS → COMPRESSION

TIME

J12G12D Z1X2 RECT AR=.95R0/PERTV=1.E-10/NOV

TOOHIST 01:09/15/93 15:28:42

PRESSURE COLORSCALE
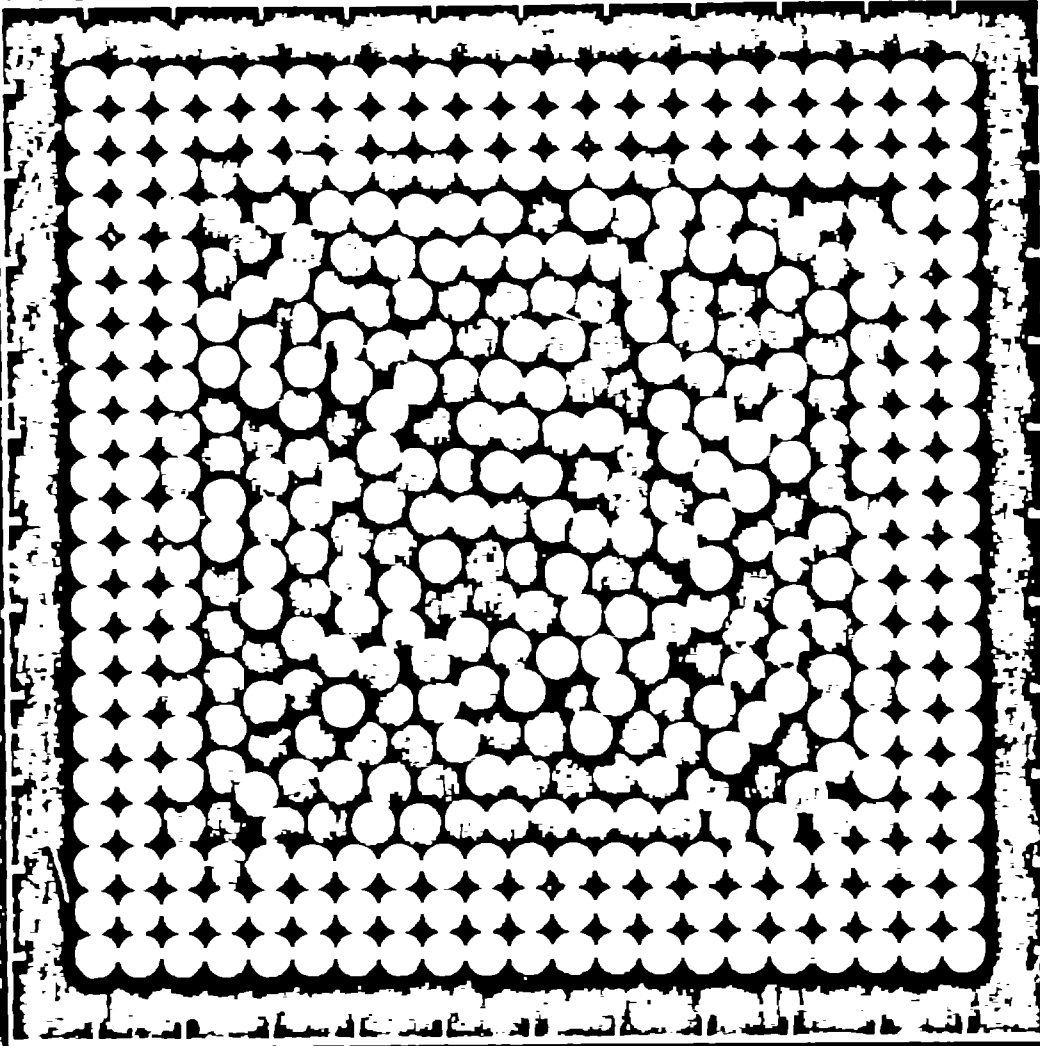
X COORDINATE

Z COORDINATE

CYCLE = 230 TIME= 1.000E-02
GB2GAS BUBBLE STABILITY - NO VISC
SMPLOT U1 08/10/93 13:03:21

Stress, Force, and Area Vectors

$$\vec{F} = \sigma \bullet \vec{A}$$

$\vec{A}$ is normal to surface with magnitude equal to area
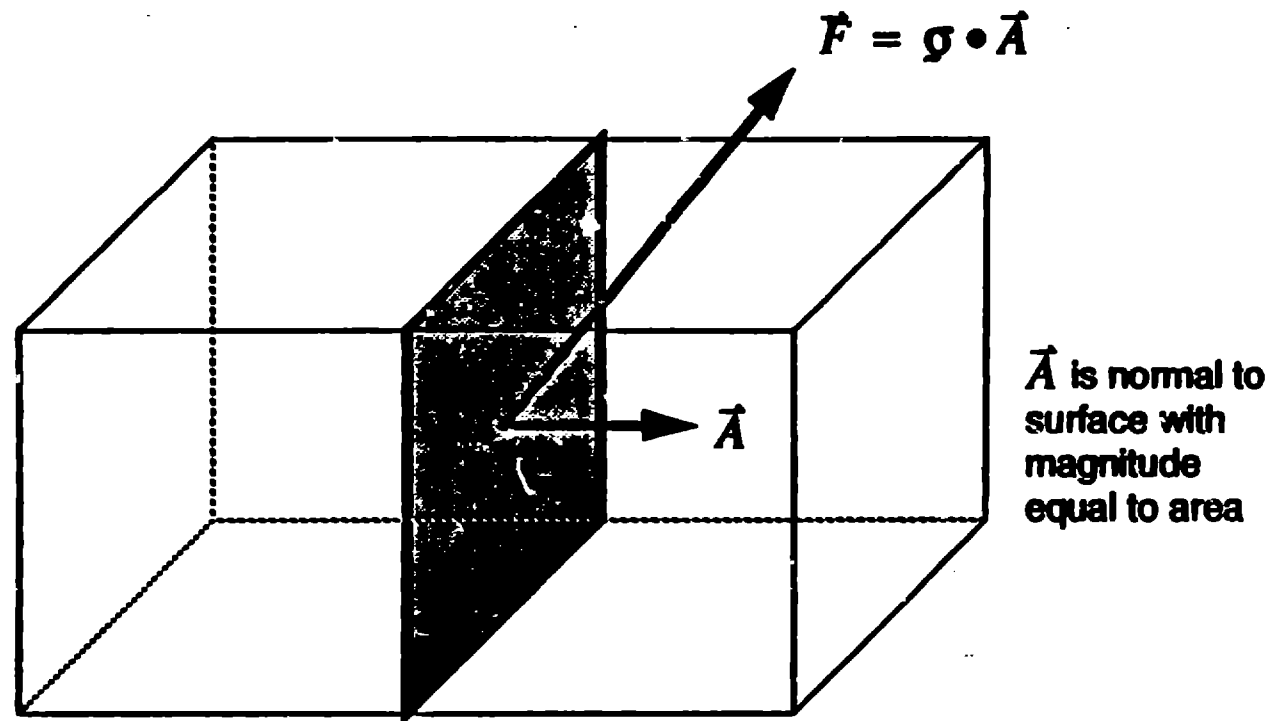
Total force: sum over all areas

$$\vec{F}_t = \sum_{i=1}^{n} \sigma_i \bullet \vec{A}_i$$

SPH and Area Vectors

$$\vec{F}^{IJ} = \sigma^{IJ} \bullet \vec{A}^{IJ}$$

$$\vec{A}^{IJ}$$

J

I

Interaction area between particles I and J
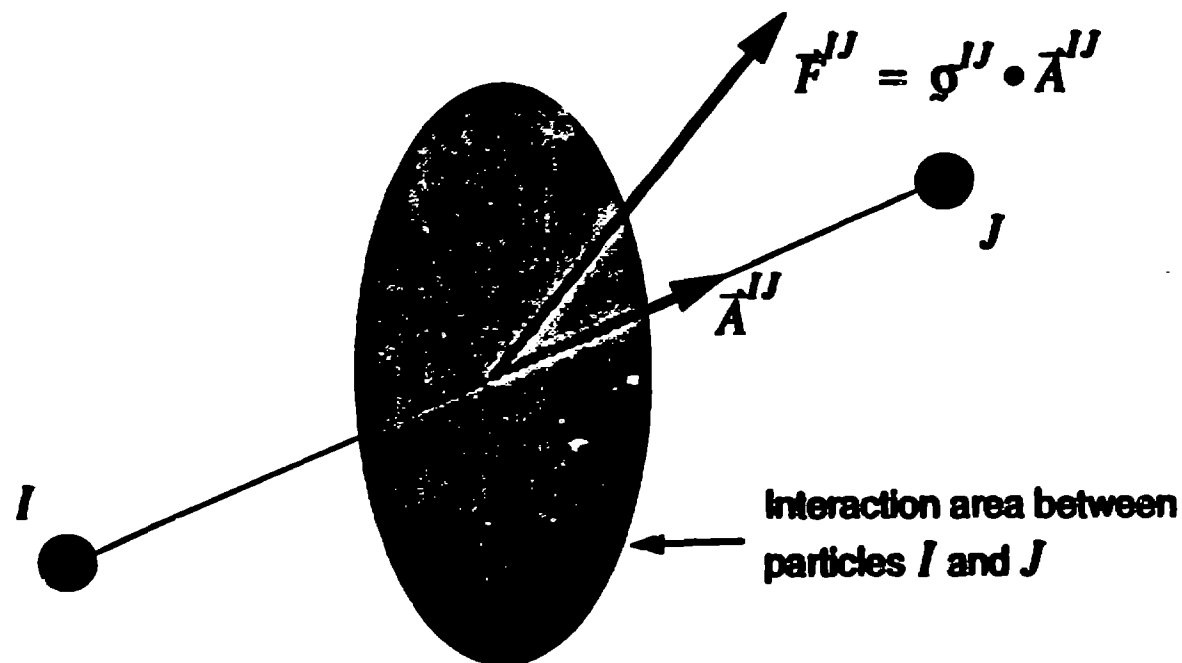
Kernel function defines area vectors

$$\vec{F}^I = m^I \vec{a}^I = -\sum_{J=1}^{N} \frac{m^I m^J}{\rho^I \rho^J} \sigma^{IJ} \bullet \nabla_J W = \sum_{J=1}^{N} \sigma^{IJ} \bullet \vec{A}^{IJ}$$

$$\Longrightarrow \quad \vec{A}^{IJ} = -\frac{m^I m^J}{\rho^I \rho^J} \nabla_J W = -Vol^I Vol^J \nabla_J W$$

Sandia National Laboratories

Area Vectors in 1D
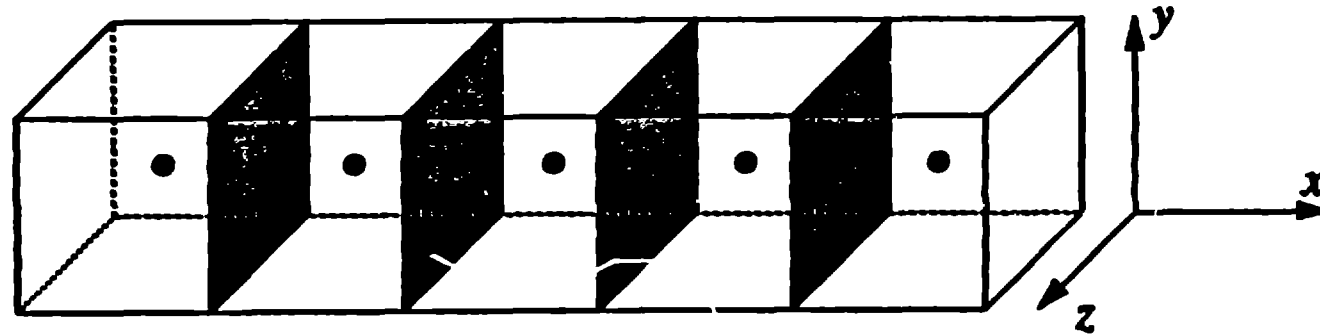
- No y, z motion means areas are constant by definition
- SPH areas depend on the interparticle separation
- Variable smoothing length reduces area variations
    - areas are still not constant if h is density-based
    - still unstable in tension
- Setting area vectors constant removes instability
    - spatial difference scheme is Lax-Wendroff

Multi-dimensional Area Vectors
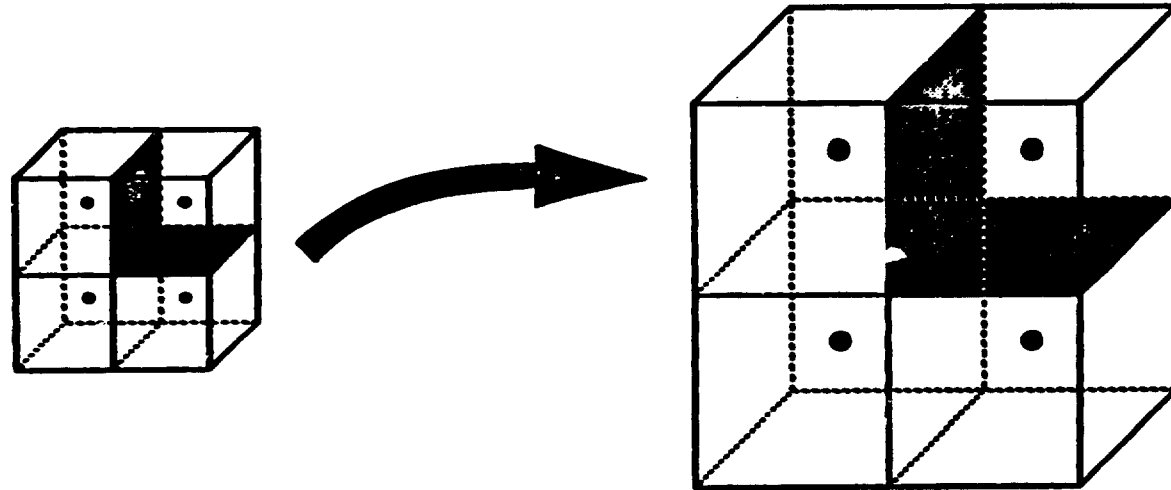
- **Areas should increase in uniform expansion if body is intact**
  - **SPH areas decrease**
- **Areas should depend on transverse dimensions**
  - **SPH areas depend only on particle separation**
- **Method based on estimation of areas might be useful approach**
  - **begins to look like free Lagrange method**

Consistency

Definition of consistency: *the discretized forms reduce to the differential forms*

Continuum equation of motion

$$\rho \ddot{x}^J = \nabla \bullet \sigma$$

Symmetrized SPH equation of motion

$$\ddot{x}^J = -\sum_{J=1}^{N} m^J \left[\left(\frac{\sigma}{\rho^2}\right)^J + \left(\frac{\sigma}{\rho^2}\right)^I \right] \bullet \nabla_J W$$

The above SPH form of the equation of motion is not consistent with the continuum equation.

-204-

Example: Accelerations at a Material Interface
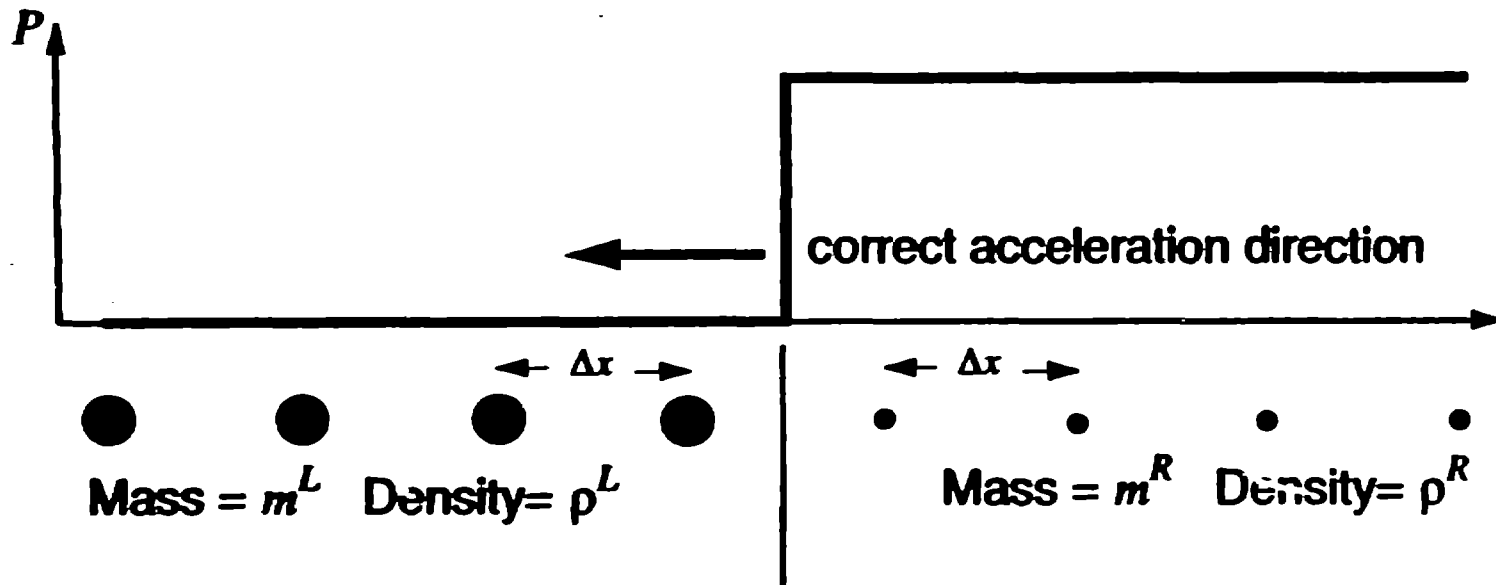
- Standard SPH accelerations do not correspond to $-\Delta P/(\rho\Delta x)$

- Low mass particle is accelerated in wrong direction if $m^L > 2m^R$

- Accelerations are obtained even if P is constant across interface

Sandia National Laboratories

Alternate Equation of Motion

Standard SPH equation of motion responds to density gradient

$$\ddot{x}^I = -\sum_{J=1}^{N} m^J \left[\left(\frac{\sigma}{\rho^2}\right)^J + \left(\frac{\sigma}{\rho^2}\right)^I \right] \bullet \nabla_J W \implies \ddot{x}^I \sim \nabla \bullet \left(\frac{\sigma}{\rho}\right)$$

Direct derivation leads to asymmetric form

$$\langle \nabla \bullet \hat{f} \rangle = -\sum_{J=1}^{N} \frac{m^J}{\rho^J} f^J \bullet \nabla_J W \implies \ddot{x}^I = -\sum_{J=1}^{N} m^J \left(\frac{\sigma^I}{\rho^I \rho^J}\right) \bullet \nabla_J W$$

Alternate symmetrization

$$0 \approx -\sum_{J=1}^{N} \frac{m^J}{\rho^J} \nabla_J W \implies \ddot{x}^I = -\sum_{J=1}^{N} m^J \left(\frac{\sigma^I + \sigma^J}{\rho^I \rho^J}\right) \bullet \nabla_J W$$

This form seems to behave correctly at density discontinuities.

-206-

PRESSURE COLORSCALE

Y COORDINATE

Z COORDINATE

MATERIALS

X COORDINATE

Z COORDINATE

$TIME = 1.000E-02$

FIG. 2D. ROUND AIR BUBBLE IN TANK 1.7 KBAR-REG EOV
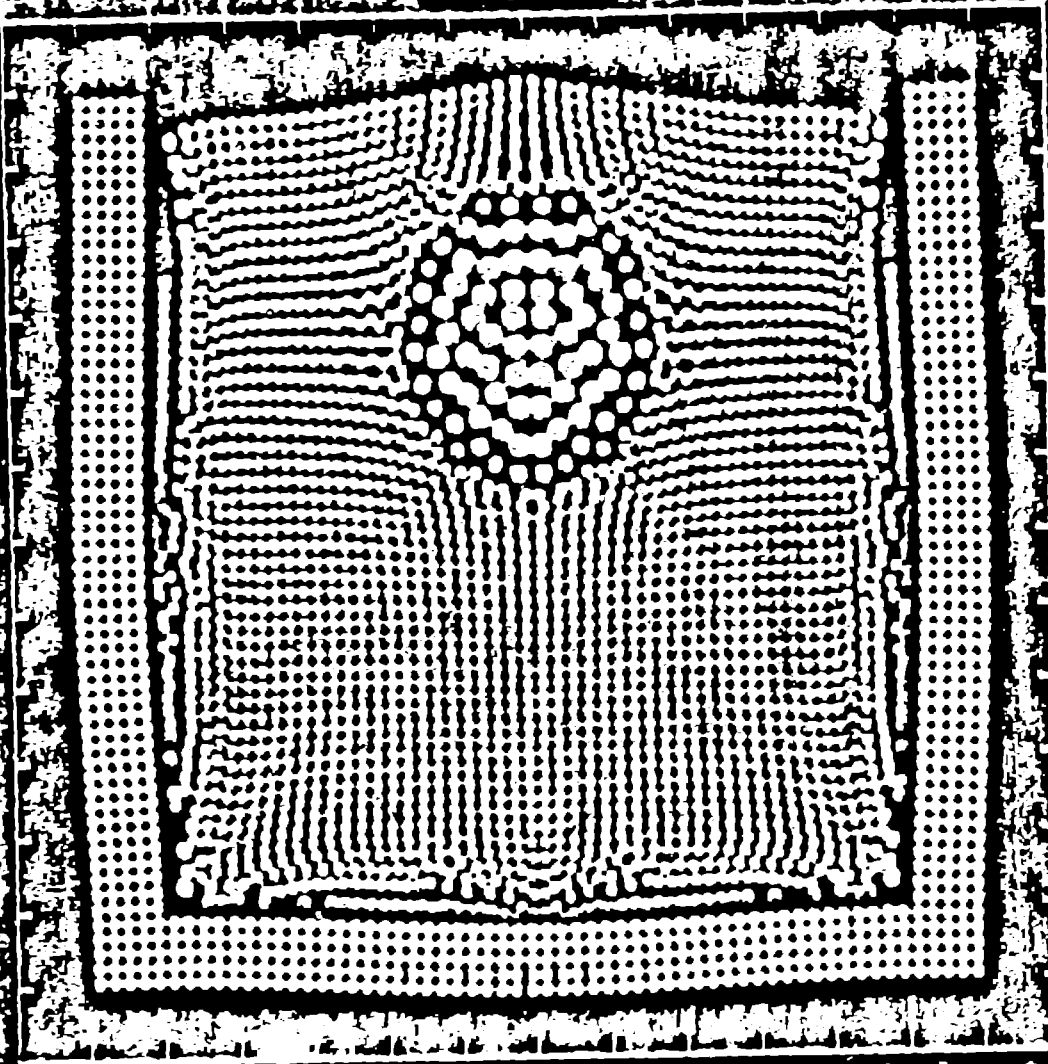
SV-LOT UI 09/14/93 14:02:21
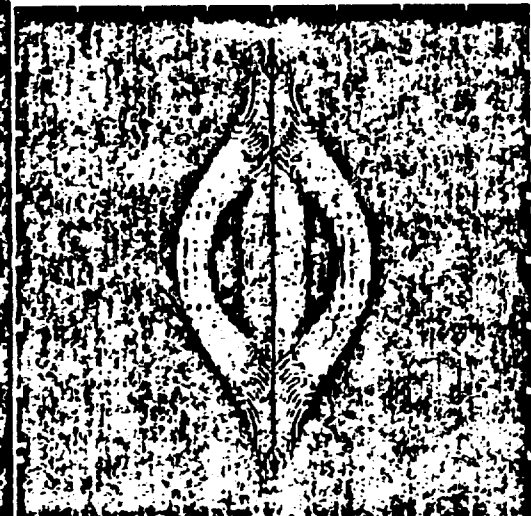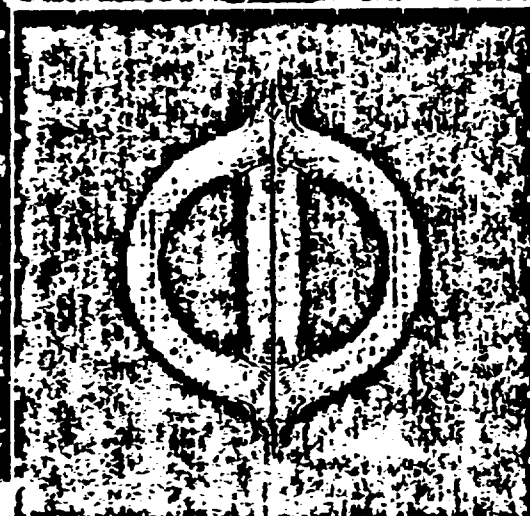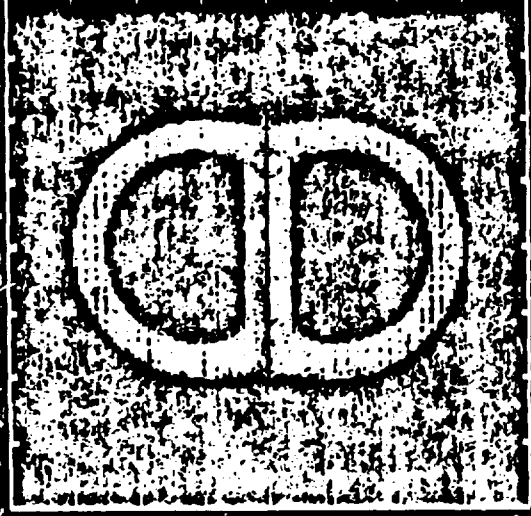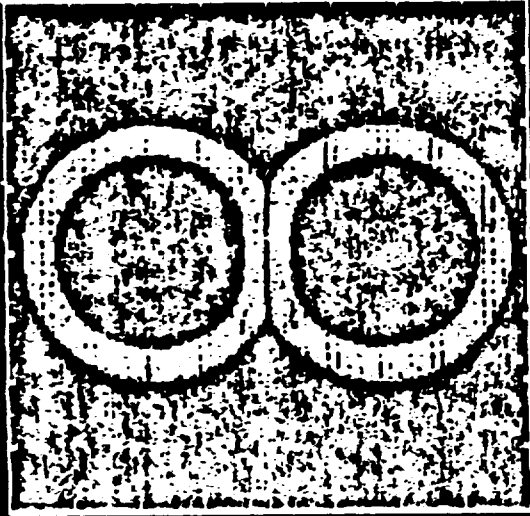
Consistency and the Kernel Function

Normality condition

$$\int W(x, h)\, dx = 1$$

Consistency requirement

- in 1D ($h = \Delta x$), consistency (correct gradient) requires

$$W'(x = h) = -\frac{1}{2h^2}$$

Consistency and normality are not equivalent

- cubic b-spline (W_4) satisfies both consistency and normality

- solving $\dfrac{\dot{\rho}}{\rho} = -\nabla \bullet \vec{V}$, not $\rho(x) = \displaystyle\sum_{J=1}^{N} m^J W(x - x^J, h)$ for density

$\Longrightarrow$ normality condition is irrelevant, since W never appears

Adjustable Factors in SPH Numerics

- *Resolution*
- *Viscosity coefficients*
- *Stability criterion (stable time step factor)*
- Smoothing length/particle spacing ratio (3)
- Constant smoothing length **vs.** variable smoothing length (2)
- Kernel sum density **vs.** continuity equation (2)
- Von Nuemann Richtmyer viscosity **vs.** SPH (Monaghan) viscosity (2)
- Initial particle packing (rectangular, hexagonal, radial) (2)
- Ordered particle distribution **vs.** perturbed particle distribution (2)

- Equation of motion symmetrization ($\left(\dfrac{\sigma}{\rho^2}\right)^I + \left(\dfrac{\sigma}{\rho^2}\right)^J$, $\dfrac{\sigma^I + \sigma^J}{\rho^I \rho^J}$, etc.) (2)

- Velocity gradient symmetrization ($\dfrac{m^J}{\rho^I}(V_i^I - V_i^J)\dfrac{\partial W}{\partial x_j^I}$, $\dfrac{m^J}{\rho^J}(V_i^I - V_i^J)\dfrac{\partial W}{\partial x_j^J}$) (2)

- Kernel function (splines, exponential, gaussian, super-gaussian) (3)

Number of combinations = 3 x 2 x 2 x 2 x 2 x 2 x 2 x 2 x 3 = 1152

-214-
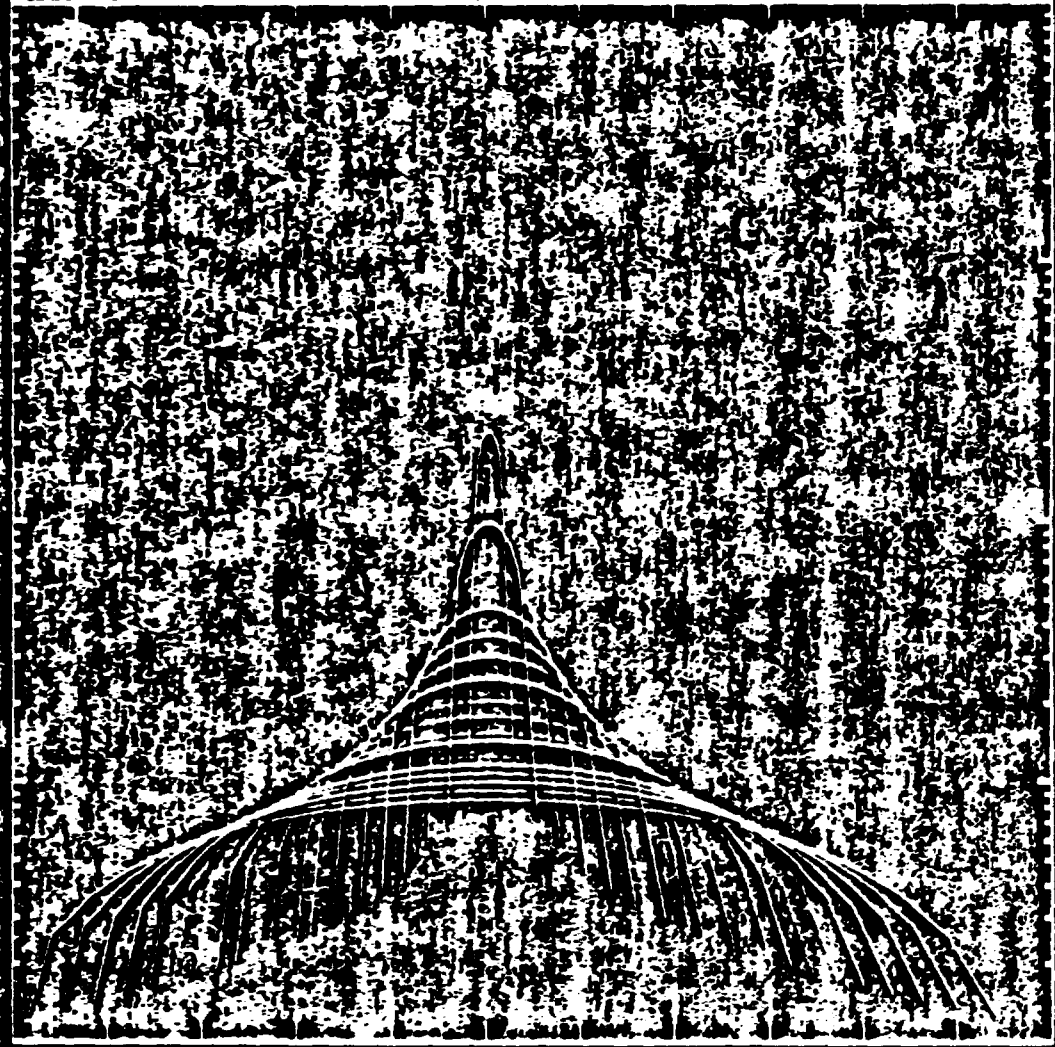
DENSITY (COLORSCALE)

-216-

LINE PLOTS ALONG U=Z AT FIXED TIMES

DENSITY

Z COORDINATE

CYCLE   265   TIME   0.33E+02

FREE RECT COORD BUBBLE KBAR

Calculational Matrix

	$h = \Delta x$	$h = 2\Delta x$
Continuity equation	Continuity $h = \Delta x$	Continuity $h = 2\Delta x$
Kernel sum density	Kernel sum $h = \Delta x$	Kernel sum $h = 2\Delta x$
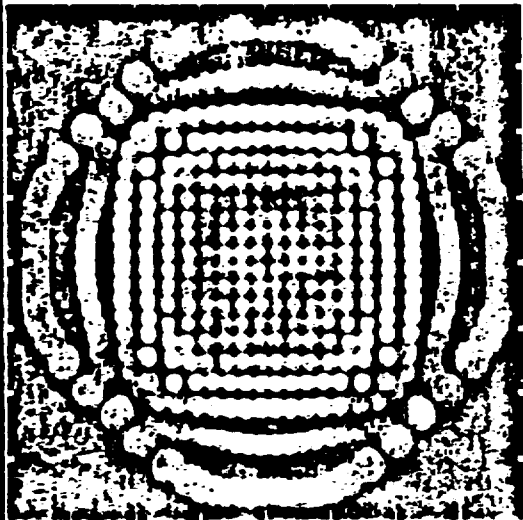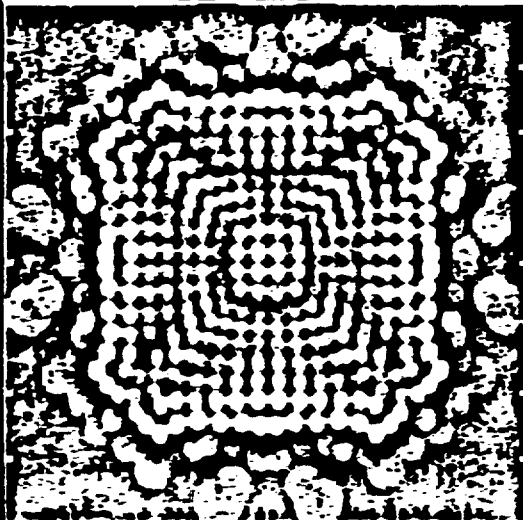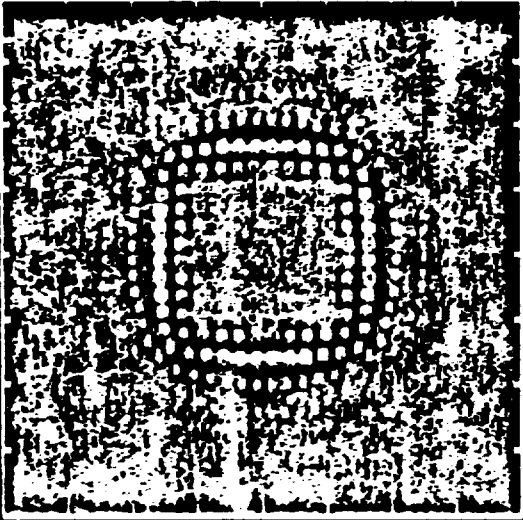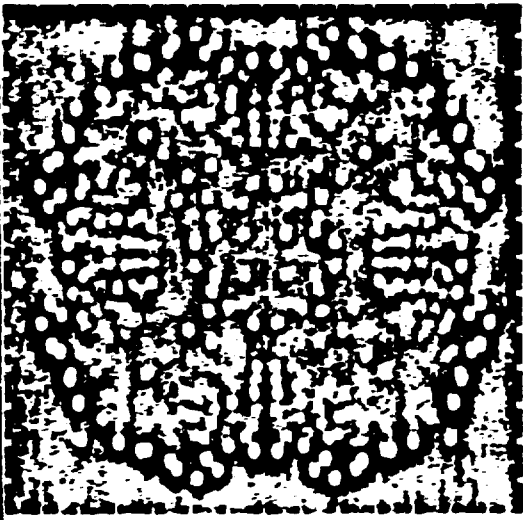
-217-
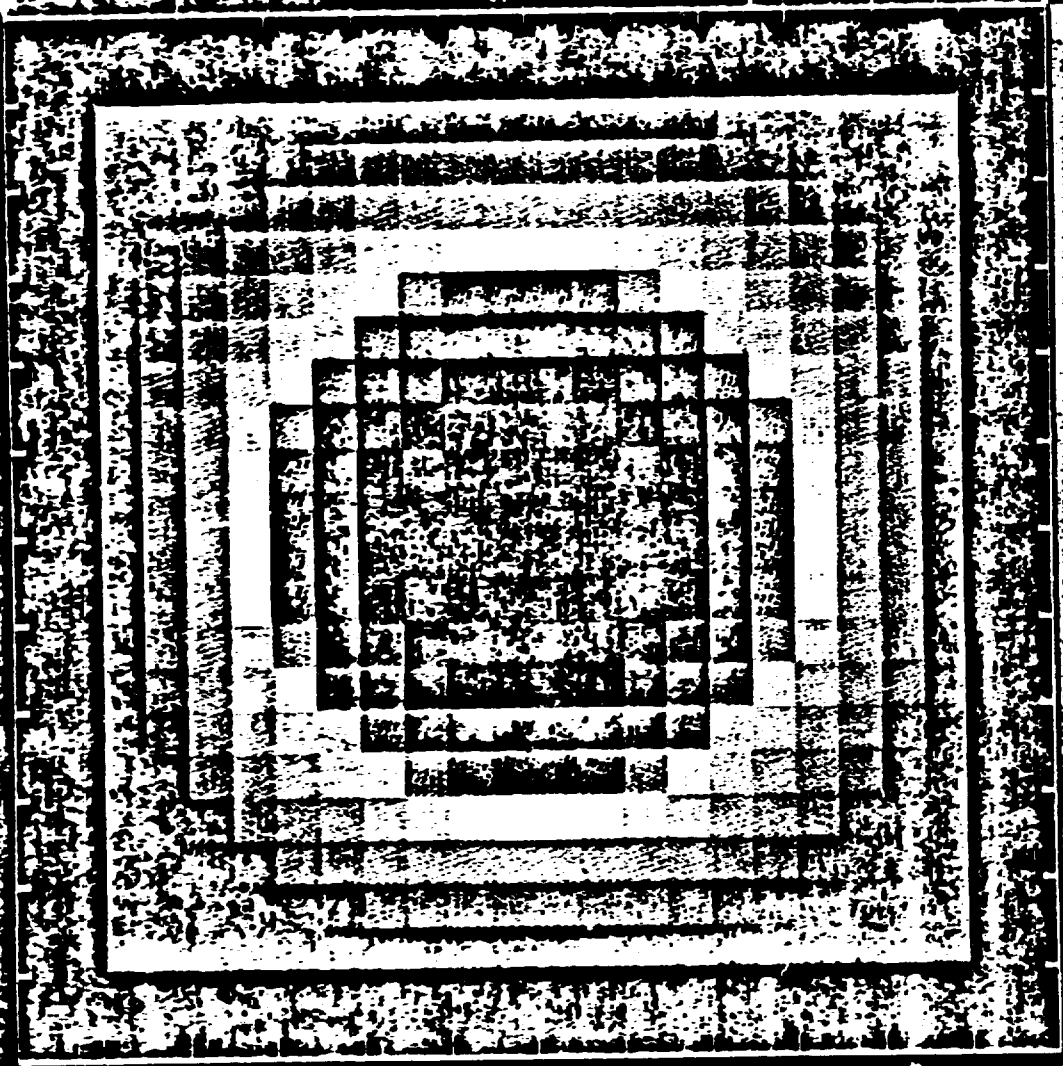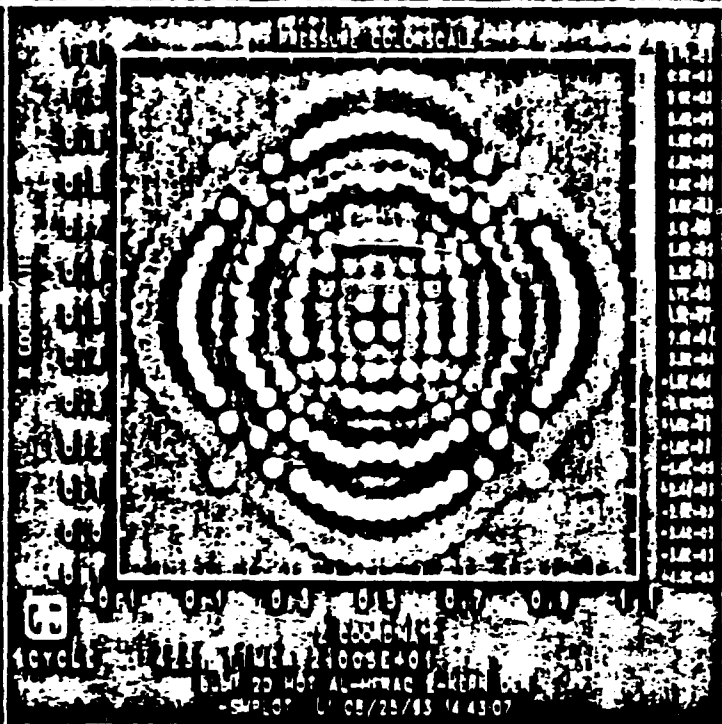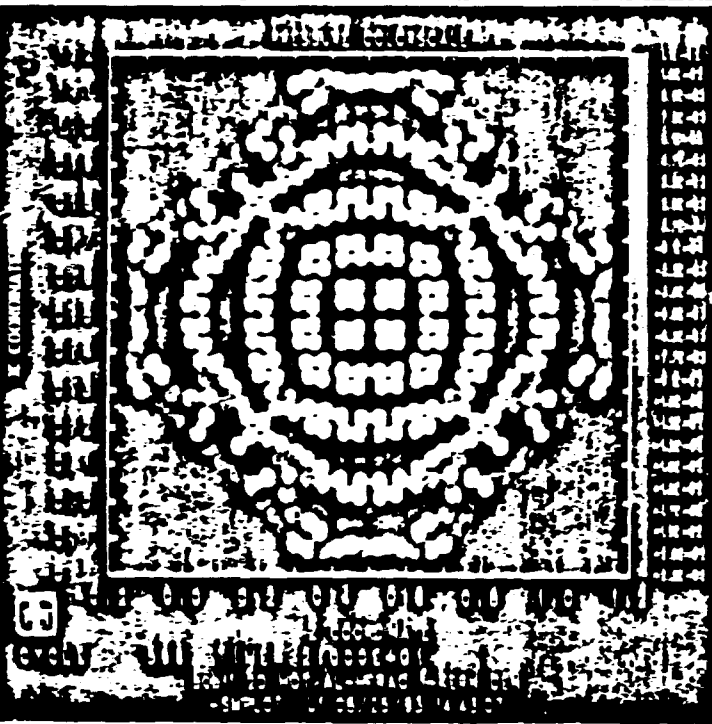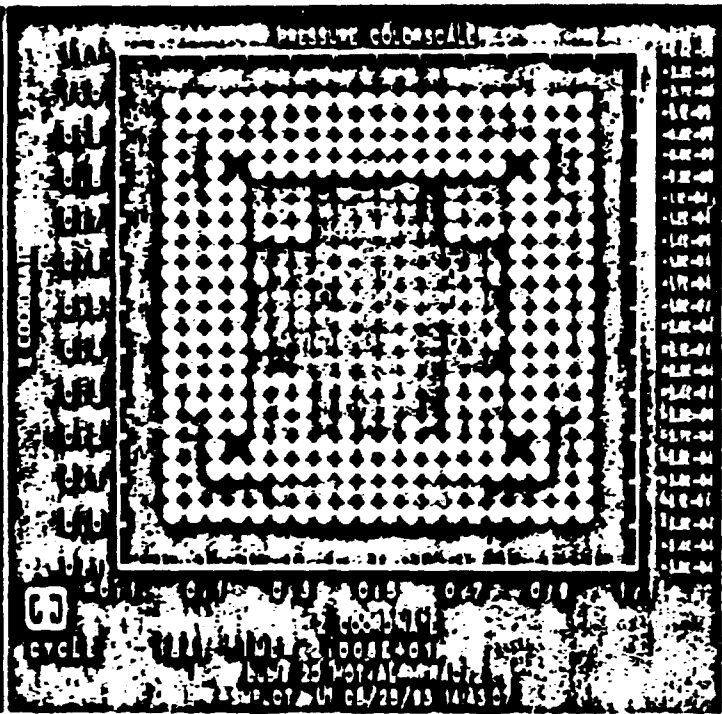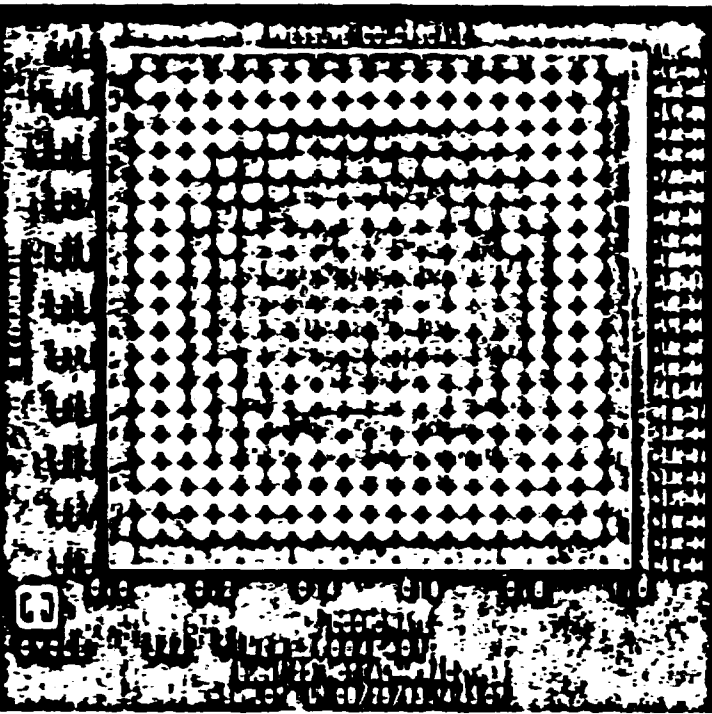
Conclusions

A numerical method must be:

- **Stable**

- **Consistent**

- **Conservative**

Satisfying one or two of these conditions is relatively easy. The challenge is to make SPH meet all three simultaneously.

JWS:1562:9/16/93

SPH: Instabilities, Wall Heating, and Conservative Smoothing

by

D.L. Hicks, J.W. Swegle, S.W. Attaway

(September 22, 1993)

Outline

I. Instabilities in SPH.

II. Conservative Smoothing can stabilize SPH.

But is there anything left except FLATLAND?

III. Test Problems

Instabilities in SPH

Sufficient condition for instabilities:

- Nearest neighbor case:

$$\sigma W'' < 0$$

- Many neighbors case:

$$\sigma \sum_{odd\_\ell} W_\ell'' < 0$$

where $W_\ell'' := \left(W_{j,+\ell}'' + W_{j,-\ell}''\right)/2$.

This analysis is for a uniform stress:

$$\sigma = p + q$$

Note: instabilities are possible for both cases

$$\begin{cases} \sigma > 0, \ positive \\ \sigma < 0, \ negative \end{cases}$$

Conservative smoothing[*] can stabilize SPH.
But is there anything left except FLATLAND?

- Conservative smoothing on the s.mom. of the artifical viscosity type:

$$smom_j = smom_j$$
$$+csm_{j+\frac{1}{2}} * (smom_{j+1} - smom_j)$$
$$-csm_{j-\frac{1}{2}} * (smom_j - smom_{j-1})$$

- Conservative smoothing on the s.i.erg. of the artifical heat conduction type:

$$sierg_j = sierg_j$$
$$+csie_{j+\frac{1}{2}} * (sierg_{j+1} - sierg_j)$$
$$-csie_{j-\frac{1}{2}} * (sierg_j - sierg_{j-1})$$

[*] Introduced in 1969 in AFWL-TR-69-20 by D.L. Hicks.

- Conservative smoothing on the s.vol. of the artifical strain relaxation type:

$$\tilde{svol}_j = svol_j$$
$$+csv_{j+\frac{1}{2}} * (svol_{j+1} - svol_j)$$
$$-csv_{j-\frac{1}{2}} * (svol_j - svol_{j-1})$$

Our analysis shows that we can stabilize SPH with conservative smoothing of the type described above. The result boils down, approximately, to the following timestep restriction for an ideal gas ($\gamma = 1.4$) in compression:

$$C_{FL} \le \frac{1}{2}.$$

Full blown conservative smoothing[*] ($cs_{j+\frac{1}{2}} = 0.25$) was assumed to get this result. We decided to test this theory with some numerical experiments.

[*] $0 \le CS \le .25$

Test Problems

Several years ago, we developed a set of hydrocode test problems [Hickr & Pelzl (1968): AFWL-TR-68-112].

These test problems have seven categories:

SCTP I Single Shock Wave Problems

SCTP II Single Rarefaction Wave Problems

SCTP III Accelerating Wave Problems

SCTP IV Decelerating Wave Problems

SCTP V Riemann's Resolution of the Discontinuity Problems

SCTP VI Shock Collision Problems

SCTP VII Shock Overtake Shock Problems

Along with these test problems (whose solution's are known exactly) we developed a procedure for quantitatively comparing hydrocodes using the $\ell_1, \ell_2, \ell_\infty$ norms to measure the error in various functions. We compared a von Neumann-Richtmyer code with a Lax-Wendroff code.

Next we show some samples of the tables and graphs from that comparison.

Table I-8

ERRORS ON SCIP-I-8

PUFF

Problem time = 1. x 10⁻³ sec
Computer time = 74 sec (CP time on CDC 6600)

Cycle = 1463
Number of Active Zones = 197

	Sum Abs. Error *	Sum Sqr. Error **	Maximum Error ***	Position of Maximum Error
Pressure	1.06	.683	+ .644	Current shock position
Velocity	1.86	1.08	+ .850	Current shock position
Density	1.78	.799	+ .577	Current shock position
Energy	2.76	1.32	+ .865	Current shock position

	Sum Int. Energy	Sum Kin. Energy	Sum Tot. Energy	
EXACT	3.09498×10^{12}	3.09324×10^{12}	6.18823×10^{12}	← in ergs
PUFF	3.09791×10^{12}	3.08713×10^{12}	6.18504×10^{12}	← in ergs

LAX-WENDROFF

Problem time = 1. x 10⁻³ sec
Computer time = 661 sec (CP time on CDC 6600)

Cycle = 1762
Number of Active Zones = 302

	Sum Abs. Error *	Sum Sqr. Error **	Maximum Error ***	Position of Maximum Error
Pressure	1.33	.695	- .663	Current shock position
Velocity	.721	.396	- .372	Current shock position
Density	1.91	.636	- .492	Current shock position
Energy	1.67	.611	+ .449	Initial shock position

	Sum Int. Energy	Sum Kin. Energy	Sum Tot. Energy	
EXACT	3.09498×10^{12}	3.09324×10^{12}	6.18823×10^{12}	← in ergs
LAXWEN	3.09016×10^{12}	3.08281×10^{12}	6.17297×10^{12}	← in ergs

* l_1 norm, nondimensionalized with max. value of exact solution

** l_2 norm, " " " "

( )*** l_∞ norm, " ( ) " " ( ) "
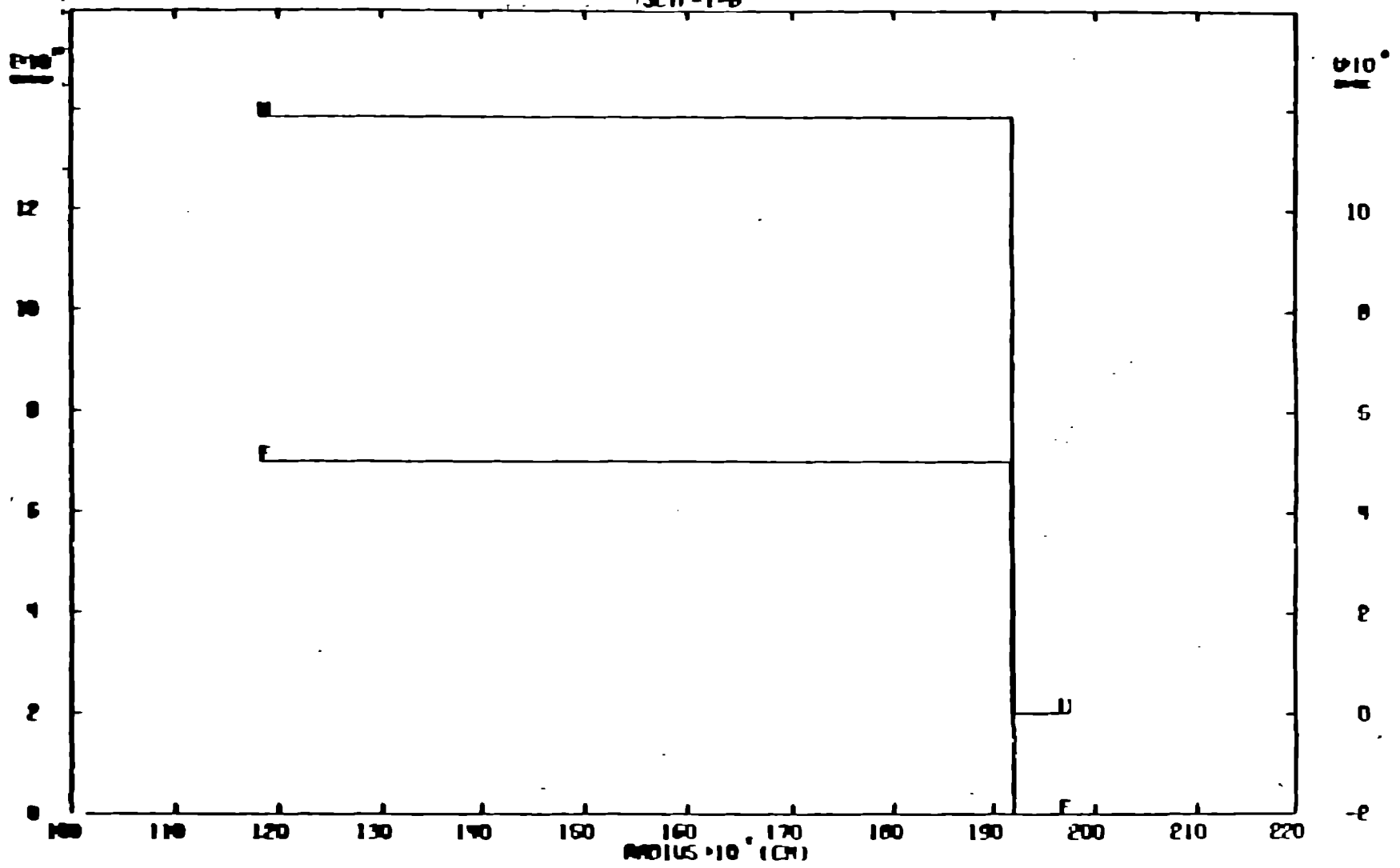
Figure 1-8. PB-EXACT

Figure I-4L VE-EXACT

Figure 1-8. PB-PUFF

CYCLE 1963   TIME 1.000×10⁻²
PUFF 66 == RCTP-1-0

Figure 1-8. VE-PUFF

Figure I-B. VE-LAX-WENDROFF

EXACT SOLUTION   TIME   7.000×10⁻⁴

SCTP-VI-8

Figure VI-8.   PB-EXACT

EXACT SOLUTION   TIME   7.000*10^{-6}
SCTP-VI-8

RADIUS *10^{9} (CM)
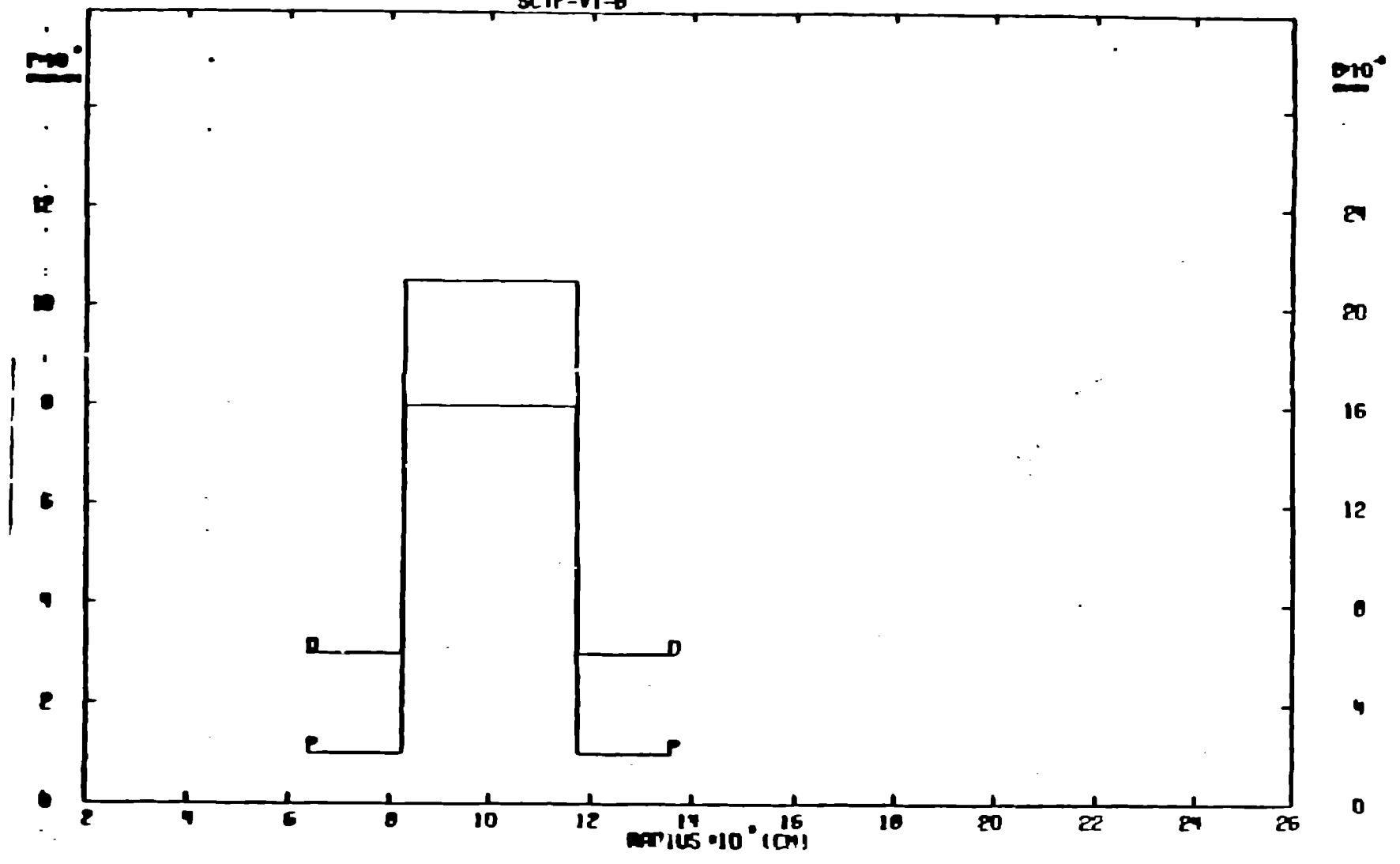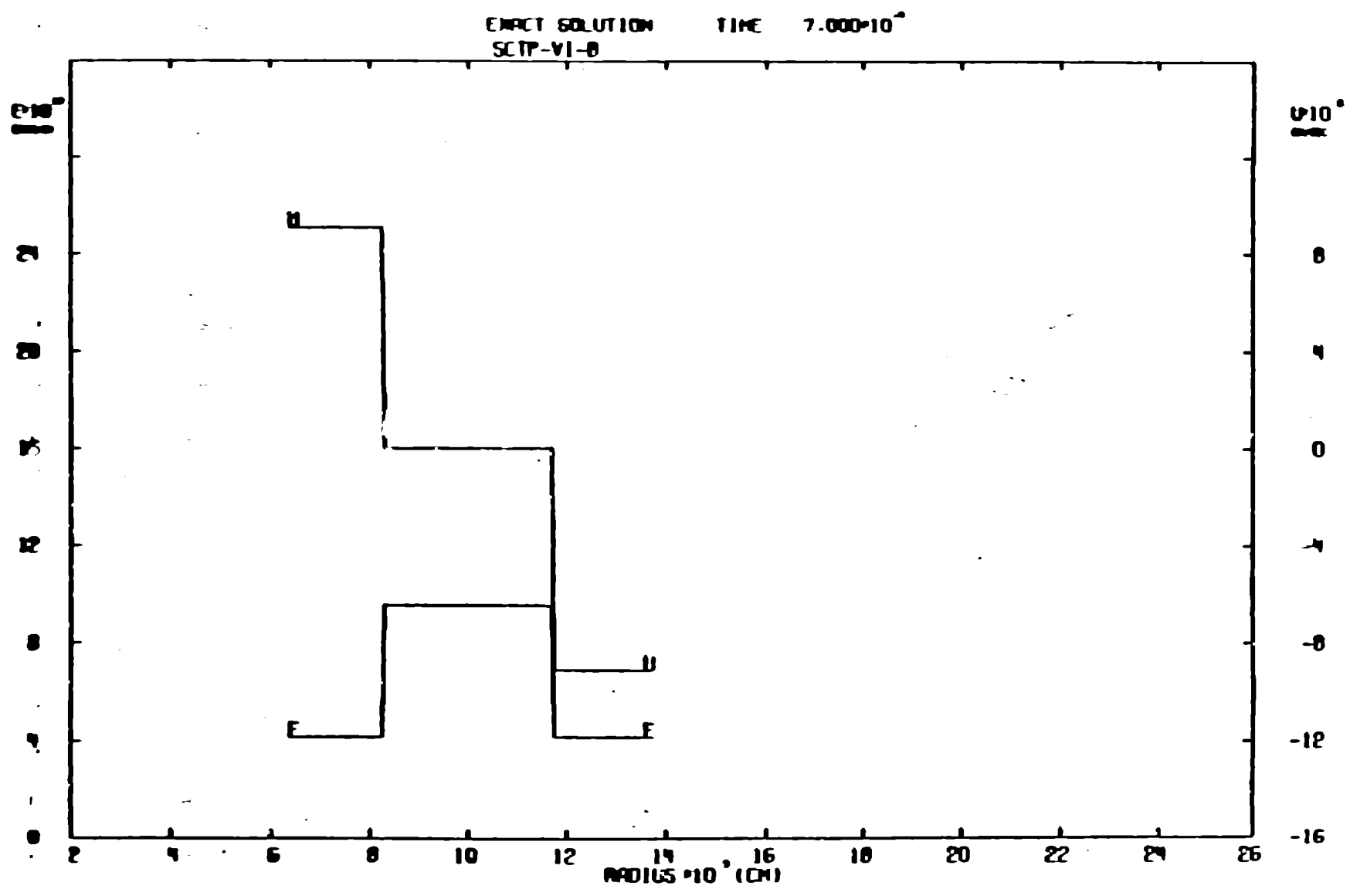
Figure VI-8. VE-EXACT
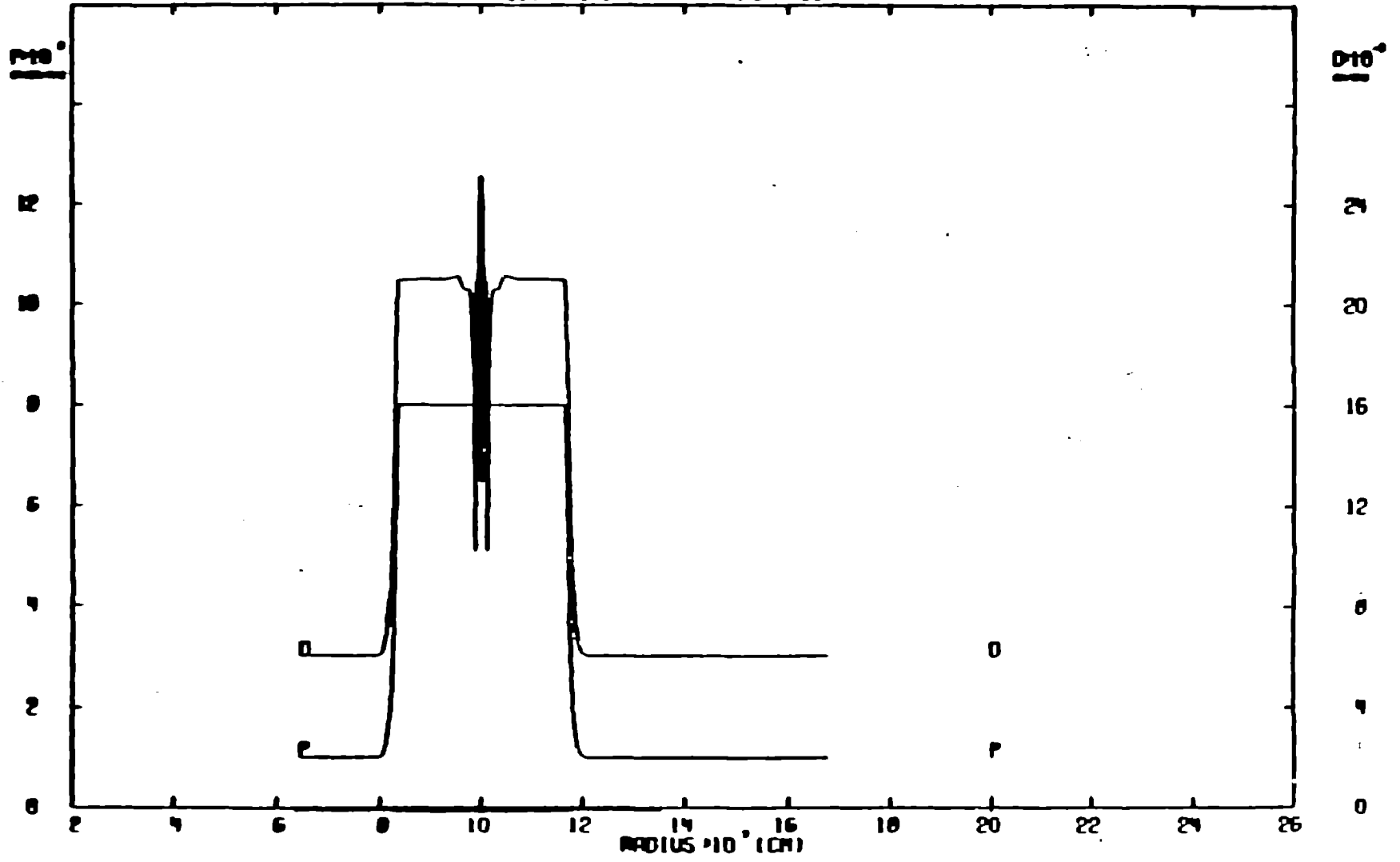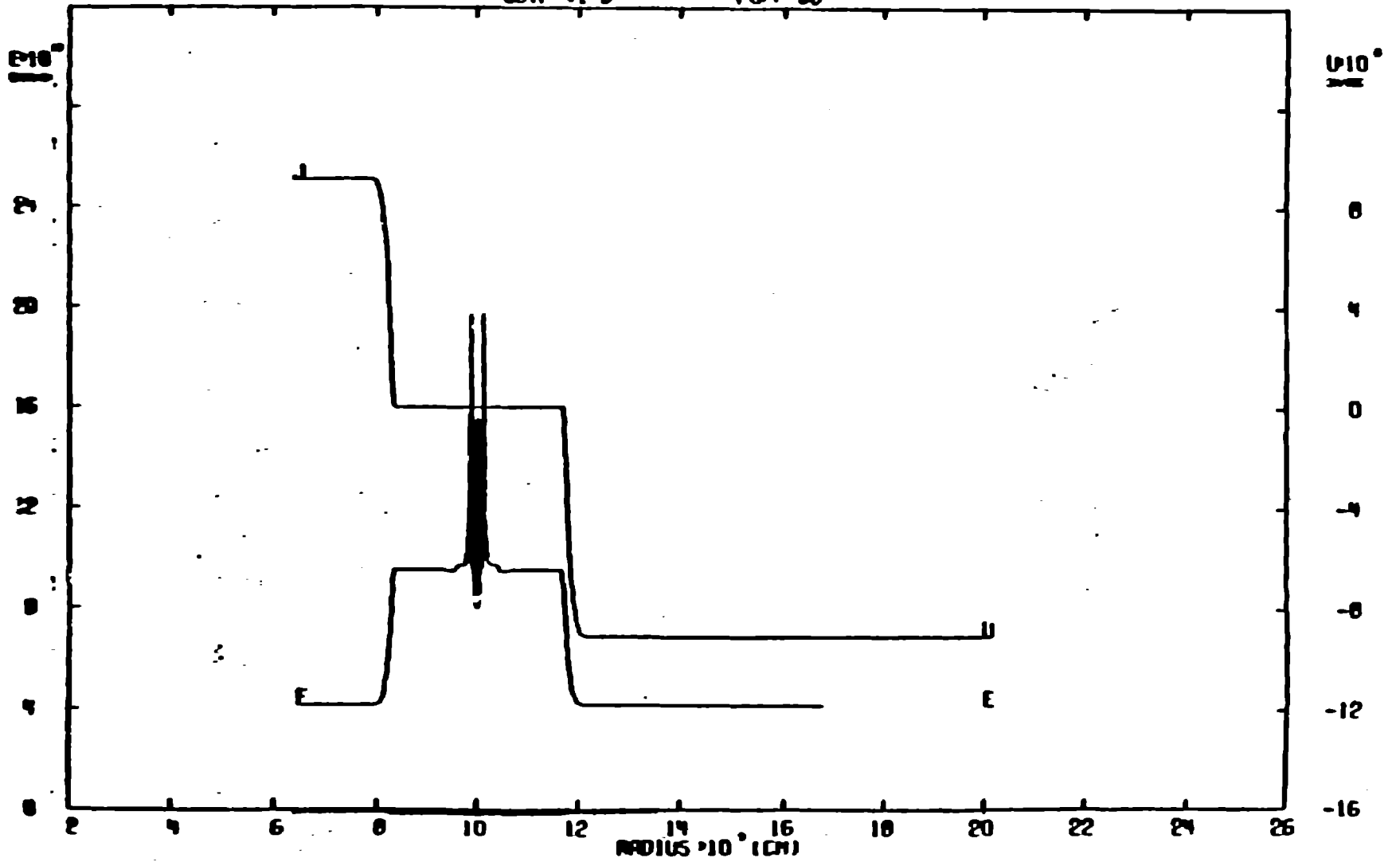
Figure VI-8, PB-PUFF

Figure VI-8. VE-PEFF

Figure VI-B, P0-LAX-WENDROFF

Figure VI-8. VE-LAX-WENDROFF

Recently we tried to run an SPH calculation on SCTP VI-B. Our SPH calculation is of the following form:

$$\mathbf{U}^T = (V, \mathbf{u}, E)$$

$$\mathbf{F}^T = (-\mathbf{u}, \sigma, \mathbf{u} \bullet \sigma)$$

$$\rho\dot{\mathbf{U}} = -div\ \mathbf{F}$$

$$m_j\dot{\mathbf{U}}_j = \sum_{i=1}^{N_p} \left(\frac{\mathbf{F}(x_i) + \mathbf{F}(x_j)}{2} \right) \bullet \mathbf{A}_{ij}$$

$$\mathbf{A}_{ij} = 2Vol_iVol_jgrad_{x_i}W_{ij}$$

$$W_{ij} = W(x_i - x_j, h)$$

The results were as follows.

final time =   1.000000E-07   (936161.952)

x-axis: material-mass-coordinate

legend: computed —— exact •
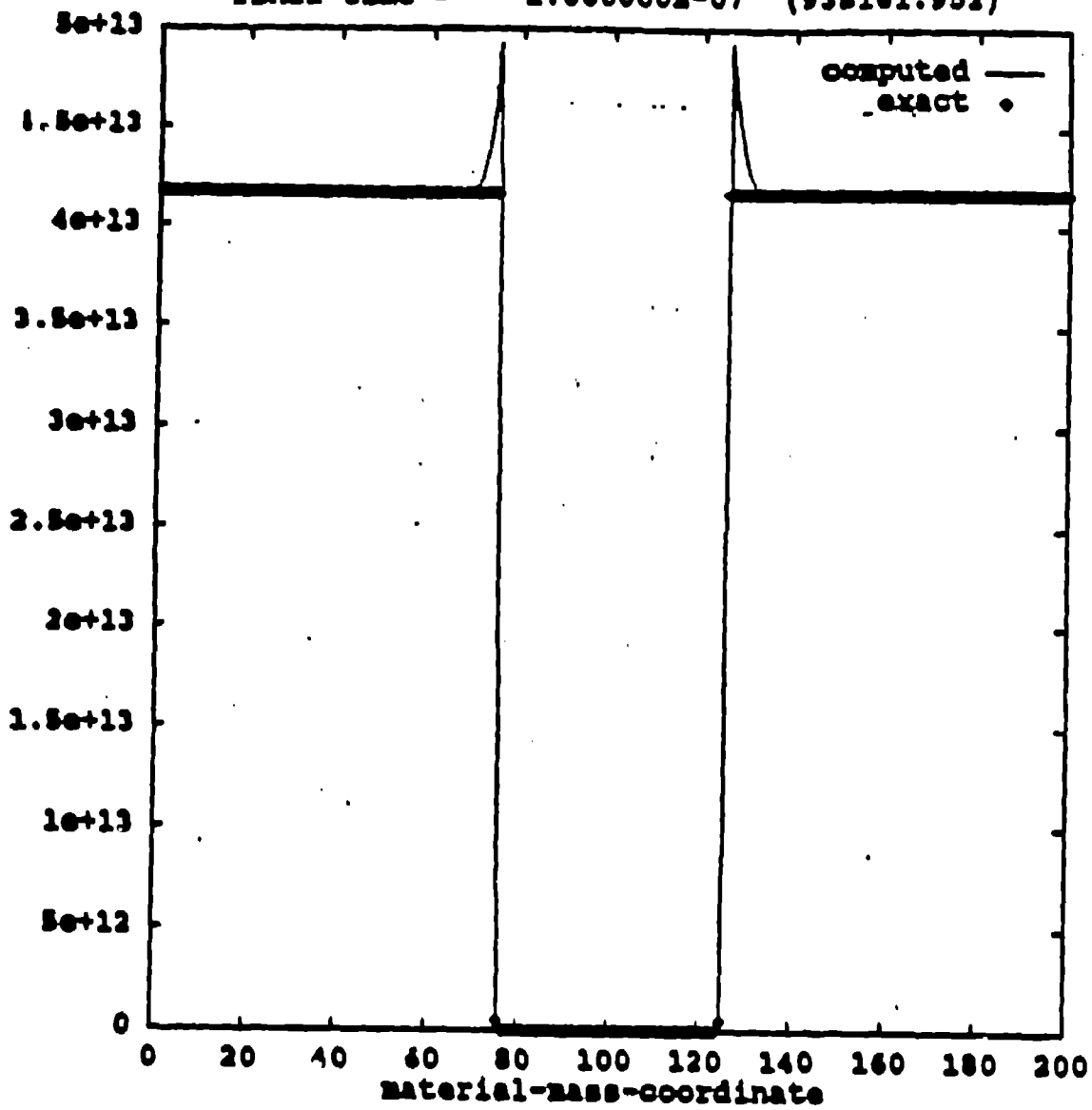
Carvis1 = Carvis2 = 3.0

nzones = 200
ncycles = 15
left shock   started at 75 meters
right shock   "   " 125 meters

-243-

final time = 3.500000E-08 (93s152.301)
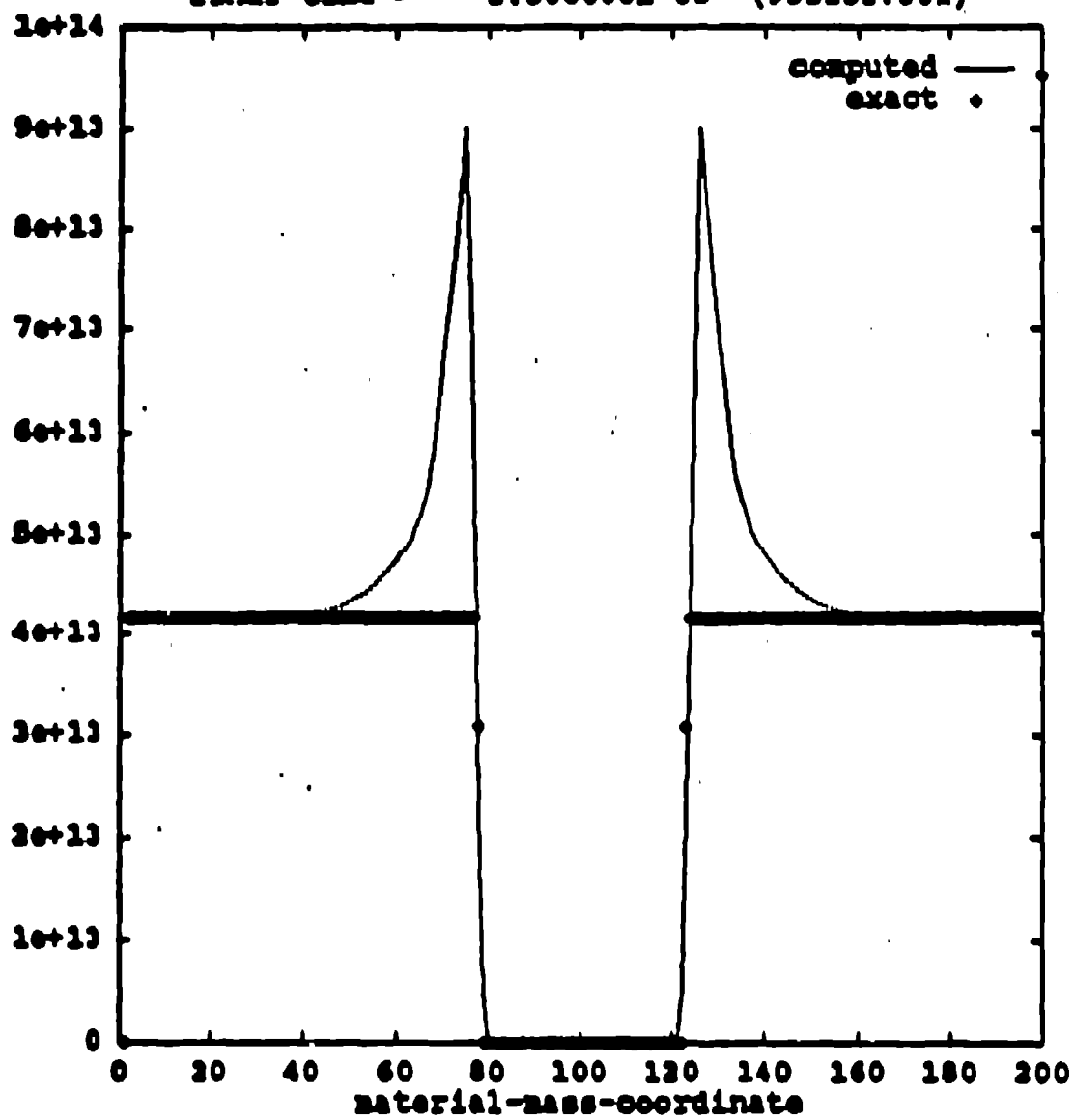
s.i.erg.

ncycles = 382
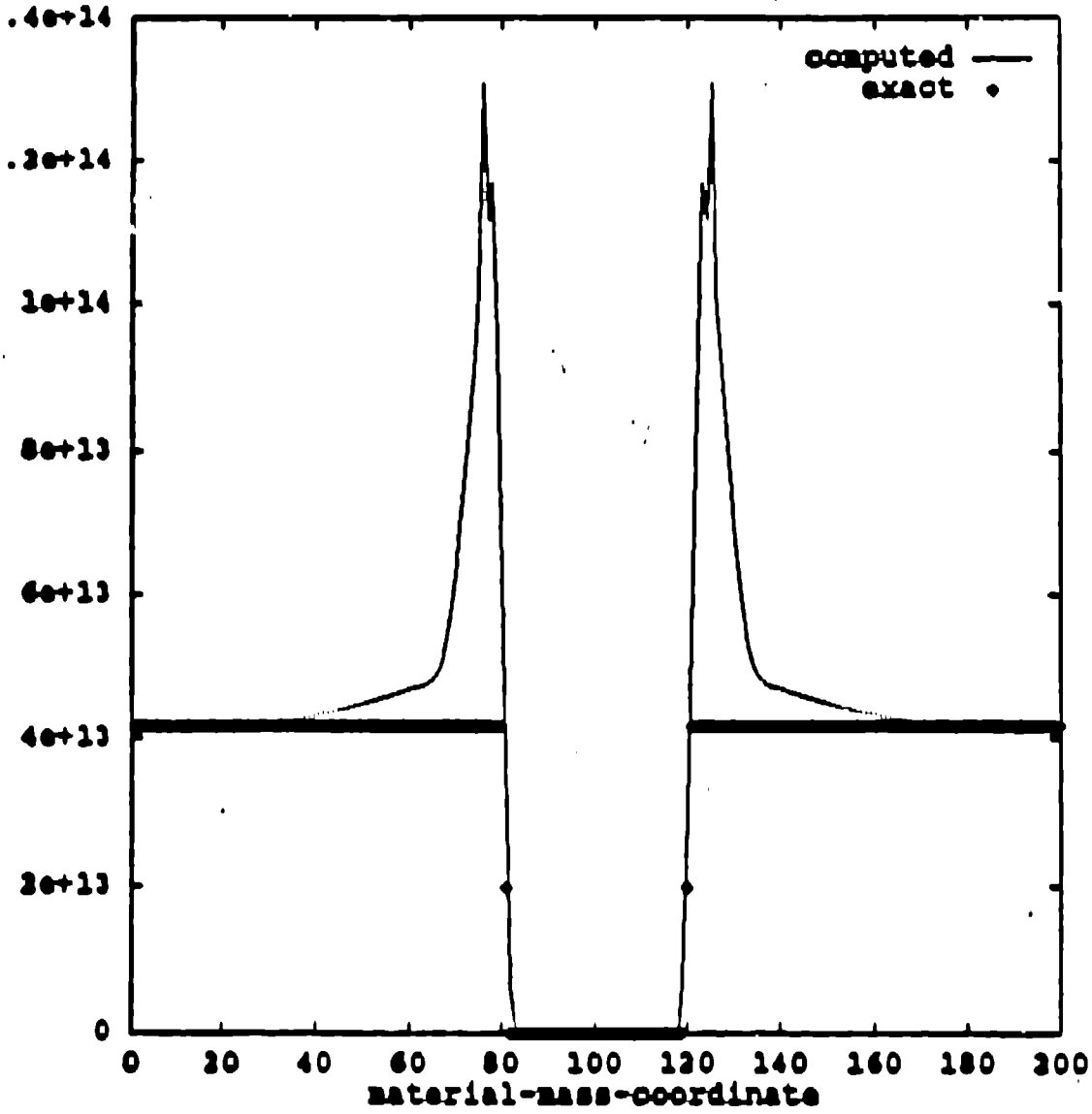
S.i.erg.

ncycles = 647

final time = 1.000000E-04 (93s161.329)
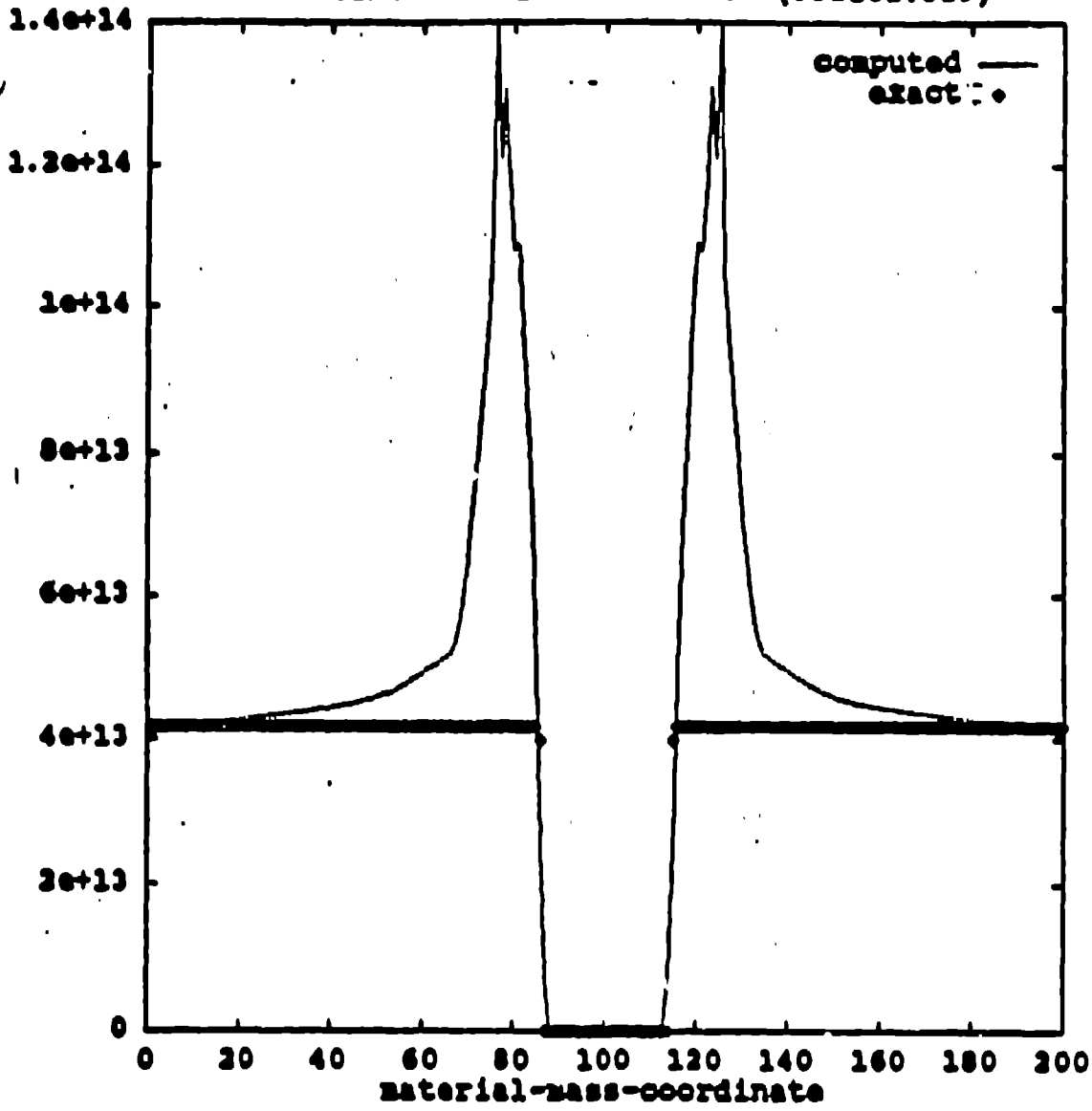
s.i.erg
ncycles = 1518

time = 2.06E-04

(93s152.023)

computed ———
exact •

material-mass-coordinate
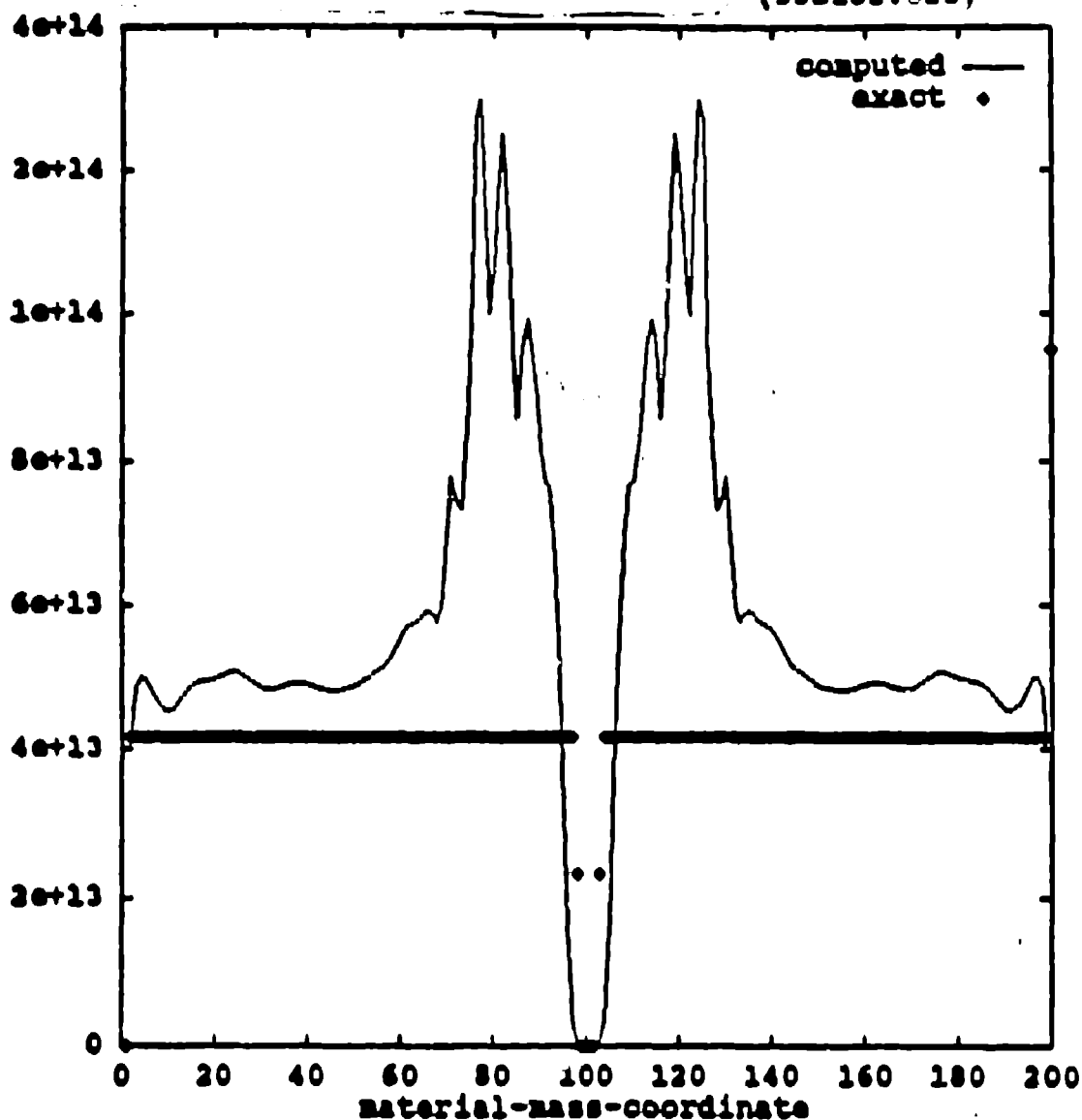
s.i.erg.

ncycles = 4347

Computation failed: $x(2) > x(3)$

$t_{collision} \doteq 2.28e-4$

$t_{last} = 7.e-4$

s.i.erg. obviously under smoothed

final time = **2.06E-04** (936152.023)
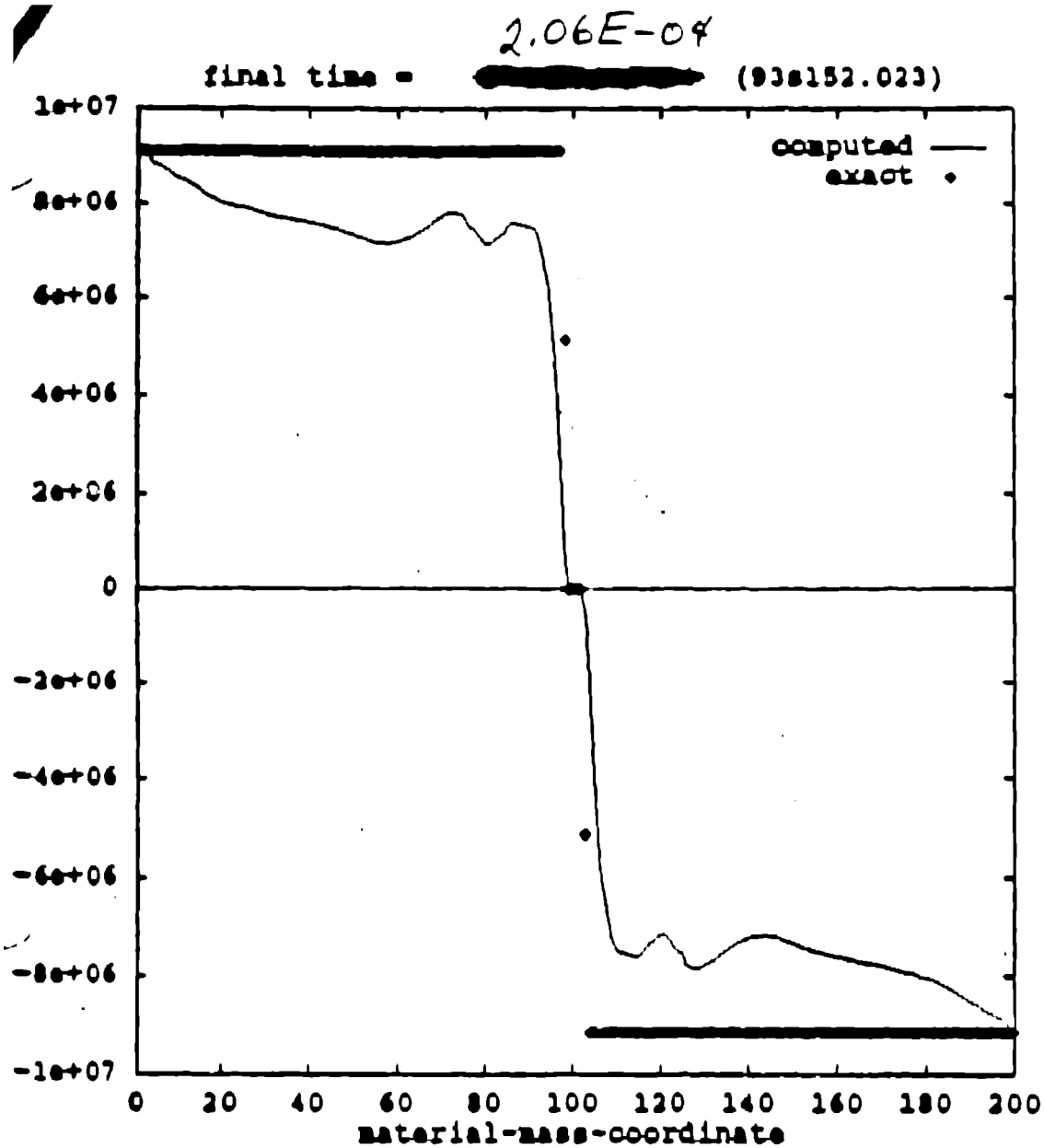
s. mom.

$ncycles = 4347$

computation failed: $x(2) > x(3)$

$t_{cd} \doteq 2.28e-4$

$t_{last} = 7.e-4$

s. mom obviously over smoothed

final time = (938152.023)
$\chi(2) > \chi(3)$

computed ——
exact •

material-mass-coordinate
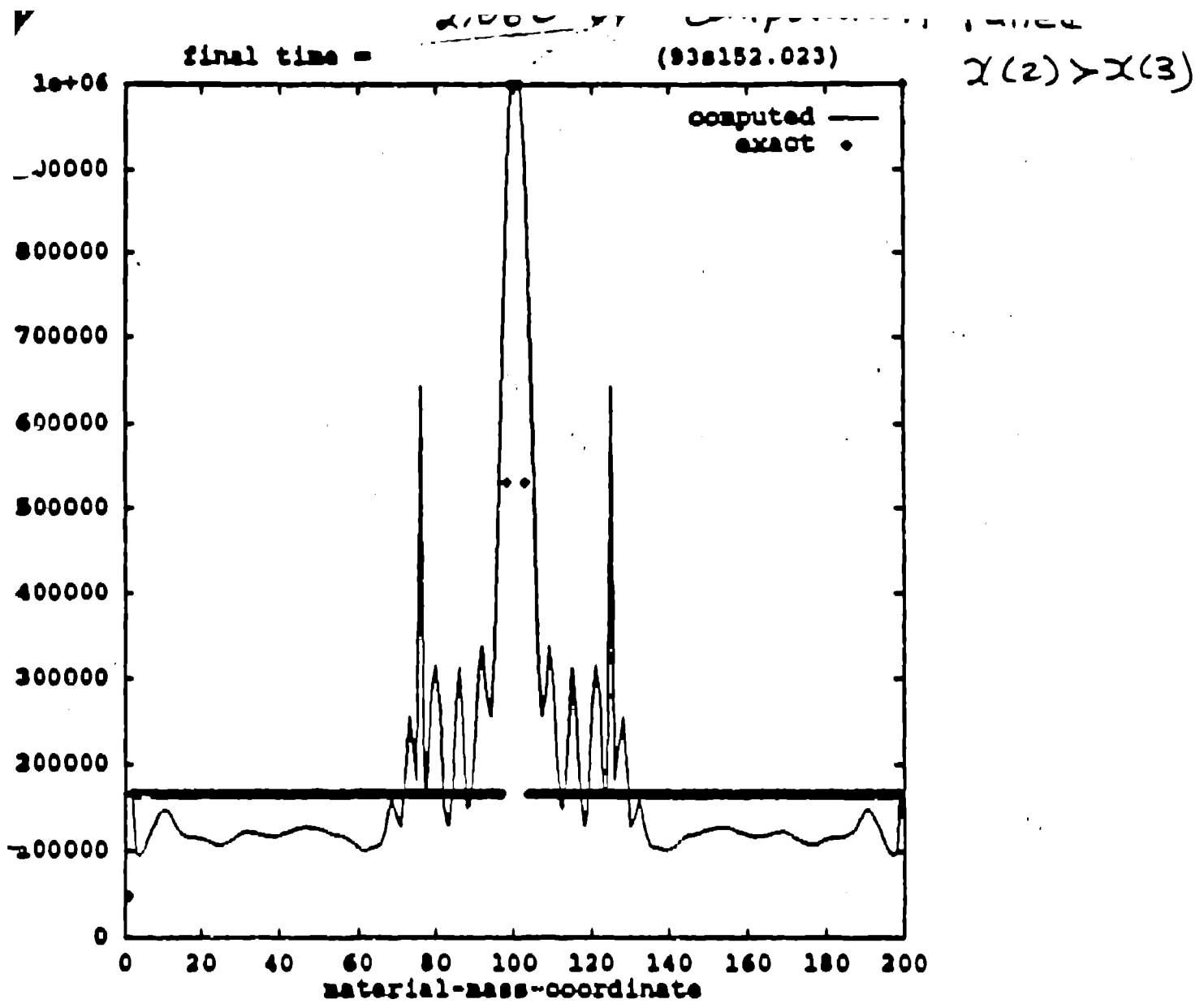
s. vol.

$n\,cycles = 4347$
computation failed: $\chi(2) > \chi(3)$

$t_{cal} \doteq 2.28e-4$

$t_{last} \doteq 7.e-4$

s. vol. obviously under smoothed
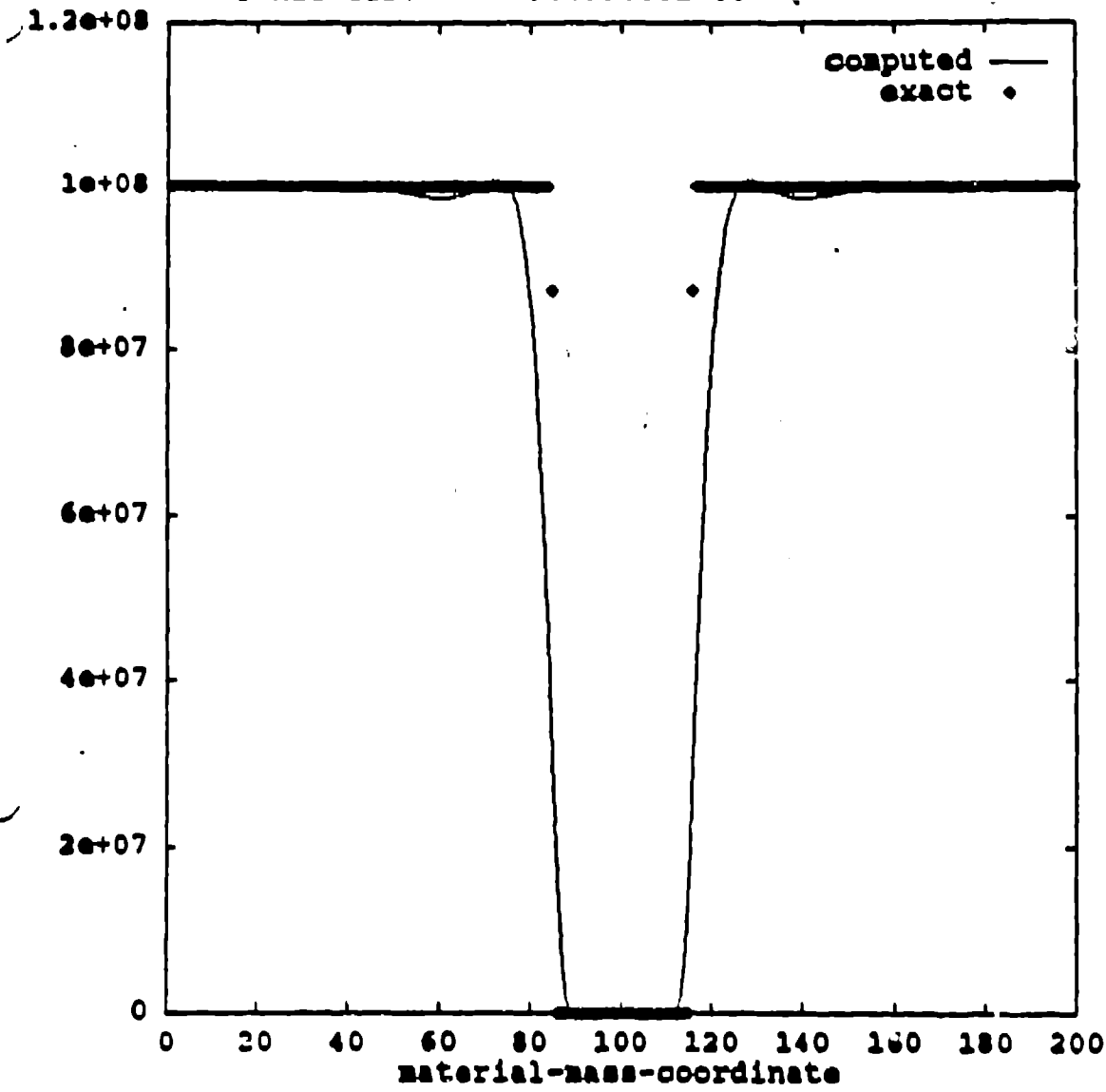
computed ——
exact •

material-mass-coordinate

10ZP , 0,0, 2^{-9} , 2^{-7} , 2^{-8}

carwist → carwis 2 → csvol → csmom → csierg

shock has travelled (or propagated) 10 zones

final time = 9.012235E-05 (93s192.033)

material-mass-coordinate

final time =   9.012235E-05   (93s192.033)

material-mass-coordinate

computed ——
exact •
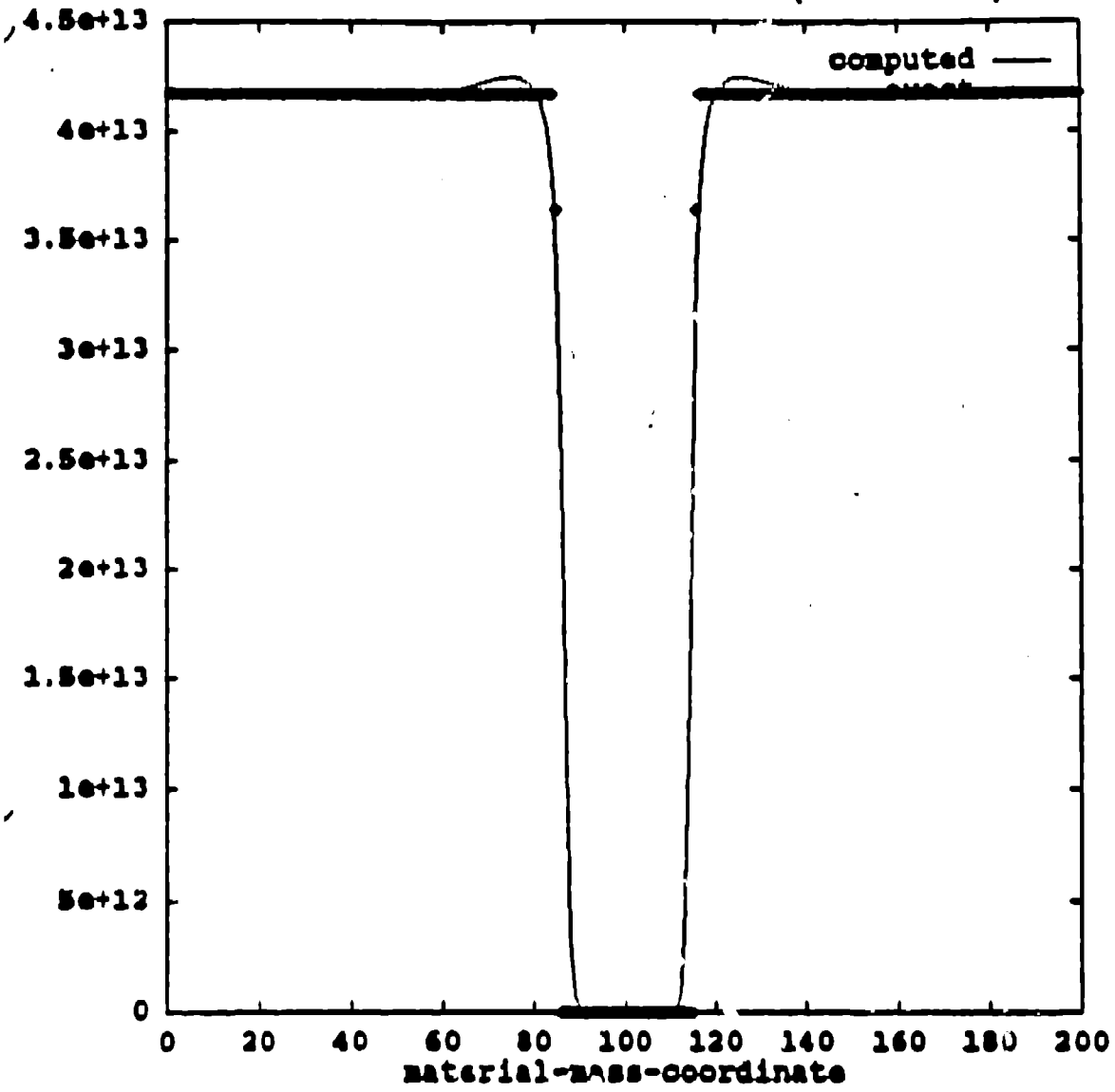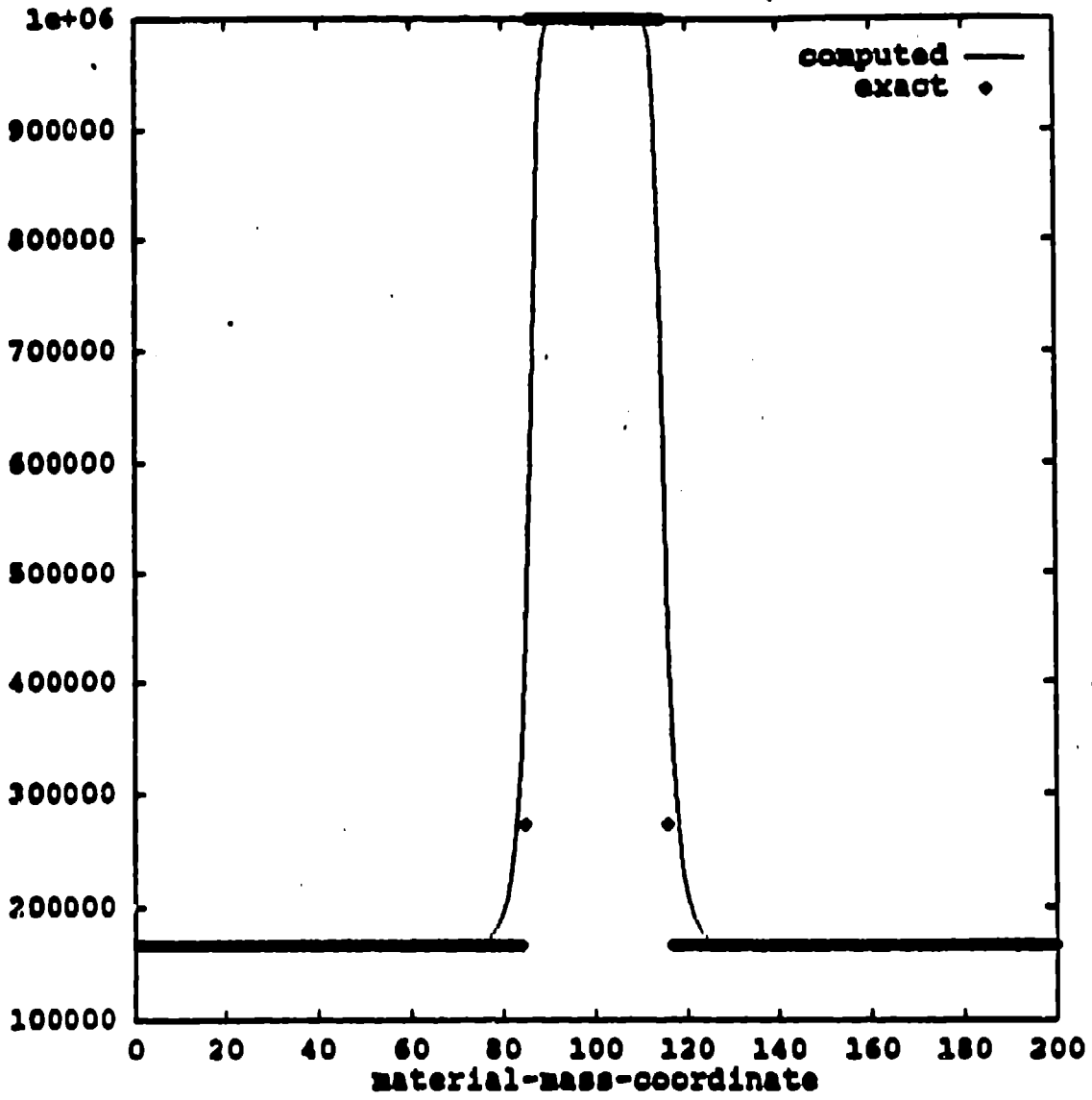
final time = 9.0122.15E-05 (93s192.033)

material-x1ss-coordinate
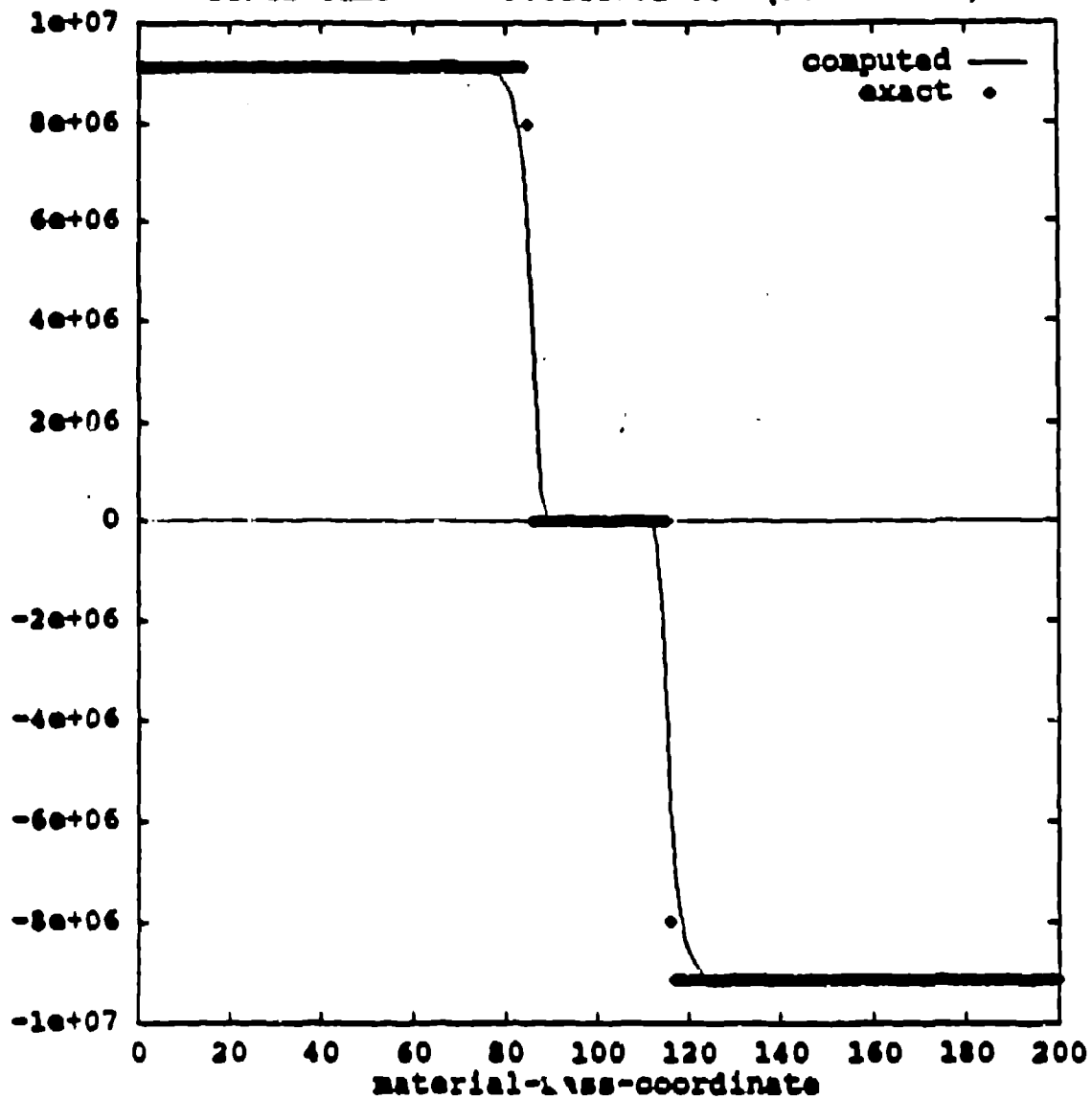
final time = 1.802039E-04 (93s192.045)
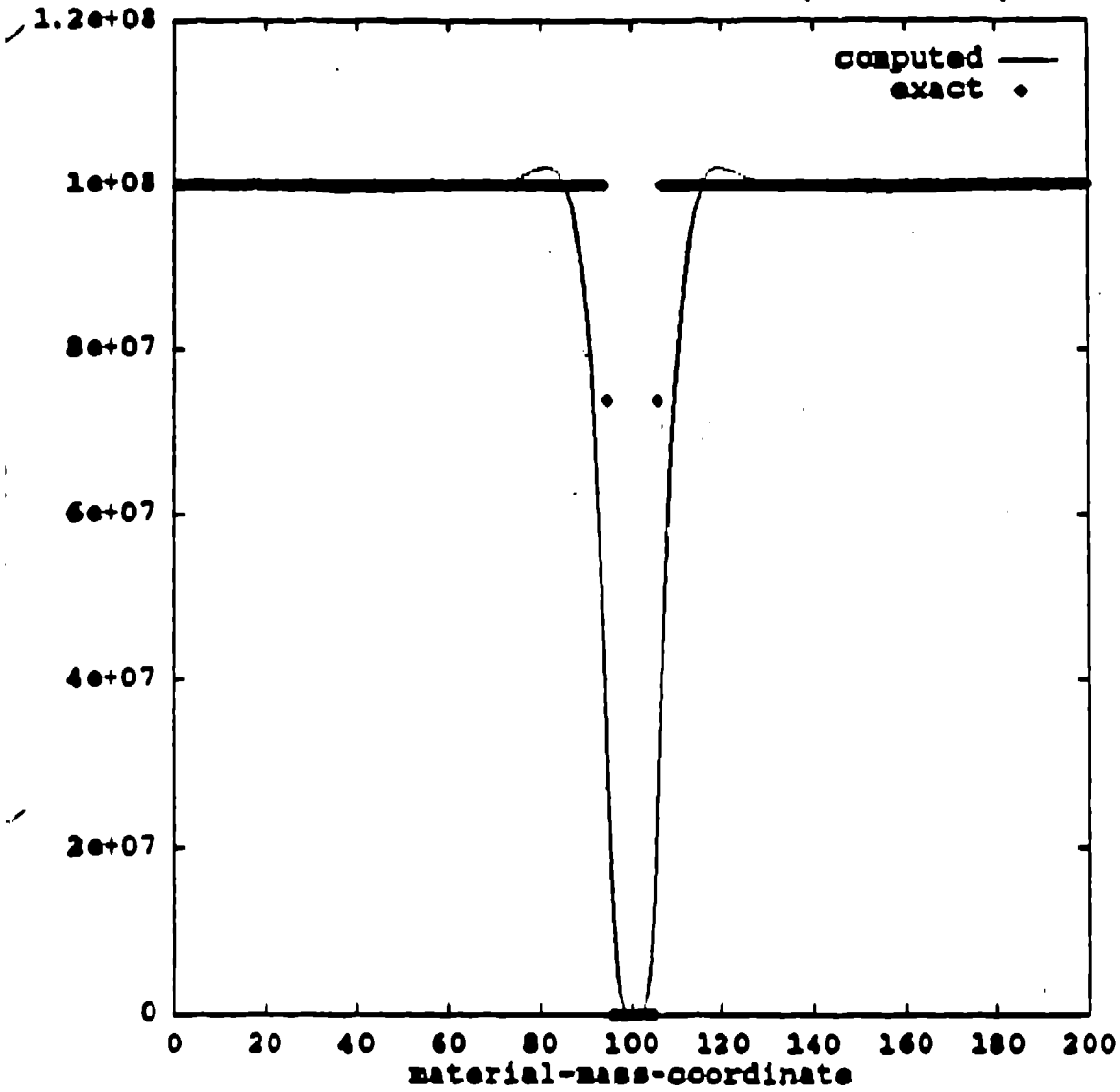
20ZP

final time = 2.301284E-04 (93s192.053)
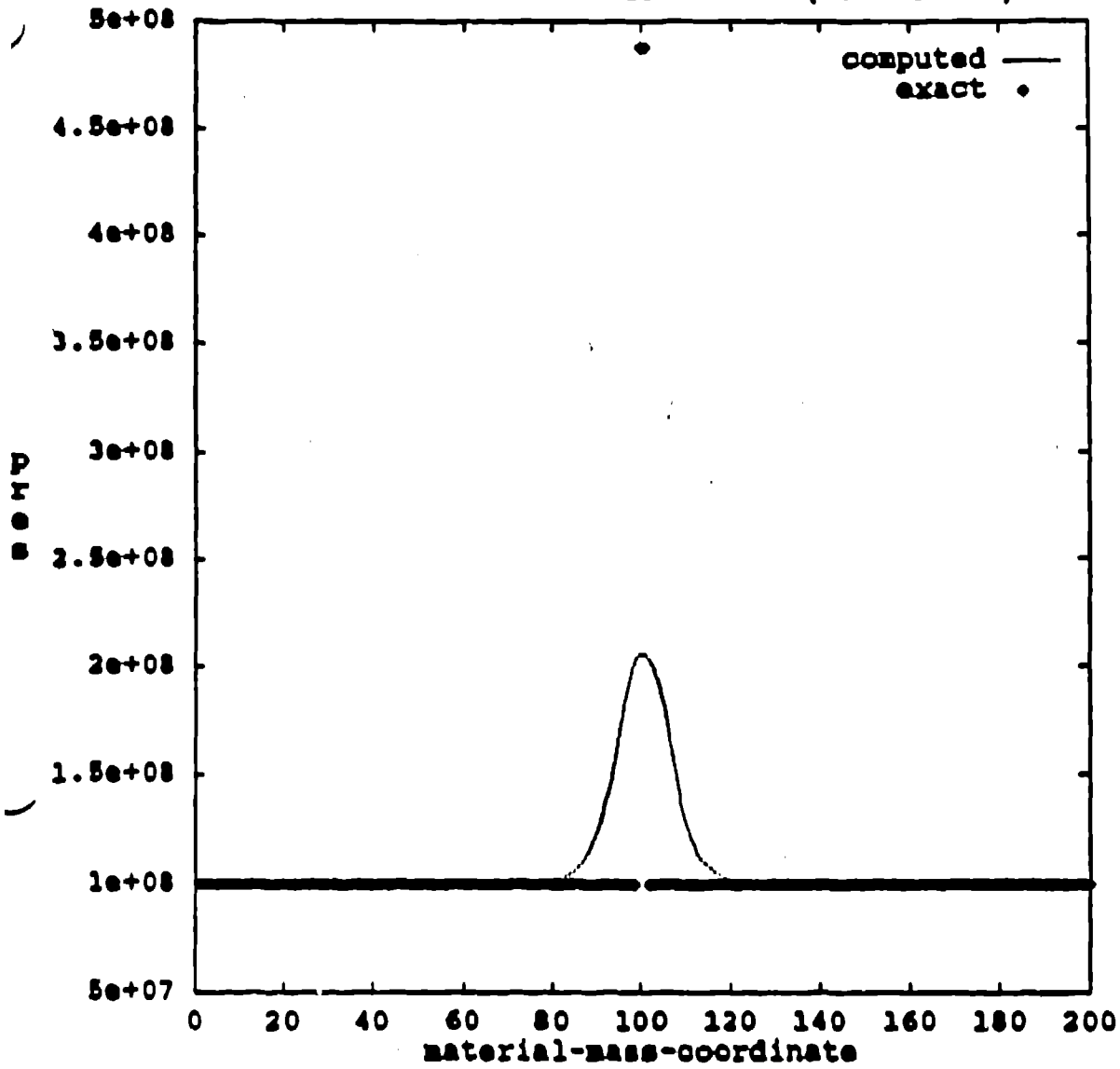
B.I.B.O. ≡ B-spline In, B-spline Out

final time = 2.700087E-04 (93s192.108)
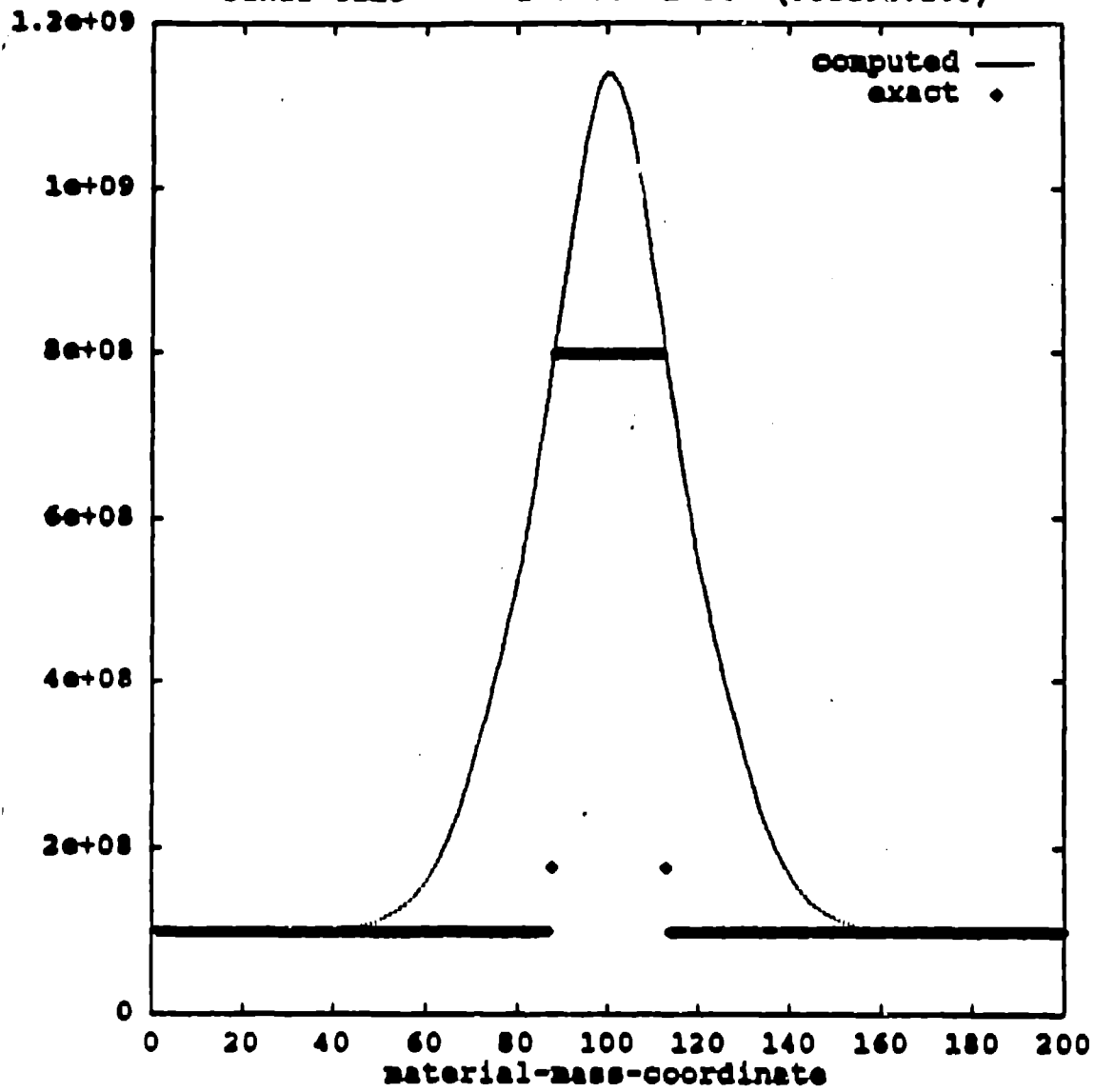
B.I.B.O.

TENSOR SPH

W. Benz, U of A
M. Davies, Caltech

Outline:

1) Motivations

2) Implementation

3) Tests

4) Conclusions

Motivations

Currently SPH uses spherical interpolants:

$$W = W(\vec{r}, h)$$

$$\downarrow$$

scalar

➤ Any given particle contributes isotropically to local averaging.

Note: this is even true when
$$h = \tfrac{1}{2}(h_i + h_j)$$

➤ works best for "isotropic" flows !?!

$$(h \sim \rho^{-1/3})$$

However, there is no such thing as an isotropic flow!!

→ Flows have a preferred direction
   $(x, y, z, r, \ldots)$

→ increase resolution along that direction.

Good for: • Impacts
             • Shock waves
             • Objects with aspect ratios
               $\neq 1$
             etc...

Equivalent of a fully adaptive grid!

Idea:

Replace the scalar h by a tensor $\underline{h}$ and write an evolution equation for each of its components:

$$h \longrightarrow \underline{h} = \begin{pmatrix} h_{xx} & h_{xy} & h_{xz} \\ h_{xy} & h_{yy} & h_{yz} \\ h_{xz} & h_{yz} & h_{zz} \end{pmatrix}$$

$$\frac{dh}{dt} \longrightarrow \frac{d\underline{h}}{dt}$$

Note: Because $\underline{h}$ has real eigenvalues, the tensor is symmetric!

Spheres $\longrightarrow$ Triaxial ellipsoids
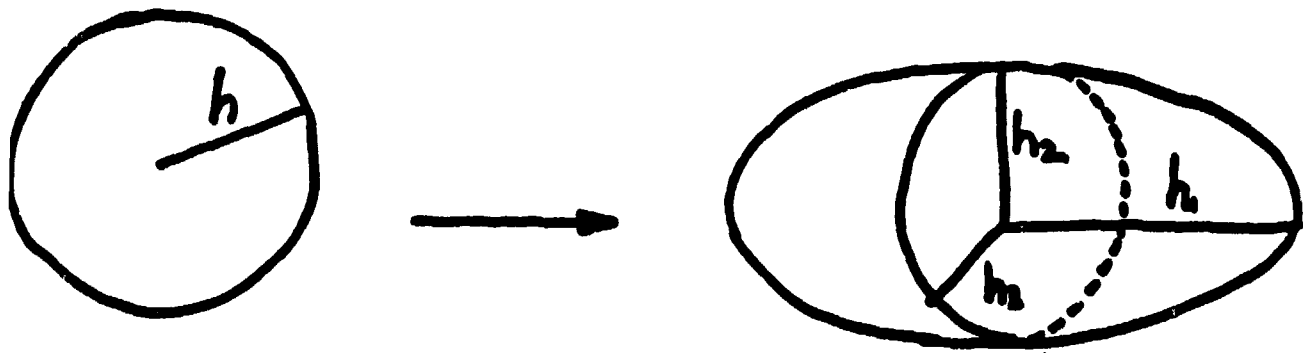
h: radius of sphere

h_1, h_2, h_3 principal axes of ellipsoid.

→ h_1, h_2, h_3 scale with the flow independently!

→ list of neighbors remains nearly constant.

but: added complexity, i.e. SPH is no longer as easy as advertised!

Implementation

) Diagonalize $\underline{\underline{h}}$:

$$\begin{pmatrix} h_{xx} & h_{xy} & h_{xz} \\ h_{xy} & h_{yy} & h_{yz} \\ h_{xz} & h_{yz} & h_{zz} \end{pmatrix} \longrightarrow \begin{pmatrix} h_1 & & \\ & h_2 & 0 \\ 0 & & h_3 \end{pmatrix}$$

h_1, h_2, h_3 : eigenvalues of $\underline{\underline{h}}$

The eigenvectors define a transformation from lab. to a frame in which $\underline{\underline{h}}$ is diagonal.

$$\underline{\underline{V}}h = \begin{pmatrix} U_{1x} & U_{1y} & U_{1z} \\ U_{2x} & U_{2y} & U_{2z} \\ U_{3x} & U_{3y} & U_{3z} \end{pmatrix}$$

$$\vec{x}' = \underline{\underline{V}}_h \cdot \vec{x}$$

kernel frame   lab. frame

2) Get kernel values:

$$W_{tot} = \frac{1}{2}\left(W_i + W_j\right)$$

where W_i is the contribution from particle i and W_j · · · · · · j.

Define $\left(\vec{r}_{ij}\right)'_i = \underline{V_h^i}\,\vec{r}_{ij}$

        kernel i space   lab. space

$$\longrightarrow \quad U_i = \left|\left(\vec{r}_{ij}\right)'_i\right| = \left(\frac{x'^2_{ij}}{h_1^{i^2}} + \frac{y'^2_{ij}}{h_2^{i^2}} + \frac{g'^2_{ij}}{h_3^{i^2}}\right)^{\frac{1}{2}}$$

get $W = W(U_i, h_1^i, h_2^i, h_3^i)$ using B-spline kernel

Note: locii of iso-W are really triaxial ellipsoids.

The procedure is repeated for W_j.

3) Get kernel gradients

$$\vec{\nabla} W_{tot} = \frac{1}{2}\left(\vec{\nabla} W_i + \vec{\nabla} W_j\right)_{(\nabla_i W_{ij} = -\vec{\nabla}_j W_{ij}}$$

use same procedure to get υ_i and υ_j

use $\vec{\nabla} W = \dfrac{dW}{d\upsilon} \cdot \vec{\nabla}\upsilon$

with $\vec{\nabla}\upsilon = \dfrac{1}{\upsilon}\begin{pmatrix} x_{ij}'/h_1^2 \\ y_{ij}'/h_2^2 \\ z_{ij}'/h_3^2 \end{pmatrix}$ (in kernel frame)

Note: unless $h_1 = h_2 = h_3$, the gradient of W is not aligned with $\vec{r}_{ij}$

rotate kernel components into lab frame

$$(\vec{\nabla} W)_L = \underline{V}_h^{i\,-1}\,(\vec{\nabla} W)_i$$

The procedure is repeated for ∇W_j

4) Time evolution of h

Just as in the spherical case with $h \propto N_n^{-1/3}$ setting h by looking at the neighbor distribution is too noisy. $\Rightarrow$ differential form.

Transformation:
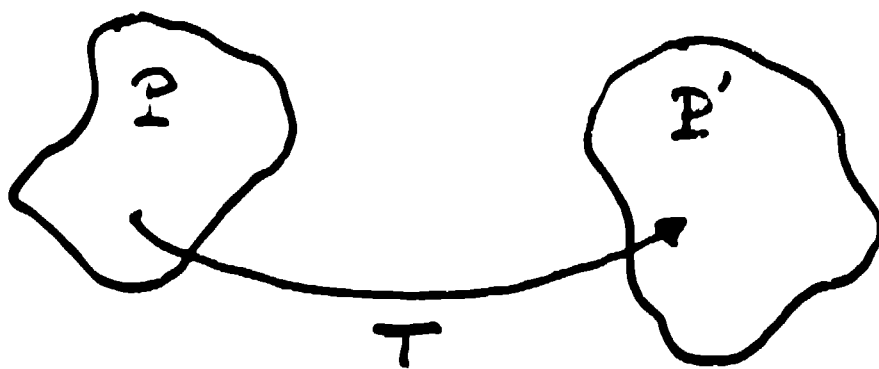
$$T = D + R$$

pure deformation   pure rotation

We assume "small" deformations and rotations (during 1 timestep.)

Deformation:

$$D: \quad \dot{\varepsilon}^{\alpha\beta} = \frac{1}{2}\left(\frac{\partial v^\alpha}{\partial x^\beta} + \frac{\partial v^\beta}{\partial x^\alpha}\right)$$

strain rate tensor

Rotation:

$$R: \quad \dot{R}^{\alpha\beta} = \frac{1}{2}\left(\frac{\partial v^\alpha}{\partial x^\beta} - \frac{\partial v^\beta}{\partial x^\alpha}\right)$$

rotation rate tensor

Naive idea for deformation:

$$\dot{h}^{\alpha\beta} = \dot{\varepsilon}^{\alpha\beta} \cdot h^{\alpha\beta} \qquad (\text{no sum!})$$

Trouble: if $h^{\alpha\beta} = 0$ initially, will remain 0 at all times!

Solution:

) Diagonalize $\dot{\varepsilon}^{\alpha\beta}$

$\quad\quad \dot{\varepsilon}_1, \dot{\varepsilon}_2, \dot{\varepsilon}_3$: eigenvalues of $\dot{\varepsilon}^{\alpha\beta}$ (real)

$\quad\quad \underline{V}_\varepsilon$: transformation matrix defined by

$\quad\quad\quad$ the eigenvectors associated with

$\quad\quad\quad\quad \dot{\varepsilon}_1, \dot{\varepsilon}_2, \dot{\varepsilon}_3$

) Transform $\underline{h}$ into frame of ref. in which

$\dot{\varepsilon}^{\alpha\beta}$ is diagonal

$$\underline{h}' = \underline{V}_\varepsilon^{-1} \, \underline{h} \, \underline{V}_\varepsilon$$

) In this frame, obtain $\underline{\dot{h}}'$

$\quad\quad \dot{h}'_{xx} = \dot{\varepsilon}_1 \cdot h'_{xx}$

$\quad\quad \dot{h}'_{yy} = \dot{\varepsilon}_2 \, h'_{yy}$

$\quad\quad \dot{h}'_{zz} = \dot{\varepsilon}_3 \, h'_{zz}$

<u>note</u>: in this frame $\underline{h}'$ is diagonal!

4) Rotate $\underline{h}$ into lab. frame:

$$\dot{\underline{h}} = \underline{V}_\varepsilon \, \dot{\underline{h}}' \, \underline{V}_\varepsilon^{-1}$$

note: $\dot{\underline{h}}'$ is symmetric $\Rightarrow$ $\underline{h}$ will remain symmetric!

+ Add rotation terms

$$\dot{\underline{h}}{}^{\alpha\beta} = \dots + h^{\alpha\delta} \, R^{\beta\delta} + h^{\beta\delta} \, R^{\alpha\delta}$$

"Jauman stress rates equivalent"

Application: compression of a cylinder
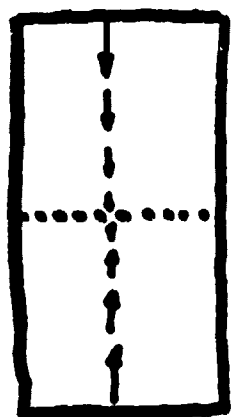
$v_y \propto y$: homologous compression.

Analytical sol: constant density

$$\rho_t = \frac{M}{V} = \frac{M}{\pi R^2 (L - v_y \cdot t)}$$

Note: At $t = 180$ ms, we have

Standard SPH $\quad h \approx 5000$

Tensor SPH $\quad h_{yy} = 500$

$\Rightarrow$ 10x resolution increase !

but since $h \propto N^{-1/3}$ standard SPH would need $10^3 = 1000$ times more particles to achieve similar resolution!

Standard GFR
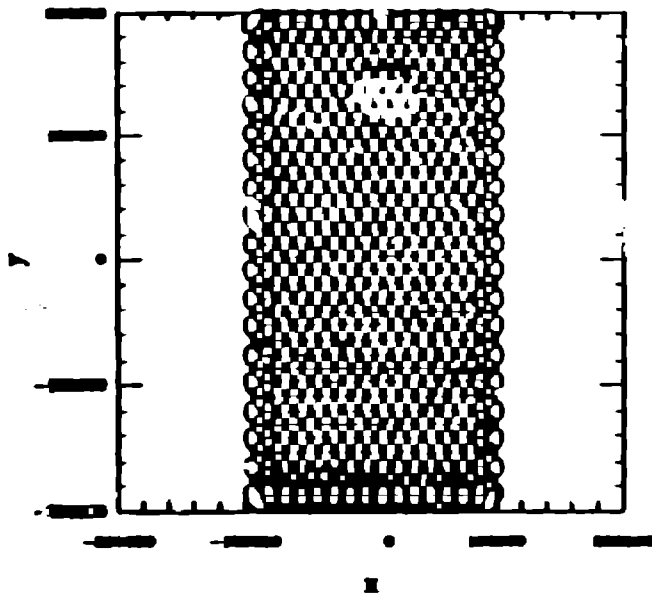
h-tensor Time = 0 ms
(Lev. 2)

h-tensor Time = 78.554 ms
(Lev. 2)
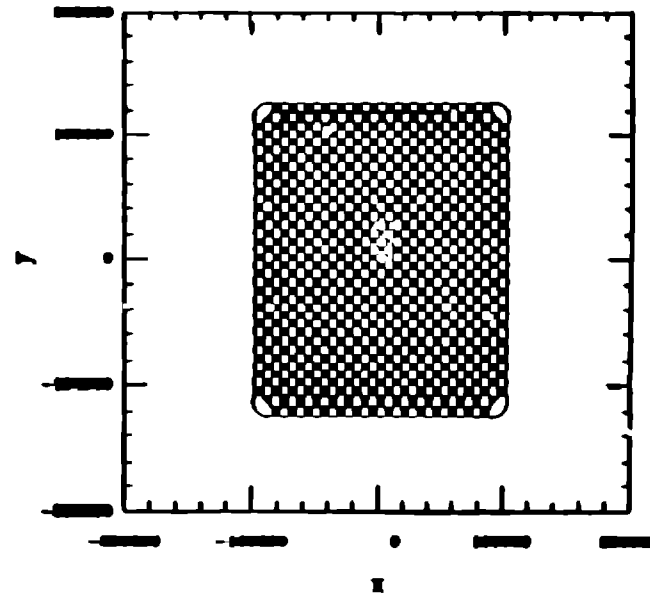
h-tensor Time = 120.991 ms
(Lev. 2)
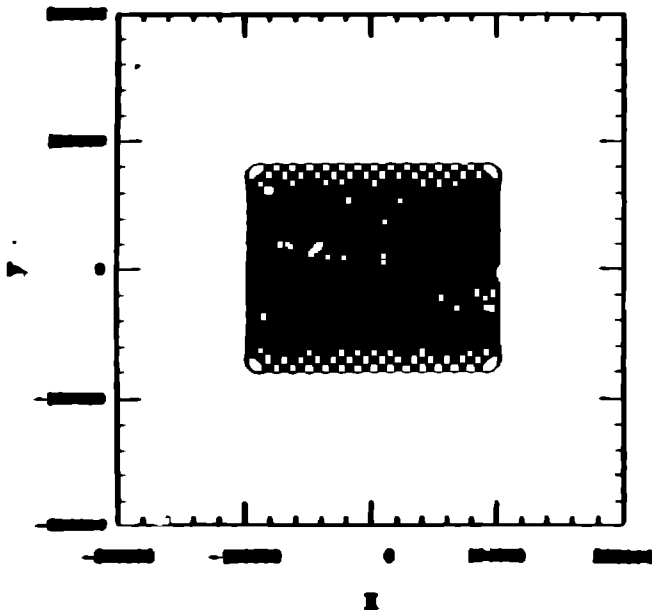
h-tensor Time = 160.663 ms
(Lev. 2)
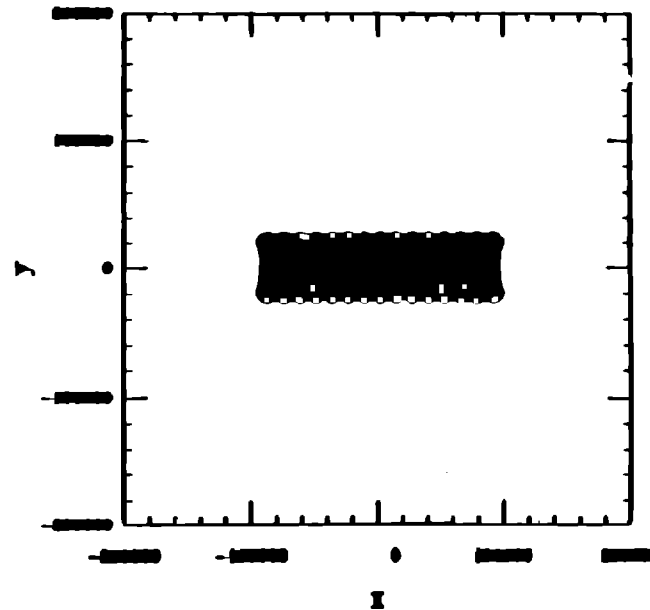
h-tensor Time = 0 ms
(test 1)
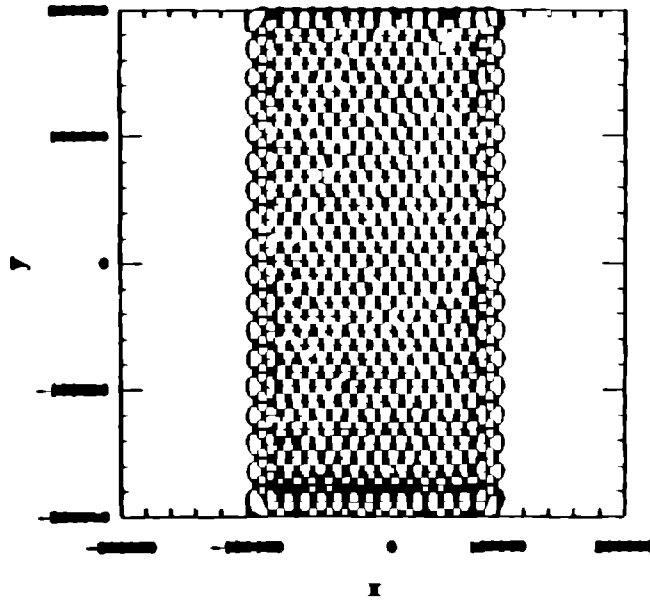
h-tensor Time = 61.69 ms
(test 1)
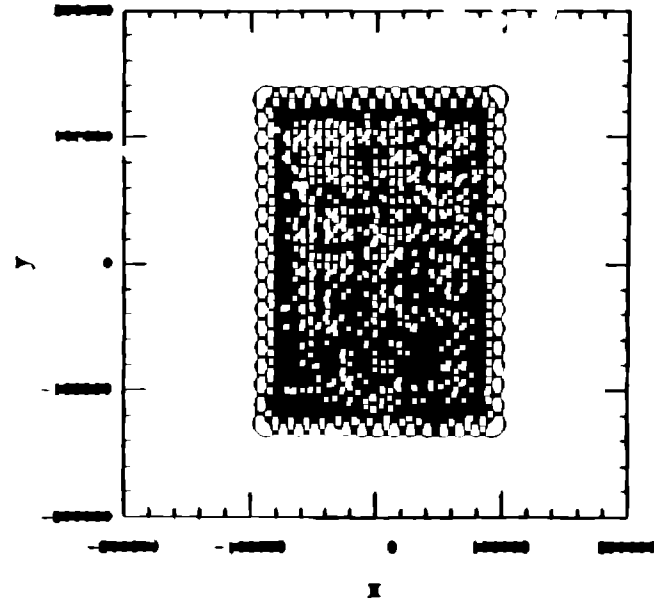
h-tensor Time = 126.311 ms
(test 1)
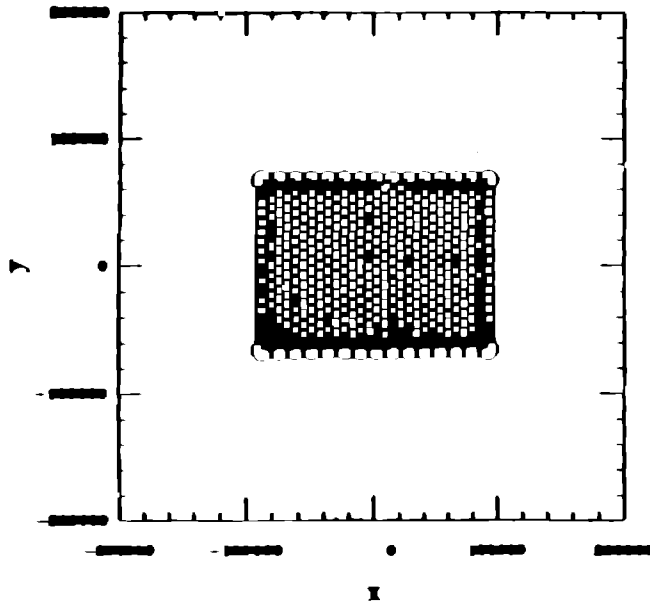
h-tensor Time = 180.358 ms
(test 1)
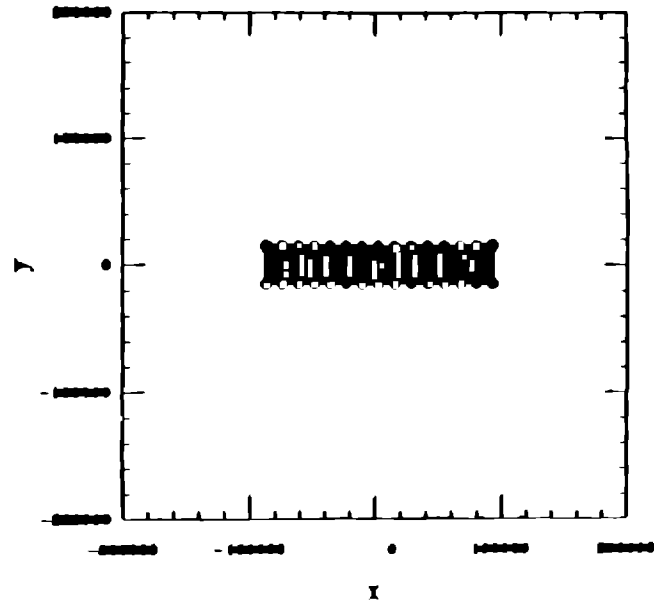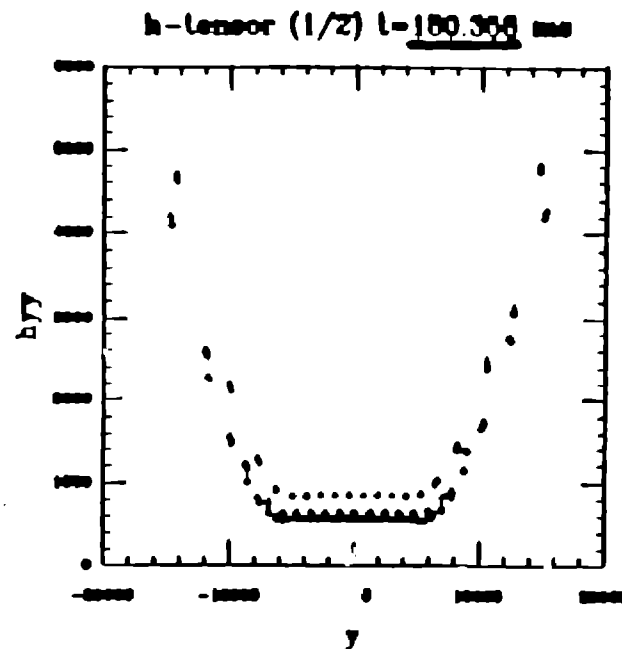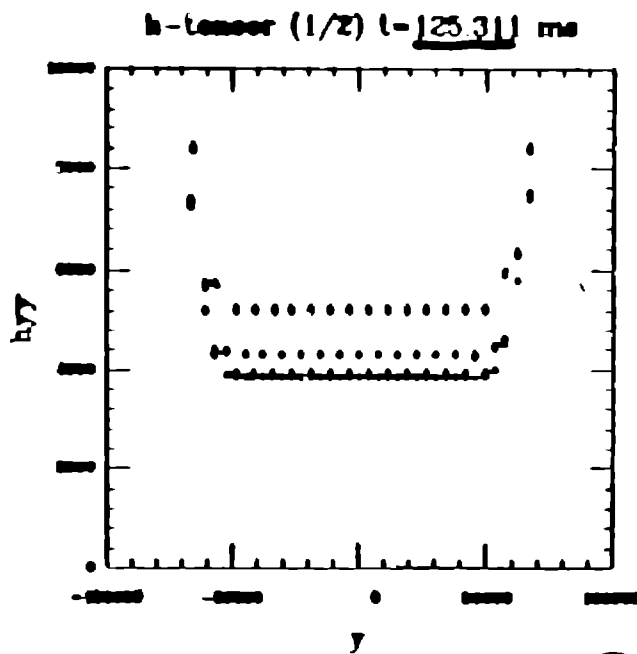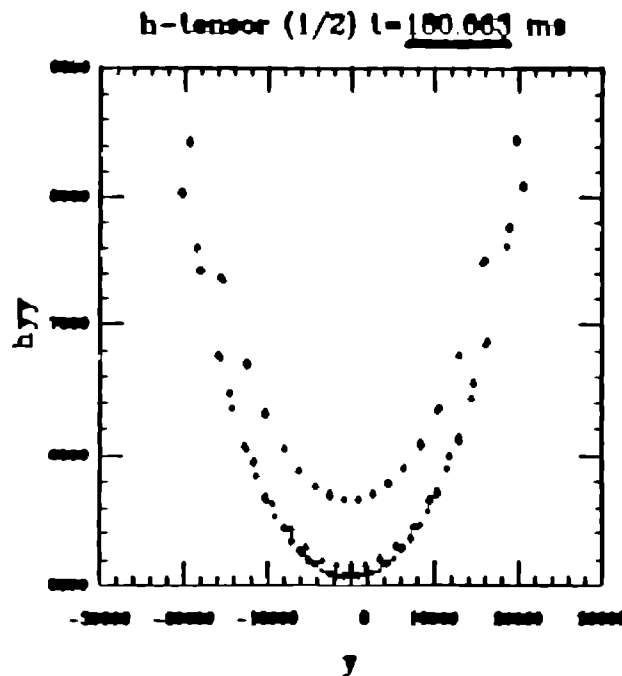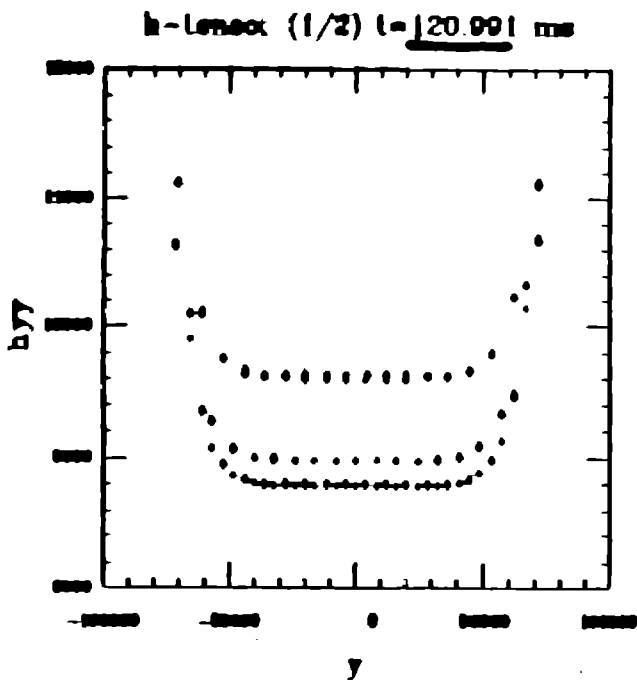
Tensor SPH

h-tensor (1/2) t=125.311 ms

h-tensor (1/2) t=150.300 ms

Standard SPH

h-tensor (1/2) t=120.991 ms

h-tensor (1/2) t=150.003 ms

Tensor SPH

h-tensor (1/2) t=125.311 ms

h-tensor (1/2) t=160.366 ms
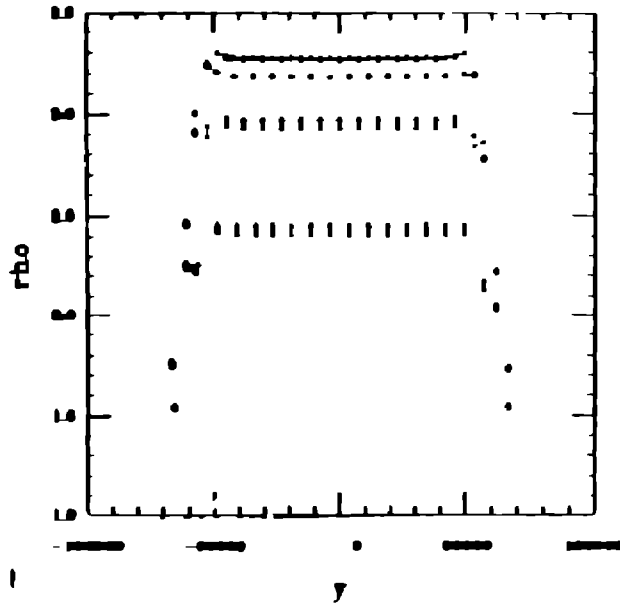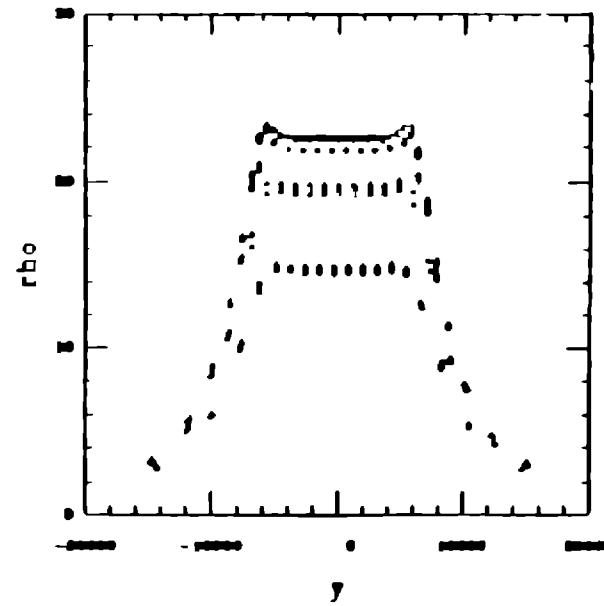
Standard SPH

h-tensor (1/2) t=120.991 ms
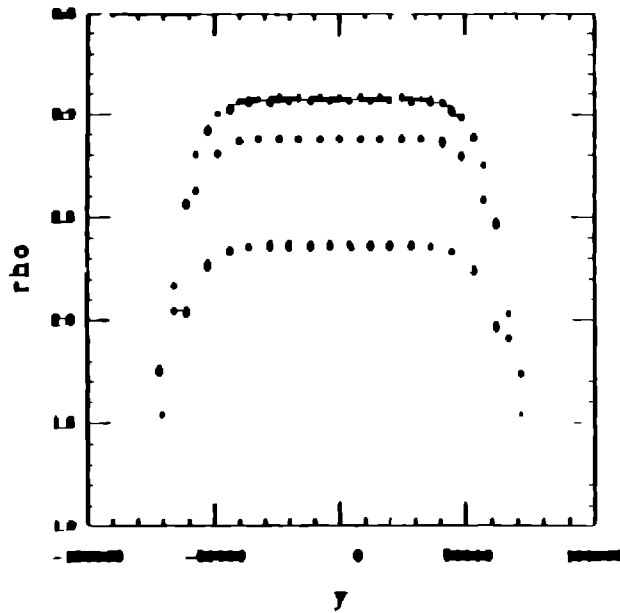
h-tensor (1/2) t=100.003 ms
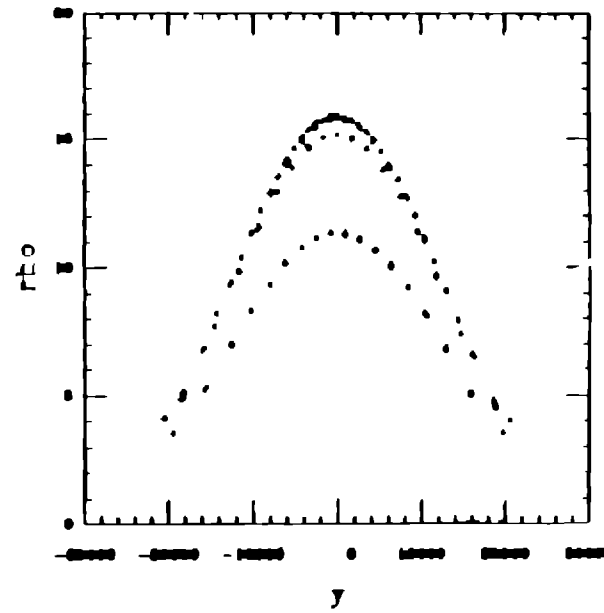
Rotating Disk

Set: $\frac{H}{R} = 0.2$

$\Omega = 2\pi \cdot 10^{4} \Rightarrow P = 10^{-4} s$
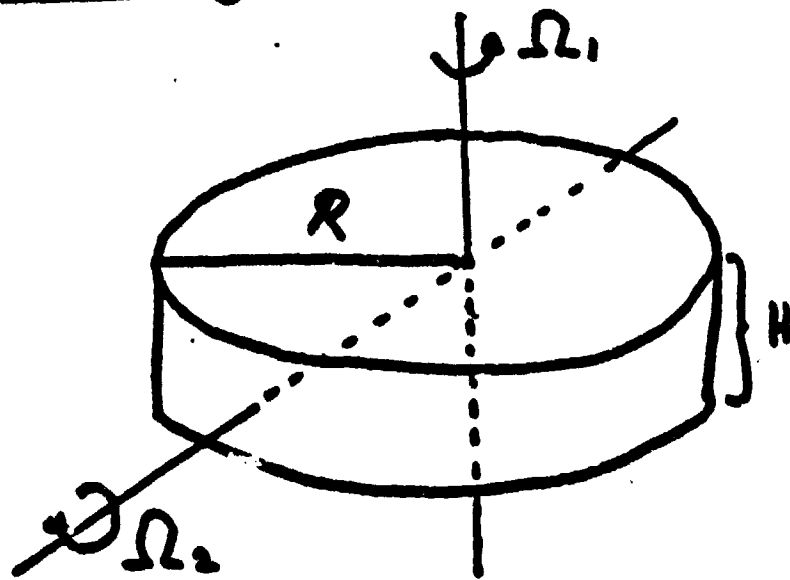
Tillotson eos for water.

Result:

1) Rotation around Ω_1 conserves momentum and angular momentum exactly

2) Rotation around Ω_2 __does not__ conserve angular momentum!

Why?   1) $\vec{\nabla} W$ is not along $\vec{r}_{ij}$

2) Rotation terms for h are poor!

Rotating Disk: t=5 μs
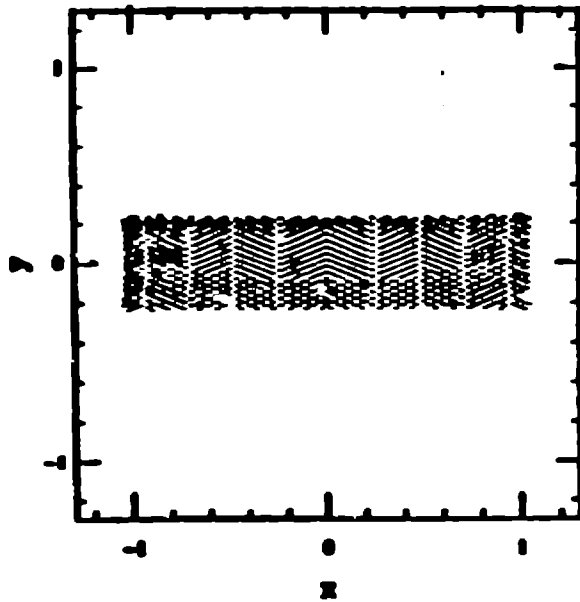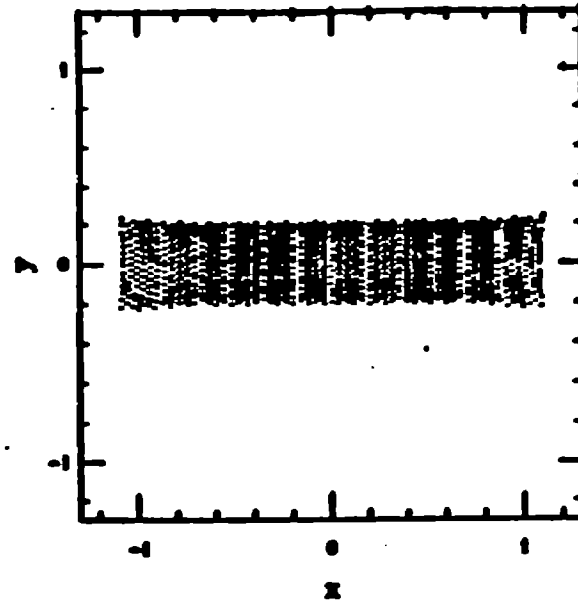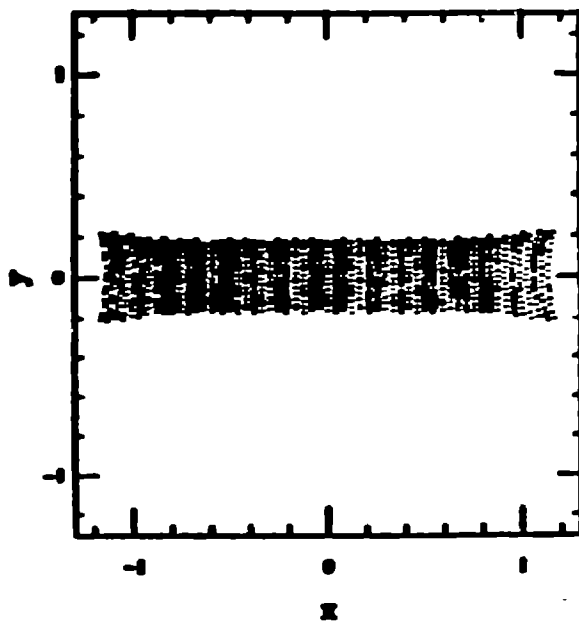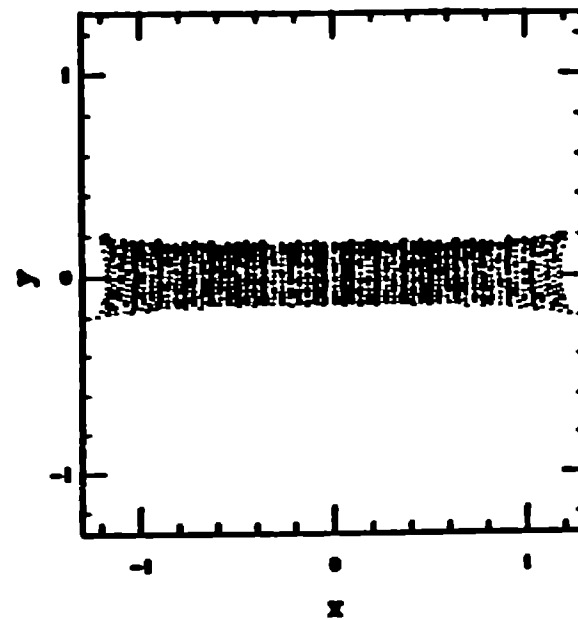
Rotating Disk: t=8 μs

Rotating Disk: t=10 μs

Rotating Disk: t=13 μs

Rotating Disk: t=13 μs
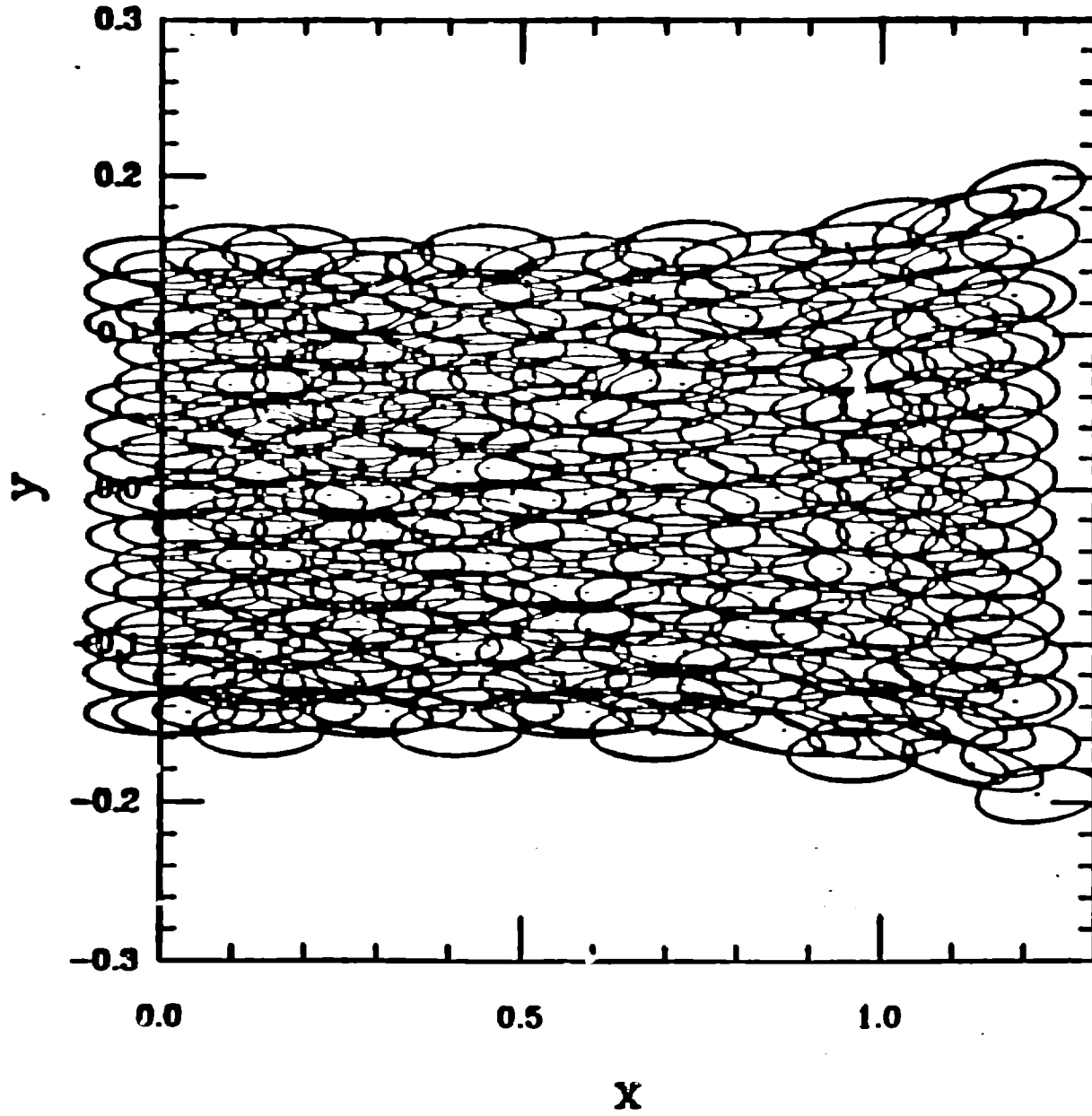
Rotating Disk: t=3 μs
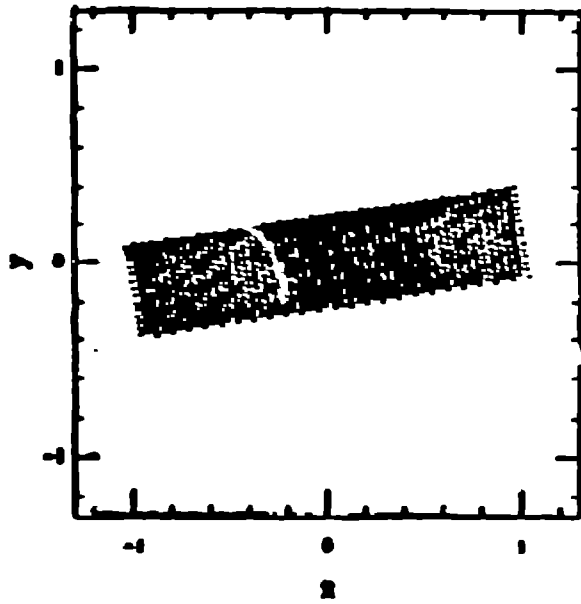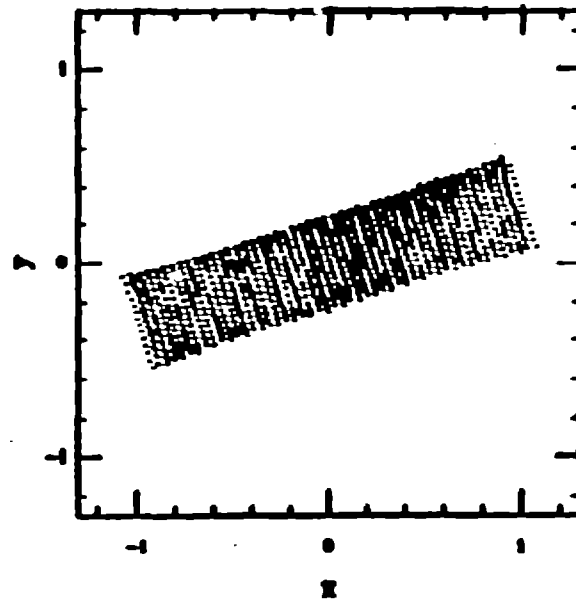
Rotating Disk: t=5 μs
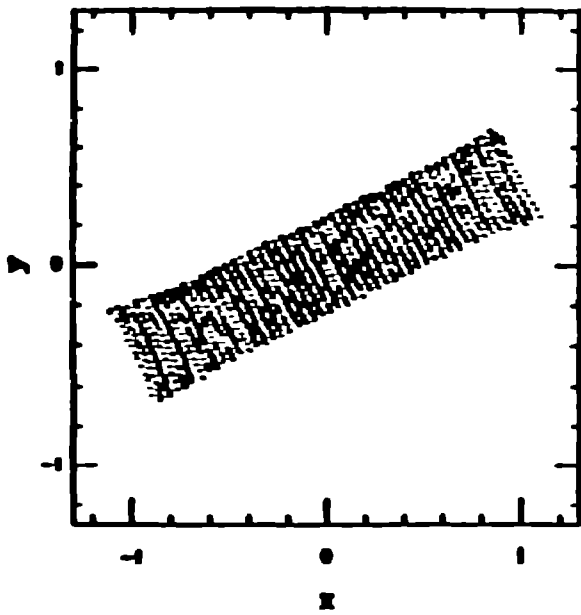
Rotating Disk: t=8 μs
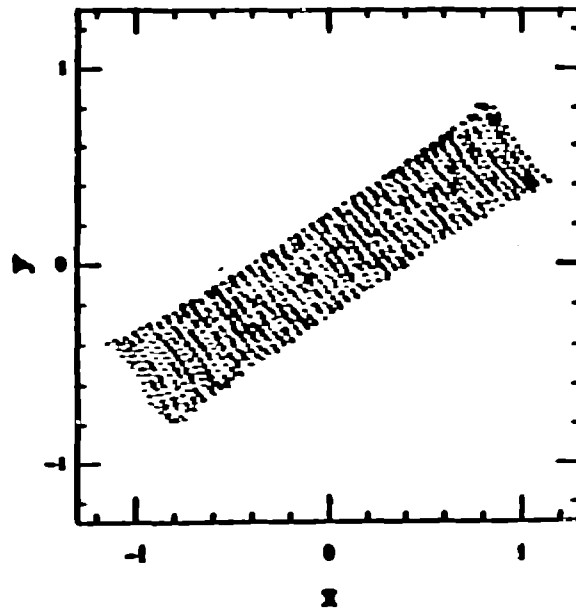
Rotating Disk: t=10 μs

Rotating Disk: t=10 μs
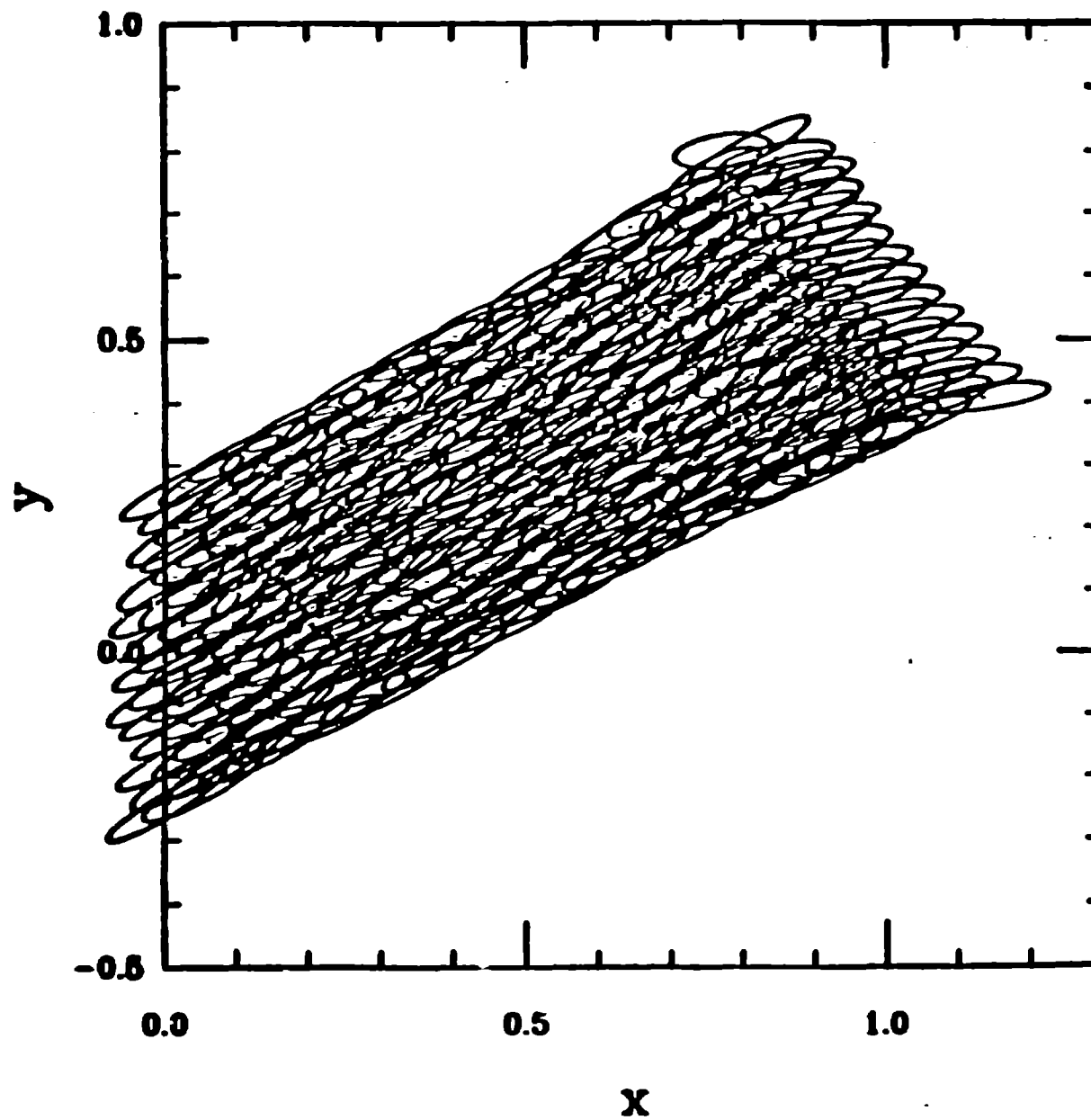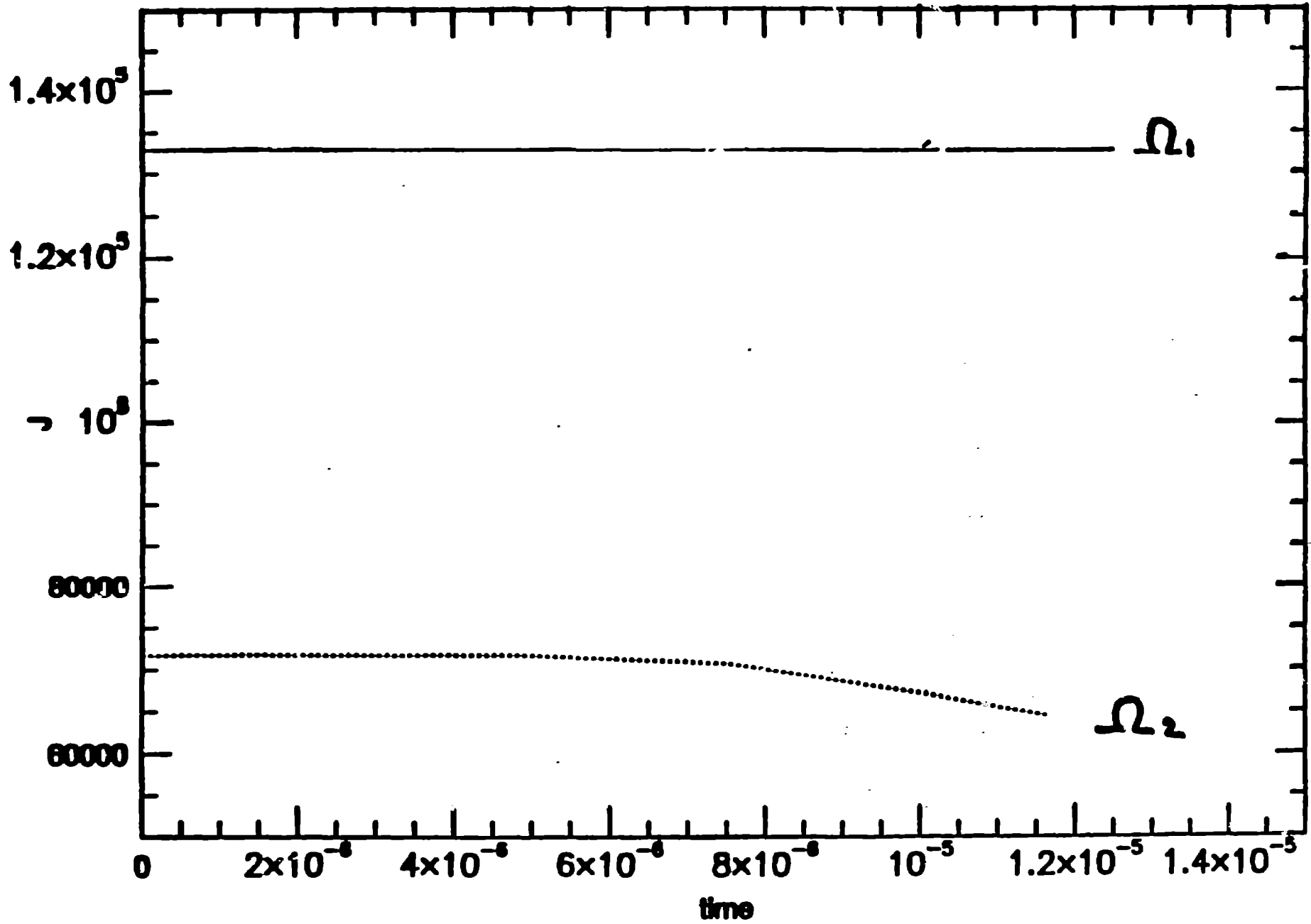
Angular Momentum

Conservation of Angular Momentum

Total angular momentum:

$$J = \sum_a M_a \vec{r}_a \times \vec{v}_a$$

Conservation implies: $\dfrac{dJ}{dt} = 0$

$$\rightarrow \frac{d}{dt} \sum_a M_a \vec{r}_a \times \vec{v}_a = \sum_a M_a \vec{r}_a \times \frac{d\vec{v}_a}{dt}$$

Assume 2D + gaussian kernel

$$y_a \cdot \frac{\partial v_a^x}{\partial t} = - \sum_b M_b \vec{v}_{ab} \frac{(x_a - x_b)}{h_x^2} W_{ab}$$

$$x_a \frac{\partial v_a^y}{\partial t} = - \sum_b M_b \vec{v}_{ab} \frac{(y_a - y_b)}{h_y^2} W_{ab}$$

So that conservation becomes

$$\frac{dJ}{dt} = \sum_a M_a \left(y_a \dot{v}_a^+ - x_a \dot{v}^y \right)$$

putting everything together:

$$\frac{dJ}{dt} = -\sum_a \sum_b m_a\, m_b\, \sigma_{ab}\, W_{ab} \left[\frac{y_a(x_a - x_b)}{h_x^{a^2}} - \frac{x_a(y_a - y_b)}{h_y^{a^2}} \right]$$

rewrite it as

$$\frac{dJ}{dt} = -\sum_a m_a\, x_a\, y_a \left[\frac{1}{h_x^{a^2}} - \frac{1}{h_y^{a^2}} \right] \cdot \sum_b m_b\, \sigma_{ab}\, W_{ab} \left(\frac{x_a y_b}{h_y^{a^2}} - \frac{y_a x_b}{h_x^{a^2}} \right)$$

clearly if $h_x = h_y \implies \frac{dJ}{dt} = 0$

the 2nd sum can be written as an integral:

$$\int \rho_b\, \sigma_{ab}\, W_{ab} \left(\frac{x_a y_b}{h_y^{a^2}} - \frac{y_a x_b}{h_x^{a^2}} \right) d\underline{r}_b$$

$$\rightarrow \quad \frac{x_a}{h_y^{a^2}} \int Q_{ab} \cdot W_{ab}\, y_b\, d\underline{r}_b - \frac{x_a}{h_x^{a^2}} \int Q_{ab}\, W_{ab}\, x_b\, d\underline{r}_b$$

$$Q_{ab} = \rho_b \cdot \sigma_{ab}$$

° $Q_{ab} =$ constant $\implies \frac{dJ}{dt} = 0$!

° $Q_{ab} \neq$ constant   use Taylor expansion

$\quad Q_{ab} = Q_{ab}(a) + (x_b - x_a)\left(\frac{\partial Q}{\partial x}\right)_a + (y_b - y_a)\left(\frac{\partial Q}{\partial y}\right)_a + \ldots$

All but the second order terms will vanish!

→ Error term of order h^2 !!

Blast wave

To remove problem with angular momentum conservation, use only the component of $\vec{\nabla} W$ that is along $\vec{r}_{ij}$

$\longrightarrow$ wrong dynamics!

Shock speed varies with direction as given by underlying lattice!

$\longrightarrow$ Do not use only radial component!

Radial only
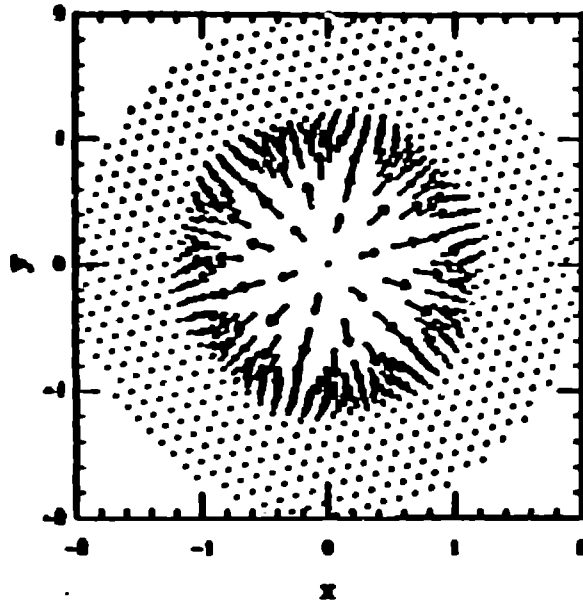
Full
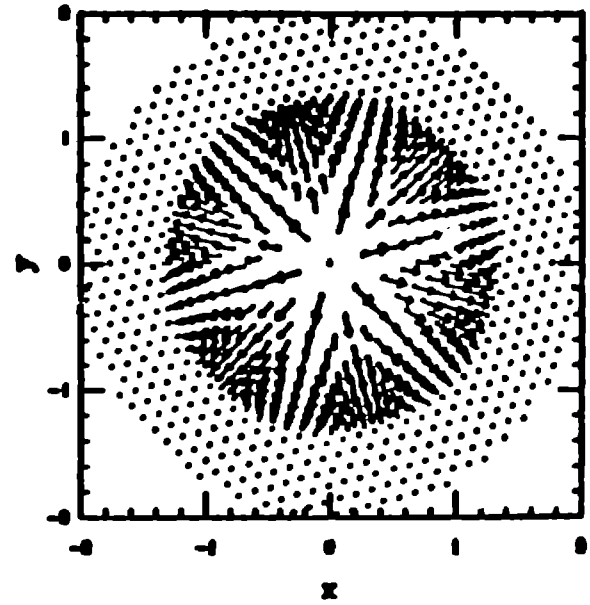
Standard SPH
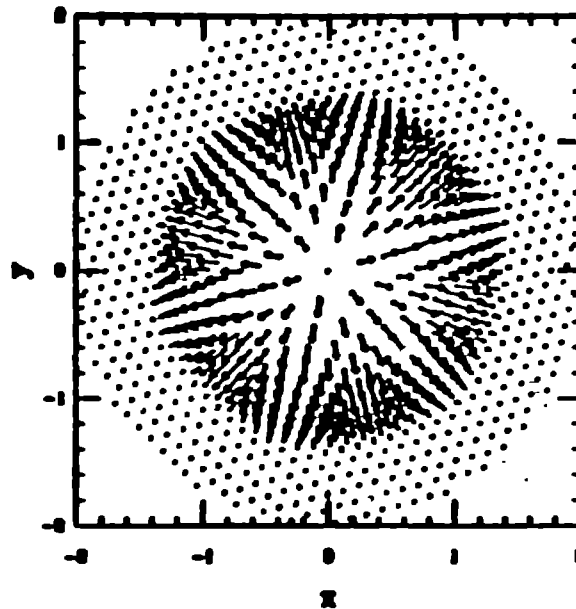
Radial only
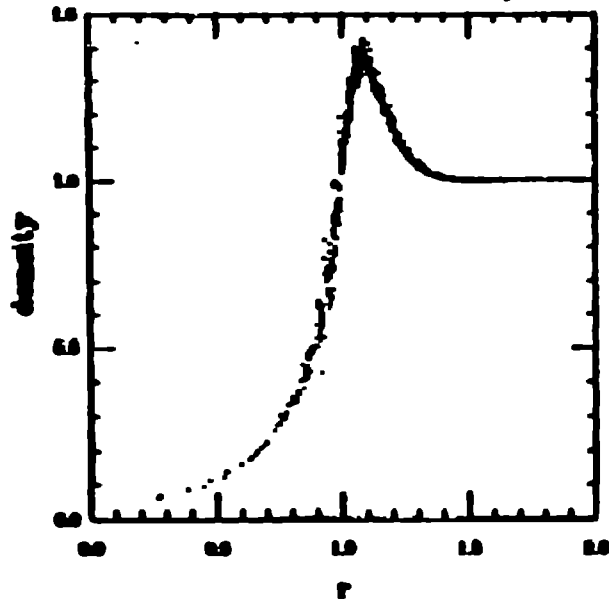
Full
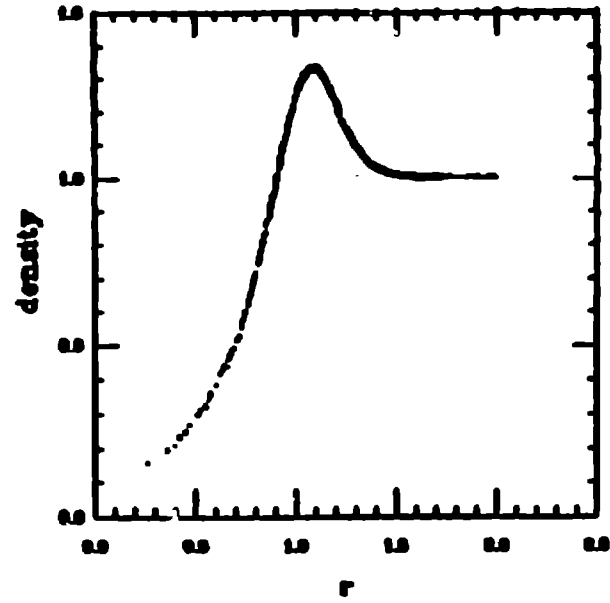
Standard
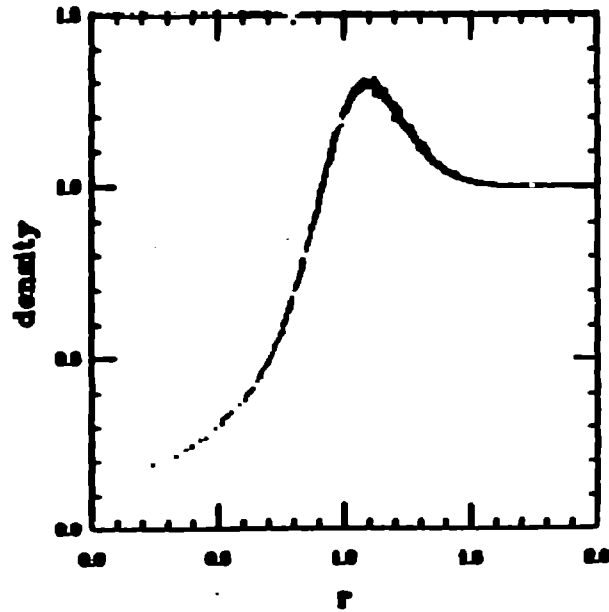
Radial only
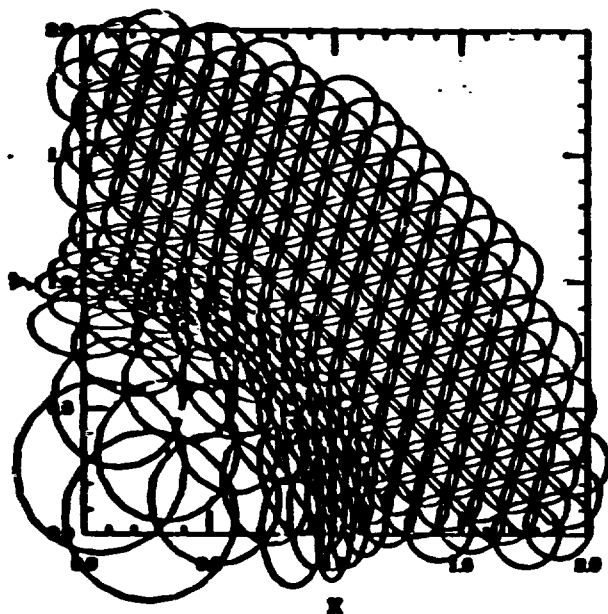
Full
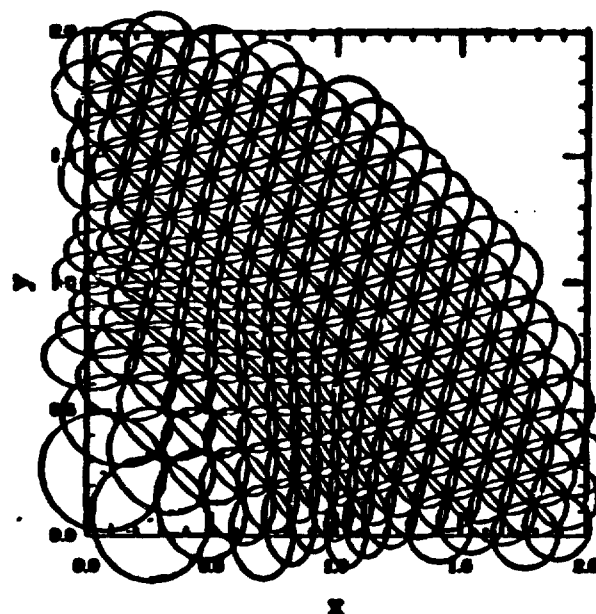
Standard
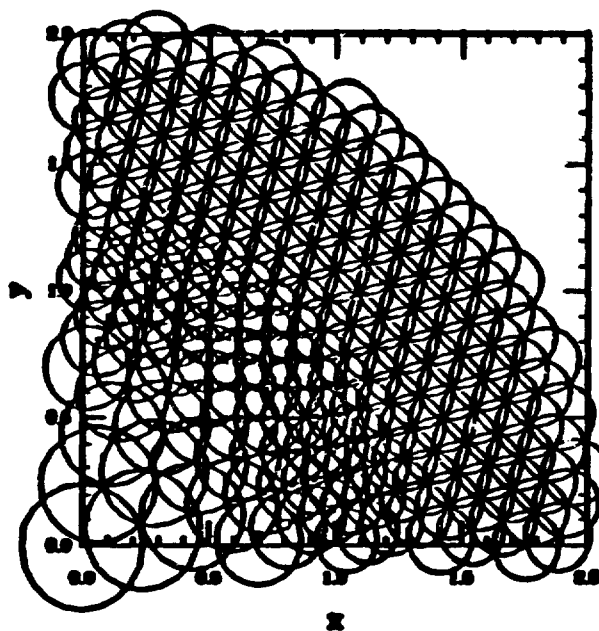
Tidal Disruption of stars

W. Benz
M. Fullbright

Top view:

star

BH

Roche
Limit

Side view:

BH

$\vec{F_1}$

star
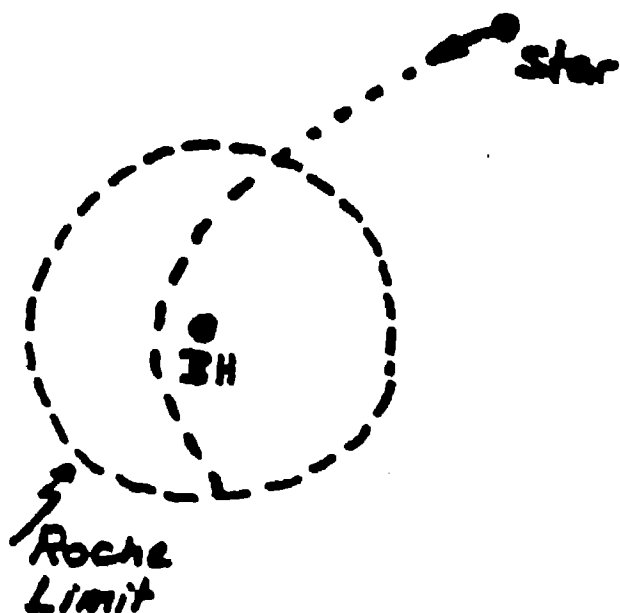
Flattening +
Stretching
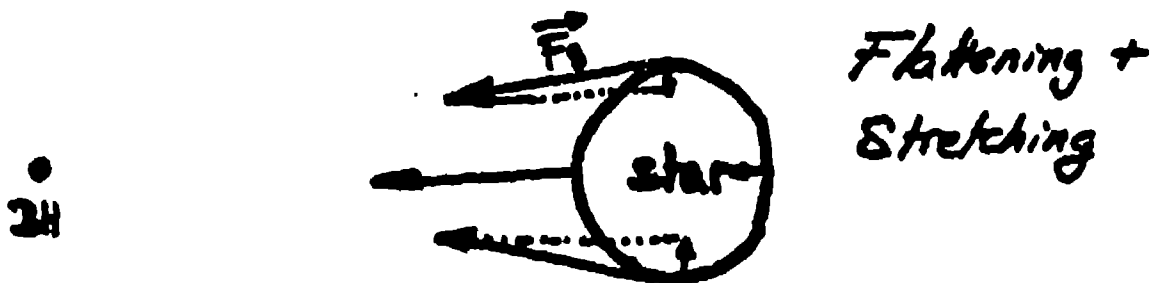
For $\dfrac{M_{BH}}{M_*} \gg 1$ Very, very strong flattening !

Question of astrophysical interest:

1) Amount of material captured

2) Ejection velocity and distribution of debris not captured

3) Density spike (red herring!)

Compression faster than stretching
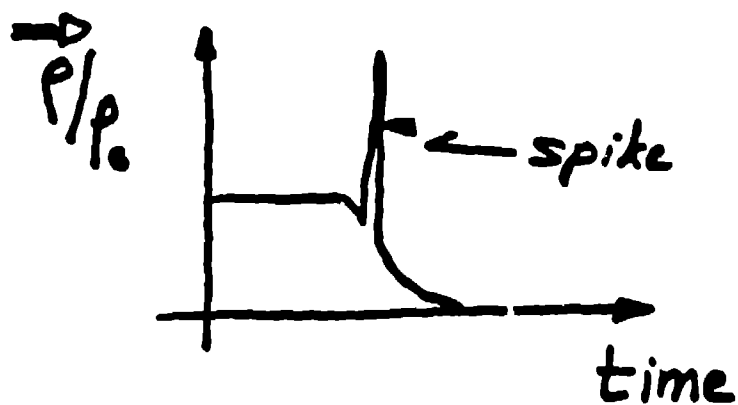
→ Numerical difficulties: 1D compression

$$\frac{z}{R} \ll 1 \quad \text{in fact} \quad z < h \; !!$$

→ ideal case for ellipsoidal kernels

(Bicknell Gingold)

Sphere t=0 ms
(h_scalar)
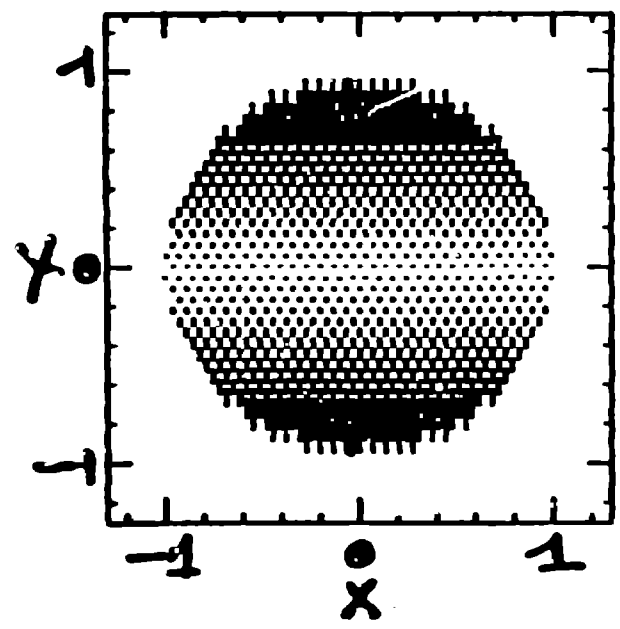
Sphere t=6.625 ms
(h_scalar)
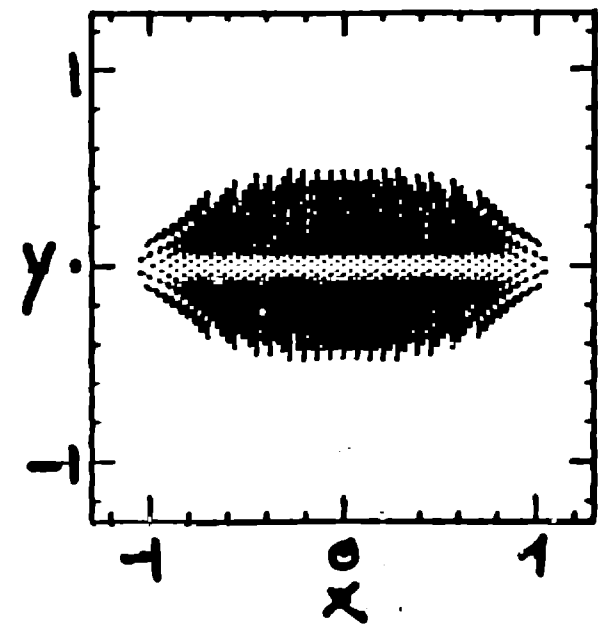
Sphere t=9.237 ms
(h_scalar)
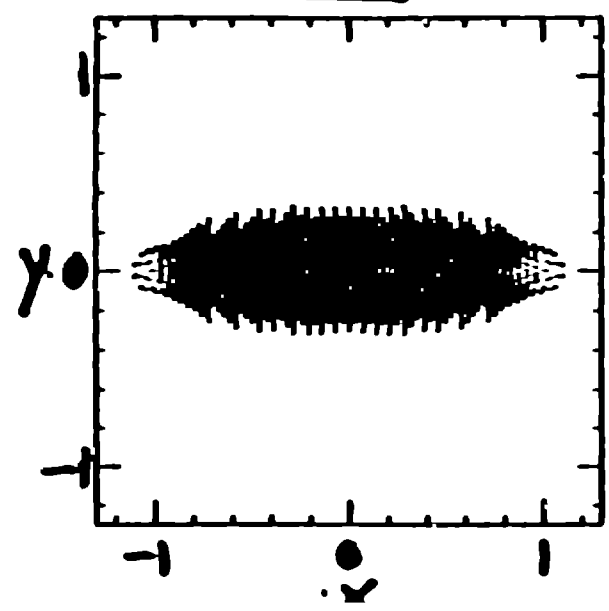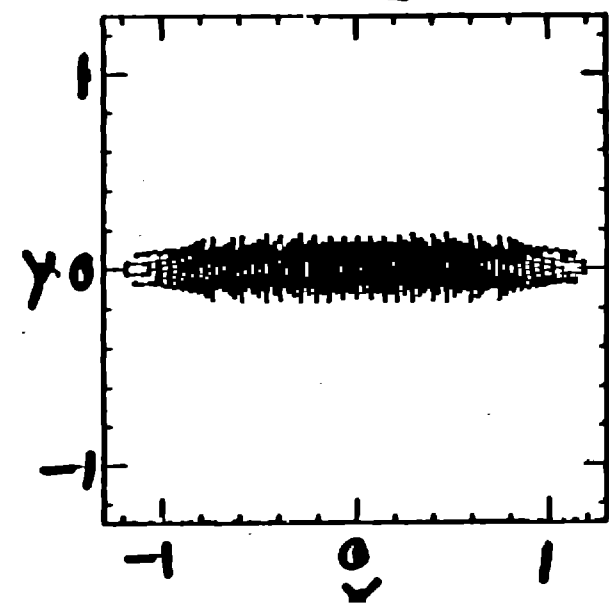
Sphere t=12.014 ms
(h_scalar)

Sphere t=0 ms
(h tensor)
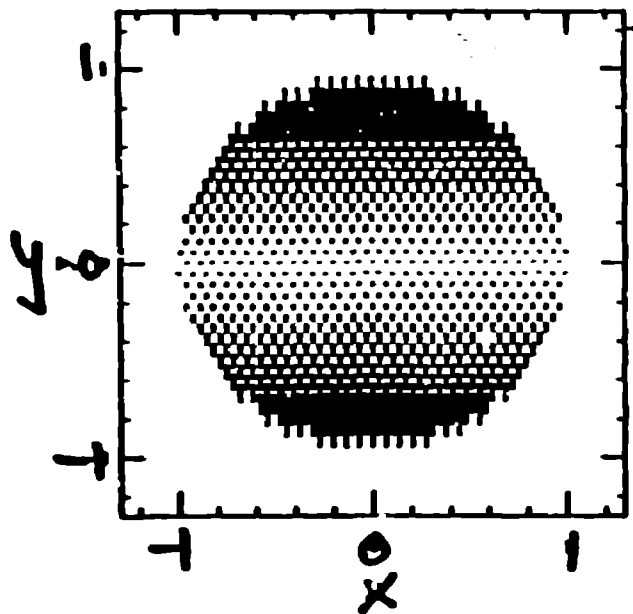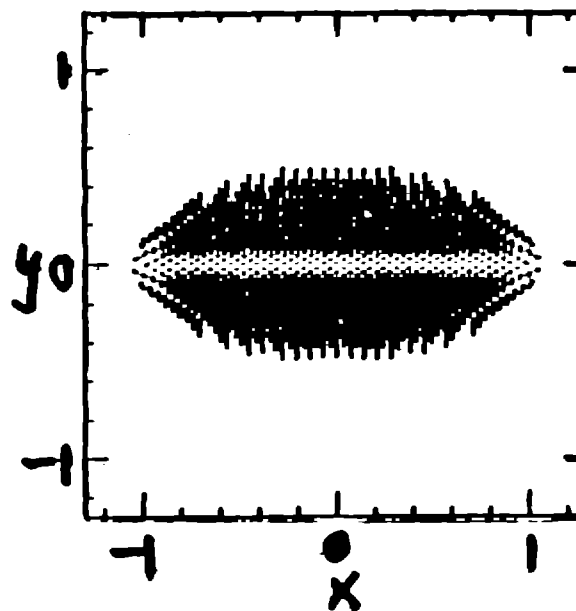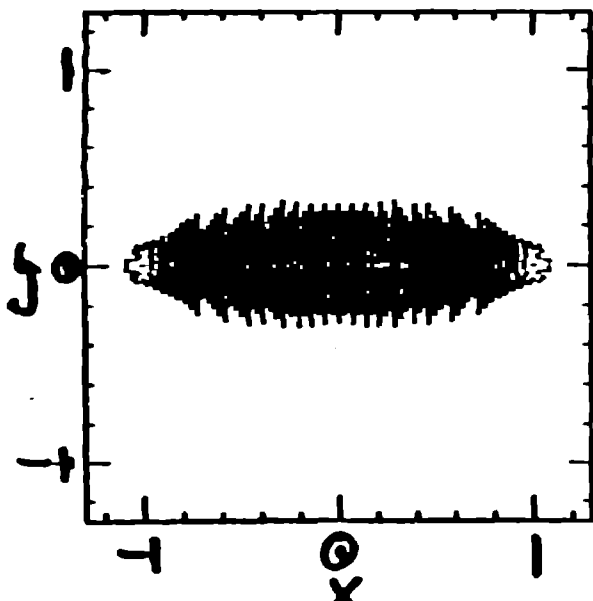
Sphere t=6.646 ms
(h tensor)

Sphere t=9.296 ms
(h tensor)

Sphere t=12.029 ms
(h tensor)

Sphere t=0 ms
(h tensor)

Sphere t=6.646 ms
(h tensor)

Sphere t=9.296 ms
(h tensor)

Sphere t=12.029 ms
(h tensor)

Sphere t=0 ms

(h scalar)

Sphere t=6.626 ms
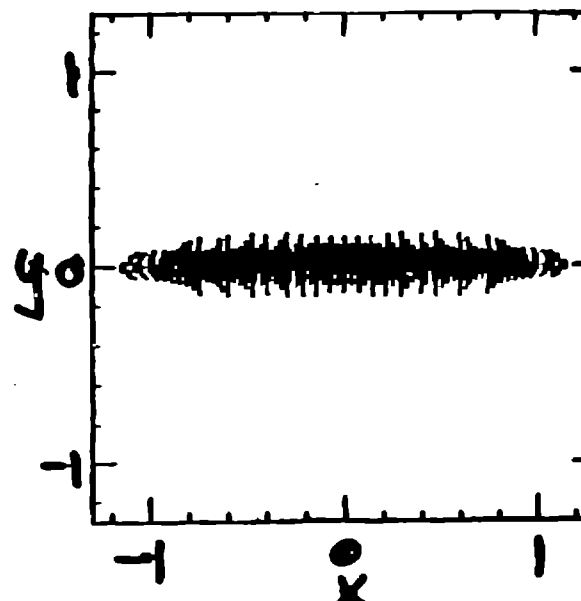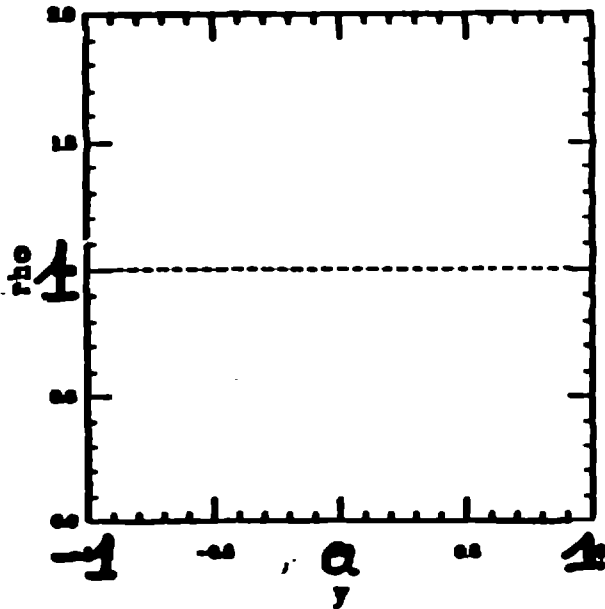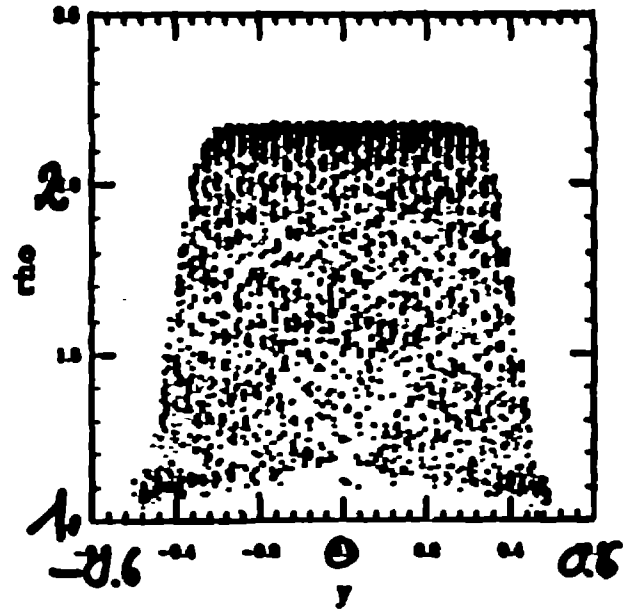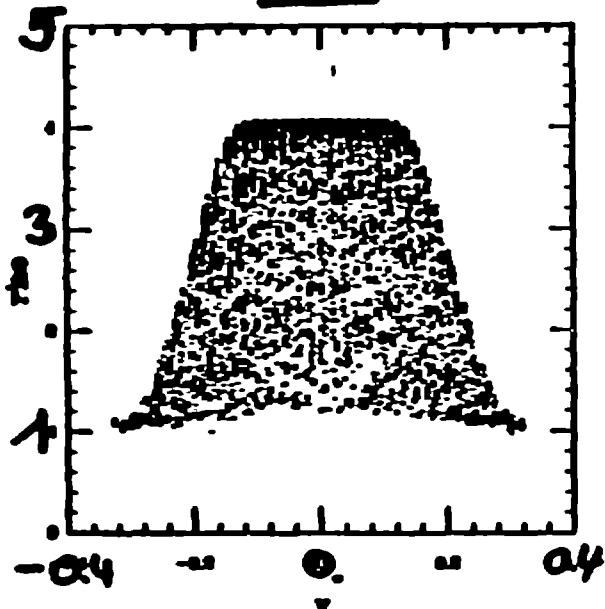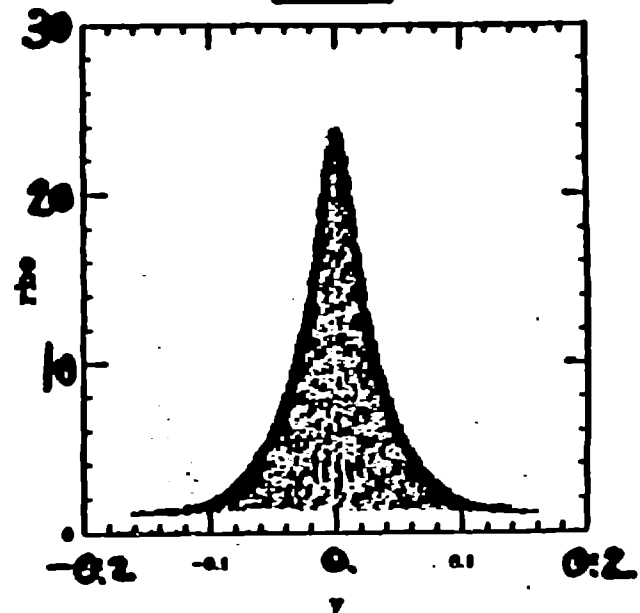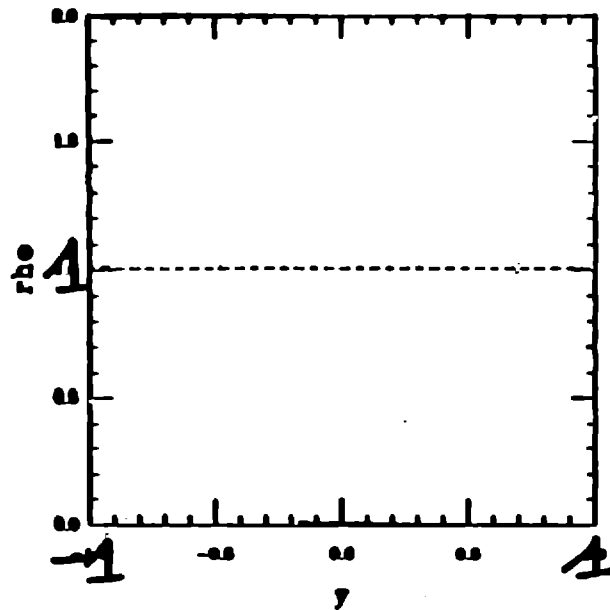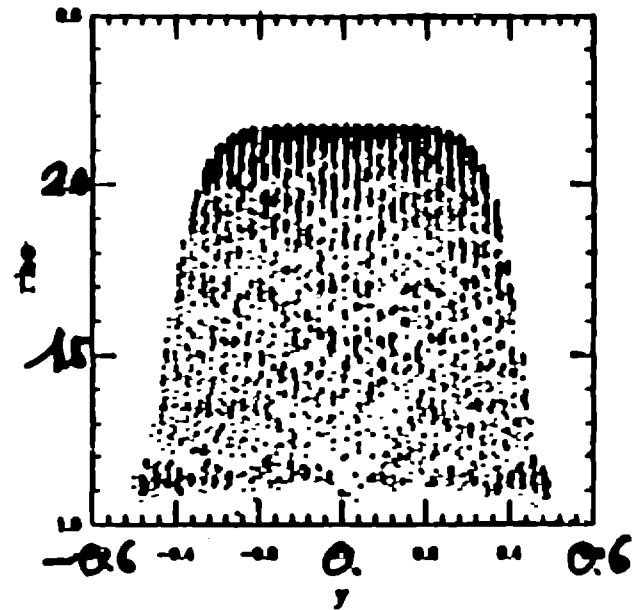
(h scalar)

Sphere t=9.237 ms
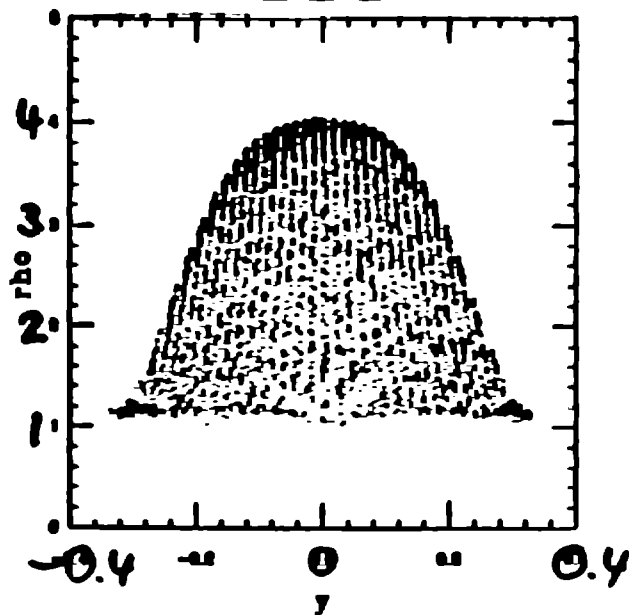
(h scalar)

Sphere t=12.014 ms

(h scalar)

$\beta = 5$, $N=611$, $M_{bh} = 10^5 M_\odot$

Standard
Tensor

$\alpha = \beta = 10^{-2}$

$\alpha = 1; \beta = 2$

$\alpha = \beta = 10^{-2}$

$\alpha = 1; \beta = 2$

$\log(\rho/\rho_c)$

Code Time (1 approx. eq. 1/2 hour)
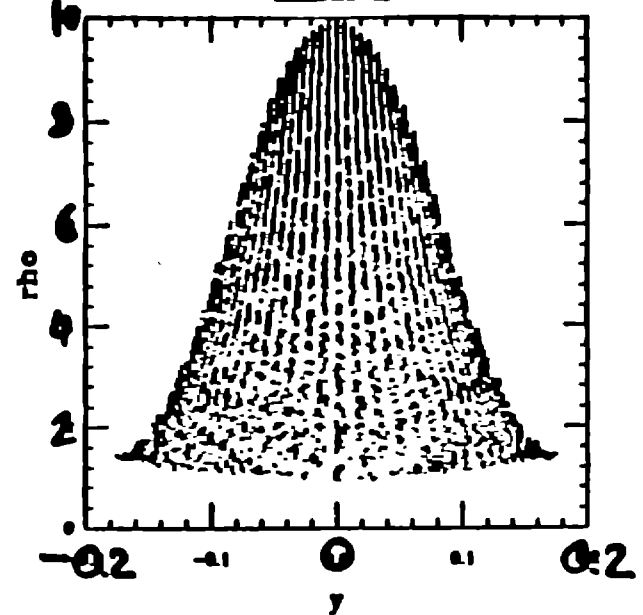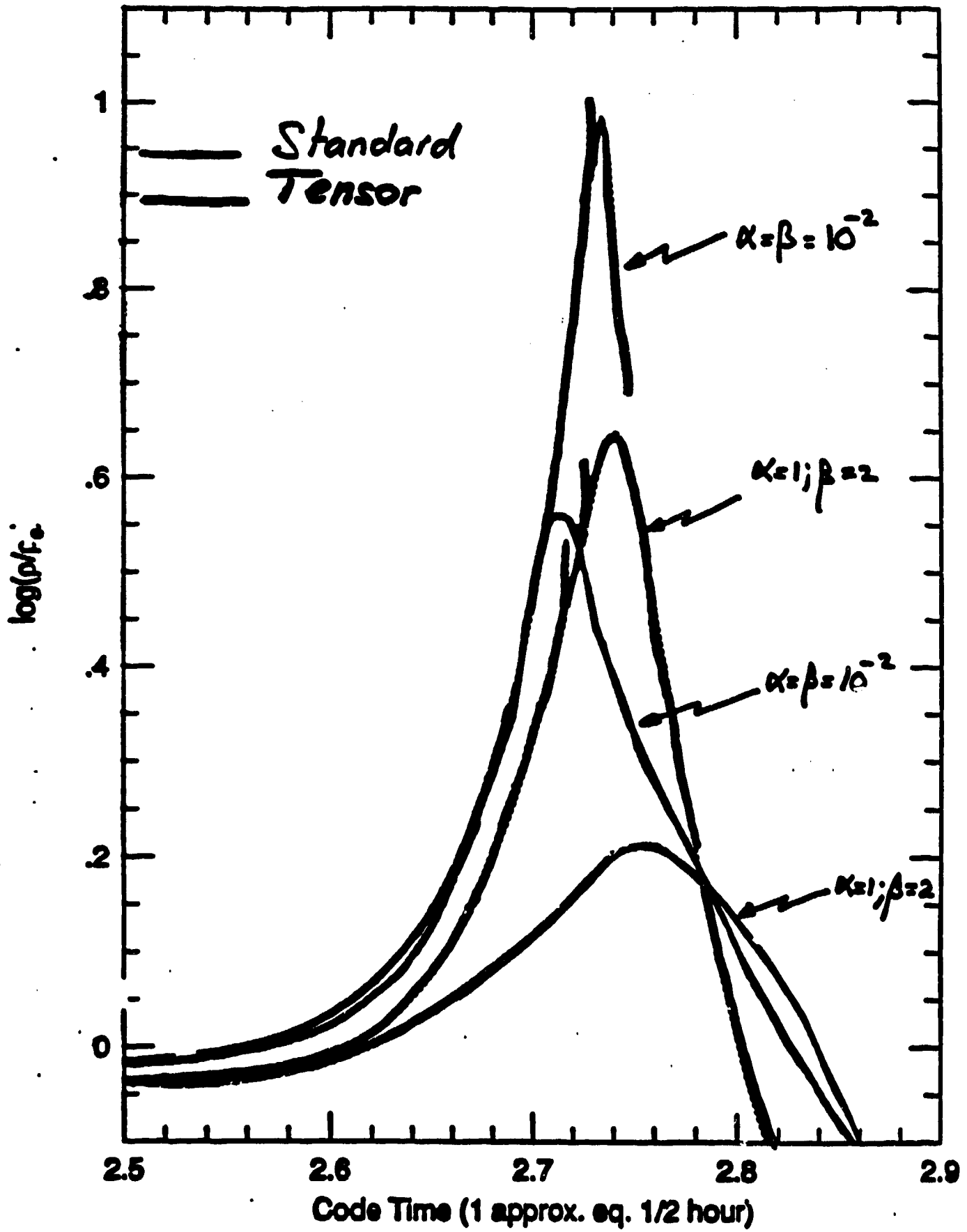
1) Resolution

with $N \approx 611$ $h \approx 0.16$ in standard SPH
(at maximum ρ)

$h_{zz} = 0.02$ in tensor SPH

$\Rightarrow$ resolution increase ~ 8
$\Rightarrow$ Standard SPH $\sim N \sim 31,000$ particles!

2) Artificial Viscosity

If shocks are present, dissipation will increase

entropy $\Rightarrow$ resist further squeezing!

but.... there are no real shocks $\neg$s the star

gets squeezed homologously...

$\rightarrow$ results should be indep. of α, β.

but they are not!
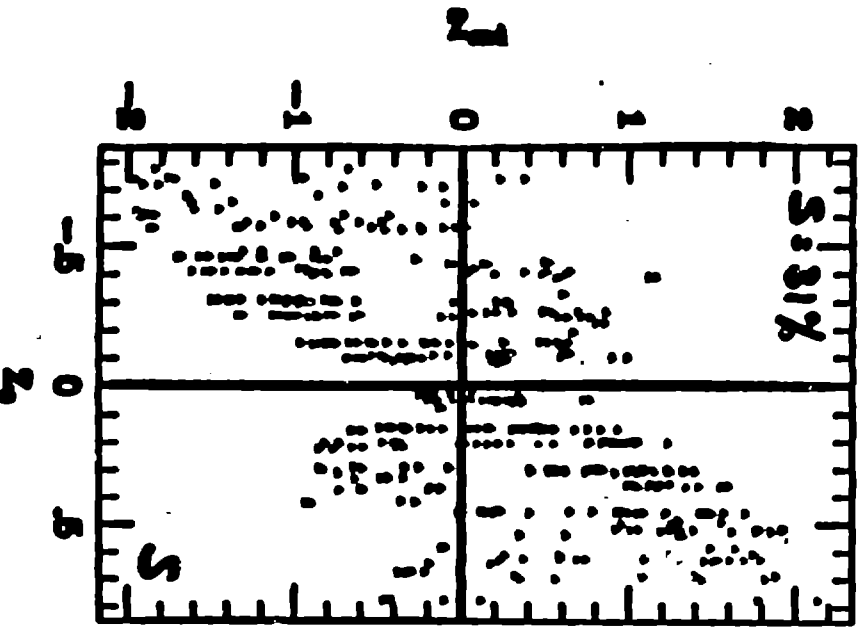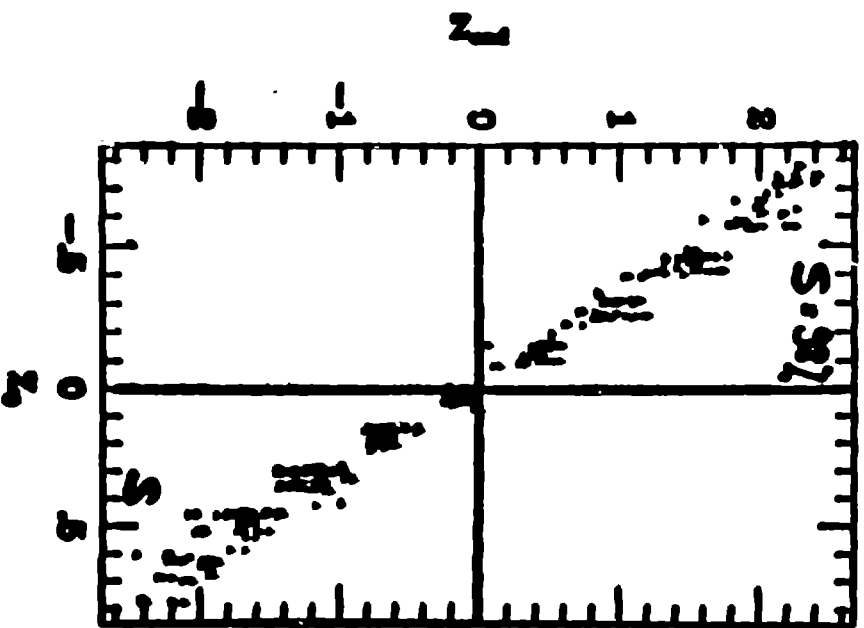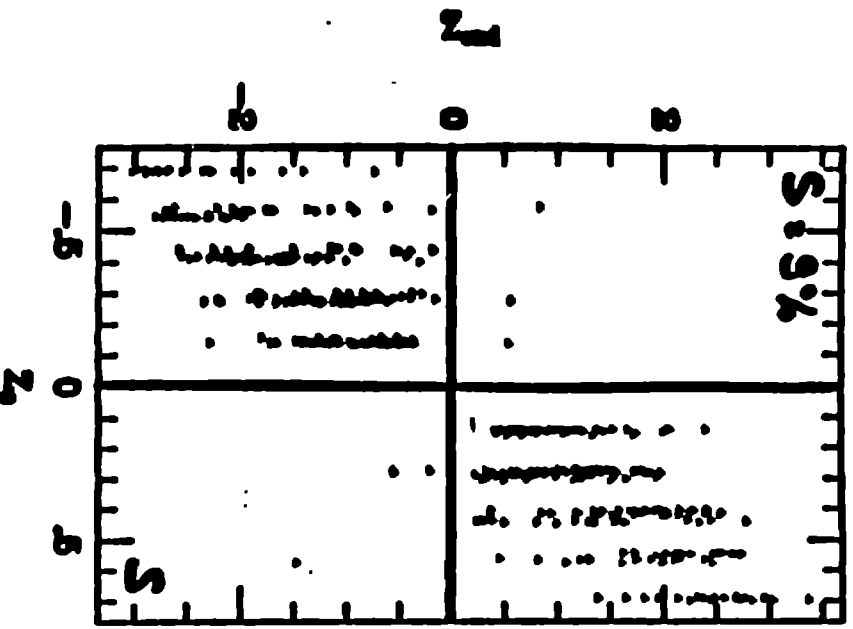
STANDARD STH
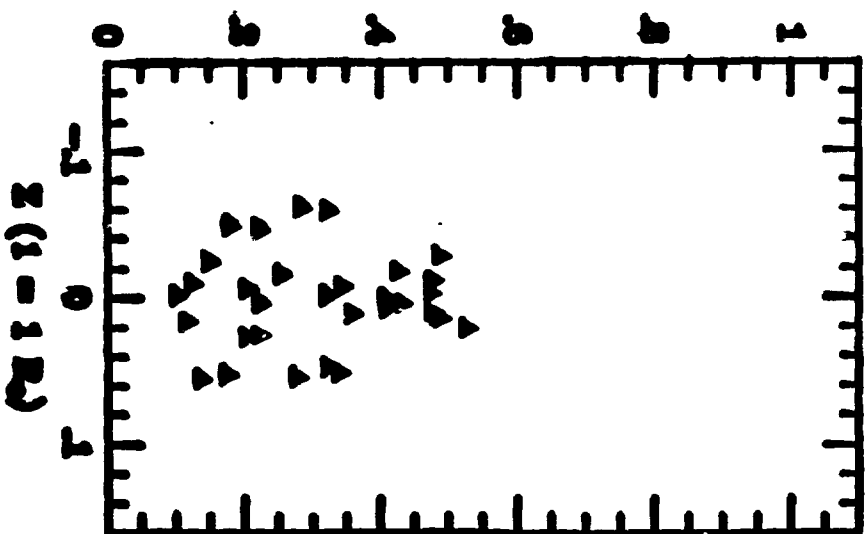
TENSOR STH
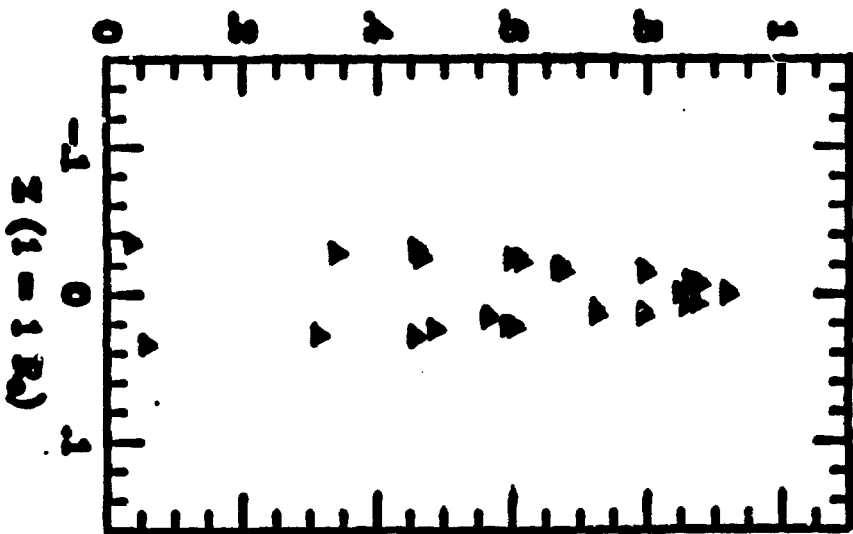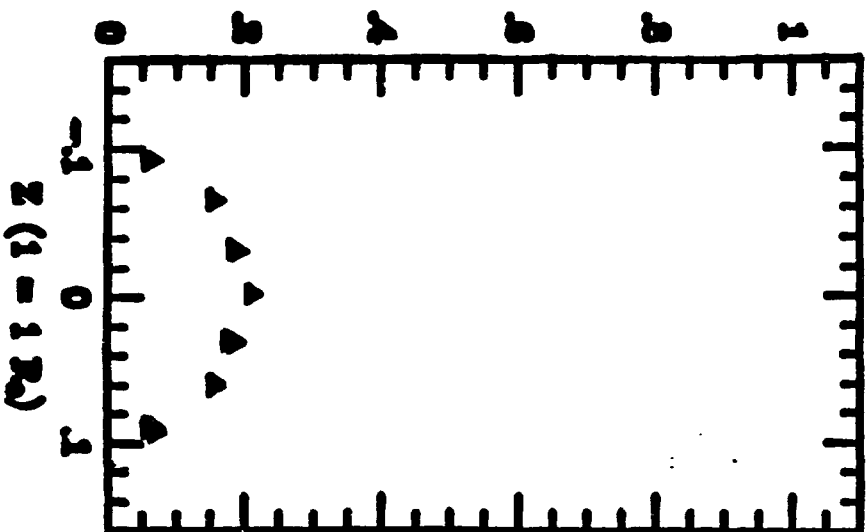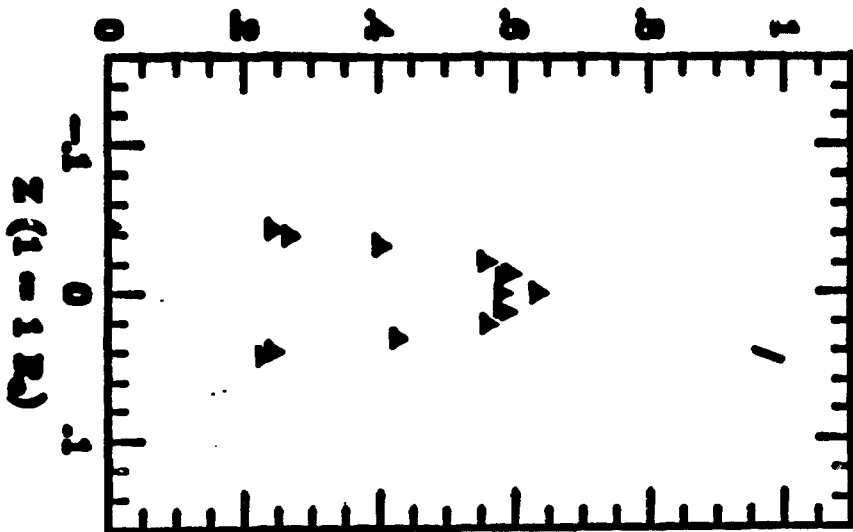
$\beta = 5$, $N=611$ & 1231, $M_n = 10^6$ $M_\odot$
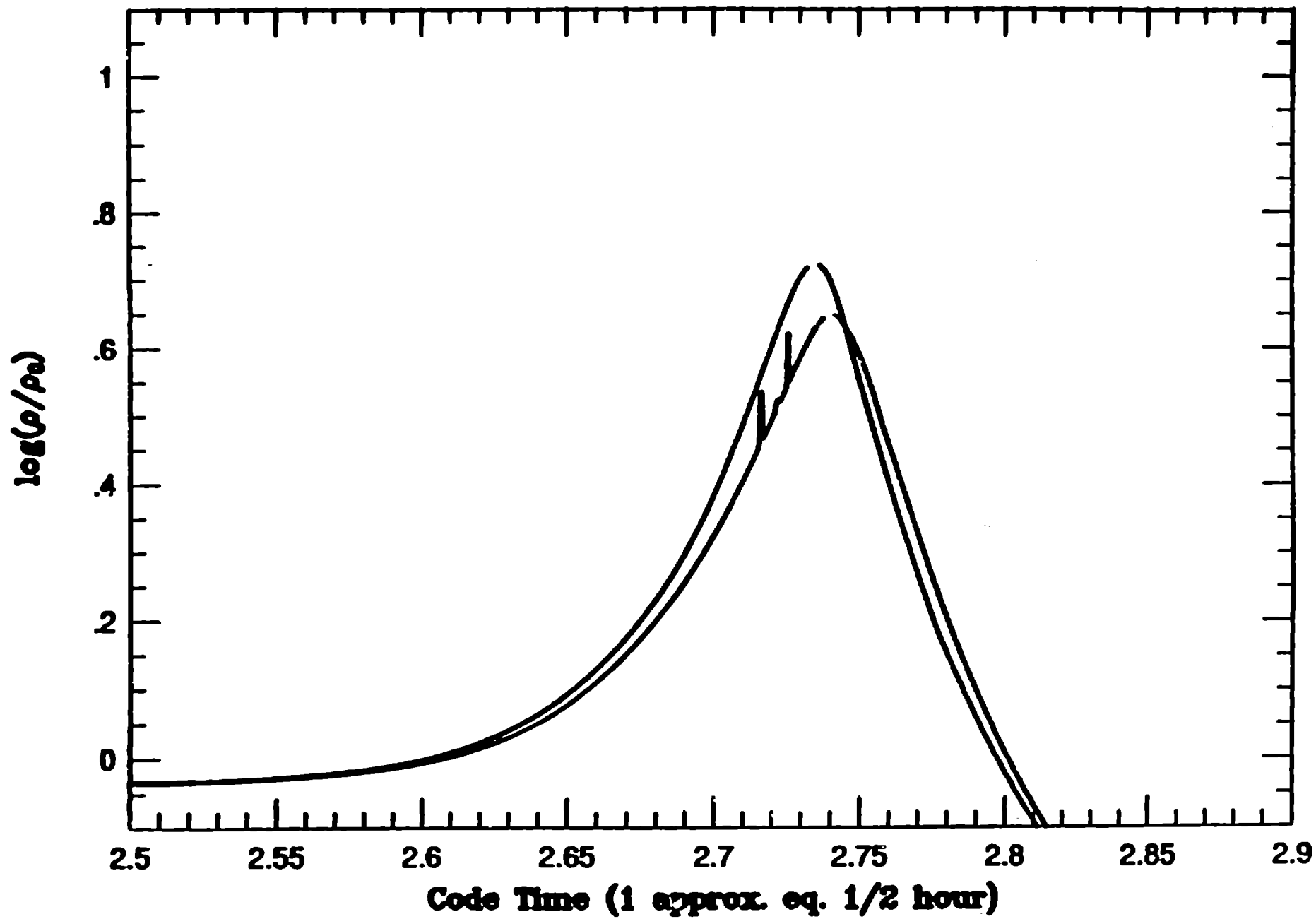
Results:

Higher densities with low values for α, β.

but... not really hydrodynamics as particles stream through the plane...

<u>Note:</u> Using the "tank stopper" XSPH is not a real solution as this does not conserve energy!

→ <u>Bottom line</u>: fix artificial viscosity to remove heating in homologous flows!

Breaking the 10,000,000 particle limit in SPH

Mike Warren (LANL T-6, UCSB)

`msw@eagle.lanl.gov`

W. H. Zurek, J. G. Hills, W. A. Miller (LANL T-6)

J. K. Salmon, M. B. Davies (Caltech)

P. Laguna (Penn State)
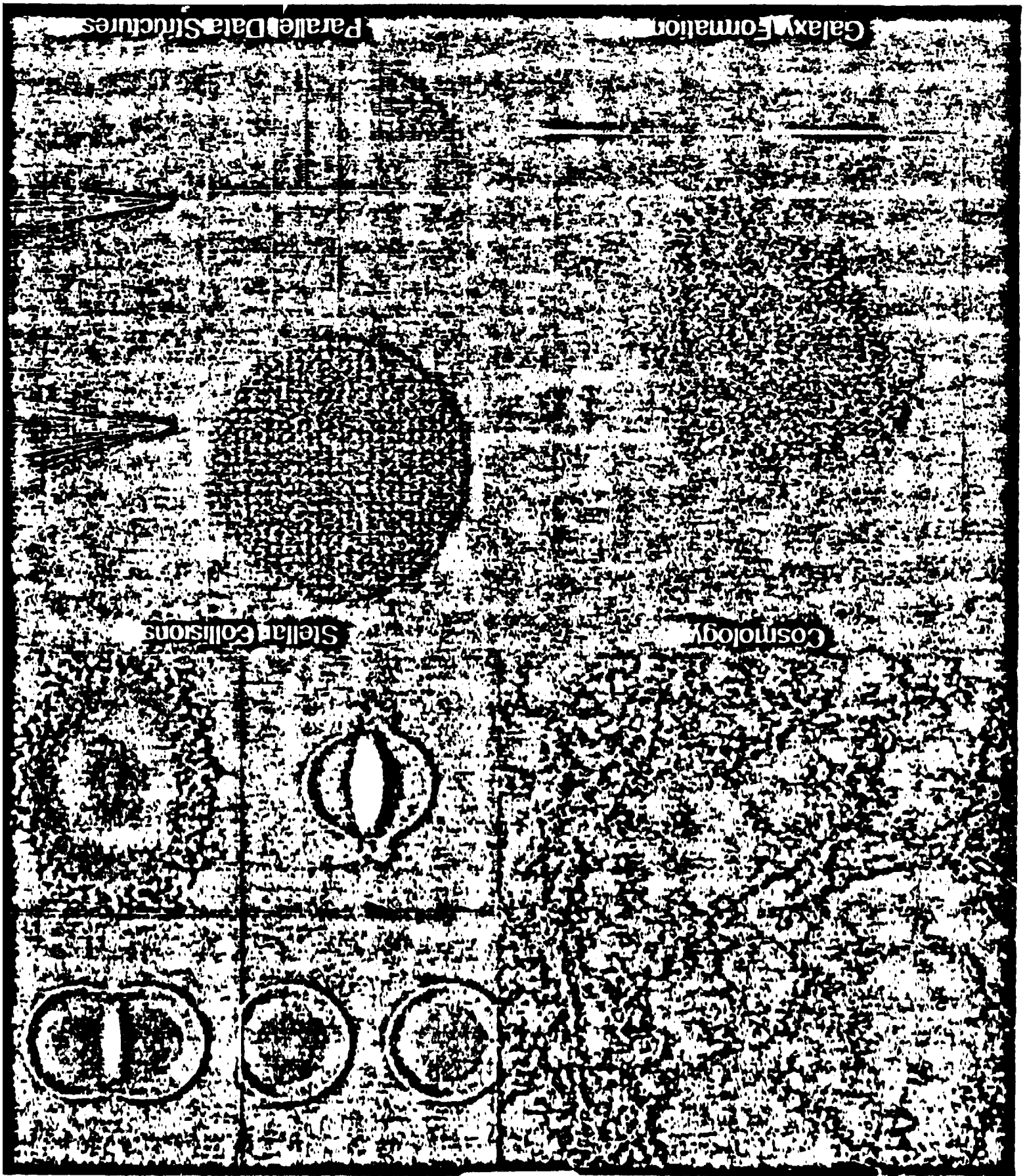
Numerical Solution

(You supply $F(i,j)$)

```
for (i=0; i<N; i++) {
    for (j=i+1; j<N; j++) {
        F(i,j);
    }
}
```

```
      DO 10 I=1,N
         DO 20 J=I+1,N
            CALL F(I,J)
10       CONTINUE
20    CONTINUE
```

The N-body Problem
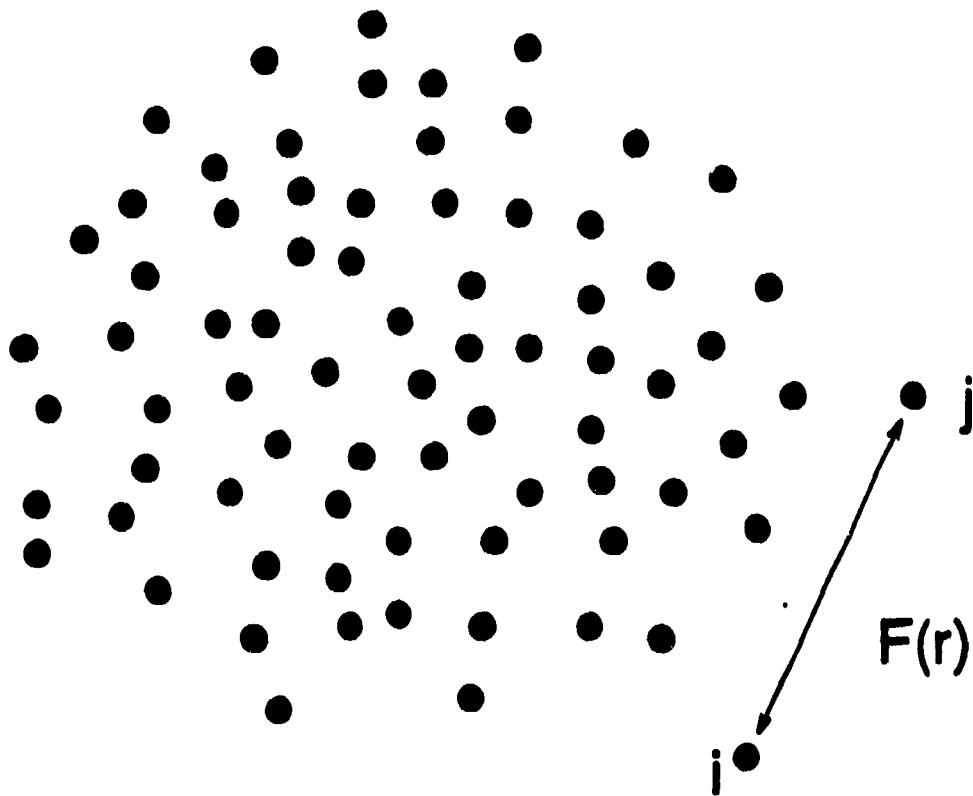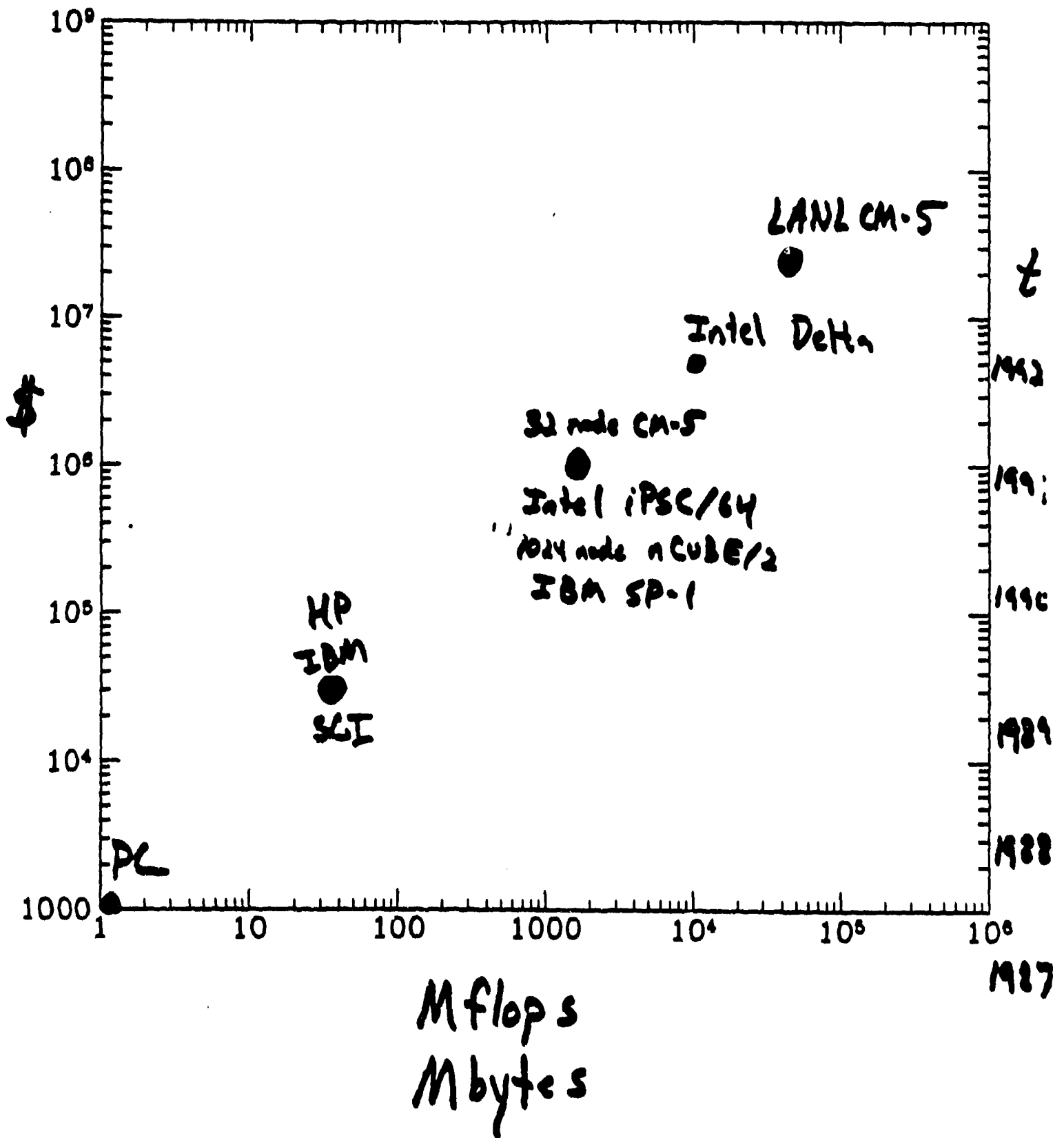
Make $\dfrac{N^2}{2}$ calls to $F(i,j)$

How long for $N = 10^7$?

Simplest useful $F(i,j)$ is finding r_{ij}^2 , which takes 8 flops.

$$\frac{(10^7)^2}{2} \cdot 8 = 4 \times 10^{14}$$

Fastest computer in existence can do $\sim 3 \times 10^{10}$ flops per sec.

$$3.7 \text{ hours}$$

Multipole Approximation

Treecodes, Apples, Satellites and Recursion
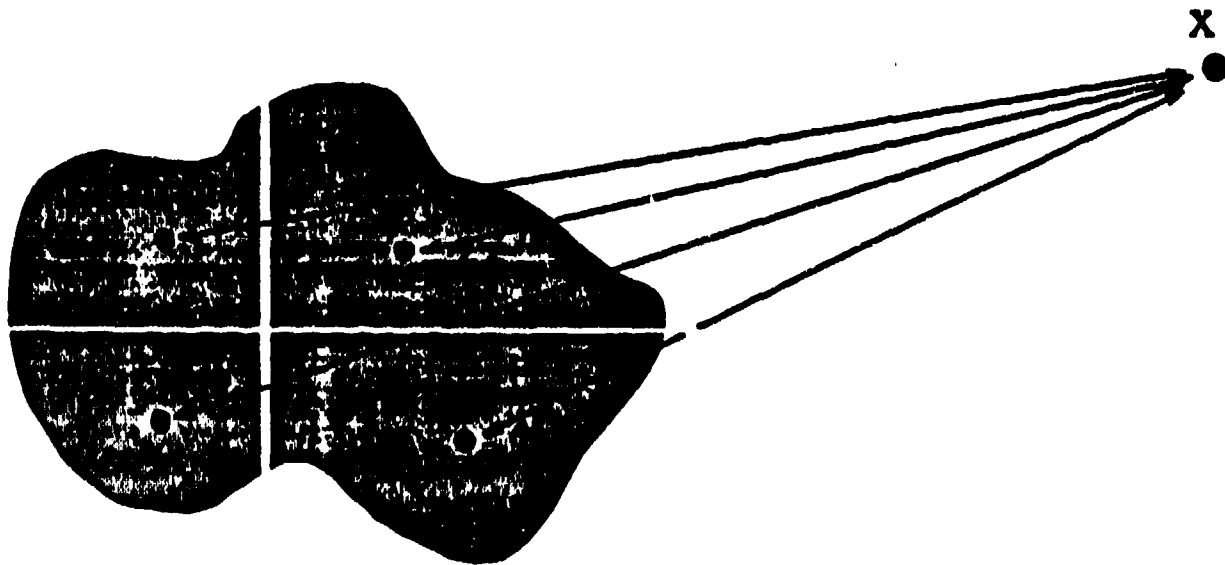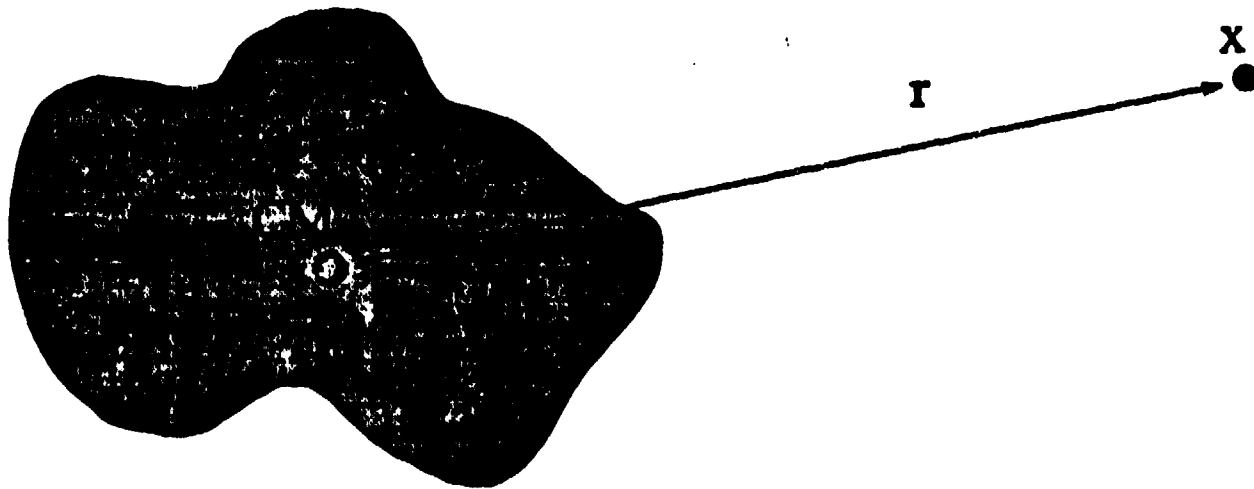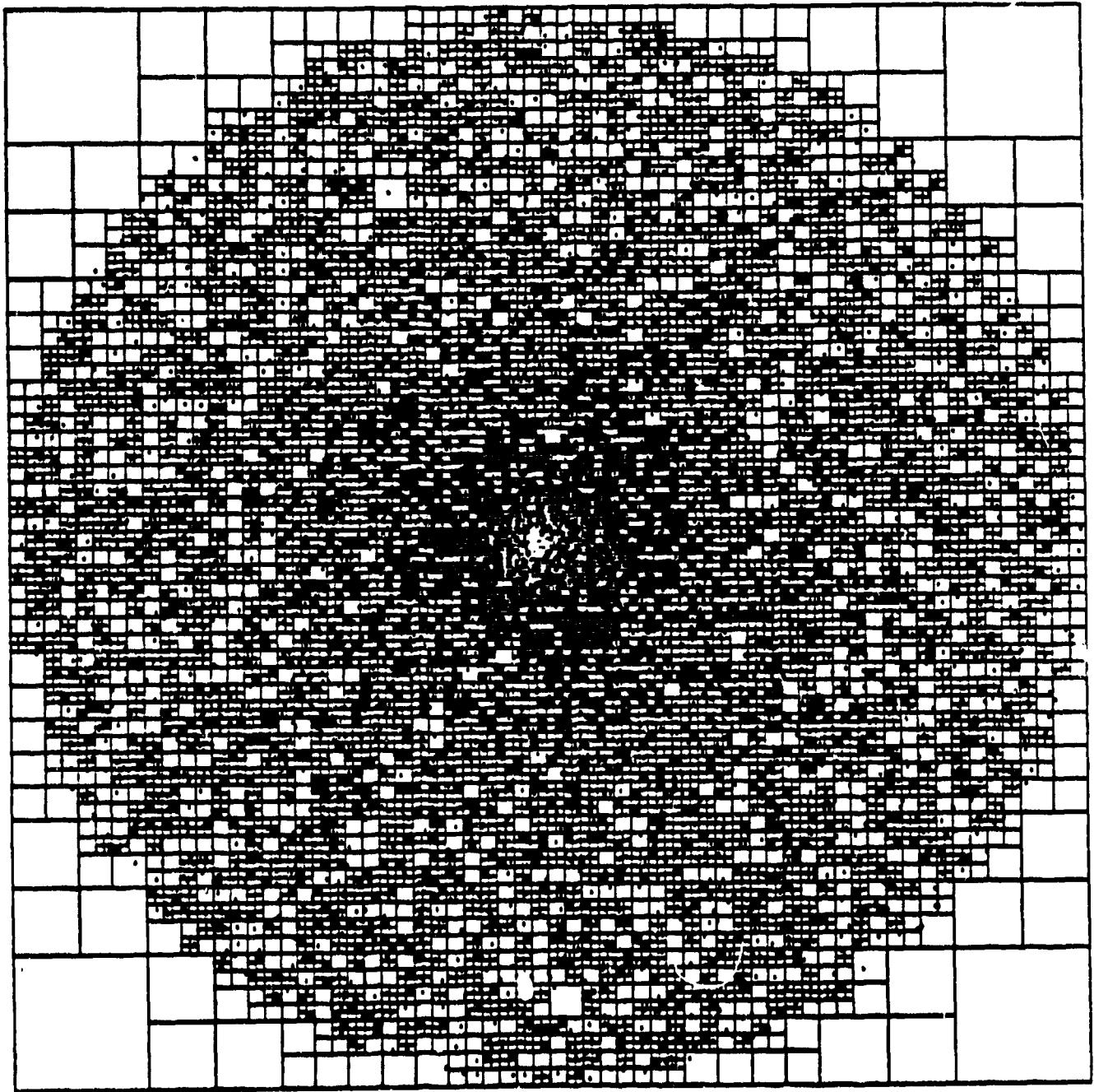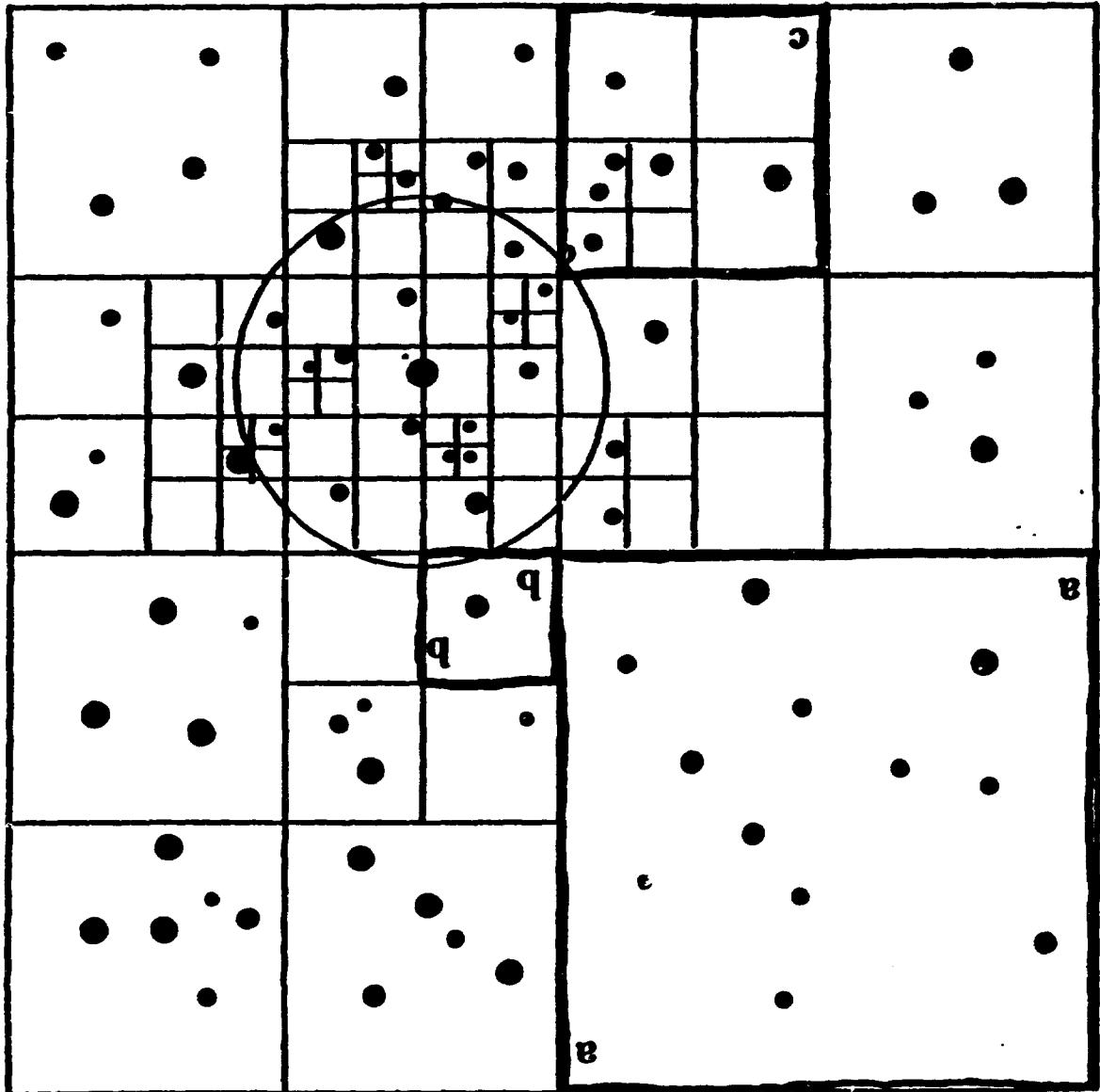
Parallelism?

There's obviously plenty of opportunity for parallelism.

- Bodies are independent

- Moments are independent (when cells are non-overlapping)

But it won't be easy

- Highly irregular

- Time dependent

- Global and local information

- Array operations won't do the job

binary coordinate representation

x	y	z
10011001	01101001	11101100

place-holder bit

bit interleave

1.101.011.011.100.111.001.000.110   binary key

0153347106   octal key
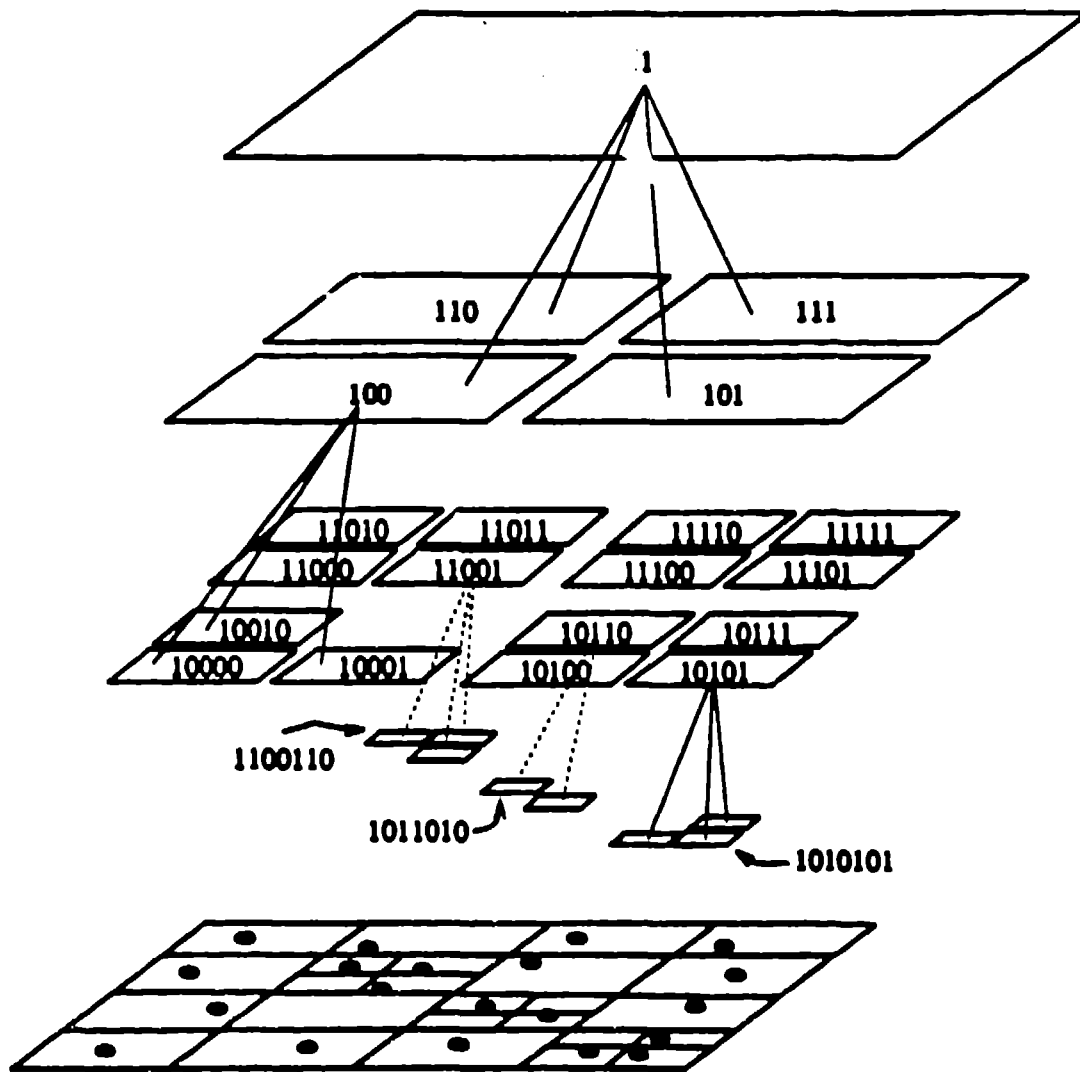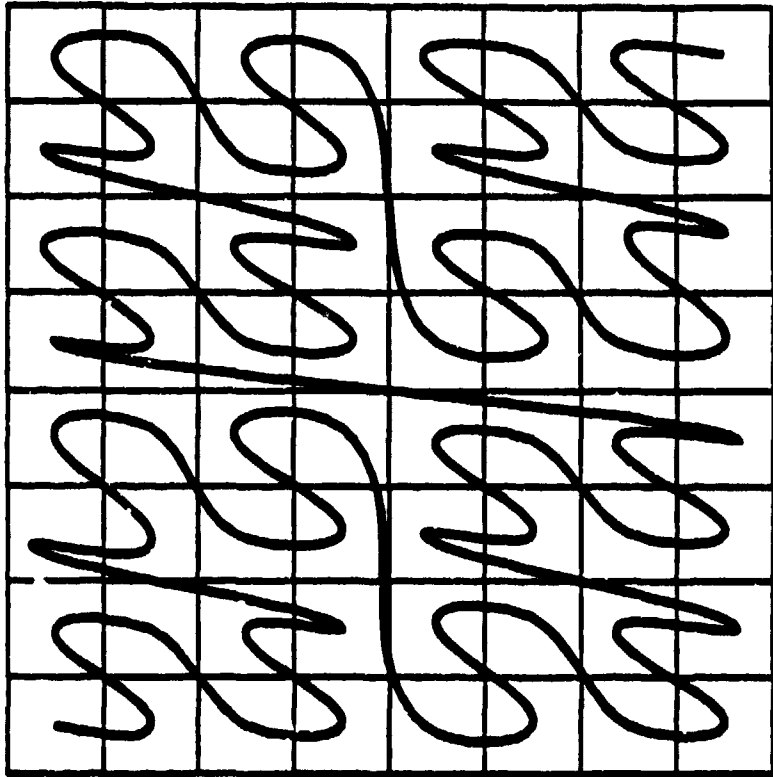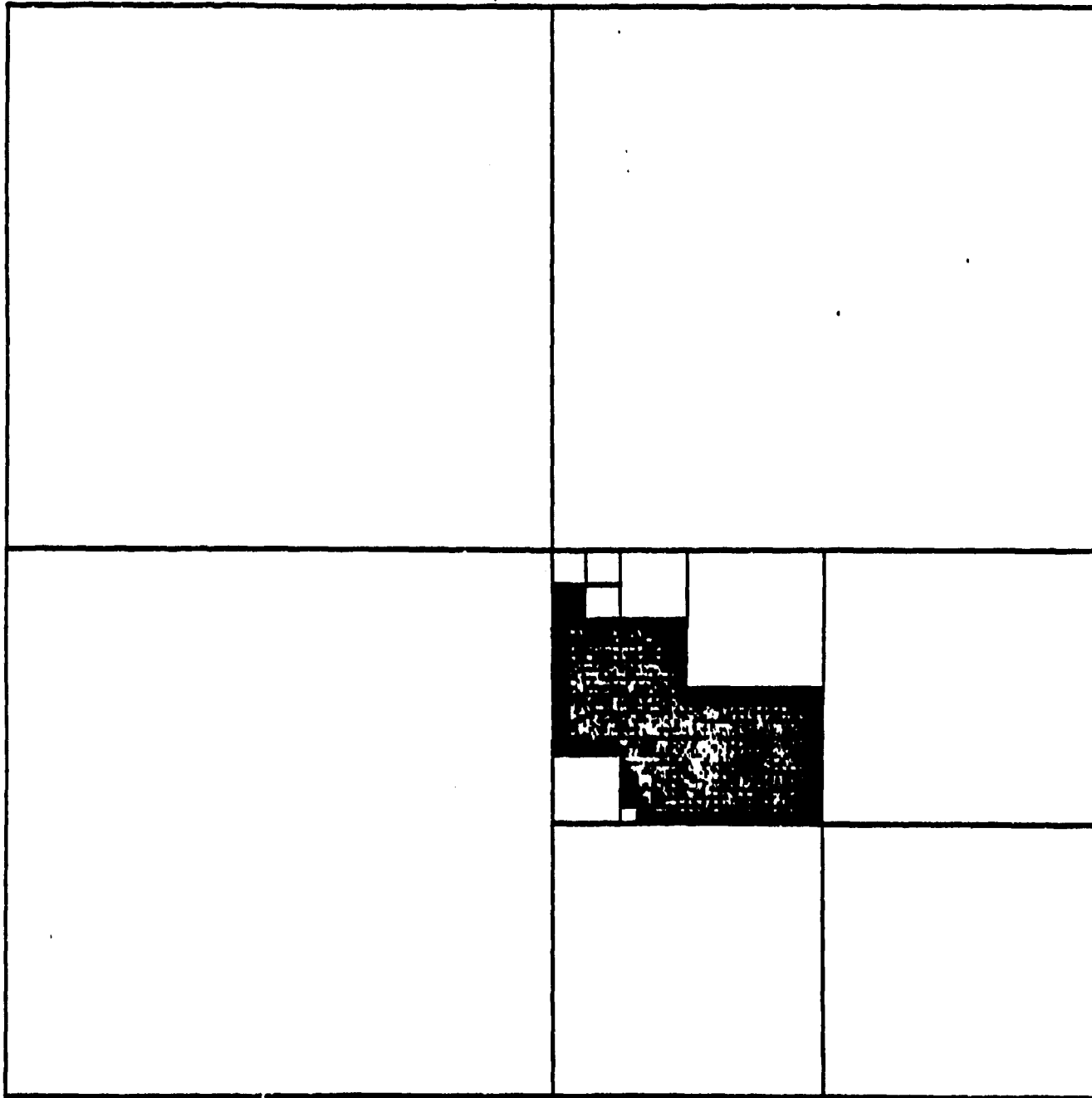
```
sampsont ls include
Assert.h            error.h             macr.h              stk.h
IOinit.h            fastflpt.h          malloc.h            sysdep.h
Malloc.h            files.h             physics_generic.h   tensop.h
Msgs.h              gc.h                pqsort.h            timers.h
SDF.h               gccextensions.h     protos.h            tree.h
SDFwrite.h          getparam.h          randoms.h           vop.h
byteswap.h          gnusort.h           randoms2.h
chn.h               heap.h              rddata.h
collective.h        key.h               signals.h

   2475 total

sampsont ls libtree
comm.c          pqsort.tix.c    traverse.c      walk.c
pqsort.c        pqsortmem.c     tree.c

   2569 total

sampsont ls libsw
Malloc.c        chn.c           go.c            memmove.c       stk.c
Msgs.c          collective.c    gnusort.c       randoms.c       timers.c
SDFwrite.c      error.c         heap.c          randoms2.c
alloca.c        files.c         key.c           rddata.c
byteswap.c      finite.c        malloc.c        signals.c

   3707 total

sampsont ls libSDF
ls *.[ch]
SDF-lex.c       SDFfuncs.c      copyright.h     mmalloc.h
SDF-parse.c     SDFget.c        fseekrd.c       obstack.c
SDF-private.h   alloca.c        kwds.h          obstack.h

   4681 total

sampsont ls sphf14
cofm_sph.c      integrate.h     physics_sph.c   rdtest.c
grav_sph.c      macs_sph.c      physics_sph.h   sph.c
integrate.c     main_sph.c      print.c         walk_sph.c

   2865 total

sampsont ls sysdep
data.c                  sysdep_eui.c        sysdep_srv.c        timers_mclock.c
ivfprintf.c             sysdep_express.c    timers_clock.c      timers_ntime.c
singlPrintf_srv.c       sysdep_ncube.c      timers_cm5.c        timers_readrtc.c
singlPrintf_unix.c      sysdep_nx.c         timers_gettimer.c
sysdep_cm5.c            sysdep_seq.c        timers_hwclock.c

   1847 total
```

SPH Performance

N	10^4	10^4	10^7	1.6×10^7
Machine	sparc2	sparc2	Δ	Δ
stage		time (sec.)		
Tree Build	3.4	1.7	37	95
Rho	43		160	270
Force	44	46	164	279
(Imbalance)			30	60
(Comm.)			14	18
Total	91	49	365	650

~ 120 bytes / particle

```
typedef struct {
    float mass;
    float pos[NDIM];
    float vel[NDIM];
    float h;
    float rho;
    float pr;
    float vsound;
    float rho_est;
    Key_t key;

    float acc[NDIM];
    float phi;
    float u;
    float udot;
    float pos_last[NDIM];
    float udot_last;
    float drho_dt;
    float hdot;
    unsigned int ident;
    unsigned int nterms;
    unsigned int nbrs;
} body, *bodyptr;
```

Modelling Relativistic Collapse: SPH vs FEM

Patrick J. Mann

Department of Applied Mathematics

University of Western Ontario.

Now, here, you see, it takes all the running you can do, to keep in the same place. If you want to get somewhere else, you must run twice as fast as that. *"Through the Looking Glass", Lewis Carroll, 1871*

Rationale

Einstein's Equations

- Extremely non-linear

- complicated

- few analytic solutions in non-linear regimes

Therefore

Two Possibilities

1. Self-Checking codes:

2. Code-Code comparison: ****

Self-Checking Codes

- M. Choptuik: multi-grid methods
- Spherical, Vacuum, Scalar fields.
- Advanced Numerical Methods.

Code-Code Comparison

- Spherical Symmetry: done
- A handful of non-spherical simulations.
- Basic Method finite differences

Alternate Methods

- *Spectral Methods* J. Marck, S. Bonnazola
- *Multi-grid Methods* M. Choptuik, A. Lanza
- *Finite Element Methods* P. Mann
- *Particle Methods* P. Mann, M. Dubal, W. Miller, A. Kheyfets

Direct Comparison

- *FEM vs SPH* P. Mann

Choice of Methods

- self-gravitating fluid
- Evolution equations + elliptic constraints
- non-spherical
- robust, Easy (at least 2 codes)

Finite Element Method: FEM

- Standard, Well-developed
- Particularly good for non-symmetric problems
- Equations appear only in quadrature routines

Smoothed Particle Hydrodynamics: SPH

- Astrophysical standard
- Easy physical basis
- Wonderful for gravity (clustering)

Which SPH?

- Relativity: problem with length. (proper vs coord vs ...)

- Therefore must extend classic SPH

There are two generic approaches

1. Physical particles

   - Particles move on fluid characteristics
   - Particles move with locally flat coords
   - ...
   - (see Kheyfets, Miller)

2. Numerical Interpolation

   - "Particles" parametrize an interpolation
   - Interpolation solves set of pde's

ADM 3+1

The sph interpolation requires:

- time: initial value
- space: boundary value *forget Einstein*
- mass: conserved

therefore:

- ADM 3+1 space-time split
- *Standard, Universally used*

ADM 3+1 (cont'd)

J.W. York, "Kinematics and Dynamics of General Relativity" in *Sources of Gravitational Radiation*, ed. *L. Smarr*

This Project:

- Spherical metric

- Schwarzschild Coordinates

- $t = $ time at infinity

- $r = $ areal radius

- $x = r cos(\theta)$, etc.

- 2 elliptic equations on a time slice

- particles averaged onto 1d, spherical grid

- FEM solver for metric

- metric interpolated onto particles

Metric:

$$ds^2 = -b^2(1-2m/r)dt^2 + dr^2/(1-2m/r) + r^2 d\Omega^2$$

where $b = b(r,t)$ and $m = m(r,t)$.

Fluid Equations

Euler's Equation

$$S_{a,t} + \nabla \cdot (\vec{v} S_a) = -bp_{,a} + \frac{1}{2} w D u^t \;[$$

$$1 \; - \frac{x^a}{r} \left(2b \frac{\partial b}{\partial r} \left(1 - \frac{2m}{r} \right) + \right.$$

$$\frac{\frac{\partial}{\partial r}\left(1 - \frac{2m}{r}\right)}{\left(1 - \frac{2m}{r}\right)^2} \left(b^2 \left(1 - \frac{2m}{r} \right)^2 + (v^r)^2 \right) \right)$$

$$+ 2f \frac{\partial v^r}{\partial r} \frac{1}{r} \left(v^a - \frac{\partial v^r}{\partial r} \frac{x^a}{r} \right)$$

$$]$$

Internal Energy Equation

$$E_{,t} + \nabla \cdot (E \vec{v}) = -p A \nabla \cdot \vec{v} - p \frac{dA}{dt}$$

Mass Conservation

$$D_{,t} + \nabla \cdot (D \vec{v}) = 0$$

where

$$A = u^t \sqrt{-g} \qquad S_\alpha = D w \, u_\alpha$$

$$\text{3-velocity} = v^\alpha = u^\alpha / u^t$$

$$E = A e \qquad D = A \rho_0$$

$$\rho = \rho_0 + e$$

$$w = (p + \rho)/\rho_0$$

S, A, v Relationships

$$A = \frac{1}{wD}\sqrt{\frac{(wD)^2 + S^2 - \frac{2m}{r}S_r^2}{1 - 2m/r}}$$

$$v^a = \frac{b}{A}\frac{1}{wD}\left(S_a - \frac{2m}{r}S^r\frac{x^a}{r}\right)$$

- Nasty

- All variables involved (fluid, metric, even pressure)

- Iterate corrector (twice)

SPH: Density

D gives a conserved rest mass. Therefore write

$$D = \sum_k m_k W_k$$

where

- $W_k = W\left(|\vec{r} - \vec{r}_k|, h_k\right)$
- $m_k(t)$: particle *rest* mass
- $\vec{r}_k(t)$: particle position
- $h_k(t)$: smoothing length

SPH: Momentum
Internal Energy

$\vec{S}$ is a momentum: $\vec{S} = D\vec{Z}$

Therefore

$$\vec{S} = \sum_k \vec{Z}_k m_k W_k$$

where $\vec{Z}_k(t)$ are interpolation parameters.

Also $E = D\epsilon$ so

$$E = \sum_k \epsilon_k m_k W_k$$

- mass-weighted interpolations

- Only $\vec{S}$ and E used as physical quantities, not the parameters $\vec{Z}_k$ and ϵ_k

- no divisions by $D(\vec{r}_i)$

Discretization of Fluid Equations
Weighted Residual Method

- Insert approximation in equation
- Multiply by weight $F_i(\vec{r}, t)$
- Integrate over slice

$$\int E_{,t} F_i \, dV = \int (-\nabla \cdot \vec{v} E - ...) F_i \, dV$$

Time Derivative explicit differentiation:

$$E_{,t} = \sum_k \dot{\epsilon}_k W_k + \epsilon_k \frac{d}{dt} W_k$$

Weight Galerkin

- $F_i = W(\vec{r} - \vec{r}_i, h_i)$
- Local support: h_i

Integration

- (Gauss Quadrature: overlapping particles)
- "particle position" quadrature ***

Therefore

$$\sum_j \left(\sum_k \dot{\epsilon}_k W_{jk} \right) W_{ij} = -\sum_j ((\nabla \cdot \vec{v})E)_j \, \dot{W}_{ij}$$

$$- \text{ time derivative terms}$$

- Matrix equation
- Sparse, but varying pattern
- Use condensation ("mass-lumping")

$$\sum_j \sum_k \dot{\epsilon}_k W_{jk} W_{ij} = \dot{\epsilon}_i \sum_j \sum_k W_{jk} W_{ij}$$

End up with

$$\dot{\epsilon}_i = ...$$

Similarly for

$$\vdots$$

- $\dot{Z}_i(t)$
- $\dot{m}_i(t)$

Code
(Predictor-Corrector)

1. Define $\ddot{\vec{r}}_i, \dot{h}_i$ and update h and r

2. Predict:

   (a) Predict Z_i, ϵ_i, m_i

   (b) Sum S_i, D_i, E_i

   (c) Compute $A, \vec{v}_i$

   (d) Metric solution

3. Correct:

   (a) Define $\ddot{\vec{r}}_i$ and update positions

   (b) Compute $\dot{m}_i, \dot{Z}_i, \dot{\epsilon}_i$

   (c) Sum S_i, D_i, E_i

   (d) Compute $A, \vec{v}_i$

   (e) Metric solution

   (f) Re-compute $A, \vec{v}_i$

Iterate corrector: "$P(EC)^2$"

NOTES

- Interpolations used *only* as interpolations
    - Kernel defined in coordinate space
- Choose $\frac{d}{dt}\vec{r_i} = \vec{v_i}$
    - (not necessary)
- h_i using standard schemes
- Final v_i evaluation is necessary
- Modified weight: include $r^2 D$, etc.

C++ vs Fortran

- Codes in both C++ and Fortran
- **FEM C++ is twice as fast as Fortran!!!**
  - Fortran data structure: d(n), e(n), ...
  - C++ data structure: node[n].d, node[n].e,
    ...
- **SPH C++ is slightly faster (insignificant)**
  - Double Sum!
  - Same difference in data structure.
- C++ is as advertised
  - Carefully thought out objects
  - Local objects
  - understandable code
  - Many more compiler errors, fewer runtime errors
  - Reusable (eg. FEM/SPH i/o, Spherical solver)

Tests

1. Shock Tube: SPH vs. FEM (done)

2. Spherical Symmetry: SPH vs. FEM (done)

3. 3d Collapse: SPH vs. FEM (in progress)

4. 3d Collision: SPH (in progress) vs. FEM (not yet)

Summary

- Comparable results

- SPH smooths more than FEM

- FEM is more sensitive to instability

- FEM is much faster for equivalent resolution
  - (but no binning in SPH yet)

- SPH better during horizon formation
  - Robust, Co-moving
  - (almost freefall)

Future

- Non-spherical Tests *in progress*

- Gravitational Radiation estimates *in progress*

- Gravity → Perturbed → Poisson's Eq'n : *Colliding neutron stars*

- Gravity → 2d Axisymmetric *in progress*

- Gravity → 3d (Huge job here)

SPH without H

Pablo Laguna
Penn State

I.. Introduction (why SPI?)

II.. SPI $\begin{cases} \text{a.. Truncation Errors, Convergence} \\ \text{b.. kernel} \end{cases}$

III.. Wave Equation $\begin{cases} \text{a.. Eulerian Tests} \\ \text{b.. Lagrangian Tests} \end{cases}$

IV.. Advection

V.. Conclusions and Future Work

THEOREM:

Let SPH be smoothed particle hydrodynamic: with a $C^{(n)}$ kernel W, if H is not singular then SPI (smoothed particle interpolation) exists for n-th order differential eqs.

PROOF:

a.. H non-singular $\Rightarrow$ $\det(H) \neq 0$ $\Rightarrow$

H^{-1} exists $\Rightarrow$ $HH^{-1} = I$

b.. $SPH H^{-1} = SPI$ ✓

SPH :

  1.. Computes derivatives without a grid.

  2.. Lagrangian nature.

  3.. Easy implementation.

Fully adaptive SPH : $\begin{cases} \bullet \text{ Variable } h \\ \bullet \text{ Non-spherical } W \\ \quad\quad \Downarrow \\ (\text{ easy implementation? }) \end{cases}$

Q.M. $\cdot$ $\begin{cases} \bullet \text{ Particles} \\ \bullet \text{ Waves} \end{cases}$

S.P.H. $\cdot$ $\begin{cases} \bullet \text{ Particles (Physics)} \\ \bullet \text{ Interpolation (Numerics)} \end{cases}$

$$SPH + \begin{cases} \text{FD: Hydro + Gravity} \\ \qquad\qquad\text{Rasio} \\[2em] \text{FE: Hydro + Gravity} \\ \qquad\qquad\text{Monn} \\[3em] \text{N-body: HDM + CDM} \\ \qquad\qquad\qquad\text{Warren et. al.} \end{cases}$$

⋮

Why not   SPH + SPH ?

Hydro + Magnetic Fields
Stellingward

Kernel Estimation:

$$\langle \phi \rangle = \int \phi' W \, dx'$$

$$\left\langle \frac{d\phi}{dx} \right\rangle = \int \frac{d\phi'}{dx'} W \, dx' = \int \phi' \frac{dW}{dx} \, dx' = \frac{d}{dx} \langle \phi \rangle$$

$$\left\langle \frac{d^2\phi}{dx^2} \right\rangle = \int \frac{d^2\phi'}{dx'^2} W \, dx' = \int \phi' \frac{d^2W}{dx^2} \, dx' = \frac{d^2}{dx^2} \langle \phi \rangle$$

In general

$$\left\langle \frac{d^n\phi}{dx^n} \right\rangle = \frac{d^n}{dx^n} \langle \phi \rangle$$

provided W is of class C^n; that is, its n-th derivatives exist and are continuous.

Also

$$\left\langle \frac{d^n\phi}{dx^n} \right\rangle = \frac{d^n\phi}{dx^n} + \Theta(h^2)$$

Trivial for $W \propto e^x$

-339-
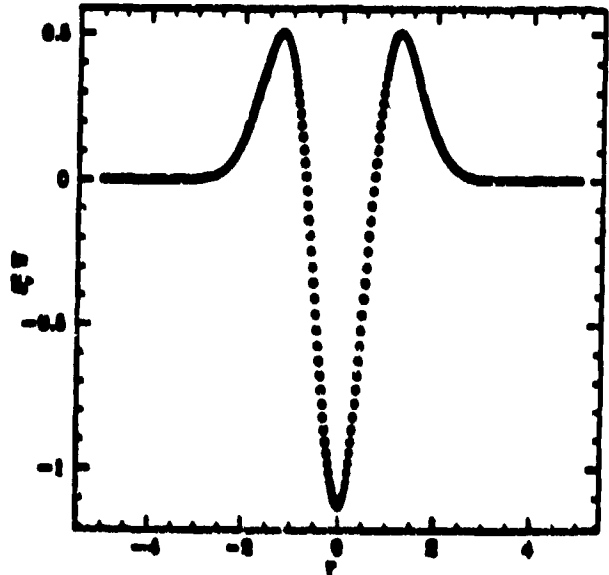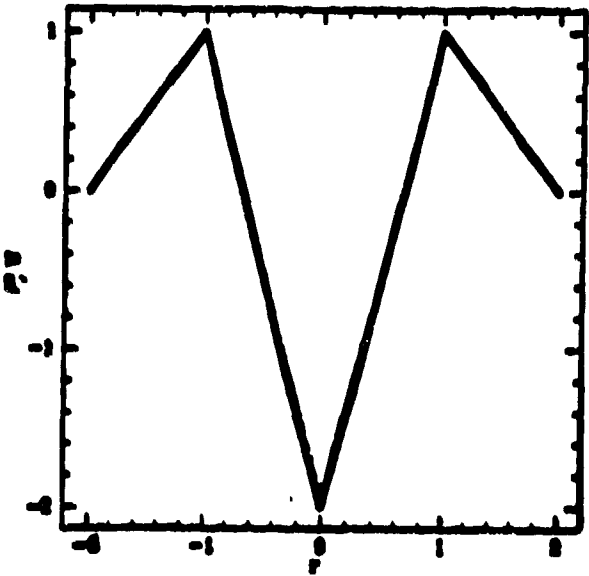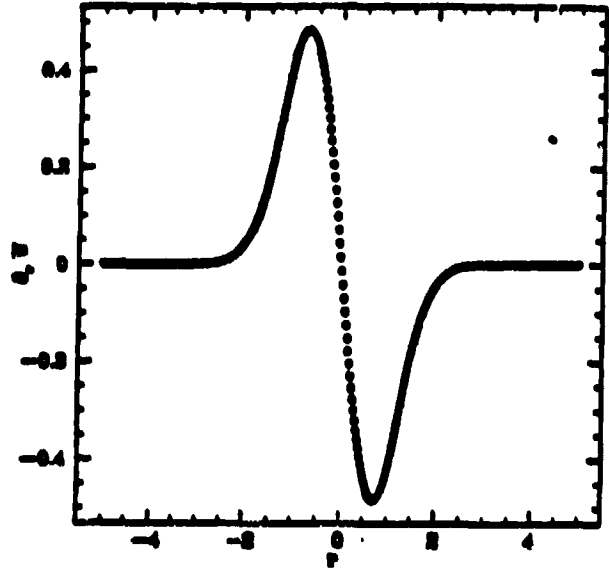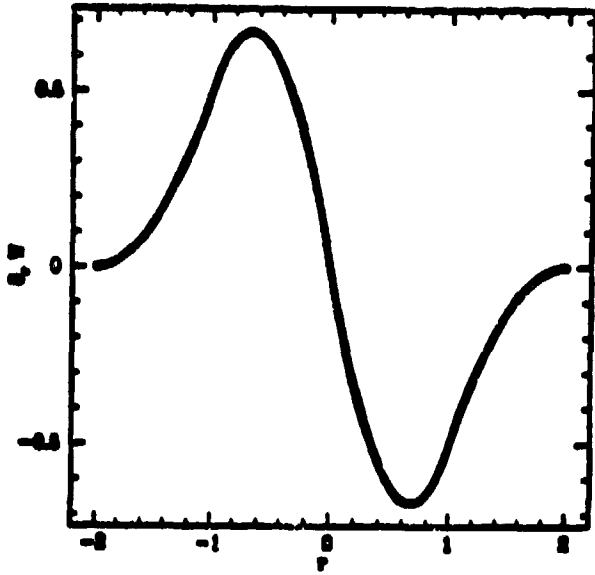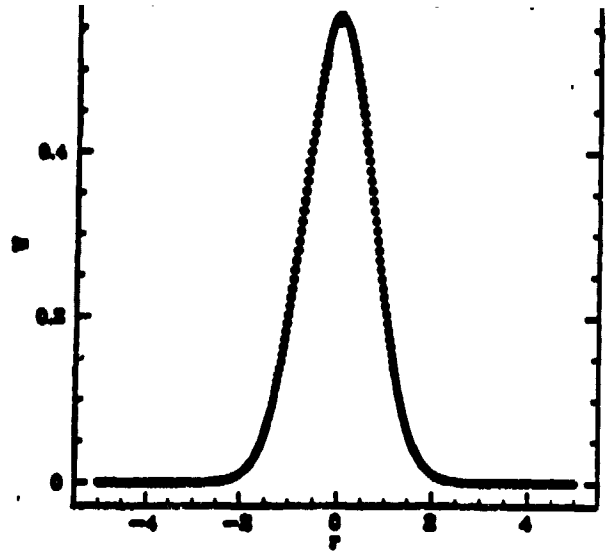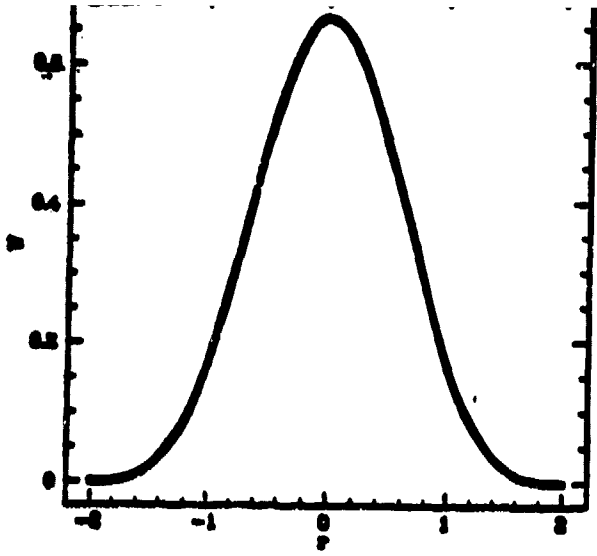
Spline   **Gaussian**

ERRORS and CONVERGENCE

$$\mathcal{L}\phi = 0 \qquad \mathcal{L}: \text{differential operator}$$

$$\hat{\mathcal{L}}\hat{\phi} = 0 \qquad \hat{\mathcal{L}}: \begin{Bmatrix} FE \\ FD \\ SPI \end{Bmatrix} \text{representation of } \mathcal{L}.$$

Truncation Error $\qquad \hat{\jmath} = \hat{\mathcal{L}}\phi$

Solution Error $\qquad \hat{e} = \phi - \hat{\phi}$

A discretization scheme is OPTIMALLY CONVERGENT if

$$\theta(\hat{e}) = \theta(\hat{\jmath})$$

Is SPI optimally convergent?

Wave equation YES if the # of neighbors is large enough.

Neighbons = 20

$$\left\langle \frac{d\phi}{dr} \right\rangle - \frac{d\phi}{dr} = \gamma_1$$

W=spline

$$\left\langle \frac{d\phi}{dr} \right\rangle - \frac{d\phi}{dr} = J.$$
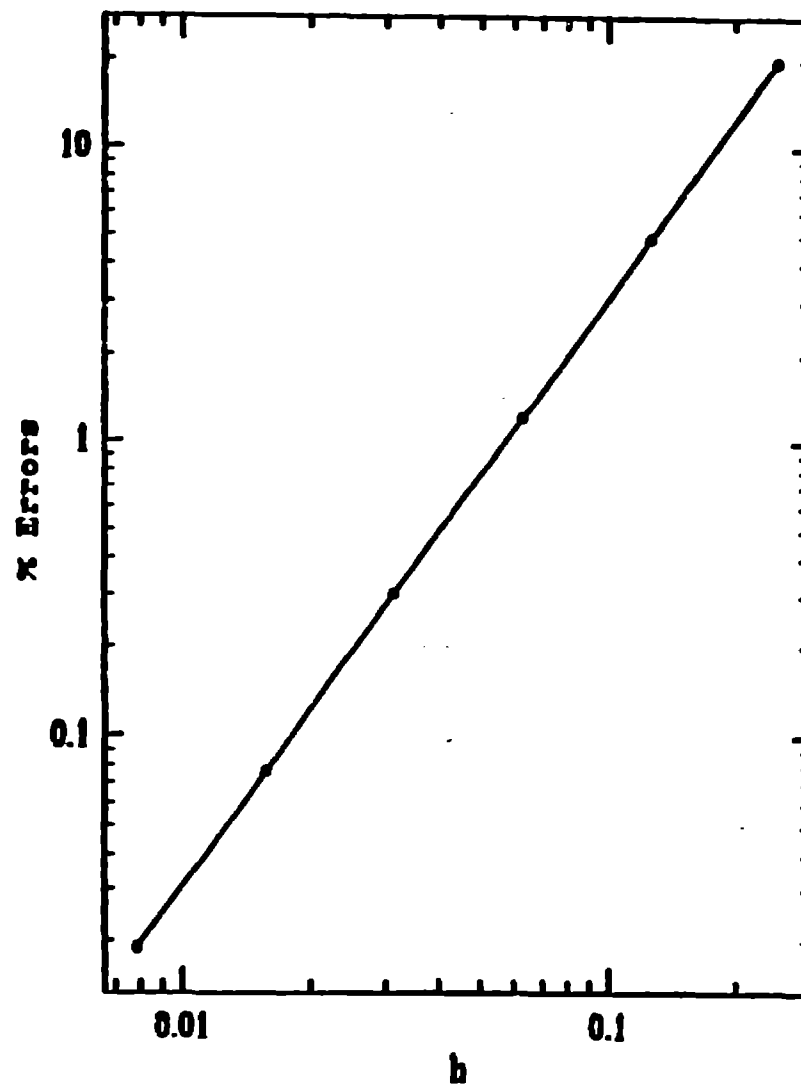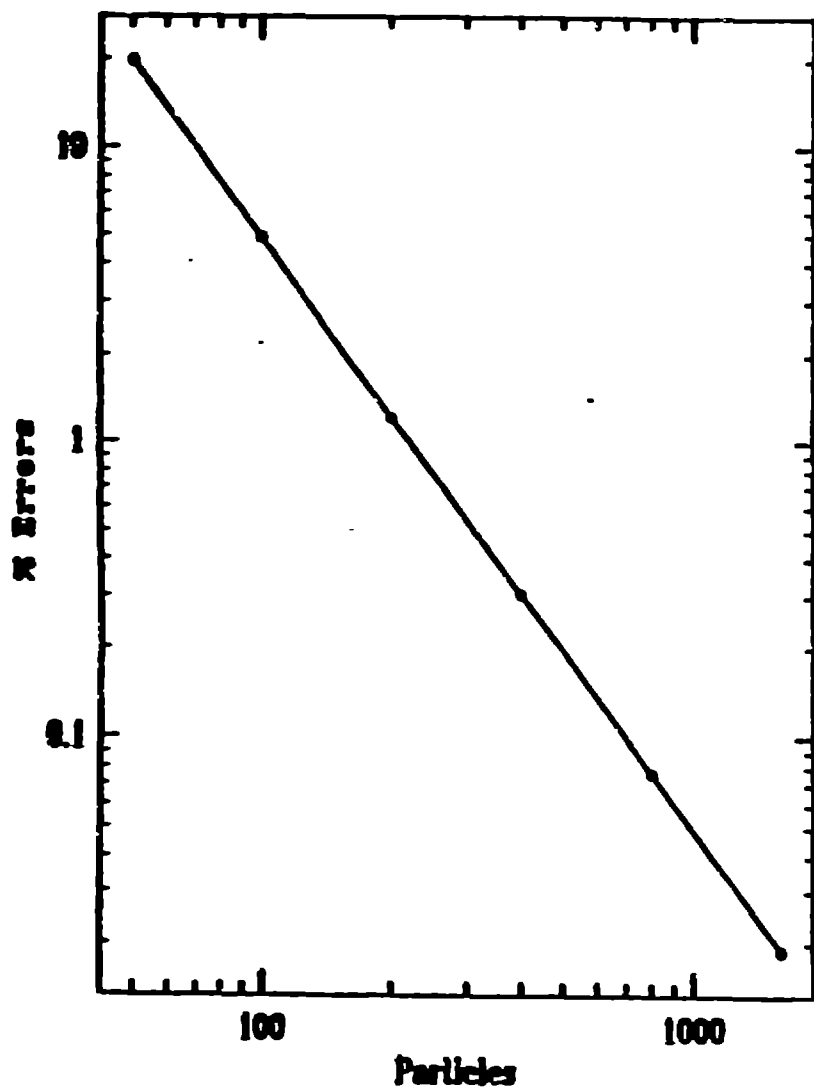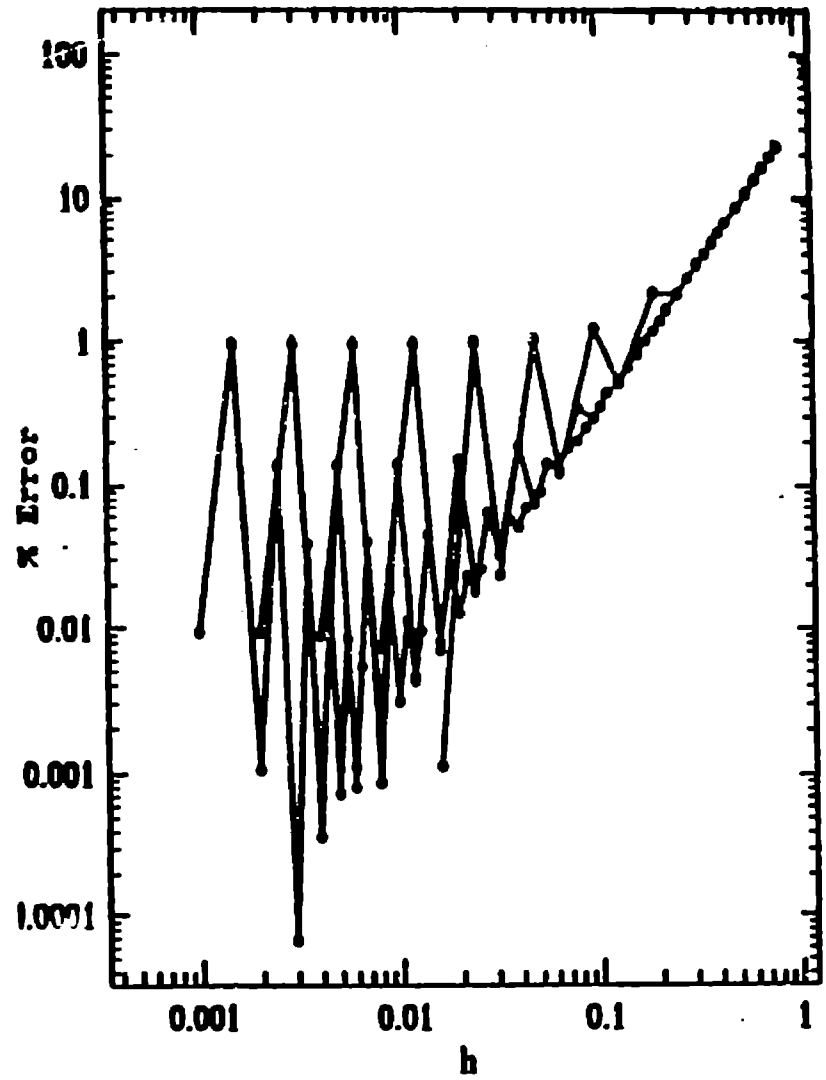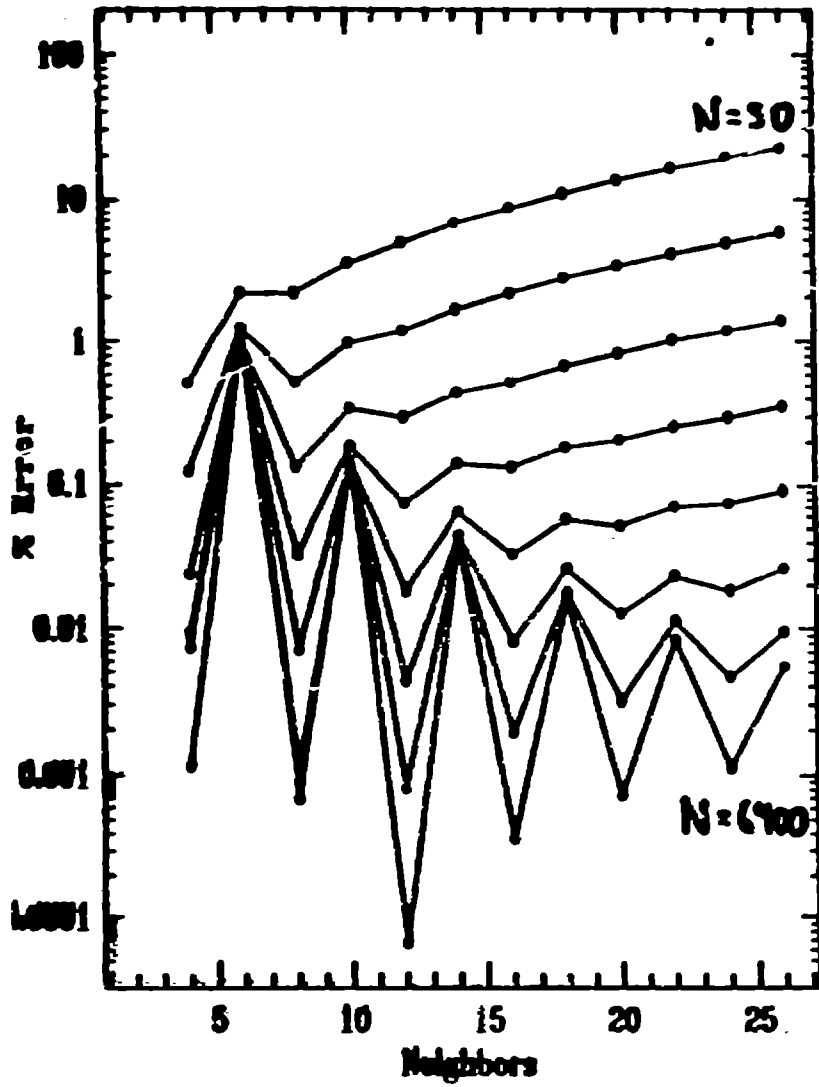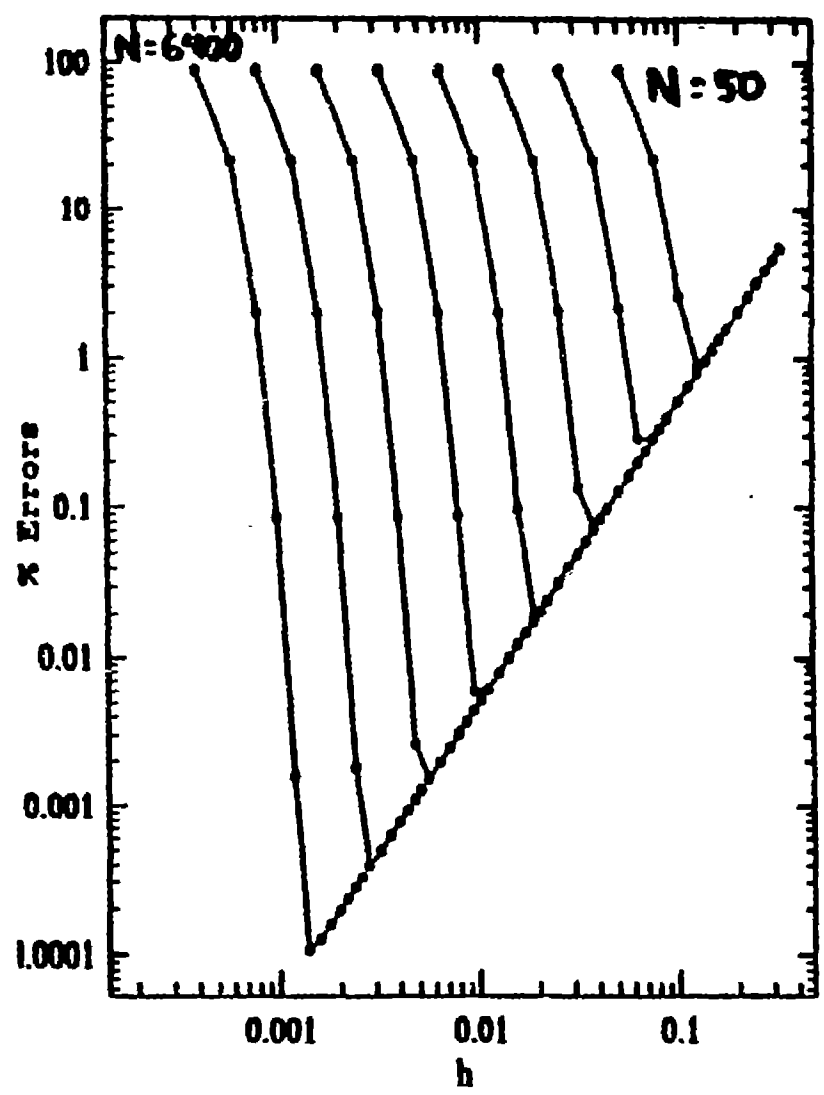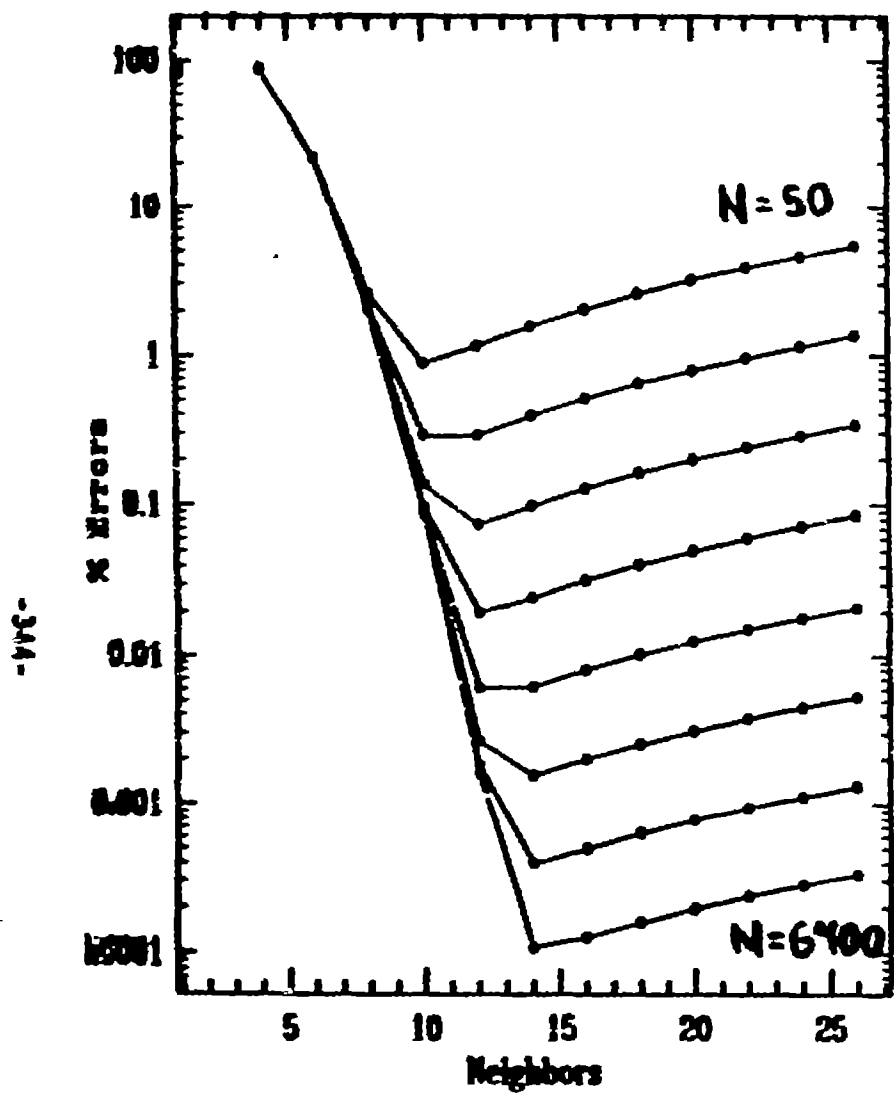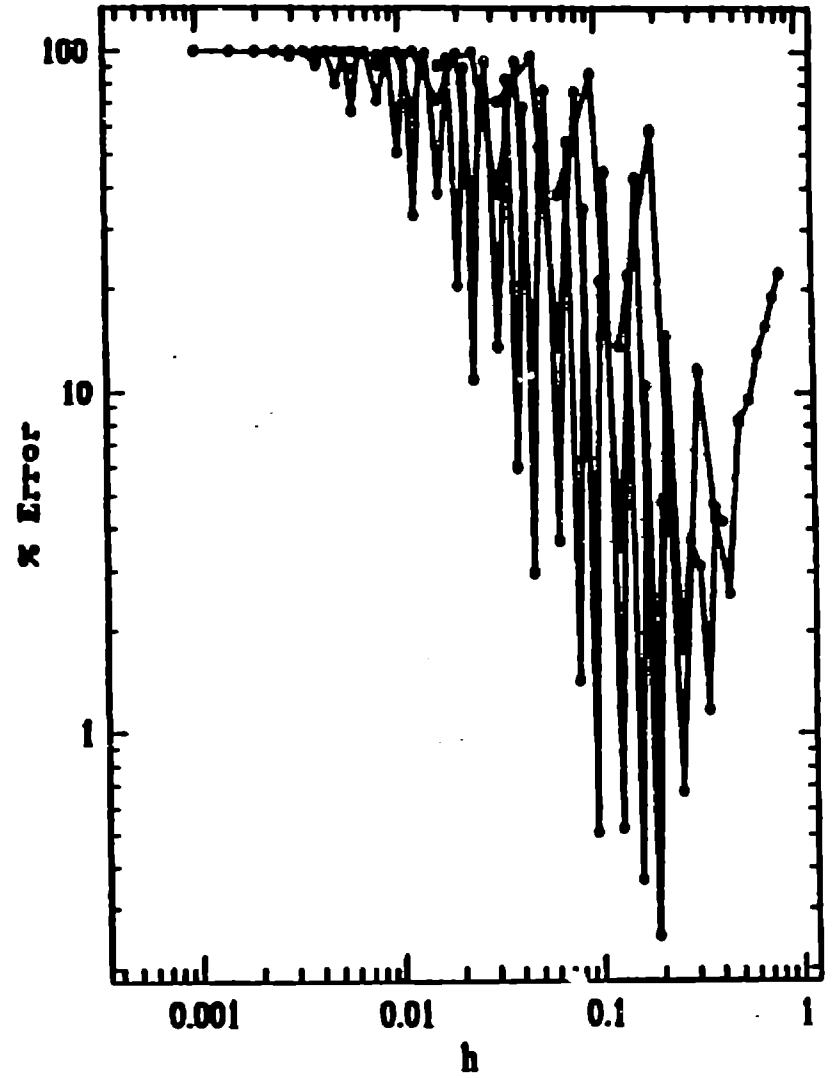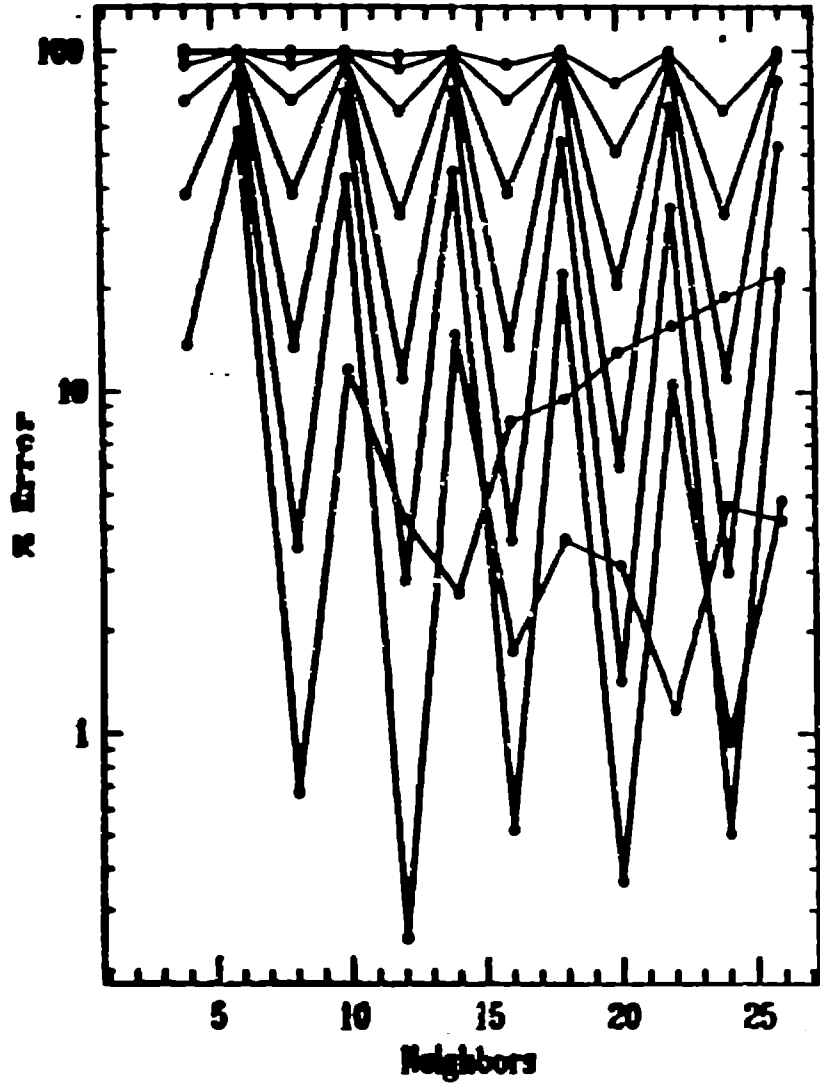
$$\left\langle \frac{d^2\phi}{dr^2} \right\rangle - \frac{d^2\phi}{dr^2} = T_2$$

W= spline
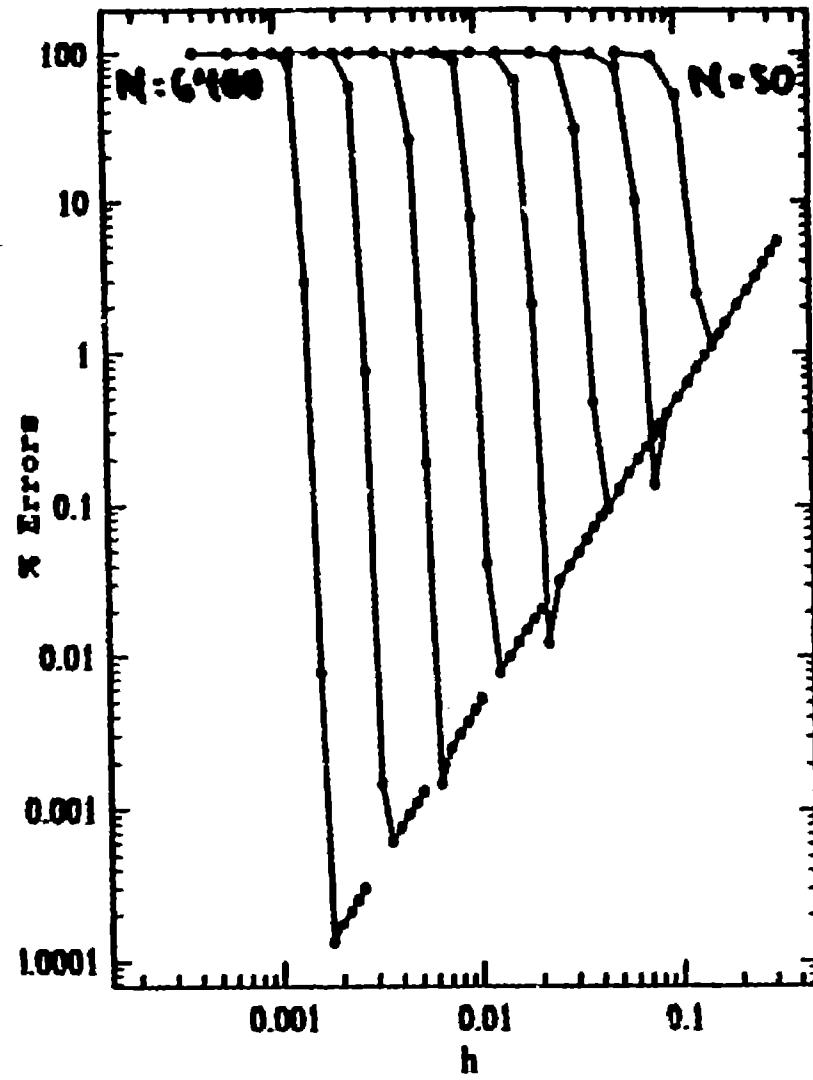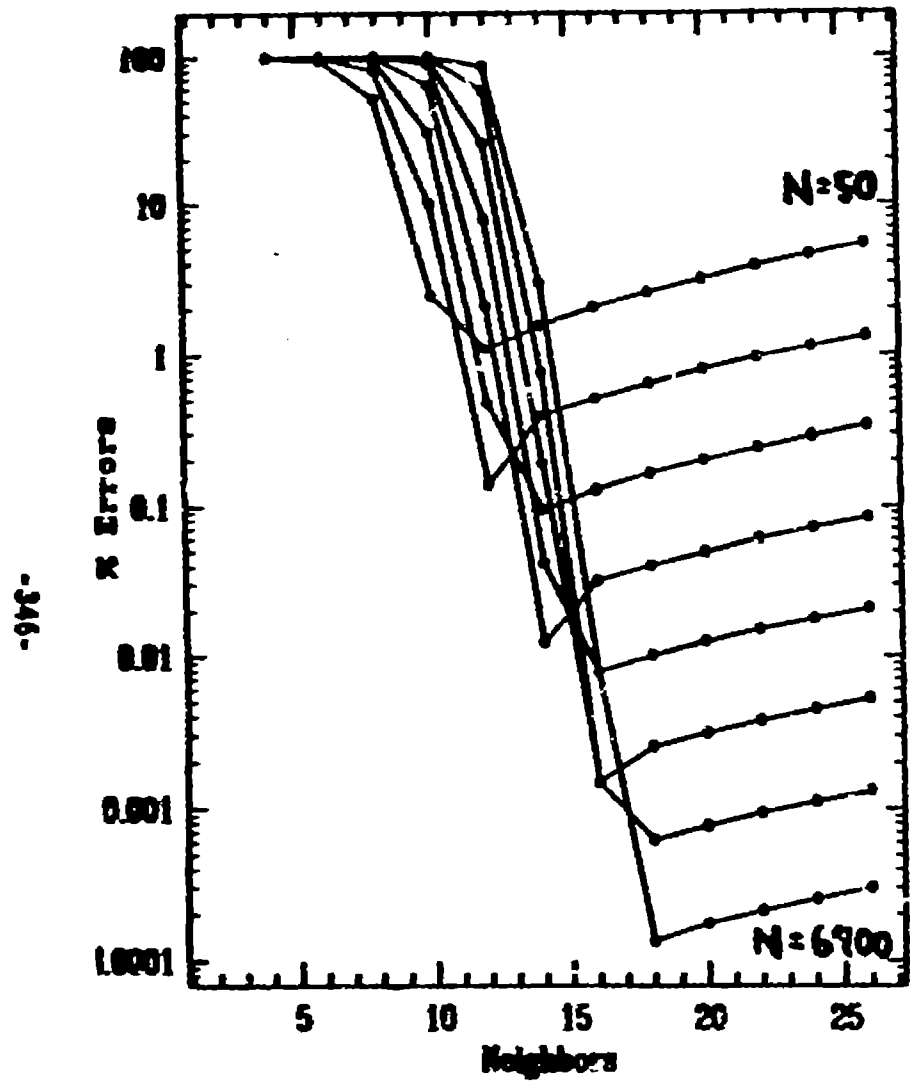
$$\left\langle \frac{d^2\phi}{dr^2} \right\rangle - \frac{d^2\phi}{dr^2} = \mathcal{J}_2.$$

W = gaussian

WAVE EQUATION $\qquad \dfrac{\partial^2 \phi}{\partial t^2} - c^2 \Delta \phi = 0$

Let $\Pi = \dfrac{\partial \phi}{\partial t}$, then
$\begin{cases} + & \dfrac{\partial \phi}{\partial t} = \Pi \\[2mm] + & \dfrac{\partial \Pi}{\partial t} = c^2 \Delta \phi \end{cases}$

$\qquad\qquad\qquad\qquad\qquad\qquad$ Eulerian form

Applying SPI one gets

$$\dfrac{\partial \phi_i}{\partial t} = \Pi_i$$

$$\dfrac{\partial \Pi_i}{\partial t} = c^2 \sum_j \dfrac{\phi_j}{n_j} \Delta_i W_{ij}$$

Time integration using staggered leapfrog.

$*$ Courant Condition : $\qquad v \Delta t \leqslant h$

$$\qquad\qquad\qquad\qquad\qquad\qquad \uparrow$$

$\qquad\qquad\qquad\qquad\qquad\qquad$ not Δr

Wave Equation and Moving Particles

$$\partial_t \phi = \Pi$$

$$\partial_t \Pi = c^2 \Delta\phi$$

$\left.\vphantom{\begin{array}{c}a\\a\end{array}}\right\}$ Fixed Particles, in general non-uniform spatial distribution

If particles move

$$\partial_t \phi - \vec{v}\cdot\nabla\phi = \Pi$$

$$\partial_t \Pi - \vec{v}\,\nabla\Pi = c^2\Delta\phi$$

$$\frac{d\vec{x}}{dt} = \vec{v}$$

$\left.\vphantom{\begin{array}{c}a\\a\\a\end{array}}\right\}$ the velocity field $\vec{v}(\vec{x})$ is, in principle, arbitrary

e.g. $\vec{v}$ = constant

$\vec{v} = \nabla\phi$ or $\nabla\Pi$
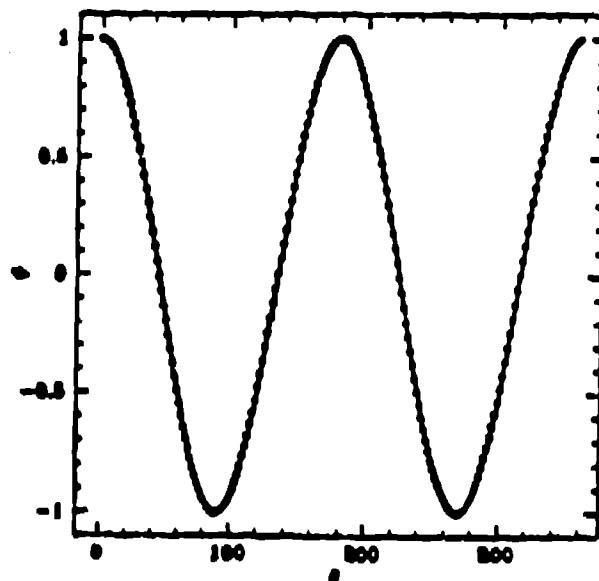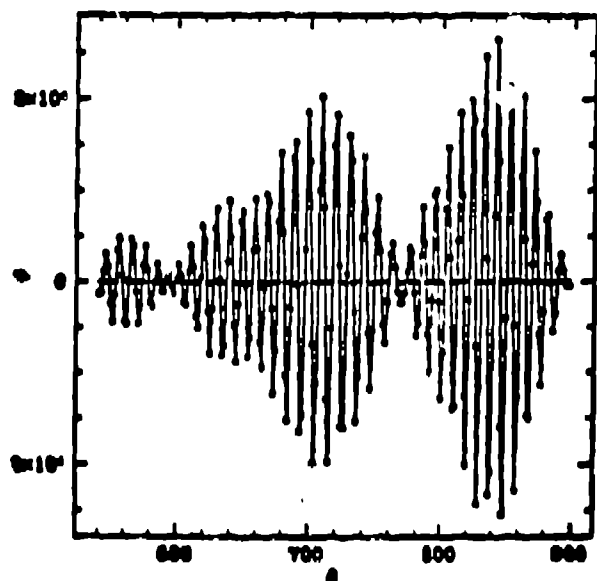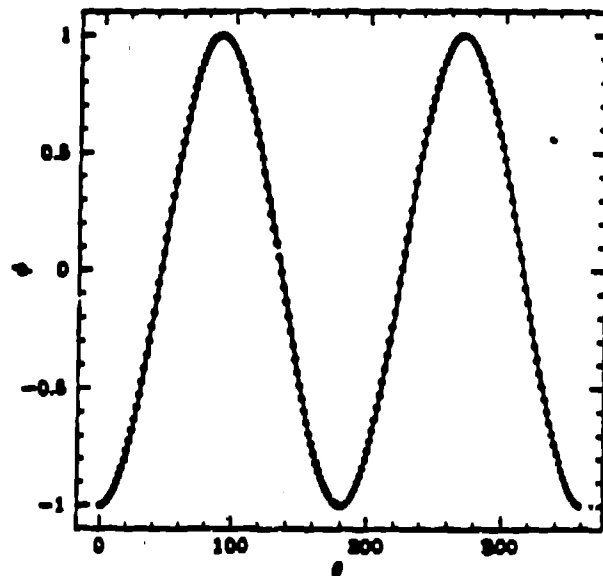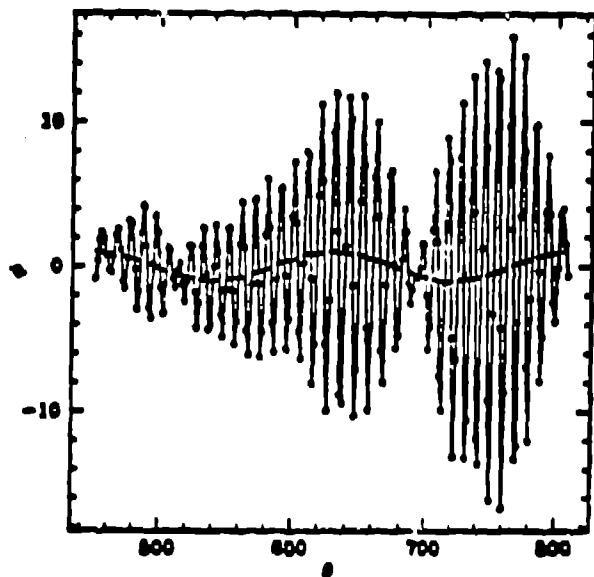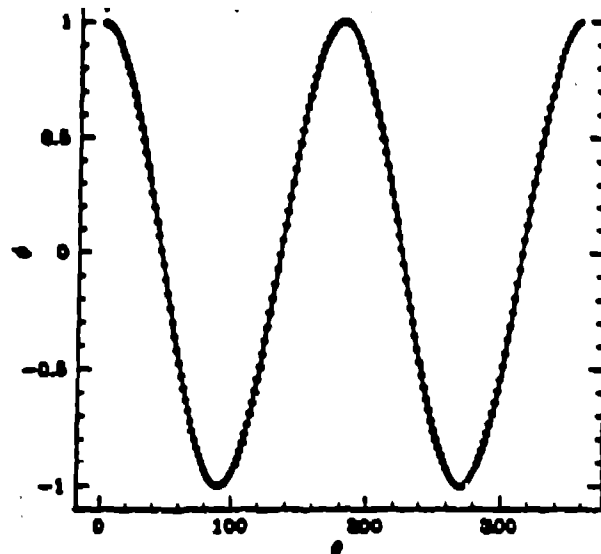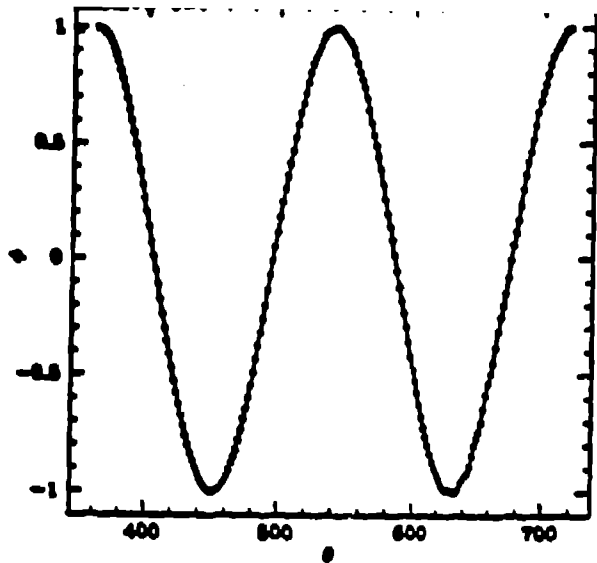
N ≈ 200

ADVECTION :

$$\frac{\partial \phi}{\partial t} + v \frac{\partial \phi}{\partial r} = 0$$

Finite Difference

$$\frac{(\phi_j^{n+1} - \phi_j^n)}{\Delta t} + v \left(\frac{\partial \phi}{\partial r}\right)_j^{n+\frac{1}{2}} = 0$$
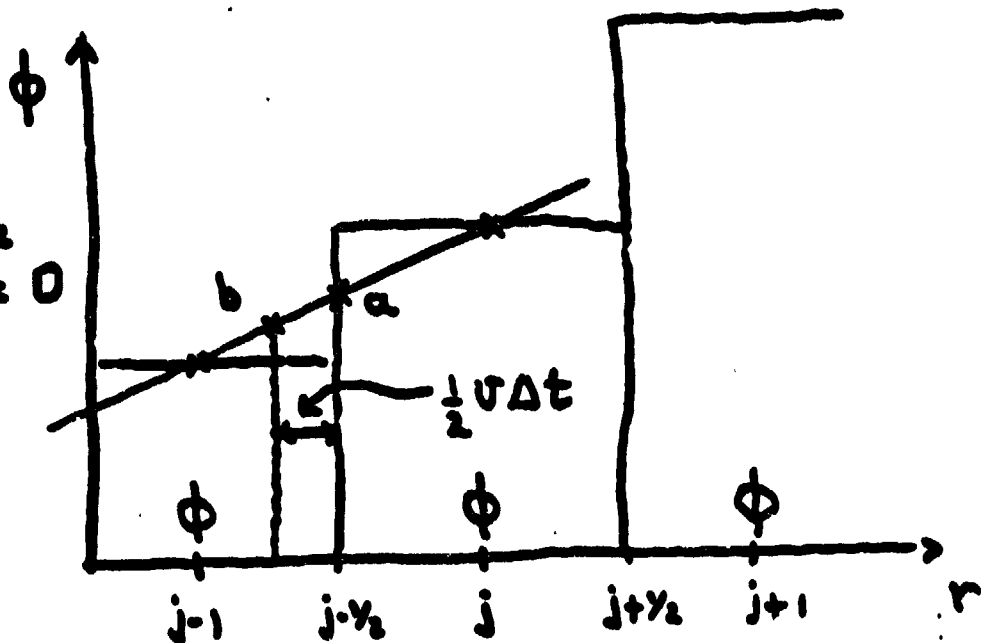
We need

$$\left(\frac{\partial \phi}{\partial r}\right)_j^{n+\frac{1}{2}} = \left(\frac{\phi_{j+\frac{1}{2}}^{n+\frac{1}{2}} - \phi_{j-\frac{1}{2}}^{n+\frac{1}{2}}}{\Delta x}\right) \qquad \text{but } \phi \text{ is } \{\phi_j^n\}$$

a.. Let $\quad \phi_{j-\frac{1}{2}}^{n+\frac{1}{2}} = \frac{1}{2}\left(\phi_j^n + \phi_{j-1}^n\right) \quad \Rightarrow \quad$ unstable

b... Let $\quad \phi_{j-\frac{1}{2}}^{n+\frac{1}{2}} = \frac{1}{2}\left(\phi_j^n + \phi_{j-1}^n\right) - \underbrace{\frac{1}{2}\left(\frac{\Delta t \, v}{\Delta x}\right)}_{c}\left(\phi_j^n - \phi_{j-1}^n\right)$

then

$$\frac{\phi_j^{n+1} - \phi_i^n}{\Delta t} + v\left(\frac{\phi_{j+1}^n - \phi_j^n}{2\Delta x}\right) - \frac{1}{2}\Delta t\, v\left(\frac{\phi_{j+1}^n + \phi_{j-1}^n - 2\phi_j^n}{\Delta x^2}\right) = c$$

which is the finite difference representation of

$$\frac{\partial \phi}{\partial t} + v\frac{\partial \phi}{\partial r} - \frac{\Delta t\, v}{2}\frac{\partial^2 \phi}{\partial r^2} = 0$$

$$\underbrace{\hspace{3cm}}_{\text{Diffusion}}$$

in SPH one can then:

A.. Add diffusion terms to the equations.

B.. Move particles a "distance" $v\frac{\Delta t}{2}$.

ut, is the intrinsic numerical dissipation of SPH
    enough to cure the instability?

$$\frac{\phi_j^{n+1} - \phi_j^n}{\Delta x} + \upsilon \sum_{k=j-N}^{j+N} \frac{\phi_k^n}{n_k} \frac{\partial W_{jk}}{\partial r} = 0$$

for a <u>uniform</u> distribution of particles

$$\frac{\phi_j^{n+1} - \phi_j^n}{\Delta x} + \upsilon \sum_{k=1}^{N} \left(\frac{\phi_{j+k}^n - \phi_{j-k}^n}{n_j} \right) \frac{\partial W_{j,j+k}}{\partial r} = 0$$

UNSTABLE !

Future Work

- Random distribution of particles
- Non-uniform particle density
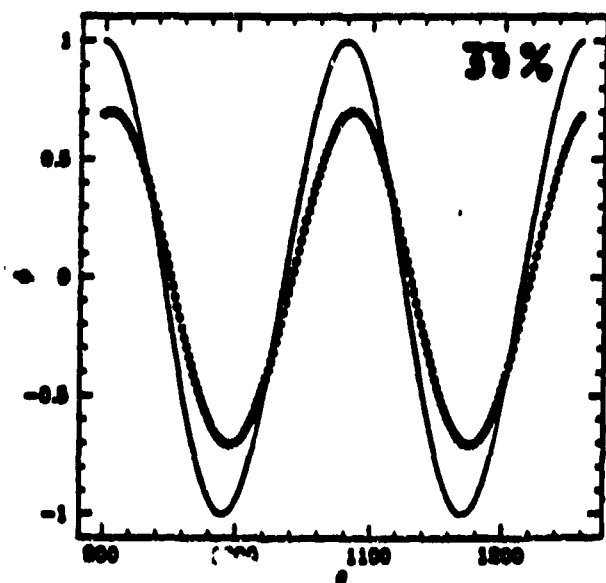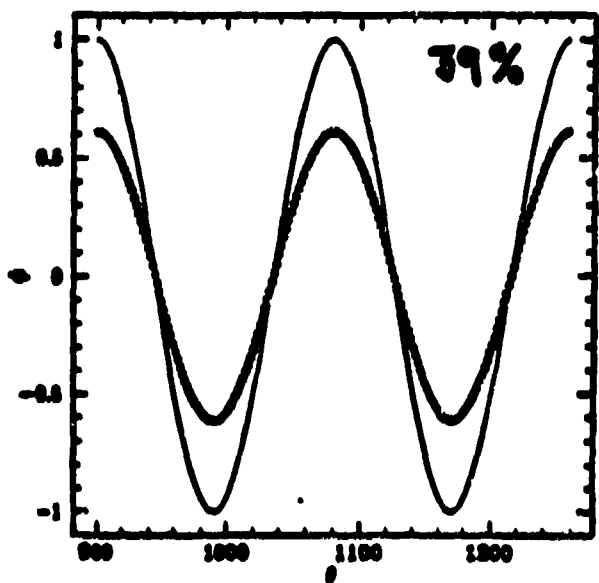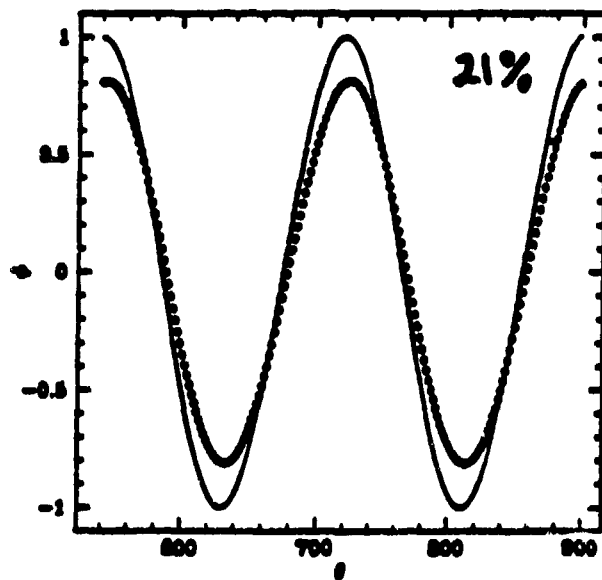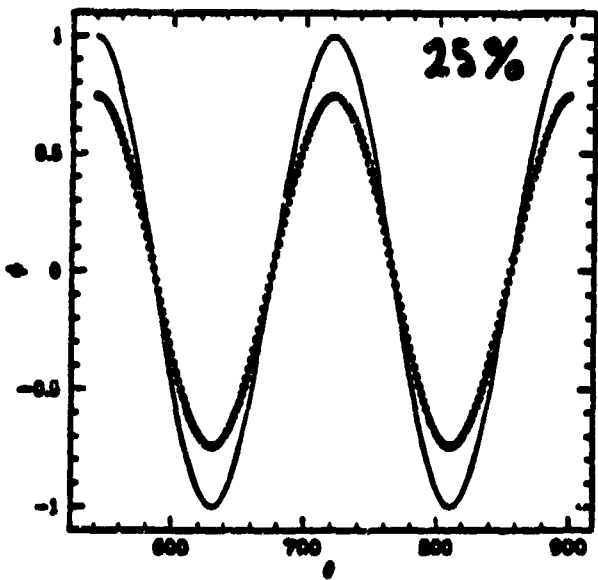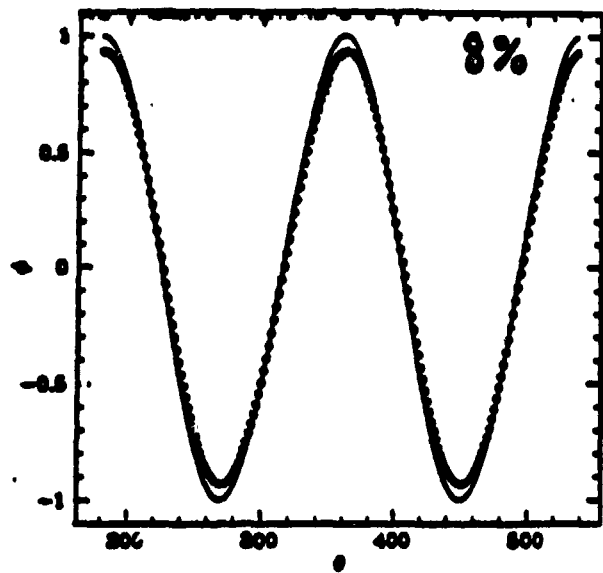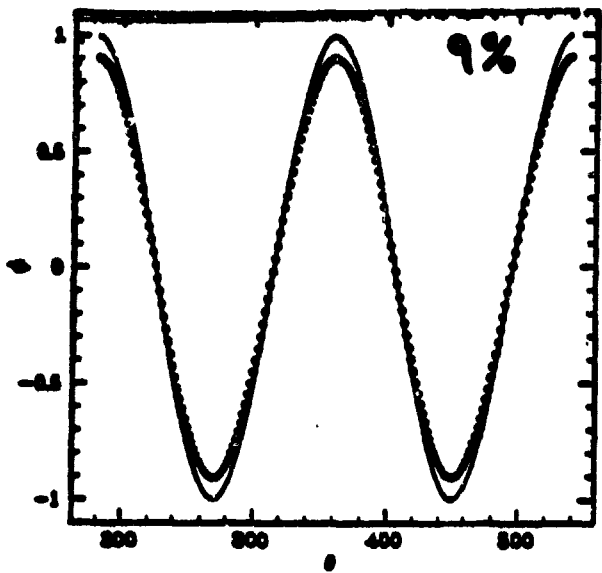
N = 200

CONCLUSIONS:

- Higher derivatives seem more expensive (Neighbors > few) under SPI.

- Advection terms represent the main challenge

  + Modify the continuum eqs.

  + Work with particle "fluxes"

FUTURE WORK:

- Variable h

- Higher dimensions

- More general velocity fields $\vec{v} = \vec{v}(\vec{x})$

APPLICATION: Numerical Relativity
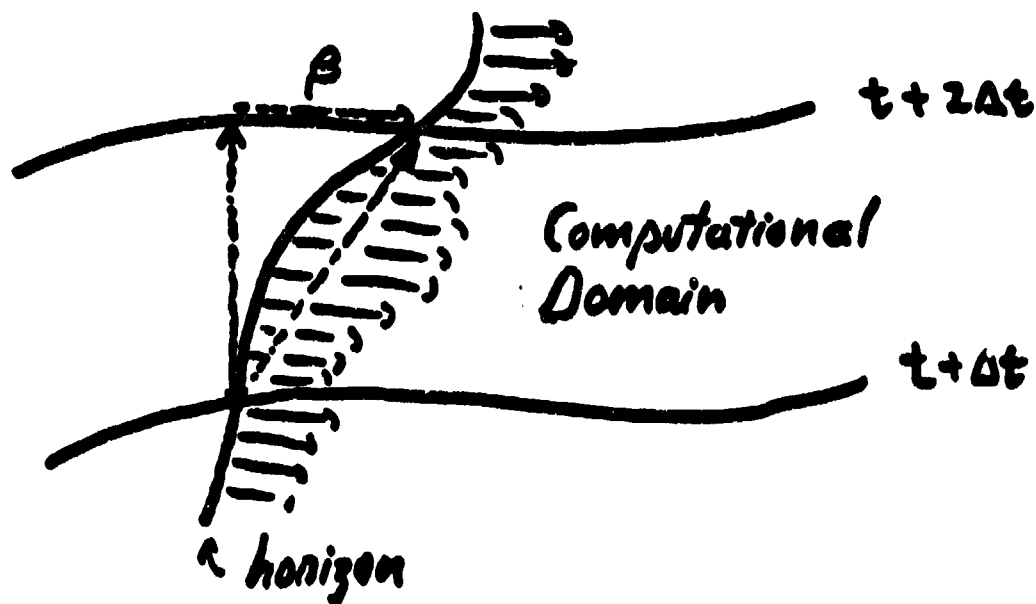
Einstein Eqs.

$$\frac{\partial}{\partial t}\phi - \vec{\beta}\cdot\nabla\phi = \ldots\ldots$$

$$\underbrace{\qquad\qquad}_{\text{"advection"}}$$

GOAL: Use the shift vector (coord. velocity)
        to lock the horizon (boundary cond.)

RELATIVISTIC SPH

AVOIDANCE OF VELOCITY-BIASED KERNELS

Arkady Kheyfets, Warner A. Miller and Wojciech H. Zurek

Our contention is that any truly relativistic application of SPH should reflect the following three requrements:

1. The kinematics of the smoothed particles should be relativistic;

2. The state equation for the fluid should be relativistic; and

3. The interactions between the smoothed particles should be treated in a Lorentz–covariant fashion.

The Lorentz covariant treatment of interactions between the smoothed particles can be achieved if one assumes that the relativistic hydrodynamical contact interactions are mediated by kernels whose supports reside in the local frame comoving with the fluid.

SEMI-RELATIVISTIC SPH

It appears to us to be common practice to satisfy only the first requirement and to neglect the other two.

- The first requirement is ordinarily taken care of automatically via applying the SPH discretization technique to the Lorentz covariant hydrodynamic equations (e.g. the Wilson equations).

- The equation of state is typically assumed to be either non-relativistic or ultrarelativistic. This should be more or less reasonable excluding problems involving variations in the temperature from non-relativistic to relativistic (collision of two clouds of cold gas moving with respect to each other at ultrarelativistic speeds). At mildly relativistic temperatures this could lead to quantitative errors, but probably, one could get away with this qualitatively. This is not a serious problem since these assumptions are made explicitly and can be easily corrected.

- The short range forces responsible for hydrodynamic interactions are ordinarily represented by spherical kernels in the proper space of an observer, or in an arbitrary spacelike section of spacetime. This procedure is obviously not relativistically invariant, as it depends on the choice of observer. It does not allow one to make any sound judgments concerning the scale of the kernels and does not allow one to draw any conclusions concerning the applicability of the SPH technique for any particular case.

EQS. of GENERAL RELATIVISTIC HYDRODYNAMICS

Baryon Conservation:

$$\partial_t D + \frac{1}{\sqrt{\gamma}} \partial_i (\sqrt{\gamma}\, D V^i) = 0$$

Energy Conservation:

$$\partial_t E + \frac{1}{\sqrt{\gamma}} \partial_i (\sqrt{\gamma}\, V^i E) + P \partial_t W + \frac{P}{\sqrt{\gamma}} \partial_i (\sqrt{\gamma}\, V^i W) = 0$$

Momentum Conservation:

$$\partial_t S_j + \frac{1}{\sqrt{\gamma}} \partial_i (S_j V^i \sqrt{\gamma}) + \alpha \partial_j P + \frac{1}{2} (\partial_j g^{\mu\nu}) \frac{S_\mu S_\nu}{S^t} = 0$$

X (1.476×10^14 M_⊙ cm)

Y (1.476×10^14 M_⊙ cm)

X (1.476×10^14 M_⊙ cm)

Y (1.476×10^14 M_⊙ cm)

Z (1.476×10^14 M_⊙ cm)

Y (1.476×10^14 M_⊙ cm)
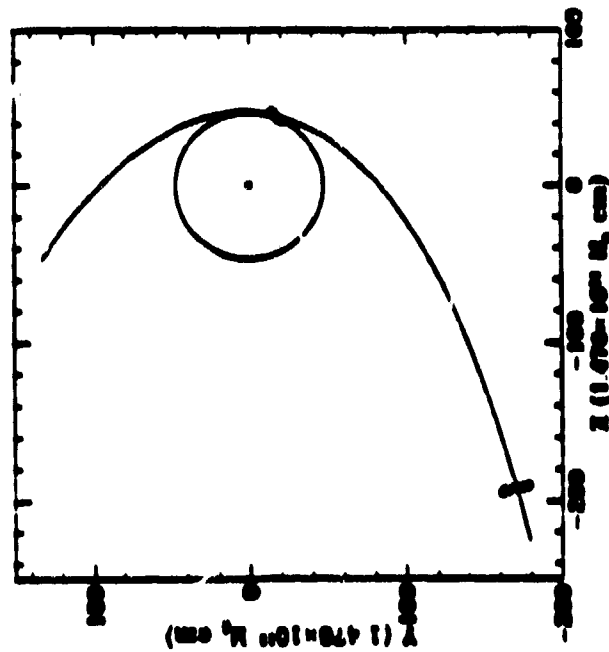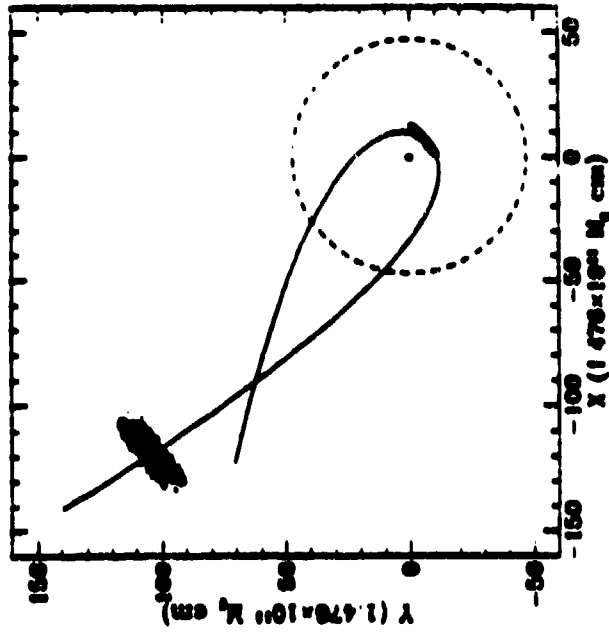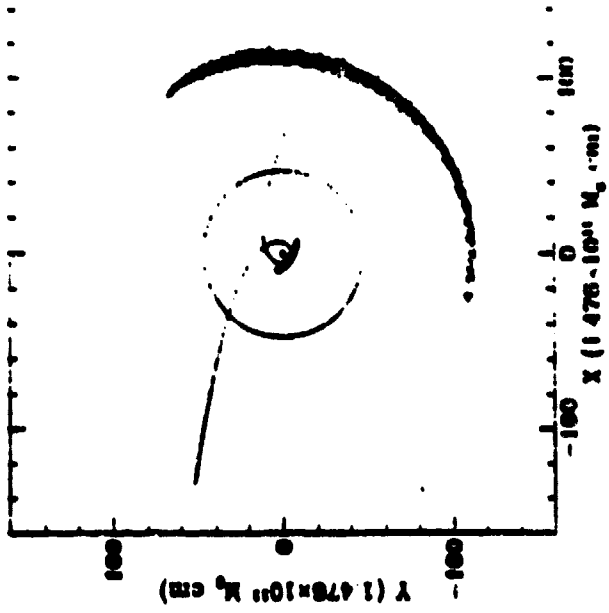
RELATIVISTIC SPH

The SPH representation of contact (hydrodynamical) forces can be made relativistically invariant if one one assumes that the relativistic hydrodynamical contact interactions are mediated by kernels whose supports reside in the local frame comoving with the fluid.

The discretized SPH equations for a 1-dimensional relativistic isentropic fluid

$$n_k L(m\xi_k) = \text{const}$$

$$c^{-2}\frac{du_l}{d\tau} = -\frac{1}{mn_l G(m\xi_l)} \sum_k \frac{\alpha_k}{\xi_k} \nabla_l w_{lk}$$

$$c^{-2}p_k = \frac{n_k}{\xi_k}$$

$$\rho_k + c^{-2}p_k = mn_k G(m\xi_k)$$

$$n_k V_k = \alpha_k = \text{const}$$

$$\mathbf{u}_l \cdot \mathbf{u}_l = -c^2$$

where

$$G(m\xi) = \frac{K_3(\xi)}{K_2(\xi)}$$

$$L(m\xi) = \frac{m\xi}{K_2(m\xi)} \exp\left[-\frac{m\xi K_3(m\xi)}{K_2(m\xi)}\right]$$

$$\xi = \frac{c^2}{kT}$$

and $K_n(m\xi)$ is the n-th hyperbolic Bessel function.

Number Density

Velocity

Temperature

Pressure
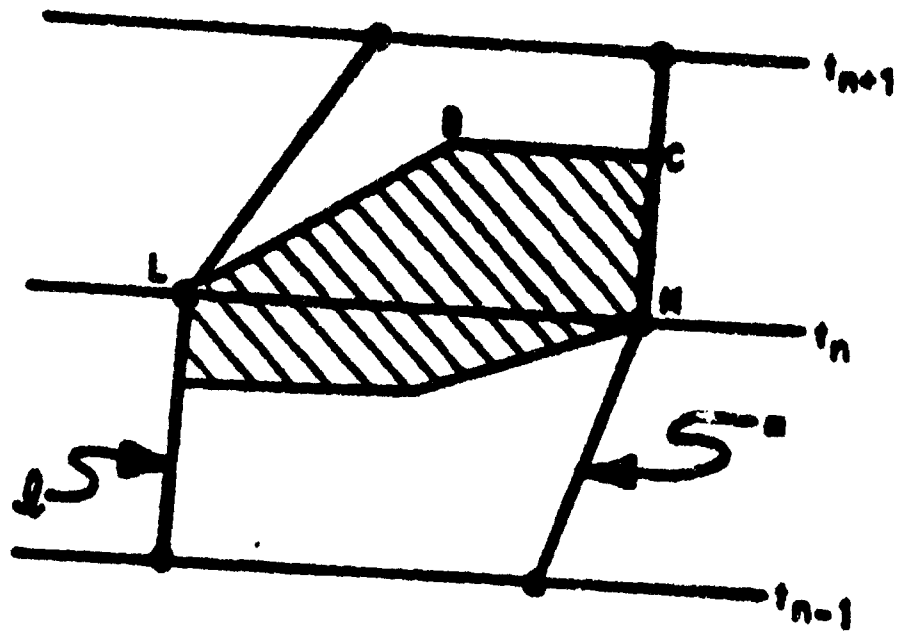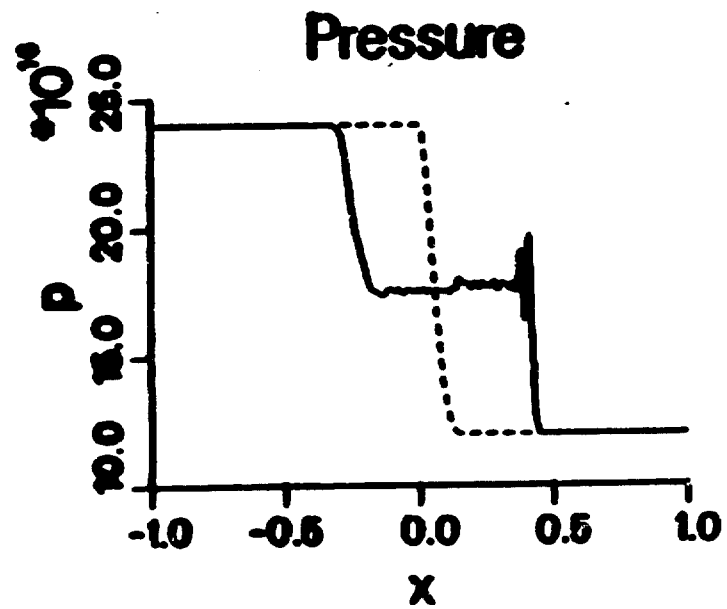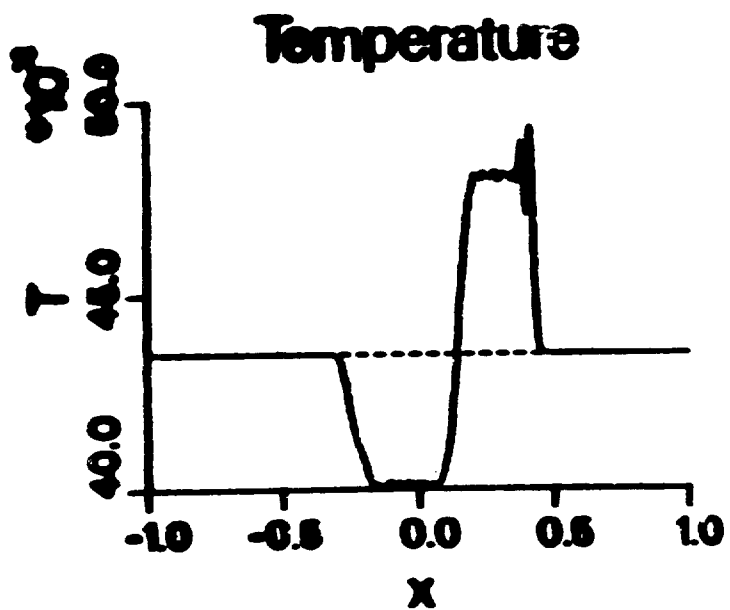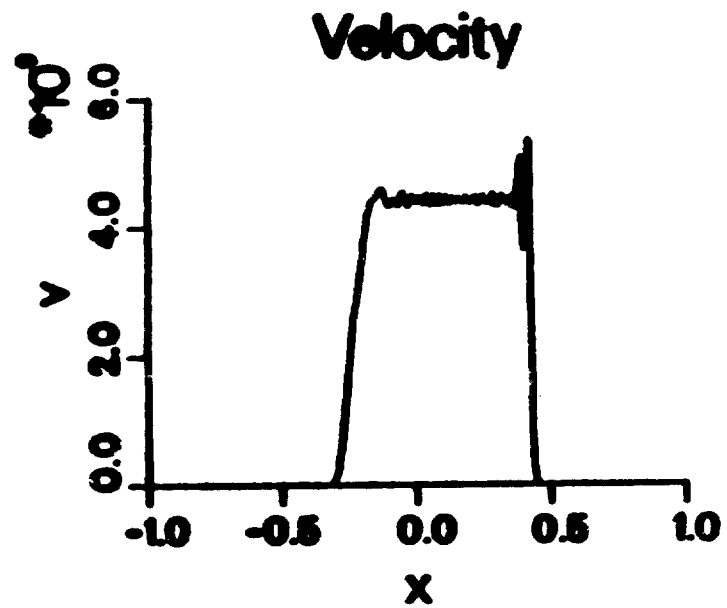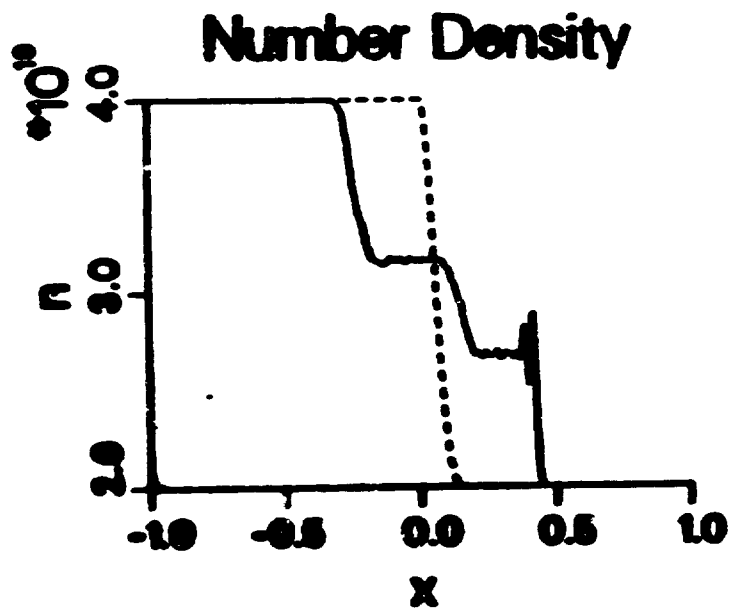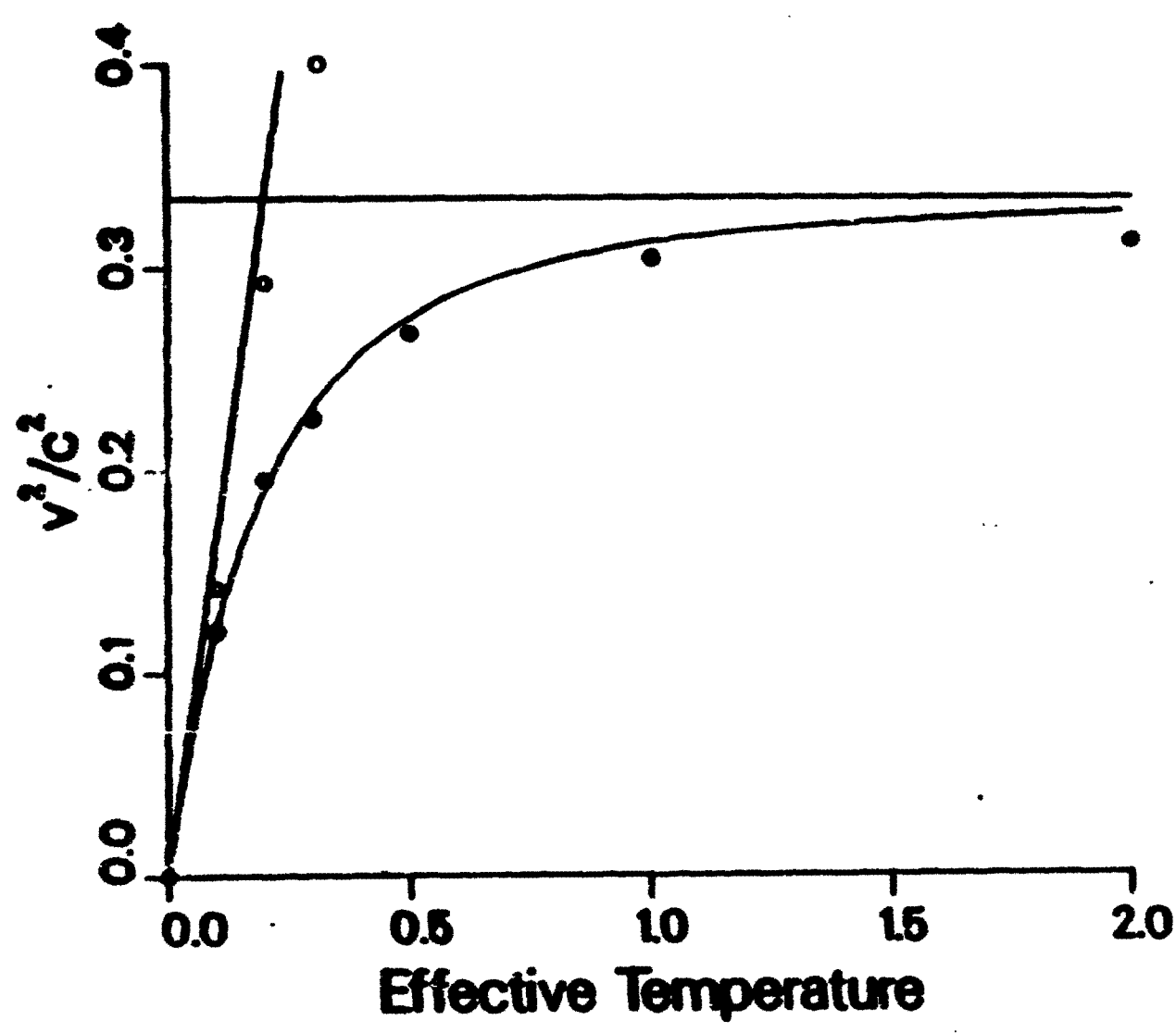
DISCUSSION

The main problem :

The kernels depend on the choice of observer. Their supports, if projected on the comoving frame of the fluid, become ellipsoidal. The ellipticity depends on the choice of the observer.

Statement.
For any choice of the smoothing length for the kernel (spherical kernels) in the observer's proper space, the observer can be picked in such a way that the smoothed particle approximation brakes down.

For any given scale, one can pick an observer such that in the direction of his motion the smoothed particles will become decoupled. The suggestion to start from an observer and to choose the scale such that there will be a sufficient number of particles in the direction of the observer's motion will ordinarily lead to silly situations (the scale of the smoothed particle becomes smaller than the baryon size, etc).

A suggestion to pick a "reasonable observer" is sometimes forwarded. However, a "reasonable observer" in this context means the one that does not move too fast (relativistically) with respect to fluid.

Statement.
The most "reasonable" observer is the one that does not move with respect to the fluid, i. e. the observer of the comoving frame.

CONCLUSION

- Truly relativistic SPH is necessary for the problems that involve interactions of parts of fluid moving relativistically with respect to each other (no "reasonable" global observer exists).

- Truly relativistic SPH contains intrinsic criteria of its applicability. Such a criterion is totally absent in semirelativistic SPH.

- When using semi-relativistic SPH one should employ the fully relativistic SPH theory when picking a "reasonable" observer. When parts of the fluid move at relativistic speeds with respect to each other this should be done locally.

Tidal compression and disruption of stars near a supermassive rotating black hole

Hanno Sponholz[*]

Institut für Theoretische Astrophysik
der Universität Heidelberg
Im Neuenheimer Feld 561
D—69120 Heidelberg

Abstract

Capture and tidal break-up of stars by a supermassive black hole (SBH) and the subsequent accretion of the dispersed matter onto the central object may provide a crucial mechanism for the fuelling of active galactic nuclei (AGN). It is generally assumed that very bright AGN contain a central rotating SBH. Because relativistic effects become important for the Roche-process for $SBH \geq 10^6 M_\odot$ we present a first hydrodynamical computation of the tidal encounter of a main-sequence-star with a rotating black hole.

To consider qualitatively new effects, especially to include additional effects by a Kerr black hole, we apply the Smoothed Particle Hydrodynamics (SPH) technique for a fixed background metric. Within the framework of SPH, the star is modelled as a polytrope — the Kerr metric of the rotating black hole is taken into account by using components of the Riemann-Tensor in a special chosen parallel-propagated tetrad-frame along the centre-of-mass trajectory of the star.

Beside tests and stability investigations of the code, a comparison between the Newtonian and the relativistic investigation is presented, as well as detailed calculations of the efficiency of tidal disruptions and their dependence on the angular momentum of the SBH for a moderate rotating $5 \cdot 10^7 M_\odot$ SBH. The tidal disruption of a $1 \cdot M_\odot$ polytrope by an extremely rotating $1 \cdot 10^9 M_\odot$ SBH is considered and the fate of the resulting debris of the star is shortly discussed. Some results of the relativistic generalisation of the problem of tidal squeezing of a star closely encountering a Kerr black hole are sketched. Finally the range of validity of these relativistic SPH-applications for tidal simulations around a SBH is derived in terms of the radius of curvature and the inhomogenity scale of the external metric.

[*]E-mail: sponholz@epikur.ita.uni-heidelberg.de

1 Tidal Processes around Black Holes – The scenario

In addition to free gas accretion, tidal interaction between a compact object and a star (Rees, 1988) may play an important role in the process of fuelling active galaxies – concerning this fundamental process there exist the following lines of research: On one side there is the application of the theory of tides to incompressible bodies in both the relativistic (e.g. Fishbone, 1973, Mashhoon, 1975) and the classical context. On the other side we have the sophisticated works with the compressible affine star model (e.g. Luminet and Carter, 1986) where the star is assumed to keep always an ellipsoidal density-shape, even during a very close encounter. Later, this application has been extended to a relativistic version (Luminet and Marck, 1985) in the environment of a Schwarzschild-BH[1], using an earlier formulation for relativistic tidal forces (Marck, 1983).

A third treatment of such 3D-problems with a reasonable computational effort has become more and more common — even if they are not that accurate as conventional hydrodynamic codes, mostly applied to restricted problems with less dimensions: The recently introduced particle methods (Lucy, 1977, Monaghan, 1992) are very helpful to understand gross effects of this intrinsic 3D-process.

Although we have principle difficulties to treat self-gravitating systems in General Relativity properly, it seems to me useful to include the formulation for tidal forces (Marck, 1983) in such a particle program. An older short description of simple SPH-simulations for tidal actions of Schwarzschild- and Kerr-Black-Holes on polytrope stars (Sponholz, 1991) is here presented as more extended and elaborated paper. An actual application in the vicinity of a Schwarzschild-BH is described in Laguna et al., 1993

2 Tidal Processes around Black Holes – motivation

Earlier it has been argued (Hills, 1975) that for the fuelling of AGNs, tidal disruption may be only effective if $M_{BH} < 10^8 M_\odot$ (if the mass M_{BH} of the central Schwarzschild black hole exceeds $3.2 \times 10^8 M_\odot$, the radius of the innermost stable orbit becomes larger than the tidal radius and the star will be captured wholly, without emitting radiation). However, tidal disruption of infinitesimal, incompressible fluid bodies is not excluded for a more massive Kerr BH with $M_{BH} < 2 \times 10^9 M_\odot$, because for co-rotating orbits the Roche limit increases while the radius of the last stable orbit decreases with increasing angular momentum of the Kerr black hole. Thus, of principle interest are the fraction of the star's mass which falls directly

---

[1]One of the results: a multiple compression of the star instead of the single one in the former Newtonian case of a very close encounter.

into the hole, the fraction which is ejected into outer regions or at times, before the disk has fully evolved [CA90], and the fraction, which remains in the disk.

We consider as primary body a massive black hole (BH) with a mass of $10^6 \ldots 10^9 M_\odot$, optionally with angular momentum. To model the secondary star as a polytrope, we divide the star into a number of fluid elements and simulate an encounter of the secondary star with the black hole; this means, that we solve the equations of motion in the combined field of (i) the black hole and (ii) the star itself.

3 The Method: Smoothed Particle Hydrodynamics

A recently introduced numerical method (Lucy, 1977, Benz and Hills, 1987, Evans and Kochanek, 1989) — Smoothed Particle Hydrodynamics (SPH) — uses a Lagrangian description to simulate the evolution of gaseous systems — the medium is modelled without a numerical grid as a collection of N gaseous parcels, elements, moving interpolation points or particles. To solve the exact real system one has to use an infinite number of such elements. For a computational method with a finite number of elements, we have to perform local averaging over finite volumes, consequently, we have to introduce a procedure for smoothing out local fluctuations in the particle number.

a) If the value of a physical field $f(r')$ is known at the radius vector r', the mean value at r can be obtained by averaging over a kernel $W_h(r - r')$:

$$\langle f(r) \rangle = \int f(r') W_h(r - r') dr' \tag{1}$$

b) The derivatives of the function f are obtained by smoothing with the derived kernel:

$$\left\langle \frac{\partial f(r)}{\partial x} \right\rangle = \int \frac{\partial f(r')}{\partial x'} W_h(r - r') dr' \tag{2}$$

(after integration by parts:)

$$\left\langle \frac{\partial f(r)}{\partial z} \right\rangle = \int f(r') \frac{\partial}{\partial z} W_h(r - r') dr' \tag{3}$$

c) If we choose the mass density ρ as smoothed function $W_h(r - r_j)$ known at a finite number of discrete points r_j, include the Poisson equation and an equation of state[3] then we may write down a system of ODE's, approximating the equations of hydrodynamics, including the Lorentz-invariant modifications (cp. Mann, 1991).

To model the secondary star as a polytrope, we divide the star into number of fluid elements or "smoothed particles" and simulate an encounter of the secondary star with the black hole.

---

[3] For now, we take the polytropic equation of state: $p = K \rho^{1 + \frac{1}{n}}$.

4 Geodesics around a Black Hole and tidal efficiency

If that the star is much smaller[3] than the BH, it is reasonable assumption that the star moves along a geodesic around the BH. The trajectory for a small main-sequence star orbiting in the equatorial plane ($\theta = \pi/2$ and $\dot\theta = 0$) around a massive BH is given by Carter's integrals of motion:

$$ \dot t = \frac{(AE - 2MraL)}{\Delta r^2} \quad , \tag{4} $$

$$ \dot r^2 = \frac{[E(r^2 + a^2) - aL]^2 - \Delta(\mu^2 r^2 + K)}{r^4} \quad , \tag{5} $$

$$ \dot\phi = \left[\frac{2M}{r}aE + \left(1 - \frac{2M}{r}\right)L\right]\frac{1}{\Delta} \quad , \tag{6} $$

where $(x^0, x^1, x^2, x^3) \equiv (x^t, x^r, x^\theta, x^\phi) \Rightarrow (t, r, \theta, \phi)$ denote the Boyer-Lindquist-coordinates and for the mass of the BH we have $M_{BH} = M$. For the constants we use the convention $G = c = 1$. μ^2, E, L are the rest mass, energy, and angular momentum about the axis of symmetry per unit mass, respectively; K is Carter's third integral: $K = (aE - L)^2$. The dot denotes the differentiation with respect to the proper time τ_{rel}. Without restriction we set $\mu = 1$. Physically motivated — the star is assumed at rest in infinity distance — we use a "parabolic" orbit: $E = 1$.

The geodesics may be obtained either as the formal solution or by numerical integration of the eqs. of motion (4) – (6). The numerical integration — here we use a *Runge-Kutta*-scheme — seems to be reasonable stable even close to unstable orbits. (For Schwarzschild-geodesic an orbit close to the marginal bound orbit at $r_{mb} = 4 = L_{mb}$ is shown in Boyer-Lindquist-coordinates (Fig 1).) Already from the shape of geodesics we may discuss the influence of relativistic effects and of the Black Hole's rotation on the tidal problem: The following three effects appear and may discussed even by considerations about the geodesics:
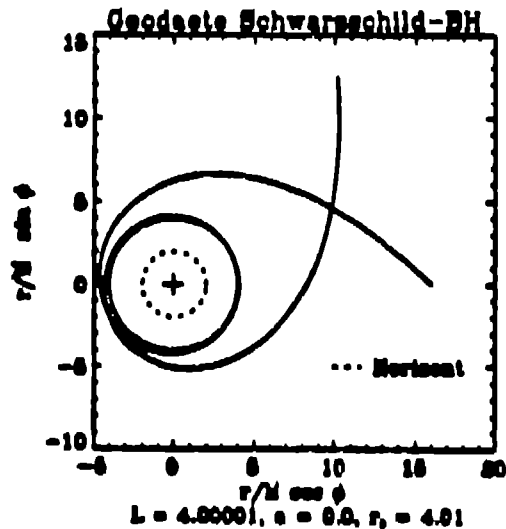
Figure 1: Schwarzschild-geodesic (periastron $r_p = 4.01$)

$L = 4.00001, a = 0.0, r_s = 4.01$

---

[3] For applicable conditions see sect. 6

(1) The geodesics of test-particles change by the influence of the curvature effects of the space-time as well as by the angular momentum of the BH. In Boyer-Lindquist-coordinates e.g. all the typical radius of prograde test-particle-orbits goes to one Schwarzschild-radius for an extreme ($a \approx 1$) rotating BH.

Increasing angular momentum of the BH *decreases for prograde orbits the marginal bound radius* r_{mb}: This enables a smaller periastron-distance
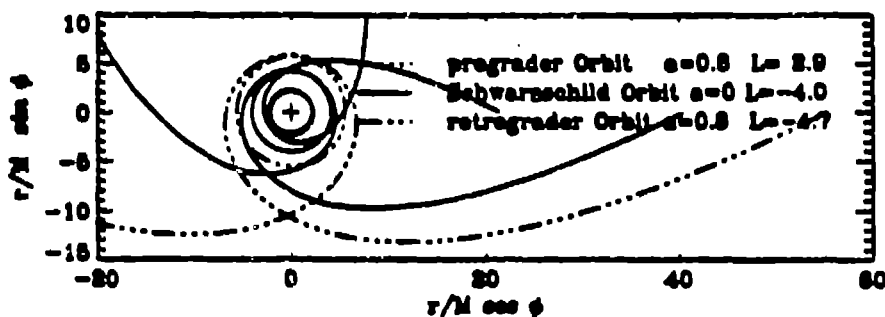
Figure 2: Critical unbound geodesics & different spin-parameters.

r_p between star and BH (Fig. 2). Potentially tidal effects on extended bodies increase roughly with decreasing distance from the compact object according to r_p^{-3}.

(2) Fixed periastron-distance:
* Relativistic orbits: the geodesic tends to wind around the BH (Fig. 1).
* Dependent from the spin-parameter of the BH; for retrograde orbit and chosen distance from the compact object, this tendency increases with the spin of the BH (Fig. 3).
* The closer the star reaches the marginal bound radius *the longer is the time it spends near the BH*. Increases time-efficiency of tidal effects.
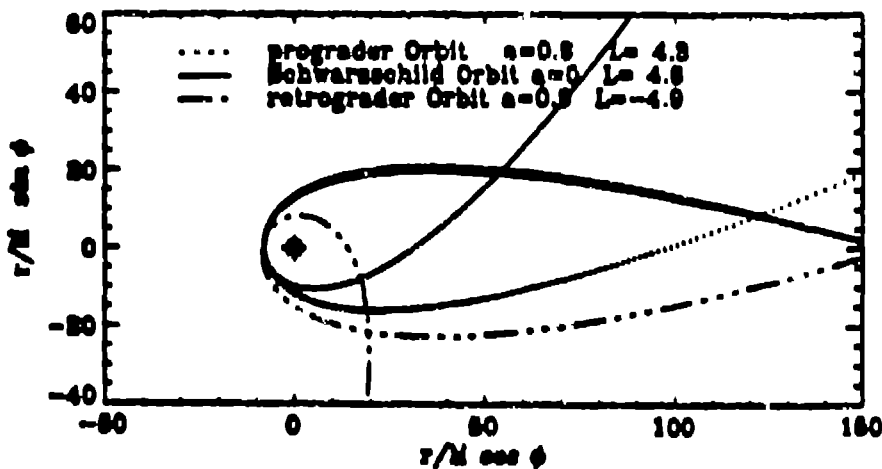
Figure 3: Geodesics $r_p = 7.0$

(3) A non-vanishing spin-momentum a of the BH results in the known "Frame-Dragging" effect; the horizon shifts inwards and on the former
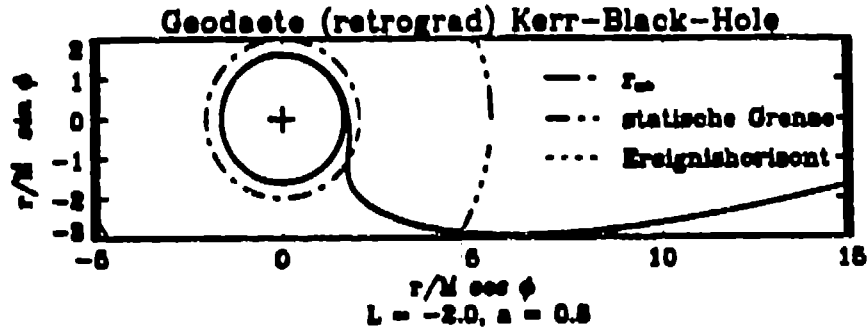
Figure 4: Kerr-geodesic (retrograde)

radius $2M$ locates the "static limit", the "border" of the ergosphere. The Boyer-Lindquist-coordinate "t" changes from a time-like to a space-like coordinate. This reflects the strong coupling of the individual orbits to the given space-time of the BH and results in a *stronger tidal force* for the retrograde orbits compared to Schwarzschild ones and in all cases stronger than for a comparable (the same penetration factor β) newtonian constellation.

5 The tidal field of the SBH Kerr-space-time

The tidal problem is treated in a test-particle approximation — we assume that the space-time of and around the compact object is negligible disturbed by the secondary star. This is the condition to consider the orbit of the star as a geodesic given by Carter's formulae (4) – (6). With other words: the condition to include the self-gravitation of the star in a local flat way leads to the demand for a small extension and spatial scales of the star against the radius of curvature of the primary metric (sect. 6).

The relative (tidal) acceleration of a hydrodynamical element of the star may be obtained by the equation of geodesic deviation. An orthonormal tetrad, locally defined and parallel-propagated along the centre-of-mass trajectory allows to derive a tidal tensor in terms of the Riemann tensor from the equation of geodesic deviation. The separability properties of a Kerr Black Hole make it possible to construct such a tetrad analytically (Marck, 1983):

$$\lambda^{(\mu)}_{[0]} = \frac{1}{r\sqrt{\Delta}}[E(r^2 + a^2) - aL]\delta^\mu_0 + \frac{r\dot{r}}{\sqrt{\Delta}}\delta^\mu_1 + \frac{aE - L}{r}\delta^\mu_3 \quad ,$$

$$\lambda^{(\mu)}_{(1)} = e^{(\mu)}_{[1]}\cos\Psi - e^{(\mu)}_{[3]}\sin\Psi \quad ,$$

$$\lambda^{(\mu)}_{(2)} = -\frac{aE - L}{\sqrt{R}}\delta^\mu_3 \quad ,$$

$$\lambda^{(\mu)}_{(3)} = e^{(\mu)}_{[1]}\sin\Psi + e^{(\mu)}_{[3]}\cos\Psi \quad . \tag{7}$$

$$e^{(\mu)}_{[1]} = \frac{r^2 \dot{t}}{\sqrt{\Delta(r^2 + K)}}\delta^{\mu}_0 + \frac{E(r^2 + a^2) - aL}{\sqrt{\Delta(r^2 + K)}}\delta^{\mu}_1 \quad , \tag{8}$$

$$e^{(\mu)}_{[3]} = \frac{\sqrt{K}[E(r^2 + a^2) - aL]}{r\sqrt{\Delta(r^2 + K)}}\delta^{\mu}_0 + \frac{\sqrt{K}r\dot{t}}{\sqrt{\Delta(r^2 + K)}}\delta^{\mu}_1 + \frac{\sqrt{(r^2 + K)}}{r}\frac{aE - L}{\sqrt{K}}\delta^{\mu}_3 \tag{9}$$

For the angular-velocity of the coordinate-system we have:

$$\dot{\phi} = \frac{E\sqrt{K} - a\,\text{sign}(aE - L)}{r^2 + K} \tag{10}$$

For a rather high velocities in the local tetrad system it is appropriate to use a further extended equation of geodesic deviation (Hodgkinson, 1972, Mashhoon, 1977), which gives the following equations for tidal acceleration of hydrodynamical elements with respect to the local tetrad system:

$$\boxed{\frac{d^2 X^i}{d\tau^2} + C^i_j X^j = 0}$$

The tidal tensor

$$C_{ij} = \tilde{C}_{i0j0} + 2(\tilde{C}_{ikj0}\dot{X}^k + \tilde{C}_{0ij0}\dot{X}^i\dot{X}^k)$$

$$+ \frac{2}{3}(\tilde{C}_{ikjl}\dot{X}^k\dot{X}^l + \tilde{C}_{0kjl}\dot{X}^i\dot{X}^k\dot{X}^l) \quad . \tag{11}$$

is derived in terms of the Riemann tensor with respect to the parallel-propagated tetrad:

$$\tilde{C}_{\mu\nu\rho\sigma} = R_{(\alpha)(\beta)(\gamma)(\delta)}\lambda^{(\alpha)}_{\mu}\lambda^{(\beta)}_{\nu}\lambda^{(\gamma)}_{\rho}\lambda^{(\delta)}_{\sigma} \tag{12}$$

Explicitly, some non-vanishing independent components of the tidal tensor are given by the following

$$\tilde{C}_{1010} = \left[1 - 3\frac{(r^2 + K)}{r^2}\cos^2\phi\right]\frac{M}{r^3} \quad , \tag{13}$$

$$\tilde{C}_{2020} = \left[1 + 3\frac{K}{r^2}\right]\frac{M}{r^3} \quad , \tag{14}$$

$$\tilde{C}_{3030} = \left[1 - 3\frac{(r^2 + K)}{r^2}\sin^2\phi\right]\frac{M}{r^3} \quad , \tag{15}$$

$$\tilde{C}_{1030} = \tilde{C}_{3010} = -3(r^2 + K)M/r^5\cos\phi\sin\phi \quad , \tag{16}$$

$$\tilde{C}_{0131} = -\tilde{C}_{0113} = \tilde{C}_{1310} = -\tilde{C}_{3110} = -3\sqrt{K}\sqrt{r^2 + K}M/r^5\cos\phi \quad \cdots etc.$$

6 Range of Application

The nonexact treatment of general relativity especially the flat (Newtonian) treatment of self-gravitation of the star reflects in the following conditions for range of application:

- The object moves on a test-particle trajectory around the BH and

- Self-gravitation can be treated in a locally flat way and

- Production of gravitational and electromagnetic radiation is negligible

only if: the length-scale of the star $R_*(> M_*)$ is small compared to the length scale of the metric. The external metric has a vacuum Riemann tensor characterised by the following three length scales:

- $\mathcal{R}$ = Radius of curvature: $\mathcal{R}^2 \sim \frac{1}{R_{,\theta\theta}}$.

- $\mathcal{L}$ = Inhomogenity scale: $\mathcal{L} \sim \frac{R_{,\theta\theta}}{R_{,\theta\theta,i}}$.

- $\mathcal{T}$ = Time scale: $\mathcal{T} \sim \frac{R_{,\theta\theta}}{R_{,\theta\theta,0}}$. In terms of the Kerr-metric this conditions can be easily derived from the components $((13) - (16))$ of the Riemann-tensor with respect to the used tetrad system:

$$\mathcal{R} \sim r\sqrt{r/M_{BH}} \ , \quad \mathcal{L} \sim r/3 \ , \quad \mathcal{T} \sim \infty \ .$$

The condition for the star's length scale R_*

$$R_* \ll \mathcal{R} \ , \quad R_* \ll \mathcal{L} \ .$$

is a real restriction for very close encounters, because the length-scale of the deformed star increases by orders of magnitude especially during a very close encounter.

The following table relates the typical stellar data to curvature-radii of SBH with corresponding mass.

RANGE OF APPLICATION FOR TIDAL TENSORS — EXAMPLES

Example [a]	M_* $(M_\odot)$	R_* $(R_\odot)$	M_R $(M_\odot)$ [b]	β_{max} [c]	M_{BH} $(M_\odot)$ [d]
B0 V	18.	7.5	$3.5 \cdot 10^6$	1.22	$1.6 \cdot 10^9$
A0 V	3.2	2.6	$1.2 \cdot 10^6$	0.75	$7.5 \cdot 10^8$
G0 V	1.1	1.1	$0.5 \cdot 10^6$	0.46	$3.5 \cdot 10^8$
M0 V	0.5	0.6	$0.3 \cdot 10^6$	0.32	$2.1 \cdot 10^8$
F0 III	2.5	5.	$2.3 \cdot 10^6$	1.58	$2.3 \cdot 10^9$
K0 III	3.5	16.	$7.5 \cdot 10^6$	4.51	$1.1 \cdot 10^{10}$
M0 III	5.0	40.	$1.8 \cdot 10^7$	10.0	$3.7 \cdot 10^{10}$
A0 I	16.	40.	$1.8 \cdot 10^7$	6.80	$2.0 \cdot 10^{10}$
F0 I	12.	60.	$2.8 \cdot 10^7$	11.2	$4.3 \cdot 10^{10}$
RGiant (ζAur)	16.	245.	$1.2 \cdot 10^8$	41.7	$3.1 \cdot 10^{11}$

[b] Mass of a black hole with curvature-radius $\mathcal{R} \sim r^{3/2} \cdot R_*$.

[c] Maximal koeff. of penetration $\beta_p = \frac{r_*}{r_p}$ für $r_p = 1.1$, $M_{BH} = 10^9 M_\odot$

[d] Maximal mass of a black hole for a koeff. of penetration. $\beta_p = 0.5$, $r_p = 2.0$

$$\frac{M_{BH}}{M_\odot} = \sqrt{\frac{M_*}{M_*}}\left(\frac{R_*}{\beta_p r_p M_{s\odot}}\right)^{3/2}$$ ($M_{s\odot}$: Schwarzschild-radius of the sun)

6.1 Classical treatment, non-relativistic case vs. Geodesic, Riemann-tensor

As simple test let's compare the classical treatment with the complete newtonian tidal forces to a similar computation using the integrated geodesics and the Riemann-tensor.
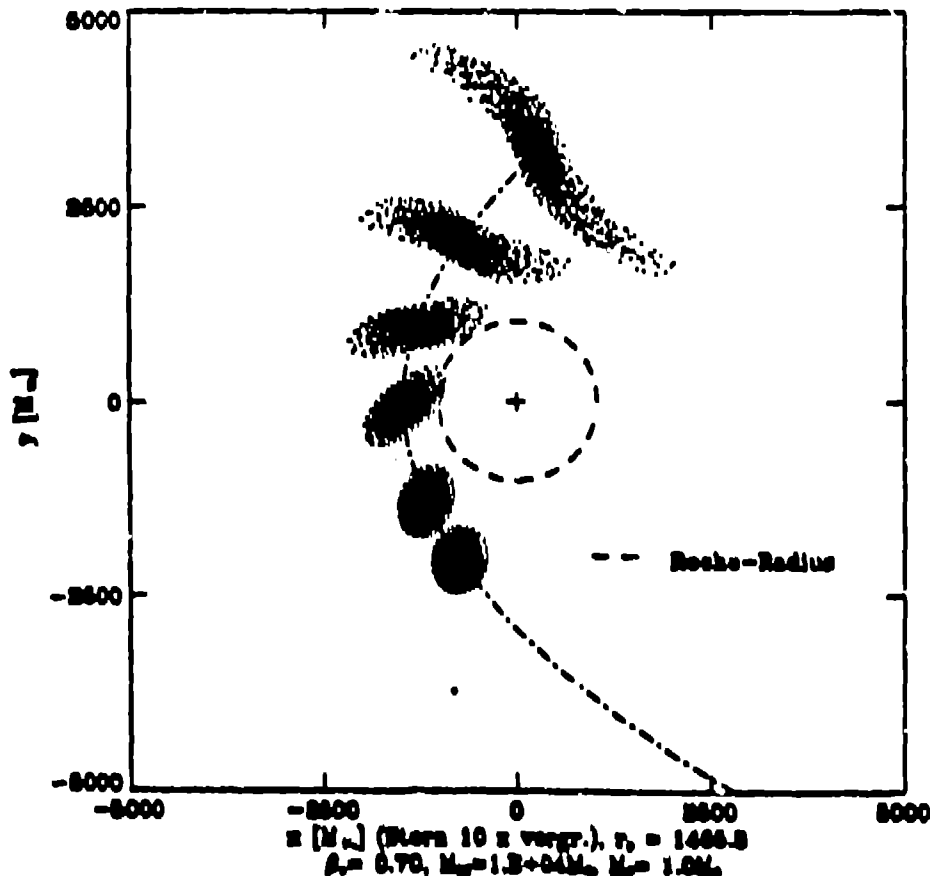
Both computations should show the same results in a classical, linear case: The linear nonrelativistic encounter happens, if $(M_{BH} \ll R_* \ll r_p)$. In Fig. 5 the formal Keplerian Orbit is shown; the computation uses the exact (non-linear) Newtonian tidal forces.

This is a computation with 1000 particles; the SPH-width $2h$ corresponds ≈ to the length of the ticks at the axis — all the length scale units are in units of the Schwarzschild radius M_{BH}; the projection of the interpolation-points onto the equatorial-layer is enlarged by the factor of 10.

The simulation has to be compared with Fig. 6.

Fig. 6 uses the geodesic equations; the tidal forces are used as components of the Riemann tensor for the same configuration (classical, linear case) as Fig. 5. Both computations show essentially the same particle distribution.
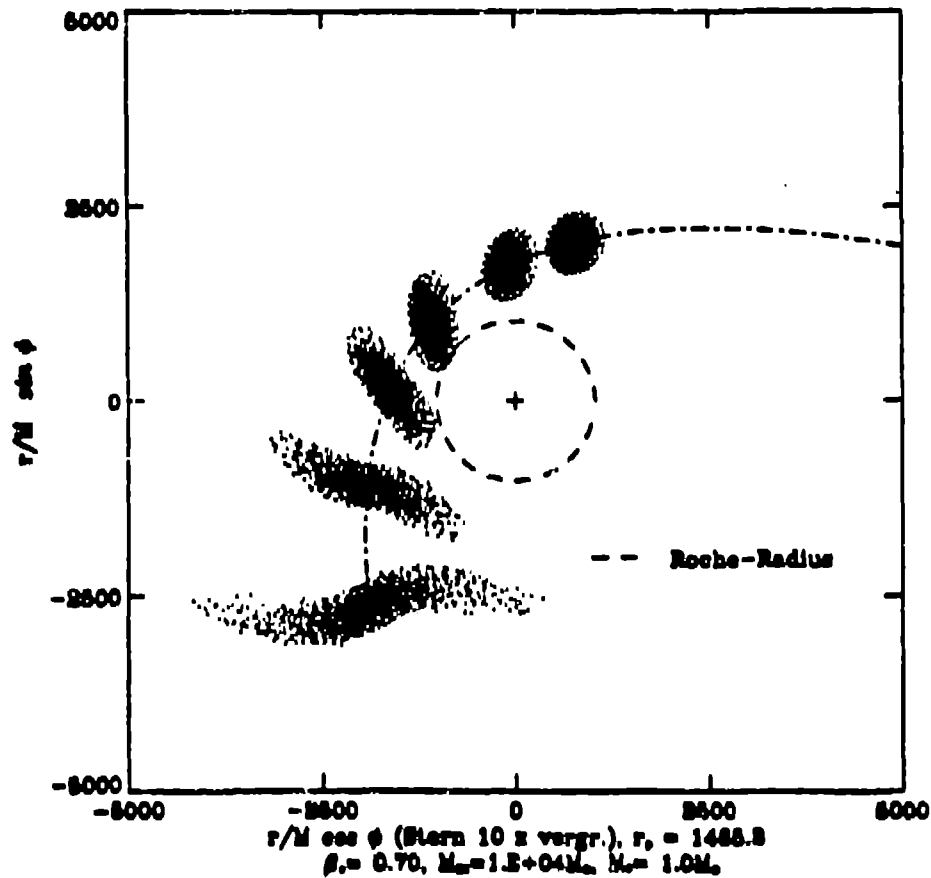
Figure 6: General relativistic encounter in the Newtonian Limit

Although the number of particles (1000) is rather restricted, the simulations gave a simple test for the correctness of the derivation of the (relativistic) tidal forces and the used time- and length-scales.

7 Nonlinear Newtonian encounter

— Very deep penetration of the star into the Roche lobe were discussed in connection with
  · tidal induced nuclear processing of the star's matter ("Nuclear

$\beta_r = 18.00, M_{\bullet} = 1.E+04 M_{\odot} M_{\bullet} = 1.0 M_{\odot} r_p = 64.1$
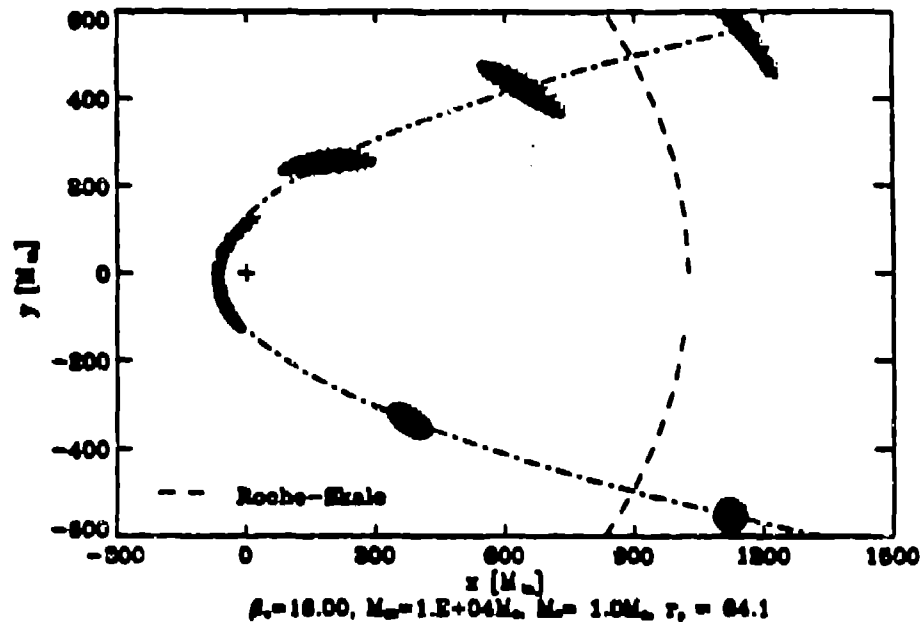
Figure 7: Nonlinear Newtonian encounter

runaway"-scenario [Luminet and Carter, 1986]) and
  · γ-bursts (Carter, 1992).
— It is assumed, that the regime of the tidal interaction is essentially controlled by the penetration factor β_p or "Roche coefficient"

$$\beta_p = \frac{R_R}{r_p}$$

with the typical length scale in the tidal field:

· The "Roche"-scale
$$R_R = R_{\bullet} \left(\frac{M_{BH}}{M_{\bullet}}\right)^{\frac{1}{3}} = \left(\frac{4\pi}{3} \frac{M_{BH}}{\bar{\rho}_{\bullet}}\right)^{\frac{1}{3}}$$

· For very close $(\beta_p \gg 1)$ and nonlinear $(r_p \simeq R_{\bullet})$ encounters the polytrope is stretched along the orbit and severely compressed in the vertical direction. This reflects in an increase for the central density just after the closest approach, before being dissolved.

· The particles are forced into individual Keplerian orbits and to cross a small area, which leads to the compression-effect.

· Particles go rather a "eye of a needle" than being compressed as a "pancake". (Fig. 8 shows a view onto the radial-vertical layer of the encounter Fig. 7.)
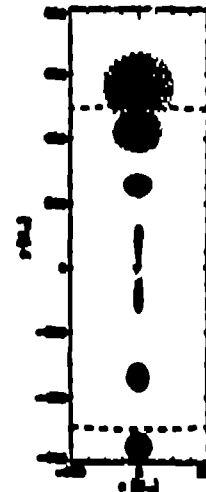
Figure 8:

8 Tidal compression — relativistic case

For the very close encounters in the vicinity of a BH, this transition of the several hydrodynamical elements through the equatorial layer occur repeated. Thus, the corresponding size of the vertical principal axis will have several minimums (Fig. 10). The coordinate-time t of such event (Fig. 9) is mostly very similar to the proper time τ_{rel} — if such violent process appear it must be observed with the same time-scale of several $5 \cdot M_6 s$ (where M_6 is the mass of the BH in $M_\odot$). A multiple peak in the density of the star could not be resolved, probably due to the low resolution of the simulation.
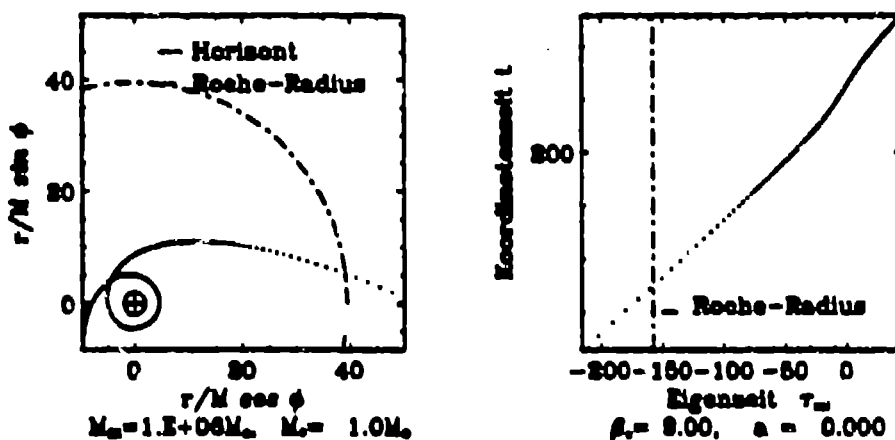
Figure 9: Geodesic for very close encounter. $\beta_p = R_R/r_p = 9$. Proper-time remains nearly unchanged.
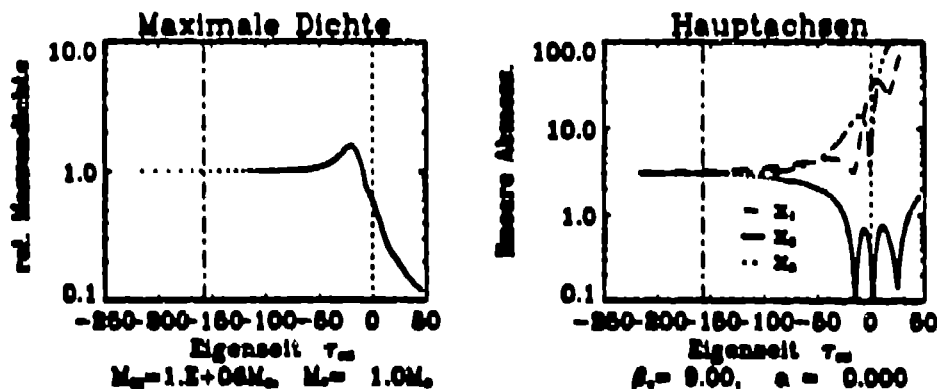
Figure 10: Time dependence of the central density and the length of axis for very close encounter (Fig. 9). The closer the marginal bound orbit is reached, the more tidal vertical compressions occur. (1000 Particles.)

9 Influence of BH-Rotation on Tidal compression

For the compression of the star there are influences already by the rotation-modified orbit of the star: For retrograde orbits, the orbit of the star is closer to the marginal bound orbit for a given perihel-distance compared to a nonrotating or a co-rotating BH. The phenomenon of several compressions are therefore reached more easily.
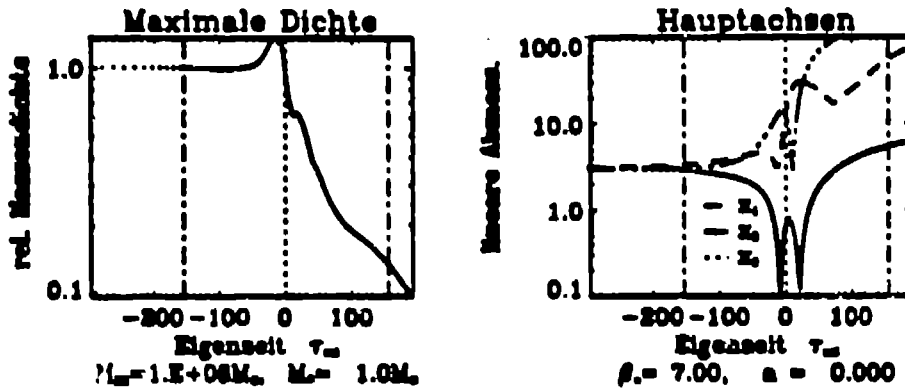
Figure 11: *Density vs. time and relative magnitudes of the principal axes of the star for the encounter with the Schwarzschild BH (Cp. Fig. 12. $\beta_p = R_R/r_p = 7$. 1000 Particles.)*
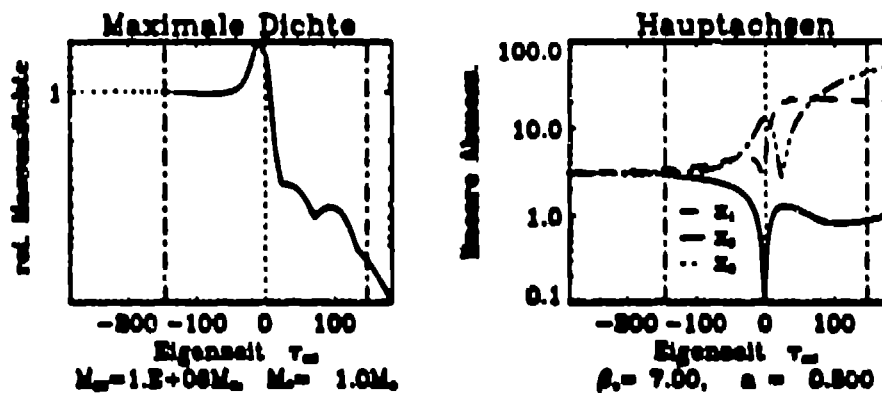
Figure 12: *Density vs. time and relative magnitudes of the principal axes of the star for the prograde encounter with the Kerr BH (Cp. Fig. 11). $\beta_p = R_R/r_p = 7$.*

For the very close encounter we obtain due to the non-linear — in the local frame velocity-dependent tidal forces (eq. (11)) — a curved shape of the compressed and tidal stretched star (see also Laguna et al., 1993) as shown in the figure 13. However we have to be carefully about the range of application (sect. 6), because for the presented examples we went easily
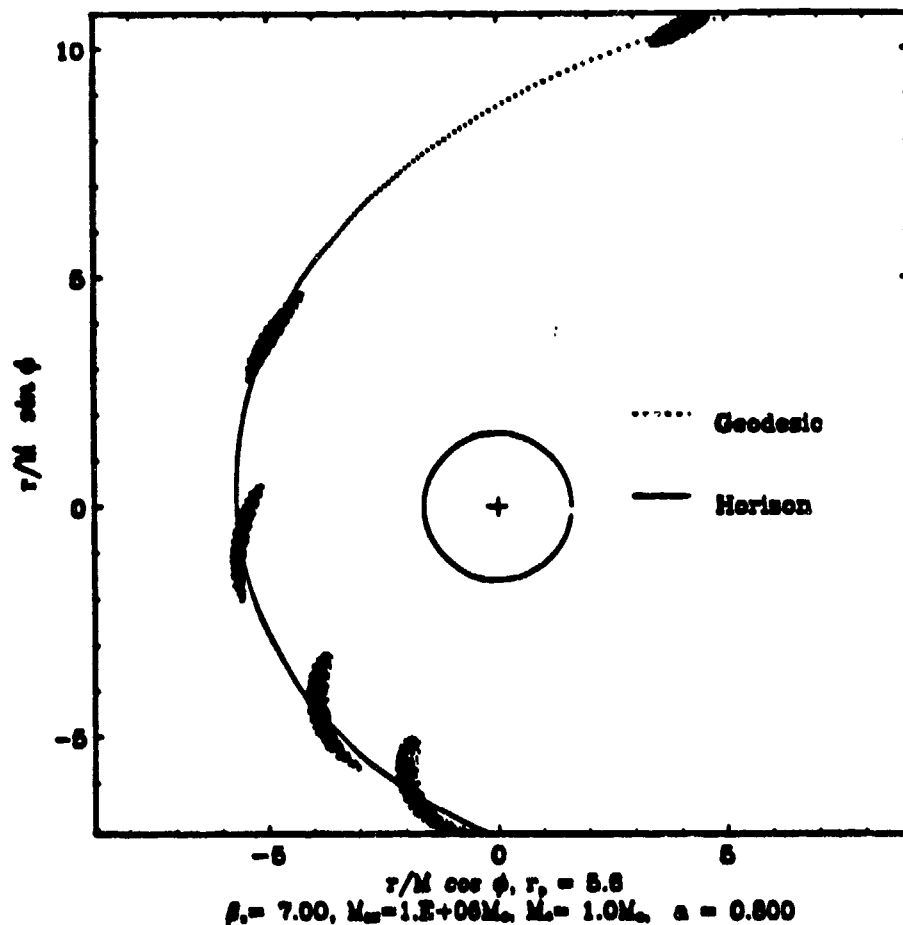
Figure 13: *Non-linear treatment for Kerr-BH $a = 0.8$, $\beta_p = R_R/r_p = 7$.*

into the dangerous region, where the length scale of the star has same order of magnitude as the inhomogenity scale, radius of curvature, respectively.

10 Tidal disruptions

To estimate Roche-limits the linear treatment ($R_o \ll \mathcal{R}$, $R_o \ll \mathcal{L}$) is applicable for computations of tidal disruptions ($\beta_p \approx 1$) of Main-Sequence-Stars and remains in the range of application. The influence of relativistic trajectories on tidal disruptions has been discussed already in sect. 4:

- Minimal *distance of the periastron* is effected by spin of the SBH.

- Orbits near the marginally bound became nearly "circular" and the tidal time-efficiency encreases.

- Tidal forces *increase* with respect to the Newtonian case.

- Tidal forces *increase* with spin of the SBH for *retrograde* trajectories (Frame-dragging).

- Examples:

1) SBH $M_{BH} = 50 \cdot 10^6 M_\odot$.

   - Simulations with the same β_p but different angular momentum of the SBH (figs. 14–19).

2) Extreme Kerr-SBH $M_{BH} = 10^9 M_\odot$ (figs. 20–22).

A rough impression for the angular momentum-influence of the SBH onto the tidal process may be obtained from the figs. 14–19. We identify the event of a successful disruption of the star as the increase of the total energy E_{tot} above zero (figs. 15,17,19) and the decrease of central stellar mass-density as well as a run-away of the principal axis of the star (figs. 14,16,18).
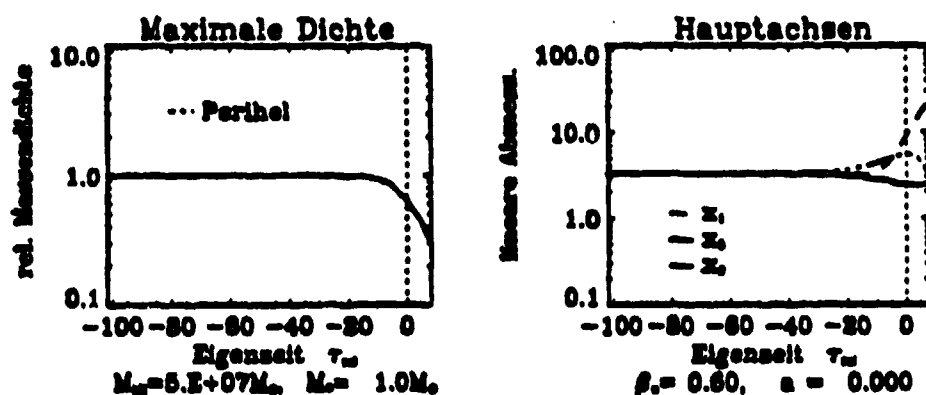
Figure 14: *Density vs. time and relative magnitudes of the principal axes of the star for the encounter with the Schwarzschild BH. Transition of perihel at $\tau = 0$.*
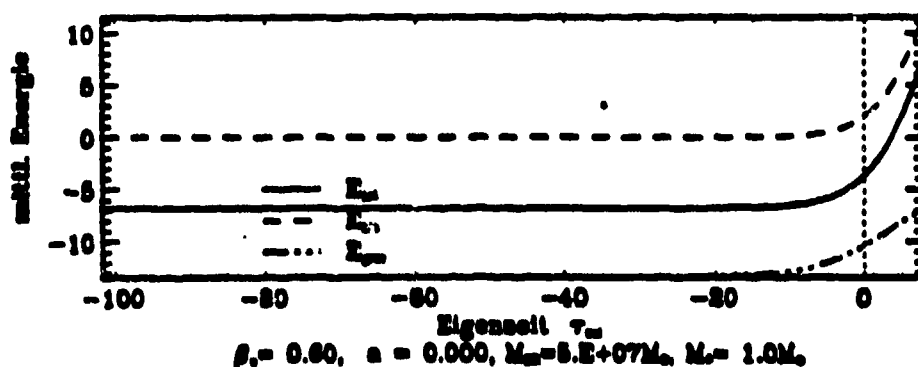
Figure 15: *Kinetic, gravitational and total energy vs. time. Encounter with the Schwarzschild BH. Roche-limit if $E_{tot} \geq 0$ shortly after transition of perihel. (5000 Particles.)*

Indeed, this disruption-event occurs for a Schwarzschild-hole (figs. 14, 15) a moment after the transition of the star through the periastron. With

the same Roche-coeff. β (the same perihel-distance), but for a prograde orbit (figs. 16, 17), the tidal disruption-event happens a considerable time later (after the periastron-transition) for an encounter with a moderately rotating Kerr-BH. On a related retrograde orbit (figs. 18, 19), disruption occurs a reasonable time prior to the transition through the periastron (in all the computations, we interrupt the simulation, if the star is disrupted.
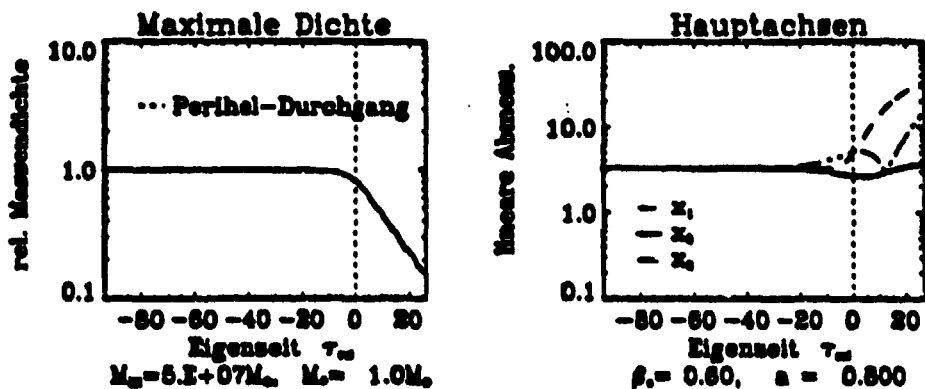
Figure 16: *Density vs. time and relative magnitudes of the principal axes of the star for a prograde encounter with the Kerr BH. Transition of perihel at $\tau = 0$.*
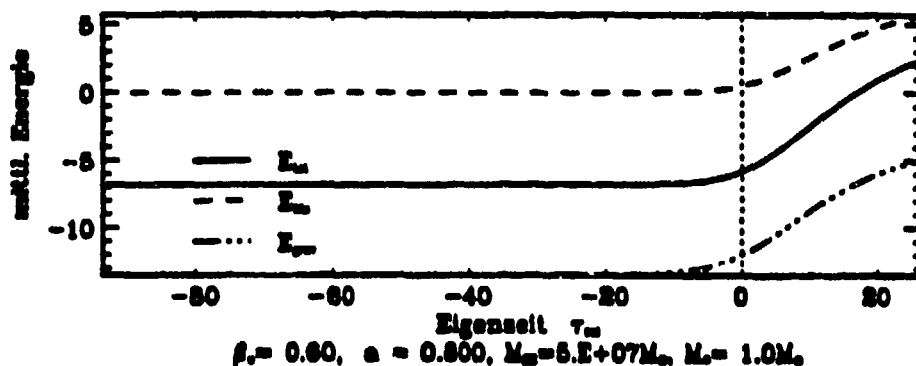
Figure 17: *Kinetic, gravitational and total energy vs. time. Prograde encounter with the Kerr BH. Roche-limit if $E_{tot} \geq 0$ longer time after transition of perihel. (5000 Particles.)*

11   Tidal disruptions by a $10^9 M_\odot$ Kerr-BH

The encounter of a $1 M_\odot$ main-sequence-star encounter with a $10^9 M_\odot$ extreme Kerr-BH (figs. 20 – 22) results in a clear tidal disruption-event. (Positive total energy, decreasing density of the star, increasing principle axis.) In connection with the fuelling of AGN we assume, that the tidal disruption events of stars are *important as fuelling process* also for the
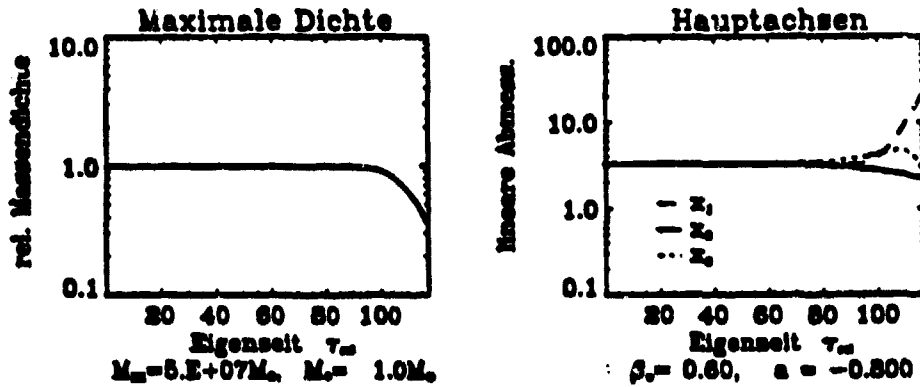
Figure 18: *Density vs. time and relative magnitudes of the principal axes of the star for a retrograde encounter with the Kerr BH. Star being dissolved before reaching the periastron.*
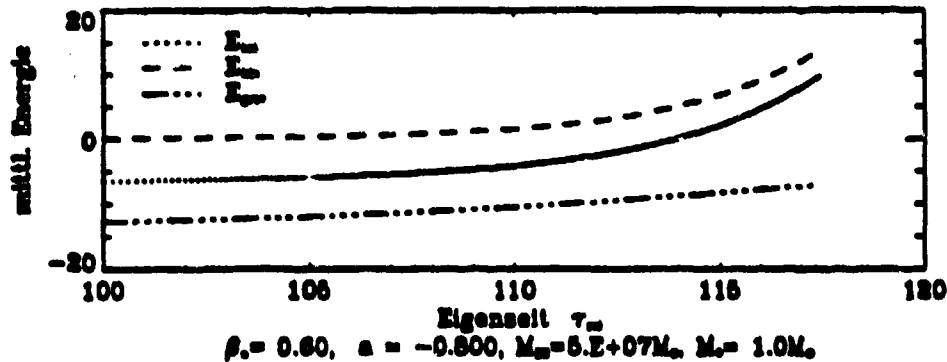
Figure 19: *Kinetic, gravitational and total energy vs. time. Retrograde encounter with the Kerr BH (a = −0.8, 5000 particles) Roche-limit $E_{tot} \geq 0$ reached before transition of perihel . (5000 Particles.)*

brightest AGN's (if the mass of the corresponding SBH is assumed for such BH's to be about $10^9 M_\odot$ and if it is rapidly rotating.) For such assumed SBH's, the mass-range for the tidal disruption event (due to the arguments given in Hills, 1975) will be extended in one order of magnitude.

The process may go to even higher masses of the BH, if one takes instead of a main-sequence-star a less dense star, e.g. a red giant.

For tidal-events, the energy-distribution $E = -p_t$ and the orbital angular momentum-distribution $L_s = p_\phi$ of the debris may be calculated by the back-transformation by $p_\mu = \lambda_\mu^{(e)} X_e$. For events close to the Roche-limit, the energy-distribution of the debris of the star is nearly the same as the energy of the former star: No dramatic changes occur for such limiting case. The fate of the stellar debris is essentially the same as it would have been for the star itself; if the star were on a geodesic, that is swallowed completely into the hole, than the fate of the debris will be the same and

vice ver·a. For the above example e.g. the distribution in energy and angular momentum is $\frac{\Delta E}{E} \simeq \frac{\Delta L}{L} \simeq 10^{-4}$, respectively.

For the example described in (figs. 20 - 22), we expect as result of the tidal process that the debris leave the close environment of the BH on similar geodesic as the former star ((fig. 20). The resulting highly elongated fragment of an accretion-disk may be later very fast transformed into a circular accretion disk fragment due to perihel-shift-effects and viscosity (Syer et al., 1991).
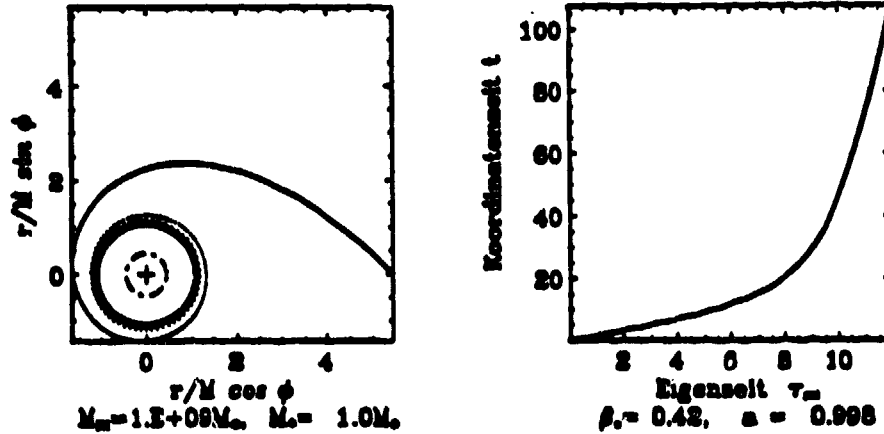
Figure 20: *Trajectory of the centre of mass of the star. Position of the Schwarzschild-BH and its Schwarzschild radius. massereichen Schwarzen Lochs. Roche-coeff. $\beta_p = R_R/r_p = 0.42$, "canonical" Spin of the Kerr-SBH $a = 0.998$. $r_p = r_{mb} + 0.1$*
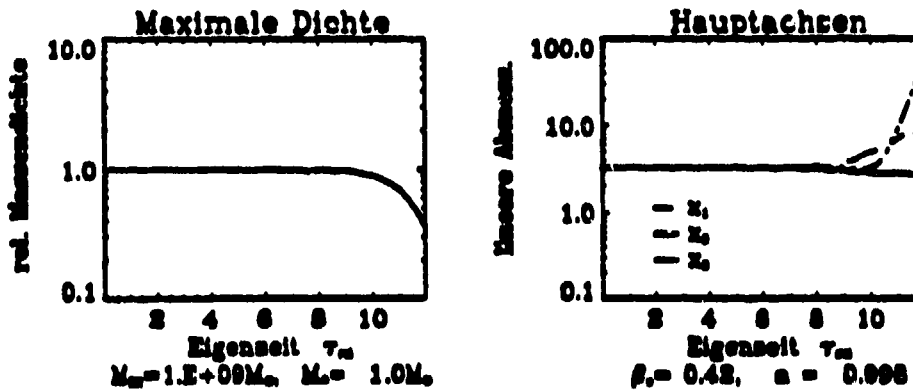
Figure 21: *Kinetic, gravitational and total energy vs. time. Prograde encounter with the Kerr BH. Roche-limit if $E_{tot} \geq 0$. Trajectory (Fig. 20, 5000 Particles)*

Figure 22: *Kinetic, gravitational and total energy vs. time. Prograde encounter with the Kerr BH (Fig.20). Roche-limit if $E_{tot} \geq 0$. (5000 Particles.)*

References

Benz, W. and Hills, J. (1987). *The Astrophysical Journal*, **323**:614.

Carter, B. (1992). *The Astrophysical Journal*, **391**:L67.

Evans, C. and Kochanek, S. (1989). *The Astrophysical Journal*, **346**:L13.

Fishbone, L. (1973). *The Astrophysical Journal*, **185**:43.

Hills, J. (1975). *Nature*, **254**:295.

Hodgkinson, D. E. (1972). *Gen. Rel. and Grav.*, **3**:351.

Laguna, P., Miller, W. A., Zurek, W. H., and Davies, M. (1993). *The Astrophysical Journal*, **410**:L83.

Lucy, L. (1977). *The Astronomical Journal*, **82**:1013.

Luminet, J.-P. and Carter, B. (1986). *The Astrophysical Journal Suppl. Series.*, **61**:219.

Luminet, J.-P. and Marck, J.-A. (1985). *M.N.R.A.S.*, **212**:57.

Mann, P. (1991). *Comput. Phys. Commun.*, **67(2)** :245–260.

Marck, J.-A. (1983). *Proc R. Soc. London*, A **385**:431.

Mashhoon, B. (1975). *The Astrophysical Journal*, **197**:705.

Mashhoon, B. (1977). *The Astrophysical Journal*, **216**:591.

Monaghan, J. (1992). *Ann. Rev. Astron. Astrophys.*, **30**:543.

Rees, M. (1988). *Nature*, **333**:523.

Sponholz, H. (1991). Gas release through tidal disruption of stars. In Duschl, W. and Wagner, S., editors, *Physics of Active Galactic Nuclei*, page 244. Berlin/Heidelberg/New York.

Syer, D., Clarke, C., and Rees, M. (1991). *M.N.R.A.S.*, **250**:505.

Relativistic SPH
Viscosity and Energy

J.J. Monaghan
Monash University

jjm@vaxc.cc.monash.edu.au

Leo Brewin, Anthony Lun
Monash.University

PROGRAM

- **BASIC EQUATIONS**
  SPH EQUIVALENTS

- **VISCOSITY, BARYON-BARYON SCATTERING**
- **NUMERICAL**

- **REGGE CALCULUS**

SPH Relativistic Simulations

- N. Lahy   M.Sc. Thesis. Monash Univ.

- P. Mann   Comp. Phys. Comm <u>67</u>, 245, (1991)

- P. Lugano, W. Miller, W. Zurek
         Ap. J. <u>404</u>, 678, (1993)

- J.J. Monaghan   Comp. Phys. Rep.
                  Ann. Rev. Astr. Ap. 1992

P.I.C. Simulations

Clare and Strottman   Phys. Rep. <u>141</u>, 177, (1986)

Nix and Strottman.   LA-UR-81-3452

Amsden, Harlow, Nix   Phys. Rev. C <u>15</u>, 2059, (1977)

Landau, Lifshitz Fluid Mechanics
J Wilson.

$$T^{\mu\nu} = (n m_0 c^2 + n\hat{e} + P) U^\mu U^\nu + P g^{\mu\nu}$$

$g_{00} = -1$, $g_{11} = g_{22} = g_{33} = 1$

$U^0 = \gamma$, $U^i = \gamma v^i/c$, $\gamma = \dfrac{1}{\sqrt{1 - v^2/c^2}}$

$U_\nu U^\nu = -1$

From

$$\frac{\partial T^{\mu\nu}}{\partial x^\nu} = 0.$$

$N = \gamma n \leftarrow \text{not}$
$\nearrow \qquad \text{frame}$
Lab Baryon
N° density

Get

$$\frac{d\vec{q}}{dt} = -\frac{1}{N} \nabla P \qquad \text{Momentum}$$

$$\frac{d\mathcal{E}}{dt} = -\frac{1}{N} \nabla \cdot (P \vec{v}) \qquad \text{Energy}$$

Where

$$\vec{q} = \frac{\vec{v}\, \gamma^2 (P + n\hat{e} + n m_0 c^2)}{c^2 N}$$

$$\mathcal{E} = \frac{\gamma^2 (P + n\hat{e} + n m_0 c^2) - P}{N}$$

and
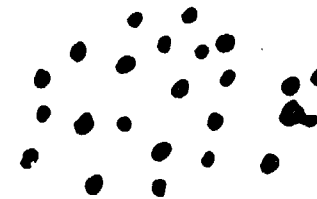
$$\frac{d}{dt} N = -N \nabla \cdot (v) \qquad \text{Continuity}$$

EQUATION OF STATE

$$P = (\Gamma - 1) n \hat{e} \quad \geq 0$$

- S. Chandrasekhar (Intro. To Stellar Structure)
  For Relativistic Gas.

- Amsden, Harlow, Nix, Strottman for
  Γ nuclear equ. of state.

SPH Equations

Cloud of
Baryons

contains
$\mathcal{N}_a$ Baryons

$$\frac{d\vec{q}}{dt} = -\sum_b \mathcal{N}_b \left[\frac{P_b}{N_b^2} + \frac{P_a}{N_a^2} \right] \vec{\nabla} W_{ab}$$

$\mathcal{N}$ of Baryons in SPH particle 'b'

The Energy Equation can be
written in more than 1 way.

TOTAL ENERGY

$$\frac{d}{dt}\mathcal{E}_a = -\sum_b \mathcal{v}_b \left\{ \right\} \cdot \nabla W_{ab}$$

$$\frac{P_a \vec{v}_a}{N_a^2} + \frac{P_b \vec{v}_b}{N_b^2}$$

$$\frac{P_a \vec{v}_b}{N_a^2} + \frac{P_b \vec{v}_a}{N_b^2}$$

$$\left(\frac{P_a}{N_a^2} + \frac{P_b}{N_b^2} \right) \left(\frac{\vec{v}_a + \vec{v}_b}{2} \right)$$

↗ average of the other two equations

$$\boxed{ \frac{d\mathcal{E}}{dt} = -\frac{1}{N} \nabla \cdot (P \vec{v}) }$$

Thermal Energy

$$\frac{d}{dt}\hat{e}_a = -\frac{P_a}{N_a}\frac{d\gamma_a}{dt} + \gamma_a \sum_b \nu_b \left\{ \qquad \right\} \cdot \vec{\nabla} w_{ab}$$

$$\frac{P_b}{N_b^2}(\vec{v}_a - \vec{v}_b)$$

$$\frac{P_a}{N_a^2}(\vec{v}_a \cdot \vec{v}_b)$$

Preferred

$$\frac{1}{2}\left(\frac{P_a}{N_a^2} + \frac{P_b}{N_b^2}\right)(\vec{v}_a \cdot \vec{v}_b)$$

$$\boxed{\gamma \vec{v} \cdot \frac{d\vec{q}}{dt} - \gamma \frac{d\varepsilon}{dt} = -\frac{d\hat{e}}{dt} - \frac{P}{N}\frac{d\gamma}{dt}}$$

Landau, Lifshitz
Eckart   } Based on Elegance
Weinberg, Carter

$$T^{\mu\nu} = (n m_o c^2 + n\hat{e} + P)U^\mu U^\nu$$
$$+ (P - \zeta\theta)g^{\mu\nu}$$

$$\frac{1}{c}\frac{d\gamma}{dt} + \frac{\gamma}{c}\nabla\cdot\upsilon$$

All Unstable

Hiscock, Lindblom   Phys. Rev D
Olson, Hiscock $31, 725, (1985)$
$t \sim 10^{-34} s.$ $41, 3687, (1990)$

Numerical

Hawley, Smarr, Wilson   Ap. J. Supp
$$P_{art} = \gamma \ell^2 (\nabla\upsilon)^2 [n m_o c^2 + n\hat{e} + P]$$

Laguna, Miller, Zurek ; Lahy (n. sc)
$$P_{art} = N\{\alpha \ell c |\nabla\cdot\upsilon| + \beta \ell^2 |\nabla\cdot\upsilon|^2\}$$
$$\text{if } \nabla\cdot\upsilon < 0$$
$$\text{otherwise zero}$$

These work okay, for $\upsilon \lesssim 0.8c$.

$$\boxed{\text{P.I.C. dissipation}}$$

Two Fluid Relativistic PIC

Nuclei
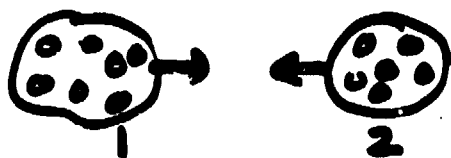
Strottman
Amsden
Harlow
Nix

$$\frac{d}{dt}\vec{q}_1 = -\frac{1}{N_1}\nabla P_1 - \frac{R_{coll}}{N_1 Y}K\left(\gamma_1 \vec{v}_1 - \gamma_2 \vec{v}_2\right)$$

$$\frac{d}{dt}\mathcal{E}_1 = -\frac{1}{N_1}\nabla\cdot(P_1\vec{v}_1) - \frac{R_{coll}}{N_1 Y}K\left(\gamma_1 - \gamma_2\right)c.$$

$$\boxed{\begin{array}{l} R_{coll} = n_1 n_2 \gamma_1 \gamma_2 \sigma v_{rel} = N_1 N_2 \sigma v_{rel} \\[6pt] v_{rel}^2 = (\vec{v}_1 - \vec{v}_2)^2 - \dfrac{(\vec{v}_1 \times \vec{v}_2)^2}{c^2} \\[6pt] Y = (1 - \vec{v}_1 \cdot \vec{v}_2)\gamma_1 \gamma_2 \end{array}}$$

Invariant v_{rel}.

$$v_{rel}^2 = \frac{\left[(\vec{v}_1 - \vec{v}_2)^2 - \dfrac{(\vec{v}_1 \times \vec{v}_2)^2}{c^2}\right]}{\left[1 - \dfrac{\vec{v}_1 \cdot \vec{v}_2}{c^2}\right]^2}$$

SPH Form of Baryon Drag

Use

$$\Pi_{ab} = \frac{-\mu_{ab}}{\overline{\pi}_{ab}} \overline{\pi}_{ab} \left\{ \overline{c}_{ab} + |\mu_{ab}| \right\}$$

Could use $|\vec{v}_{rel}|$

Note

$$\mu_{ab} = \frac{(\gamma_a \vec{v}_a - \gamma_b \vec{v}_b) \cdot (\vec{r}_a - \vec{r}_b)}{(\vec{r}_a \cdot \vec{r}_b)^2 + \eta^2}$$

Same form as Non Relativistic Viscous Term.

Equations

$$\frac{d\vec{q}_a}{dt} = -\sum_b \nu_b \left\{ \frac{P_a}{N_a^2} + \frac{P_b}{N_b^2} + \Pi_{ab} \right\} \vec{\nabla}_i W_{ab}$$

$$\frac{d N_a}{dt} = +\sum_b \nu_b (\vec{v}_a - \vec{v}_b) \cdot \nabla W_{ab}$$

$$\frac{d \hat{e}_a}{dt} = -\frac{P_a}{N_a} \frac{d \gamma_a}{dt}$$

$$+ \frac{\gamma_a P_a}{N_a^2} \sum_b \nu_b (\vec{v}_a - \vec{v}_b) \cdot \nabla W_{ab}$$

$$+ \gamma_a \sum_b \nu_b \, \Pi_{ab} \, \tfrac{1}{2} (\vec{v}_a - \vec{v}_b) \cdot \nabla W_{ab}$$

- Spline Kernel

- Iteration on $\hat{e}$ and $d\gamma/dt$

- $h_{ab} = \tfrac{1}{2}(h_a + h_b)$

  or
  $$h_{ab} = \frac{2 \, h_a h_b}{h_a + h_b}$$

  or
  $\bullet \; \bullet \; \bullet \; \bullet \; \bullet \; \bullet \; \bullet \bullet$

Experiments

- Sound Wave. $(D=1, \hat{E}=0.2, \Gamma=\frac{5}{3}$

$$\Delta v = 0.05 \exp\left(-\frac{x^2}{\ell^2}\right)$$

- Shock Tube

- Colliding Cold Streams

Smoothing

$$N(x) = \frac{[N\ell + Nr \exp(x/\ell)]}{1 + \exp(x/\ell)}$$
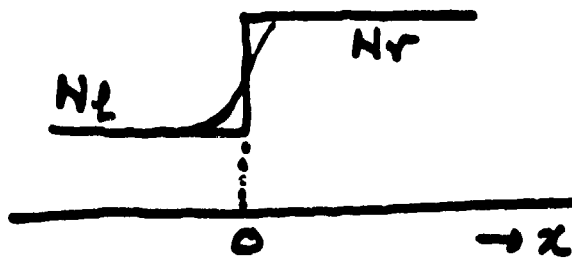
nmodel= 120   n= 201   h= 0.010   time= 4.5135E-01 $\alpha = 1$ $\beta = 2$
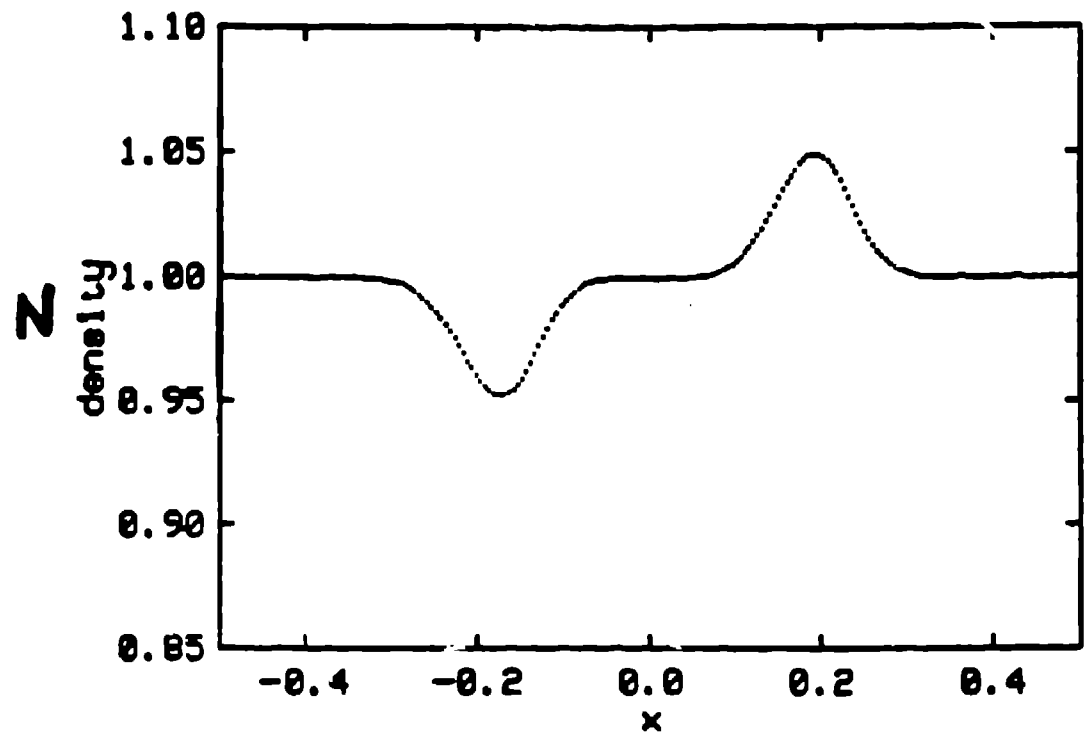
PROPAGATION OF SOUND WAVE IN A RELATIVISTIC GAS.

Speed 0.414

$42\,m$
$\cdot \delta = 90m$
$\frac{42}{40} \times \cdot \delta$ ...

26-AUG-93

$\frac{42}{40} \times \cdot 4$
$\frac{}{16 \cdot 8}$

speed = $\frac{\cdot 187}{1 + \cdot 15}$
$= 0.414$

$S = \sqrt{\dfrac{\frac{5}{6} \cdot \frac{4}{8} \cdot 2}{1 + \frac{5}{6} \cdot 2}}$
$= 0.408$

26-AUG-93

$x=1, p=2$
$p=q=0.1$ $r=5/3$, $\hat{e}=0.2$

nmodel= 200   m= 600   h= 0.150   time= 1.1474E+01

small v ~10^{-4}

vx

0.000

-0.001

-0.002

-0.003

-0.004

-0.005

-30   -20   -10   0   10   20   30

x
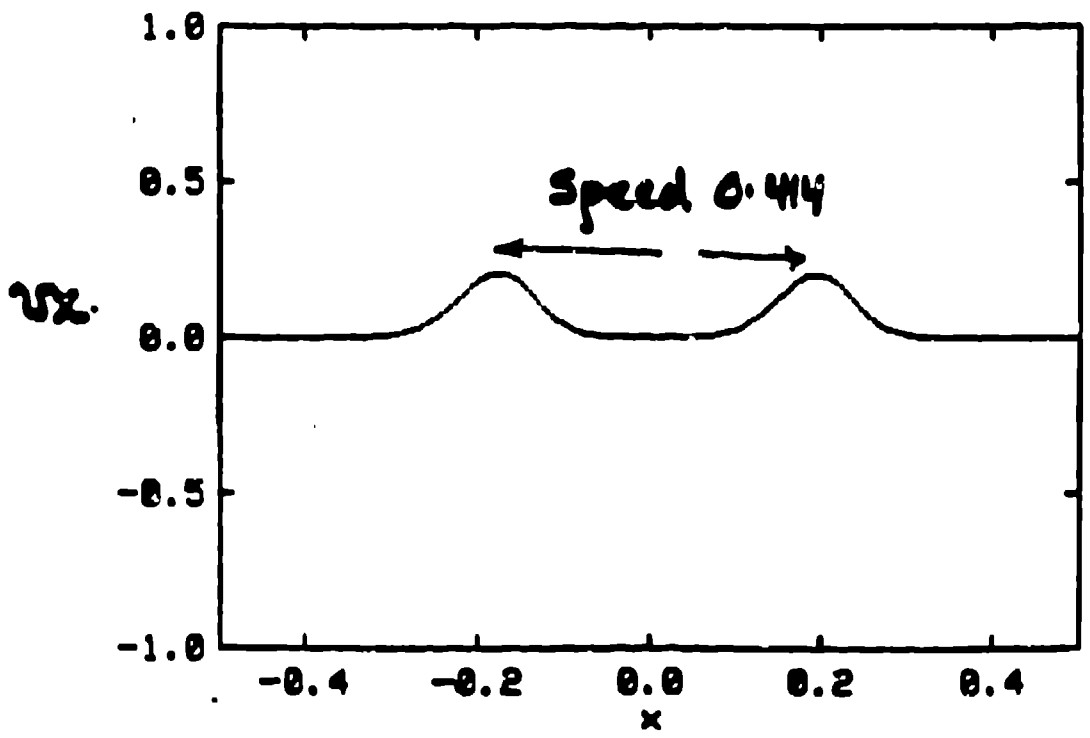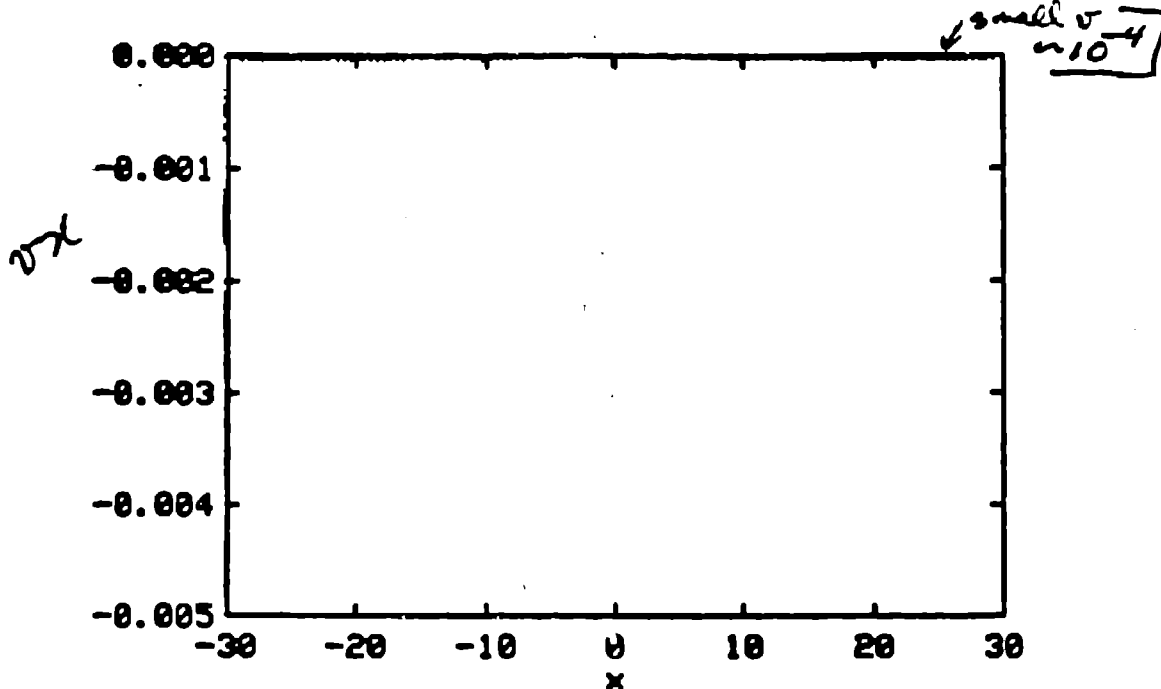
25-AUG-93

Why are the errors small for x=0 ?

nmodel= 200   n= 600   h= 0.150   time= 1.1474E+01

density

1.04

1.02

pattern slopes

1.00

.005

.002

Vx .0001

factor 20 smaller

0.98

0.96

-30   -20   -10   0   10   20   30

x
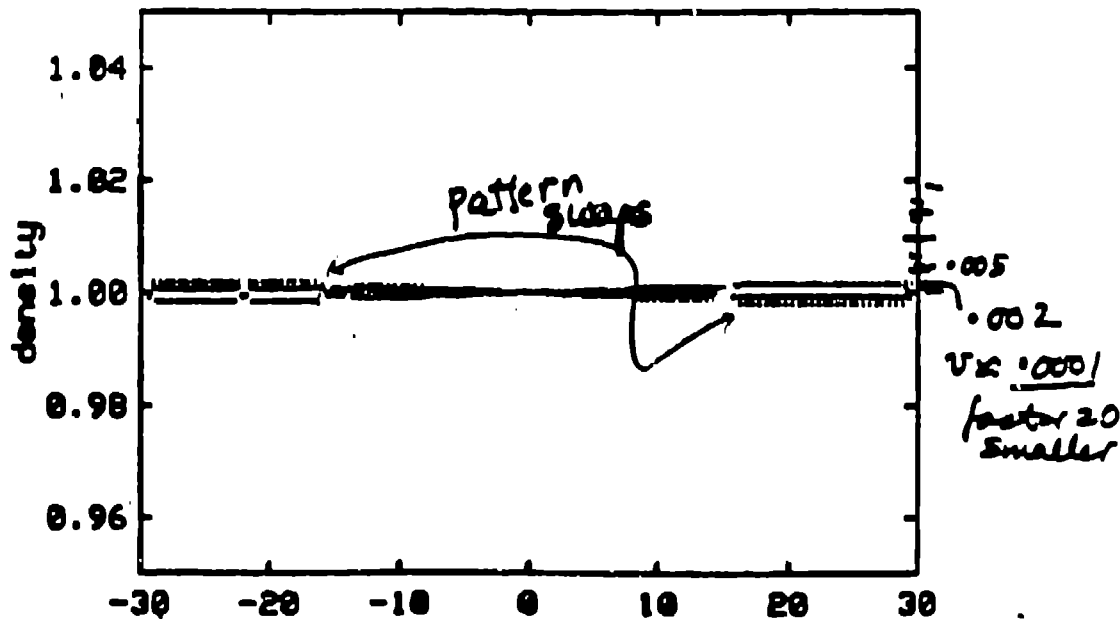
25-AUG-93

nmodel= 200   n= 600   h= 0.150   time= 1.1471E+01

$\tau \chi$
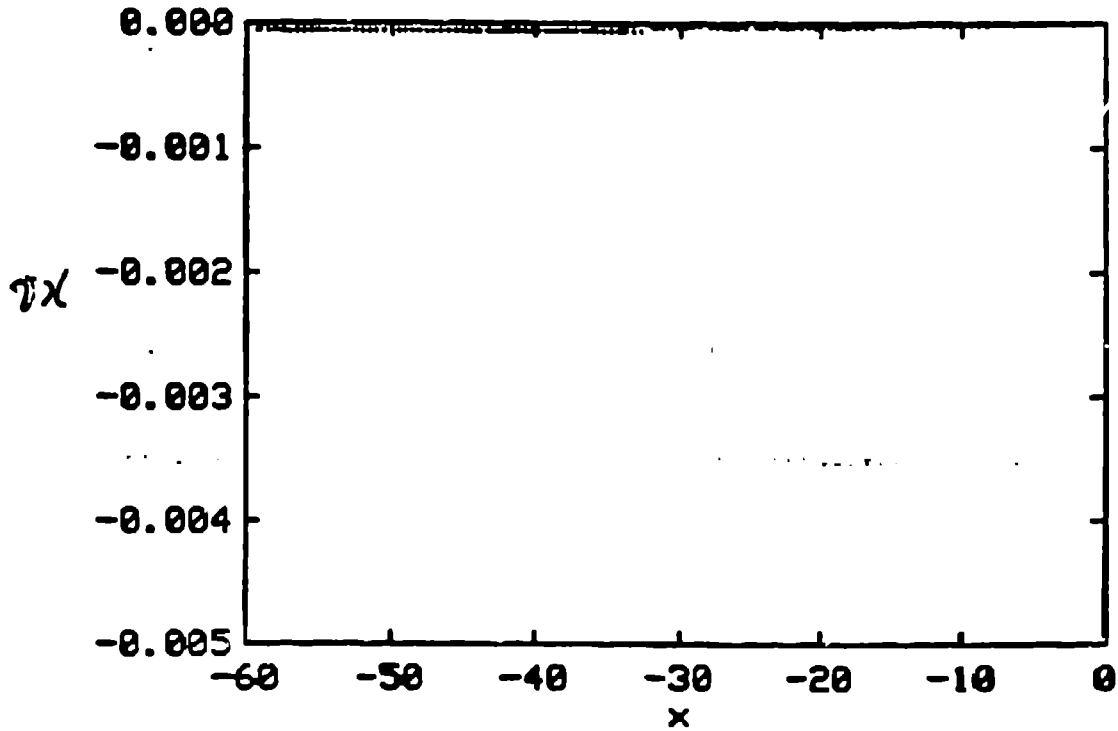
25-AUG-93

No initial perturbations!

nmodel= 200   m= 600   h= 0.150   time= 1.1471E+01
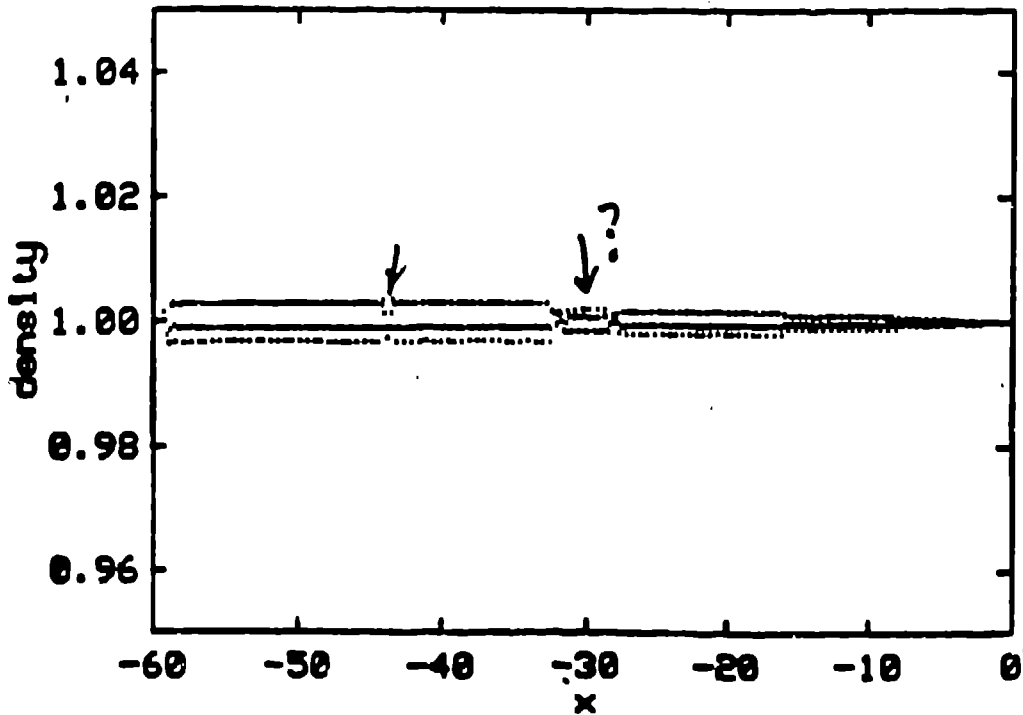
pattern
changes

contains
oscillations
$\lambda \sim \pi \lambda$

-402-

25-AUG-93

nmodel= 800   n= 551   h= 0.020   time= 3.0983E-01

$\Delta x_i = \frac{2\mu}{E}$

$\frac{E_{kin}=0}{\alpha = 1}$

$\frac{\rho^{e_1}}{\ell_{int}}$

$h = 2\lambda$

density

10-SEP-93

$\hat{\varepsilon} = 10^{-6}$
$N = 1$

$r_b = \frac{3}{4}$
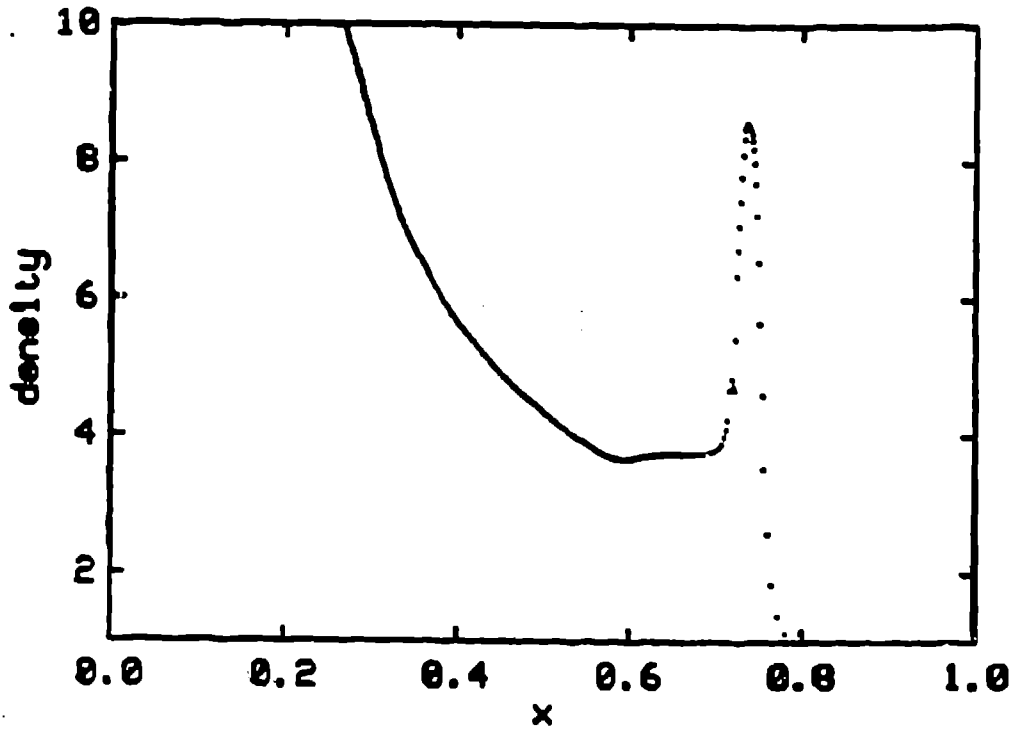
nmodel= 800   m= 551   h= 0.020   time= 3.0983E-01

v

Error
< 1%

10-SEP-93

$$h_{ab} = \frac{1}{2}\left(h_a + h_b\right)$$

$\mathcal{E} = \mu^{-4}$
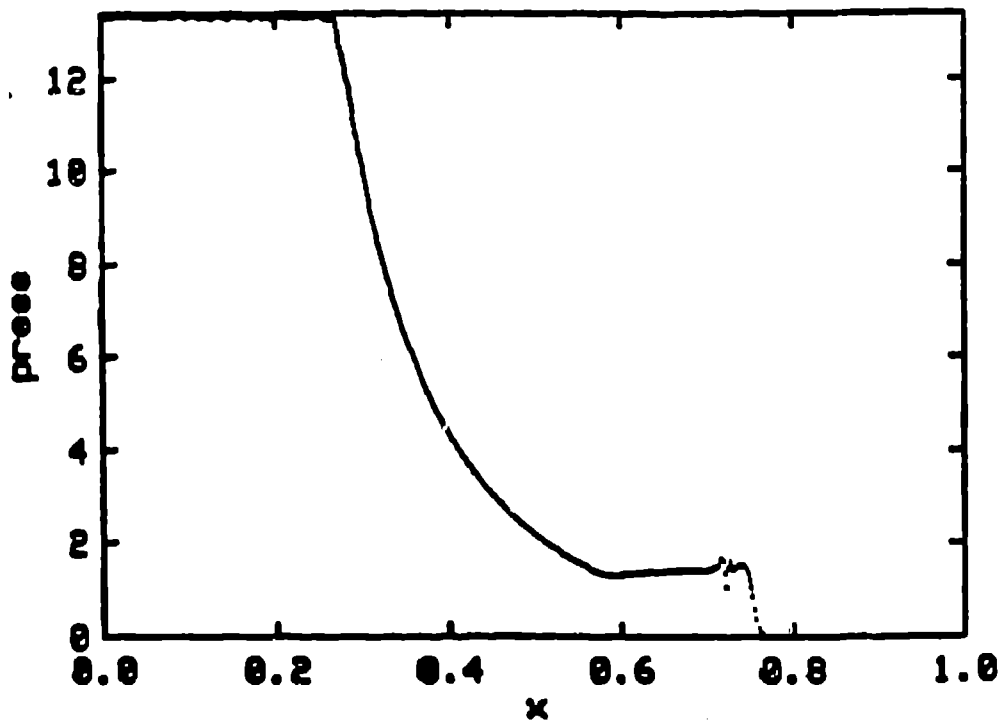
nmodel= 400   n= 101   h= 0.015   time= 3.6499E-01
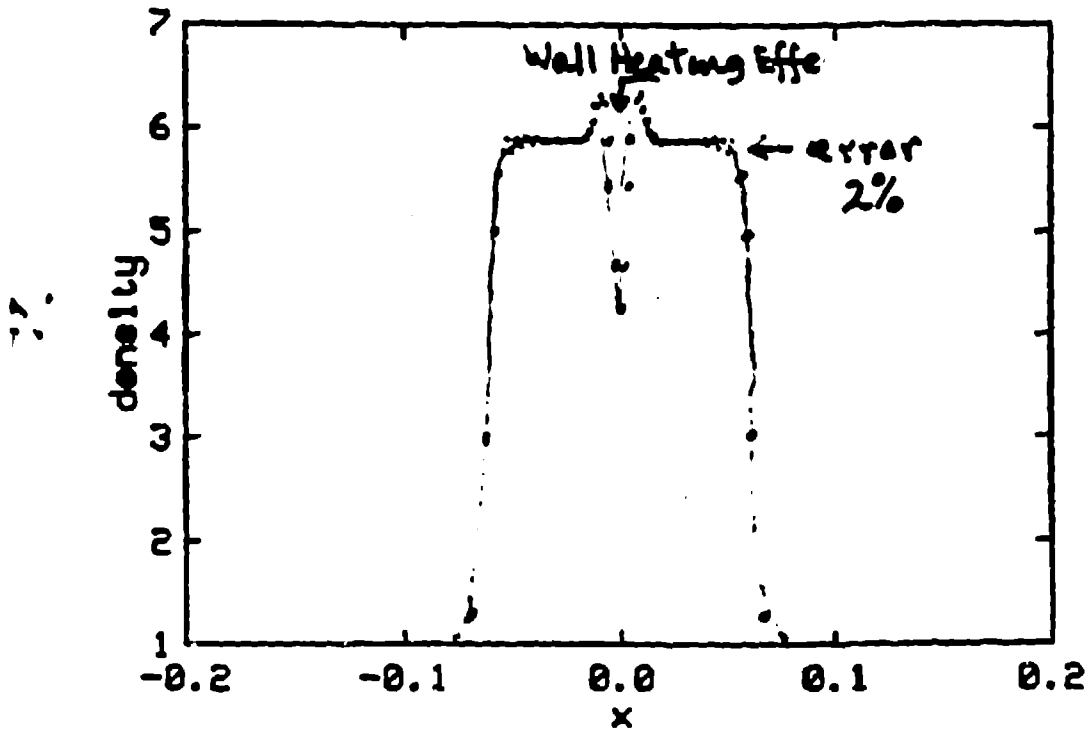
$$h_{ab} = \frac{2h_a h_b}{h_a + h_b}$$

Hawley et al.
get larger errors

nmodel= 400   n= 101   h= 0.015   time= 3.6499E-01
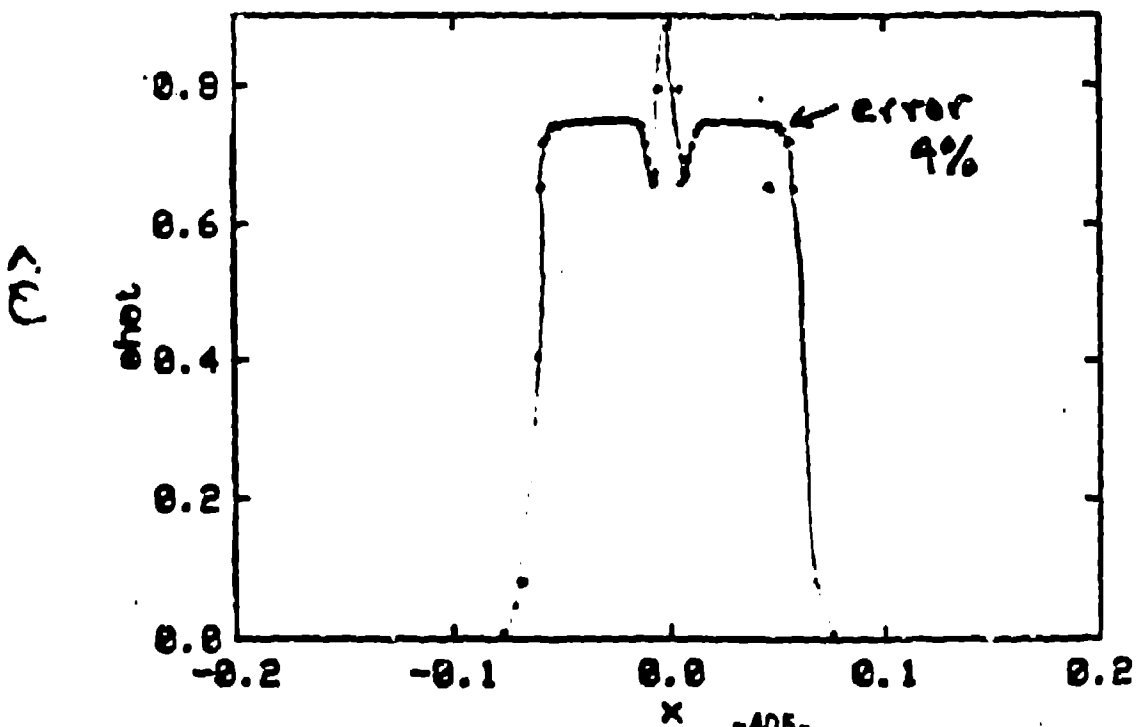
CONCLUSIONS

- The Baryon-Baryon Viscosity is known to work with $v \leq 0.95\,c$

- The results are comparable to those of Hawley et.al. — often better!

- We need to decide best rule for choosing h_{ab}

- We definitely need a good heat conduction — for any method

- The calculations show integrating the continuity equation works o.k. for strong shocks.

1) Constructing particle paths for Schwarzschild + FRW spacetimes
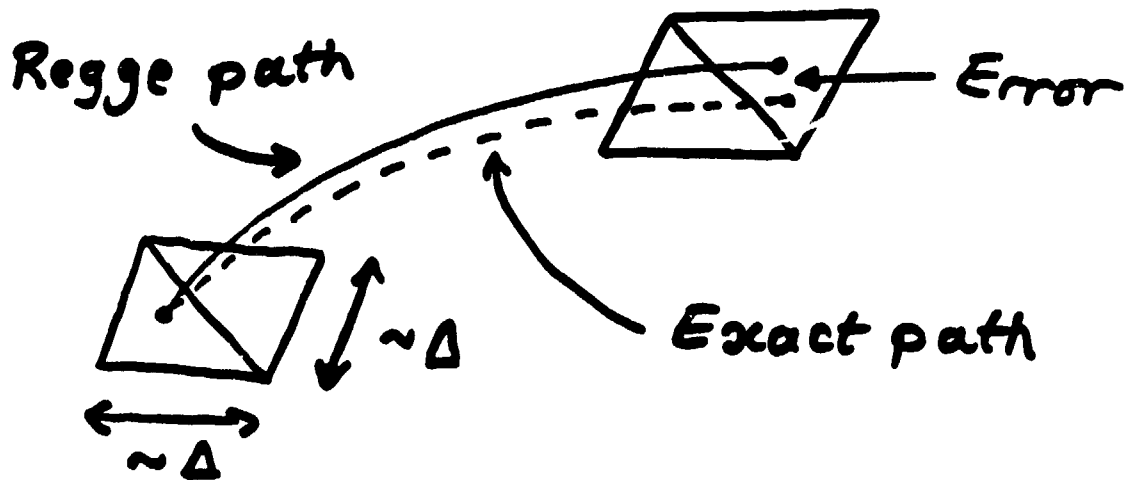
We showed that the global error $\sim O(\Delta)$
The Regge equations can be modified to give a global error $\sim O(\Delta^2)$

2) Boundary conditions
Is there a systematic way to translate

$$\frac{\partial \phi}{\partial r} + \frac{\phi - 1}{r} = 0$$

into some BC on the L_{ij}'s ?
How can r and L_{ij} be related ?

We have a program that evaluates, for <u>any</u> 4-D simplicial space

i) all areas, volumes and defects

ii) all the field equations and

iii) all the derivatives of the field equations — required for Newton-Raphson.

The program takes about 6×10^{-9} s per equation (+ derivatives).

Next step — port it to a CM5.
         — apply it to 2 BH problem.

"Mountains

Fertile Plains
of Gas Dynamics

SPH

Path of SPH
Viscosity

Swamp of
Penetration

Shocks

Star formation

Relativity

TREECODES

Cosmology

?

Baker's
Exit

Swegle
Ravine
of Metals

Variable .h

Elastic-Fracture.

Resolution
Rapids

Ellipsoidal
Kernels
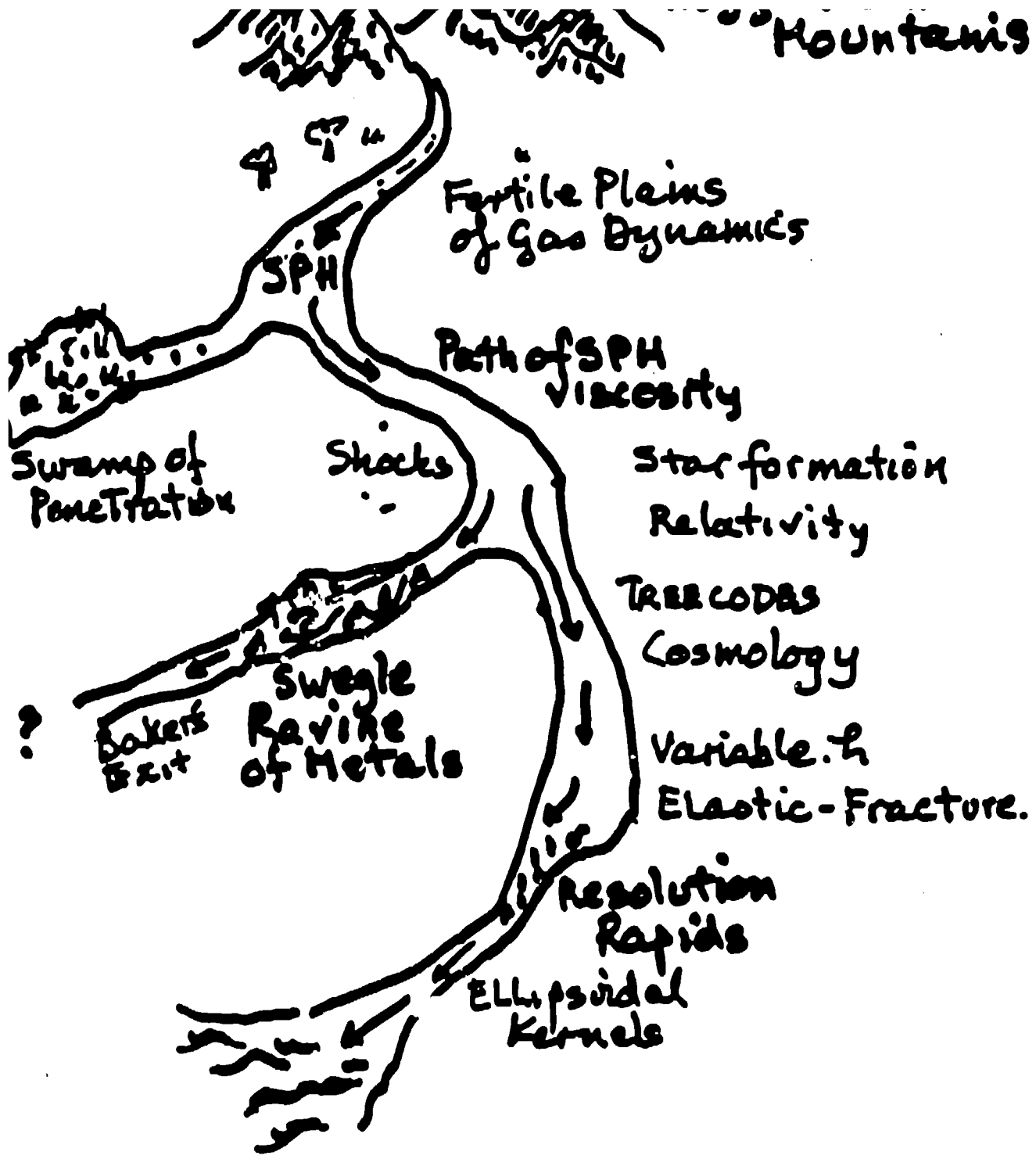
Caltech
130-33
Pasadena, CA 91125

Melvyn B. Davies
mbd@tapir.caltech.edu

Cray Research, Inc.
Suite 830
6565 Americas Parkway, N.E.
Albuquerque, NM 87110

Phil Campbell   505-883-8700
          pmc@crayalb.cray.com
Dave Shirley   505-883-8700
          dshirley@crayalb.cray.com

Dagonet Software
2904 La Veta Dr. NE
Albuquerque, NM 87110-3110

Lou Baker   505-883-0381
          505-846-2018
          baker@jake.plk.af.mil

Kachina Technologies
1420 Carlisle Blvd. NE
Suite 202
Albuquerque, NM 87110

Tony Giancola   505-268-8982
          tony@objectsci.com

Kaman Sciences Corporation
1500 Garden of the Gods Rd.
P. O. Box 7463
Colorado Springs, CO 80933

Nasit Ari   719-599-1637
Sheldon Jones   719-599-1911
          jonesm@ksc.com
Joe Secary   719-599-1647

Laboratoire de Physique de la Matiere Condensee
Universite de Nice Sophia-Antipolis
Parc Valrose
06108 NICE Cedex 2 France

Christian Vanneste   33 93 52 99 72
          vanneste@calypso.unice.fr

Lawrence Livermore National Laboratory
PO Box 808
Livermore, CA 94550

Leigh Brookshaw   MS L-413
Bill Hoover   MS L-794
Alan Spero   510-423-2999
Joseph S. Oliveira
          jso@ocfmail.ocf.llnl.gov

Los Alamos National Laboratory
Los Alamos NM 87545

Stirling Colgate   505-665-5254   MS B275
Necia Cooper   505-667-1447   MS M708
Rich Davidson   505-667-7438   MS K557
          rich@lanl.gov
Mike Garcia   505-667-7965   MS C931
Jack Hills   505-667-9152   MS B288

LIST OF ATTENDEES AND OTHERS

This list inlcudes people who attended the SPH workshop and people who were interested in the workshop but could not attend. This also constitutes the distribution list. This list is organized by company or institution. Following this list is a list organized by name.

Advanced Sciences Incorporated
6739 Academy Rd., NE
Albuquerque, NM 87109

Mehdi Eliassi

Air Force Institute of Technology
2950 P Street
Wright-Patterson Air Force Base
Dayton, Ohio 45433-7765

Michael Stoecker   513-255-3636 ext 4514
            Department of Mathematics and Statistics
            mstoecke@afit.af.mil
Dave Fulk
            AFIT/ENC
            dfulk@afit.af.mil

Alliant Tech Systems Inc. (MN 11-2925)
600 2nd St NE
Hopkins, MN 55343

Gordon Johnson   612-931-5905

Alme and Associates
2 Stevens Forest Professional Center
9650 Santiago Road
Columbia, MD 21045

Marv Alme   410-740-1118

Applied Research Associates
4300 San Mateo Blvd. NE
Suite A-220
Albuquerque, NM 87110

Ted Carney   505-883-3636

Battelle
505 King Avenue
Columbus, OH 43201-2693

Mike Fisher   614-424-3620
            fisher@tomahawk.dst.battelle.org
Doug Everhart   614-424-3214
            doug@dragon.dst.battelle.org
Chuck Hargraves   614-424-4953

Brad Holian	505-667-9237	MS B268
Kathy Holian	505-665-4616	MS B295
Norman Johnson	505-667-9094	MS B216
Mike Jones	505-667-7760	MS F645
Bob Karpp		MS F663
Jerry Kerriak	505-665-8709	MS F663
Ron Kirkpatrick	505-667-7208	MS F645
Raymond Leflamme	505-667-3394	MS B288
Peter Leonard	404-667-1472	MS B288
Larry Luck	505-667-3563	MS K557
Dave Mandell	505-667-7145	MS F663
dam@lanl.gov		
Warner Miller	505-667-3747	MS B288
wam@regge.lanl.gov		
B. Nadiga	505-667-9466	MS B213
Joe Repa	505-667-4494	MS K574
Larry Schwalbe	505-667-0325	MS F663
Barry Shafer	505-667-1074	MS K574
Charles Snell	505-667-9841	MS F665
cms@beta.lanl.gov		
Warren Sparks	505-667-4922	MS F663
wms@lanl.gov		
Bob Stellingwerf	505-667-8905	MS F645
rfs@lanl.gov		
Robert Swift	505-665-7871	MS F665
bswift@beta.lanl.gov		
Harold Trease	505-667-8062	MS F663
het@lanl.gov		
Mike Warren	505-665-5023	MS B288
Doug Wilson	505-667-4370	MS F645
dcw@lanl.gov		
Chuc Wingate	505-667-8954	MS F645
caw@lanl.gov		
Wojciech Zurek	505-667-6837	MS B288

Louisiana State University
Dept. of Mechanical Engineering
Baton Rouge, LA 70803

Robert Courter   504-388-5891

Michigan Tech. University
Math Department
Houghton, Michigan 49931

Darrell L. Hicks   906-337-5817
liebrock@cs.mtu.edu

Mission Research Corporation
1720 Randolph Road, SE
Albuquerque, NM 87106-4245

Tom Hughes   505-768-7719

Monash University   Joe Monaghan   03 565 3867
Mathematics Department   jjm@vaxc.cc.monash.edu.au
Clayton, Vic.3168
Australia

NASA Ames Research Center   Erik Asphaug   415-604-0786   MS 245-3
Moffett Field, CA 94035   asphaug@cosmic.arc.nasa.gov

NM Institute of Mining and Technology   Larry Libersky   505-835-5941
Center for Explosives Technology Research   larry@illusion.nmt.edu
Socorro, NM 87801

Northwestern University   Ted Beletchko   708-491-7270
Dept. of Mechanical Engineering   Wing Kam Liu
2145 Sheridan Rd.   Yun Yun Lu   708-491-5164
Evanston, IL 60208-3111   yunlu@tam4.mech.nwu.edu

Ohio State University   Mike Owen   614-292-7881
Dept. of Astronomy   owen@payne.mps.ohio-state.edu
174 W 18th Avenue   Jens Villumsen
Columbus, OH 43210   jens@payne.mps.ohio-state.edu

Phillips Lab   Firooz Allahdadi   505-846-2016
PL/WSSD   Dave Amdahl   505-846-2017
Kirtland Air Force Base   amdahl@jake.plk.af.mil
Albuquerque, NM 87117   Charles Luehr   505-846-2017
                                                luehr@jake.plk.af.mil
                                          David Medina
                                          James Ninter
                                          Brad Smith   505-846-2016
                                                bsmith@jake.plk.af.mil

Purdue University   Patrick Fox   317-494-0697
Dept. of Civil Engineering   pfox@ecn.purdue.edu
West Lafayette, IN 47907

Rice University   Hank Alme   713-665-0133
Baker College   almehj@owlnet.rice.edu
6320 South Main St.
Houston, TX 77005

Sandia National Laboratory
P. O. Box 5800
Albuquerque, NM 87185

Steve Attaway   505-844-9288   Dept. 1425
                 swattaw@sandia.gov
Jeff Swegle   505-844-9369   Dept. 1562
                 jwswegl@sandia.gov

Tetra Corporation
3701 Hawkins St. NE
Albuquerque, NM 87109-4512

Gary Hess   505-345-8623

University of Arizonia
Steward Observatory
Tucson, Arizona 85721

Willy Benz   602-621-6530
                 wbenz@ptolemy.as.arizona.edu

University of Heidelberg
Institut fur Theoretishche Astrospyaik
Im Neuenheimer Feld 561
D - 69120 Heidelberg
Germany

Hanno Sponholz   49 (6221) 56 2974
                 sponholz@epikur.ita.uni-heidelberg.de

University of New Mexico
Dept. of Chemical/Nuclear Engineering
Farris Engineering Center
Albuquerque, NM 87131-1341

Rita Smith   505-821-0416
                 rsmith@aquarius.unm.edu
A. Sharif Heger
                 heger@hydra.unm.edu

University of Pennsylvannia
Dept. of Astronomy and Astrophysics
525 Davey Laboratory
University Park, PA 16802

Pablo Laguna   814-863-8470
                 pablo@astro.psu.edu

University of Texas
Dept. of Mechanical Engineering
ETC 5.160
Austin, TX 78712

Eric Fahrenthold   512-471-3064
                 meed522@hermes.chpc.utexas.edu

University of Western Ontario
Department of Applied Mathematics
London, Ontario, Canada, N6A 3K7

Patrick Mann
                 pjm@monty.apmaths.uwo.ca

LIST OF ATTENDEES AND OTHERS

This list is the same as the previous list but organized by individual name.

Firooz Allahdadi	Phillips Lab
Hank Alme	Rice University
Marv Alme	Alme and Associates
Dave Amdahl	Phillips Lab
Nasit Ari	Kaman Sciences Corporation
Erik Asphaug	NASA Ames Research Center
Steve Attaway	Sandia National Laboratory
Lou Baker	Dagonet Software
Ted Beletchko	Northwestern University
Willy Benz	University of Arizona
Leigh Brookshaw	Lawrence Livermore National Laboratory
Phil Campbell	Cray Research, Inc.
Ted Carney	Applied Research Associates
Stirling Colgate	Los Alamos National Laboratory
Necia Cooper	Los Alamos National Laboratory
Robert Courter	Louisiana State University
Rich Davidson	Los Alamos National Laboratory
Melvyn B. Davies	Caltech
Mehdi Eliassi	Advanced Sciences Incorporated
Doug Everhart	Battelle
Eric Fahrenthold	University of Texas
Mike Fisher	Battelle
Patrick Fox	Purdue University
Dave Fulk	Air Force Institute of Technology
Mike Garcia	Los Alamos National Laboratory
Tony Giancola	Kachina Technologies
Chuck Hargraves	Battelle
A. Sharif Heger	University of New Mexico
Gary R. Hess	Tetra Corporation
Darrell L. Hicks	Michigan Tech. University
Jack Hills	Los Alamos National Laboratory
Brad Holian	Los Alamos National Laboratory
Kathy Holian	Los Alamos National Laboratory
Bill Hoover	Lawrence Livermore National Laboratory
Tom Hughes	Mission Research Corporation
Gordon Johnson	Alliant Tech Systems Inc.
Norman Johnson	Los Alamos National Laboratory
Mike Jones	Los Alamos National Laboratory
Sheldon Jones	Kaman Sciences Corporation
Bob Karpp	Los Alamos National Laboratory

Jerry Kerrisk	Los Alamos National Laboratory
Ron Kirkpatrick	Los Alamos National Laboratory
Pablo Laguna	University of Pennsylvannia
Raymond Leflamme	Los Alamos National Laboratory
Peter Leonard	Los Alamos National Laboratory
Larry Libersky	NM Institute of Mining and Technology
Wing Kam Liu	Northwestern University
Yun Yun Lu	Northwestern University
Larry Luck	Los Alamos National Laboratory
Charles Luehr	Phillips Lab
Dave Mandell	Los Alamos National Laboratory
Patrick Mann	University of Western Ontario
David Medina	Phillips Lab
Warner Miller	Los Alamos National Laboratory
Joe Monaghan	Monash University
B. Nadiga	Los Alamos National Laboratory
James Ninter	Phillips Lab
Joseph S. Oliveira	Lawrence Livermore National Laboratory
Mike Owen	Ohio State University
Joe Repa	Los Alamos National Laboratory
Larry Schwalbe	Los Alamos National Laboratory
Joe Secary	Kaman Sciences Corporation
Barry Shafer	Los Alamos National Laboratory
Dave Shirley	Cray Research, Inc.
Brad Smith	Phillips Lab
Rita Smith	University of New Mexico
Charles Snell	Los Alamos National Laboratory
Warren Sparks	Los Alamos National Laboratory
Alan Spero	Lawrence Livermore National Laboratory
Hanno Sponholz	University of Heidelberg
Bob Stellingwerf	Los Alamos National Laboratory
Michael Stoecker	Air Force Institute of Technology
Jeff Swegle	Sandia National Laboratory
Robert Swift	Los Alamos National Laboratory
Harold Trease	Los Alamos National Laboratory
Christian Vanneste	Laboratoire de Physique de la Matiere Condensee
Jens Villumsen	Ohio State University
Mike Warren	Los Alamos National Laboratory
Doug Wilson	Los Alamos National Laboratory
Chuck Wingate	Los Alamos National Laboratory
Wojciech Zurek	Los Alamos National Laboratory